Lehrstuhl für Ingenieurgeologie

Sediment dynamics in Lago Calafquén and Lago Villarrica (Northern Patagonia – Chile):

A baseline study on sedimentological processes and considerations in assessing palaeoenvironmental change

Sabine Volland

Vollständiger Abdruck der von der Fakultät für Bauingenieur- und Vermessungswesen der Technischen Universität München zur Erlangung des akademischen Grades eines

Doktors der Naturwissenschaften (Dr. rer. nat.)

genehmigten Dissertation.

Vorsitzender:	Univ.-Prof. Dr. rer. nat., Dr. rer. nat. habil. J. H. Kruhl
Prüfer der Dissertation:	
1.	Univ.-Prof. Dr. rer. nat. K. Thuro
2.	apl. Prof. Dr. phil. M. Sturm, Eidgenössische Technische Hochschule Zürich/Schweiz

Die Dissertation wurde am 23.11.2005 bei der Technischen Universität München eingereicht und durch die Fakultät für Bauingenieur- und Vermessungswesen am 31.03.2006 angenommen.

To all of you who always believed in me,
to my sister and her family,
to my mother,
to my friends.

Life is what we make it!

ACKNOWLEDGEMENTS

This work was done on material that was initially retrieved from a pilot seismic, sediment sampling, and coring campaign of the 'Sediment Research Group' of the Technische Universität München (TU), together with the Universidad Austral de Chile (UACH) in Valdivia, Chile. The campaign took place in southern autumn 2001 (northern spring) in the northern Chilean Lake District and was initiated to begin a long-time monitoring program involving the quantification of recent sedimentation processes by sediment traps. Furthermore, the planned project included palaeoenvironmental and -climatic reconstructions from long sediment cores (Kullenberg piston cores) of these lakes, to improve the understanding of the regional development since the end of the last glaciation in that area. Due to unpredictable developments, the proposal never went beyond the planning phase. The former head of this project and of the 'Sediment Research Group' of the TU München, Dr. *Jens Müller*, died suddenly and unexpected in May 2002, shortly after the field work in Chile.

I continued working with the rough seismic data and the sediments we had taken provisionally from both lakes, not knowing if they would reveal any significant results for my PhD study. I applied the 'routine' sediment analyses that could be done in our sedimentological laboratory of our research group, which was closed in October 2004. In this spirit, I have to say that I am more than indebted to *Jens Müller*, not only for taking the samples during the Chilean field work campaign, but rather for the experience I gained from all the project work I did with him and for him, for teaching me the basics of lake sedimentology and what it is all about. This helped me to conduct other projects without him, to continue working in and maintain the sedimentology section of the institute at the TU München after his death – together with my colleague *Johannes Wallner* – until the section was finally closed. Gathering all this experience, from doing a lot of welcome and also definitely unwelcome work, is one essential 'core' that I take with me. It made me richer in personality and broadened my mind.

Eventually, serendipity was one of the driving factors that kept me continuing with what I did, keeping me curious and interested, and bringing this work to an end. In this sense I owe tribute to a lot of people who were in the background all that time, who provided helping hands, technical and logistical – and above all – mental support during all those years.

My cordial thanks go to:

- Prof. Dr. *Kurosch Thuro*, Lehrstuhl für Ingenieurgeologie, Technische Universität München, who accepted the supervision of this PhD work after taking over the management and leadership of this institute in February 2004. He provided me a study carrel, and with his approval, I could use the facilities of the institute. He supported my application for the women's funding scholarship of the TU München, thus allowing completion of this work.

- I am acutely indebted to Dr. *Mike Sturm*, EAWAG Dübendorf, Switzerland, who appeared out of the blue one day in February 2004. Mike took over the professional supervision of this PhD work in April 2004, and supported me by giving me the chance to improve existing and conduct additional analyses that make up the sedimentology and multi-proxy parts of this thesis. He allowed me to use all necessary analytical facilities and equipment of the EAWAG laboratories and the Malvern grainsizer at the ETH

Zürich, funded the geochemical and sedimentological analyses, as well as the radionuclide Cs- and Pb-dating. Furthermore, he supported my trips to Zurich during my last year and made it possible for me to attend congresses. Mike also supported my scholarship application. I am grateful to his fruitful comments, his patient and redundant discussions with me, his generous manner and for integrating me into the 'Sedimentology Group' of the EAWAG. In this sense I also thank Brian Sinnet and Alex Blass from the EAWAG as well as Raphael Bühler for supporting the 'lab' work and solving technical problems that occurred sometimes with the analytical equipment.

- My thankfulness goes to the women's representative of the Technische Universität München, Fr. Dr. Ute Lill, who funded completion of this work by granting a one-year scholarship after the HWPII of the Women's Research Funding Programme 2004/2005, 'Chancengleichheit für Frauen in Forschung und Lehre' ('Equal opportunity for women in research and teaching').
- The 'Deutscher Akademischer Austausch Dienst' (DAAD) supported my stay and field work in Chile during 2001 by granting a six-month postgraduate scholarship of the HSPIII Programme.
- To Prof. Dr. Mario Pino from 'el Instituto de Geociencias de la Universidad Austral de Chile' in Valdivia I cannot express enough thankfulness to meet satisfaction. He provided logistical support for the lake campaigns, allowed me to use the facilities of the institute at the UACH, advised my 'lab' work over there, and cared for me during all my stays in Chile. Moreover, Mario helped me to contribute a Spanish abstract in this thesis. I owe him for his inexpressibly kind of humor and everlasting friendship.
- Robert Brümmer from 'el Instituto de Geociencias de la UACH', technically supported our field work and gave me logistical support in Valdivia, which was much appreciated.
- Rolf Klee, Landesamt für Umweltschutz (formerly: Bayerisches Landesamt für Wasserwirtschaft) in Wielenbach, put a lot of effort into Part 3 of this thesis. He made all the SEM photographs, introduced me to the basics of diatom identification, taught me sample preparation, and helped me identifying all the newly found species in the sediments of Lago Calafquén and Lago Villarrica.
- Dr. Emmanuel Chapron, Geological Institute, ETH Zürich, Switzerland, gave a lot of comments on the seismic sections, advised me at the Malvern grainsizer, took time for professional discussions that were beyond the call of duty. Thanks for the little but easy meetings and talks.
- Dr. Thomas Kulbe, EAWAG Dübendorf, Switzerland, often discussed and explained to me, very patiently, some of the secrets of geochemical and sedimentological behaviour (I really could pester him with my questions…). I appreciate his cooperativeness and am very grateful for the accommodation he provided me during the turn of my day- and nightshifts at the EAWAG laboratories.
- In this sense, I am also very grateful to Dr. Ruth Prelicz for also providing me endless accommodation during the weeks of marathon sample analysis, for her selfless offers, the permanent exchange and her friendship.
- I am deeply grateful to Dr. Markus Heinrichs, Canada, for the work he did to improve the English text of this thesis and the submitted manuscript on the seismics of Lago

Calafquén, for spending a lot of time to show me patiently how to do DCA and PCA-analyses, and all the ideas he came up with upon the biology of the studied lakes. Furthermore, his scientific and encouraging support during his stays at the Limnological Station of the TU München in Iffeldorf helped all PhD students there and me to continue working motivated and continuously.

- Dr. Gerhard Daut, Institut für physische Geographie, Friedrich-Schiller-Universität, Jena, is thanked for the AAS analyses of both sediment cores. Moreover, his commitment to further project work on the Bavarian lakes is gratefully acknowledged.
- Dr. Dirk Merten, Geologisches Institut, Friedrich-Schiller-Universität, Jena, is thanked for the ICP-MS analyses on the core samples.
- Prof. Dr. Marc De Batist, RCMG Gent, Belgium, and François Charlet took time and looked with me at the seismic data of both lakes several times. I am very grateful to both for helping me between 2002 and 2003, and for providing a study carrel whenever it was necessary. Furthermore, I am very grateful to Marc for the critical, precise and fruitful review of the submitted manuscript that still is subject to much improvement.
- PD Dr. Martin Grosjean, NCCR Climate, Universität Bern, Switzerland, is thanked for all the discussions, comments, and advice on my work, for the time he took, and for the critical review of the submitted manuscript on Lago Calafquén.
- Dr. Sven Lukas, School of Geography and Geosciences, University of St Andrews, Scotland, soon Geologisches Institut, Universität Bern, Switzerland, did an intense amount of work on the submitted manuscript of the seismics of Lago Calafquén. He explained me some of the secrets of 'glacial terminology'. Furthermore, he helped me a lot with the text on the Quaternary development of the study area in this thesis. Thanks for the great time during the congresses we attended.
- Prof. Dr. Jörn Kruhl, Fachbereich für Tektonik und Gefügekunde, Technische Universität München, was always there when needed. He also supported my scholarship application. I am grateful to his permanent encouraging words and the philosophical discussions on big and general questions about the 'why and what and what for', and for taking me to Corsica.
- Mark Peternell, Fachgebiet für Tektonik und Gefügekunde, and John Singer, Lehrstuhl für Ingenieurgeologie, Technische Universität München, exerted themselves on the Surfer bathymetric maps and GIS DTM models of both lakes, though they really had better things to do, as they are busy enough with their own PhD, assistance works, etc. You two did a bunch of work that wasn't yours!
- Dr. Jürgen Froh, formerly Lehrstuhl für Allgemeine, Angewandte und Ingenieur-Geologie, Technische Universität München, took the SEM pictures in Part 3, Chapter 7 and 8.
- Prof. Dr. Georg Spaun, formerly Lehrstuhl für Allgemeine, Angewandte und Ingenieur-Geologie, Technische Universität München, is thanked in this sense, as he had let me stay after Jens Müller's death and allowed me to continue my work at the institute until he retired.

My further thanks go to:

- Dr. Katja Held for her great energetic work she did with me during the last two years and all her C.E. workshops, for keeping me focused on the essential things, and for coaching the hidden parts of my personality.
- Dr. Christine Vornehm for the friendship, the endless and patient mutual exchange during all the good and bad times for both of us, and all the fun we had. There will be different times!
- Dr. Markus Scholz, for supporting me in necessary times, for solving some engineering geological problems in some of my work projects, and for being the friend he is.
- Ivan Zibra, Università di Pisa, Italy, for more than 40 days of pasta at my house, for all the bikes, and for introducing me to the geology of Corsica.
- Dr. 'Ted' Button, Institute of Engineering Geology, ETH Zürich, Switzerland, for the all the night filling conversation on 'all the world and his brother' and the easy time.
- All my friends and colleagues, who had been there during my PhD time and still are, who backed me up with small and big things, with helping hands, or with just being.
- My house mates Alex, Nicola, Christine, and Chrissi, who suffered from me during the last months (though I've actually moved to my office…), for their blithesome manner, their invitations, and for being the great house mates they were.
- Manfred Nadler, who eased the last but decisive months of this work with his enjoyable and caring manner, and simply with his presence.
- My last thanks concern my beloved one and only sister, and her husband, my two nieces, and my mother. All of you did a lot for me and I cannot do more than honour it.

Table of contents

Part 1:

III. Seismic stratigraphic investigation of Lago Calafquén and Lago Villarrica

Part 2:

IV. Sedimentation processes of Lago Calafquén and Lago Villarrica

Part 3:

V. Diatom assemblages: Considerations in assessing environmental change

Table of figures

Tables

ZUSAMMENFASSUNG

An den Seen Lago Calafquén und Lago Villarrica in Nordpatagonien (süd-zentral Chile) wurden limnogeologische Grundlagenstudien durchgeführt. Diese beinhalten 3,5 kHz hochauflösende Flachseismik, texturelle Untersuchungen von Oberflächenproben des Seebodens, 'multi-proxy' Untersuchungen an Sedimentkernen und eine qualitative, zeitbezogene Beschreibung der Diatomeenvergesellschaftungen.

Ablagerungen von Massenbewegungen und großräumige Deformationsstrukturen konnten in den Seesedimenten anhand der seismischen Profile kartiert werden. Diese Strukturen sind am deutlichsten in den südlichen und südwestlichen Beckenbereichen der Seen Lago Calafquén und Lago Villarrica identifizierbar. Erdbeben induzierte Deformationsstrukturen umfassen mehrfache Massenverlagerungen, großräumige Sedimentverflüssigungsstrukturen (Liquefaktion) und Turbidite. Aufgrund der regionalen Geologie des Einzugsgebietes sind die Hänge und das Hinterland beider Seen anfällig für häufige Hangrutschungen und Felsstürze. Diese Strukturen können auch in Satellitenbildern der umliegenden Nachbarschaft beider Seen beobachtet werden.

Rezente Sedimentationsprozesse beider Seen wurden auf der Grundlage von texturellen Sedimentuntersuchungen an Oberflächenproben rekonstruiert. Ihre Texturmuster spiegeln die Wechselwirkungen beider Seen mit ihrem Einzugsgebiet, der Größe des Einzugsgebietes und der Sedimentverfügbarkeit wider. Ablagerungen aus bodennahen Dichteströmen (underflows) beeinflussen die Sedimentation des Profundalbereiches beider Seen. Turbiditablagerungen kommen nur untergeordnet an den südwestlichen Enden beider Seebecken vor. Die normale lakustrine Sedimentation wird in diesen Bereichen überwiegend von Ablagerungen aus Trübstoff führenden Strömungen kontrolliert, die sich entlang der Thermokline einschichten (interflows). Klastischer Sedimenteintrag durch die saisonale Entwässerung der Vulkanhänge 'verdünnt' die normale biologisch kontrollierte lakustrine Sedimentation in beiden Seen. Dies kann anhand von Konzentrationsminima des gesamtorganischen Kohlenstoffgehaltes räumlich kartiert werden. Kleinere und überwiegend saisonal wasserführende Zuflüsse transportieren mitunter große Mengen an grobkörnigem Material in die Seebecken, wo sie sich als mächtige Turbidite großräuming verteilen. Anhand der sedimenttexturellen Muster können ihre Transportrichtungen und Ablagerungsbereiche bis weit ins Profundal verfolgt werden.

'Multi-proxy' Analysen wurden an kurzen Sedimentkernen beider Seen durchgeführt mit dem Ziel, zeitbezogene Sedimentationsprozesse zu erfassen und zu beschreiben sowie mögliche Umweltveränderungen während des späten Holozäns aufzuzeigen. Die datierten Sedimentablagerungen aus Bohrkernen beider Seen umfassen eine Zeitspanne bis max. 1200 Jahre (Lago Villarrica) und 3000 Jahre (Lago Calafquén). Häufig eingeschaltete Tephralagen unterbrechen die normale lakustrine Sedimentation und reflektieren eine starke vulkanische Aktivität während dieser Zeiträume. Beide Seen zeigen signifikante Reaktionen auf Veränderungen in ihrem lokalen Einzugsgebiet. Da die Einzugsgebiete beider Seen sehr unterschiedlich sind, können Reaktionen auf überregional greifende Umweltveränderungen nur spezifisch und individuell für jedes Einzugsgebiet betrachtet werden. Dennoch ist ein allgemeiner langzeitlicher Trend in der biogenen Produktion zwischen AD 800 und AD 1500 beobachtbar. Dies kann auf übergreifende Steuerungsmechanismen zurückgeführt werden, welche die internen Prozesse beider Seen kontrollieren, wie z. B. Klimaschwankungen.

Lago Calafquén und Lago Villarrica zeichnen sich durch eine artenarme Diatomeenvergesellschaftung aus. Vulkanischer Einfluss durch Ascheregen verursacht keine

Veränderungen in der Diatomeenabundanz; es werden nur Arten durch andere bereits existierende ersetzt. Das zeigt sich insbesondere in Ablagerungen einer monospezifischen Diatomeenpopulation, die über nahezu jeder Tephralage sedimentiert. Darüber hinaus werden keine Veränderungen in der Diatomeenstratigrafie verzeichnet, die größer als die natürliche Schwankungsbreite ist. Zeitbezogene stratigrafische Diatomeenuntersuchungen ermöglichten Interpretationen über denkbare Umweltbedingungen, die während dieser Zeiträume um die untersuchten Seen herum geherrscht haben könnten. Schwankungen in Diatomeenvergesellschaftungen stimmen mit Schwankungen in den gesamt- und biogenen Sedimentakkumulationsraten weitestgehend überein. Aufgrund von relativen Schwankungen zwischen schwer- und leichtschaligen Diatomeenarten könnten für den Lago Calafquén zwischen ~ BC 50 und ~ AD 1350 evtl. Bedingungen abgeleitet werden, die auf Turbulenz und Auftrieb in der Wassersäule hindeuten, wie z. B. starke Windaktivitäten und/oder Seespiegelschwankungen. Diatomeenvergesellschaftungen des Lago Villarrica könnten auf den Beginn der permanenten Besiedlung des Sees zum Ende des 18. Jahrhunderts/Beginn des 19. Jahrhunderts hinweisen.

ABSTRACT

A limnogeological baseline study of Lago Calafquén and Lago Villarrica, located in a geodynamically active setting in Northern Patagonia (south-central Chile), was carried out comprising 3.5 kHz high-resolution seismic stratigraphic investigation, texture analyses of surface sediments, multi-proxy analyses of sediment cores, as well as qualitative and chronological characterizations of diatom assemblages.

Mass movement deposits and large-scale soft sediment deformation structures mapped in the seismic data can be related to large seismic events that affect the southern and south-western slopes of the basins of Lago Calafquén and Lago Villarrica. Earthquake-induced deformation features comprise multiple mass-flow deposits, large-scale liquefaction structures, and turbidite deposits. According to site geology, the catchment of both lakes is prone to frequent landslide activity, which can also be deduced from structures in the lake's proximity mapped in Landsat images.

Modern sedimentation processes of both lakes are characterized by mapping sediment texture from surface sediment samples. Texture patterns reflect the interaction of the lake with its catchment, catchment size, and sediment availability. Underflow deposits accumulate in the deep basin plains of both lakes. Interflow deposits dominate along the south-western end of both basins, areas that are less affected by turbidite deposition. Clastic sediment input derived from seasonal drainage from the volcano flanks dilute the normal biologically-controlled lacustrine sedimentation, which is mapped by concentration minima of total organic carbon. On occasions small and mainly seasonal water-bearing tributaries deliver vast amounts of coarse-sized material into the basins, forming large turbidites. Deduced from textural patterns, their pathways can be traced far into the deep basin plain.

The multi-proxy studies on short sediment cores from both lakes were completed in order to characterize chronological sedimentation processes and to track possible environmental changes during the late-Holocene. Cores from Lago Calafquén and Lago Villarrica comprise a sediment record of the last 3000 and 1200 years, respectively. Strong volcanic activity during this period is unmistakable, as frequent tephra layers interrupt the normal lacustrine sedimentation. Both lakes show significant response to changes in the local catchment. As catchments of both lakes differ greatly, responses to regional spanning changes of environmental conditions are unique, but a general large-scale trend in biogenic productivity during AD 800 to AD 1500 is apparent. This is associated with a single driving force that controls internal processes of both lakes simultaneously, such as climate change.

Diatom assemblages of Lago Calafquén and Lago Villarrica have particularly low species diversity. Volcanic impact by tephra fall-out does not trigger changes in diatom abundance; only shifts in relative abundance occur, as observed by layers of monospecific diatom assemblages that were deposited above nearly every tephra layer in the sediment. Little change in the diatom stratigraphy, greater than the 'natural variation', was detected. Fluctuations in the diatom stratigraphy were consistent with fluctuations in the total and biogenic mass accumulation rate, enabling the interpretation of environmental conditions that might have prevailed. Shifts between heavy and light valve diatom species indicate turbulence and up-welling might have occurred between ~ BC 50 to ~ AD 1350 in Lago Calafquén. Diatom assemblages of Lago Villarrica indicate the onset of permanent settlement around the lake by the 18th/beginning 19th Century.

RESÚMEN

Se llevó a cabo un estudio limnogeológico en los lagos Calafquén y Villarrica, ambos ubicados en una zona de geodinámica activa de los Andes norpatagónicos. Estos análisis incluyen estratigrafía sísmica de alta resolución (3,5 kHz), análisis textural de sedimentos superficiales, análisis de testigos sedimentarios empleando variados proxies y caracterización de asociaciones temporales de diatomeas.

Depósitos de movimientos en masa y estructuras sinsedimentarias de gran escala reconocidas en los datos sísmicos pueden ser relacionadas a grandes eventos sísmicos que afectaron los bordes sur y suroeste de las cuencas de los lagos Calafquén y Villarrica. Tales estructuras de deformación inducidas por terremotos incluyen múltiples depósitos de flujo de masas, liquefacción de gran escala y turbiditas. Depósitos de flujos piroclásticos correspondientes a la actividad volcánica del Villarrica son identificados por múltiples reflectores de alta amplitud en los registros sísmicos. De acuerdo a la geología local las cuencas fluviales de ambos lagos son propensas a originar caídas de rocas y frecuentes deslizamientos de tierras, los cuales también pueden ser interpretados en la cercanías de ambos lagos a partir de imágenes satelitales Landsat.

Los procesos de sedimentación moderna en ambos lagos han sido caracterizados por medio de análisis textural de los sedimentos superficiales. Los patrones texturales reflejan la interacción de ambos lagos con sus cuencas, incluyendo el tamaño de las mismas y la disponibilidad de sedimentos en ellas. Depósitos de flujos profundos dominan las planicies sedimentarias profundas en ambos lagos. Por otra parte, depósitos de aguas intermedias se identifican a lo largo del borde suroccidental en ambos lagos, áreas que muestran una menor contribución de turbiditas. Ingreso de sedimentos clásticos derivados de drenajes estacionales desde los flancos del volcán Villarrica diluye la típica sedimentación biogénica lacustre, la que fue mapeada empleando la concentración mínima del Carbono orgánico total. Pequeños tributarios principalmente estacionales transportan ocasionalmente enormes cantidades de material grueso hacia ambas cuencas lacustres, originando grandes depósitos turbidíticos. Sus características texturales permiten trazar las direcciones de transporte hacia las planicies sedimentarias profundas de los lagos.

Con el propósito de investigar posible cambios ambientales holocénicos tardíos se analizaron con variados proxies testigos cortos de ambos lagos. Los testigos de ambos lagos registran la secuencia sedimentaria de los últimos 3000 (Lago Calafquén) y 1200 (Lago Villarrica) años, respectivamente. La fuerte actividad volcánica es evidenciada por frecuentes niveles de tefra que interrumpen la sedimentación lacustre normal. Los depósitos de ambos lagos han mostrado respuestas significativas a los cambios en las condiciones de las cuencas fluviales. Ya que tales cuencas difieren fuertemente, las respuestas a los cambios ambientales son individuales, pero en general se reconoce una obvia tendencia de gran escala en la productividad biogénica entre 800 AC y 1500 AC. Esto está asociado con los forzamientos generales que controlan los procesos internos en ambos lagos, tales como las fluctuaciones climáticas.

Las asociaciones de diatomeas en los lagos Calafquén y Villarrica tienen muy poca variedad. El impacto volcánico por caída de tefra no origina cambios en la abundancia de las diatomeas, solamente se observa desplazamiento de las especies preexistentes por otras diferentes. Esto se registra en láminas de poblaciones monoespecíficas de diatomeas sobre prácticamente cada uno de los múltiples niveles de tefra muestreados en cada testigo. Además, no se detectaron cambios en la bioestratigrafía de diatomeas que resulten mayores que la variabilidad natural. Sin embargo, estos análisis permitieron un interpretación de las posible condiciones ambientales que pueden haber ocurrido en ambos lagos. Las fluctuaciones en las asociaciones de diatomeas son consistentes con la

variabilidad en los tasas de acumulación de masa total y biogénica. Debido a la alternancia de asociaciones de especies de diatomeas con valvas livianas y densas es posible deducir condiciones de turbulencia y surgencia durante el intervalo de tiempo desde ~50 AC y a hasta ~1350 DC en el lago Calafquén. Las asociaciones de diatomeas del Lago Villarrica podrían indicar el inicio de los asentamientos permanentes en los bordes de este lago en el lapso entre el siglo 18 y el comienzo de siglo 19.

I. Prologue

1. Introduction

Palaeoenvironmental and palaeoclimatological reconstructions have advanced and improved during the last few decades with the shift to, and intense study of, lake sediments. Numerous measurable parameters within lake sediments have been recognised as important tools in documenting environmental and climatic variability. Many of the parameters investigated are sensitive to atmospheric influences, and may reflect changes in precipitation, atmospheric moisture balance, or temperature. External forces, such as intense volcanism, may mask the proxy signals found in normal lacustrine sedimentation. A reconstruction of palaeoenvironmental and –climate changes is generally done by high-resolution sediment studies. High-resolution studies are only valid for a certain period of time (Lotter and Sturm, 1994). Moreover, the reliability of the results achieved from these studies is highly dependent on the sample density of the sediments. Dense sub-sampling of sediments omits chronological biases and enables to establish a good model of past changes. But to generalize deduced prevailing climatic conditions on a large spanning transect should be done carefully, because parameters for high-resolution studies to reconstruct palaeoenvironmental and –climatic conditions are only local and, therefore, are individual, as they differ greatly in nature (Soon and Baliunas, 2003).

The Chilean Lake District located in northern Patagonia (south-central Chile) comprises around 20 glacial and tectonic born lakes. First sedimentological and palaeoenvironmental studies were conducted recently on Lago Puyehue (Chapron et al., 2004a, Bertrand, 2005, Bertrand et al., 2005). Furthermore, the entire Lake District is subject to recent and recurring volcanism. Effects of volcanic eruptions on these lakes and their ecological systems have not been studied. Thorough sedimentological studies and multi-proxy palaeoenvironmental investigations of the entire Lake District are in the very beginning. The overall goal of this thesis is to establish a baseline study that contributes to close this gap.

2. General context

In the context of ongoing discussions on global climate change, various interdisciplinary research projects have focussed on modelling of climate variability in the near future. Comparisons of reconstructed palaeoenvironments and/or palaeoclimates can play a vital role in improving the modelling of atmospheric circulation patterns and their teleconnections and associated climatic effects on terrestrial, lacustrine, and marine environments (Branconnot et al., 2004; Notaro et al., 2005; Gallimore et al., 2005). As the term 'climate' only refers to direct changes in the atmosphere, precise climate signals of the past are difficult to verify. Methane and oxygen isotope-based temperature estimates from ice cores of the northern and southern hemisphere, as well as temperature estimates derived from calcareous shells and siliceous algae, result in differing temperature (or climate) development patterns since the Last Glacial Maximum, throughout the Holocene, until the present day (e.g. Blunier et al., 1998; v. Grafenstein, 1996,1998).

Palaeoenvironmental conditions are often reconstructed via indirect or proxy data, as temperature and precipitation cannot be obtained directly in the ancient past. Proxy-data may record seasonal or annual changes of climate. Variables that lead to a better understanding of 'climate-data' as proxies are manifold, and include sediment accumulation rates, pollen, and fossil marine flora and fauna. Lake sediments form special high-resolution proxy-data archives, often containing information on the variablity of local environmental systems and climate.

Those archives have supported local, regional, and hemispheric studies, though most have been performed in the northern hemisphere. In the last decade, attention has turned towards the

southern hemisphere (PAGES, PEP-1, PEP-11, PEP-III). South America and New Zealand have become important regions of climate research, as the Antarctic Ocean with its large ice cover, thermohaline ocean circulation and cold ocean currents play a vital role for global climate events (Gersonde et al., 1996).

2.1 The westerlies and ENSO phenomena

The westerlies are dominant winds of the mid-latitudes of the northern and southern hemisphere. On the southern hemisphere, they form an important trajectory bringing moisture to South America. These winds move from the subtropical highs to the subpolar lows from west to east, prevailing between of about 35° and 60° south latitude (Fig. I-1). The westerlies are variable and produce stormy weather. Recent studies have examined the establishment of the westerlies, in the context of reconstructing environments, as a major force shaping the South American climates from the Late Glacial Maximum to the present day (e.g. Anderson and Archer, 1999; McCulloch et al., 2000; Hulton et al., 2002;).

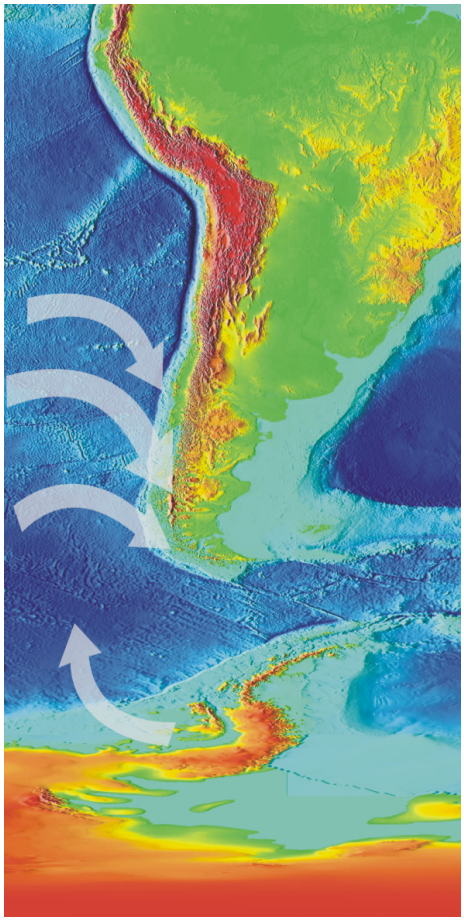

Fig. I-1: Westerly trajectory along the Chilean Pacific coast and climatic influence through the Antarctic continent. Map source: http://ngdc.noaa.gov/image/2minrelief.htm

A second important climate phenomena on the southern hemisphere is the 'El Niño Southern Oscillation' (ENSO). ENSO refers to irregular warming of sea surface temperatures from the coasts of Peru and Ecuador to the equatorial central Pacific. This causes a disruption of the ocean-atmosphere system in the tropical Pacific, having important consequences for weather around the globe. This phenomenon is not totally predictable, but on average occurs once every four years, lasting for about 18 months. ENSO alternates between positive 'El Niño' and negative 'La Niña' climate anomalies. They especially affect the western and eastern Pacific. Among all oceans, the Pacific Ocean is affected by the strongest surface temperatures anomalies, which may last over several months to several years, with considerable effects on the global climate. ENSO events have been studied predominantly in the lower and mid-latitudes (cf. Anderson et al., 1992; Cook, 1992; Ortlieb and Machare, 1993; Diaz and Markgraf, 2000, etc.). A better understanding of the ENSO pattern requires detailed and high-resolution studies of various constrasting settings, as its effects are regionally very variable (e.g. humid conditions in northern Peru and contemporaneous storms in central Chile).

The regional effects of ENSO and its atmospheric patterns along the Chilean Pacific coast during the last centuries were the subjects of various recent multi-disciplinary research projects (e.g. PEP1; PAGES). Climate proxies from lakes and marine sediments along the coast (e.g. Lamy et al., 2001, 2002; Abbott et al., 2003) and east of the Andes (e.g. Marwan et al., 2003) were studied in terms of large-scale patterns of climate variability during the Late Glacial and Holocene. In the last decade, analyses of tree-rings (Villalba, 1994), lake sediments (e.g. Jenny et al., 2002; Grosjean et al., 2003) and moraines (Koch and Kilian, 2005) have provided high-resolution information on climate fluctuations of the late Holocene. These studies focussed on abrupt climatic variations, such as the 'Medieval Warm Period'

and the 'Little Ice age' as a teleconnected climate phenomena of the northern and southern hemisphere. These teleconnections have been reported by Soon and Baliunas (2003).

South-central Chile might be a key region for monitoring past climate and environmental changes and the impact of ENSO events, as the transition from moderate/dry (central Chile) to moderate/humid climate occurs in the Chilean Lake District, Northern Patagonia. In addition to the Andean topography, the westerlies control the very high annual precipitation received in the Chilean Lake District. Lamy et al. (2001) report a southern shift of the westerlies during 'La Niña' years that causes pronounced storm trails and reduced winter precipitation in central Chile. For 'El Niño' years, they describe a northern shift of the 'Westerlies' linked to strong precipitation in central-Chile.

Any investigation of ENSO signals in lake sediments of the Chilean Lake District first requires a high-resolution baseline study on the general spatial and chronological sedimentological processes that occur.

2.2 High-resolution palaeoenvironmental studies

Lake sediments are an important archive, preserving evidence of the natural variability of local or regional environments. High-resolution palaeolimonolgical studies require a narrow sample density and are only of importance for specific time-frames that comprise significant changes in geological, geochemical, and biological parameters (Lotter and Sturm, 1994). Most parameters react very sensitive to disturbances of terrestrial and atmospherical systems. Catchment activity is strongly connected to sediment accumulation rates in the lake basin. They are a decisive parameter for temporal resolution to a seasonal, annunal, or decadal spanning chronology (Lotter and Sturm, 1994).

2.3 Volcanism and palaeoenvironmental reconstruction

Chile is a young and active volcanic region. Within its 4 000 km north-south extension, many active volcanoes are located in nearly all climatic zones, playing a vital ecological role by both destroying and creating new habitats. Volcanic activity on environments is generally extremely rapid, and volcanic eruptions can directly influence the environment via lava flows, lahars, and pyroclastic flows influence directly their surrounding and damage physically. They can also indirectly influence environments in a more subtle manner, ejecting aerosols (La Marche and Hirschboeck, 1984; Baillie and Munro, 1988) and fine ash particles into the atmosphere, resulting in short-lived climate change by reducing albedo. These indirect effects still are controversial and subject to ongoing discussions (cf. Birks, 1994; Hall et al., 1994; Caseldine et al., 1998).

Volcanic ashes leave characteristic sedimentological, geochemical and magnetic signals in lakes. Direct ash fall-out into lakes may have a significant impact on internal biological, chemical and physical processes. Increased diatom productivity caused by direct subaerial tephra deposition into the lake and associated increase in silicon content of the lake water is reported from various regions (e.g. Halfiddason and Einarsson, 1989; Hickman and Reasoner, 1994; Lotter et al., 1995; Heinrichs et al., 1999). Reduction of vegetation via tephra deposition and/or remobilisation of deposited tephra may increase erosion rates of soils within the catchment area. This causes changes in depositional processes in the lake basin (Hardardóttir et al., 2001). Such volcanic signals may mask environmental signals that reflect erosion- and sediment accumulation rates, which normally are proxies for changes in precipitation, and hence climate. For sensible reconstructions of past environmental changes in areas of active volcanism, these studies should consider volcanism-based changes in lake productivity, erosion, and vegetation that may mask the normal environmental and climate-related variability,

before proxies (such as pollen, diatoms, or sediment accumulation rates) from lake sediments are used to model past environmental conditions.

The Chilean Lake District has a high potential for unravelling the past environmental and climatic history since the end of the last southern hemispheric glaciation. Conducting studies on these lakes would close a data gap between the low (Grosjean et al., 2003) and high latitudes (cf. Kilian et al., 2003; Koch and Kilian, 2005).

2.4 Ecological effects of volcanic ash fall-out on aquatic systems

Direct influences of volcanic eruptions on lacustrine ecosystems have only been partially investigated. Short-termed increases in diatom productivity due to increased silica input (Lotter and Birks, 1993; Hickman and Reasoner, 1994; Lotter et al., 1995), as well as reducted phyto- and zooplankton (Wissmar et al., 1982) due to phosphorus and oxygen deficits after eruptions (Edgar and Keeley, 1998), have been reported. Regeneration time to return to pre-eruptive conditions can last between 10 and 20 years (Wissmar et al., 1982; Lotter et al., 1995) or 66 and 90 years (Hardardóttir et al., 2001) if sustained tephra influx from the catchment to the lake system occurs. These studies only address discrete eruptions, and do not consider the long-term, sustained effects on ecology and geology of a lake basin with a background of recurring eruptions and ash input into the lake – conditions that prevail in this Chilean study area.

3. Aims and questions

Little information on lake development and internal limnological and sedimentological processes on lakes from the Chilean Lake District is available. The purpose of this thesis is to perform a baseline study on spatial and time-related sedimentation processes on Lago Calafquén and Lago Villarrica in northern Patagonia (south-central Chile). Other than some basic limnological studies performed in the early 80's by Campos et al. (1980, 1983, 1984), no information on these two lakes is available.

The unique geological setting of these lakes makes a general geolimnological study necessary. Both lakes are located between the flanks of Volcano Villarrica, considered to be one of the most active volcanoes of South America. Its recurring eruptions and frequent, strong earthquakes disturb the ambient aquatic conditions and geology surrounding both lakes.

This thesis is divided into three major parts. The first part focuses on geodynamic effects, examined by seismic investigations of the lake basins. Seismic stratigraphy analysis characterizes the basin infill and reveals sediment disturbances. The second part focuses on the sedimentological development of both lakes. General modern lacustrine sedimentation patterns and effects of geodynamic activity on the lake basins will be assessed by the textural analysis of surface sediments. Results provide information on current patterns and areas of deposition and mass movements within the lake basin. Multi-proxy analysis will evaluate time-related sedimentation processes and assess the palaeoenvironmental and palaeoecological development of both lakes. The third part of this thesis focuses on the effects recurrent volcanic ash fall-out deposition has on ecosystems in both lakes. Diatom assemblages will be investigated to ascertain impacts of such strong volcanism on productivity. Furthermore, the diatom population changes after volcanic impact or ash deposition will be examined to determine the nutrient effect of silica input. A preliminary assessment of environmental change by using diatom analyses will be done.

II. Geodynamical, geological, and palaeoclimatological background

1. Introduction

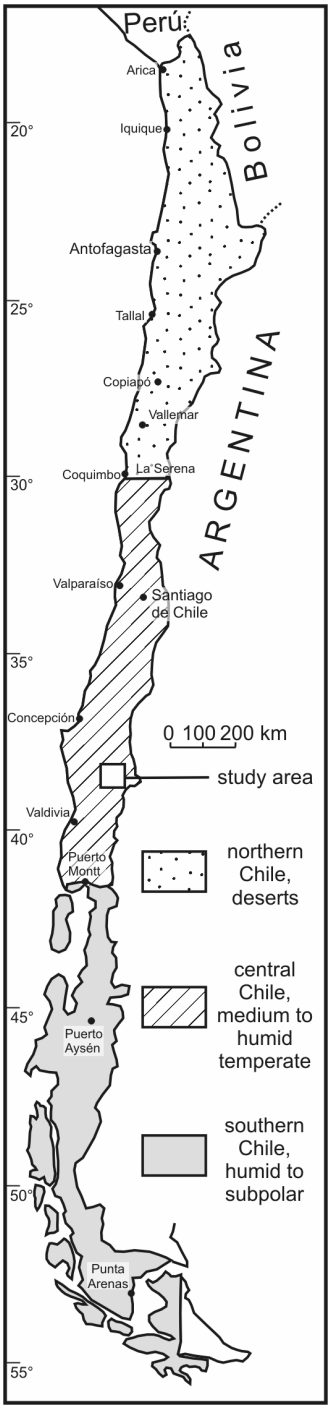

Fig. II-1: Simplified Chile map with geographic and climatic zones (*modified after* Zeil, 1964)

Over an extension of 4,300 km in length and approx. 180 km in maximum width, Chile comprises a broad spectrum of climatic conditions, from the xeric north (Atacama desert), a medium-to-humid temperate zone in central Chile (cultivated midland), and the humid subpolar south (Patagonia, and Tierra del Fuego) (Fig.II-1). The geotectonic configuration of the South American west coast makes Chile morphologically unique. In the central to southern-central Chile Palaeogene lateral extension tectonic separates the crust into three geomorphological units: the coastal cordillera in the west, the central valley (longitudinal valley), which sets in south of Santiago de Chile, and the main cordillera of the high Andes and their foothills.

The study area is located in south-central Chile, ~ 150 km north-eastwards of the city of Valdivia. Situated between the flanks of active Volcano Villarrica Lago Calafquén and Lago Villarrica are one of the first big and deep, glacial lakes of the northern Chilean Lake District (Fig.II-2). The area is marked by a humid temperate climate with annual winter precipitation rates of ~ 2,000 mm/yr, which may increase to values up to ~ 5,000 mm/yr during exceptional years (Moreno, 1993). Undisturbed vegetational cover comprises native species of *Araucaria*, *Nothofagus*, *Laurel*, *Pinus,* and perennial shrubs. Intense land clearing during the last century led to a change in soil stability, increasing erosion rates. Due to the high precipitation, soil weathering is high and converts the interstadial volcanic ashes into residual rank soils, as can be observed in the outcrops along the main road between Lago Calafquén and Villarrica.

Agriculture and tourism are the primary economic activities in the study area. Situated at the eastern shore of Lago Villarrica, Pucón (Fig.II-2) is the third most frequented site of Chilean tourism in the past 100 years. Interest has expanded to the surrounding lakes and has impacted the lake's ecology. In Lago Villarrica catchment development initiated eutrophication in some of the lakes embayments (Campos et al., 1983; Woelfl et al, 2003). This ecological shift is detected in the increased diatom abundance of both lakes, even considering the natural eutrophic-like state due to the silica- and nutrient-rich volcanic environment (Rumrich et al., 2000) of the study area.

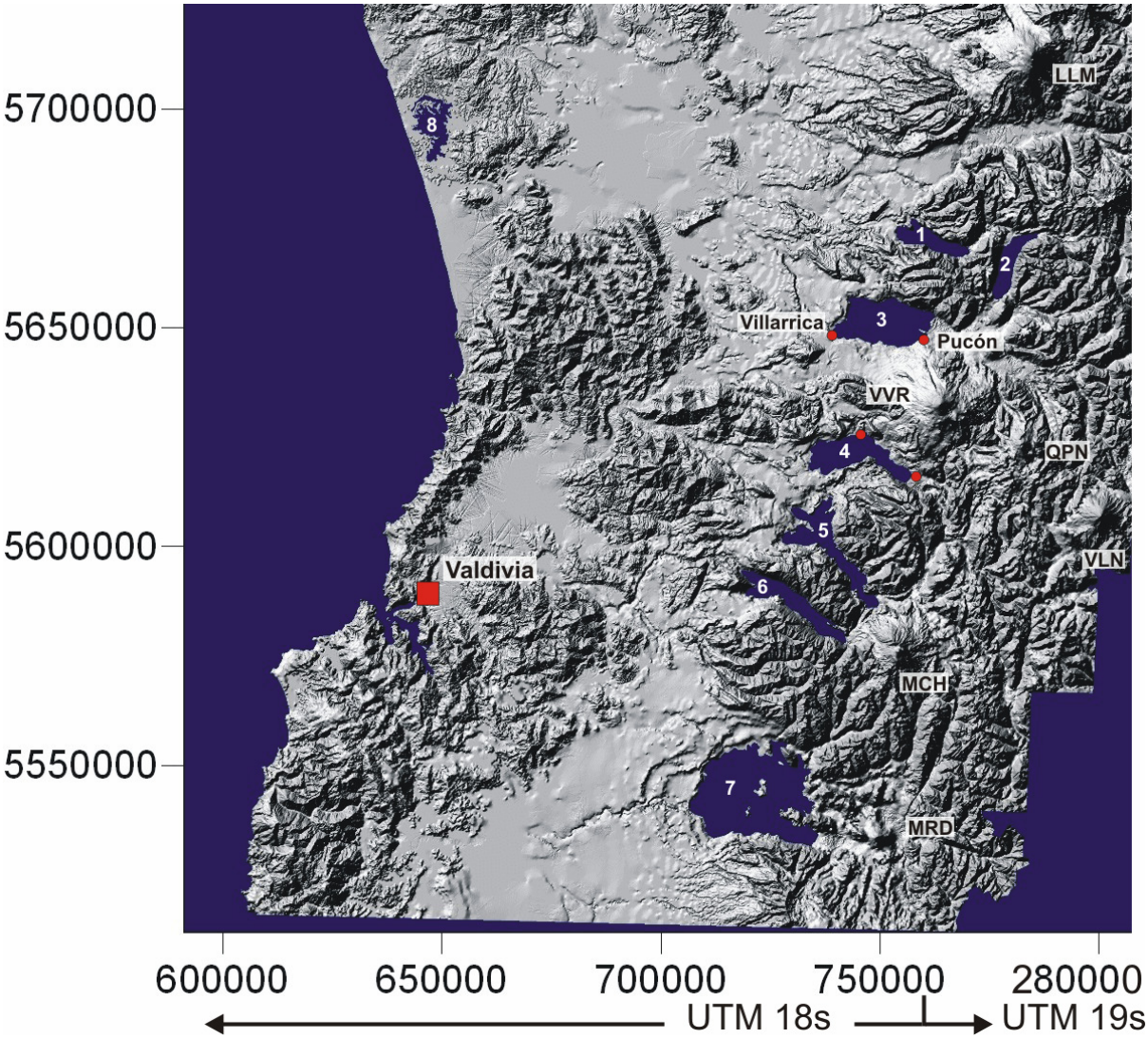

Fig. II-2: Shaded relief map of the northern to central Chilean Lake District with the most prominent lakes and volcanoes. Localities mentioned in the text are indicated with red dots and squares. Lakes: 1=Colico, 2=Carburga, 3=Villarrica, 4=Calafquén, 5=Panguipulli, 6= Riñihue, 7=Ranco, 8= Budi. Volcanoes: LLM=Llaima, VVR=Villarrica, QPN=Quetrupillán, VLN=Lanín, MCH=Mocho-Choshuenco, MRD=Mirador. Data and map base was provided by and *modified after* Lindhorst (2004), University of Hamburg, Germany

2. Geological and tectonic background

2.1 Tectonic setting

The Andes are an example of recent orogenic development in an active continental margin. The ongoing process of subduction of the Nazca plate beneath the South American plate and uplift causes differences in the morphological, geological and magmatic structure of the Andean orogene. The height and width of the orogene decrease rapidly from north to the south. In the northern Andes, the highest peaks (6,885 m, Nevado Ojos de Salado/Atacama desert) are concentrated around 18 - 30°S latitude. This contrasts with the south-central Andes around 38°-40°S (location of study area), where the average peak height is ~2,000 m, formed by the summits of the active stratovolcanoes in the main range.

2.1.1 Plate tectonic situation

The Nazca plate began formation during the upper Oligocene (24 Ma). From north towards the south, decreasing ages of the Nazca plate are observed, with 25 Ma at 38°S to virtually 0 Ma at 46°S, where the Chile rise is subducted (Cembrano et al., 2000) (Fig. II-3).

The Chile rise is a ~ 1,400 km long spreading zone, extending from 46°-35°S, where it is connected to the East Pacific rise by a transform fault zone. From 20 to 12 Ma, rapid migration of the Nazca plate occurred, beginning at the Chiloé fault zone towards the Valdivia fault zone (Fig. II-3), and at 5 Ma to the J. Fernandez fault zone towards the north.

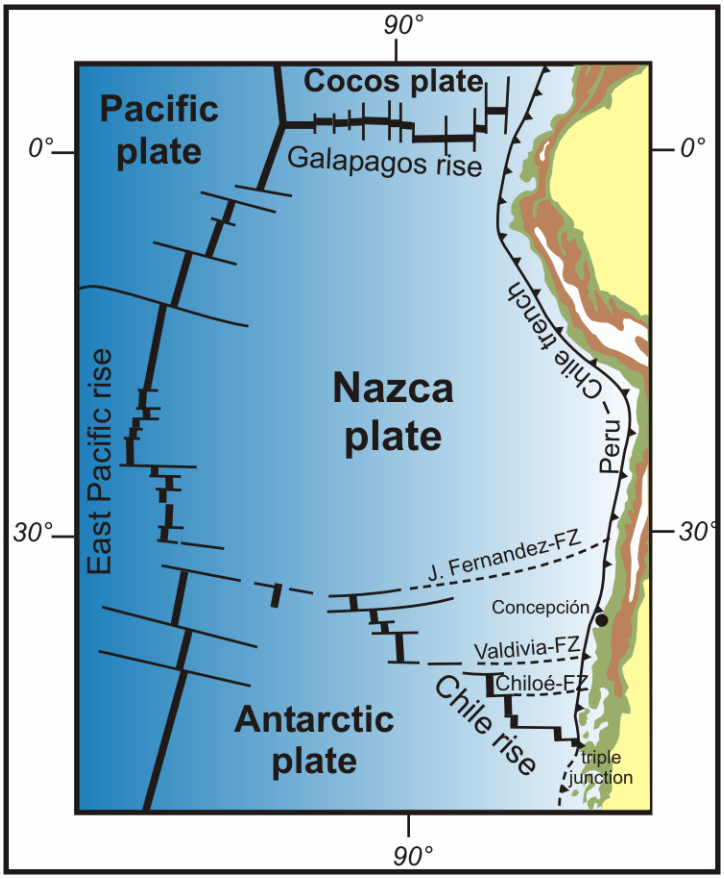

Fig. II-3: Plate tectonic situation along the Chilean continent (*modified after* Gonzales-Ferran, 1995 and Potent, 2003).

At the south-central plate boundary a segmentation of the Nazca plate into two formerly transform faults (Fig.II-4) took place. The 60° striking Mocha fault zone was formed at the former East Pacific ridge, separating the older oceanic crust (31 Ma) in the north from the younger crust (26 Ma) in the south. The second fault system, the 80° trending Valdivia fault zone, was formed at the Chilean ridge and reveals a maximum age of ~ 20 Ma near the deep sea trench. The Valdivia fault zone is part of a parallel striking system of several transform faults that have interrupted short rifting periods.

The Cenozoic subduction history of the Nazca plate indicates relatively steady right-oblique subduction (Cembrano et al., 2000). The present-day convergence rate of the Nazca plate under the South America plate is ~ 80 mm/yr (Hervé, 1994), with a slab dip of 20° (DeMets et al., 1994). South of the Chile triple junction, the Antarctic plate is subducted beneath the South American plate with convergence rates of 20 mm/yr. The difference between subduction velocities leaves imprints in the magmatic and tectonic evolution south of the Chile triple junction (Hervé, 2000).

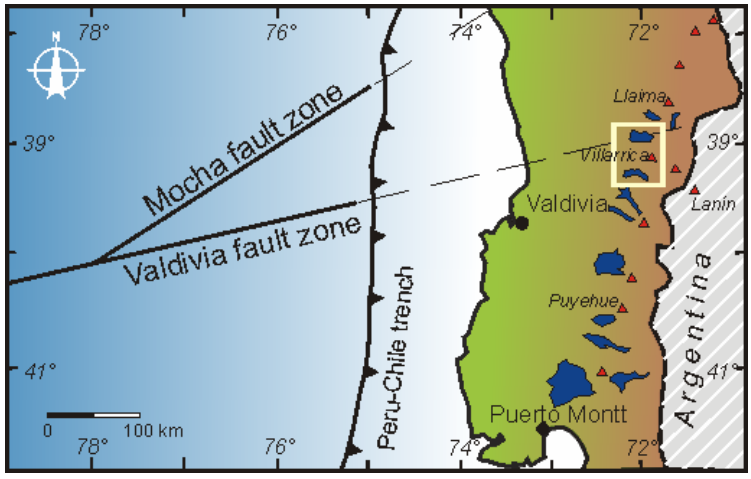

Fig. II-4: Structure of the Nazca plate near the study area (*modified after* Bohm et al. (2002) and Potent, 2003).

2.2 Regional geology and volcano-tectonic setting of the study area

As the Andes orogene originated from an ocean-continent collision system, its inventory is primarily made up of magmatites. Subordinate sediments and metamorphites are found in the coastal range and in the deeper parts of the Andean main cordillera. As the deformation structure of the Chilean Andes can be referred to as being brittle rather than ductile, only little folding occurs, and is found mostly in the metamorphites of the coastal cordillera and less in the main cordillera (Hervé, 1994). Large Neogene to Quaternary volcanic nappes and lava flows, together with glacial sediments and Cretaceous to Jurassic granites, form the main geologic units of the study area (Fig. II-5).

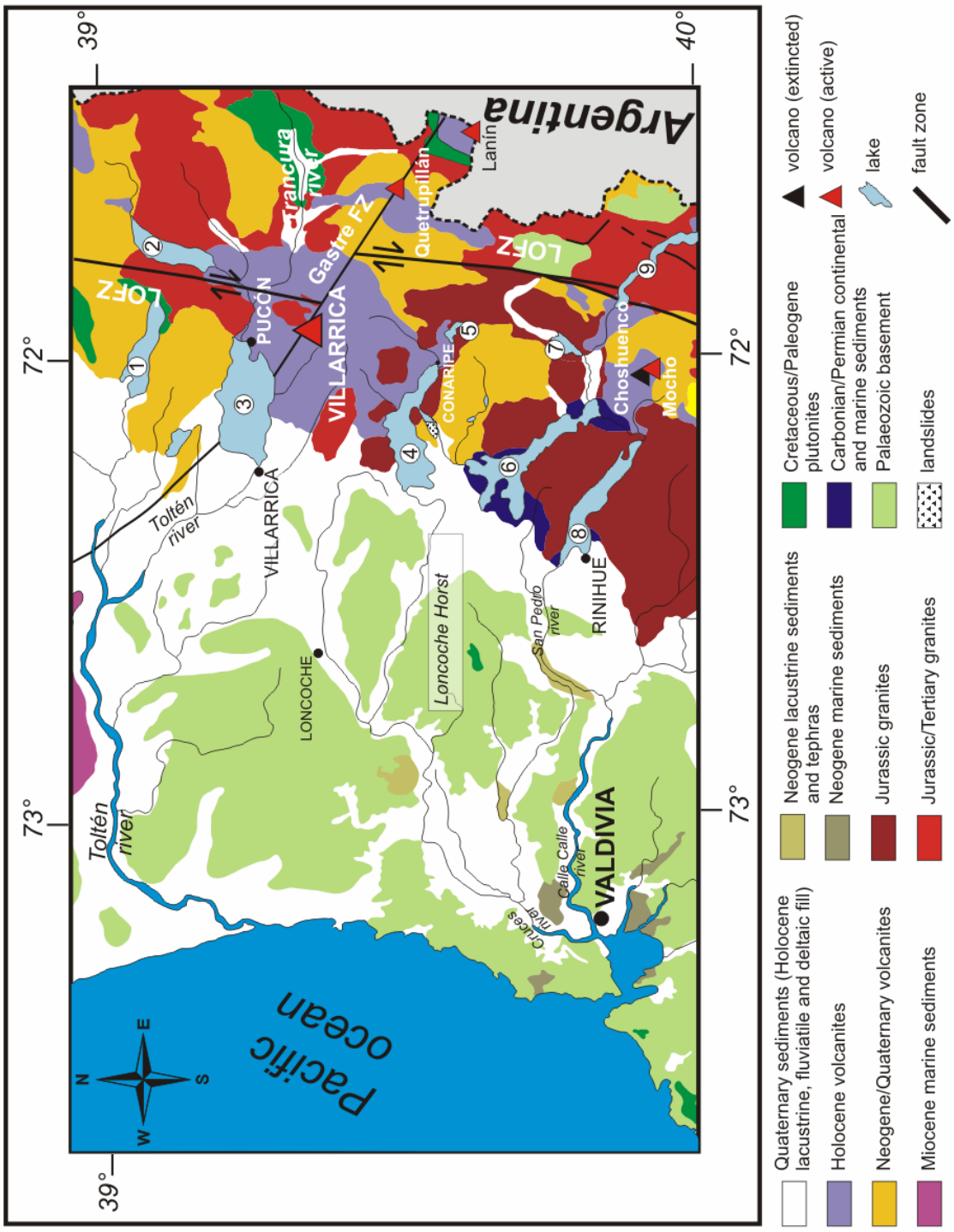

Fig. II-5: Geologic map and tectonic lineaments of the northern Chilean Lake District with the most prominent volcanoes (red and black triangles) and lakes. 1=Lago Colico, 2=Lago Carburga, 3=Lago Villarrica, 4=Lago Calafquén, 5=Lago Pellaifa, 6= Lago Panguipulli, 7=Lago Neltume, 8=Lago Riñihue, 9=Lago Pirihueico. *Modified after* SERNAGEOMIN (1982): Mapa Geológico de Chile 1:1000000, Hoja 4, Pineda (1983), *and* Bohm et al. (2002).

2.2.1 South Andean structural development

The original formation of the Andes occurred during upper Triassic/lower Jurassic period. Movements along the Gastre fault zone, located north of the study area (cf. Fig.II-5), had been associated with the up-break of Gondwana (Rapela and Pankhurst, 1992; Storey et al., 1999). The present day subduction geometry formed during the Jurassic formed the magmatic arc within the Palaeozoic accretionary wedge of the main cordillera. During the opening of the southern Atlantic Ocean in the mid-Cretaceous, the first compressional movements in the main cordillera occurred. The real Chilean type high-stress subduction zone was formed at the same time (Ramos, 1989; 2000). Further compressional movements occurred during upper Cretaceous and at the transition of Miocene/Pliocene.

2.2.2 The Liquiñe-Ofqui fault zone (LOFZ)

The Liquiñe-Ofqui fault zone (Fig.II-6) is a NNW-SSE striking dextral transform fault that parallels the magmatic arc northwards for > 1000 km (Hervé, 1994; Cembrano et al., 2000). It originates at the Nazca–South America–Antarctic triple-junction (46°S), where the Chile Ridge is currently subducted (Cembrano et al., 2000), and trends northward in the form of a strike-slip duplex structure (Cembrano et al., 1996) until 38°S, where the structure of the fault systems gradually diminishes (Potent, 2003). The oblique subduction of the Nazca plate beneath the South American plate drives the dextral displacement along the LOFZ (Cembrano et al., 1996; Cembrano et al., 2000, and references therein). First movements are associated with the Mesozoic period (Potent, 2003, and references therein), but Cenozoic dextral shear development since the Eocene (Lavenu and Cembrano, 1999) gives a further rise to exhumation of the basement. The LOFZ controls the magmatic activity (Moreno et al, 1994a,b; Melnick et al, 2002) at its main and subsequent failure zones throughout the Cenozoic and permits magmatic up-lift at the stratovolcanoes and the subordinate satellite cones.

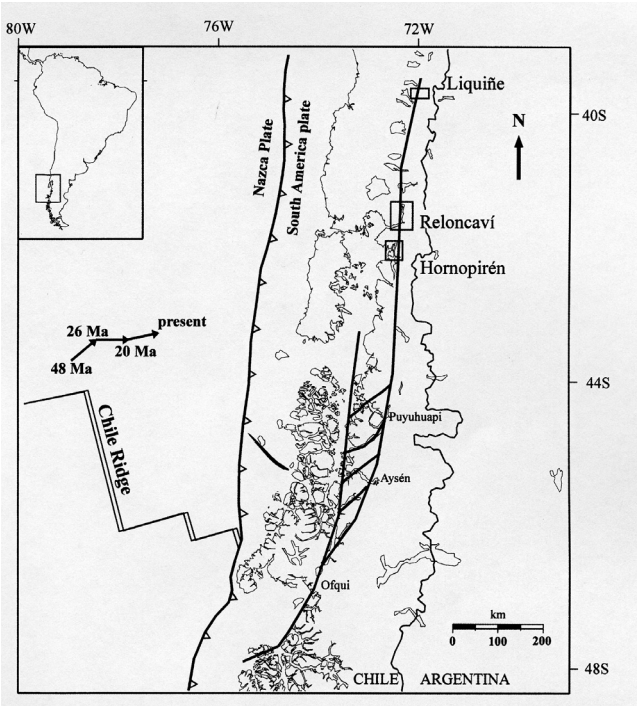

Fig. II-6: Geotectonic setting of the southern Andes and regional geometry of the Liquiñe-Ofqui fault zone (Cembrano et al., 2000).

2.2.3 Morpho-tectonic structure

The Arauco-BíoBío Trench-Arc-system, in which the study lakes are located, can be divided into four major morphotectonic units, incipient from the deep sea trench to the Chilean-Argentinean border: a basin-and-rise area with the continental shelf, the Palaeozoic coastal cordillera, the central valley, and the main cordillera comprising the active magmatic arc.

A) Basin-and-rise area and the continental shelf

The deep sea trench is located ~150 km (on average) from the Chilean coast in > 6,000 m water. East of the trench, a basin-and-rise area is filled by upper Cretaceous to Quaternary sediments. Nearer to the Chilean coast, the continental shelf base is a metamorphic complex of the late Palaeozoic accretionary wedge. The shelf is characterized by several forearc basins that have up to 3,000 m of sediments covering the metamorphic basement. The oldest ages are upper Cretaceous, and detailed descriptions of these basins are given by Mordojovich (1974).

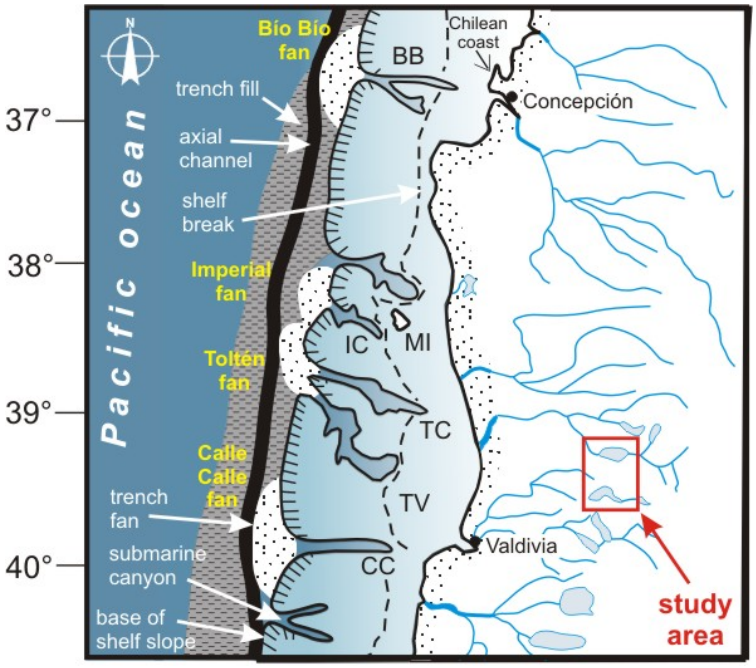

Fig. II-7: Submarine canyons and fans along the Chilean coast. Canyons: BB= Bío Bío canyon, IC= Imperial canyon, TC= Toltén canyon, CC= Calle Calle canyon. Valley: TV= Toltén valley. MI= Mocha island. *Modified after* Thornburg et al., 1990)

Within the Valdivia basin, confined to the north by the Mocha High, are several submarine canyons (Fig. II-7) cross the shelf striking in E-W or NW-SE direction. The largest are the BíoBío canyon, Toltén canyon (Río Toltén forms the outlet of Lago Villarrica) and the CalleCalle canyon (Fig. II-7), and they deliver terrestrial sediments into the deep sea trench. Geomorphologically, most of these canyons are exposed from a distance from the coast, as they were created by intense Pleistocene glaciation at low sea level (Potent, 2003; Lindhorst, 2004). A petrographical north-south separation of the terrestrial canyon sediments reflects the change in the catchment and the sediment source area. The BíoBío canyon sediments consist of volcanic material, whereas in the CalleCalle canyon in front of Valdivia, increased alluvial input of metamorphic and plutonic sands is recorded (Thornburg et al., 1990; Lindhorst, 2004). Together, the basin-and-rise area and the shelf form the outer forearc.

B) Coastal cordillera

The coastal cordillera is located parallel the Pacific coast and is the continuation of the outer forearc (Fig. II-8). It separates the central valley from the ocean. Based on lithology and metamorphic zonation, the coastal cordillera can be separated into western and eastern metamorphic complexes. Lowgrade metamorphic conditions of the western complex reached greenschist facies; locally high-pressure conditions were achieved. Lithology comprises meta-basite and -chert, serpentinite, and micaschist, which are attributed to protoliths consisting of pelite, greywacke, chert and basic volcanites. Furthermore, ophiolitic sequences consisting of metamorphic pillow lava, associated with diabase, serpentinite, and metachert (Frutos and Alfaro, 1985) are observed as outcrops. The eastern metamorphic complex includes meta-greywacke, phyllite, gneiss and hornfelse, indicating high-temperature metamorphism from greenschist to granulite facies. Shelf and flysch sediments bearing an alternating succession of pelite and greywacke are interpreted as possible protoliths.

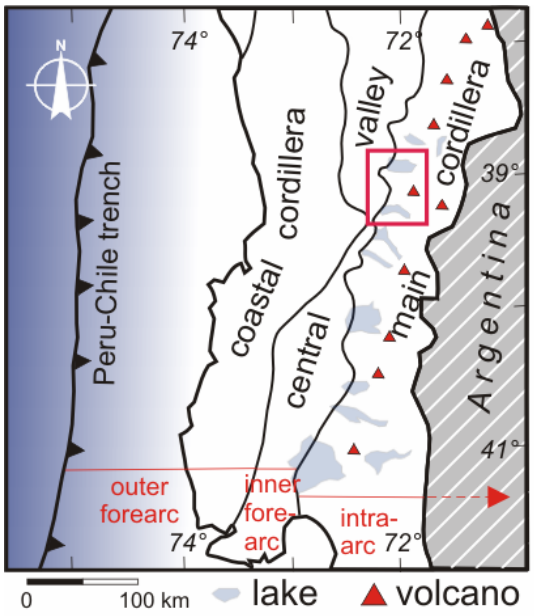

Fig. II-8: Morpho-tectonic structure of the study area (red square) and the surroundings (*modified after* Lopez-Escobar et al., 1995).

The metamorphic units are interpreted as a coupled metamorphic belt of late Palaeozoic subduction zone (Martin et al., 1999, Potent, 2003). The western complex is considered to be the accretionary wedge, whereas the eastern complex is interpreted as the transition to the former magmatic arc (Willner, 2000).

C) Central valley (longitudinal valley)

The central valley, also known as 'longitudinal valley', is a ~ 1,000 km long and ~ 60 km wide (averaged) graben forming the inner forearc (Fig. II-8). The northern part is confined by a subduction segment not bearing any volcanism and only minor earthquakes, which is located north of Santiago de Chile. The southern part of the central valley trends below sea level, south of Puerto Montt. The basement of the central valley is composed of the same greenschist metamorphic complex that forms the coastal cordillera. Covered by a thick sequence of Oligocene/Miocene to Quaternary sediments, the continuity of the central valley is interrupted near the study area by the Loncoche Horst (39°3'-40°S), formed by the same metamorphic rocks making up the coastal cordillera. North of Loncoche Horst (cf. Fig. II-5), sediments of the central valley achieve thicknesses of ~ 3,000 m; to the south, next to Puerto Montt, 4,000 m of basin fill are reported by Illies (1967). The formation of the central valley is attributed to a phase of far-ranging extension in the upper Oligocene/lower Miocene (Potent, 2003; and references therein).

This is confirmed by crustal thinning under the sedimentary infill of the central valley (Araneda et al., 2000). The relatively diffuse contact of the central valley with the coastal cordillera and the magmatic arc suggests that the central valley is not a continuous basin, but rather a combination of several individual basins. Therewith associated is a later opening and subsidence of the central valley. The transition of the central valley to the coastal cordillera is described by a NNW-SSE striking and eastwards dipping shallow normal fault (McDonough et al, 1997). Muñoz and Araneda (2000) describe Neogene normal faults with an offset of ~ 1 km for the central valley. Due to coverage by large amounts of volcanites and lava the contact of the central valley to the main cordillera remains diffuse and speculative.

Volcanism, spreading from the magmatic arc into the central valley, continued throughout the Pleistocene until the present day. Pleistocene glaciation has left various till deposits in the central valley and the main cordillera. Intercalations of volcanites (ashes, lavas, lahars, and pyroclasitc flows, etc.) in the glacial sediments can be recognized throughout the study area and along the sidewalls of the lakes. This combined lithology is responsible for the rock and soil mechanical properties and the susceptibility to landslides of the side slopes of the investigated lakes. Holocene sediments that make up the present day cover are best observed from exposures along the river beds and roads. These sediments are formed by intense weathering of the volcanic soils in the central valley and at the foot of the main cordillera, and are found throughout the Chilean Lake District.

D) Main cordillera and magmatic arc

The primary folding phase of the main cordillera began during the lower to upper Cretaceous (*Cenomane*) and was followed by uplift during the upper Miocene/lower Pliocene (Paskoff, 1977). The magmatic arc of the main cordillera developed during the Jurassic and was since remained stable (Potent, 2003; references therein). Jurassic to Holocene volcanites and plutonites comprise a large part of the geologic formation of the main cordillera. Palaeozoic basement outcrops occur in the vicinity of the study area (southwards of 39°3'S) but are lacking northwards in the main cordillera. The active volcanoes of the magmatic arc form the highest peaks around the study area, with heights up to 3,000 m. Quaternary volcanism is confined to a narrow part of the main cordillera. Volcanoes are located around 90 km above the descending plate, on a distance of ~ 285 km away from the deep sea trench (Stern, 1989). Andesites, basaltic andesites and basalts form the common volcanites; some acidic volcanites occur as a result of magmatic differentiation (Hickey-Vargas et al., 1989; Lopez-Escobar et al., 1995). Volcanoclastic deposits, ashes, and lava flows make up most of the surficial sediments and are also recorded in the Quaternary nappes of the central valley. Large extended lahars formed at the foot of the magmatic arc and reached the Pacific coast several times during the past (Pino 2003).

2.3 Seismicity and Earthquakes

As a result of the strong coupling between the Nazca and the South American plates along the subduction zone of the Chilean coast, destructive earthquakes occur, strongly affecting large cities like Concepción, Valdivia and Santiago de Chile. North of 38°S, seismicity and earthquake epicentres increase in depth eastwards with the east-dipping slab (Baranzangi and Isacks, 1976; Bohm et al., 2002; Potent, 2003). Earthquakes arising in the central valley and the main cordillera south of 38°S occur at shallow depths, located in the upper continental crust (Baranzangi and Isacks, 1976). Potent (2003) suggests earthquakes occurring in the main cordillera south of 38°S are possibly due to movements along the LOFZ.

During time of Hispanic colonization, approximately around 127 earthquakes were historically recorded (cf. Muñoz Christi (1956) in Weischet, 1970), many of which were reported to have been devastating. The 1960 Valdivia earthquake (May 22nd) caused damage from Concepción to Puerto Montt and destroyed the city of Valdivia. The rupture length of the pronounced earthquake extended from 37°S over 1,000 km southwards, estimated from the distribution of aftershocks and crustal deformation (Bohm et al., 2002). Since instrumental monitoring coverage was incomplete, localization of the epicentres of the most important pre- and main shocks is not known. Barrientos and Ward (1990) and Cifuentes (1989) assume a relationship between the 1960 main shocks and the former transform faults of the oceanic crust. Others locate the main shock epicentres on or near the continental plate (e.g. Plafker and Savage, 1970; etc.). Weischet (1970) reports a more than three minutes duration for the most devastating main shock, which was followed by > 90 aftershocks within the following 18 hours. In the succeeding four weeks, 56 seismic shocks of magnitudes $M \geq 5$ were recorded (Weischet, 1970). Several strong aftershocks also occurred in direct proximity and succession of the study area (cf.. Plafker and Savage, 1970).

As a result of the main and aftershocks in 1960, the outlet of Lago Riñihue (cf. Fig. II-5) was completely blocked by 5×10^6 m³ of landslide and rockfall debris. Within two months, a lake level rise of 28 m was recorded, eventually leading to a breakthrough of the blocked gorge and causing a flooding of the adjacent foreland by 3×10^9 m³ of water. Earthquake magnitudes around Lago Calafquén and Lago Villarrica frequently exceed $M_w = 7$ and leave also a clear imprint on the

sedimentary infill of the lake basin (Volland et al., subm.), which will be discussed in the following chapters.

2.4 Volcanism

Magmatic activity in the Andean main cordillera occurs as a consequence of rising magma from the subducting plate through the overriding plate. The result is a separation of the Andes into four major volcanically-active segments: the northern (6°N-8°S) and central volcanic zone (16°-28°S), the southern (33°-46°S) volcanic zone, in which the study area is located (Fig. II-9a), and the austral volcanic zone (49°-55°S). Volcanism is intense in the southern volcanic zone, as it is made up of a ~ 1 300 km chain of recent volcanoes, located approx. 270 km away from the Chile Trench (López-Escobar et al., 1995) (Fig. II-9a). Numerous stratovolcanoes and clusters of minor eruptive centres, such as satellite cones, form parallel to the LOFZ, but others aligned oblique with respect to the magmatic arc axis, such as the Villarrica-Quetrupillán-Lanín volcanic chain of the study area (Fig. II-9b), which strikes N50°-60°W (López-Escobar et al, 1995; and references therein). This zone represents a crustal weakness and is responsible for a 18 km western displacement and the morphologic change of the LOFZ (Moreno et al., 1994a) (cf. Fig. II-5). It probably corresponds to an inverse active transcurrent fault zone that trends into a central depression and represents the northern boundaries of the Valdivia-Loncoche-Paillaco tectonic block, which penetrates into the Andes (Moreno et al., 1994a). Volcanic activity increases from the SE towards the NW with a decreasing SiO_2 content of 60-65% at Volcano Lanín in the east, to 51-57% at Volcano Villarrica (Moreno et al., 1994a) in the west. Magmas from Volcano Lanín differ geochemically from those of Volcano Villarrica, the former having a higher incompatible element abundance (Hickey-Vargas et al., 1989).

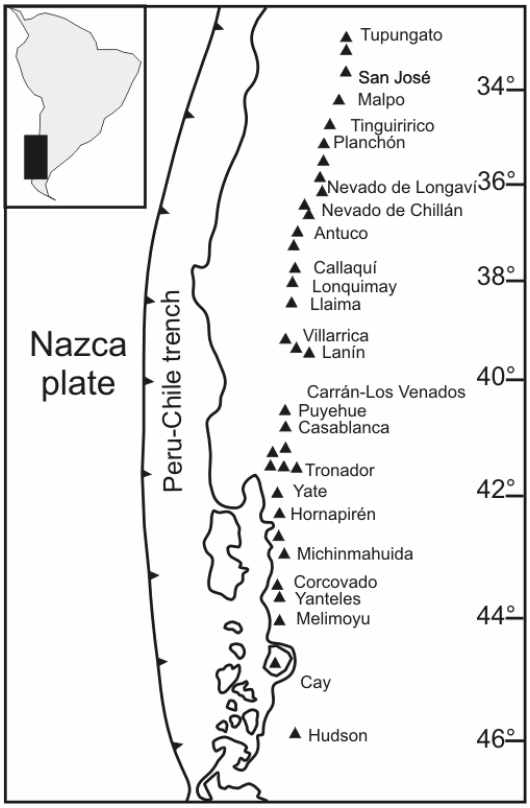

Fig. II-9a: Southern Volcanic Zone of the Andes; the Peru-Chile trench is indicated by a thick black line (*modified after* Lopez-Escobar et al., 1995)

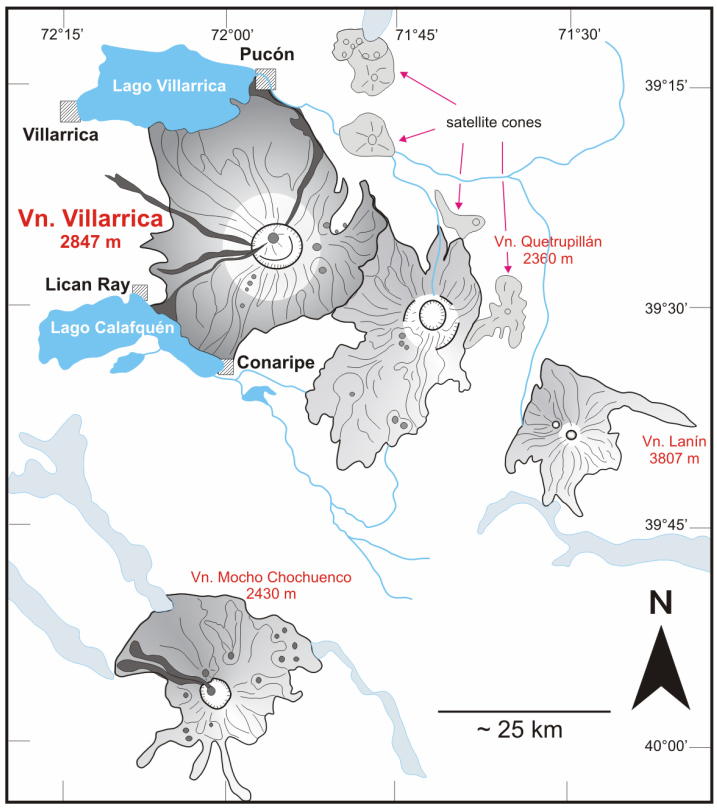

Fig. II-9b: Study area with the Villarrica-Quetrupillán-Lanín volcanic chain aligning oblique with respect to the magmatic arc axis (*modified after* Gonzales-Ferran, 1995).

Volcano Villarrica is part of the southern volcanic zone (cf. Fig. II-9a) and is considered one of the most active volcanoes in South America, as more than 70 eruptions have occurred in historic time (Petit-Breuilh and Lobato, 1994; http://www.volcano.si.edu). The latest eruption occurred a strong seismic shocks during 28.03.-06.04.2005, strombolian explosions, and hurled volcanic bombs (http://www.volcano.si.edu/reports/usgs/index.cfm?content=archive&volcano=villarric; www.povi.org). Since the beginning of Villarrica's magmatic activity during Pleistocene, ~ 90,000 yr BP (Moreno et al., 1994a), activity nearly has been constant until present day. Based on morphological and chronostratigraphical features, Moreno et al. (1994b) distinguish three major geological units during the evolution of Volcano Villarrica. Unit 1 is considered to be of pre-glacial origin, continuing through the Last Glacial Maximum, comprising the period of the largest volume of effusive volcanites production. Effusive basalts and andesites with porphyrites of plagioclase are characteristic of Unit 1. Unit 2 (Fig. II-10) corresponds to Holocene age and describes a time interval of explosive magmatism that started with the eruption of the major ignimbrite Licán at 14,000 yr. BP (Moreno et al., 1994b) followed by numerous large and significant pyroclastic flows and surges (Fig. II-11). With the deposition of ignimbrite Pucón at 3,700 a BP (Moreno et al., 1994b) the period of Unit 2 had ended and a change to an eruptive mode dominated by lava flows and lahars marks the onset of Unit 3 (Fig. II-10).

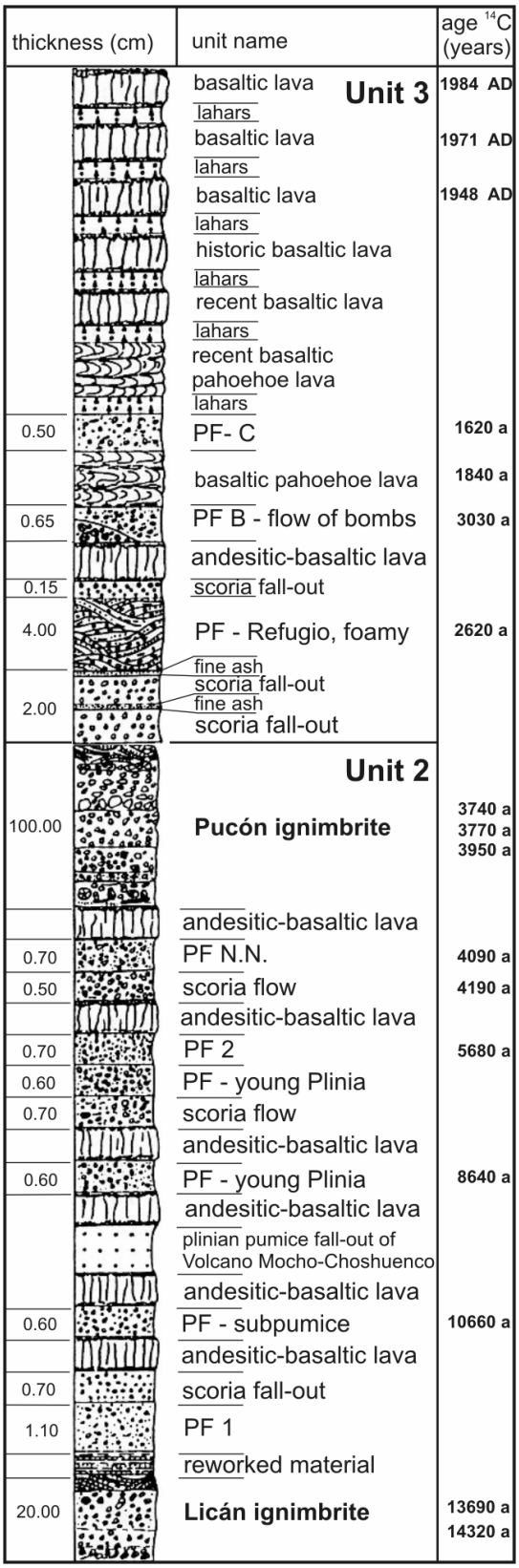

Fig. II-10: Stratigraphic Units 2 and 3 of Volcano Villarrica (*modified after* Moreno et al., 1994b)

Volcano Villarrica is a composite stratovolcano whose eruptions significantly influence the sedimentation of the surrounding fluviatile catchment and lacustrine setting significantly. Groundwater supply from the glaciated summit to the magma chamber of the volcano results in repeated phreatomagmatic eruptions (e.g., Gonzales-Ferran, 1995) generating violent pyroclastic surges and flows of basaltic to andesitic composition, which are rare in the world. Large plinean and strombolian ash clouds, as well as the aforementioned pyroclastic surges and flows, cover the study area with thick blankets of scoria, tephra and ash-fallout that also accumulate in lake basins. Lahars contribute to lake sedimentation, as they enter the lake basins of Lago Calafquén and Lago Villarrica in the form of devastating debris flows, deduced from laharic sequences in the river bed of Río Carmelito (Part 1, Chapter 2.2, Fig. III-3, site map) near Pucón (Fig. II-12,13). This outcrop shows large loosely lahar deposits with successions of debris avalanches, debris flows and hyperconcentrated

flow units that are mostly produced by more waterly flow. The latter are typically generated by dilution of the debris flow front, as described by Smith and Lowe (1991).

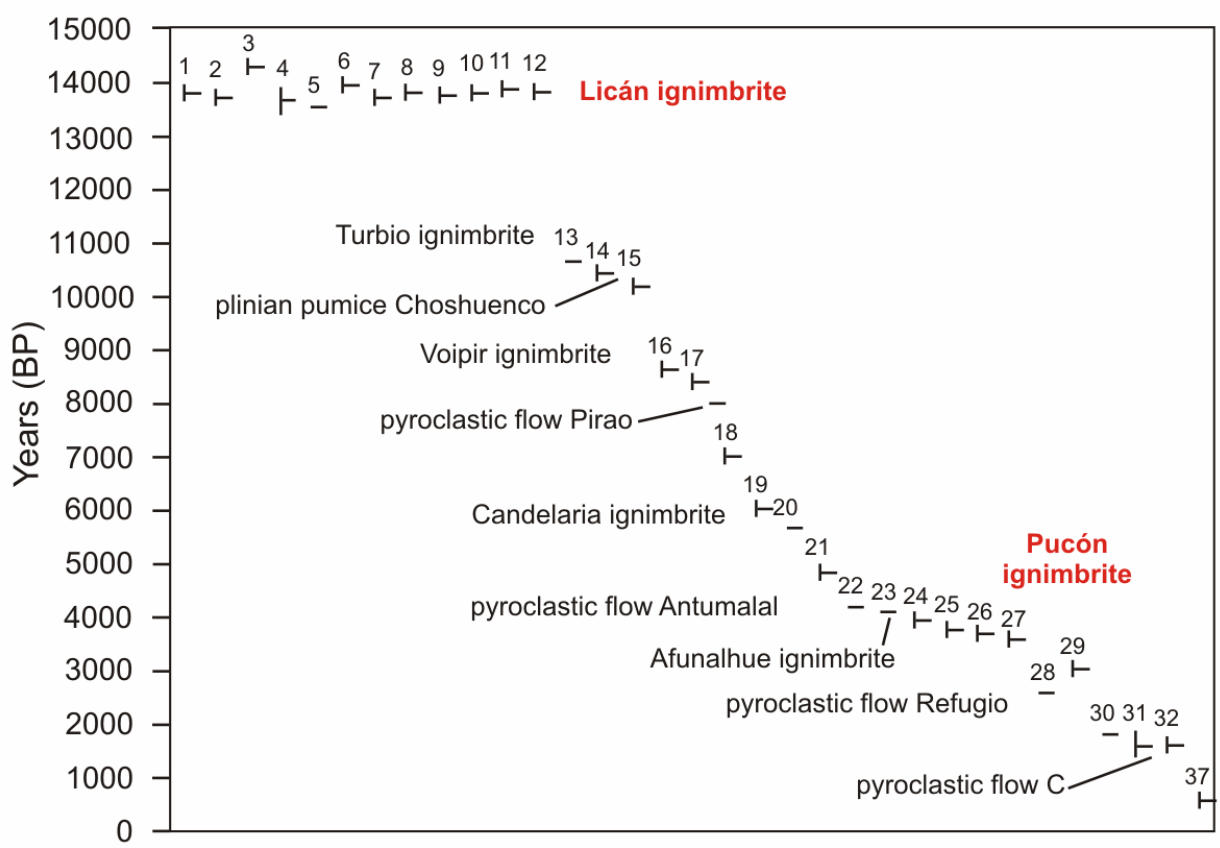

Fig. II-11: Succession of ignimbrites and pyroclastic flows of Volcano Villarrica during the Holocene (*modified after* Pino et al., subm.).

Increase in volcanic activity prior to large earthquakes occurring, related to earthquake magnitude, is reported by Acharya (1982; references therein). Increases in eruptions appear to be followed by an increase in small earthquakes, probably in response to conditions related to the preparatory processes prior to earthquake rupture (Acharya, 1982). Kimura (1978) reports a precursory time of major volcanic activity to large earthquakes of about one to two decades. Indeed, the present-day active volcanoes surrounding the study area (e.g. Llaima and Villarrica) noted a significant rise in activity during the 1930's to 40's, prior to the large 1960 Valdivia earthquake. On the other hand, volcanic eruptions followed the large seismic shock of 1960, as reported from Volcano Puyehue (Zeil, 1964; Weischet, 1970) and from Volcano Villarrica, for the large 1920 earthquake with magnitude M=7.4. Nevertheless, volcanic activity is strongly connected to seismic events and forms a decisive part of the geodynamic setting of the study area. Its effects on the lacustrine systems of Lago Calafquén and Lago Villarrica will be emphasized in the following chapters.

Fig. II-12: Laharic sequences of Volcano Villarrica in the riverbed of Río Carmelito, southern shore of Lago Villarrica near Pucón. For locality see sitemap Part 1, Chapter 2, Fig. III-3b).

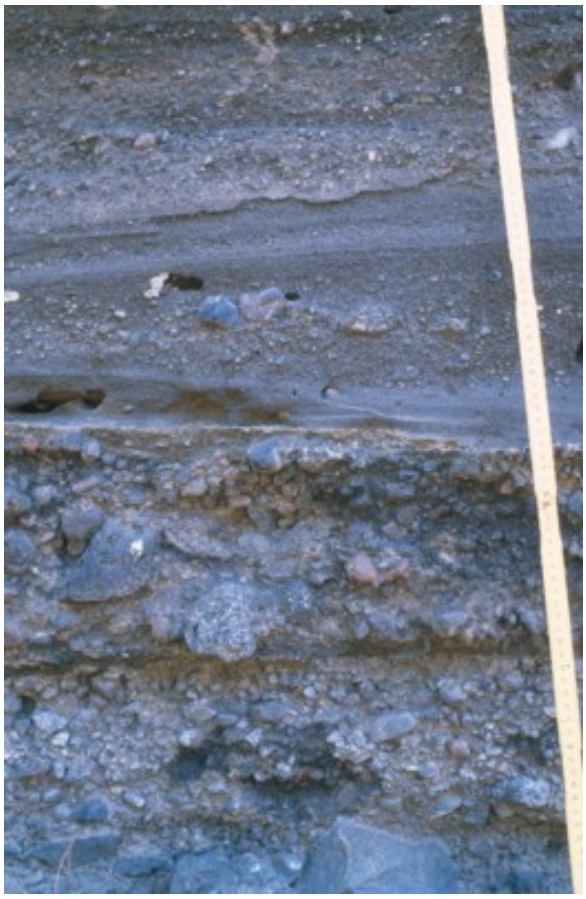

Fig. II-13: Magnification: Hyperconcentrated flow units produced by more waterly flows overlie massive basal debris flow deposits.

3. Quaternary environment and palaeoclimatology

The history of South America's Quaternary glaciation is rather complex. Numerous studies, in southern South America, e.g. the Strait of Magellan (Markgraf, 1993; Clapperton et al., 1995; Heusser et al., 1996; Benn and Clapperton, 2000; McCulloch et al., 2005; etc.) or Patagonia (Heusser, 1995; Pendall et al., 2001; Kaplan et al., 2005; etc.) provide insight into glacial development from the Pleistocene. A comprehensive overview on the Quaternary evolution of the Chilean Lake District is given by various authors (e. g. Lauer, 1968; Laugenie, 1982; Mercer 1976, 1983; Porter, 1981; Rabassa and Clapperton, 1990; Clapperton, 1994; Lowell et al., 1995; Bentley, 1996; Denton et al., 1999a,b; Moreno et al., 1999; 2001; McCulloch et al., 2000; Villagrán, 2004; etc.).

Glaciation in South America began during the upper-mid Pliocene, around 3.5 Ma (Mercer, 1976), followed by several pulsing advances and retreats. For the Pleistocene, at least four glacial ages are known for the southern Chilean Lake District (Mercer, 1976). Onset of Pleistocene glaciation is assumed around 1.2 – 1 Ma BP (Mercer, 1976) without radiometric support. During the Last Glacial Maximum (LGM), an ice sheet 1,800 km long spread along the Andes from the southern south tip to the Chilean Lake District (McCulloch et al., 2000; Hulton et al., 2002; Sudgen et al., 2002). Cool, humid climatic conditions responsible for glaciation of the Andes at ~ 41°S were cursed by a northward shift of the westerlies to lower latitudes around 50°-45°S (Denton et al., 1999b; McCulloch et al., 2000) that increased precipitation, whilst in the higher latitudes (55°-50°S) snowfall decreased at the same time (McCulloch et al., 2000). Ashworth & Hoganson (1993) suggest that the Chilean Lake

District was not fully covered by a large extended Antarctic ice dome, but rather with ice-stream fields, nourished by expanded glaciers from the Andean Cordillera, stretching across the Lake District into the lowlands of the central valley (cf. Laugenie, 1982). Empirical models of the extent of the Patagonian icesheet by Hulton et al. (2002) and Sudgen et al. (2002) brought similar results and strengthen this assumption. Maximal ice extent during the LGM is best recorded in the Chilean Lake District at Lago Llanquihue, near Puerto Montt (Denton et al., 1999a,b; Hulton et al., 2002;), and is the type-locality for the so-named last glacial age during the late-Pleistocene (Llanquihue stage I to III) (Fig. II-14). A detailed study of stratigraphic glacial geomorphologic features by Denton et al. (1999a) provides many ^{14}C dates around the Lago Llanquihue area (41°30'S). A series of four advances during the last 30,000 years has been identified, with the last glacial advance occurring at 14,805-14,550 ^{14}C yr BP (Denton et al., 1999b; McCulloch et al., 2000), when lake basins were buried under ice. Glacial and palaeoenvironmental evidence from pollen (Heusser et al., 1996; Moreno et al., 1999) and beetle studies (Ashworth and Hoganson, 1993; Hoganson and Ashworth, 1992) indicate a rapid, three-step glacier retreat with the first and decisive temperature upheaval at 14 600 ^{14}C yr BP (Denton et al., 1999a; Moreno et al., 1999; McCulloch et al., 2000). After a 1 600 yr transitional period with high precipitation rates (Mc Culloch et al., 2000), a second warming pulse occurred at 13 000 -12 700 ^{14}C yr BP with temperatures close to those of today's, linked to a spread of warmth-favouring forest trees over the lowland of the Chilean Lake District (Moreno et al., 1999). At 12 310 ^{14}C yr BP ice had withdrawn to within 10 km of their sources in the Andean Cordillera (Lowell et al., 1995).

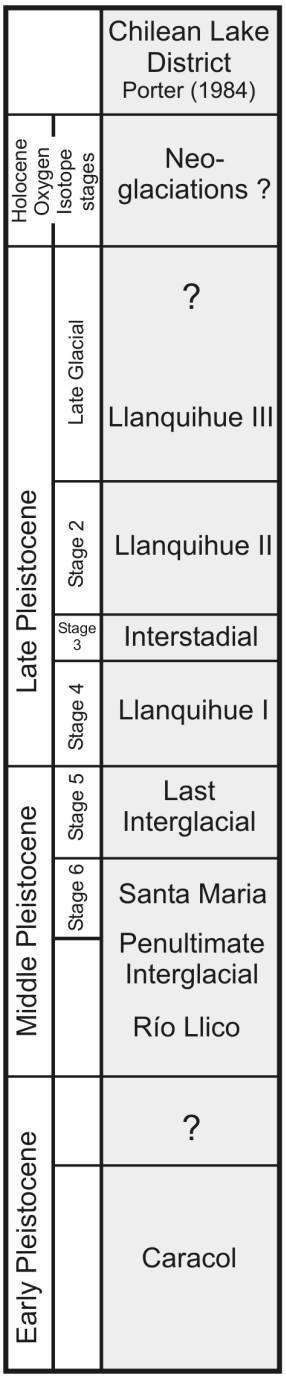

Fig. II-14: Glacial sequences of the Chilean Lake District. *Modified after* Rabassa and Clapperton 1990.

There is an ongoing controversy regarding the certainty of a Younger Dryas phenomenon in South America, similar to the northern hemispheric event (e. g. Heusser, 1974; Mercer, 1976; Heusser and Rabassa, 1987; Markgraf, 1989, 1991; Hoganson and Ashworth, 1992; Denton et al., 1999b; Heusser et al., 1999; Moreno et al., 1999; Benett et al., 2000; Glasser et al., 2004). For the Younger Dryas stage, no glacier re-advance is described in the southern Chilean Lake District, but in Argentina on the eastern side of the Andean Cordillera, Ariztegui et al. (1997) observed a small re-advance of Mt. Tronador's glacier at Lago Mascardi. A reverse to lateglacial climate between 12 200 ^{14}C yr BP, continuing into early Younger Dryas (Denton et al., 1999b) with a drop of temperature that restructured the forest communities in the lowlands, is reported by Moreno et al. (1999). At 10 000 ^{14}C yr BP, a third warming step is recorded from the entire Chilean Lake District to the Strait of Magellan (40°-55°S) (McCulloch et al., 2000).

The mid- and late Holocene underwent further, well-documented fluctuations at 5000 - 0 yr BP (Glasser et al. 2004). The last neoglacial advance during the LIA culminated by AD 1600 to AD 1900 (Glasser et al., 2004), with an extensive glaciation in late AD 1800's (Irvins and James, 1999).

In contrast to the detailed investigations of the southern Chilean Lake District, vast and incomplete information is available on the Quaternary evolution for the northern Lake District. Laugenie (1982) expanded the knowledge base geomorphologically for the area between Lago

Villarrica (39°18'S) and Lago Llanquihue (41°30'S), but provided no radiometric dating including the Quaternary evolution of Lago Calafquén and Lago Villarrica.

3.1 Glacial history of the region

Evidence for glaciation in the vicinity of both lakes is clearly marked by the glacially overridden granitic basement of the surroundings (Fig. II-15, 16). Attributed to the combined volcanic and tectonic activity during the Holocene, the glacial landscape features are yet not as striking as in other mountain ranges, e.g. the European Alps (Penck & Brückner, 1901/1909) or the Scottish Highlands (Benn, 1992; Lukas, 2004), Iceland (Beylich, 2000) or the Scandes mountains (André, 2002).

Fig. II-15: Glacial overridden morphology of the granitic basement at Lago Villarrica. View from the tributary Río Trancura towards the north.

Fig. II-16: Glacial overridden catchment of Lago Calafquén: view towards south-east at the river bed of Río Pellaifa forming the tributary of Lago Calafquén.

3.1.1 Moraines of Lago Villarrica

Clearly rounded and continuous arcuate moraine ridges, with heights of up to 30 m, limit the western end of Lago Villarrica. The surface of these moraines is covered by occasional subangular boulders (Fig. II-17), however, due to active grazing most of these moraines were not accessible to more detailed examination. Tree cover made it difficult to map them from the satellite imagery. Exposures in this area are limited to the immediate vicinity of the lake shores. Grey, matrix-supported, visually overconsolidated, massive diamicton is exposed along the southern shore of Lago Villarrica. It contains numerous bullet-shaped clasts, edge-rounding is common and only very few very angular clasts are present (Fig. II-18).

Fig. II-17: Moraines at the western end of Lago Villarrica.

Fig. II-18: Diamicton at the western shoreline of Lago Villarrica with bullet-shaped and subordinate angular shaped clasts.

3.1.2 The Villarrica glacier system

The glacier field of Lago Villarrica is dominated by the confluence of: the Trancura and Carburga glaciers. Episodically, active, bifurcating valley glaciers of the high Andean cordillera merge in the Currarehue basin, thus forming the main accumulation area of the Trancura glacier system. Carburga glacier, as the second main glacier source, joins the large Trancura glacier tongue in the basin of Minetue, where both tributary ice-source fields merged into the open and wide ablation area of the large Villarrica piedmont glacier tongue (Fig. II-19).

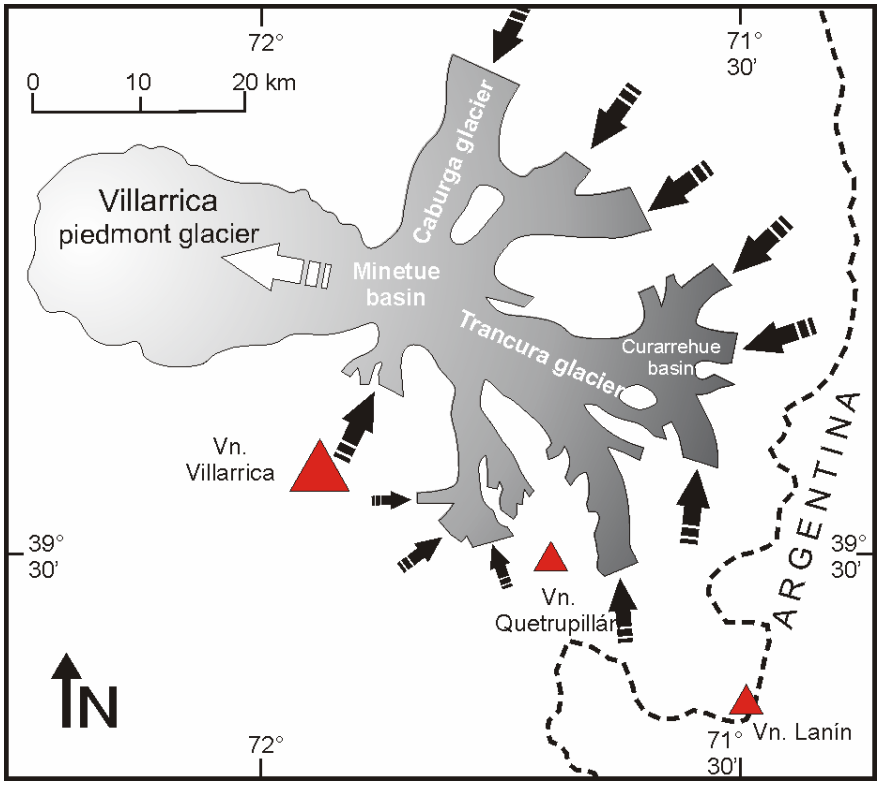

Fig. II-19: The Villarrica piedmont glacier system (*modified after* Laugenie, 1982). Red triangles mark volcanoes; black and white arrows give the ice-flow direction.

3.1.3 Glacial landforms around Lago Calafquén

As visible in satellite images, similar moraines to Lago Villarrica exist in a zone of ~ 5 km around the western perimeter of Lago Calafquen (see Fig. A-2, Appendix) mimicking the shape of the western lakeshore. Evidence for the maximum extent of the last glaciation (presumably around the LGM) comes from several – at least three – clear morphological arcuate ridges (see Fig. A-2, Appendix) that are identified as frontal moraine walls of different glacial retreat stages (Laugenie 1982). Fluvioglacial terraces in the proximity of today's shoreline support this observation (Fig. II-20). Just southeast of Lago Calafquen, NW-SE trending moraines cross-cut moraines that trend SW-NE, producing a glacial palimpsest landscape (cf. Kleman, 1992). Laugenie (1982) recognizes at least three moraine systems along the northern shore of Lago Calafquén, with elevations up to 400 m a.s.l. The southern shore is confined by steep sided walls of glacial sediments

Fig. II-20: Fluvioglacial terraces near Cantera, proximal vicinity of the western shore of Lago Calafquén. Picture was provided by Mario Pino, UACH Valdivia, Chile.

intercalating with volcanic material. The former originated from a confluence of the Panguipulli glacier from the adjacent southern valley with Calafquén glacier. A detailed description of the moraine formation and its structure is given by Laugenie (1982).

3.1.4 Glacial history of the Lago Calafquén's vicinity

The Calafquén glacier merged with the Panguipulli glacier on the piedmont field during the last glaciation (Laugenie, 1982). During glacial retreat, this 'lake-triplet' system of Calafquén-Panguipully-Riñihue drained primarily to the west. Calafquén also used the early-developed subglacial outlet of Mañedehue, intersecting the frontal moraine walls (Fig. II-21). Located at ~ 230 m a.s.l. between the lateral moraines of Calafquén and Panguipulli, palaeolake Pullinque was formed, but as the older shorelines cut below this height, Laugenie (1982) deduces an inclination of the Calafquén basin against the basin of Lago Panguipulli.

Glacial retreat was probably oscillatory, as can be deduced from the presence of several bifurcating moraines (see Landsat image, Fig. A-2, Appendix) (cf. Bennett and Boulton, 1993; McDougall, 2001; Lukas, 2003, 2004). However, cross-cutting relationships between Lago Calafquen and Lago Panguipulli indicate that localised re-advances occurred and that glacier retreat was asynchronous and probably highly dynamic, thereby supporting the notion of incremental, oscillatory retreat.

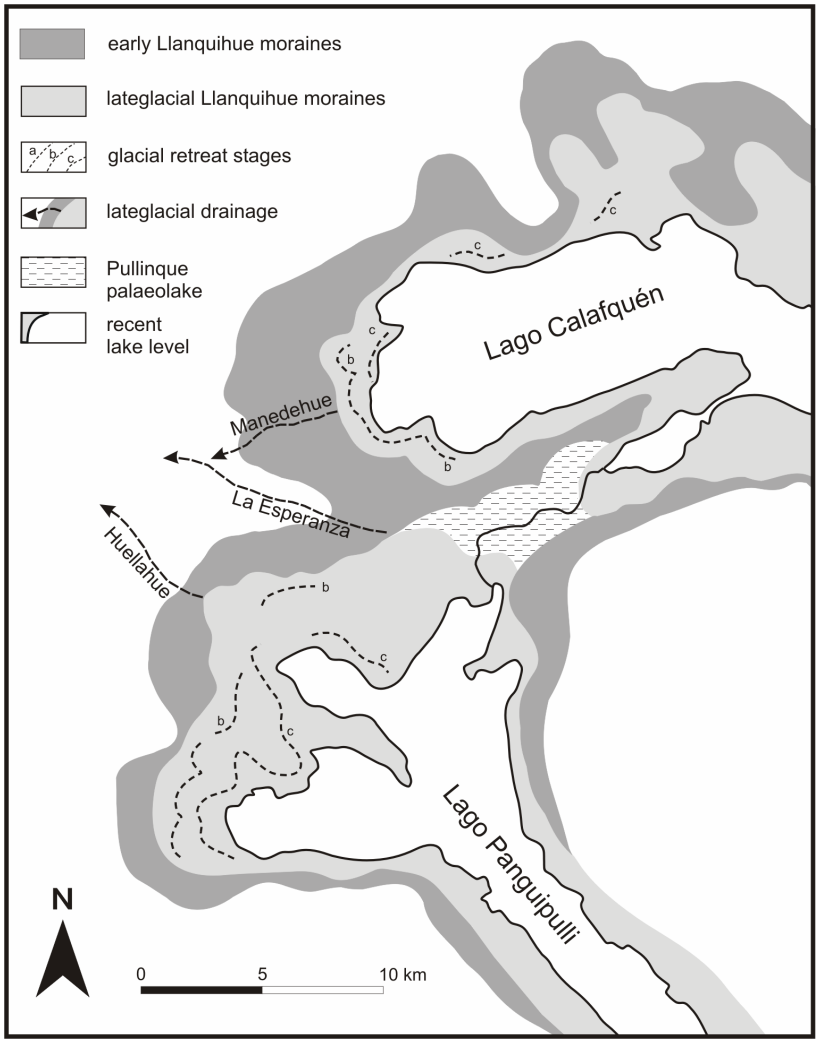

Fig. II-21: Palaeogeographic constellation of the glacier front of Lago Calafquén and Lago Panguipulli. *Modified after* Laugenie (1982).

PART 1

III. Seismic stratigraphic investigation of Lago Calafquén and Lago Villarrica

Seismic stratigraphy of Lake Calafquén was submitted to *Quaternary International* as:

Volland, S., Sturm, M., Lukas, S., Pino, M., Müller, J. 2007. "Geomorphological and sedimentological evolution of a lake basin under strong volcano-tectonic influence: The seismic record of Lago Calafquén, (south-central Chile)". Quaternary International, 161. *In press.*

The seismic text was modified for publishing of the aforementioned paper after peer review. Modifications are <u>not</u> fully included in this dissertation. For details, please see published paper.

Pre-publishing has been accepted and approved by the dean of the faculty “Bauingenieur- und Vermessungswesen”, Technische Universität München, with notification from 09.06.2005.

1. Introduction

Landscapes continually evolve over shorter and longer geological time periods to produce modern topography via processes such as earthquakes, volcanism, and landslides. These endogenic forces accelerate reshaping of the land surface, as earthquakes and active volcanism create a landscape which in turn is eroded and destroyed by subsequent seismic events. They also can cause abrupt changes that result in sudden reshaping of topography and subsurface (Siebert, 1984; Keefer, 1999; Korup, 2005). Volcanic eruptions deposit loose tephra, accelerating erosion and favouring the development of debris flows during intense rainfall events. Furthermore, eruptions trigger rockslide debris avalanches, as reported from the 1980 Mt. St. Helens eruption (Voight et al., 1981; Wieczorek, 1996; and references therein). Eruptive explosions can also cause seismic shocks that affect (sub)surface structures, (re)activate faults and slides on various scales (Waldron, 1967; Belousov and Belousova, 1996).

In mountainous regions and their forelands e.g. in the European Alps, Andes or New Zealand, geological and glacial forces interact. Glacial activity impacts are found on both valley bottoms and flanks, as glacial erosion oversteepens slopes, removes talus deposits, and thus mitigates slope shear-strength. Due to a lack of abutments, earthquakes can trigger large-scale landslide events, rockfalls and slumps, cause earth spreads, earth block slides or slumps (Wieczorek, 1996). They may also liquefy regolith or blankets of volcanic ash, giving rise to further landslide activity. Mass wasting has been triggered in the sediments of European alpine lakes by earthquakes with magnitudes of $M_w = 5$ to 7 (e.g. Siegenthaler et al., 1987; Chapron et al., 1999, 2004a; Monecke et al., 2004; Schnellmann et al., 2002, 2005, and references therein; etc.).

This chapter focuses on the interaction of landscape evolution and topographic features in two lacustrine settings within the geodynamically active environment of the northern Chilean Lake District. Chile, and the Chilean Lake District in particular, are regions with high deformation rates and short seismic cycles, though regional seismic investigation is still in its infancy. The first combined seismic-sedimentological investigations in the Chilean Lakes District were from Lago Puyehue (Charlet et al., 2003; Chapron et al., 2004b) and Lago Icalma (Charlet et al., 2003, 2004). Assessing climate and environmental evolution from lake sediments is rather complex in geodynamically active settings where endogenous processes may overprint climatic control. Earthquake magnitudes around Lago Calafquén and Lago Villarrica frequently exceed $M_w = 7$ and leave a clear imprint on the sedimentary infill of the lake basins. Thus, the future use of these lake sediments as an environmental and climatic archive necessarily requires a pre-investigation of the sedimentary basin infill. The seismic surveys on Lago Calafquén and Lago Villarrica were performed with the aim to 1) assess the effects of landscape remodelling processes, 2) select suitable coring sites for detailed sedimentary analysis, 3) revise the existing bathymetric mapping (Campos et al., 1980, 1983), and 4) test the lake's archival potential for palaeoenvironmental reconstruction.

2. Study area

2.1 Volcano-tectonic setting

Chile's active continental margin (Fig. III-1a) comprises the ~ 1,000 km-long N-S striking Liquiñe-Ofqui fault zone (LOFZ), dominating the tectonics and volcanism of the study area. The LOFZ is a dextral strike-slip fault system that is crosscut by the secondary NW-SE trending Gastre fault zone (GFZ) (Melnick et al., 2002). The volcanic lineament of Villarrica-Quetrupillán-Lanín (Fig. III-1b; cf. Fig. II-5) is located southwards of the GFZ. The LOFZ is the result of the oblique subduction of the Nazca plate (Cembrano et al., 2000) and ridge-push stress from the Chilean rise (Nelson et al., 1994), whereas the GFZ represents an inherited structure formed in Palaeozoic times (Melnick et al., 2002). The Chilean Lake District is located south of the Valdivia fault zone (cf. Fig. II-4). Plate convergence, subduction and stress concentration control the location and frequency of intense earthquakes with high destruction potential in an area between Concepción and Valdivia. The 1960 Valdivia earthquake, with intensity I > VIII (Modified Mercalli Scale) and Mw 9.5/Ms 8.5 (Barrientos and Ward, 1990), was the highest-ever recorded magnitude earthquake worldwide. The epicentre was located in the vicinity of the study area and several strong aftershocks occurred in direct proximity and succession (cf. Plafker and Savage, 1970). A frequency distribution of earthquakes Ms ≥ 7 for the past 400 years between Santiago de Chile and Puerto Montt (Fig. III-2a) shows that the strongest earthquakes around the study area are mostly located on the southern side of Lago Calafquén (Fig. III-2b). Note that historic earthquake registration was dependent on population density before instrumental seismic monitoring was installed and, therefore, has to be considered as incomplete, especially in a country with such a complex colonization history as Chile. In the Andean Cordillera only a few shallow earthquakes occur that might predominantly relate to movements along the LOFZ (Potent, 2003). Volcanic activity of the Villarrica-Quetrupillán-Lanín lineament increases from the SE towards the NW, and concentrates in the proximity of the LOFZ. Groundwater supply to the magma chamber results in repeated phreatomagmatic eruptions of the basaltic-andesitic Volcano Villarrica (Moreno et al., 1994a; Gonzales-Ferran, 1995).

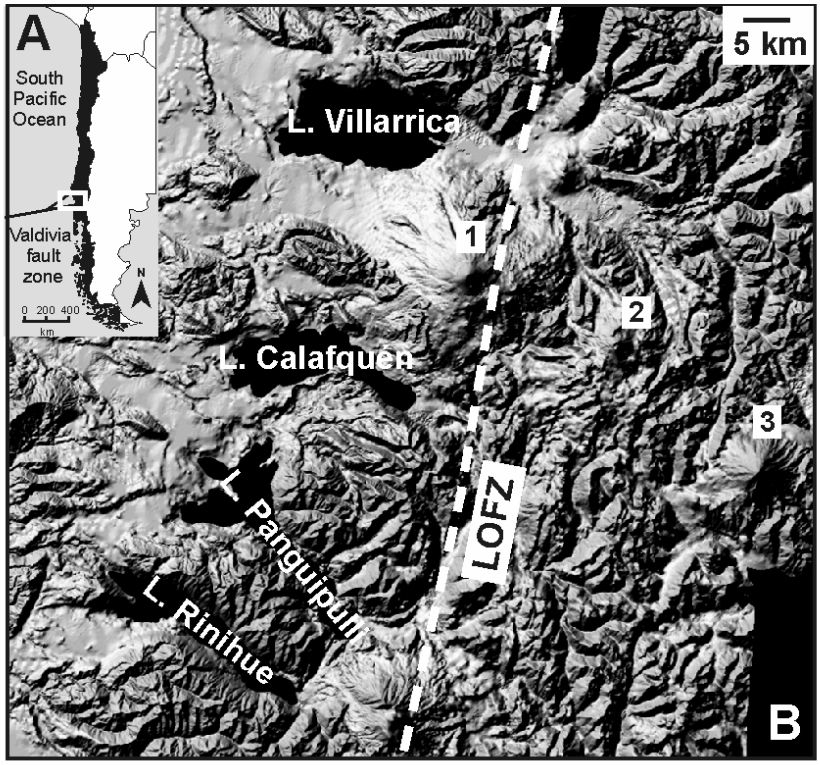

Fig. III-1: Shaded relief map of the study area with major volcanoes and tectonic lineaments. Volcanoes: 1=Villarrica, 2= Quetrupillán, 3=Lanín.

2.2 Lake description and climate

Lago Calafquén (39°32'S, 72°09'W) and Lago Villarrica (39°18'S, 72°05'W) are located in the northern Chilean Lake District, comprising a 500 km-long transect of more than 20 lakes between Temuco in the north and Puerto Montt in the south. The climate is humid-temperate with a mean annual precipitation of ~ 2,000 mm/yr (cf. Chapter II, p.1), which together cause deep weathering of the bedrock and volcanic soils. Further details of climatic and hydrographic aspects are found in Campos et al. (1980, 1983). Lago Calafquén (22 km long, 3 to 7 km wide, and 212 m deep) is the largest fjord-lake (Hutchinson, 1957; cf. Campos et al., 1980) of the hydrologically-interlinked system of three overdeepened glacial lakes (Lago Calafquén, Lago Panguipulli and Lago Rinihue; cf. Fig. III-1b). The outlet of Lake Pellaifa forms the main tributary, whilst discharge of Lago Calafquén proceeds via the gorge of Hueninca into Lago Pullinque to the south (Fig. III-3a). The waters of Calafquén indirectly enter the Pacific ocean via discharge of Lago Riñihue (cf. Fig. II-2) into its outlet River San Pedro. Lago Villarrica (21.5 km long, 9 to 11 m wide) is a typical piedmont lake of type 28c after Hutchinson (1957) (cf. Campos et al., 1983, 1984), with the natural tributary River Trancura, originating in the volcanic hinterland of the Andean cordillera (Fig. III-3b). Lago Villarrica drains to the Pacific ocean via its outlet of Río Toltén (Fig. III-3b).

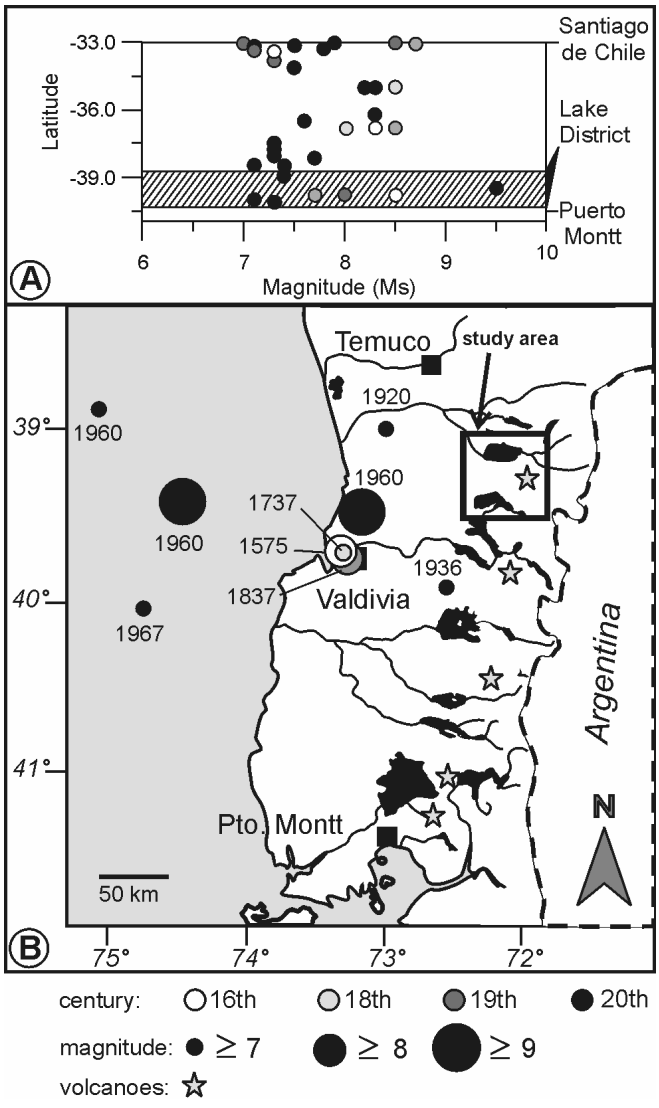

Fig. III-2: Chilean earthquake catalogue A) of the area from Santiago de Chile to Puerto Montt and B) of the study area for the past 400 years for earthquakes with magnitude M_s>7.0. Data source is based on historical and instrumental observation during the period AD 1570-1995 *(source: Servicio Sismológico Universidad de Chile, http://ssn.dgf.uchile.cl/home/sismohisto.html).*

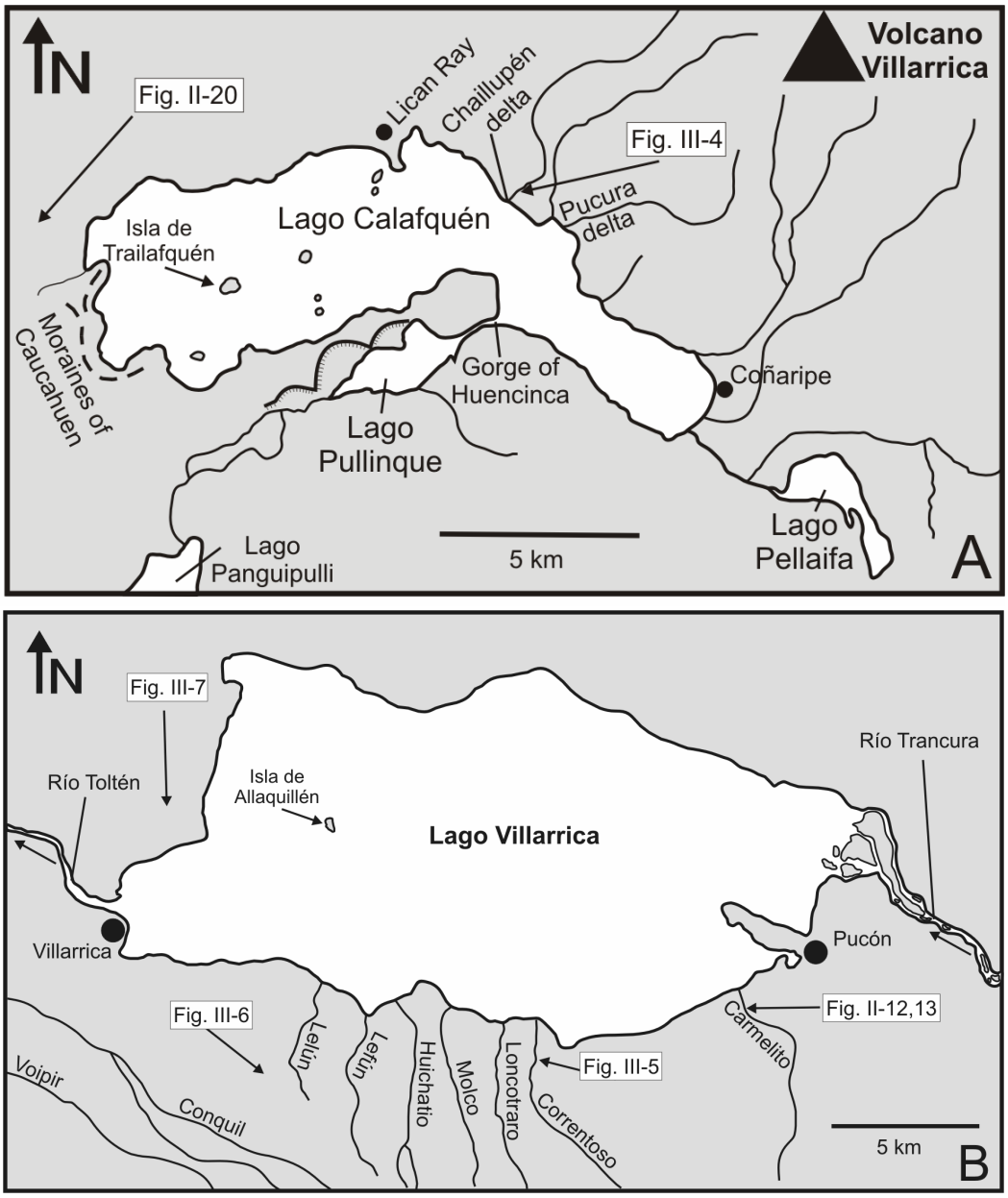

Fig. III-3: Sitemaps of A) Lago Calafquén and B) Lago Villarrica with characteristic localities mentioned in the text.

2.3 Regional geology

The south to south-eastern side of Lago Calafquén is bounded by 400 to 1000 m-high slopes made up of Jurassic granites (cf. Fig. II-5). The lake's south-western side is primarily formed of steep walls of inclined, alternating layers of volcanic lava flows, ashes, breccias and tuffs, partly covered by glacial sediments of the last glaciation. Foothills of the active Volcano Villarrica bound on its north-east shore. Seasonally water-bearing river beds that stretch from Chaillupén to Coñaripe (Fig. III-3a) substantially influence lake sedimentation, as they form the predominant trajectories for lahars, slumps, debris flows and avalanches triggered by heavy precipitation, volcanic eruptions or earthquakes (Fig. III-4). Furthermore, deposition from recurring Plinean ash-fallout contributes to the lacustrine sedimentation processes.

Fig. III-4: Bed of Río Chaillupén (here in half width) forms the major trajectory for lahars and heavy seasonal meltwater runoff. View towards the east, in an upstream direction to the volcano flank.

The northern side of Lago Villarrica is made up by gravel deposits that are related to glacial activity in the catchment. Likewise, deposits found on the south lake side of the Correntoso river bed may indicate ice-marginal sedimentation processes (Fig. III-5). These deposits are overlain or intercalate with highly weathered volcanic sediments. Alteration of the ashes is strong, and locally they have formed water impenetrable clay-like bearing soils (Fig. III-6) that give rise to or support soil creeping processes and rotational to translational landslides. The western shore of Lago Villarrica is bound by high moraine walls (cf. Fig. II-17) that bear overconsolidated till deposits (cf. Fig. II-18) with healed polygonal fissures and a cemented matrix (Fig. III-7).

Fig. III-5: Bed of Río Correntoso on the southern side of Lago Villarrica with gravel deposits and a delta-like embankment that might indicate ice-margin sedimentation.

Fig. III-6: Strongly alterated volcanic soils near the southern side of Lago Villarrica. Locally, they have formed clay-like soils with nearly water impenetrable blankets of weathered volcanic ashes. Location is indicated in Fig. III-3b.

Fig. III-7: Over-consolidated till deposits with a cemented matrix near the western shore of Lago Villarrica, revealing healed fissures. For location, see Fig. III-3b.

2.4 Geomorphological features

Glacial activity has left a clear imprint on the study area landscape. Several moraines and steep sided valleys can be found in the lakes' vicinity. At least two hazardous geomorphologic features developed on the eastern and southern side of Lago Calafquén. A significant landscape feature is the postglacial separation of Lago Pellaifa from the primary Calafquén basin by large alluvial landslide activity that resulted in the fluviatile damming of Lago Pellaifa (Campos et al., 1980). An enormous alluvial cone is also clearly identifiable on aerial photographs and Landsat images, showing evidence of large debris flows and flood events caused by melting snow and glacial ice, perhaps triggered through volcanic eruptions (see Fig. A-3, Appendix).

The present-day outlet of Lago Calafquén, draining into Lago Pullinque (cf. Fig. III-3a) was formed when the former Pullinque lake basin was confined by huge rockslides (Laugenie, 1982). Due to a lack of volcanic ash on the debris ridges, Laugenie (1982) regards this event as late postglacial or (sub)recent, triggered by a seismic event similar to the 1960 Valdivia earthquake. Evidence of rockslides is clearly identifiable on Landsat images (Fig. III-8) and GIS models (Fig. III-11) in the near proximity of the shores. Laugenie (1982) reports a lake-level rise in Calafquén linked to the enormous slide events of Pullinque, which might have blocked the outlet of Lago Calafquén into Lago Pullinque. He associates the drowning of parts of the moraine belt of Caucahuen (cf. Fig. III-3a), which today is marked by stagnant and swampy water of the western end of the lake basin, with this rapid water-level rise.

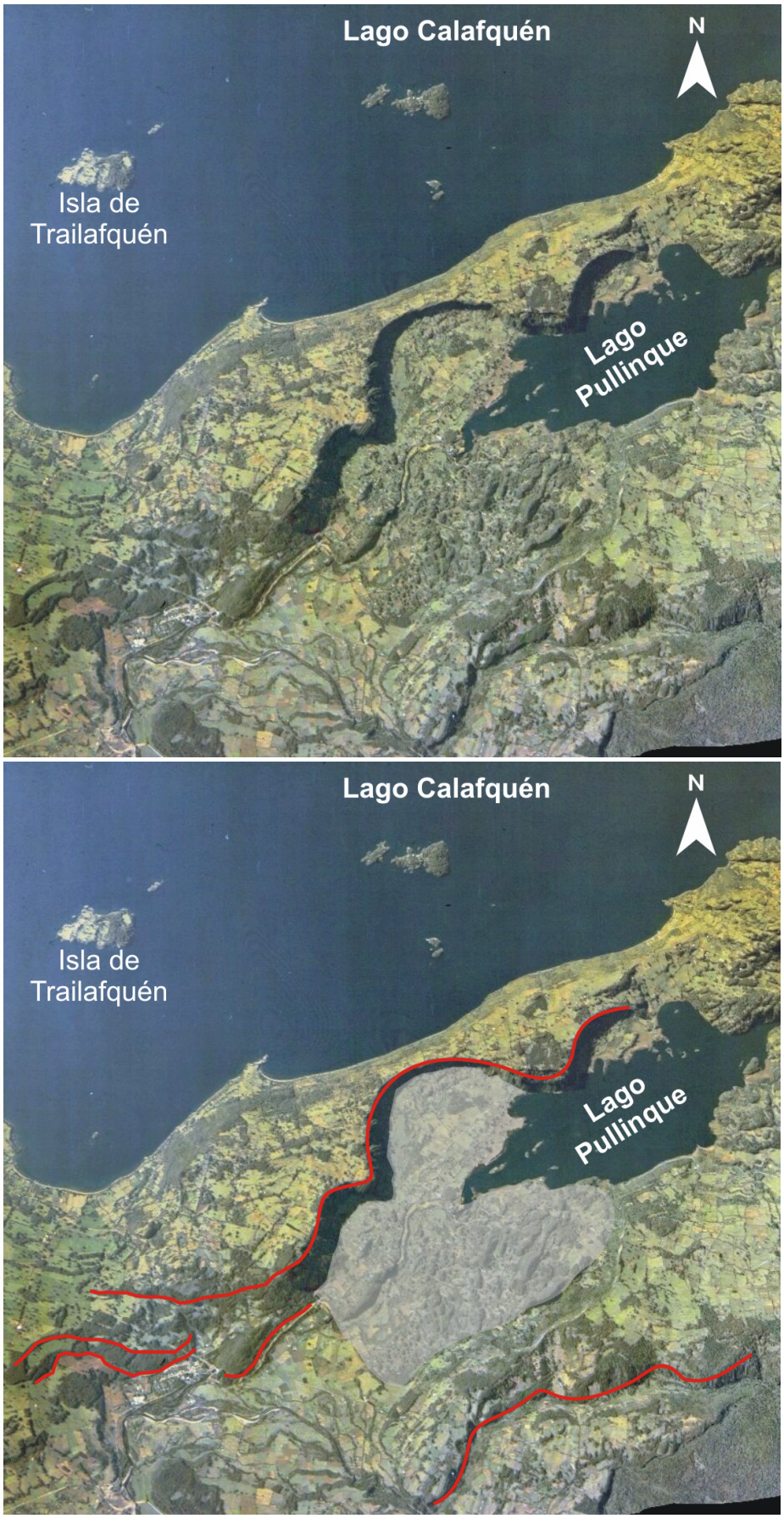

Fig. III-8: Above: Clipping of the south-western shore of Lago Calafquén. Below: Evidence of rockslides is clearly marked by steep failure scarps (red line) and large debris accumulation (grey colour) that confine the present day shore of Lago Pullinque. *Source landsat images: www.sinia.cl*

The vicinity of Lago Villarrica lacks such drastic rockslide events like the aforementioned, but does exhibit strong susceptibility for landslide acitivity around the western to eastern shoreline. The entire southern side is prone to repeated slumps and debris avalanches of different origins. In addition to the main tributary of Río Trancura, the river bed of Río Carmelito (Fig. III-3b,) forms another major trajectory for debris flows and lahars (Moreno, 2000) during volcanic eruptions (cf. Fig. II-13). Emparán (1980) defines an area of risk for natural hazards along the southern side of Lago Villarrica (Fig. III-23; Fig. A-4, see Appendix). The smaller rivulet beds and creeks stretching from Río Correntoso to Lelún, that usually drain the northern to western flanks of Volcano Villarrica, are identified as the main trajectory zones of repeated landslides, debris flows and avalanches. The area between Lelún and Lefún creeks are considered highly susceptible for fast slumps and landslides caused by seismic events. The south-eastern to eastern side of Lago Villarrica is frequently impacted by lahars and lava flows. The most recent and large lahar of 1971 destroyed the campsite of Pucón, causing several deaths and blocking the river bed of Río Trancura completely, drowning the surrounding region.

These pronounced features around both lakes mark large changes in the lake's catchment, and evidence of its timing and severity may exist in the lake sediment of either basins. Therefore, seismic analysis is employed to investigate and characterize infill sediments.

3. Seismic methods

Seismic profiles were shot on Lago Calafquén during March 2001 and on Lago Villarrica during April 1997 using a 3.5 kHz high-resolution system with an ORE 137b electromagnetic pinger with varying outgoing pulse length between 0.2 to 2 ms and varying velocities between 0.5 to 0.25 s at 2.5 kW. Data acquisition was monitored onboard by simultaneous paper recording using a Raytheon LSR 1811-2 linescan recorder. Positioning on Lago Calafquén was obtained by GPS navigation of KODEN. On Lago Villarrica, navigation was achieved by the internally installed FURUNO radar. Due to technical problems, the FURUNO coordinates of the shotpoints were noted by hand and the profiles had to be re-positioned manually in the track plot. The seismic paper records were scanned with a high resolution endless scanner and processed by graphics programs (Corel Photo-Paint® V.11, Adobe Photoshop® V.7) to filter the contrast of the grey colour plots, providing details of the basement and sediment structure. Bathymetric data obtained by the seismic surveys were combined with the existing bathymetry published by Campos et al. (1980, 1983) to create a revised bathymetric map (Fig. III-9a,b). The data were compiled to a 3D basin model using Surfer® V.8 (Fig. III-10a,b) and a digital terrain model (DTM) with ArcGIS (Fig. III-11a,b) to image the lake floor topography.

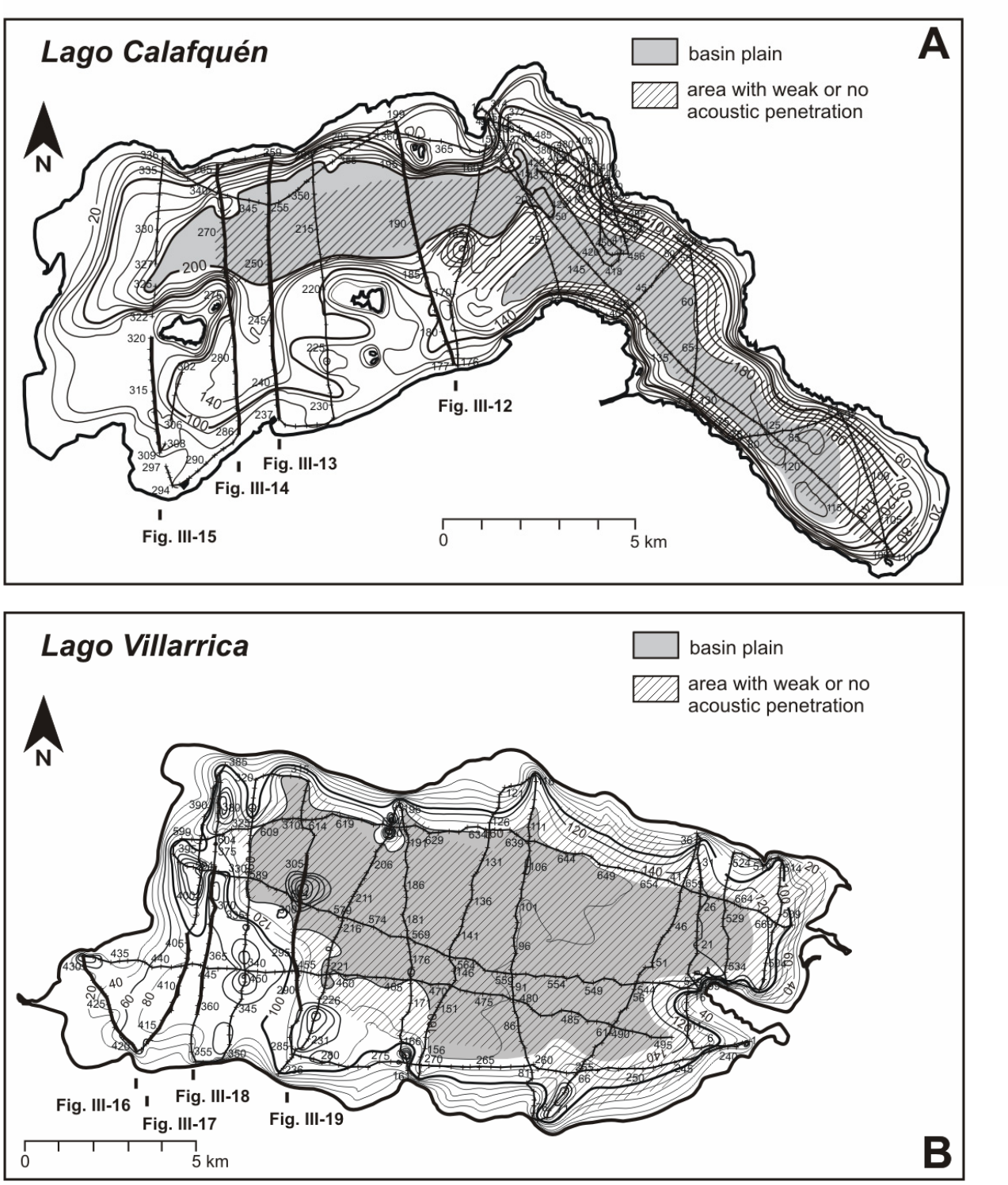

Fig. III-9: Bathymetric maps and seismic survey grids of A) Lago Calafquén and B) Lago Villarrica with track marks and shot points. Grey colour marks the basin plain, hatched lines indicate the area without or with minor acoustic penetration. Thick black lines mark the seismic sections discussed in the text.

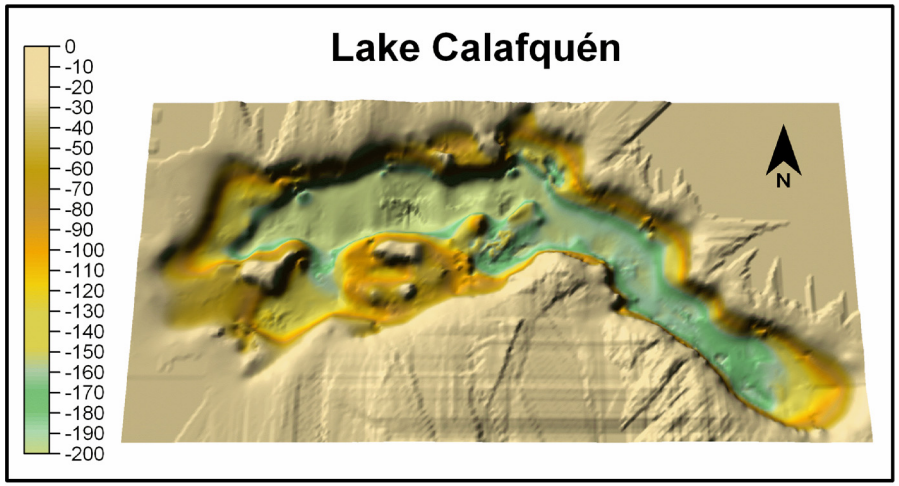

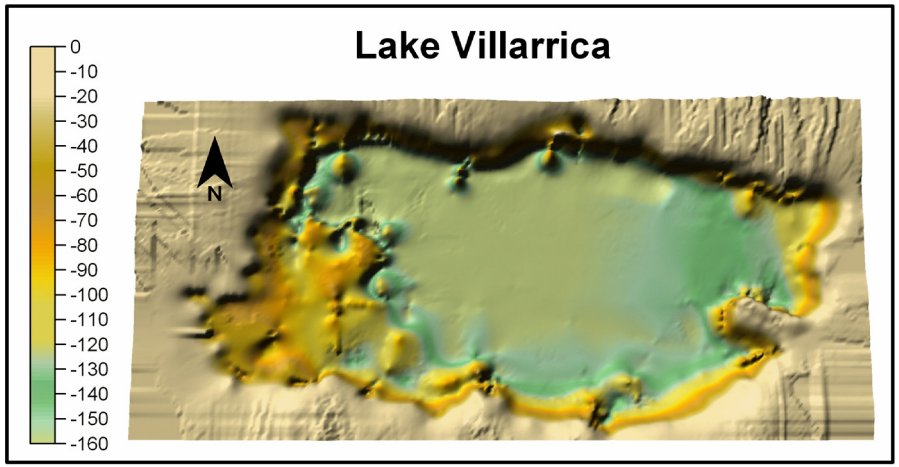

Fig. III-10: Bathymetric models obtained by data combination of the seismic surveys and the published bathymetry by Campos et al. (1980, 1983). A) 3D basin model of Lago Calafquén and of B) Lago Villarrica.

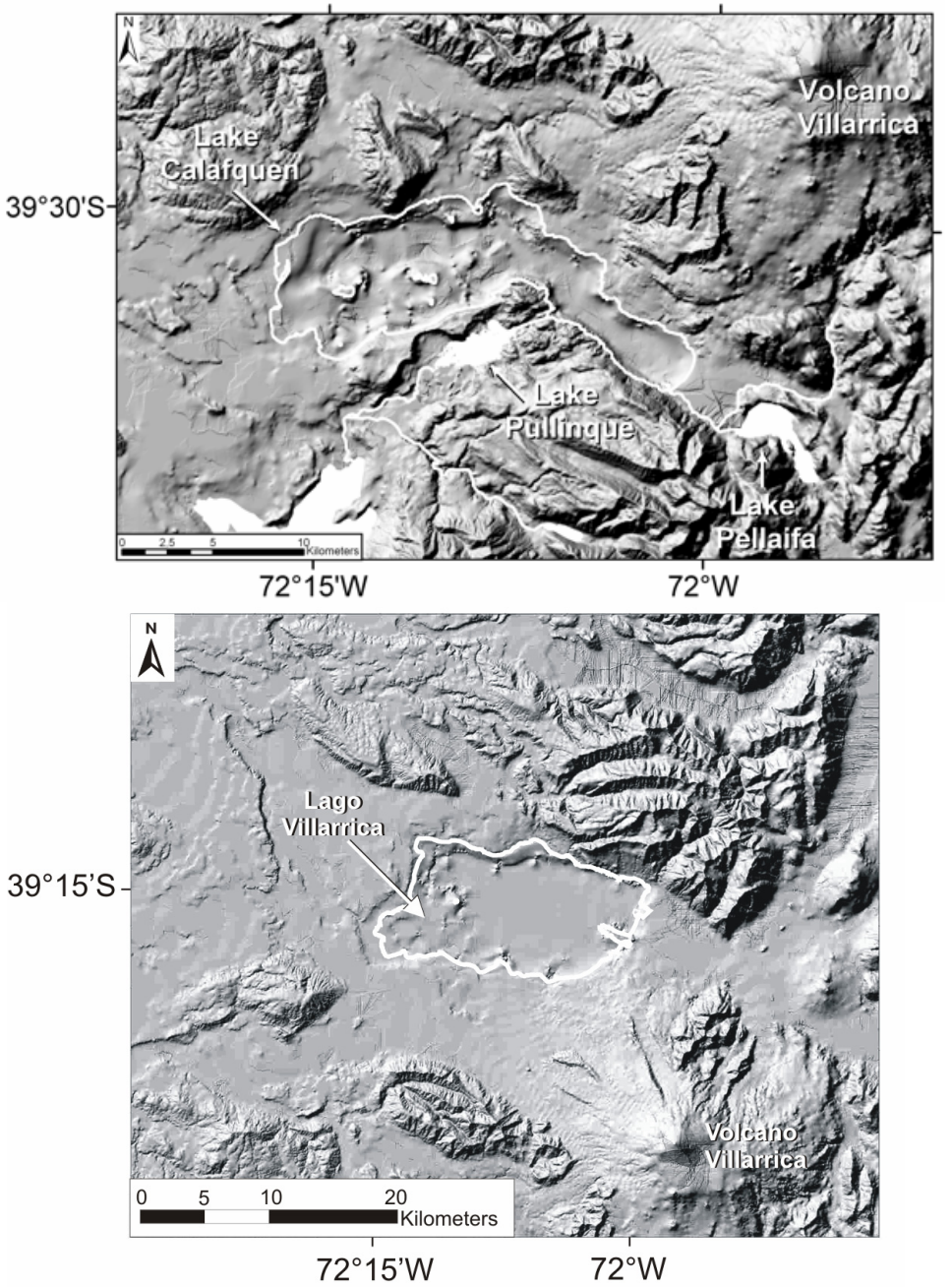

Fig. III-11: Digital terrain models (DTM) of A) Lago Calafquén and B) Lago Villarrica.

4. Seismic results

Around 100 km of seismic profiles were shot for Lago Calafquén and ~ 130 km for Lago Villarrica. Although the acoustic seismic properties of the lake sediments are similar in their general acoustic characterization, some differences in the unit distinction and in the soft-sediment deformation have been observed. For this reason the seismic results and the trigger mechanism for sediment deformation of both lakes will be discussed separately. The surveys on both lakes comprise the entire basin (Fig. III-9a,b), on Lago Calafquén, a special focus of shot points around the Chaillupén delta (cf. Fig. III-3a). The seismic signal penetrates the upper 30 – 40 m of the lake sediments with a resolution ≤ 50 cm, faintly detecting the acoustic basement. The deep basin plain, deltas, and areas with chaotic layering, as well as gas-rich sediments, absorb rapidly the pinger energy (cf. Giovanoli et al., 1984). These areas appear acoustically opaque or as areas with minor penetration in the seismic records (Fig. III-9a,b).

4.1 Lago Calafquén

4.1.1 Lake floor topography

a) Bathymetry

Lago Calafquén is divided into two sub-basins: a narrow and planar elongated eastern basin and a wide and open western lake basin that has a complex morphological structure (Fig. III-9a to III-11a). The eastern basin is characterized by a deep basin plain confined by steep slopes. The basin plain extends into the western lake basin where it reaches a maximum depth (Z_{max}) of 212 m, but has mostly low seismic penetration (Fig. III-9a) and acoustic opaqueness in some profiles. A morphological ridge delineates the basin plain towards the south (Fig. III-9a to III-11a). Resolution of seismic data becomes better near the south-western and western shores. Despite these problems on the northern shore and eastern basin, acoustically stratified sediments can be identified in parts of the basin plain. They are overlain by strata that show a chaotic seismic signal of varying amplitude.

b) The basement

The basement appears in variable forms along the southern lake side (Figs. III-9a to III-11a). A narrow succession of lateral en-echelon spreads rises in the mid-southern part (Fig. III-12; shotpoint 177 to 185; ~ 28 m water depth; cf. Fig. III-9a), showing large cracks and linear depressions that separate individual basement blocks. The incisions are filled by > 30 m of sediment. The whole succession progrades to an increasing water depth of 90 m over a distance of 2.5 km, and has an inclination of about 3 % (Fig. III-12). Debris consisting of openwork blocks and rocks has accumulated at the foot of the basement blocks at a depth of 165 m. The cracks widen towards the west and reveal enlarged voids for sediment deposition with a slightly increased inclination of 3.5 % over a distance of 2.8 km (see Appendix, Fig. A-8). A small plateau at ~ 11 m sub-bottom extends over 320 m (shotpoint 237/238; Figs. III-9a, III-13) into the lake, followed by a sudden transition to a steep slope. At the foot of the slope in +/- 280 ms (approx. 46 m sub-bottom), the surface is hummocky and chaotic blocks have accumulated. Farther westward, side wall deformation of the basement shows a linear graben-like depression of broad size (Figs. III-9a, III-14) whose probable acoustic basement is detected at ~ 270 ms (> 40 m sub-bottom). Sediments with a thickness ≥ 40 m fill this depression. This morphology continues to the western end of the lake basin but rises to a horst-like elevation in +/- 140 ms (equivalent to 28 m sub-bottom) (Fig. III-15).

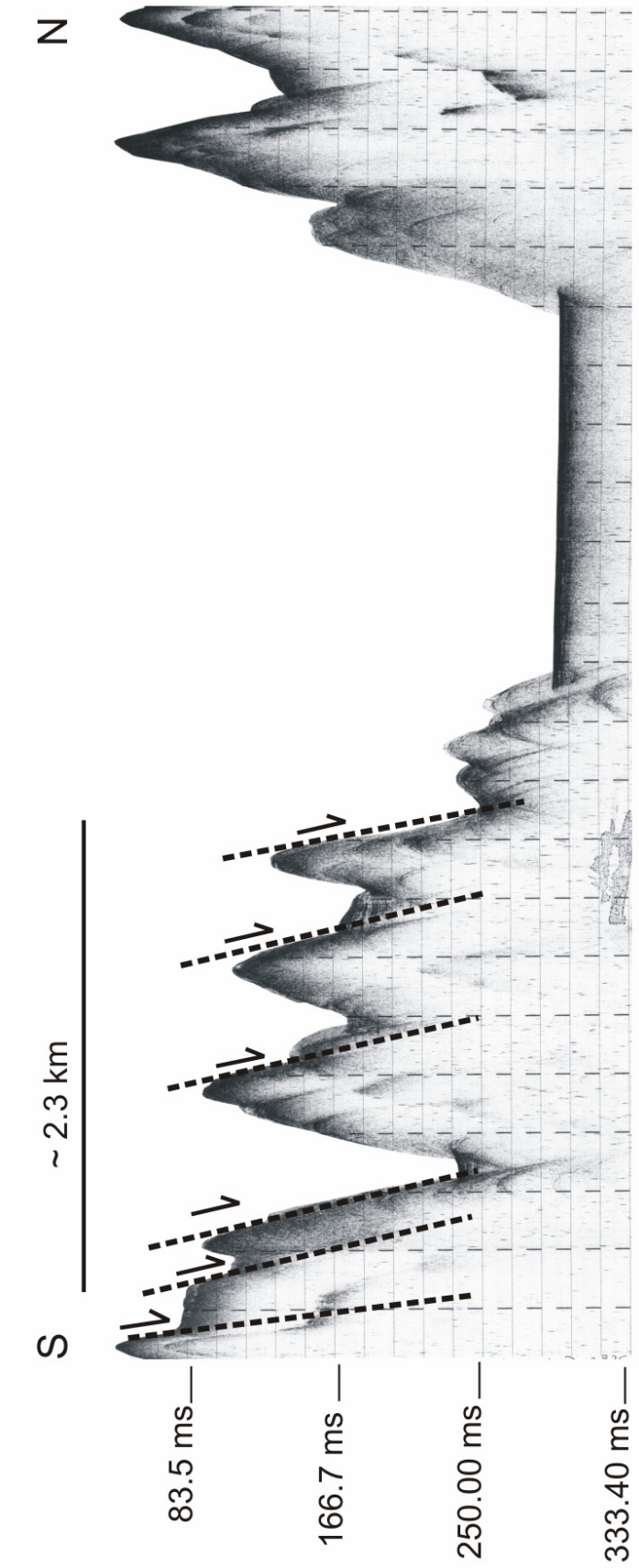

Fig. III-12: 3.5 kHz seismic line through a narrow succession of lateral en-echelon spreads (narrow dashed lines). Relative movements of the individual basement blocks are indicated by black arrows. The position of the seismic section is indicated in the track plot in Fig. III-9a.

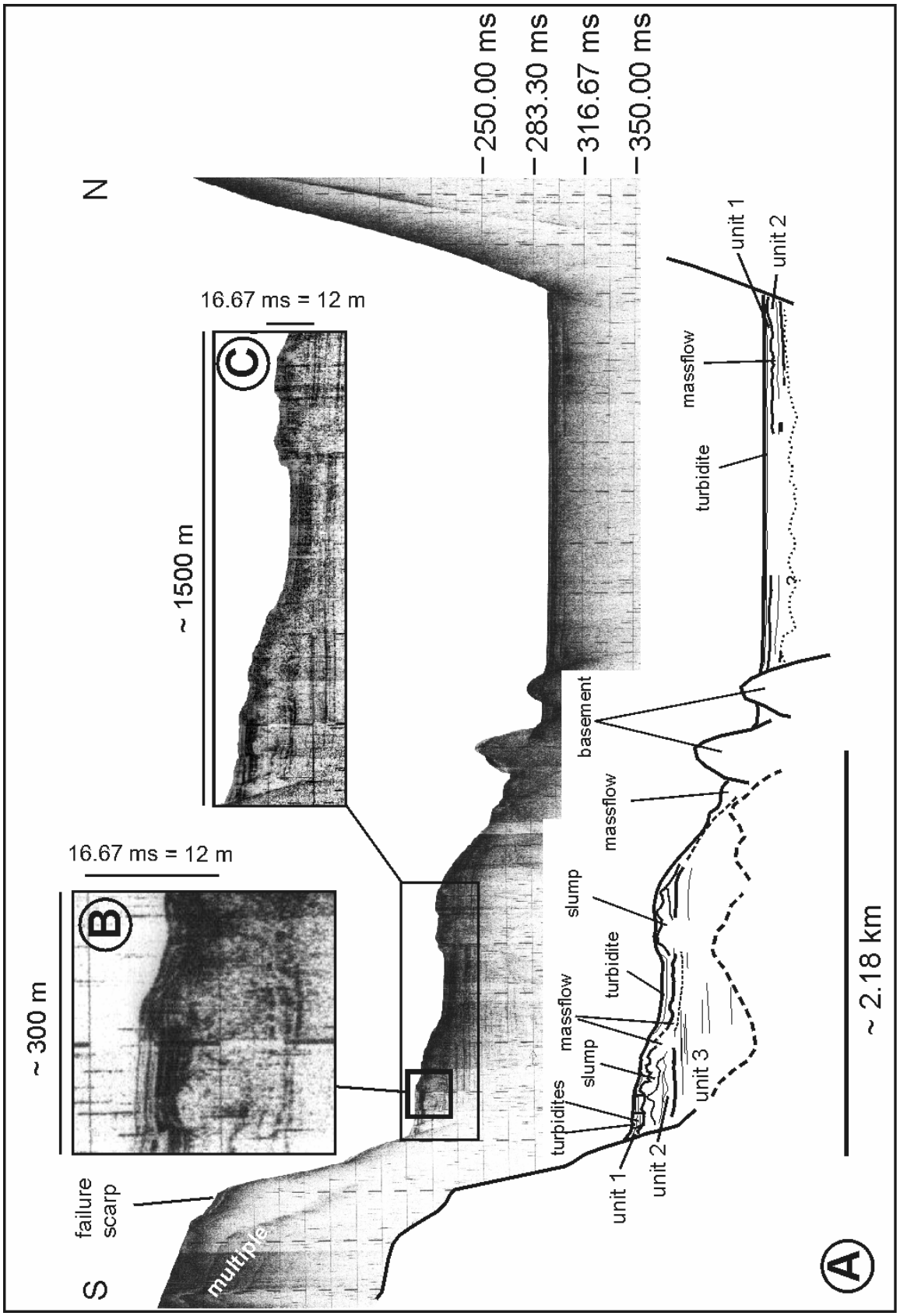

Fig. III-13. A: Slumps and mass-flow deposits in Unit 2 form a chaotic acoustic facies and a hummocky surface with high-amplitude reflectors and side echoes at the top. B: Slump deposit deeply penetrates and rework the underlying sediment of Unit 2. C. Multiple mass-flows and liquefaction are visible in Unit 2, underlying the modern lacustrine drape. The position of the seismic section is indicated in the track plot in Fig. III-9a.

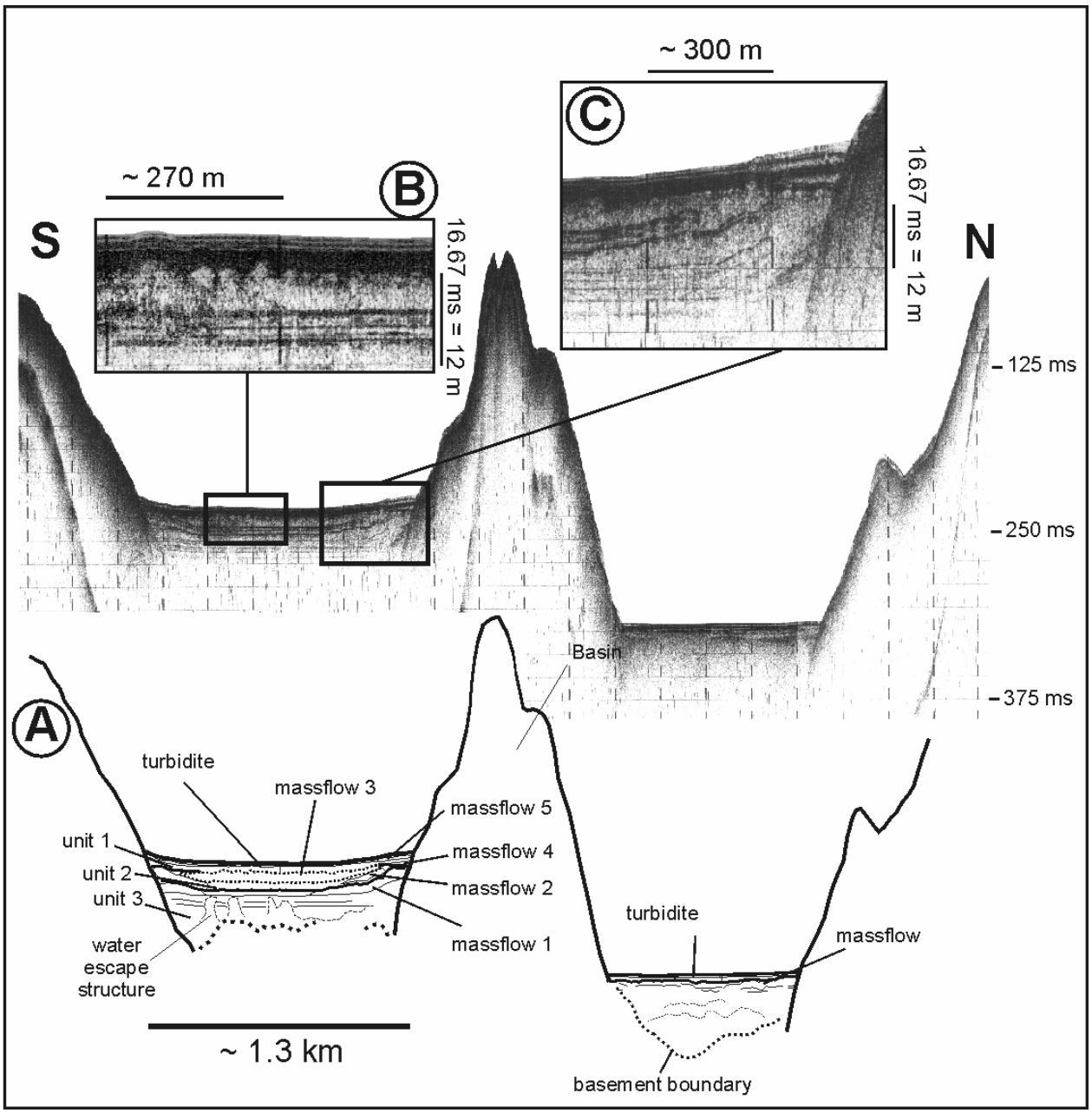

Fig. III-14. A: 3.5 kHz seismic section through an area of multiple mass-flow deposits (1-5) in the westward extension beyond the slump affected area. B: Large-scale liquefaction pattern with diapiric structures bulging into the overlying Unit 1. C: Discontinuous wedge-shaped sediment accumulation of chaotic to transparent seismic facies. Smaller corresponding mass-flow deposits accumulate at the southern side margin. The position of the seismic section is indicated in the track plot in Fig. III-9a.

4.1.2 Seismic stratigraphy

The seismic lines along the southern side reveal medium to good resolution and at some localities show > 40 m-thick sediments covering the basement. At some localities the basin substratum could faintly be traced. Based on the acoustic properties, a separation into four major seismic units was possible comprising a sedimentary record from Unit 1 down to Unit 4.

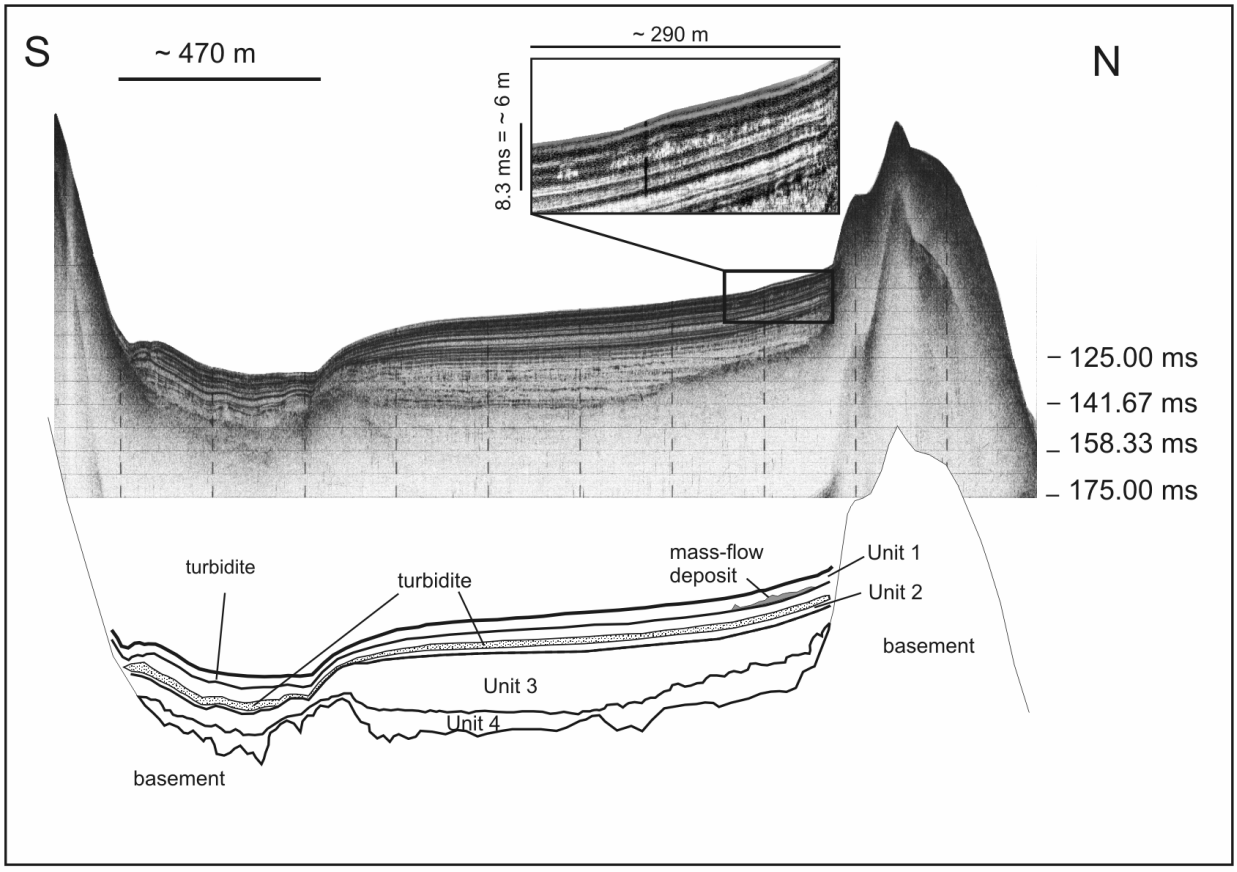

Fig. III-15: Seismic line across the western end of Lago Calafquén, revealing the general acoustic facies of four major seismic units that can be traced in all seismic lines along the southern side. The position of the seismic section is indicated in the track plot in Fig. III-9a.

The basement was only faintly detected, thus numbering of these units from top to bottom seems favourable. Due to resolution limits, a further subdivision does not appear reasonable. From the seismic stratigraphy (Fig. III-15) the lower part of the total sediment pile is apparently not or poorly stratified whereas the upper part exhibits thin but regular and continuous reflections. These sequences have been recognised in all seismic lines along the southern side and at one locality on the northern side.

Unit 1 is a concordant drape, defined by closely spaced, parallel, continuous, high-amplitude reflections that onlaps onto Unit 2. Unit 2 is transitional between its lower and upper boundaries. Depending on the locality in the seismic grid, it shows double to multiple reflections with weak transparent sub-parallel to parallel reflection of medium to low amplitude. The transition between the lower and upper boundary is delineated by a strong high-amplitude reflection. Unit 2 is characteristic of all seismic lines and can be best identified along the southern side. The middle to lower parts of Unit 3 are reflection-free to faintly-stratified and sometimes shows large-scale diffraction patterns. Onlapping the slopes of the basement, it marks an erosional truncation upwards and grades into an increasingly

stratified facies with characteristic non-continuous reflections of varying amplitude. This features were observed only at the western end of the lake but not in other seismic lines, which is probably due to resolution problems. Unit 3 comprises between 13 to > 35 m of sediments along the southern side. Thickness is lowest at the western end of Lago Calafquén and increases eastwards with a visible maximum around 40 m. The lower part of Unit 3 is smooth to hummocky and shows partly contorted, partly chaotic reflections, but is mostly reflection-free. Several non-continuous, high-amplitude reflections probably mark distinct pyroclastic layers and intercalate with all seismic units. The lower boundary of the basin substratum, defined here as Unit 4, could only faintly be detected, thereby making characterisation difficult.

4.1.3 Mass movements and soft-sediment deformation

Mass movements, such as sliding and slump events, mass-flows and large turbidites, affected the seismic stratigraphic sequences along the southern lake side and the basin plain.

a) Slumps, slides and faults

A large slump is identified in Unit 2 (Fig. III-13a,b) along a longitudinal distance of ~ 2 km at a current water depth of 145 m (5.5 m sub-bottom), underlying the modern lacustrine drape. The southern side exposes a steep rock slope with little overlying sediment, and has a failure scarp of ~ 8.8 m maximum height at 48 m current water depth (Fig. III-13a). Adjacent to the foot of the slope, a large slump was recognised in Unit 2 that reveals a chaotic-to-transparent acoustic facies. Internally propagating frontal thrusts are identified that have formed on the lake floor during the slump event, comparable to internal structures of basin plain deformation like they are described by Schnellmann et al. (2005). As the lateral extent is not known, volume determination of the slump was not possible. Deeply penetrating deformation structures and reworking of the underlying sediment in Unit 2 has been recorded (Fig. III-13b). Locally liquefaction behaviour occurs in the underlying sequences, identifiable by bulging of the latter into overlying strata (Fig. III-13c). Mass-flow deposits occur adjacent to debris cones (Fig. III-13a) and form a chaotic facies of medium amplitude with a hummocky surface. Coalescing extensive turbidites that reveal a transparent seismic facies with thickness of ~ 1.9 ms (about 2 m) are recorded. Unit 1 drapes the entire slump-affected area and the basin plain. At the foot of the southern slope vertically offsetting thrusts deform the sediments of Unit 1 (Figs. III-13a,b).

b) Mass-flow deposits

At the foot of the steep southern slopes, mass-flow deposits are frequently found in the seismic profiles. They mostly form discontinuous, wedge-shaped sediment accumulation of chaotic-to-transparent seismic facies (Fig. III-14). Multiple mass-flow deposits (1 to 5) are recorded in seismic stratigraphic Units 1 to 3 (Fig. III-14c). These mass-flows also occur as smaller bulges on the opposite side, implying coeval deposition (Fig. III-14a,c). They grade into turbidites with a transparent seismic signal at the distal end of the slope, and some spread into the distal northern sub-basin forming turbidites. Thick, chaotic-to-transparent seismic double reflections separated by a distinct high-amplitude layer are characteristic of Unit 2. This seismic facies is identified in all seismic lines throughout the southern side of the basin. The uppermost strata of Unit 1 comprise larger mass-flows and turbidites between 0.8 to >1.5 m thick that are identified in the same seismic stratigraphic levels in various seismic sections (cf. Figs. III-12, III-13) and can also be recognized in the basin plain.

c) Water-escape features

Water-escape structures are frequently recorded in the seismic sections and are related to liquefaction processes of loosely packed, non-consolidated lake sediments. These structures can be observed in various seismic sections along the southern lake side, where they form locally well-defined vertical pipes rising from the deeper sediment sequence and migrate into the modern lacustrine drape beneath the lake floor. Mass-flow deposit 3 (Fig. III-14b) shows a large-scale liquefaction pattern with diapiric structures bulging into the overlying Unit 1.

4.2 Lago Villarrica

4.2.1 Lake floor topography

a) Bathymetry

Contrasting the complex basin geometry of Lago Calafquén, Lago Villarrica forms a relatively simple, typical piedmont-like, U-shaped lake basin, not revealing any large subdivision. The eastern basin is characterised by the wide and planar basin plain with a maximum depth (Zmax) of 160 m. The plain continues towards the north-western end but shows minor seismic penetration and acoustic opaqueness in nearly all seismic profiles from the eastern and central areas. A morphologic elevation rise delineates the basin plain, from a plateau at the south-western lake shore, stretching from Huichatio creek beyond the northern bay of Villarrica (cf. Fig. III-3b; Fig. III-10a). Acoustic resolution becomes better along the morphologic rise at the south-western shore, revealing seismic profiles of acoustically stratified sediments.

b) The basement

In contrast to the heterogeneous basement formation of Lago Calafquén, the basement substratum of Lago Villarrica is less complex. The entire plateau-like formation in the south-western to western lake basin (Fig. III-3b, III-10b) is made up by chaotically arranged openwork blocks and rocks. They interfinger and are tilted against each other, thus forming depressions and ridges (Fig. III-16). Large basement blocks are surrounded by vast debris masses (Fig. III-17). Trending eastwards along the southern shore, the hummocky surface of the basement changes into a smooth plain, forming a ground level (shotpoints 367 to 373, Fig. III-18) which might be identified as the acoustic basement, but due to the limited acoustic resolution this cannot be confirmed. Individual separated blocks drift towards the central basin plain (Fig. III-19). Their formation and arrangement, together with the debris accumulation suggests a large spreading event linked to a large landslide was responsible for the formation of the morphologic rise in the south-western and western basin of Lago Villarrica (Fig. III-20).

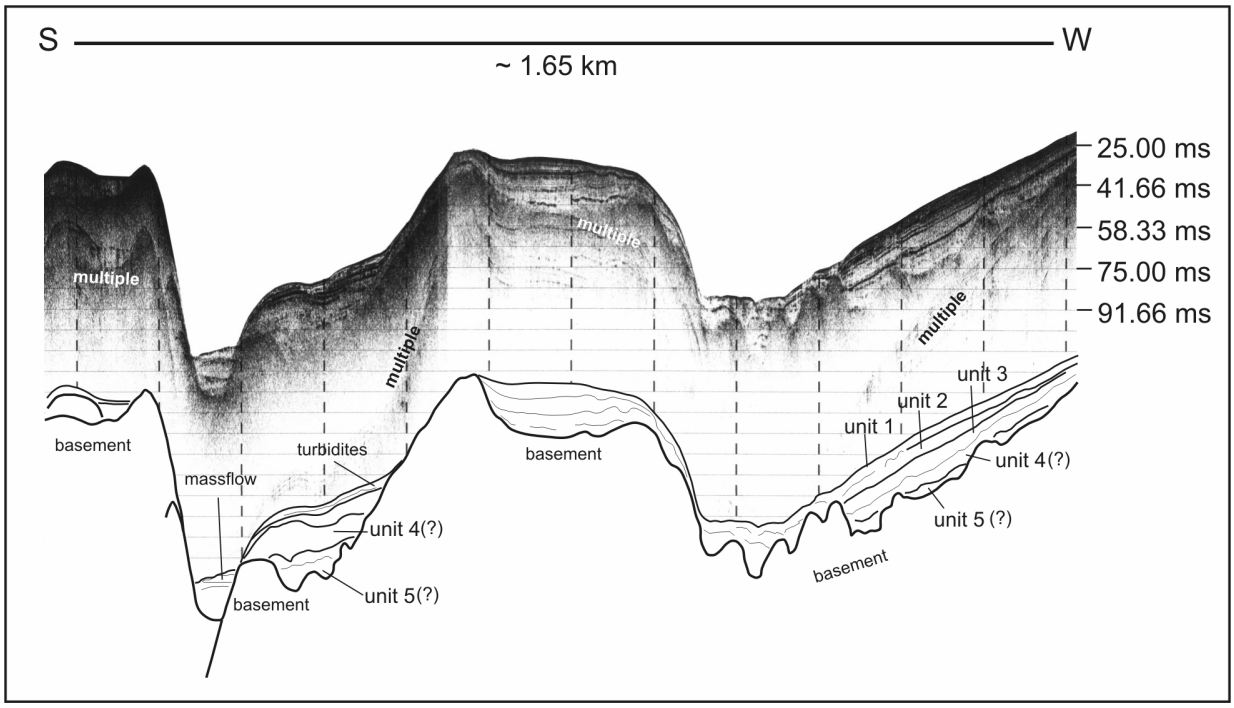

Fig. III-16: Basement formation in the bay of Villarrica. Chaotically arranged openwork blocks and rocks are tilted against each other and interfinger, hence forming depressions and ridges (shotpoints 436-452).

4.2.2 Seismic stratigraphy

Along the plateau-like elevation in the south-western to western basin, the seismic lines achieved good penetration. Sediment between ≥ 35 to > 50 m thick covers the basement and fills the voids and cracks of the tilted openwork blocks and the debris masses. The acoustic basement was only faintly traced. Separation into at least five seismic units was possible and their classification generally resembles those described from Lago Calafquén.

A full seismic stratigraphic sequence from Unit 1 until Unit 5 is recorded in the seismic profiles. They comprise a sedimentary record from Unit 1 down to Unit 4 (Fig. III-17). Deposits of Unit 5 are not clearly identified, but presumably were detected in some areas (e.g. shotpoint 409-411; Fig. III-17b) up to ~ 12 m thick.

In the general succession of the acoustic seismic stratigraphic units, the lower part of the sediment pile is poorly stratified or reflection-free, whereas the upper part exhibits thinly but regular and continuous reflections Fig. III-17b. These sequences have been recognised in the longitudinal seismic lines along the south-western side and at some localities on the northern side. Unit 1 forms a concordant drape ~ 5 m thick, defined by closely-spaced, parallel, continuous, high-amplitude reflection that onlaps onto Unit 2. Unit 2 is ~ 11 m thick and shows double to multiple reflections with weak, sub-parallel to parallel, medium to low amplitude, transparent reflections. The transition between the lower and upper boundary is delineated by a strong high-amplitude reflection, akin to the sub-division of Unit 2 that was observed in Lago Calafquén. Unit 2 is characteristic of all seismic lines along the plateau-like elevation, but it blurs towards the eastern margin of the rise (Fig. III-19). The ~ 11 m thick Unit 3 is faintly-stratified and shows low-amplitude reflections with poor continuity. At least two large-scale, medium-amplitude diffraction patterns of poor continuity that mark distinct reflectors, are recognised in Unit 3. Unit 4 forms a ~15 m thick, completely reflection-free sediment succession that reveals isolated chaotic seismic signals towards the southern shore. Unit 5 forms a smooth to hummocky surface at the

boundary to Unit 4 and is poorly stratified to reflection-free. Irregular contorted, low-amplitude reflections of very poor continuity are detected in Unit 5 that achieve thicknesses of ~ 12 m (Fig. III-17b). Various non-continuous, high-amplitude reflections are recorded in all seismic units. They cover the upper limits of the basement up to Unit 4 where they mimic the original topography.

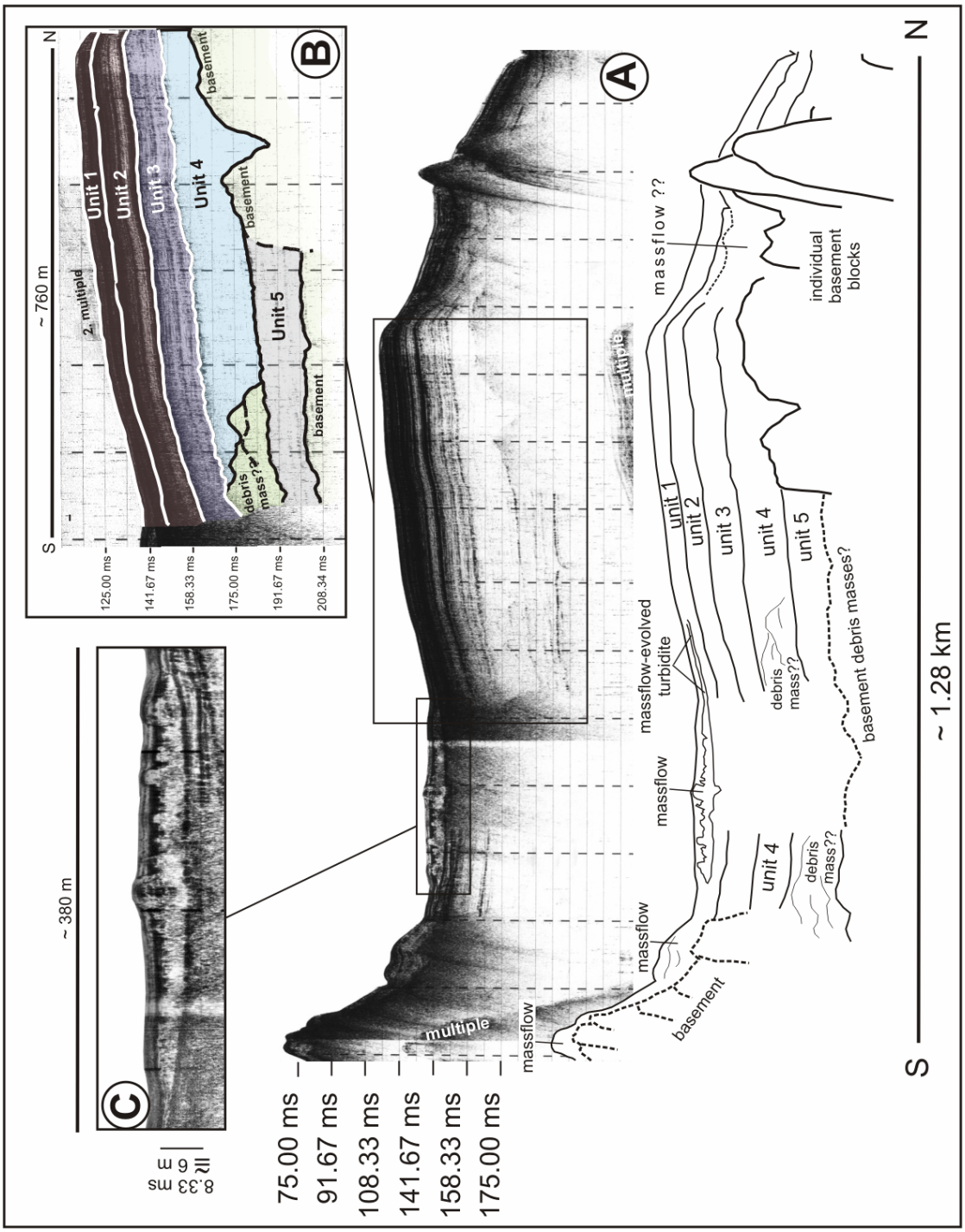

Fig. III-17. A) Seismic line of shotpoints 404-417. Large basement debris masses accumulate on the basement. B) The basement is overlain by a succession of sediments which reveal a classification of at least five seismic stratigraphic units. Reflection-free Unit 4 comprises a large debris mass, suggesting that this area was affected by repeated large shallow landslides. C) Large-scale liquefaction pattern with diapiric structures bulge into the overlying sediments.

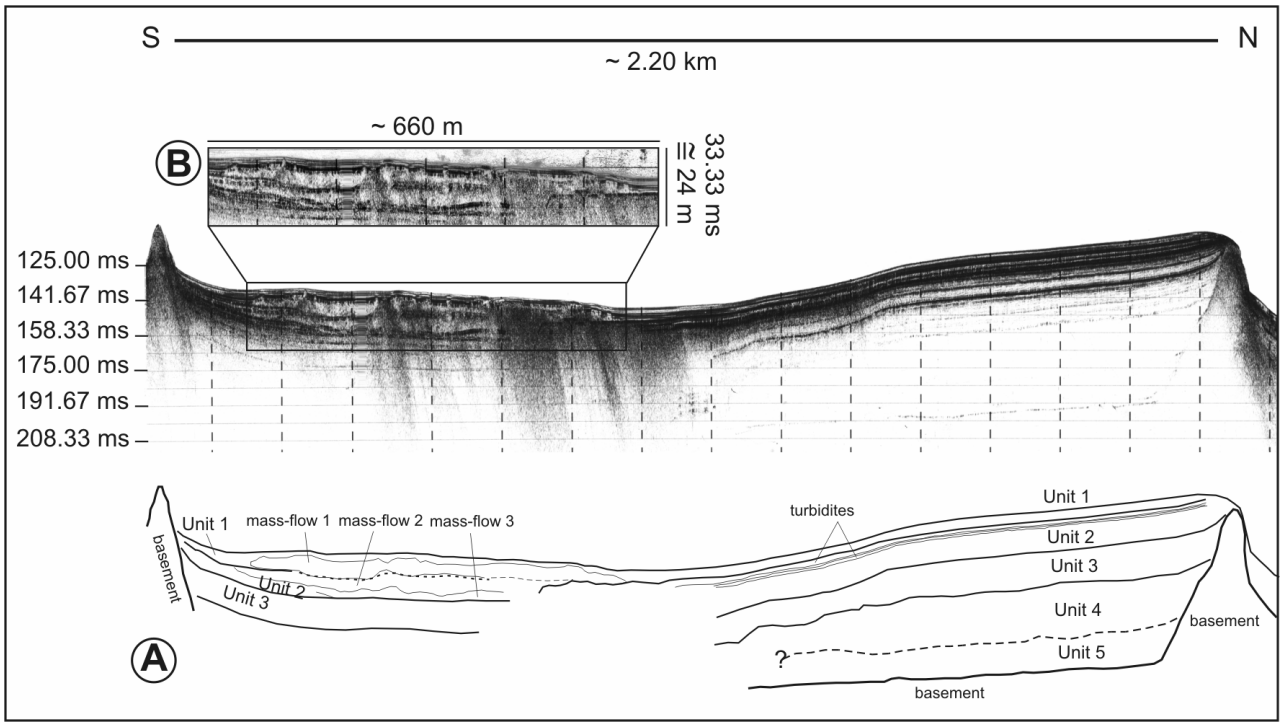

Fig. III-18. A) Seismic line of shotpoints 359-374. The hummocky surface of the basement changes into a smooth plain, forming a ground level which is identified as acoustic but not necessarily as geologic basement. B) Succession of three mass-flow deposits. The largest mass-flow 1 encompasses a volume of $3.2 \times 10^6 m^3$.

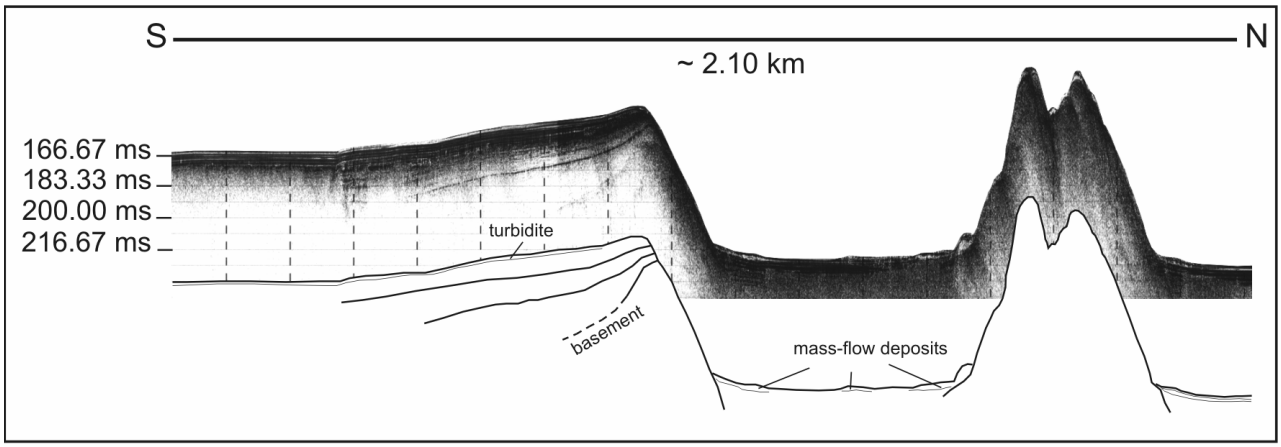

Fig. III-19: Beyond the continuous morphologic rise, individually separated blocks detached from the sidewalls drift towards the central basin plain.

4.2.3 Mass movements and soft-sediment deformation

In Lago Villarrica, soft-sediment deformation is not so drastic or destructive as observed in the seismic lines of Lago Calafquén. In the basin of Lago Villarrica, soft-sediment deformation is identified in the modern Units 1 and 2, and is restricted to the south-western side. The affected zone stretches along a small area next to the bay of Villarrica. Soft-sediment deformation is linked to mass movements. Mass-flow deposits affect the entire eastern basin plain, entering the lake via the small and main tributaries. Associated with mass-flows are large turbidites that form isolated, reflection-free bodies intercalating with the lacustrine stratified sediments.

a) Mass-flow deposits

Mass-flow deposits in Lago Villarrica are restricted to a small area between the mouth of Lelún creek and the bay of Villarrica (cf. Fig. III-3b). Three distinct locations of isolated mass-flow deposits (Tab.III-1, Fig. III-21) are traced in the seismic profiles (Fig. III-17 to III-19) but are obviously not connected to each other as they do not appear at the same geographic latitude. At least three major generations of mass-flow deposits (1 to 3) can be distinguished (Fig. III-21). Mass-flow deposit 1 forms a discontinuous, wedge-shaped sediment accumulation of chaotic-to-transparent seismic facies in Unit 1 (Fig. III-17,18), whereas Unit 2 comprises both mass-flow deposits 2 and 3 (Fig. III-18b). Acoustic facies of mass-flow deposit 2 are rather chaotic and less transparent, revealing low- to medium-amplitude reflection. The top and the base of mass-flow deposit 3 are made up by an irregular hummocky surface, and thickness varies from 2.2 to 3.6 m. The internal structure of the body is partly acoustically transparent and partly chaotic. The top of mass-flow deposit 3 is delineated by a strong, high-amplitude reflection.

The largest body of mass-flow deposit 1 in Unit 1 was detected at location 2 (Figs. III-18b,21a), covering an area of ~ 0.63 km² (Fig. III-21a). By cross-cutting a lateral seismic section, a minimum volume of $\sim 3.2 \times 10^6 m^3$ (Tab. III-2) could be estimated. Mass-flow deposit 1 detected in locations 1 and 3 (Fig. III-17,21a) stretchs from 230 to 330 m in longitudinal distance. As the lateral extension is not known, a volume estimation of the isolated debris masses was not possible. The mass-flow deposits caused a poor resolution in the seismic signature, thus no lateral extension for mass-flow deposits 2 (Fig. III-21b) and 3 (Fig. III-21c) could be achieved. Only location 2 and 3 allow longitudinal mapping of mass-flow deposit 2 (Fig. III-18,21b). Detailed mapping of the longitudinal expansion of mass-flow deposit 3 was not possible.

All of the mass-flow deposits are detected at nearly the same acoustic sub-bottom depth of the distinct seismic stratigraphic unit, implying coeval deposition. The minor variation in the recording depth is attributed to the irregular basement topography caused by the subjacent tilted openwork blocks. Details on average depth and thickness for mass-flow deposits 1 to 3 are given in Table III-1. Note that this data only provides a rough estimate as analyses were done manually on paper plots and not with computerized filtering methods. Due to resolution problems, these estimates can only be considered approximate values.

The mass-flow deposits grade into turbidites with a transparent seismic signal at the distal end of the rise (Fig. III-17 to III-19). They likely also spread into the distal central basin plain. In Unit 2, they achieve minimum thicknesses up to 1.6 m. Akin to the seismic stratigraphic unit of Lago Calafquén, thick, chaotic-to-transparent, seismic double reflections separated by a distinct, high-amplitude reflector form a characteristic acoustic inventory of Unit 2. This seismic facies is identified in all seismic lines along the plateau-like elevation in the south-western basin area. The uppermost strata of Unit 1 comprise large turbidite bodies trending along the southern shore into the central basin. They are identified by an acoustic transparent facies.

The basin plain along the southern shore shows a chaotic seismic signal and interfere acoustically stratified sediments. These units are identified and described as mass-flow deposits and large turbidite bodies that cause reduction in acoustic penetration. Turbidite deposition

location	average depth (ms)	varying depth (ms)	depth subbottom (m)	average thickness (m)
mass-flow 1	136	130.9-144.2	4	2.5
mass-flow 2	142	132.7-154.2	7.2	4.2
mass-flow 3	144	142.9-146.6	11	2.9

Tab. III-1: General characterisation of mass-flow deposits in Lago Villarrica. Averaged depth and thicknesses are rough estimations. Due to resolution problems and manual analyses, the estimates can only be considered approximate.

by torrential flows and flood events caused by heavy seasonal rainfalls and meltwater runoffs occur more frequently in Lago Villarrica, as can be deduced by various short cores taken from different parts of the basin plain (see photographic documentation, Fig. A-6,7, Appendix). Volcanic input by debris flows (e.g. lahars) along the southern shore impedes acoustic penetration, followed by gas enrichment.

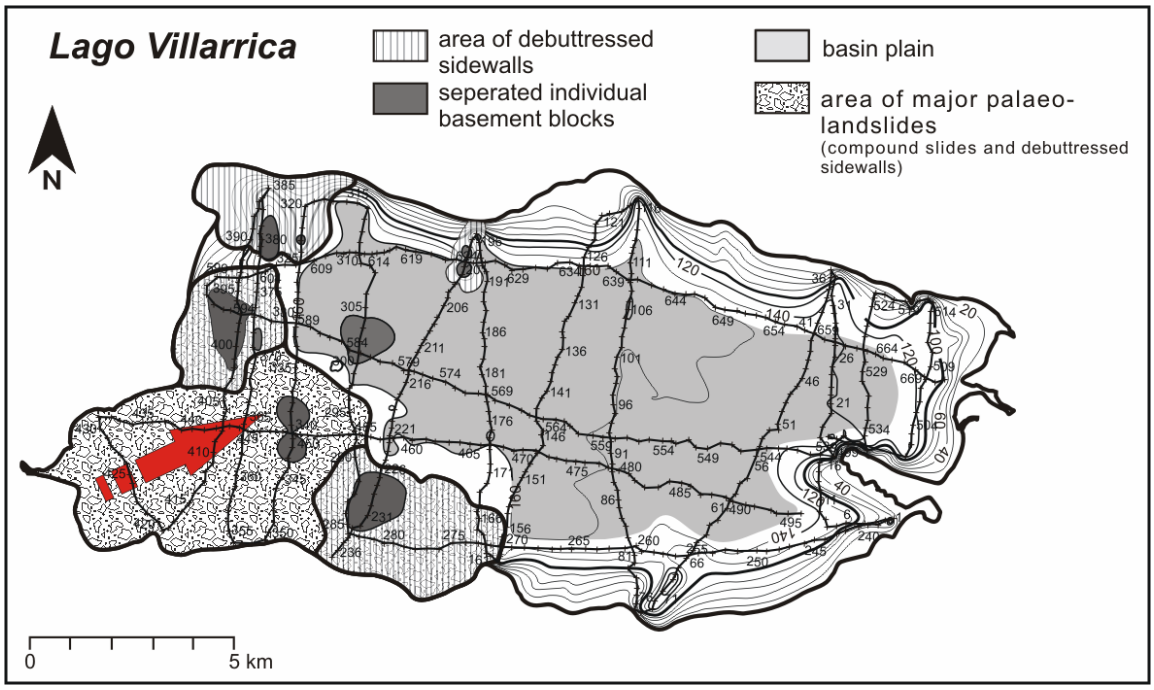

Fig. III-20: The morphologic rise in the south-western to western basin suggests large spreading events linked to a major landslide as a mechanism responsible for the formation. On the base of the filtered seismic lines areas of landslides and debuttressed sidewalls can be distinguished. The red arrow marks the probable centre of main failure.

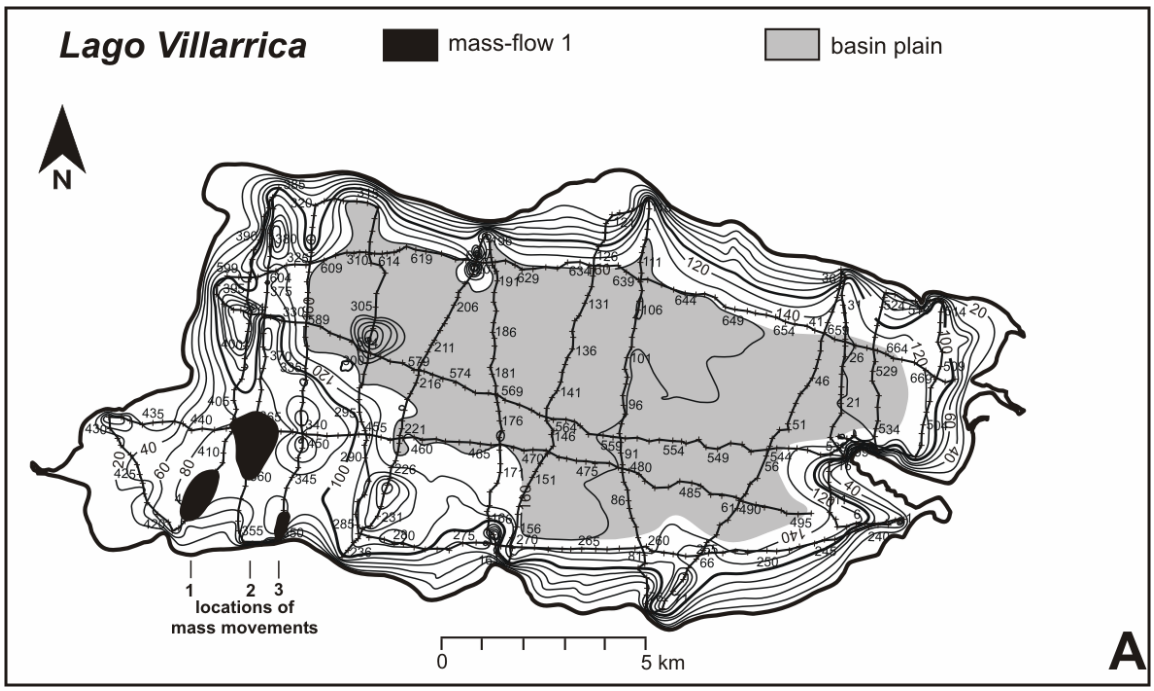

Fig. III-21a: Map of different locations with deposition of mass-flow 1.

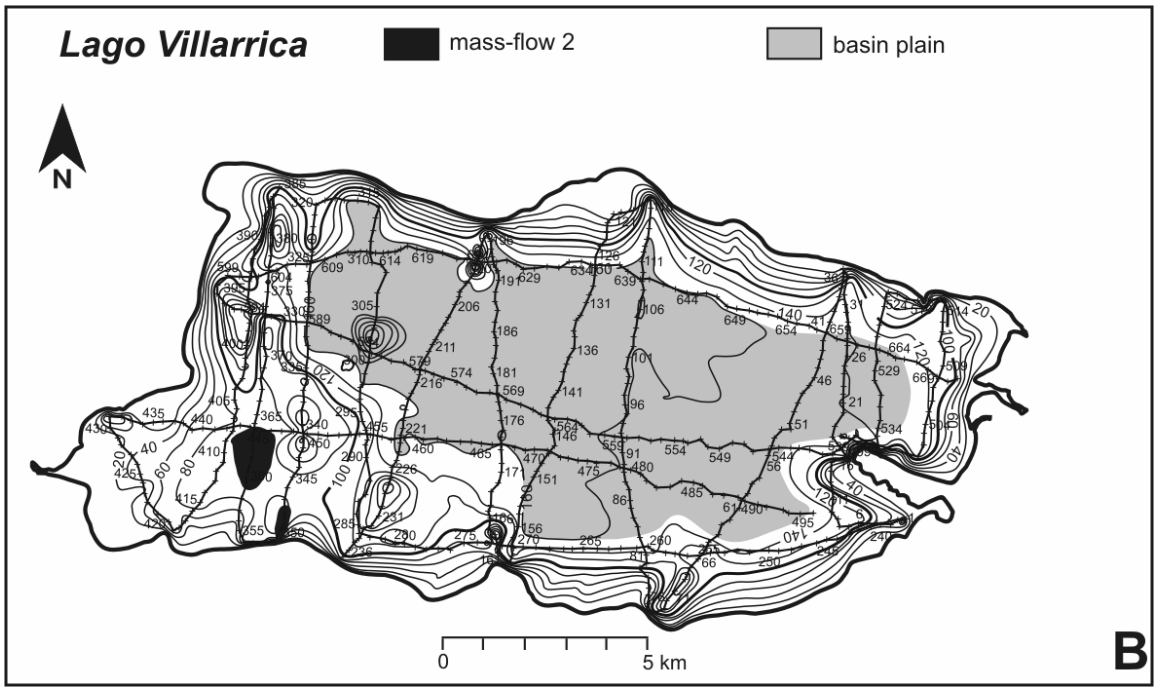

Fig. III-21b: Map of different locations with deposition of mass-flow 2.

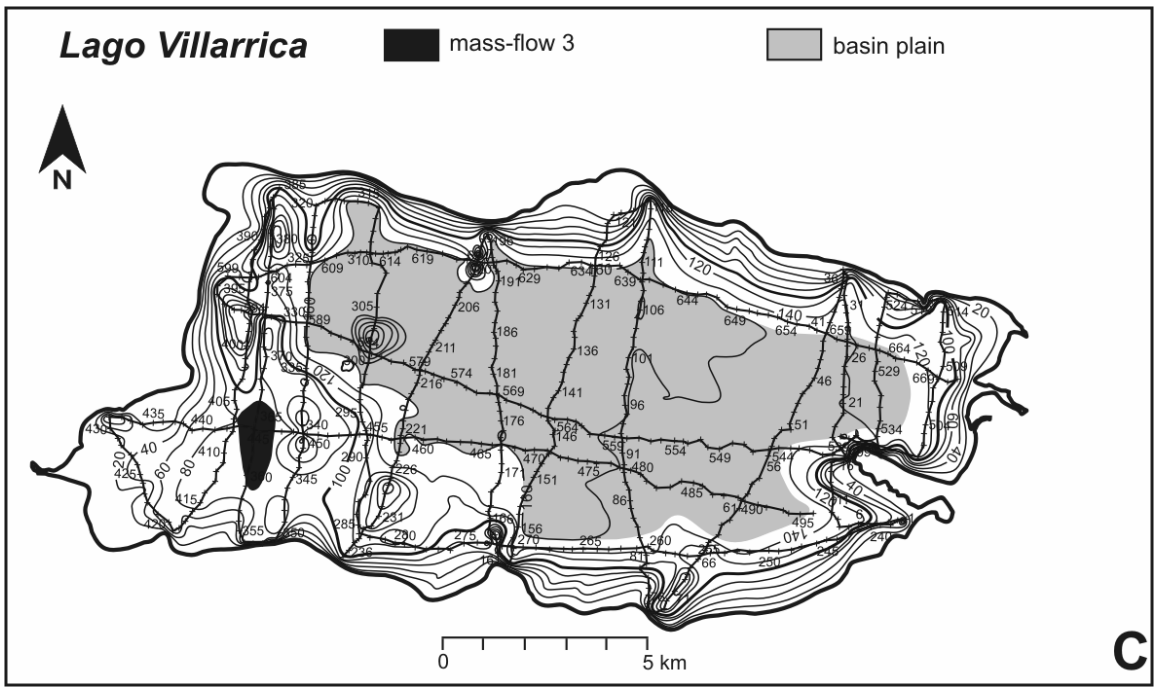

Fig. III-21c: Map of location with deposition of mass-flow 3.

b) Water-escape features

In the seismic profiles of Lago Villarrica water escape structures are restricted to the mass-flow affected areas. They are related to liquefaction processes of loosely packed, non-consolidated lake sediments. These structures can be observed clearly in mass-flow deposit 1, where they form a large-scale liquefaction pattern with diapiric structures bulging into the overlying sediments (Fig. III-17c, III-

18b). Subordinated mass-flow deposit 2 reveals the same structures, but due to acoustic resolution problems, their acoustic properties have been less clearly traced, thereby making further characterization rather difficult.

5. Triggers for mass movements

a) Lago Calafquén

Several clear horizons of distinct mass movements dominate the seismic lines in the uppermost level of Unit 3 and all of Unit 2, and persistently intercalate with Unit 1. The lower parts of Unit 3 do not reveal clear signs of intense primary deformation, thus indicate phases of low or reduced landslide activity. Since the uppermost parts of Unit 3 show major mass-flow deposits (cf. Figs. III-13,14) and related turbidite deposits, a decrease in slope stability and an apparent increase in slide frequency is noted and can be followed up to the present day. A large slump incident occurs in a locally defined area of the southern side in Unit 2 and is assumed to have left major imprints in this seismic-stratigraphic horizon throughout the lake basin. The large amounts of debris that have slid from the steep sides into the deep lake are likely to have caused strong impact waves – slump related seiches – that in turn would have produced mass-flow deposits and turbidtes of chaotic-to-transparent seismic facies. Such a relationship can be identified in Unit 2 of all acoustically transparent sections of the lake basin. Related is a large-scale mass-flow deposit that resulted in large-scale liquefaction features (Fig. III-14) and turbidites triggered by the slump event shown in Fig. III-13. At least three turbidite horizons occur in Unit 1 and can be correlated to several other parts in the lake basin as distinct seismic-stratigraphic horizons of Unit 1 (Figs. III-13b,14c,15). It is striking that the most remarkable deformation structures occur concentrated along the southern side of Lago Calafquén, north of the rockslides that confine the present-day shoreline of Lago Pullinque.

b) Lago Villarrica

Clear signs of primary sediment deformation are recorded in Units 1 and 2 as multiple large mass-flow deposits that occur in a narrowly defined area. They left obvious imprints in the seismic stratigraphy, at least throughout the plateau-like rise and probably along the southern shore and the entire lake basin. The deposition of mass-flow deposits resulted in large liquefaction patterns (Fig. III-17,18). The isolated bodies of these mass movements and the accumulation of a large debris mass in seismic stratigraphic Unit 4 (Fig. III-17b) imply the south-western shore is susceptible to repeated slope instability. In Lago Villarrica, the formation of seiche deposits can be assumed to have occurred due to the impact of landslides. Possibly related mass-flow evolved turbidites are identified in Units 1 and 2.

The trigger mechanism responsible for the pronounced features is important in the geological setting of Lago Calafquén and Lago Villarrica, and will be discussed below.

5.1 Seismic activity

As the study area is located on an active continental margin, serialized earthquakes of strong magnitudes occur that induce recurring landslide-related mass movements. But not only proximity to an earthquake epicentre controls landscape development, as places located far away can also be affected.

Various types of landslides, mass movements and sediment deformation can occur dependent upon a minimum exceeding earthquake magnitude in regions varying with distance away from the earthquake epicentre (Wieczorek, 1996) (Fig. III-22). Sediment deformation by seismic shocks is dependent on lithology, site characteristics and geophysical properties of the basement rocks. Exposure of the volcanic and glacial sediment lithology and related soil properties imply that the southern sides of Lago Calafquén and Lago Villarrica and their surrounding are prone to recurring destabilization of the sidewall, triggered by seismic shock events.

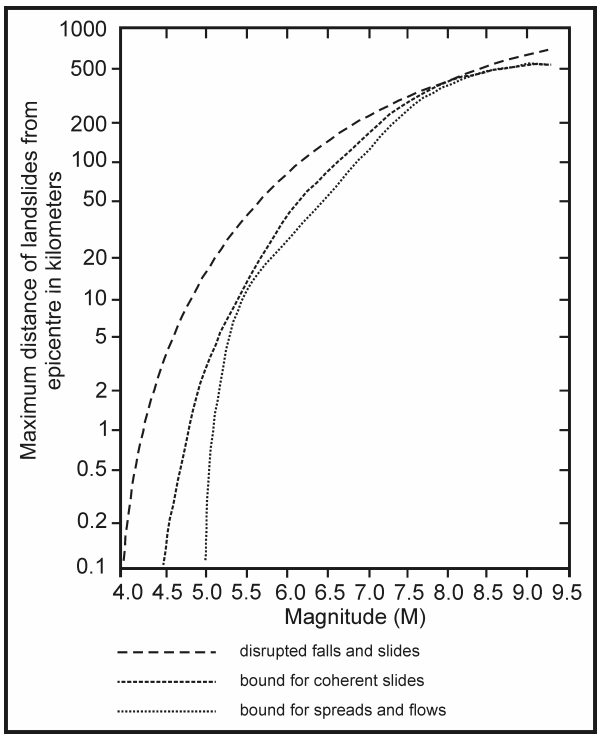

Fig. III-22: Maximum distance to mass movements and landslides from epicentre for earthquakes of different magnitude (*modified after* Keefer, 1984).

5.1.1 Effects on Lago Calafquén

The slump incident of Lago Calafquén in Unit 2 was probably triggered by a larger earthquake as several coeval mass-flow deposits and turbidites can be traced coincidently in distinct seismic horizons, similar as it is described for other seimic affected areas by Schnellmann et al. (2005, and references therein). Unit 1 further reveals coeval mass-flow deposits and turbidites. Several studies report slump and rockfall induced seiches, mass-flows and mass-flow evolved turbidites triggered by earthquakes (Siegenthaler et al., 1987; Chapron et al., 1999; Van Rensbergen et al., 1999; Schnellmann et al., 2002, 2005, in press; Chapron et al., 2004a). Following Schnellmann et al. (2002), the synchronous occurrence of these features in corresponding seismic horizons can be attributed to seismic events as the main trigger. Associated with seismic activity, widespread earthquake-induced sediment deformation by liquefaction is clearly imaged in the seismic lines. Liquefaction of sediment has been shown to occur with earthquake magnitudes Mw=5 to Mw=5.5 (Obermeier et al., 1993). However, liquefaction structures have also been reported to be triggered by strong wave action or lake level oscillations (Monecke et al., in press), as well as by seiche wave propagation. An upward-decreasing permeability, such as is present in graded turbidites, favours the development of such water-escape structures (Lowe, 1975). Although sand is most amenable to fluidization (Maltman and Bolton, 2003), water escape features are commonly found in alternating fine-to-coarse grained sediments (Lowe, 1975; Van der Meer et al., 1999). As deduced from short cores, modern sediments of Lago Calafquén comprise alternating sequences of silty sediment with frequent intercalated coarse tephra layers of high porosity, thus favouring liquefaction processes to a large extent.

5.1.2 Effects on Lago Villarrica

Subaerial shallow landslides originating from the catchment of the southern lake side are assumed to be the main trigger for the mass movements in the south-western basin of Lago Villarrica (Fig. III-17, III-18). Landslides on the southern side are thought to be triggered by seismic impacts, as the mass-flow deposits in Lago Villarrica can be traced coincidently in the distinct seismic stratigraphic horizons.

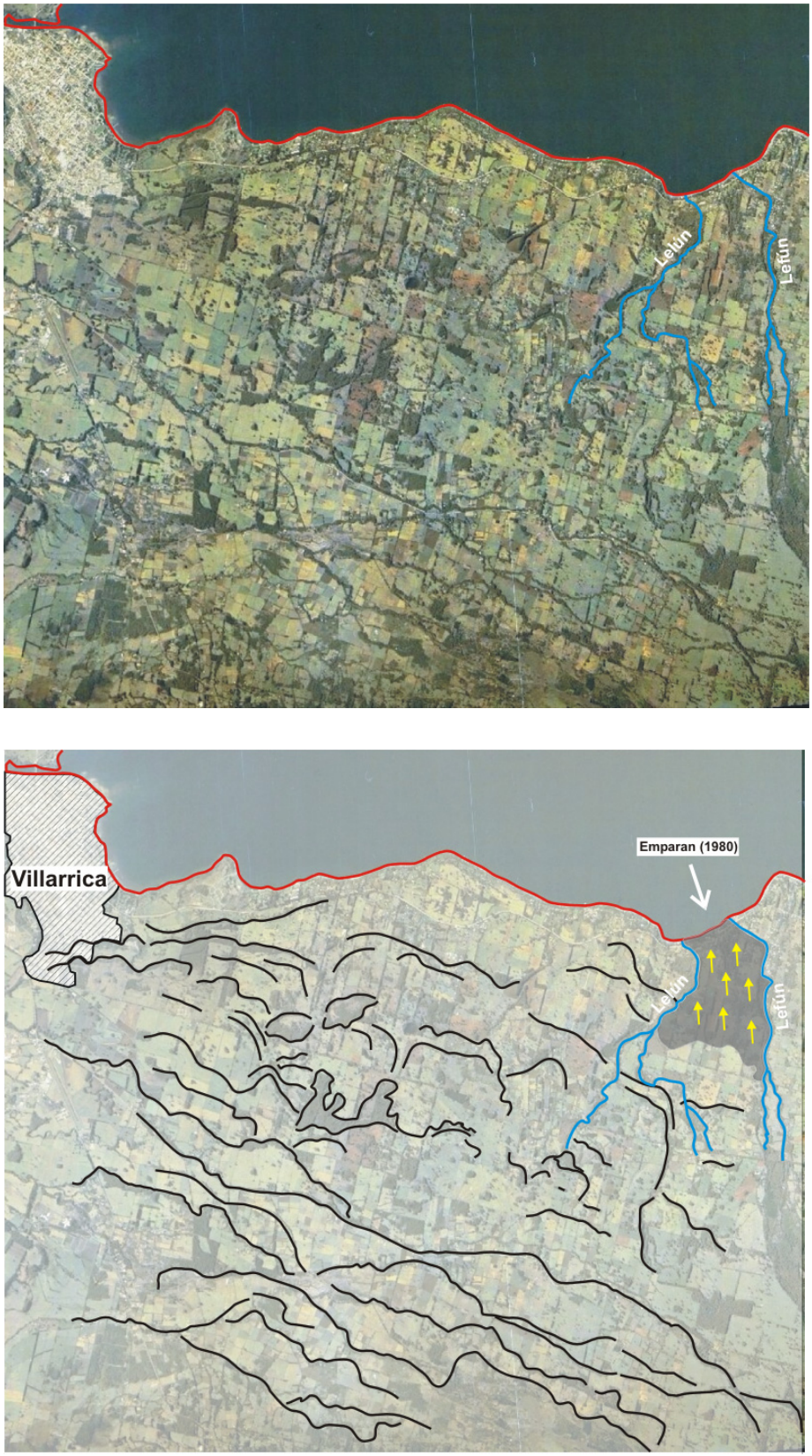

Fig. III-23: Clipping of the southern shore of Lago Villarrica, from Lefún creek to Villarrica village (above). Below: Many overgrown shallow failure scarps imply that the entire south-western side and its hinterland are strongly susceptible to recurrent shallow landslide activity. The expansion of these failure scarps suggests that frequent and recent mass movements occurred. *Source landsat images: www.sinia.cl*

The geology is made up by loosely packed, strongly weathered, volcanic regolith (lapilli to ashes), underlain by or intercalating with sandy to silty, gravel-bearing, glacial sediment. The southern region of Lago Villarrica has moderately smooth slopes which are characteristic of moderate humid to temperate climate zones. They are prone to rapid weathering and have the ability of easy soil erosion. Wieczorek (1996) suggests "landslides involving loose, saturated, cohesionless soils on low to moderate slopes commonly occur as a result of earthquake-induced liquefaction" and may be caused by a temporary rise of pore-water pressures due to earth shaking and associated reduction in soil strength. Emparán (1980) describes the area of the Lefún and Lelún creeks as highly prone to seismic induced landslide activity. Terrain mapping by Landsat images (Fig. III-23) shows that the entire south-western side and its hinterland are strongly susceptible to recurrent landslide activity. Many overgrown shallow failure scarps imply that frequent and recent incidents occur (Fig. III-23). A distinction into either rotational or translational landslide mechanism is difficult to estimate, but from exposures and the inclination of the strata, compound slides might be responsible.

5.2 Non-plate tectonic induced landslide activity

Not only seismic deformation by earthquakes leads to sidewall deformation of both lake basins and their surroundings. Landslides in the catchment could also be referred to a reduction of rock-mass strength by glacial erosion, especially for of the steep slopes on the southern side of Lago Calafquén. Tremendous slumps and rockfalls in that context are reported from the Andes, New Zealand, Alaska (Hambrey, 1994), the European Alps (Abele, 1997; Van Asch, 1997) and Scandinavia (Jarman, 2002).

5.2.1 Isostatic uplift and debuttressing effects

In contrast with the frequent seismic activity deduced from the pronounced sediment deformation and seismic stratigraphy from Unit 1 to the upper strata of Unit 3, the lower parts of stratigraphic Unit 3 in Lago Calafquén are lacking clear signs of frequent seismic events. This might reflect with a temporally reduced seismic activity of the lithosphere during this time interval. An upward increase in earthquake activity might be additionally inferred from the effects of rapid isostatic uplift after glacial retreat. For recently deglaciated areas, aseismic trembles with magnitudes from 5.9 to 7.0 may occur with rebound (Ballantyne, 1997, and references therein). Related liquefaction processes and soft sediment deformation have also been reported from tectonically-stable areas (Sissons and Cornish, 1982). The formation of the basement in Lago Calafquén and Lago Villarrica is akin to the aforementioned events. The Calafquén basement covers an area of ~ 23 km² of the southern lake basin. In Lago Villarrica, the basement fills ~ 13 km² of the south-western to western basin. The irregular morphology in both lake basins indicates that massive rock-slope failures occurred that filled the former basin, hence forming the basal lake floor topography. Sidewall deformation is related to debuttressing of the glacially oversteepened flanks. The timing of these adjustment processes remains speculative, but is assumed to have taken place possibly during the glacial advance and retreat intervals anytime prior Llanquihue stage III. This inference is based on the observation that the rock debris of the basement is covered by a sediment sequence sub-divided into 4 to 5 seismic units. Their characteristic acoustic facies might imply that these units comprise a succession covering till to modern lacustrine deposits. Most of the debris ridges that make the present-day southern basal lake floor topography in both lakes are thought to have been removed during the last glacial advance, implying that the original volume of rock debris was significantly greater than has been detected in the seismic data. The restriction of the failed rock mass to the south to south-western side of both basins could implicate failure took place

whilst a remanent glacier tongue blocked the deep original basin during the glacier oscillatory retreat and re-advance stages. Thus the detached debris and rock masses traced the glacier gradient line and therefore did not drift farther into the central basin. These topographic constraints would explain why, at some localities, spreading was induced (e.g. Fig. III-12,19) rather than a transformation into large rock avalanches. This would also provide an evidence of the farthest retreat level of the glacier body during this event. A different explanation could be that the rock masses were too large and there was no way for the glacier's central section to expand, as proposed for the giant Flims rockslide (Switzerland) by Pollet et al. (2005). A rough volume estimation of the present-day basement blocks of each lake basin, taking their present-day basin plain as a reference basal zero-value, reveals a minimum volume of debuttressed openwork blocks, rocks and debris masses of $\sim 2.1 \times 10^9$ m³ for Lago Calafquén and $\sim 1.8 \times 10^9$ m³ for Lago Villarrica. Mass movements of such a volume often result from slopes deformed by deep creep, and maintain an imminent danger of a rapid transition to sliding, similar to the enormous landslide of Koefels (Austria) (Brueckl and Parotidis, 2001). A general comparison of rock-slope failures and sliding events of different origin is given in Table III-2. The large volume of the sidewall failures of Lago Calafquén and Lago Villarrica implies sudden and major tension release by continuous creep that was controlled by pore pressure or continuous motion. Brueckl and Parotidis (2005) describe this mechanism responsible for sagging of the whole slope (Sackung failure) of the Koefels landslide. Side failure for each lake is also favoured by the alternating highly porous, strongly interstadial weathered pyroclastic material which might have formed the sliding plane and the glacial sediments. Fracture toughness could also be considered as a failure mechanism for these large rock-slope failures. Strong precipitation events and/or snow melting during glacial retreat can be considered as an additional trigger. Isostatic uplift is likewise reported as a trigger for the sturzstrom of Goldau (Switzerland) in 1806 (Thuro et al., 2005).

location	volume	event	age	references
Flims (Switzerland)	**12×10^9 m³**	rock-fall	early Holocene	A. Heim (1932)
Köfels (Austria)	**2.5×10^9 m³**	rock-fall	8700 BP	Stingl et al. (1993)
Miralago	158×10^6m³	rock-fall	Late Glacial	H.Völk (1987)
Val Pola	40×10^6m³	rock-fall	1987	Patzelt and Poscher (1993)
Goldau (Switzerland)	40×10^6m³	rock-fall and slide	1806	Thuro et al. (2005)
Randa/Zermatt (Switzerland)	30×10^6m³	rock-fall	1991	Schindler et al. (1993)
Lago Calafquén (Chile)	**2.1×10^9 m³**	rock-slope failures	pre-Llanquihue stage III??	Volland et al. (in press)
Lago Villarrica (Chile)	**1.8×10^9 m³**	rock-slope failures	pre-Llanquihue stage III??	Part 1, Chapter 5, this thesis

Tab. III-2: A general comparison of rock-slope failures and sliding events at different locations and time periods.

However, glacial erosion is not necessarily considered a direct trigger of sidewall failure. As reported by Abele (1997) and Moya et al. (1997), detachment of sidewalls by debuttressing does not follow immediately after deglaciation, but often with some delay (e.g. after 10,000 yrs for the rock avalanche of Randa, Switzerland, cf. Noverraz and Bonnard, 1991; Ballantyne, 2002). On the southern sidewalls of Lago Calafquén and Lago Villarrica the reduction of rock-mass strength caused by internal joint networks after deglaciation, possibly interacting with high cleft-water pressures, weathering and exceptional precipitation rates during drier climatic periods around the Last Glacial Maximum, might

have led to rock-slope failures. Furthermore, the reduction of soil shear strength by the reduced cohesion and internal friction of the porous pyroclastic material favours the shallow landslide processes of the southern hinterland of Lago Villarrica. The failure trigger might also have been the seismic activity of earthquakes, strong tremors from volcanic explosions or strong aseismic trembles caused by isostatic vertical motion, or a combination of the above.

5.3 Importance of volcanism

Evidence of strong volcanic impact comes from the area surrounding the lakes. In proximity of the lake basins outcrops in the watersheds show distinct horizons of ignimbrites and pyroclasitc flow deposits of late-glacial to Holocene age (Pino et al., 2004). The major Ignimbrite Licán was deposited around 14,000 BP (Clavero and Moreno, 1994) and covered more than two-thirds of Calafquén's basin and the entire basin of Lago Villarrica. Evidence comes from the island Isla de Allaquillén in Lago Villarrica, where the ignimbrite covers the eastern shore of the island (Fig. III-24). In front of the island, it had formed a concrete-like impenetrable blanket on the lake floor, which was noticed during one of the coring campaigns. The strata of pyroclastic flows, surges and ignimbrites are considered to form a noticeable part of the high-amplitude reflectors in the acoustic sequences. Further volcanic impact is deduced from inferior acoustic penetration and the chaotic facies on the basin plain. Debris flows sourced by lahars also form a portion of the turbidite system in the basin plain. Major lahar and debris flow impacts in Lago Calafquén follow the deltas of Chaillupén (cf. Fig. III-4) and Pucura (cf. Fig. III-3a) that prograde into the central sub-basin, as they do at Coñaripe (cf. Fig. III-3a) using the eastern basin plain as discharge route. At Lago Villarrica, the small southern rivulets like Río Correntoso or Carmelito (cf. Fig. III-3b,5, II-12,13) form the major trajectories. Debris flows also use the main tributary Río Trancura at the eastern lake side (Fig. III-3b). Lahar velocity reaches a maximum during subaerial flow and decreases as it enters a lake. However, velocity of these high density debris flows is sufficient to maintain an erosional, supercritical flow sensu Sturm and Matter (1978). Seasonal torrential flows and flood events are assumed to contribute to the turbidite system of the lake basin, but are supposed to generate different, probably less catastrophic events. Distinguishing lahars from flood events by their acoustic properties in the seismic sections is unfortunately not possible due to the minor acoustic penetration of the lake floor.

Fig. III-24: The major ignimbrite Lican covers the entire basin of Lago Villarrica. Its deposits crop out on the little island Allaquillén and overlay glacial till and the granitic basement.

5.4 The influence of bathymetry on sedimentary processes

The irregular bathymetry of Lago Calafquén plays a vital role in general sedimentation processes and the formation of turbidites. Catchment-triggered alluvial turbidites are defined as those derived from flood events from the surrounding catchment or by subaerial debris flows originated from sources of any kind, such as lahars, etc. They mainly follow the deep basin plains as underflows. Evidence for the basin plain as the main depositional area for turbidites comes from a short core of the eastern sub-basin (see photographic documentation, Fig. A-5, Appendix), as well as from surficial bottom sediments of the entire lake (cf. Part 2, Chapters 4,5). Following the subaqueous morphology that divides the central basin into two sub-basins, subaerial debris flows spread as underflows into the deep basin plain, where reduction of the current velocity occurs gradually until the western end of the basin. Thus, bottom currents penetrate far into the basin plain, and by doing so, transport coarse and finer fractions to the pelagic basin that in turn appears as a zone of minor penetration in the seismic sections (cf. Fig. III-9). In Villarrica, wide basin morphology allows turbidites to spread over the entire central basin plain. As turbidites enter the lake from two sides – the eastern and the southern – there is an overlapping in turbidite spreading direction. Distribution of the pronounced catchment-triggered alluvial turbidites in Lago Villarrica is blocked either by the northern shore or by the plateau-like morphologic rise in the south-western basin. Therefore, these deep basin plain turbidites are rarely thought to form part of the sediment sequence along the morphologically elevated southern to south-western side of both lakes. Turbidites deposited in these prominent areas are considered to be of genetically different types, developing from slope movements, slide processes and mass-flow deposits along the southern side and are considered to be predominantly triggered by seismic shocks. Alternatively, they may form part of the turbidite system in the deep basin plain.

6. Conclusion

The central basin of Lago Calafquén is divided into two sub-basins: a northern deep basin plain and an elevated area along the southern side. Lago Villarrica reveals a wide and open U-shaped central basin plain that is delineated by a morphologic rise in the south-western basin. The original lake floor of the southern to south-western part of both lakes is primary filled by basement with irregular and hummocky surfaces and chaotic seismic facies (ca. 23 km² in Lago Calafquén; 13 km² in Lago Villarrica). It represents massive rock-slope failures, rockslides and earth spreads events caused by debuttressing from the detachment area after glacial retreat, thus forming the initial present-day lake floor topography. The basement is overlain by sediments with maximum thicknesses of up to 50 m or even more. Seismic and tectonic activity initially triggers soft sediment deformation in the lake basins in form of mass movements. For Lago Calafquén they reveal various formations:

- A slump occurred at the southern side in Unit 2 and has deformed underlying sediments. It is likely to have caused turbidites that are identified in thick chaotic-to-transparent layers in Unit 2;
- A succession of large mass-flow deposits is recognized at the south-western side implying persistent slope instabilities. Smaller bulges on the opposite side in the corresponding seismic stratigraphic horizons implicate coeval deposition. Towards the distal northern sub-basin, mass-flow deposits grade into turbidites of transparent seismic facies that settle into the basin plain;

- Large liquefaction features along the southern side show large scale injections and vertical migrating fluid escape pipes.
- Repeated coeval mass-flow deposits, mass-flow evolved turbidites and liquefaction behaviour indicate that earthquakes might be the main trigger for sediment deformation. Furthermore, isostatic rebound after glacial retreat might also plays a vital role for enhanced earthquake activity in addition to plate tectonic processes at the active continental margin.

In Lago Villarrica seismic and tectonic activity trigger large coeval mass-flow deposits ($\sim 3.2 \times 10^6$ m³ minimum) and turbidites that show liquefaction behaviour. These mass-flow deposits are identified only along the south-western rise in the lake basin. South of Lago Villarrica, the landscape is prone to shallow landslides due to the site geology and the moderate slope formation.

Flood-related turbidites and debris flows affect the central basin plains of both lakes, but their distribution in the lake basins seem to be restricted by lake floor morphology. Volcanic impacts on the lakes is deduced from high-velocity reflectors in the seismic sections. Wide-spread turbidites sourced from subaerial debris flows, such as lahars and other loosely packed volcanic material contribute to the sediment succession in the basin plains that cause minor acoustic penetration.

The basin plain is the main depositional area for seasonal or extraordinary flood-related turbidites supplied from the surrounding catchment. Turbidites in the basin plain are supposed to be genetically different in origin from those appearing along the southern to south-western side of each lake. The latter are most probably seismically induced and contribute to sedimentation throughout the distal lake basin. Catchment triggered alluvial turbidites seem to be restricted to the deep morphologically controlled basin plain and therefore contribute little sediment to the elevated sub-basins.

The observations presented above suggest rapid and partially catastrophic mass movements in the vicinity of Lago Calafquén and Lago Villarrica. As the sediment infill is severely disrupted by serial geodynamic impacts, palaeoenvironmental and palaeoclimatic signals are thought to be disturbed strongly in certain parts of the lake basin. Thus, for reconstruction of the site histories coring sites have to be selected carefully. This should require a thorough seismic investigation of the lake basin on a dense grid.

PART 2

IV. Sedimentation processes of Lago Calafquén and Lago Villarrica

1. Introduction

The common goal of diverse lake studies is to determine how inorganic environment and lake ecosystems interact, how they relate one to another through cause and effect and through feedback mechanisms. Sediments are an important part of a lake system, controlling especially the nutrient budget, and hence the trophic status, ecology and lake evolution. Furthermore, lakes function as sediment traps that preserve information on changes in the surrounding environment. Thus, lake sediments operate as an excellent sensor of environmental and climate change.

Before applying time-related analyses to unravel a lake's history in terms of palaeoenvironmental development it is important to understand the modern processes that control the present-day sedimentation processes. To detect areal changes in a lake basin that may reflect variations in the hydrological process operating in a lake and the proximity, surface bottom sediment analyses are a useful tool. They provide information on sediment dynamics, sediment source and catchment related processes, which in turn control productivity and hence describe the lake's condition, amongst others. Several studies on lake bottom sediments focused on sediment provenance, texture analyses and sedimentation rates (e.g. Hakånson, 1977; Nelson, 1983; Nelson and Lister, 1995; etc.) to deduce general sedimentation processes or man's driven changes in the catchment by hydraulic engineering and water management (e.g. Müller and Sigl, 1977).

An actualistic conceptual dynamic model based on modern surface sediment analyses then could be applied on vertical time-related palaeolimnological sediment analyses that reveal information on past environmental and climatic changes. Palaeolimnological studies focus on stratigraphic changes in the sediment record with the primary goal to assess environmental and climatically driven changes and their impact on the lake ecosystem, information that are recorded in the lake sediment. Lacustrine palaeoclimatologic and –ecological studies based on multi-proxy analyses have become common (e.g. Gasse et al., 1987; Smol et al., 1991; Lamb et al., 1995; Birks et al., 2000; Oberhänsli and Mackay, 2005; etc.).

However, the Chilean Lake District is still lacking such lake sedimentological studies. The first study focussing on sub-recent temporal sedimentary evolution and climatic significance was conducted on Lago Puyehue (Bertrand et al., 2005), located south of the study area. Besides, no further lake sedimentological studies were carried out for this region until present-day.

This Chapter presents the first spatial and time related lake sediment investigation for the northern Chilean Lake District, performed on Lago Calafquén and Lago Villarrica. One aim of this study is to reconstruct recent general sedimentation processes in terms of sediment dynamic, spatial sediment distribution within the lake basin by surface sediment analyses, and to assess volcanic impact on lacustrine sedimentation processes. Furthermore, a multi-proxy study on sediment cores of both lakes will provide general information of time-related sedimentation processes that are controlled by changes in catchment and moisture balance. At last, a possible transfer of sedimentation processes connected to palaeoenvironmental and climate changes will be discussed carefully.

2. Hydrographic characteristics

Lago Calafquén and Lago Villarrica are located in the northern Chilean Lake District on the pre-Andean mountains in a volcanic active area (see previous chapters). According to the typical vegetation of the Lake District, these lakes are also referred as to the Araucanian lakes by Thomasson (1963). During the early 80's principal limnological studies lakes by Campos et al. (1980, 1983) and Campos (1984) on both lakes provided morphometric, physical, and chemical information on the

water bodies. Based on the classification of thermal lake types with latitude by Wetzel (1975) and because of their morphometric, physical, chemical and planktonical factors both lakes are considered as warm monomictic, oligotrophic lakes (Campos et al., 1980, 1983). But diatom investigation by Rumrich et al. (2000) report that planktonical samples from areas with active volcanic impacts, especially in Chile, rather reveal a common eutrophic trend.

In general, morphometry and geological substrates of lakes are of major importance in understanding sedimentological and geochemical processes, the sediment-water interactions and the resultant specific lake productivity. Geographical and geological information about Lago Calafquén and Lago Villarrica were provided in detail in Chapter II. General information on planktonical factors will be discussed in Part V of this thesis.

Parameter	Lake Calafquén	Lake Villarrica
Latitude	39°32' S	39°18' S
Longitude	72°09' W	72°05' W
Altitude	203 m	230 m
Maximum length (l_m)	25.10 km	23.05 km
Maximum breadth(b_m)	7.80 km	11.20 km
Shoreline (L)	76.30 km	71.20 km
Surface area (A_0)	120.60 km²	175.87 km²
Shoreline development (D_L)	1.9	1.5
Maximum depth (Z_m)	212 m	165 m
Volume (V)	13.91 km³	20.99 km³
Catchment area (A_d)	733 km²	2920 km²
Ratio A_d/A_0	6.08	16.60

Fig. IV-1: Morphometric parameters of Lago Calafquén and Lago Villarrica (after Campos, 1984).

Lake morphometry and geological substrate are important in determining sedimentological and geochemical processes, sediment-water interface interactions, and the resultant lake productivity. Geographical setting and geological substrate descriptions from Lago Calafquén and Lago Villarrica are provided in detail in Chapter II. General information on morphometry characteristics of each lake is given in Fig. IV-1. All subsequent described morphometric, physical and chemical lake characteristics refer to the studies by Camps et al. (1980, Lago Calafquén), Campos et al. (1983, Lago Villarrica) and Campos (1984, both lakes) as there are no other works about these lakes in the literature. The catchment areas of both lakes are shown in Fig. IV-2. Below, the sedimentological properties of both lakes are described, such that interpretations regarding recent sediment dynamic and lake productivity can be made.

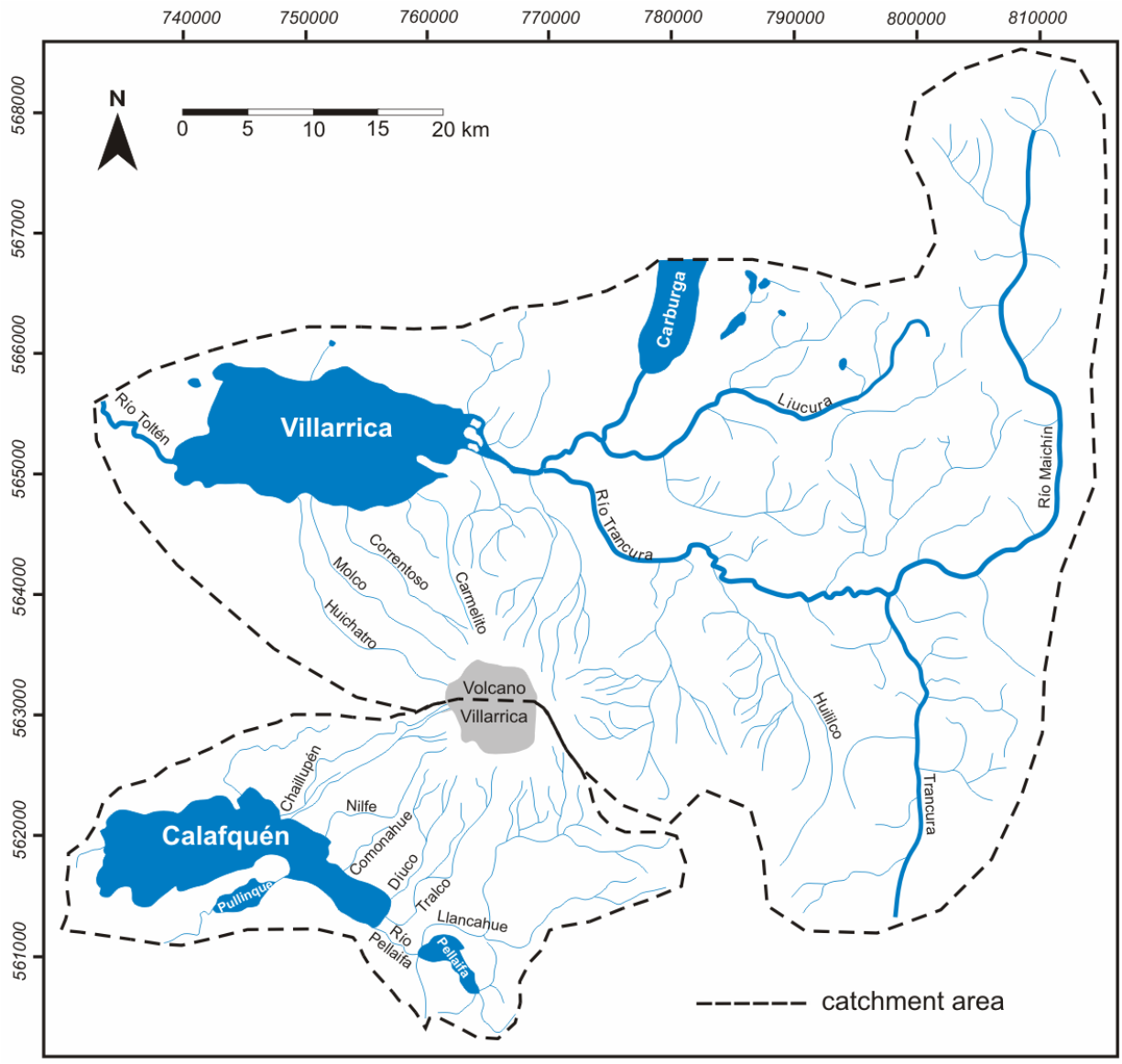

Fig. IV-2: Catchment areas of Lago Calafquén and Lago Villarrica. Modified after drainage maps of Sistema Nacional de Información ambiental, SiNIA. Source: http://www.sinia.cl/mapas/ix_region.html and http://www.sinia.cl/mapas/x_region.html.

2.1 Lago Calafquén

2.1.1 Physical properties

Lago Calafquén corresponds to lake type 28 B "fjord lake" (Hutchinson, 1957). The catchment area extends over 733 km² and comprises several small effluents that drain the area of Volcano Villarrica (Fig. IV-2). Most of them are only seasonally water-bearing, the remaining flow throughout the year. All of them can be considered as wild creeks and rivulets. The principal tributary to Lago Calafquén is Río Pellaifa, which forms the outlet of Lago Pellaifa (Fig. IV-2). In the early 1980's, the mean flow velocity of Río Pellaifa was approximately 71 m³/s, though at its outlet into Lago Pullinque (Fig. IV-2), it was approximately 68.4 m³/s (Campos et al., 1980) Considering the total volume of Lago Calafquén, the theoretical residence time is approximately six years.

Lago Calafquén was observed to have one circulation period (overturn) per year. During the summer it has a stable stratification, which broke down with winter homoiothermy. Winter

temperatures had a minimum of ~ 9.5º C, whereas mean annual temperatures were approximately 11.2° C. Secchi depth varied between 8 to 14.5 m (Campos et al., 1980).

2.1.2 Chemical parameters

From oxygen values provided by Campos et al. (1980) and from sediment cores taken from the deep basin plain it can be deduced that Lago Calafquén is not meromictic. The water has a mean pH ~ 7.1 with a tendency to acid in the deeper water body. It is very poor in electrolytes and has a total hardness is < 2°dH. Despite the little ionic concentration Calafquén's water belongs to calcium bicarbonate type. Anions correspond to the sequence bicarbonate > chloride > sulphate, cation to the sequences Ca > Na > Mg > K. Mean concentrations of Silica are high with 9.2 mg/l.

2.2 Lago Villarrica

2.2.1 Physical properties

According to Hutchinson (1957) Lago Villarrica belongs to a piedmont lake type 28 C with a U-shaped basin. Contrasting the relatively short and small tributaries of Lago Calafquén, Lago Villarrica receives its water primarily from its major tributary Río Trancura which originates in the deep Andean mountains (Fig. IV-2). It drains cross weathered volcanic soils, forests and agricultural zones. The flow velocity is seasonally dependent and varies from 490 m^3/s (spring) to 662 m^3/s (winter). Small creeks draining the northern flanks of Volcano Villarrica form additional small tributaries. The catchment expands over an area of 2920 km^2. During a seasonal cycle Lago Villarrica builds up summer stagnation and shows winter circulation with homoiothermy and a mean winter temperature of 9.7°C. Secchi depth varies between 5.5 to 11 m. Theoretically, the water body renews in a lapse of four years according to its total volume.

2.2.2 Chemical parameters

Sediment cores taken from the deep basin plain in Lago Villarrica do not show any indication of meromixis. Campos et al. (1983) observed an oxygen deficit throughout the entire water column during autumn and winter. As their sampling period only comprised one year, these measurements may reflect extraordinary conditions. Therefore, they should not be considered as representative in the subsequent chapters. The water had a mean pH ~ 7.3 and was poor in electrolytes, with a total hardness < 1°dH. The water of Lago Villarrica is considered to be of the "sodium bicarbonate" or "magnesium bicarbonate" type. Anions correspond to the sequence bicarbonate > chloride > sulphate throughout the year. Cation sequences varied with season, though the sequence Na > Mg > Ca > K was found nearly throughout the year. Dominance of sodium is variable from spring to autumn. Mean concentrations of silica, approximately 11.8 mg/l, are higher than in Lago Calafquen (Campos, 1984).

3. Methods

3.1 Sampling field methods

Sediment sampling of both lakes was conducted in March and April, 2001. In Lago Calafquén, 44 grab samples of uppermost sediment and two short gravity cores were collected (Fig. IV-3a); in Lago Villarrica, 18 grab samples and four short gravity cores were taken (Fig. IV-3b). The number of grab samples taken in Lago Calafquén is sufficient to be considered representative, described by the sample formula (1) that was introduced by Håkanson (1981).

$$n = 2.5 + 0.5 \times \sqrt{a \times F} \quad (1)$$

n = number of samples
a = surface area (km²) of the lake
F = development (*indirect measure of bottom roughness after Håkanson and Jansson, 1983*).

The results of the grab sample analysis can therefore be considered as reliable. In contrast, the number of grab samples from Lago Villarrica is too small by a factor of 2.7. Nevertheless, the results should be considered representative, as bottom roughness is consistent for more than 2/3 of the sampled area, which can be deduced a) from the seismic profiles, and b) from the sediment texture patterns described in Chapters 4.2.3 and 5.2.

Surficial bottom sediments were taken with a Van-Veen-type grab sampler, obtaining a mixed sample from the uppermost 20 cm of surface sediment. Short cores were obtained using a gravity corer equipped with 2 m long transparent PVC tubes after Meischner and Rumohr (1974). Maximum length of sediment cores retrieved using this corer was 1.62 m in Lago Calafquén and 1.14 m in Lago Villarrica, where coring problems occurred due to the impenetrable subaquatic ignimbrite blanket and cemented till cover around the island Isla de Allaquillén (cf. Fig. III-3b). Sampling on both lakes was conducted from a research vessel of the Geoscience Department of the Universidad Austral de Chile (UACH) in Valdivia. Water depth during sampling was monitored using a GARMIN humminbird fishfinder at 200 kHz; navigation and positioning was achieved using a KODEN GPS device.

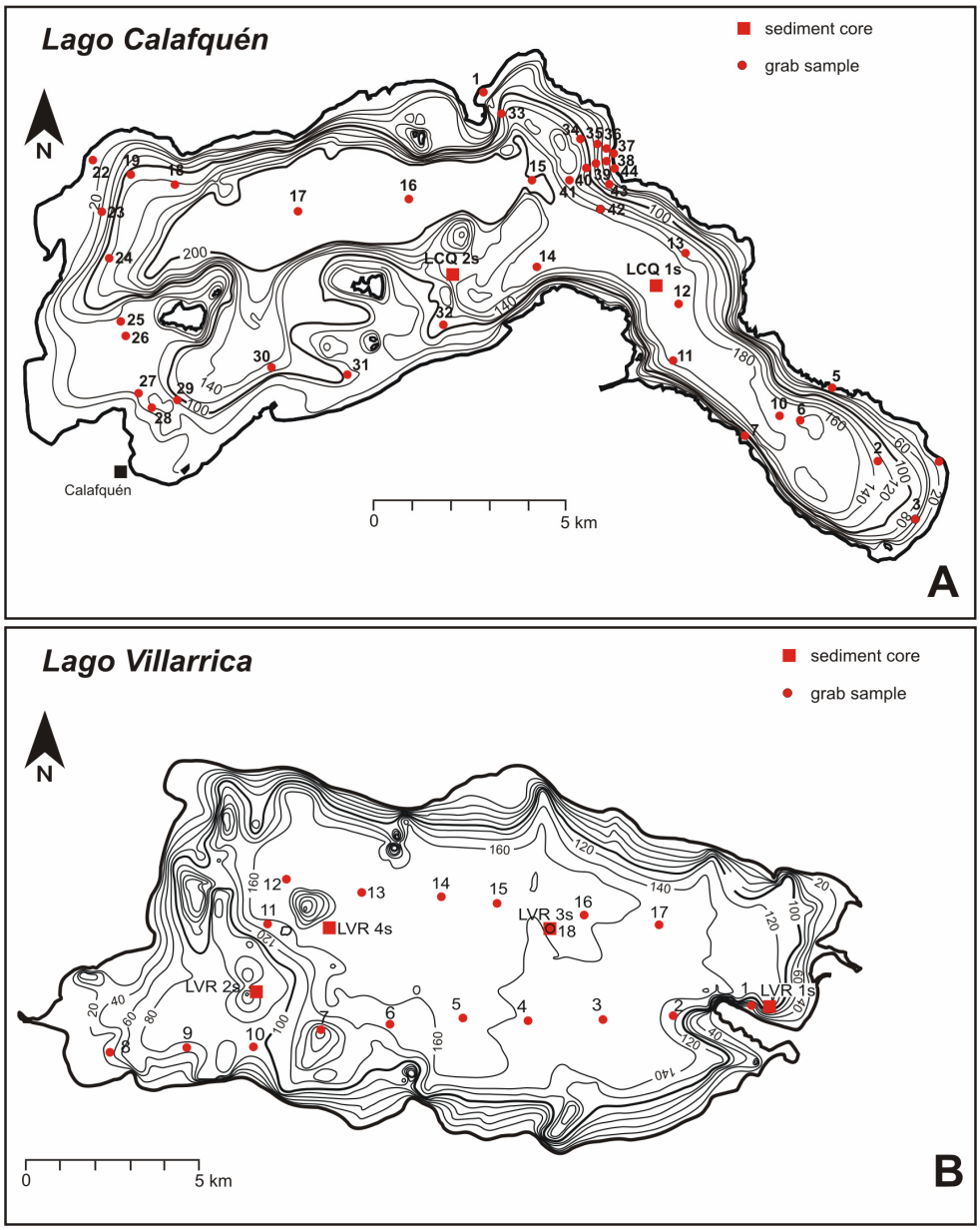

Fig. IV-3: Sample sites of A) Lago Calafquén and B) Lago Villarrica.

3.2 Sample preparation

The cores were split shortly after field sampling and sub-sampled at the UACH (Valdivia) laboratory from May to July 2001. Sampling interval was adjusted to changes in lithology and different layers were considered on an individual basis. This prevented loss of information contained in each layer and avoided mixing of information that likely derived from different processes. Immediately after sub-sampling, core samples were dried at 40°C for > 48 h to a constant weight, such that further quantitative analyses could be undertaken after transport to Europe. The archive halves of the cores were initially stored at the UACH, but in October 2003 were subsequently transferred to Europe. Further sediment analyses on the archive halves were conducted from June to September 2004 at the EAWAG laboratory in Dübendorf, Switzerland.

3.2.1 Physical sediment properties

Investigation of the physical sediment properties comprise the estimation of water content (wt.%), magnetic susceptibility (MS) and grain size analysis. These methods provide microscopic lithological information.

a) Water content

Water content was estimated on the base of equation (2), which involves the weight of the wet and dried sediment of the samples.

$$W = \frac{M_{sw} - M_s}{M_{sw}} \times 100 \qquad (2)$$

W = water content (%)
M_{sw} = weight wet sediment (g)
M_s = weight dry sediment (g)

b) Magnetic susceptibility

The amount of magnetizable (iron-bearing) material in sediment is characterized by magnetic susceptibility, measured in S.I. units. Magnetic susceptibility provides information on the terrigeneous (allochthonous) yield of the catchment area. The records reflect changes in the weathering and transport rate resulting from various environmental triggers. On the cores from Lago Calafquén and Villarrica, magnetic susceptibility was determined using a Bartington MS2 Magnetic Susceptibility System and a high-resolution MS2E/1 surface-scanning sensor at the EAWAG, Switzerland. Measurements were taken at 1 cm intervals from the core top to bottom.

c) Grain size analysis

Grain size was measured by laser diffraction with a Malvern Mastersizer X Laser Particle Analyzer at the ETH Zürich, Switzerland, providing an analytical size range from 0.02 to 2,000 µm. Before analysing, the biogenic silica fraction on all core and grab samples was removed (see Chapter 3.2.4.c) in order to avoid erroneous size fractions related to large diatom valves. After dissolution, samples were treated with 15% H_2O_2 to remove organic matter and after full oxidization, were rinsed with distilled water. To determine the grain size distribution, a small amount of each sample was added to the mixing chamber within the laser analyzer and sonicated. The suspension goes to a measuring cell, where a laser beam passes through the sample. Due to diffraction, different sized particles deflect light at different angles, striking detectors that record the signal. A computerized list of signal reflections is produced, representing the different fractions of the particle sizes measured.

3.2.2 Mineralogy

Although bulk chemistry of lake sediments is often used to provide important insights into lake chemistry and dynamics (Jones and Bowser, 1978), here it will be rather applied just to characterize the mineral components making up the sediment. This provides basic information on the sedimentological processes in space and time of both lake basins.

a) X-ray diffractometry (XRD)

Bulk chemistry was determined at the TU München, Germany, by X-ray diffraction using a Philips PW 1800 diffractometer with 20 – 40 kV at angles between 2 and 70° 2θ. For analysis, a quantity of dry sediment material was homogenized by hand to 40 µm and powder tablets were produced. For clay mineral analyses, the clay fraction, here taken to be < 2 µm equivalent spherical diameter, was separated by elutriation in Atterberg tubes, a method based on Stokes' law of particle settling. Prior to separation, organic matter from the bulk samples was removed with 15 – 30% H_2O_2. During this oxidation process, the samples were repeatedly disaggregated by ultrasound. After complete oxidation, the samples were washed with distilled water until the supernatant was only slightly turbid. To avoid flocculation during elutriation, 0.01 M $NH_4(OH)$ was used as dispersing agent. If samples resisted dispersion, the dispersing medium was changed to Na-pyrophosphate or distilled water. After a sufficient amount of clay fraction was obtained, samples were washed with distilled water. The suspension was concentrated using a Labofuge centrifuge at 6,000 rpm. From the residuum, oriented-pipette glass slides and smear slide mounts were prepared. Non-treated, Mg-acetate and K-acetate treated samples of air-dried slide mounts were X-rayed to determine exact reflection growth. To determine smectite and/or mixed-layered clays, the slides were subjected to ethylene-glycol vapour at 80°C for at least 24 h and subsequently X-rayed. If necessary, the samples underwent a final heating to 550°C for 2 h and were X-rayed to distinguish further phases. Often the material on the smear and pipette glass slides shrunk on drying regardless of treatment, with the result that the samples curled or peeled off. Application with Millipore filters and Diapor porous ceramic plates did not overcome these problems, making exact clay mineral analyses difficult.

XRD identifications of feldspar can be uncertain due to the variation in the d-values and the high crystal electron density. Thus the XRD identification of one sample was verified by Fourier Transform Infra-Red (FTIR) spectrometric measurement. The XRD identification turned out to be reliable, and therefore no additional FTIR analyses were applied.

b) Scanning electron microscope (SEM)

Characteristic special layers of the sediment cores, which suggested decisive information of grain formation, sediment aggregates, and layer boundaries were investigated by SEM analysis using a JEOL JSM-35C at the TU München, Germany. When necessary, the chemical composition was determined using an energy-dispersive X-ray spectroscopic (EDS) Röntec XFlash detector.

3.2.3 Geochemical methods

Lake sediments comprise a large variety of 'inorganic' (minerogenic components) and 'organic' matter (here considered as carbon, nitrogen, sulfur) that is either of allochthonous or autochthonous origin. 'Inorganic' geochemical investigation of the lake sediments was not applied in terms of 'inorganic geochemistry' in general, but rather in the context of 'inorganic geochemical palaeolimnology' introduced by Boyle (2001), in order to describe and quantify the environment. However, a distinction of the analysis in one or the other discipline seems not favourable for this work, as both feed into the other and support to characterize an evolution of the environment.

The relative proportion of organic matter derived from lake sediments is a function of catchment characteristics relative to lake productivity (Håkanson and Jansson, 1983). Total carbon, divided into the fractions of organic (residual remnants of plant and animal tissues) and inorganic carbon (Ca–carbonate), nitrogen and biogenic silica were analysed from sediment samples of both lakes in order to determine lake productivity and catchment influence.

a) Atom absorption spectrometry (AAS)

Elemental analysis with AAS investigation is based on absorption by free atoms of near-monochromatic light of appropriate wavelength. Main elements were determined at the University Jena (Dr. G. Daut), by a flame-AAS with graphite tube and hydride system. Total elemental concentrations were determined on 90 samples, dissolved in a mixture of nitric and hydrochloric acids.

b) Inductive coupled plasma mass spectrometry (ICP-MS)

Because of its superior sensitivity, ICP-MS analysis was used for trace element determination. This method requires samples that are brought into solution by acid digestion. The solution is sprayed into flowing argon gas, passing into a torch which is inductively heated to several 1,000° C. This causes atomization and ionization of the gas and everything in it, thus forming a plasma which provides both excited and ionized atoms. Trace element analysis was conducted at the University Jena (Dr. D. Merten), using the residual of digested samples from the AAS analysis.

c) Total carbon (TC), nitrogen (TN) and sulfur (TS) content

Organic carbon, inorganic carbon, and nitrogen were analysed simultaneously on the core samples from both lakes at the sedimentological laboratory of the EAWAG, Switzerland, using a EuroVector Elemental Analyzer. Determination is based on "dynamic flash combustion" where the sample, in a tin capsule, is melted at 1020° C in a combustion reactor. The oxidation product, CO_2, is separated by helium-based gas chromatography and detected by a Thermal Conductivity Detector. Peaks are recorded on a chromatogram and carbon is determined from area of the CO_2 peak after correction by a regression curve.

Total carbon and sulphur content of the grab samples were analysed at the TU München with a LECO CS 125 Carbon and Sulphur Analyser. A known weight of sediment sample is placed in a ceramic crucible together with iron and tungsten catalyst. The LECO system uses inductively-coupled electrically-induced combustion at >1,000° C, fed by a stream of pure oxygen gas, to completely oxidize the sample. Combustion produces carbon and sulphur dioxide, which is analyzed by infra-red absorption. The results are corrected for calibration factors and sample weight.

d) Total Inorganic Carbon (TIC)

Total inorganic carbon (TIC) was analysed using a Coulometrics Inc. CO_2 Coulometer. Sediment samples were treated with a 2N HCl solution at 70°C, producing CO_2, which is captured in the reaction chamber of the coulometer. The gas reacts with a monoethanolamine solution, generating a titratable acid. A titration current is activated to stoichiometrically generate base proportional to the amount of CO_2 content.

e) Biogenic silica (BSi)

At the laboratory of the EAWAG/Switzerland, biogenic silica was determined using inductively-coupled plasma optical emission spectrometry (ICP-OES). An alkaline treatment of the sediment was applied after the 'single-step wet-alkaline leach method' described in detail by Ohlendorf and Sturm (in press). Because of a probable additional leaching of abundant clay minerals and volcanic ashes of the samples, the extraction time had to be limited such that the biogenic silica content was dissolved but that further reaction of other silicate minerals was prevented. To control the rate of release or corrosion of clay and other silicate-bearing minerals, Na and Al were monitored

during ICP measurements. The silica value was corrected by a stoichiometric calculation of Si, Na and Al.

3.2.4 Dating and accumulation rates

For chronological control of the sediment geochemical results, and for determining accumulation rates, several radionuclide dating methods were applied.

a) ^{137}Cs and ^{210}Pb dating

A maximum in atmospheric nuclear weapons testing in 1963 as well as the nuclear accident of Chernobyl, Ukraine, in 1986, released large amounts of ^{137}Cs into the atmosphere. This nuclide was incorporated into lake sediments globally, though more abundant in the northern hemisphere (e.g. Hutchinson, 1994; Yan et al., 2002), thus allowing accurate dating of material up to 40 years old. But also a spatial variable depth incorporation of ^{137}Cs inventories is reported from the southern hemisphere (Andrello and Appoloni, 2004).

The radionuclide ^{210}Pb is naturally produced by atmospheric decay of ^{222}Rn, which falls out of the atmosphere and becomes incorporated into sediments. Its half-life of about 30 years allows dating of sediments up to 100 years (Appleby, 1997). Together, these radionuclides provide excellent chronological markers which can be found in recent sediments, though the ^{137}Cs marker is limited to the 1963 peak in Chilean sediments. Both radionuclides were measured at the EAWAG/Switzerland using gamma ray detectors.

b) AMS-radiocarbon dating

The interaction of cosmic ray particles with nitrogen, oxygen and carbon produces ^{14}C in the Earth's atmosphere. Atmospheric ^{14}C is oxidized to CO_2 and is assimilated into the carbon cycle via photosynthesis. Through herbivory, radiocarbon is integrated into materials such as chitin, bones, teeth, etc. The amount of ^{14}C incorporated does not normally change after senescence, thus the decay rate determines the abundance of radioactive carbon in organic remains. As the half-life of ^{14}C is 5,568 years (Stuiver and Polach, 1977), the effective dating range of organic material is 100 to 70,000 years.

The sediment cores were dated by Accelerator Mass Spectrometry (AMS), where a few atoms of an isotope are identified against an abundant stable isotope background. A total of eleven sediment samples were analysed. Two samples were dated at the Leibniz-Laboratory for Radiometric Dating and Isotope Research, Germany. The remaining nine samples were dated at the Van de Graaff Laboratory of Utrecht University, Netherlands. For a detailed technical and method description see http:www1.phys.uu.nl/ams/method.htm.

Ages were calibrated with CALIB Rev. 5.0.1 on the base of the calibration curve for the Southern Hemisphere (SHCal04) (Stuiver and Reimer, 1993).

c) Mass accumulation rates (MAR)

Mass accumulation rates were calculated on the base of sedimentation rates, porosity and average density of the mineral fraction. Porosity was determined after estimating the water content. Average density was not measured, but estimated on the base of the general proportionate contribution of each mineral phases to the bulk sediment. Mass accumulation rates were counted after formular (3)

$$MAR = (SR \times \rho samp \times (1 - \eta)) \times 1000 \quad (3)$$

MA	=	Mass accumulation rate
SR	=	Sedimentation rate
$\rho samp$	=	average densitiy of bulk sediment
η	=	porosity (%)

Mass accumulation rates of biogenic fractions, such as biogenic silica and TOC were calculated after forumular (4)

$$MARbio = \frac{MAR \times comp}{100} \tag{4}$$

MARbio	=	mass accumulation rate of biogenic fraction
Comp	=	biogenic component, such as BSi or TOC

4. Surface sediments

Mapping surface sediment distribution leads to a better understanding of sediment dynamics in lake basins (Håkanson, 1981). The aim of these investigations is to provide local syntheses of the lake floor environments, determine the role of lake-floor morphology in recent sedimentation processes, and to estimate spatial sediment-dispersal pathways to and within Lago Calafquén and Lago Villarrica. Reconstructing modern water current dynamics and sediment supply on a spatial scale assists in the interpretation of past changes in hydrologic regime and sediment source.

4.1 Lago Calafquén

4.1.1 Sediment composition

Bulk mineralogy using XRD diffractometry revealed that Lago Calafquén sediments comprised approximately 60% anorthite and 30% diopside. An additional approximately 10% of X-ray amorphous components was detected, consisting of volcanic glass, diatom valves and probably non-crystalline material from the allophane-imogolite category. The former two were identified by SEM-investigation. Quantification was done by FTIR-spectrometry. In the bulk samples and clay fractions, few clay minerals or other phyllosilicates were observed. The clay fractions consist of extremely small feldspars, diopside and numerous, small diatom valves (~ 2 µm; see Appendix, Fig. C-1). Only grab samples #2 and #3, taken from the bay near Coñaripe, are composed of < 5% smectite.

Diffraction patterns show a shift of the background between 20 – 34° 2θ. This varies between different sample sites in the lake basin (Fig. IV-4) and largely follows the total carbon distribution of the grab samples (see Chapter 4.1.4). TOC distribution in Lago Calafquén is linked to primary productivity. But the spatial variation in amorphous components of the sediment is referred to dilution effects due to allochthonous influence rather than changes in productivity. That is, sample sites with higher proportions of amorphous components apparently reflect sites with less allochthonous clastic input, whereas sites with lower proportions of amorphous components suggest areas influenced by higher clastic influx. An increase of volcanic glass input as an explanation for this shift is excluded, as it is not correlated with changes in the TOC content.

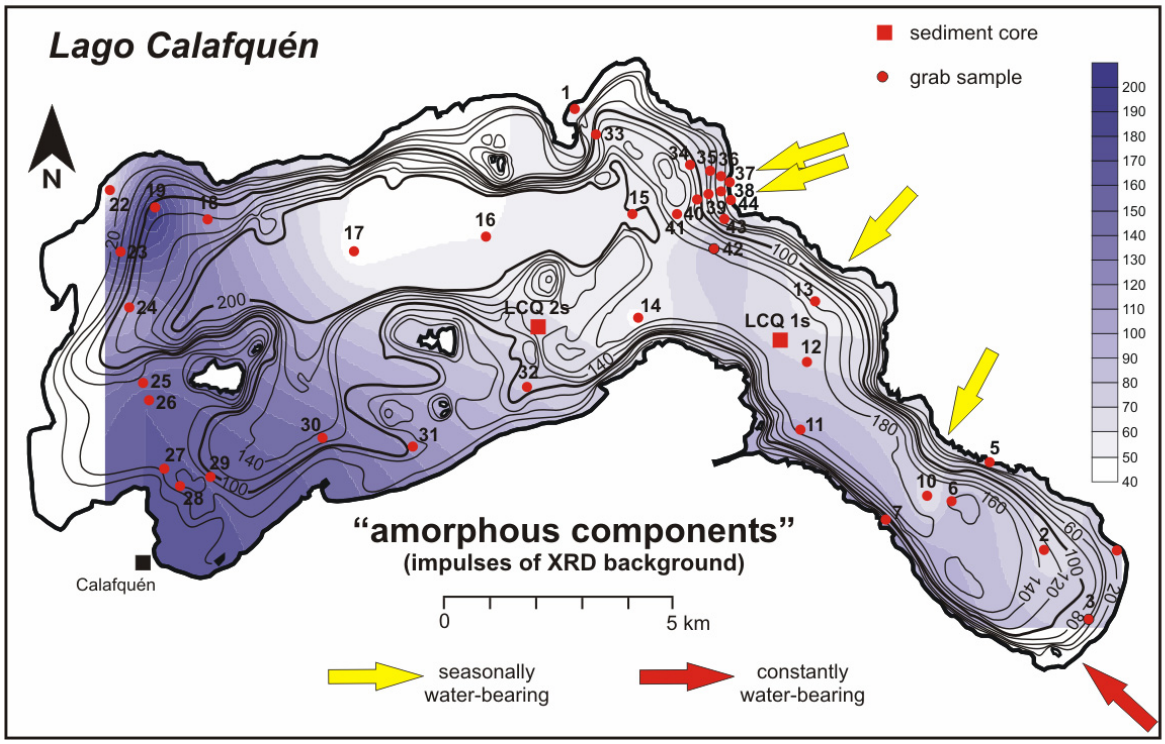

Fig. IV-4: Spatial distribution of amorphous components deduced by the background shift in X-ray diffractograms of the surface samples.

4.1.2 Sediment texture

Surface sediments of Lago Calafquén do not show a uniform size pattern. The high diatom frustule content suggests that the sediment texture of Lago Calafquén can be classified as diatomaceous silt (Fig. IV-5a,b). Triangular plots of sediment texture related to their lake-bed environment (Fig. IV-5b) show no tendency for samples from specific grain sizes (Folk, 1980). Slope sediments mostly consist of silts and sandy silts, but included a few samples of silty sands. Delta sediments of Río Chaillupén are sandy silts to silty sands. Basinal sediments are sandy silts with lesser amounts of silty sands, the latter linked to turbidite trajectories in the lake basin. Only a few samples from the basin plain can be characterized as silts. Rise sediments from the southern to south-western shelf are mainly silts, except for samples located leeward of the island Isla de Trailafquén (cf. Fig. III-3a), which consist of pure clay. Littoral sediments are primarily silt.

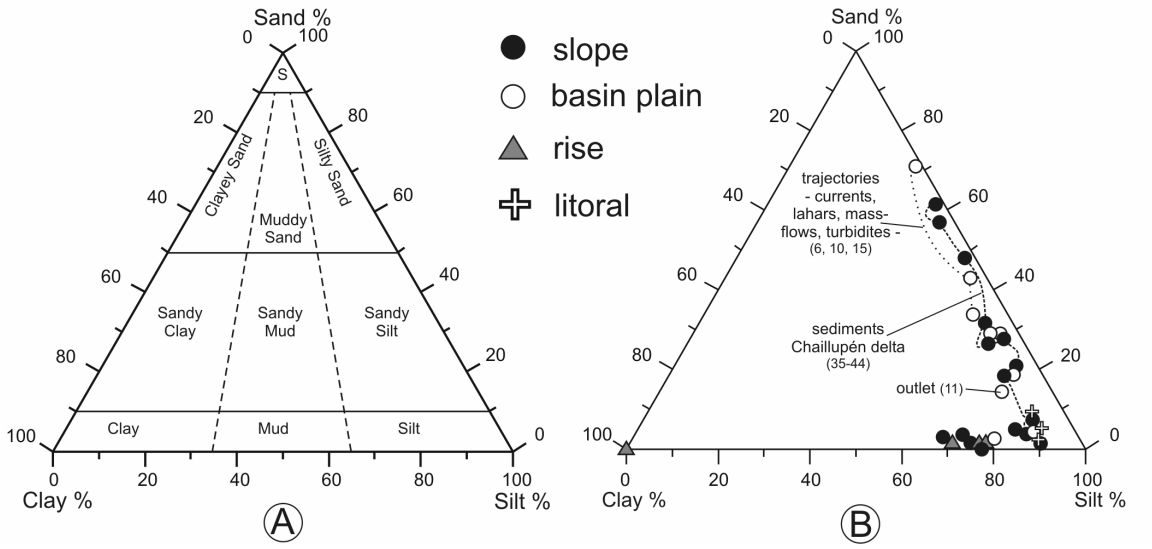

Fig. IV-5: A) Textural classification of sediments based on the composition of sand, silt and clay (Folk, 1980); B) Ternary textural diagram for Lago Calafquén surface sediments, classified according to their lake-bed environments. The sample numbers are enclosed in brackets

4.1.3 Textural trends

The spatial grain size distribution of Lago Calafquén's surface sediments shows a trend of increasing clay fraction towards the western end of the lake (Fig. IV-6). The mean grain size is largest in the south-eastern basin and central region (Fig. IV-6a). The mode (Fig. IV-6b) is taken as the most frequent occurring diameter which is useful for evaluating hydrodynamic regimes where two or more contributing sources may be involved (Folk, 1980). It shows similar depositional centres around the river mouths of Río Chaillupén and Río Comonahue (cf. Fig. IV-2). Both parameters show that sediment dispersal is systematically decreasing towards the west with distance from these inflow trajectories. Surface sediments of Lago Calafquén are poorly sorted all over the entire lake basin, except for sediments deposited leeward of Trailafquén Island, which are well sorted and consist of up to 100% clay.

Sand content is highest around the above mentioned river deltas, > 40% at Chaillupén and > 60% at Comonahue. Sand-sized material fines and decreases with distance from the river towards the basin plain of the western and the eastern lake basins. Areas affected by the seasonally water-bearing creeks Nilfe, Díuco and Tralco (cf. Fig. IV-2) have moderate sand content at approximately 10%. Across the entire south-western to western side of the central sub-basin, sand content decreases to zero. With low concentrations of 5 to 15%, clay-size material accumulates throughout the eastern to central sub-basin, but increases steadily towards the south-western to western end, achieving a maximum leeward of Isla de Trailafquén.

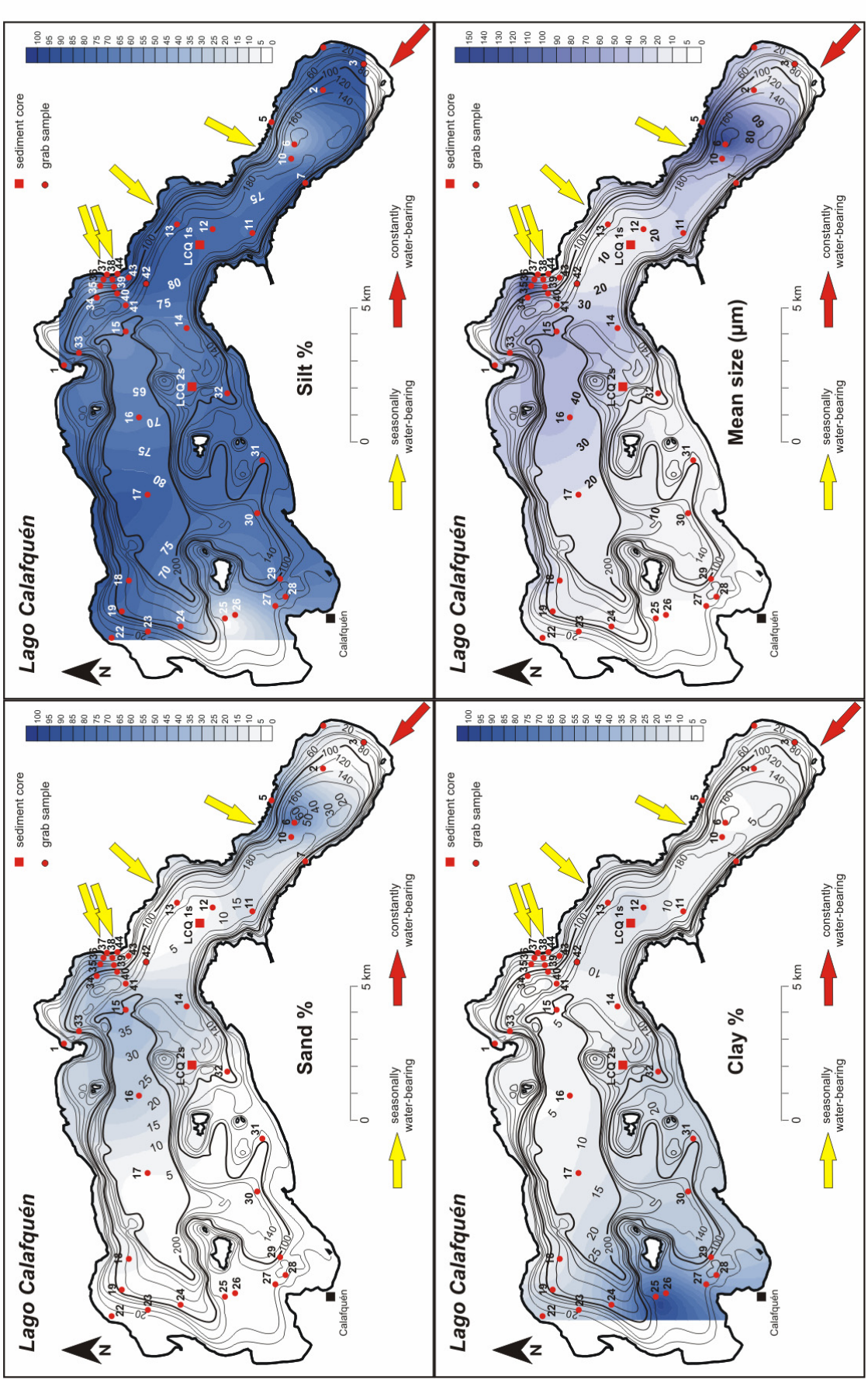

Fig. IV-6a: Sediment texture (composition of sand, silt, and clay) and mean grain size distribution of surface sediments in Lago Calafquén.

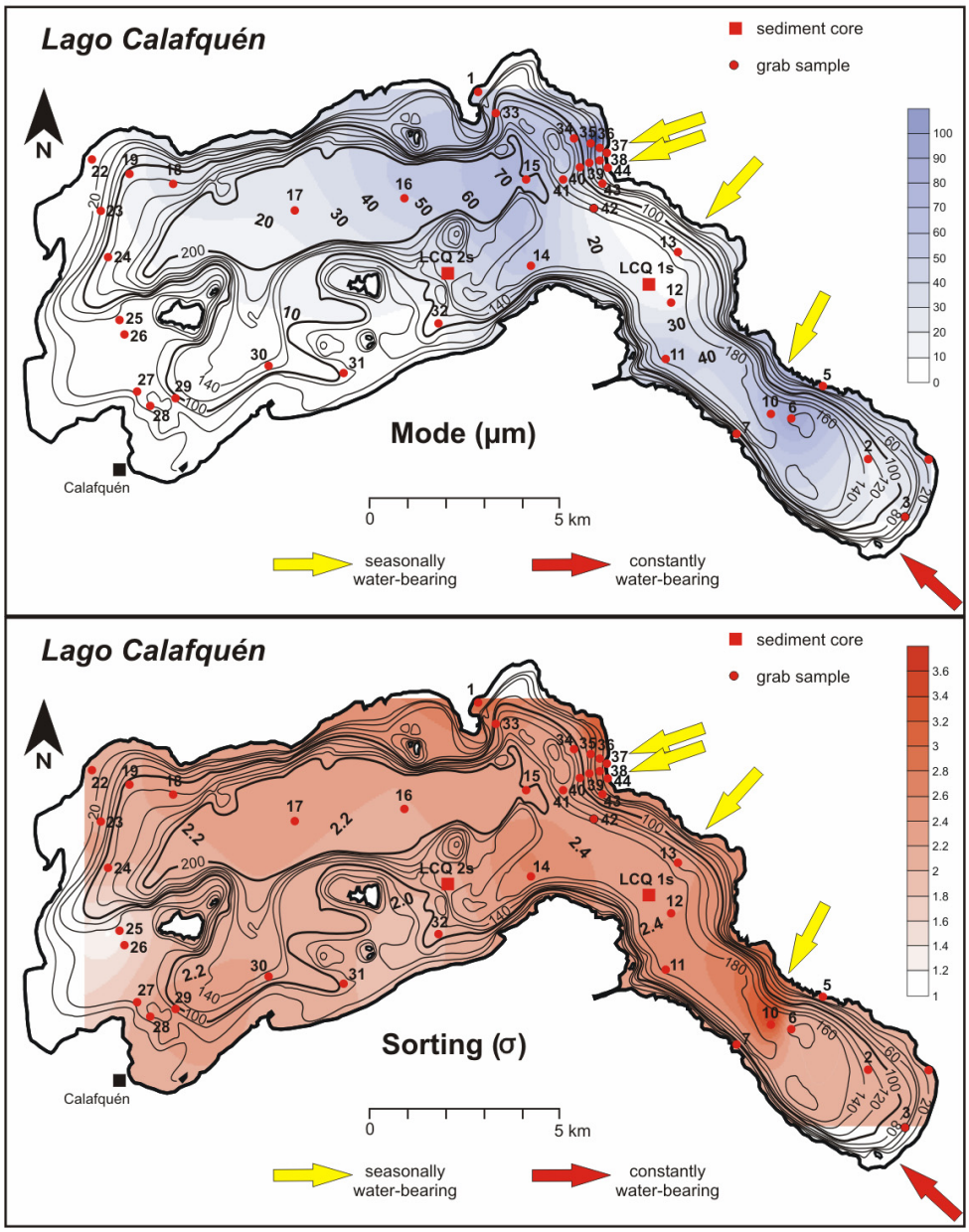

Fig. IV-6b: Mode-size distribution (upper panel) and sediment sorting (lower panel) for Lago Calafquén surface sediments.

Because silt content is relatively uniform over the entire lake basin, maps of ratios of silt and its sub-fractions to clay are more informative, as introduced by Nelson and Lister (1995) for Lake Taupo in New Zealand. Generally, ratio maps of clay and silt show, in detail, the distribution of the fine fraction. Since silt fractions are subdivided, their distribution patterns show the lake-wide interrelation of the transported material and the inflow hydrodynamics, which are discussed in Chapter 5.

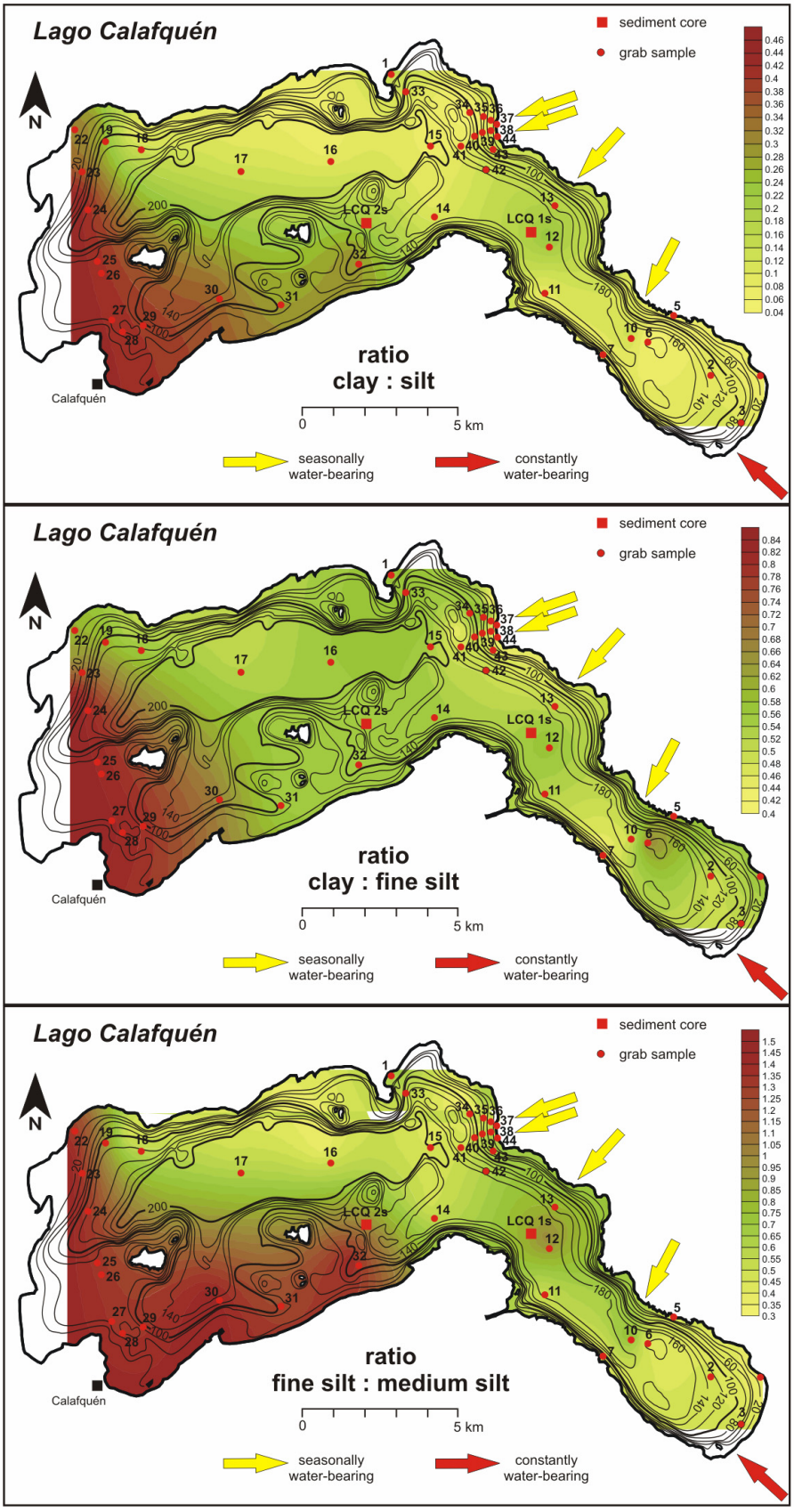

Fig. IV-7: Textural maps showing the ratio of clay:silt (upper panel), clay: fine silt (centre panel), and fine silt: medium silt (lower panel) in Lago Calafquén surface sediment samples.

Silt dominates the sediment over the entire lake basin and decreases near the river inflows where sand-sized material accumulates (Fig. IV-7). The grain size in these areas corresponds to the river flow velocity (e.g. Campbell, 1998). Accumulation of clay-sized sediments on the entire western side of the lake interferes with sedimentation along the southern shore, where it replaces the silt fraction. Two prominent size fractions, $2 - 6$ µm and $6 - 20$ µm, occur in the silt. The larger silt fraction is greater in the northern and eastern deep sub-basins and less on the southern shelf. The fine silts achieve maxima along the entire southern and south-western side of the lake. The ratios of clay to fine silt-sized material clearly show an increase of clay-sized material along the south-western edge of the basin.

4.1.4 Carbon and sulfur content

TIC analyses confirmed that the siliciclastic sediments are free of carbonate compounds, therefore the TC content of the grab samples analysed with the LECO can be considered as total organic carbon (TOC). The TOC content ranges from 0.5 to 3.0% by weight throughout the lake basin, with one extraordinary maximum of > 7%, likely related to influence of animal husbandry occurring near the shore, and is thus unrepresentative of the overall TOC (Fig. IV-8). Deposition minima occur in the central basin plain of the central sub-basin and around the areas of the river and creek deltas that drain the flanks of the volcano. In the eastern basin, TOC concentrations increase towards the southern shore, with values between 2 and 3% by weight. The increase of TOC content is not related to a decrease in water depth, nor does it follow the subaqueous bottom morphology, although TOC values become steadily higher along the southern and south-western shelf. Total sulphur content (TS) shows the presence of two depositional maxima (Fig. IV-8), possibly associated with sediment texture, as they appear related to grain-size (see mean grain size, Fig. IV-6a). One deposition centre, located in the bay near Coñaripe, is dominated by fine and medium silt-sized material. The second maximum concentrates material in the lee of the Chaillupén delta, where the eastern basin merges into the western lake basin. The TS concentration shows a decreasing east-west gradient through the central basin plain extending towards the western side, where it reaches a minimum. Values are somewhat higher in samples #22, #23 and #24, located on the north-western slope, but generally follow TOC concentrations. This increase might reflect the influx of humic material originating from the swampy stagnant water from the uppermost western shore. The ratios of TOC to S increase with distance from the tributaries and with fining size-modes towards the western lake basin, where two maxima occur (Fig. IV-8).

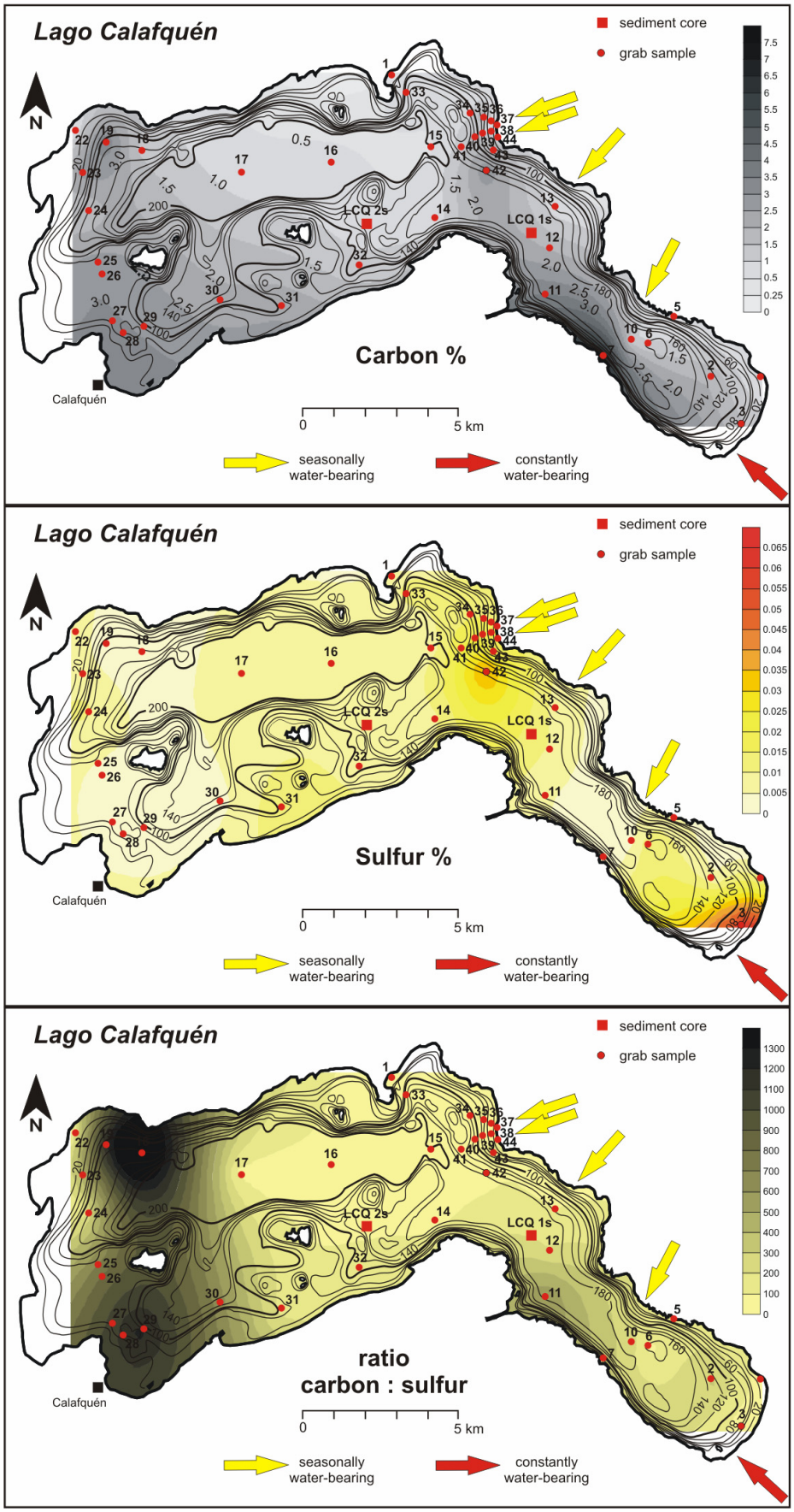

Fig IV-8: Upper panel: Total organic carbon (%) distribution of surface sediment samples from Lago Calafquén. Central panel: distribution map of total sulfur (%) derived from surface sediment samples. Lower panel: carbon to sulfur ratio from surface sediment samples.

4.2 Lago Villarrica

4.2.1 Sediment composition

Bottom sediments of Lago Villarrica show similar bulk minerals as sediments of Lago Calafquén. XRD analyses indicate that the total clay mineral contents are low, but frequently comprise a variety of clay mineral species. The intensities of the basal reflections for chlorite and smectite were confined to nine localities not exposed to the direct trajectory of erosive bottom currents (see Chapters 4.2.3 and 5). Small crystals of feldspar and pyroxenes, as well as diatom valves, contribute to the components making up these clay fractions.

Also in Lago Villarrica diffraction patterns of bulk samples show a background shift between 20 – 34° 2θ (Fig. IV-9), which is referred to a variable quantity in amorphous components. Deposition minima occur in direct proximity of the river mouths of the consistently water-bearing Río Molco and Río Correntoso, which deliver clastic material to the central lake basin. This allochthonous influx dilutes the biogenic controlled lake sediment and therefore represents areas of higher clastic influx with lower proportions of amorphous components.

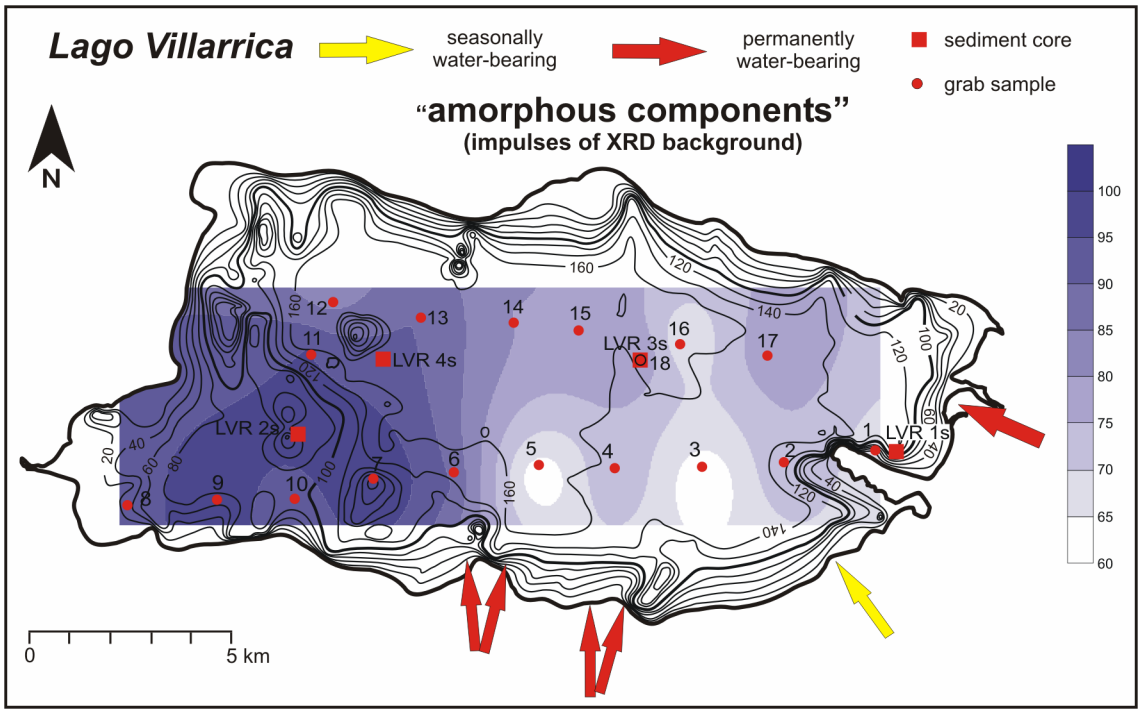

Fig. IV-9: Spatial distribution of amorphous substance in surface sediment samples from Lago Villarrica deduced by shift in the X-ray diffraction values.

4.2.2 Sediment texture

Sediments of Lago Villarrica are relatively uniform, and contain high amounts of diatom valves, thus the sediment texture is classified as diatomaceous silt (Folk, 1980). No trend in sediment texture for samples from specific environments can be identified by the triangular plots (Fig. IV-10), but they show a narrow distribution within texture fields (Folk, 1980). Due to the relatively simple structure of the basin, only a few samples were located on slopes, which were composed of silts, except for one sandy silt sample taken from a steep slope at the littoral zone in the bay of Pucón. Sediments from the basin plain are pure silts, except for those that were clustered in the direct path of

strongly erosive bottom currents, turbidites, or lahars. Samples exposed to these highly dynamic regimes are sandy silts with a trend to silt (Fig. IV-10a) and form a trajectory in the triangular texture plots (Fig. IV-10b). Samples from the elevated south-western rise are mainly silts, except for the location around the outlet of Lago Villarrica, which shows a tendency to sandy silts. Littoral sediments consist of a large silt fraction.

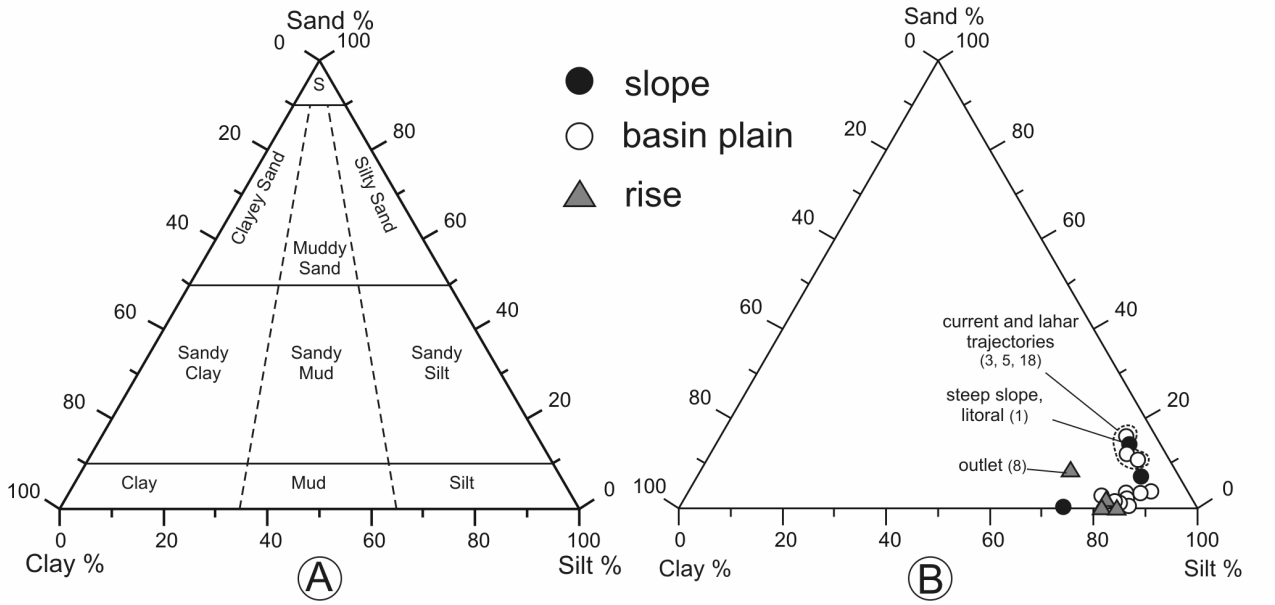

Fig. IV-10: A) Textural classification of sediments based on the composition of sand, silt and clay (Folk, 1980); B) Ternary textural diagram for Lago Villarrica surface sediments, classified according to their lake-bed environments. The sample numbers are enclosed in brackets.

4.2.3 Textural trends

A spatial summary of the grain size distribution, including mean and mode grain sizes (Figs. IV-11a,b), shows three depositional centres which lay in the direct path of the seasonally water-bearing Río Carmelito river-delta and the permanently water-bearing Río Correntoso river-delta (cf. Fig. IV-2). Both size-modes decrease towards the north with increasing distance from the deltas, and also decrease towards the west with increasing distance from the major tributary Río Trancura. Surface sediments are poorly sorted in the eastern to central part of the lake basin (Fig. IV-11b), but tend to be moderately sorted westwards, on the south-western basin shelf and leewards of Isla de Aillaquillén. The sand content of Lago Villarrica sediment is fairly low, approximately 15%, and is generally confined to the south-eastern and southern sides of the lake, around the areas that are influenced by the tributaries draining off the flanks of the volcano. The sand fraction fines and decreases towards zero across the entire western lake basin.

Clay content of the surface sediments is generally low, increasing from approximately 5% in the eastern basin to 20% at the western lake shore, along the elevated shelf.

The silt-size fraction is the prominent grain size. In the eastern lake basin, sand-sized material is restricted to the river and creek mouths (Fig. IV-12). Towards the west, the strong increase in the silt to sand ratio on the shelf reflects the lake floor morphology.

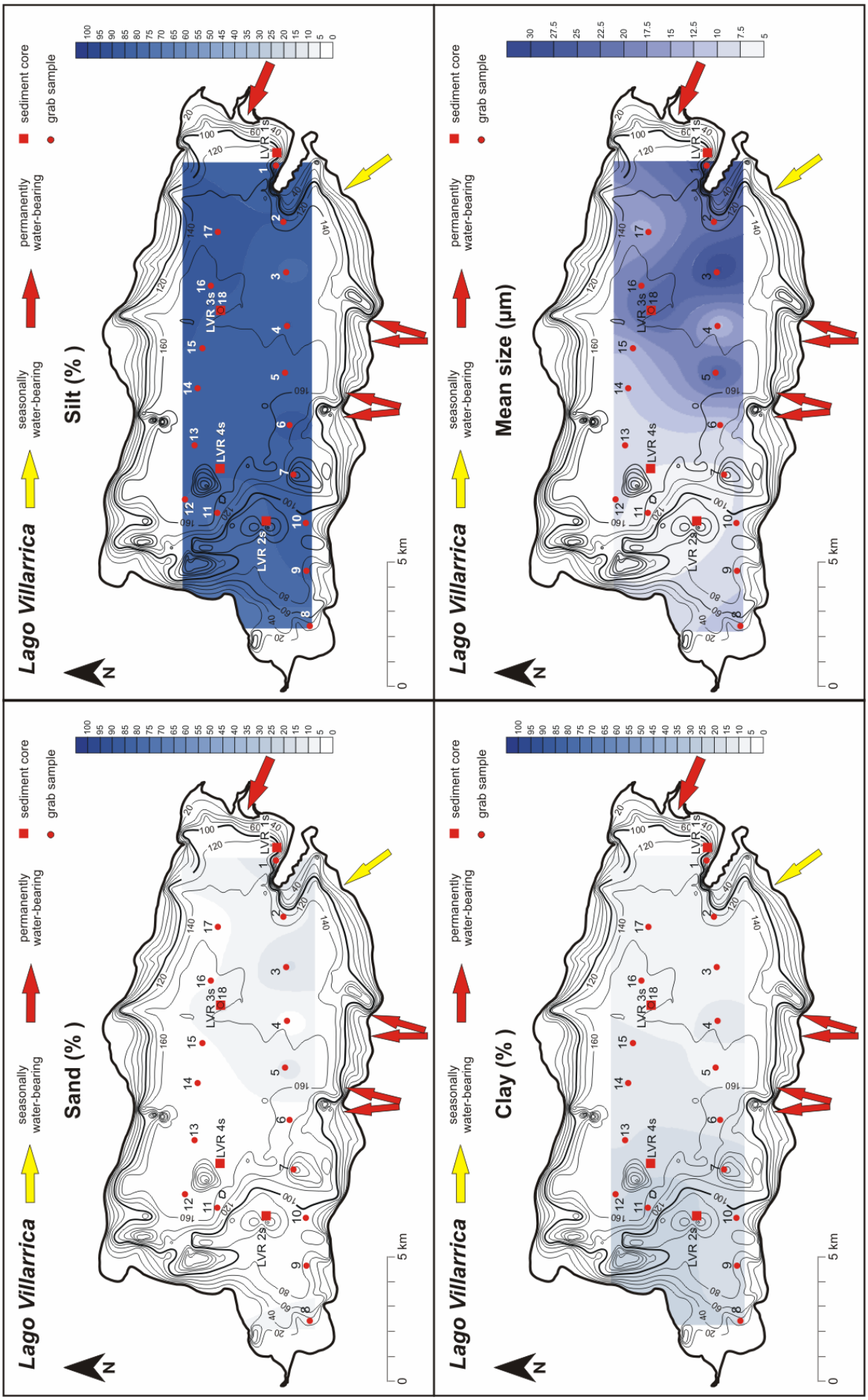

Fig. IV-11a: Sediment texture maps (composition of sand, silt, and clay) and mean grain size distribution of surface sediments in Lago Villarrica.

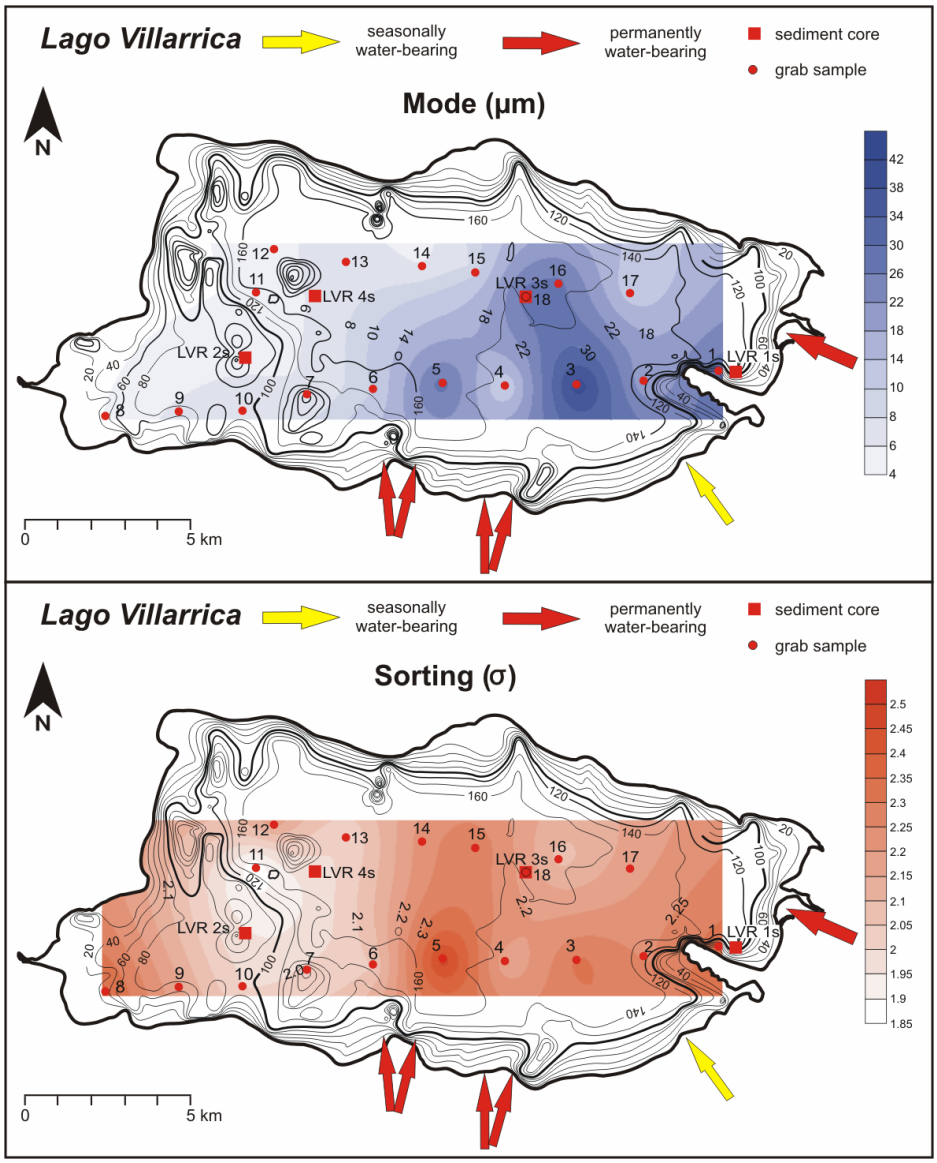

Fig. IV-11b: Mode-size distribution (upper panel) and sediment sorting (lower panel) in Lago Villarrica surface sediments.

The medium silt fraction (6-20 µm) accumulates predominantly in the deep central basin plain (Fig. IV-12), but also makes up a notable amount of the sediment on the elevated rise in the south-western lake basin. The clay to fine silt ratios achieve maxima on the western shelf but decrease eastwards toward the deep central basin plain, where clay content is negligible. Clay content in the central basin plain is limited to narrow isolated areas that obviously occur between tangential currents entering the lake from the southern side.

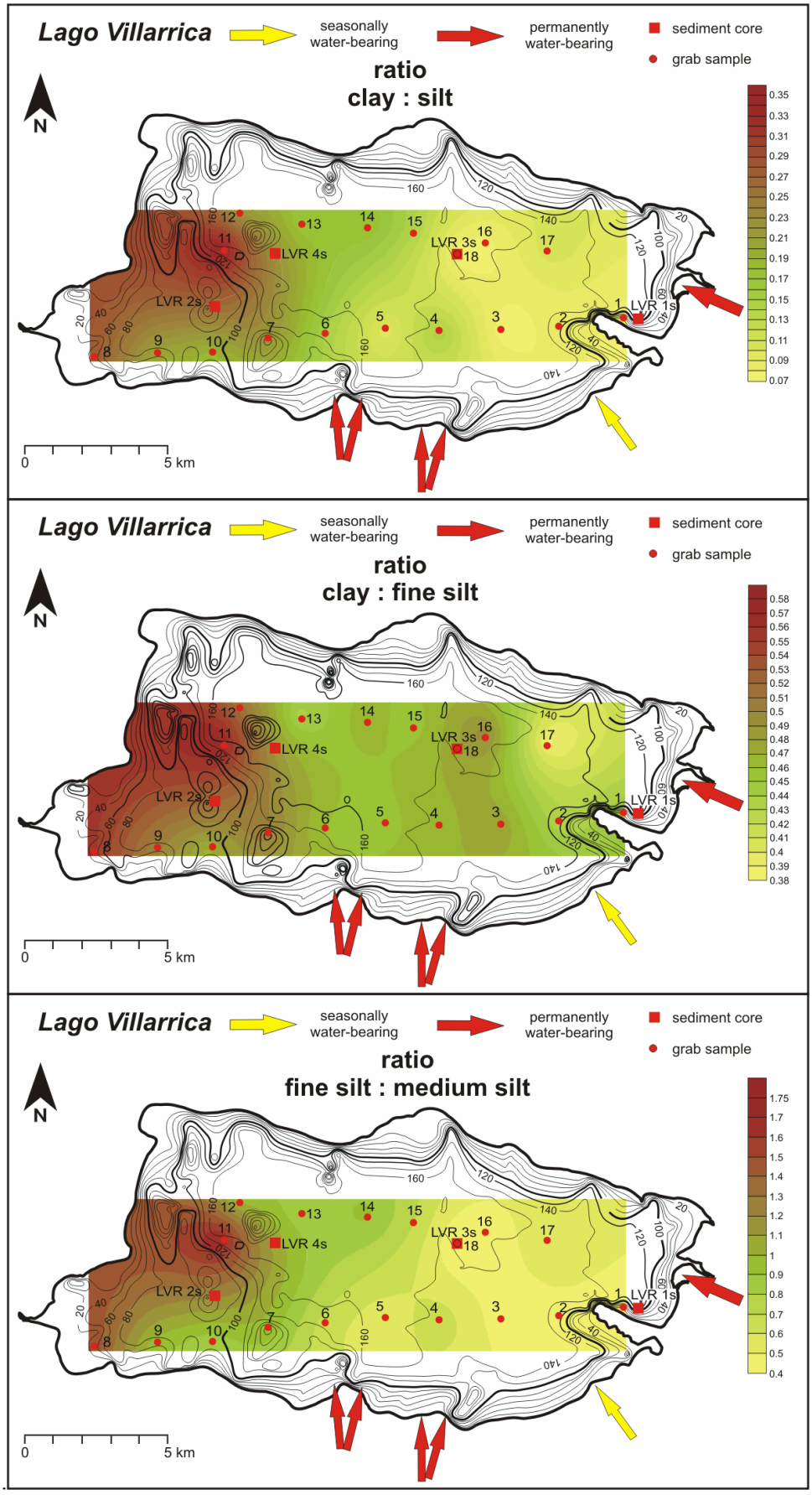

Fig. IV-12: Textural maps showing the ratio of clay:silt (upper panel), clay:fine silt (centre panel), and fine silt:medium silt (lower panel) in Lago Villarrica surface sediment samples.

4.2.4 Carbon and sulfur content

The TOC concentration in Lago Villarrica ranges from 1.1 to 3.4% by weight (Fig. IV-13a). The TOC distribution pattern shows a north-south trend, the lowest values in the south around Carmelito, Correntoso, and Molco creeks, increasing with distance along the water current trajectories. No relationship between depth or lake-bottom morphology and TOC distribution is observed, since there are isolated TOC maxima in the deep basin plain, however an increase in TOC on the south-western shelf is evident. TS content in Lago Villarrica follows the TOC distribution patterns, with similarly located concentration maxima and minima, except for the south-western shelf. There, TS content decreases towards the bay of Villarrica city, where TOC values become higher (Fig. IV-13b). The C:S ratio remains relatively constant throughout the lake basin but increases in the south-western bay at Villarrica-city (Fig. IV-13c).

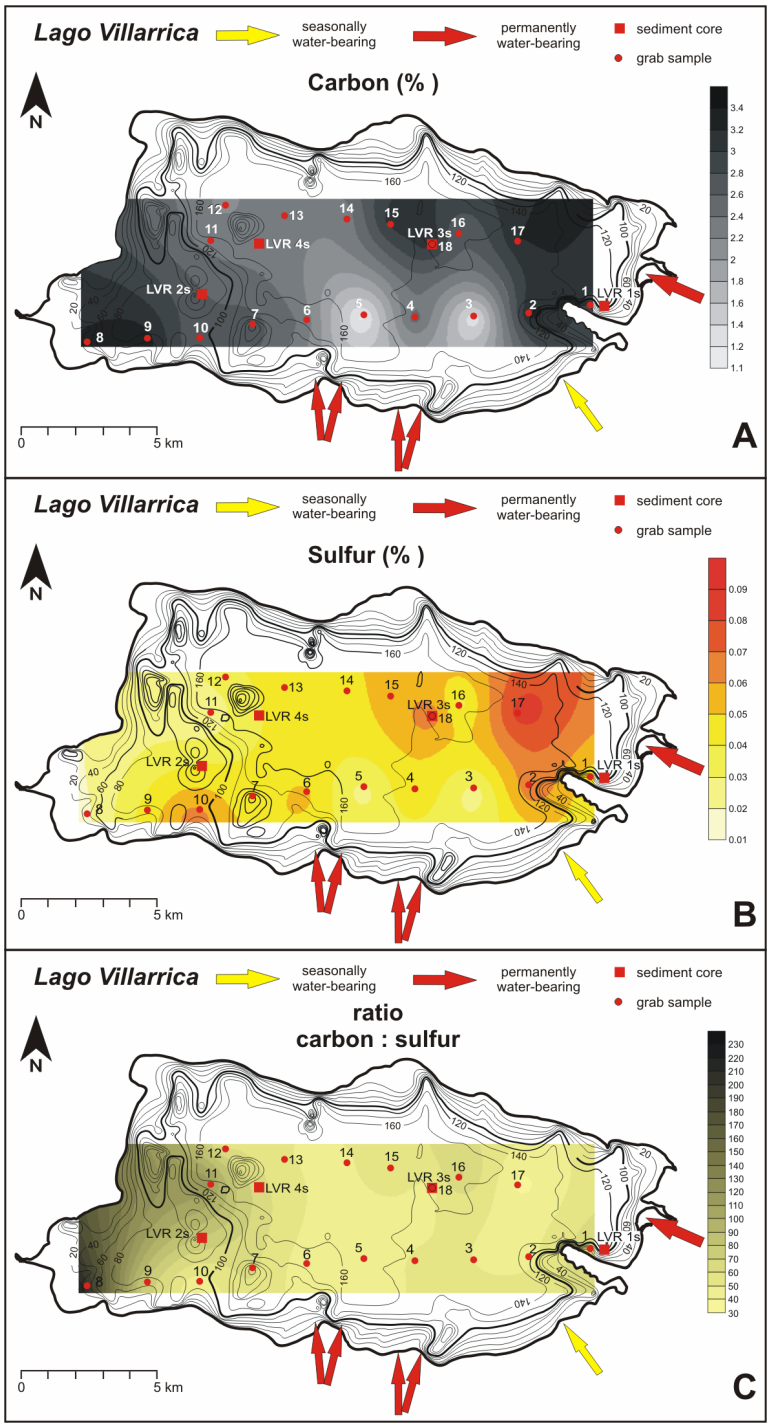

Fig. IV-13: A) Total organic carbon (%) distribution of surface sediment samples from Lago Villarrica. B) Distribution map of total sulfur (%) derived from surface sediment samples. C) Ratio of C:S from surface sediment samples.

5. Hydrodynamic reconstruction

Lake sediment texture is a function of the catchment and sorting processes during the transport of material from the source to and within the lake basin. Sorting processes of detritus particles depend on the current energy, the distance from the source, and settling velocities. Sediment composition is related to source area and is reflected in the sediment dispersal patterns on the lake

floor. The use of sediment texture and grain size parameters to determine sediment transport pathways and reconstruct hydrodynamics of the current systems is difficult, as these properties are influenced by transport independent processes such as sediment focussing, sediment mixing from different sources, or resuspension of the bottom sediments. Furthermore, geodynamic activity also may influence grain size and texture, as deposits are affected by erosion of subaqueous slopes during earthquakes or other mass movements. The sediment texture analysis forms a suitable basis for discussing and interpreting surface sediment features (Figs. IV-4 to 13).

5.1 Lago Calafquén

Sediments of Lago Calafquén are silts to sandy silts and are not clearly separated according to their depositional environment, except for deltaic deposits (Fig. IV-5). Basin plain sediments are medium silts, becoming coarser towards the deltas and other sources of terrigeneous influx, where sand content also increases. Sediments are generally poorly sorted, though they become somewhat moderately sorted towards the western and southern ends of the lake basin (Fig. IV-6). Sorting of shelf sediments increases with decreasing depth, though only slightly. In the central and western lake basin, mean grain-size decreases along an east-west trending gradient. Winnowing of mean-size in the eastern basin occurs from the northern sidewalls onto the narrowly-defined basin plain. There, mean-size becomes coarsest within an area that is affected by deposits of mass movements, as deduced from seismic investigation. Fine grain-sized material (Fig. IV-7) and organic matter content (Fig. IV-8) increases on the central sub-basin shelf and within the many small depressions appear towards the deep basin plain. Conversely, sulfur concentrations are highest around the areas of terrigeneous influx like the deltas and creeks, and decrease with distance from these sources, implying that sulfur input is related to terrigeneous influx and not to bacterial sulfur production. Distribution patterns of carbon and sulfur are not depth-dependent (Fig. IV-8), but are closely related to one another (Fig. IV-8). Mineralogical trends can only be detected by a discrepancy in background intensity of the X-ray diffractograms, synonymous for a variable quantity of amorphous components in the sediments. A close relationship between carbon content and amorphous components can be observed (Fig. IV-4).

The textural and compositional data suggest complex sediment pathways occur in Lago Calafquén. It can be deduced that currents in Lago Calafquén do not disperse uniformly, but rather function independently, controlling sedimentation and productivity of each sub-basin (east and central). Various interrelated processes and basin morphological features, lead to hydrodynamic models and sedimentation processes that will be discussed below.

a) Eastern sub-basin

The sediment texture of the eastern sub-basin is influenced by the constantly water-bearing Río Pellaifa, the seasonally water-bearing lateral tributaries that drain the flanks of the volcano, and areas that are affected by turbidity currents (Appendix, Fig. A-5,9). Underflows form the major currents in this prominent area, depositing medium- to coarse-sized materials, whereas interflows might contribute sediment to the accumulation area in the overlap of the sub-basins (Fig. IV-14). Moreover, the riverrine textural pattern is masked by coarse sediment accumulation on the northern shore, likely material winnowed from the adjacent sidewall or possibly of subaerial origin. This deposit should be interpreted as a debris flow body of unknown origin. Moreno (2000) declares the adjacent catchment area as a zone of exceptional danger for lahars during volcanic eruptions, thus implying on possible source of origin among many others.

The mean- and mode-size of the river-borne sediments of Río Pellaifa fine in SE-NW direction and indicate zones of accumulation around the area where the eastern and central sub-basins merge (Fig. IV-14).

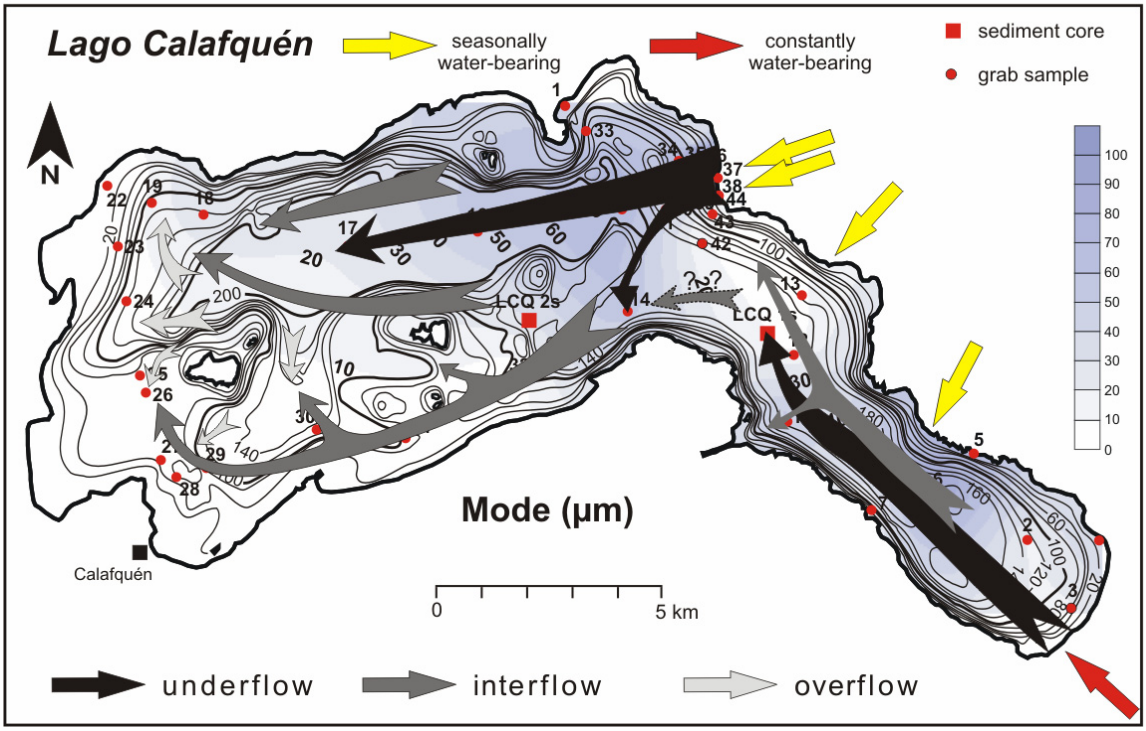

Fig. IV-14: Conceptual hydrodynamic reconstruction for Lago Calafquén based on results of sediment texture and geochemistry. Currents are indicated as underflows (in black), interflows (dark grey), and overflows (light grey). Units are mode (µm) of grain size.

b) Central sub-basin

Sediment texture maps indicate that current systems of the central sub-basin do not follow the lake bottom morphology, but are affected by thermal stratification patterns within the lake. The seasonally water-bearing Río Chaillupén delivers sediment-laden runoffs into the lake, either by melt-water or strong precipitation flows. Furthermore, it serves as the main trajectory for subaerial debris flows and lahars (Moreno, 2000) that spread in the lake basin. Following the pattern of mode, temporary strong underflows originating from the mouth of Río Chaillupén delta form a prominent current along the deep basin plain of the central sub-basin. Sediment texture follows a general E-W depositional gradient, indicating that the suspended load may be transported into the central basin plain by similar processes of extraordinary turbidites as described by Sturm and Matter (1978). It is likely that they act as underflow currents in the southern area in the extension of the delta (Fig. IV-14). Pelagic sedimentation of Lago Calafquén is controlled primarily by low-energy interflow currents in the metalimnion. They stratify and transport fine-sized fraction into the southern and western basins, depositing their sediment on the shelf, as can be deduced by the ratios of fine to medium silt (Fig. IV-7). Overflows are thought to transport the fine-sized fraction to the outer western end of the basin, as indicated by the ratio of clay to fine silt (Fig. IV-7). Variations in amorphous components of the bottom sediments correlate with the spatial distribution of TOC content. Theses variations are referred to dilution of the biogenic controlled sediment by increased clastic influx from the tributaries. Sediments deposited in areas located far away from the river mouths receive less allochthonous clastic riverrine material, hence showing a higher abundance of amorphous material, which is mostly made

up of biogenic components. A centre of increased primary productivity is restricted to the bay next to Calafquén village at the southern side, where intense growth of goldalgae was observed.

Sediment focusing as described by Viner (1989) for Lake Taupo/New Zealand as enhanced sedimentation with increasing depth, obviously does not play a significant role in Lago Calafquén. Spatial sedimentation pathways in Lago Calafquén are not controlled by depth but by distribution mechanisms characteristic of clastic sedimentation in oligotrophic lakes as introduced by Sturm and Matter (1978).

5.2 Lago Villarrica

Sediments of Lago Villarrica are silts with a slight tendency to sandy silts for areas exposed to erosive bottom currents. Sediments in Lago Villarrica are not clearly separated according to their depositional environment, as basinal and rise samples from the shelf are plotted within the same texture field (Fig. IV-10). Basin plain sediment is classified as medium silts in the eastern basin, with maxima around areas with increased terrigeneous influx i.e. near the tributaries, fining into fine silts towards the western lake basin and on the shelf (Fig. IV-11). Sediments are generally poorly sorted, becoming moderately sorted in the lee of Isla de Aillaquillén (Fig. IV-11). Mode-size decreases along an east-west trending gradient, with the fine-sized fraction increasing on the shelf and the western shore (Fig. IV-12). TOC and TS content are linked to fine fractions except in the bay near Villarrica city (Fig. IV-13). In the eastern basin, TOC and TS reflect the mode-size distribution (Fig. IV-11). Mineralogical trends in Lago Villarrica also occur in a variance of amorphous components deduced from the XRD records (Fig. IV-9).

Sediment pathways in Lago Villarrica are comprised of several cross-cutting currents (Fig. IV-15). The mode-size shows a basic E-W grading current pattern, from the main tributary, Río Trancura, to the western lake basin. This pattern is masked by the interference of sediment-laden river water from the Trancura delta, which flows along the delta foreset following the depositional gradient into the deepest part of the lake basin as an underflow, sensu Sturm and Matter (1978). Pelagic sedimentation of Lago Villarrica is primarily controlled by low-energy interflow currents, which transport fine-sized material into the western lake basin.

This general sediment pathway is interfered by S-NNW trending texture patterns of the southern tributaries. Seasonal underflows from the Río Carmelito leave the strongest imprint on depositional patterns, forming a clear trajectory that is observed by the mode-size distribution (Fig. IV-10). From the presence of terrestrial outcrops along the bed of Río Carmelito (cf. Fig. II-12,13) it can be deduced that large debris flows occur repeatedly. The constantly water-bearing Río Correntoso and Río Molco deliver coarse grain-modes to the lake and form additional minor underflow currents, injecting sediment-laden water and debris flows from the volcano flanks into the thermal stratified water body. Moreno (2000) suggests these river beds (cf. Fig. IV-2) are major trajectories and zones of exceptional danger for lahars. Interflows from the small creeks on the southern side cross-cut the main current in a NNW direction, transporting fine-sized material into the northern basin. Overflows transport and release very fine-sized sediments into areas with little influence of strong water movement, where increases in amorphous components in the sediment are traced in the bulk mineralogy.

The arrangement of water currents is clearly traced by the TOC dispersal patterns on the lake floor. The TOC and TS minima correlate to the coarse mode-size and reflect strong bottom currents along the bottom set area of the river mouths. These sediment texture patterns mask the dispersal pathway of the main tributary, the Río Trancura.

The TS content of Lago Villarrica sediments exceeds those of Lago Calafquén by almost one order of magnitude. It suggests that a clear relationship between catchment size and influx rates exists. The catchment of Lago Villarrica is 2/3 larger than that of Calafquén, likely transporting more terrigeneous material into the basin, reflected in the high TOC and TS in front of the Río Trancura delta. Further evidence is the dominance of silt-sized material accumulating along the Trancura delta bottomset. Sand content around the delta is negligible, reflecting the long distance material is transported from the source, through the catchment and into the lake reservoir.

Distribution patterns of amorphous components follow the minima around the southern tributaries, but in the western basin differ slightly from the TOC content. This suggests an additional supply of terrigeneous TOC from the south-western side.

The lake is flushed by the west-flowing current of Río Trancura, crossing the entire lake basin and discharging at the western end. This flushing has different consequences for the dynamic of the water body. The current system in Lago Villarrica is primarily driven by inter- and underflows that contribute the major part of the sediment to different parts of the lake basin. Underflows are restricted to the deep basin plain, whereas interflows transport sediments to the elevated rise in the south-western lake basin.

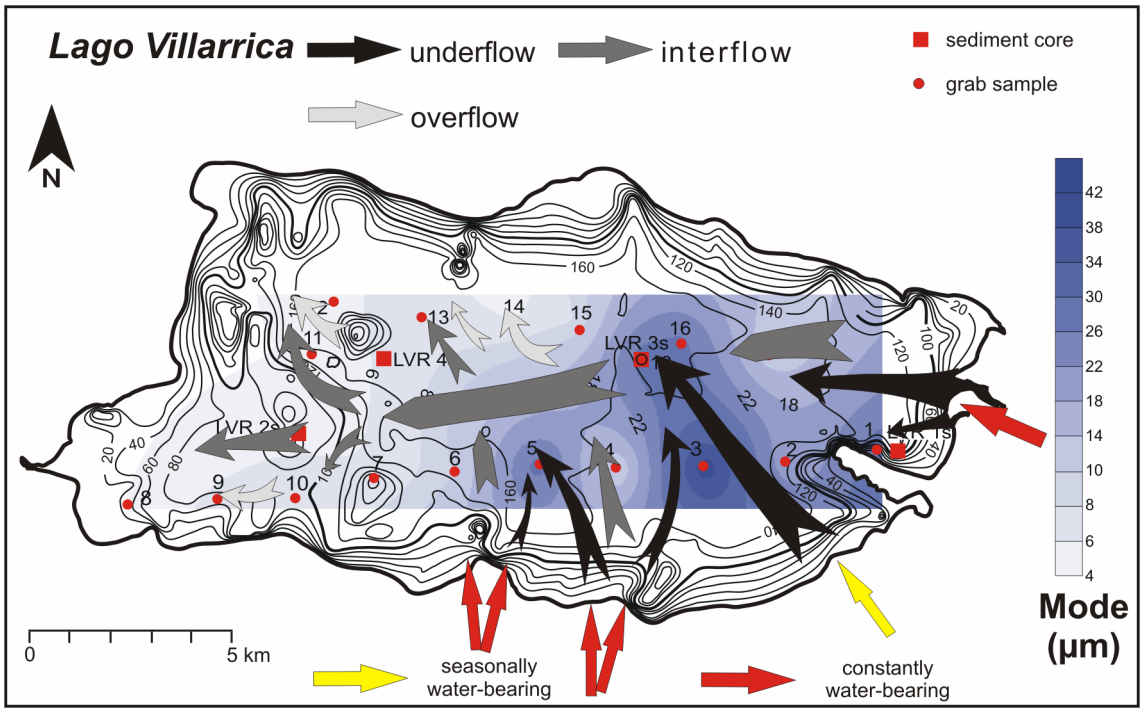

Fig. IV-15: Conceptual hydrodynamic reconstruction for Lago Villarrica based on results of sediment texture and geochemistry. Currents are indicated as underflows (in black), interflows (dark grey), and overflows (light grey). Units are mode (µm) of grain size.

From the sediment texture analyses of both lakes, it can be concluded that the sediment deposits, derived from the constantly water-bearing tributaries in the catchment, are decisively masked by the small and mainly seasonally water-bearing creeks which drain off the flanks of the volcano. They deliver vast amounts of coarse-sized material into the lake basin on occasion, forming strong bottom currents. As they mostly are the main trajectories for all kinds of debris flows, their pathways can be traced far into the deep basin plain using sediment texture pattern.

6. Multi-proxy lake study

Spatial sediment analyses of the previous chapter explained modern sedimentation processes in both Lago Calafquén and Lago Villarrica on the basis of a strong coupling between the lake and its catchment. Understanding how these processes operated in the past, and their connection to environmental and climatic variability, performing a chronological, multi-proxy analysis on the sediments of both lakes is necessary. Proxy-data is gathered using material such as pollen, tree rings, ice cores, sediments, or historical records to reconstruct past environmental changes by proxy, as no direct evidence is available. 'Proxy-material', often found preserved in lake sediments, transforms past climate and environmental conditions into relatively permanent records. A sediment-based multi-proxy approach has significant power; it generates abundant data enabling one to infer potentially integrated responses of the lake system to environmental and climatic changes.

High-resolution, multi-proxy studies were carried out on a single core from both Lago Calafquén and Lago Villarrica to better understand time-related sedimentation processes and detect regional environmental change. The analyses were performed on normal lacustrine sediment, which is delivered from the catchment into the lake basin by surface runoffs, and comprise information on sediment dynamic and availability from the catchment, erosion, nutrient supply and lake productivity. This information obtained from the different proxies is interpreted carefully in order to deduce environmental and climatic changes from the last 3000 years in Lago Calafquén and 1200 years in Lago Villarrica.

6.1 Lago Calafquén

In Lago Calafquén, short gravity cores were taken from two sites with differing predominant currents (cf. Fig. IV-3,14). High-resolution, multi-proxy analysis was applied on sediments from coring site LCQ2s (cf. Fig. IV-3a) that is not influenced by strong underflow currents. This 162 cm long core covers a continuous record of normal lacustrine sedimentation, showing distinct events that clearly reflect the geodynamic activity of the area surrounding the lake.

At the coring site in the eastern deep basin plain, strong underflows interrupt the steady normal lacustrine sedimentation processes and deposit large turbidites. Turbidites in short core LCQ1s (max. length 93 cm, see photographic documentation, Fig. A-5, Appendix) reach maximum thickness up to 31 cm. They have a coarse base and fine upwards, and often incorporate plant residue, like leaves and wooden bits, which are found mostly in the coarser parts of the strata. Turbidites are generally overlain by diatom layers. Due to the strong clastic inputs, further multi-proxy analyses on this core did not seem favourable.

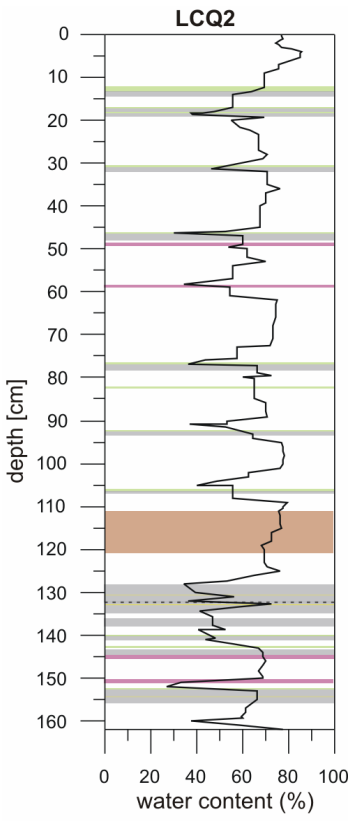

Fig. IV-16: Water content (in percent) of short core LCQ2s.

6.1.1 Water content

With uniform values of 75% to 80%, the normal lacustrine sediment reflects a water content which is typical for silt-sized material (Fig. IV-16). Characteristic extraordinary decreases to < 40% occur in the sandy tephra layers. Nevertheless, from 162 to 115 cm depth, water

content increases slightly. Between 99 and 20 cm, water content decreases, though the trend is interrupted by several small peaks between 73 to 63 cm and 45 to 35 cm, which suggests a change in grain size distribution. The increase towards the top of the core is linked to the natural diagenetic dewatering reaction.

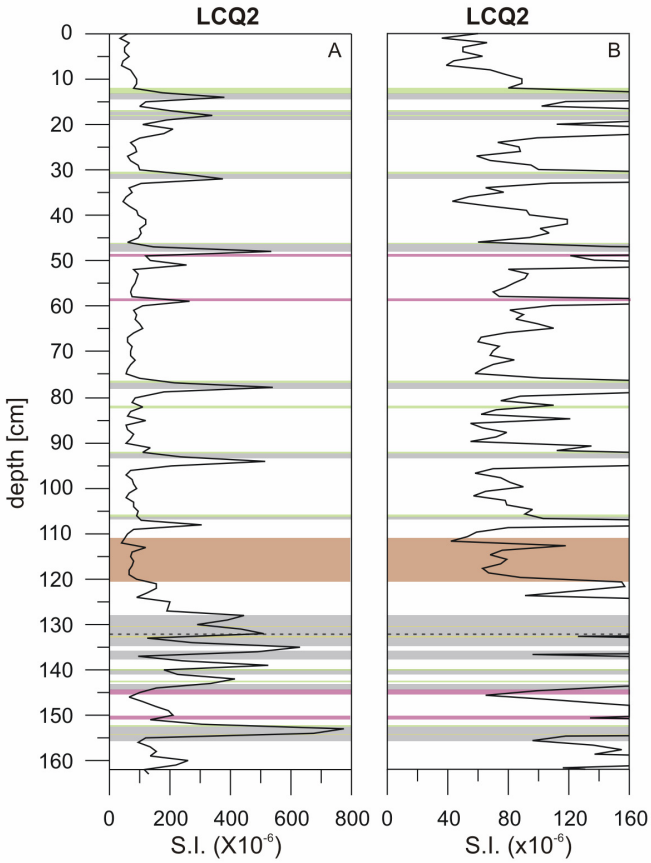

Fig. IV-17: A) Magnetic susceptibility (10^{-6} S.I.) of core LCQ2s achieves highest values in the tephra layers of the sediment core. B) Magnification of the magnetic susceptibility of the normal lacustrine sedimentation.

6.1.2 Magnetic susceptibility

The base of the core is made up of frequent deposited tephra layers which become less frequent towards the top. Values of magnetic susceptibility vary in the range from ~ 40 × 10^{-6} to ~ 800 × 10^{-6}, achieving the highest values in the volcanic ash layers (Fig. IV-17a). These peaks mask the susceptibility variation in the normal lacustrine sediment, especially in the lowest part of the core between 162 and 127 cm. Magnification of the curve show distinct peaks from 105 to 75 cm (Fig. IV-17b). From 75 cm depth, a slight but continuous increase is observed, reaching maximum values between 46 and 43 cm, though they fluctuate between 35 to 25 cm. Between 25 and 20 cm, the curve shows another small peak (Fig. IV-17a,b). From 13 cm depth to the top of the core, magnetic susceptibility decreases continuously.

6.1.3 Lithology and sediment composition

Core lithology is partly characterized by silt-sized laminated sediments. Laminations are fine in the uppermost 13 cm and from 109 to 92 cm depth, but are wider spaced from 92 cm to 24 cm (Fig. IV-18). Indistinct lamina occur between 162 to 143 cm and from 126 to 109 cm. At least 15 distinct tephra layers of different thickness repeatedly interrupt the normal lacustrine sedimentation. The lower part of the core, from 155 to 126 cm, is characterized by frequent volcanic deposits, as it comprises at least eight 0.5 to 2 cm thick tephra layers. No tephra layers were observed between 75 and 56 cm. From 56 cm to the core top, several tephra layers occur again. In this intercept the sediment core contains at least five major volcanic events. Most tephra layers are overlain by a distinct white- to slightly pink- coloured diatom layer of varying thickness, ranging between ~ 1 mm to 1 cm. Diatom layer thickness appears not to be related to the tephra layer thickness. Normal lacustrine sedimentation is clearly disturbed between 111 and 119 cm, where a homogeneous matrix with traces of black organic material occurs. Formation and internal structures of the sediment suggest an earthquake occurred, but this can only be assumed and not proven.

Mineral composition of the sediments was examined by X-ray diffraction (XRD) measurements. Sediments of core LCQ2s have the same mineral composition as the bottom sediments described in Chapter 4. Most prominent minerals are plagioclase (mostly labradorite) and pyroxene (predominatly diopside), with subordinate amorphous components comprising volcanic glass, diatom valves, and most probably amorphous clay minerals (allophone and/or imogolite). The latter has not been proven by FTIR or DTA analyses. All minerals and amorphous components appear in variable proportions throughout the core, and distinct clay mineral phases are rare. The first small peaks of smectite occur at ~ 120 cm, but form only < 5% of the entire mineral spectra. Quantification of the bulk minerals with core depth was abandoned due to the consistent solid solution series of plagioclase and pyroxene.

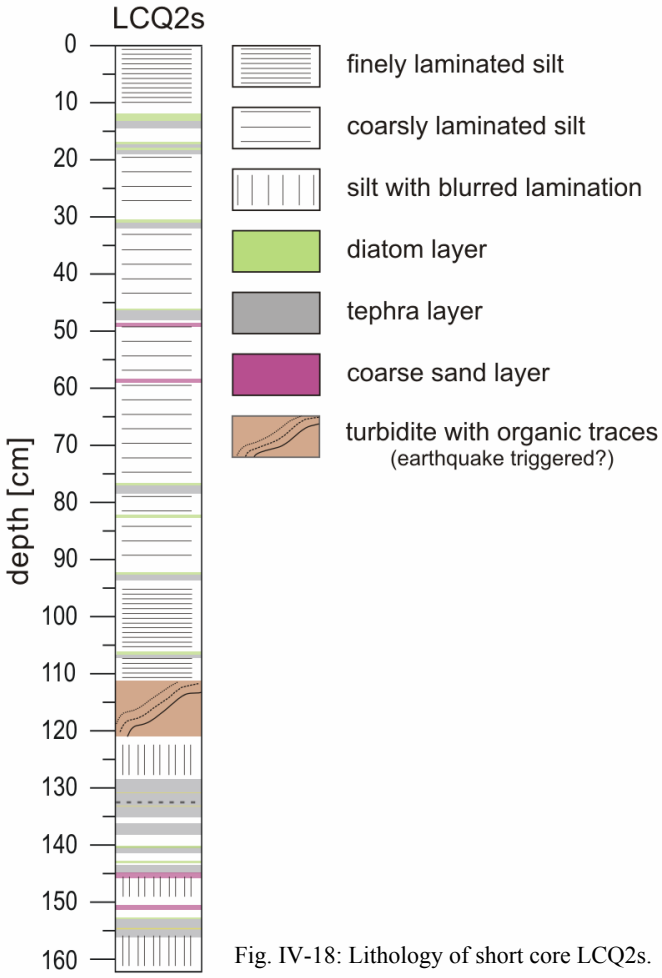

Fig. IV-18: Lithology of short core LCQ2s.

6.1.4 Grain size distribution

The general patterns for mean grain size values are also masked by the coarse tephra layers, seen in Fig. B-1 (Appendix). To detect important changes in sedimentation, the x-axis scale was magnified (Fig. IV-19). Slight changes in the normal lacustrine sedimentation are recorded as changes in the mean value (Fig. IV-19), however individual plots for each grain size fraction reveal greater changes (Fig. IV-20) and will be discussed later.

Excluding large tephra and coarse sand peaks in the grain size curve, the mean grain size of the normal lacustrine sediment ranges between 6 µm and ~ 20 µm (Fig. IV-19). Values are constant around 8 µm between 162 cm to 127 cm, except for the

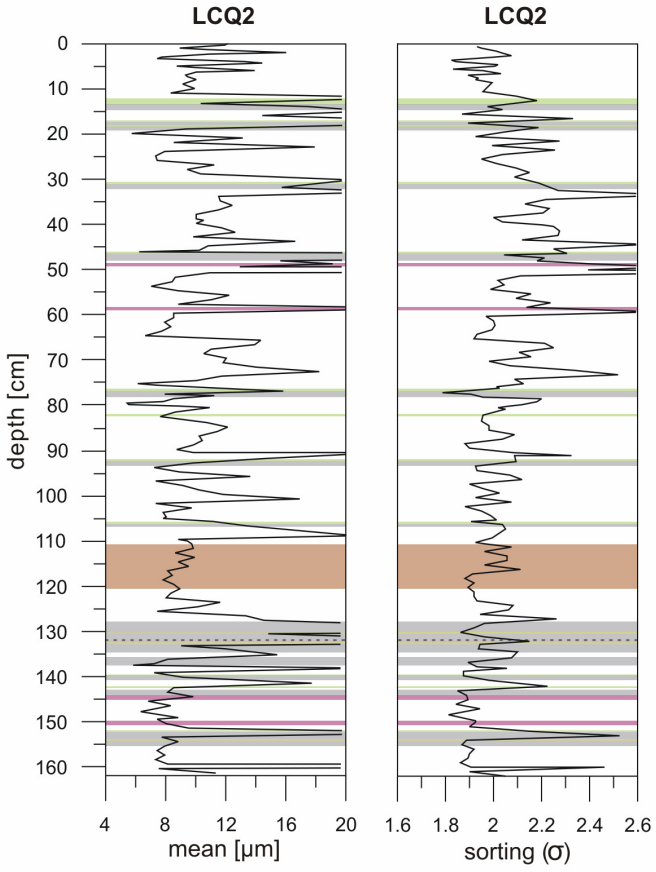

Fig. IV-19: Mean grain size (in µm) and sorting values (in standard deviation units) for short core LCQ2s. Shaded and coloured bands indicate lithology, presented in Fig. IV-18.

intercalated coarse tephra layers. From 127 cm upwards, the grain size curve shows a slight but continuous coarsening trend, which inverts to a fining trend at ~ 40 to 15 cm. From 13 cm to the top of the core, the sediment coarsens slightly. Moderate sorting (after Folk, 1980) of the sediments occurs from 162 to 127 cm. Sorting becomes gradually poorer until an inflection point at ~ 45 cm, where sediments steadily become moderately sorted towards the core top (Fig. IV-19).

Detailed grain size curves for the fractions < 63 µm show that between 162 cm and 90 cm, concentrations of clay and fine-silt are nearly constant (Fig. IV-20). The fine-silt mode follows the clay-size curve, thus suggesting coupling between both fractions. Clay concentrations increase between 90 and 55 cm, but decrease significantly between 55 and 13 cm, though this trend is interrupted by a small but distinct increasing trend between 30 and 20 cm. Towards the top of the core, the clay fraction continuously decreases whereas the fine-silt fraction remains constant, generally following the clay curve pattern. The medium-silt fraction is unchanging from the core bottom to 90 cm, after which its concentration steadily decreases. This decreasing trend inflects at 45 cm, where the concentration begins to increase towards the core top (Fig. IV-20). The coarse-silt fraction shows a slight continuous coarsening upward from the core bottom until 29 cm, with little decreasing tendency to 20 cm. The curve inversely follows the medium silt fraction except during the uppermost 13 cm, where the values remain nearly constant, similar to the medium-silt fraction.

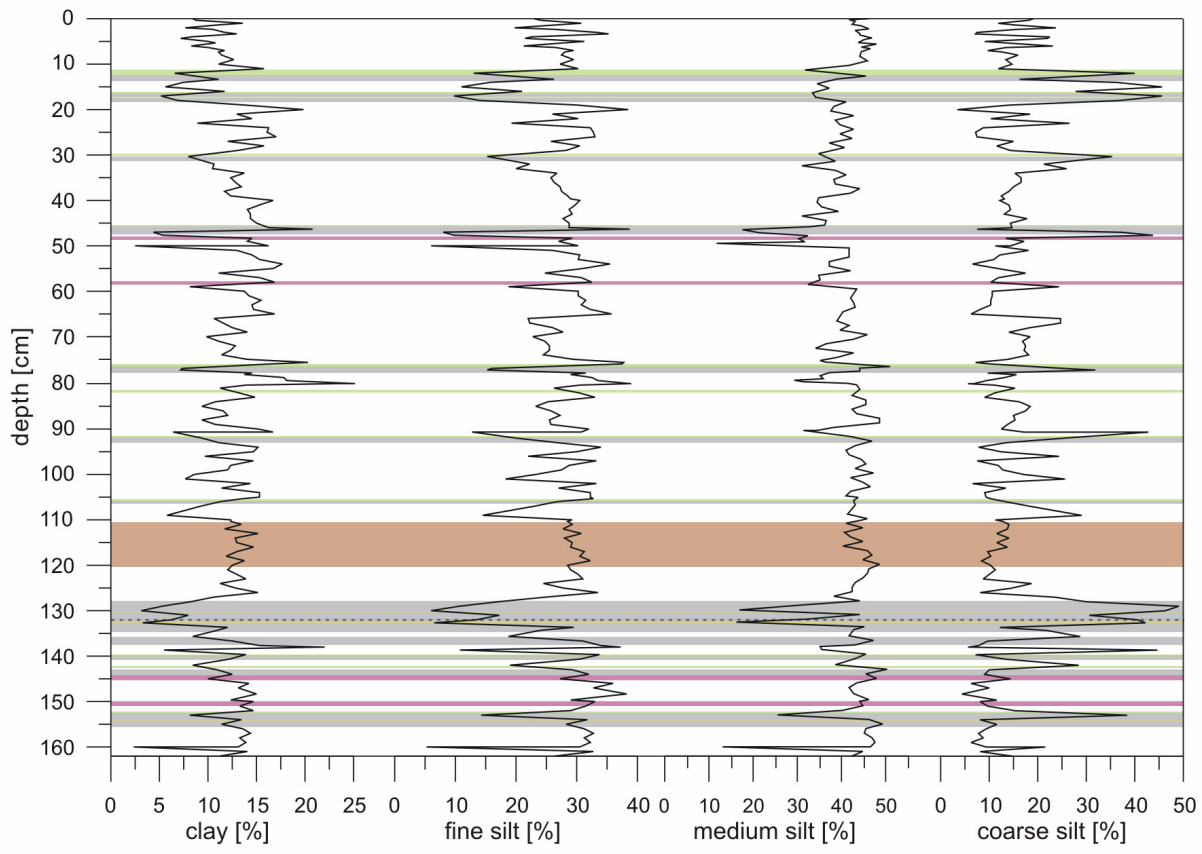

Fig. IV-20: Grain size distribution of individual grain size fractions for core LCQ2s. Shaded and coloured bands indicate lithology, presented in Fig. IV-18.

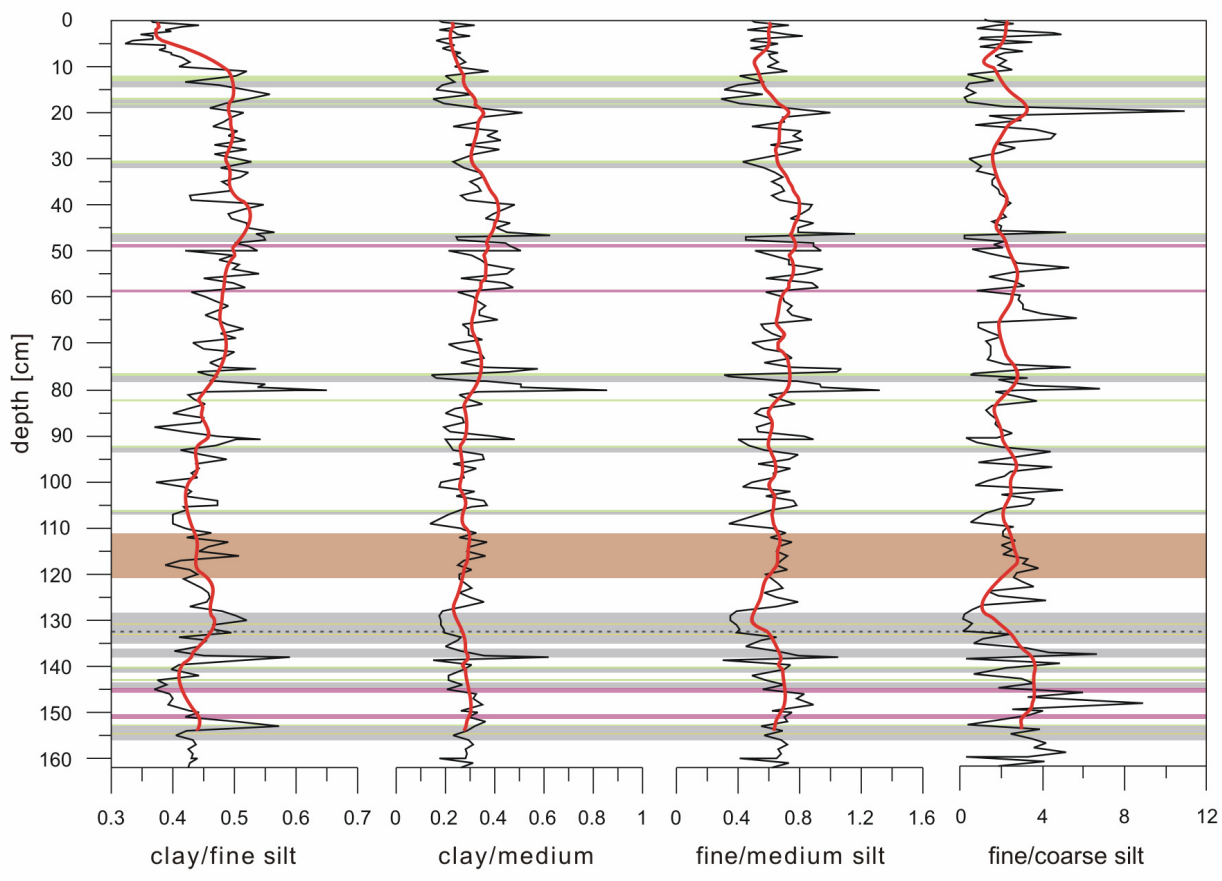

Fig. IV-21: Ratio maps with 11 sample running mean (red line) of clay to fine silt, clay to medium silt, fine silt to medium silt, and fine silt to coarse silt. Shaded and coloured bands indicate lithology, presented in Fig. IV-18.

The relative increases in the individual fractions are seen clearer by plotting ratio curves of clay to fine- and medium-silt, as well as ratios of fine- to medium- and coarse-silt (Fig. IV-21). Increased proportional sedimentation of the clay fraction from 130 to 40 cm is now apparent, as is the decreasing clay trend in the uppermost 40 cm. Increased proportions of the fine- and medium-silt fractions occur through this period (Fig. IV-21).

6.1.5 Carbon and nitrogen

Total carbon content corresponds entirely to TOC, as no TIC was identified by coulometric analyses. TOC and nitrogen curves are parallel, following the same trends throughout the core (Fig. IV-22). TOC values ranges from 0.172% to 3.832%. Extremely low values are observed from the clastic tephra layers, whereas maximum values occur in the uppermost surface layers. The same is true for nitrogen, with the highest values of 0.478% in the same stratigraphic horizon as TOC peaks, and lowest values at 0.038% in volcanic ash layers. Both plots are relatively uniform, and except for strata of tephra impact, they show little diversity. Similarly, the C/N atomic ratio in the normal lacustrine sediment does not vary significantly, but shows a slight decreasing trend from the bottom of the core which is likely a result of terrestrial influx via tephra impact and/or remobilization by the turbidite event recorded from 120 to 111 cm depth. With a total range from 4.66 to 14.53, the C/N atomic ratio achieves lowest values in coarse sand layers and highest values in volcanic ash layers near the core bottom.

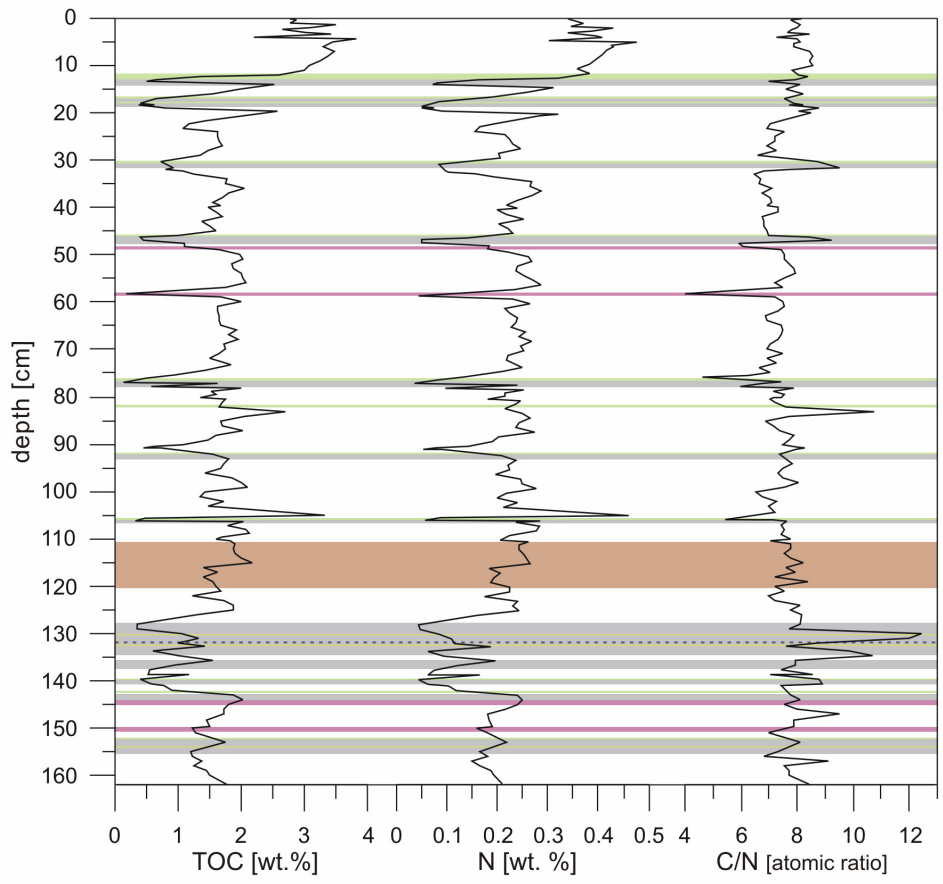

Fig. IV-22: Total organic carbon (TOC) and nitrogen (N) plots as a percent of the total weight, and the C/N atomic ratio for core LCQ2s. Shaded and coloured bands indicate lithology, presented in Fig. IV-18.

6.1.6 Biogenic silica

With an average value of ~ 30.4%, biogenic silica concentration of Lago Calafquén is very high. Concentration values vary between 0.47%, detected in the volcanic ash layers, and 76.8%, measured at the bottom of the core (Fig. IV-23). Concentration steadily decreases from 162 to 127 cm, but changes to a clear large-scale increasing trend in the normal lacustrine sediment, beginning at 127 cm and continuing to 35 cm. The curve increases on a large-scale trend, however internal fluctuations on smaller scales are noted. Between 90 and 33 cm, the highest average concentrations are achieved, with a mean value of 44.23%. Between 70 and 39 cm, the curve inverts to a minimum value at ~ 48 cm. From 13 cm to the core top, concentrations increass. BSi concentration largely follows the TOC concentration (Fig. IV-24). Points where uncoupling occurs are those with increased terrestrial influx.

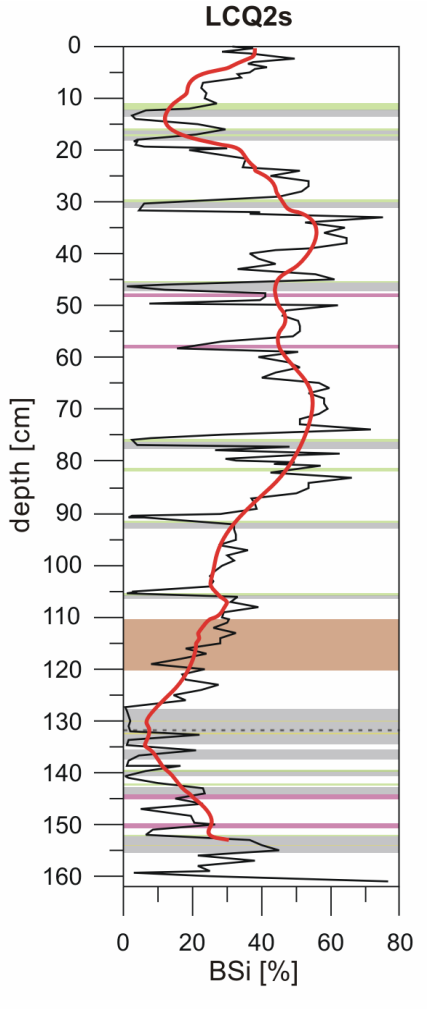

Fig. IV-23: Biogenic silica (BSi) curve of LCQ2s with 11 sample running mean (red line); peak values occur between 90 and 33 cm depth. Shaded and coloured bands indicate lithology, presented in Fig. IV-18.

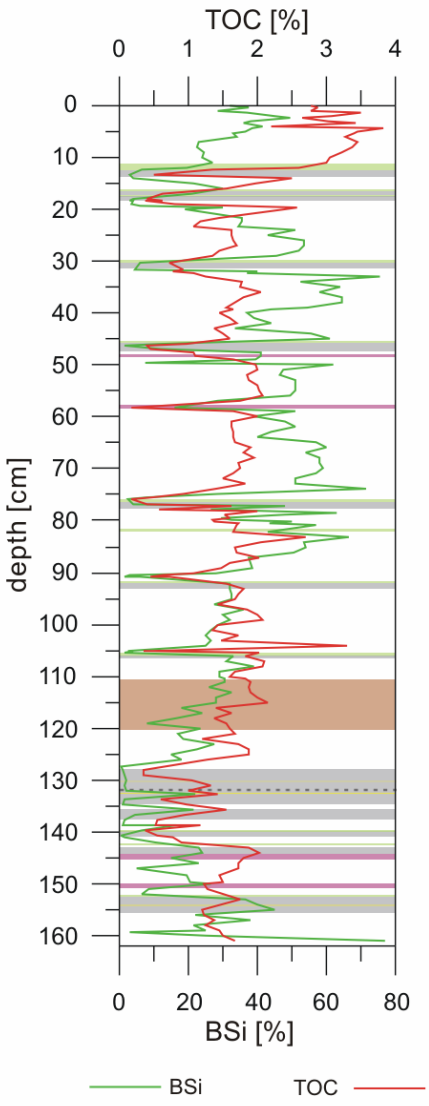

Fig. IV-24: Comparison of biogenic silica (BSi) to total organic carbon (TOC) from short core LCQ2s. Shaded and coloured bands indicate lithology, presented in Fig. IV-18.

6.1.7 Inorganic geochemistry

The catchments of both lakes are dominated by volcanic derived sediments. X-ray, elutriation, and microscopic analyses showed an enrichment in magnetite of these sediments, which leads to a high titanium content (cf. Besoain and Sepúlveda, 1983). These sediments are delivered to the lake basin by annual and seasonal flow, forming the normal lacustrine sediment of the cores. Bulk geochemistry of the sediment was measured by AAS and ICP-MS. To avoid dilution effects, all elements have been normalized against titanium. Original and normalized concentration profiles of all elements are listed in the Appendix (Fig. B-3 to B-25). Discussion is limited to the conservative elements Na and Ca, and the mobile elements Fe and Mn. Between 25 to 15 cm, a loss of sample for Lago Calafquén occurred, therefore this section was excluded in the curves.

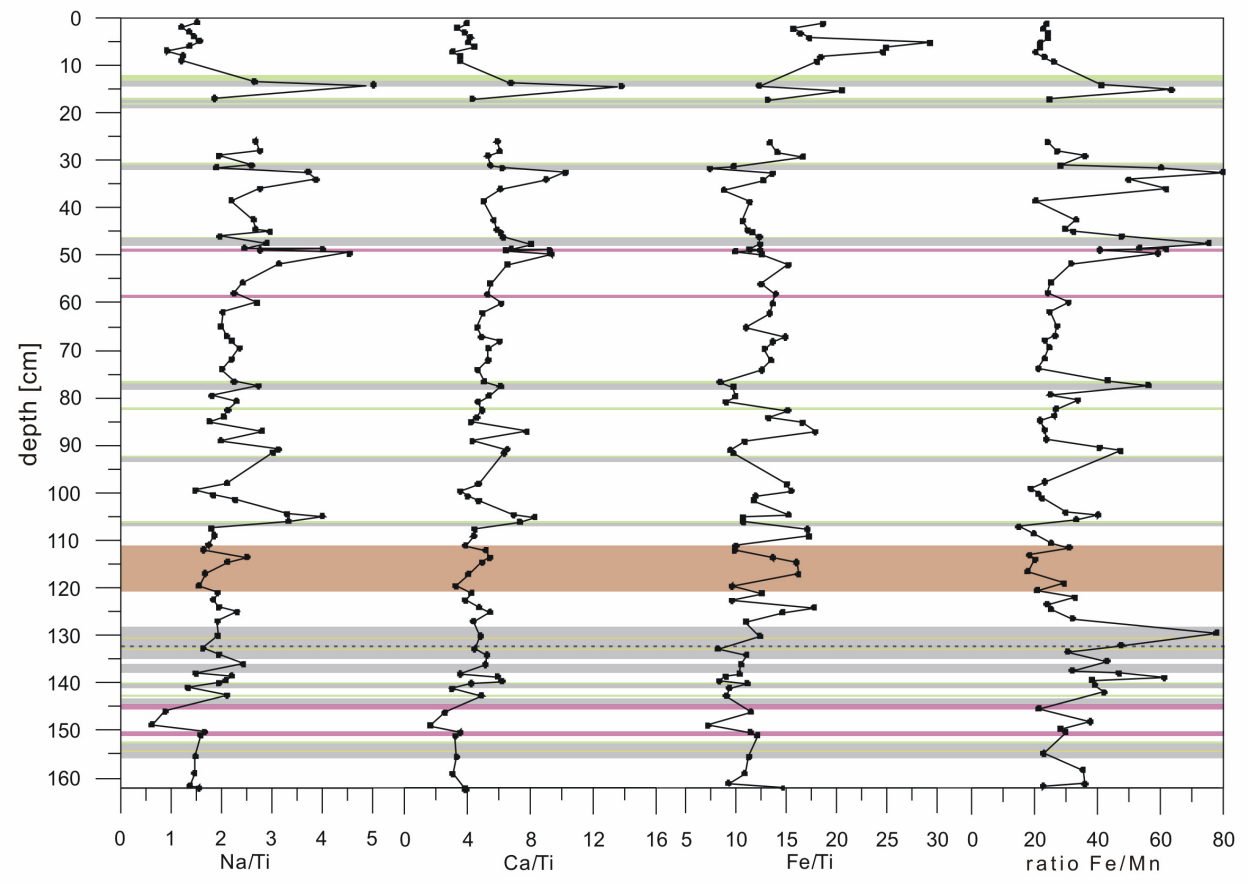

Fig. IV-25: Ti-normalized profiles of Na, Ca, and Fe, and Fe/Mn ratio from short core LCQ2s. Shaded and coloured bands indicate lithology, presented in Fig. IV-18.

In oligotrophic systems, diagenetic processes are minimal, therefore post-depositional modification of the sediments is relatively unlikely, in contrast to more trophic lake systems. The selected elements are considered to represent and/or trace changes in the environment or the lake itself. Ca and Na were selected as they make up nearly the entire mineral spectra of the catchment, bonded in plagioclase, pyroxenes, volcanic glasses and the less abundant clay and amorphous clay minerals. Na and Ca show increase upwards in the core from 1.5 to about 2.5 and 4 to 7, respectively, until an intercalated coarse sand layer at 49 cm (Fig. IV-25). Thereafter, both curves decrease until the core top. Within tephra layers major peaks occur at the base of the layer but decline strongly towards the top of the tephra layer. This might be explained with grading effects of grain size in the tephra rather than with changes in chemical conditions. Apart from the large peaks caused by tephra layers, the smaller peaks and decreases in the profiles backgrounds generally correspond to the shifts and decreases in magnetic susceptibility (cf. Fig. IV-17b). Besides, no other changing levels are observed that might point to a clear shift in catchment.

Iron and manganese form a great part of the deeply weathered soils in the catchment, but these elements are particularly sensitive to redox mobilization (Mackereth, 1966; Förstner and Wittmann, 1979; Boyle, 2001). To separate source changes from lake redox effects, these elements are compared using a Fe:Mn ratio (Fig. IV-25). According to Mackereth (1966), coincidence of peaks in Fe concentration with peaks in the Fe:Mn ratio could be explained by changes in supply from the catchment. If Fe peaks coincide with minima in the Fe:Mn ratio, reducing conditions might be inferred. However, this method is sensitive to remobilization of Fe and Mn in the sediment, and small scale changes do not necessarily relate with supply or capture (Bryant et al., 1997). The Fe:Mn ratio

follows to a large extent the Fe:Mn course for sediment sensitive to hypolimnetic O_2 of biologically-rich soils and lakes introduced by Mackereth (1966). The highs in Fe curve mostly meet minima in the Fe:Mn ratio (Fig. IV-25), probably indicating no effects of source change but rather effects within the lake itself. Peaks in Fe curve mostly meet with minima in Na and Ca and peaks in magnetic susceptibility (cf. Fig. IV-17b).

6.1.8 Age-depth model and accumulation rates

Radio-isotope dating with ^{210}Pb and ^{137}Cs for the uppermost 10 cm of the core was not significant (see Appendix, Fig. B-21), likely due to the influx of unsupported ^{210}Pb and a lack of significant marker horizons in the Southern Hemisphere, except for the 1963 event (cf. Andrello and Appoloni, 2004). Due to the large lake depth and volume, dilution might play an additional role in detection insignificance. The age-depth model (Fig. IV-26) for Lago Calafquén was established by ^{14}C-AMS dating of organic residue of the normal lacustrine sediment, as there was little distinct plant material retrieved. The oldest date, at 162 cm, was performed on a small piece of charred wood. The individual ages are listed in Table IV-1. For improved chronological comparison with other reference ages, the ^{14}C-ages were calibrated into AD/BC dates with 2-sigma error. Ages range between BC 1385 ±78 and AD 1216 ±57, and an age inversion occurred only once at 62 - 61 cm. This sample was not used in the age-depth model (indicated by a red rhombus, Fig. IV-26). The date of AD 1245 ±29 was also rejected, as the number of years that would have elapsed since the next earlier date, AD 1216, would result in an extraordinarily high sedimentation rate during the 17 cm-long section. Sedimentation and accumulation rates were counted on the base of age interval 40 – 0 cm. The time interval between BC 1385 ±78 and BC 101 ±103 (162 to 132.6 cm depth) comprises a long time span within a short core section, which causes an evident offset within the lowermost part of the age-depth model.

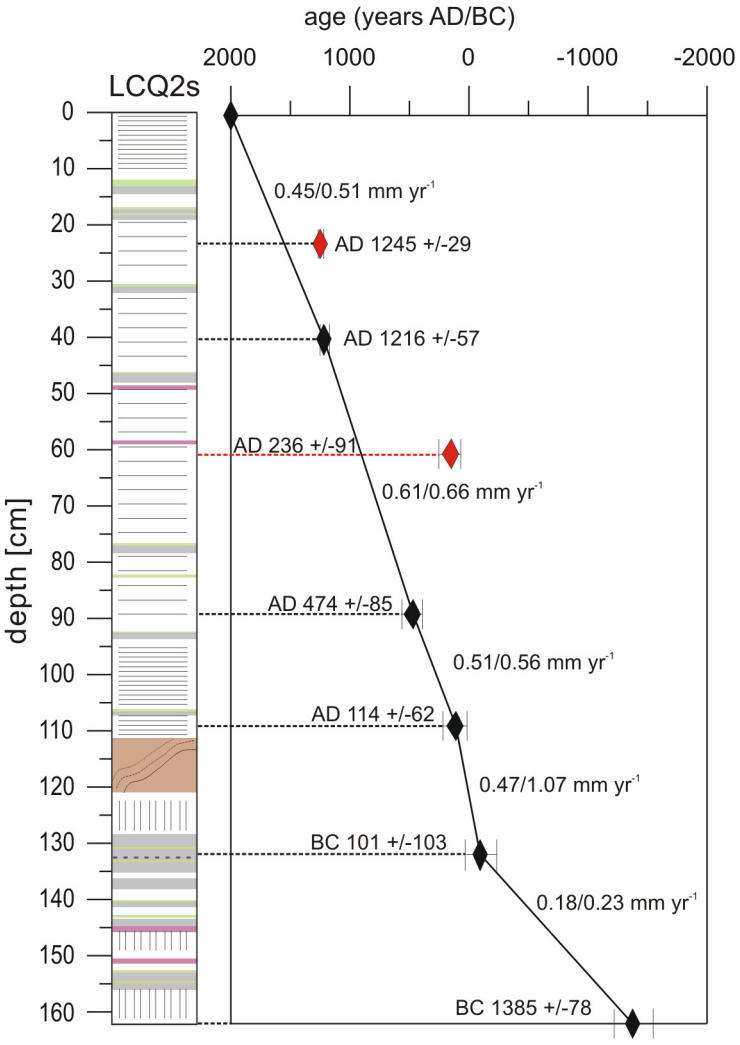

Fig. IV-26: Age-depth model (in years Anno Domini (AD) and Before Christ (BC)) for short core LCQ2s derived from ^{14}C-AMS dating of bulk organics from the normal lacustrine sediment. Numbers before slash indicate sedimentation rates excluding tephra sedimentation, behind the slash including tephra layers. Red rhombus marks indicate refused age. Core lithology is that presented in Fig. IV-18.

To determine if concentrations of the aforementioned parameters were due to changes in supply rate of one or more of the other components, mass accumulation rates (MAR) were calculated

on the basis of the water content and porosity. Mass accumulation rates were calculated for the minerogenic particles of the sediment (after dissolution of the biogenic fraction) as well as for the chemical parameters TOC and BSi. Accumulation rates express the weight of sediment per unit area (Einsele and Hinderer, 1998). Hence, absolute changes of the individual parameters can be estimated. Sedimentation rates (SR) are considered as the thickness of solid sediment during a certain time span. As several tephra layers intercalate the values of SR and MAR, values are presented including and excluding tephras (Table IV-2). The latter was done to estimate the actual catchment triggered sedimentary influx.

depth (cm)	^{14}C age BP	calendar yr. BP	calibrated age AD/BC	years
23	835 ±20	705 ±29	AD 1245 ±29	
40	870 ±31	735 ±57	AD 1216 ±57	785
61	1934 ±35	1805 ±91	AD 236 ±91	
89	1650 ±36	1476 ±85	AD 474 ±85	742
109	2103 ±40	2011 ±113	AD 114 ±62	360
132.6	2145 ±36	2050 ±103	BC 101 ±103	215
162	3180 ±30	3334 ±78	BC 1385 ±78	1284

Tab. IV-1: Uncalibrated and calibrated ^{14}C-AMS data for Lago Calafquén. Red colour indicates excluded dates.

depth (cm)	av. SR (cm a^{-1}) incl. tephra	av. MAR (mg cm^{-2}a^{-1}) incl. tephra	av. SR (cm a^{-1}) excl. tephra	av. MAR (mg cm^{-2}a^{-1}) excl. tephra
0 - 40	0.051	24.15	0.045	21.31
40 – 89	0.066	41.74	0.061	38.58
89 – 109	0.055	30.01	0.051	27.89
109 – 132.6	0.1069	63.69	0.047	28.00
132.6 – 162	0.02	14.80	0.018	13.32

Tab. IV-2: Average sedimentation rates (SR) and mass accumulation rates (MAR) for Lago Calafquén including and excluding tephra layers.

6.1.9 Concentration versus mass accumulation rates

Lake sediments components are usually measured as concentrations relative to sample mass and therefore are not independent from each other. An increase in concentration of one component relative to others mark either a change in supply rate or a decrease in supply rate of one or more of the other components (Boyle, 2001). Mass accumulation rates expressed as fluxes might overcome this problem. Although dating is available, MAR values are less precise than concentration data as not every sample interval is dated and, therefore, biases are added into the calculation. Furthermore, fluxes may vary significantly within a lake dependent from the locality the cores are taken. Therefore, representative flux rate would require the investigation of many other cores as well. According to Boyle (2001), concentration data record subtle changes of the relative importance of any component in the sediment supplied. Determining which component has changed can be approached either by expressing greatest fluxes of components with MAR data or by analyses of variation of components in concentration curves.

Sediment parameters (grain size, BSi, and TOC) from Lago Calafquén are compared using concentration profiles. Additionally, MAR values for the normal lacustrine sediment and the biogenic components were calculated to verify changes and inter-relationships. The concentration comparisons of individual grain size fractions with BSi (Fig. IV-27) and TOC (Fig. IV-28) show that both biogenic parameters inversely follow clastic sediment input. Only the interval between 45 and ~ 36 cm reveals an almost congruent course of BSi to the medium-silt fraction, but an inverse trend to all other fractions. A second correlation of BSi to fine- and medium-silt is observed between ~ 29 and ~ 24 cm, thus implying a change in grain size. After this interval, grain size and biogenic silica patterns diverge. From the core bottom to ~ 36 cm (Fig. IV-28), TOC follows the characteristics of BSi and grain size curves, but to 20 cm, the TOC curve follows the course of clay, fine- and medium-silt fractions but deviates from the BSi pattern. This suggests that TOC in this part of the core is controlled more by terrestrial supply than by autochthonous sources.

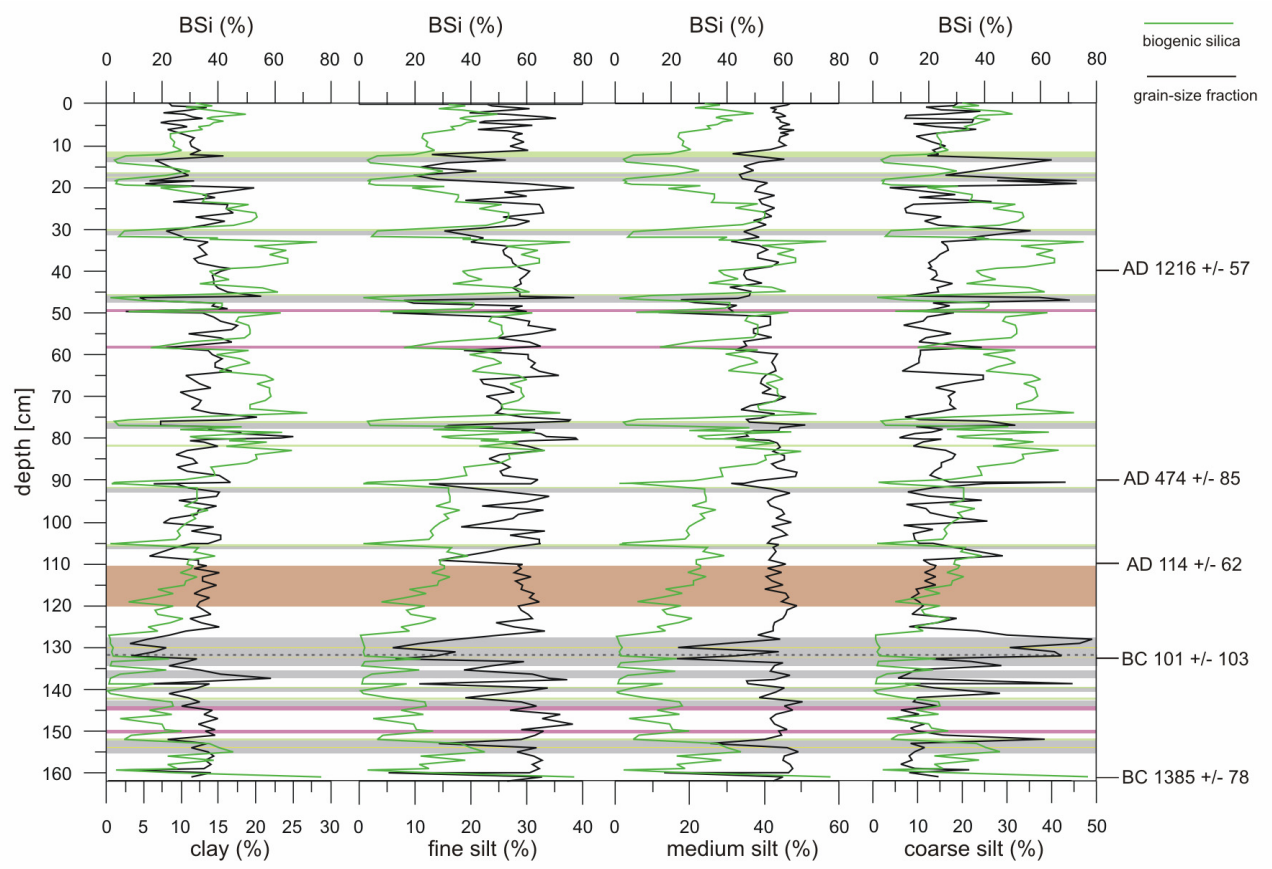

Fig. IV-27: Comparison of biogenic silica (BSi) with individual grain size fractions (percent clay, fine silt, medium silt, and coarse silt) from short core LCQ2s. Dates are those obtained using the age-depth model presented in Fig. IV-26. Shaded and coloured bands indicate lithology, presented in Fig. IV-18.

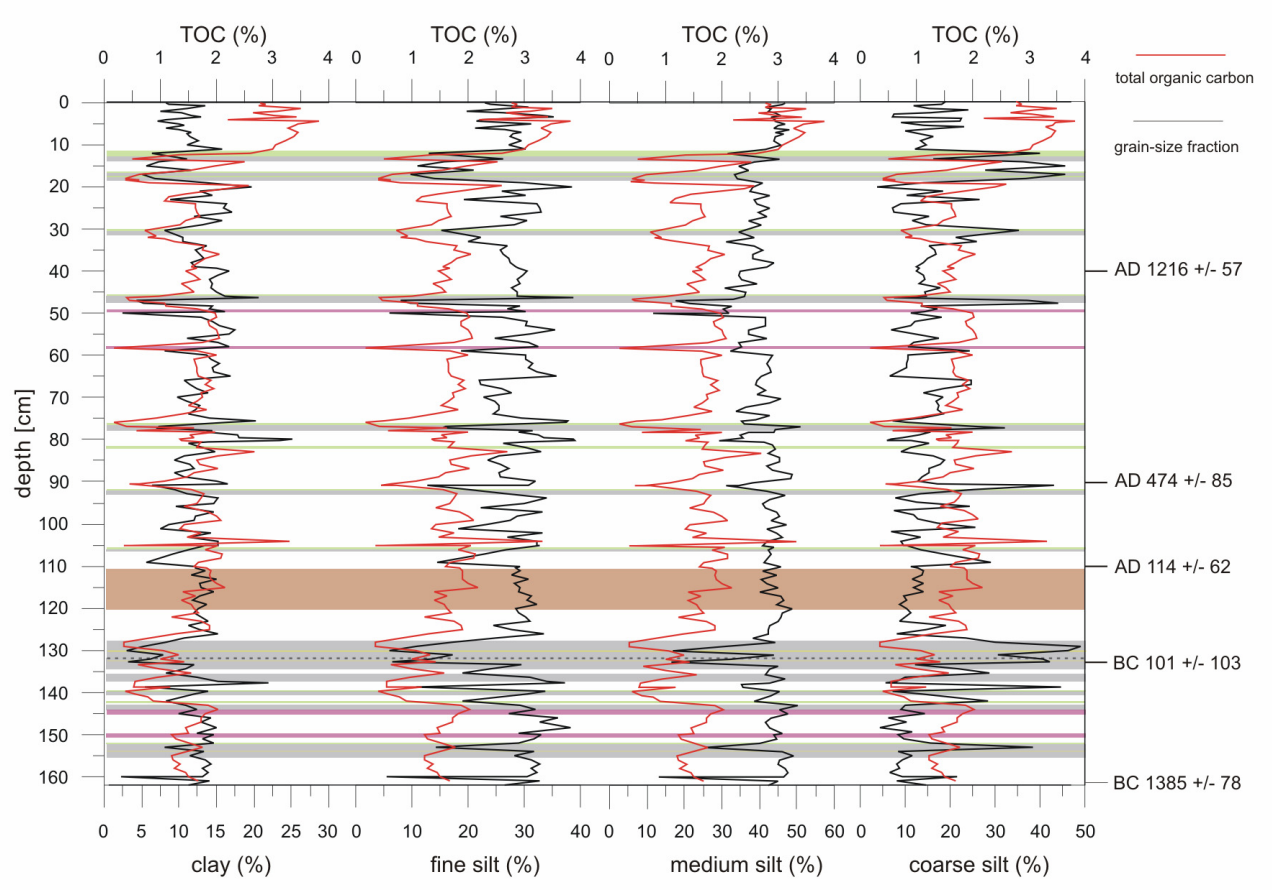

Fig. IV-28: Comparison of total organic carbon (TOC) with individual grain size fractions (percent clay, fine silt, medium silt, and coarse silt) for short core LCQ2s. Dates are those obtained using the age-depth model presented in Fig. IV-26. Shaded and coloured bands indicate lithology, presented in Fig. IV-18.

MAR profiles largely follow the BSi and TOC concentration profiles (Fig. IV-29). Increased concentrations are connected to increased mass accumulation and *vice versa*. Increases in TOC and BSi concentrations between 110 and ~ 106 cm are linked to smaller flux rates. The same is observed between 103 and 93 cm. A further small increase in BSi concentration between 100 and 95 cm is not observed in BSi MAR but rather in the TOC MAR. Between 46 and ~ 28 cm, TOC fluxes decrease as BSi flux increases and the opposite occurs from 28 to 19 cm. Nothing can be inferred for the period between 18 and 14 cm, as no data was determined. Over the entire core, BSi has an average MAR of 6.78 mg cm^{-2} a^{-1}. For the section between 90 and ~ 30 cm, which is characterized by a clear increase in concentration, the average MAR is 8.78 mg cm^{-2} a^{-1}. TOC follows a similar trend, with a whole-core MAR average of 0.51 mg cm^{-2} a^{-1} and 0.36 mg cm^{-2} a^{-1} for the section between 90 and ~ 30 cm.

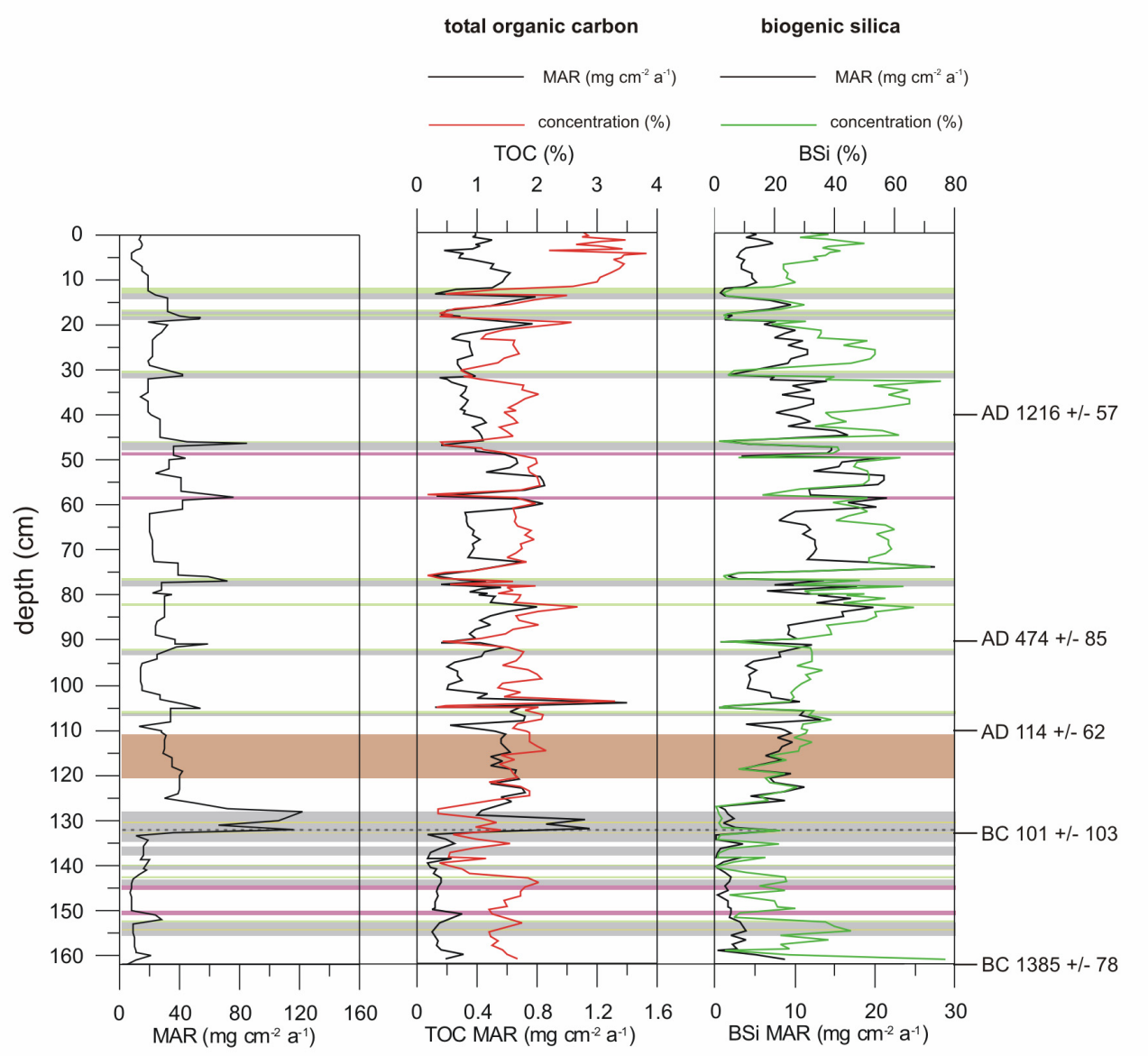

Fig. IV-29: Total mass accumulation rates (MAR), MAR of total organic carbon (TOC) versus TOC concentration, and MAR biogenic silica (BSi) versus BSi concentration profiles of Lago Calafquén, short core LCQ2s. MAR pattern largely follow the course of the concentration profile. Dates are those obtained using the age-depth model presented in Fig. IV-26. Shaded and coloured bands indicate lithology, presented in Fig. IV-18.

6.2 Lago Villarrica

In Lago Villarrica four cores were taken from all sites with differing predominant currents described in Chapter 4. High-resolution, multi-proxy analysis was applied on sediments from coring site LVR4s located next to the island Isla de Aillaquillén (cf. Fig. III-3b). This locality is less influenced by turbidites, The core covers 114 cm and comprises a continuous record of normal lacustrine sediments, which is less interrupted by extraordinary events from outside the lake.

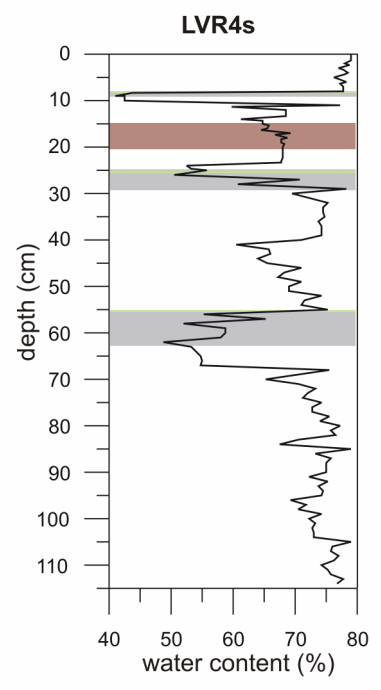

6.2.1 Water content

Water content of core LVR4s decreases up the core with variation of 65% to 82% (Fig. IV-30), and increases slightly within the first 20 cm. It fluctuates on a minor scale, but at 40 cm a sudden shift from ~ 60% to ~ 80% occurs, which continues up to 30 cm depth. Within the tephra strata water content drops to < 50%.

Fig. IV-30: Water content (in percent) of short core LVR4s.

6.2.2 Magnetic susceptibility

Values of magnetic susceptibility vary in the range between ~ 45 × 10^{-6} and ~ 550 × 10^{-6}. Strongest peaks occur in each of the ash layers (Fig. IV-31a). An enlargement of the background line shows a slight large scale increase from centimetres 114 to nearly 86 (Fig. IV-31b). This trend continues after a small decreasing offset up to centimetre 20. Since then a continuous decrease until the top of the core is observed. Fluctuation of the background line within these small intercepts might be linked to changes in the supply or within the catchment.

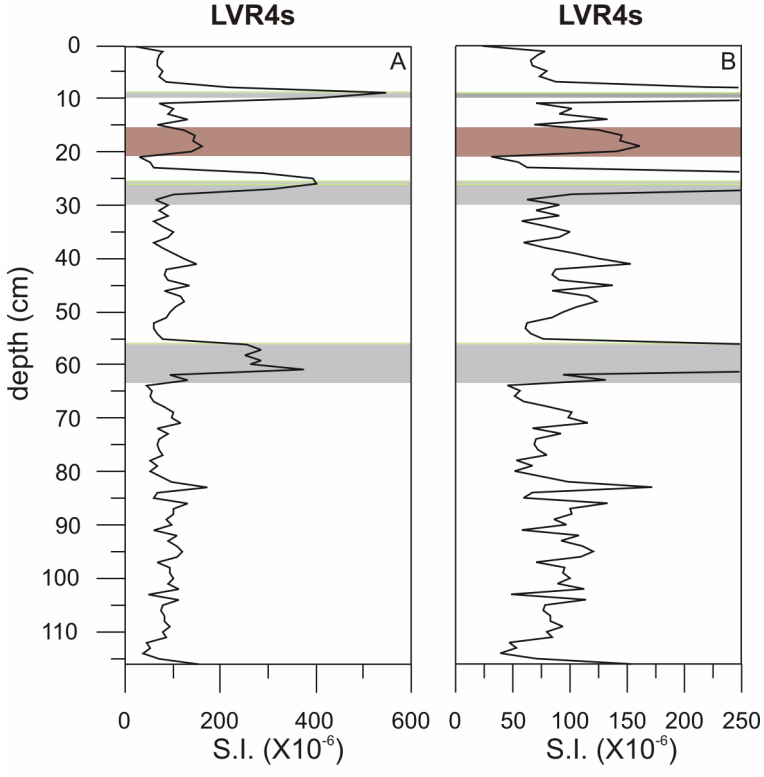

Fig. IV-31: A) Magnetic susceptibility (10^{-6} S.I.) of core LVR4s records discrete peaks within each tephra layer except for 26 cm to 29 cm. B) Magnification of the magnetic susceptibility of the normal lacustrine sedimentation.

6.2.3 Lithology and composition

Core lithology is characterized by dark grey to brown and grey to black silt-sized sediment with moderate lamination. Organic enrichment is high on the first 9.5 cm, visible by the dark colour and black traces in the sediment, although black colour recedes between 5 cm to 9.5 cm. From 15 cm to 21 cm depth the colour of the sediment suddenly changes to homogeneous light grey brown. Sediment within this depth is very aerated. Due to gas enrichment it was torn from the original sediment succession. This strata might represent a larger turbidite impact, but this cannot be definitely stated. Within the intercept between centimetres 9 to 29 three tephra layers intercalate the sediment, each of them superimposed by a diatom layer (Fig. IV-32). Grading of the last of the tephra triplet in 26 cm to 29 cm depth was clearly visible when the core was sub-sampled. From centimetre 35 to 55 sediment colour changes to lightish grey to grey brown within this intercept and sediment becomes quite stiff but lamination remains moderate. In depth 56 cm to 62 cm a major ash layer is recorded, again overlain by a diatom layer. It cannot definitely be said if this strata represents an air borne volcanic ash layer, accumulated after subaerial input or if this accumulation originates from a major turbidite, supplied by subaquatic or maybe subaerial influx. Downcore from 62 cm to 80 cm lamination of the normal lacustrine sediment becomes somewhat finer but sediment colour does not change. From 82 cm until the bottom of the core at least five light grey to pinkish diatom layers are recorded with neither a proof of underlying volcanic ashes nor turbidite evidence. Within this last intercept sediment becomes softer again. From the top until centimetre 65 the sediment is strongly aerated which is related to high gas content. Photographic documentation of all cores is found in Fig. A-5 to A-7 of the Appendix.

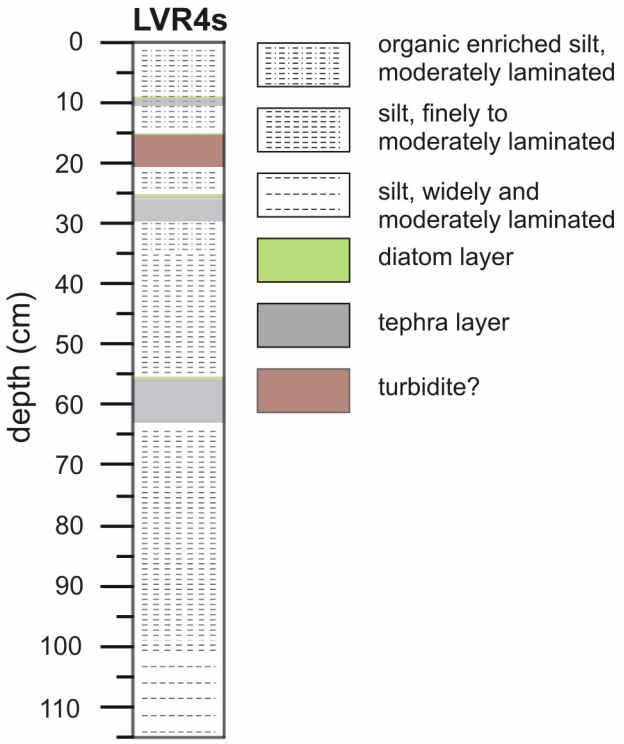

Fig. IV-32: Lithology of short core LVR4s.

Mineral composition of the sediments was examined by XRD measurements and resembles those described for the bottom sediments in Chapter 4. Also here plagioclase and pyroxene form the common mineral phases with subordinated amorphous components comprising volcanic glass, diatom valves, and most probably amorphous clay minerals.

6.2.4 Grain size distribution

Grain size variance is masked by the strongest peaks that occur in the tephra layers. For an evaluation of grain size variance it was therefore necessary to neglect the largest particles settled within the ash layers in core LVR4s. Focussing on the background line an enlargement of the mean grain size curve shows a clear fining upward between 114 cm to the base of the first ash layer in 62 cm depth (Fig. IV-33). From 55 cm depth until the top of the core a steady and continuous coarsening

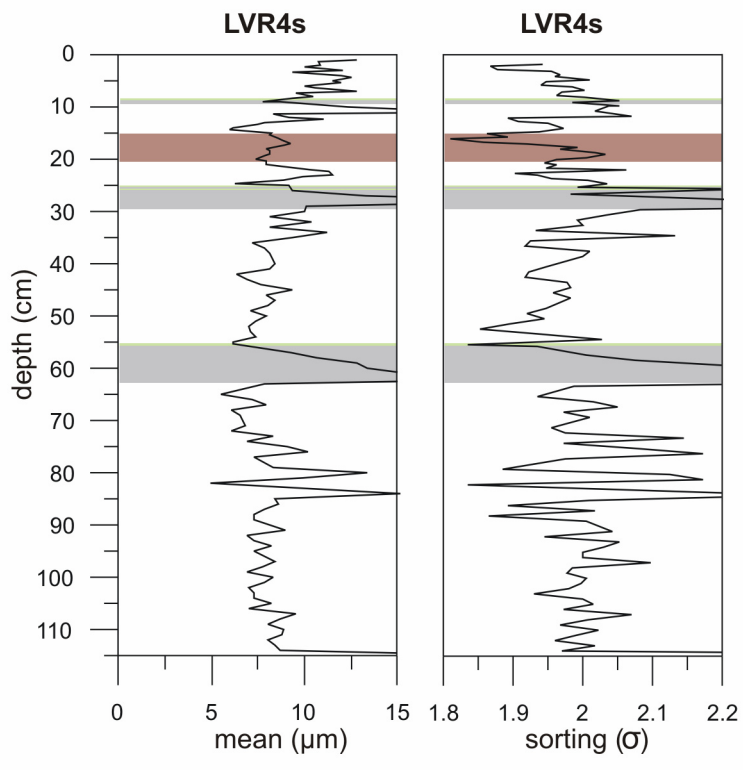

Fig. IV-33: Mean grain size (in µm) and sorting values (in standard deviation units) for short core LVR4s. Shaded and coloured bands indicate lithology, presented in Fig. IV-32.

upward is recorded. Excluding volcanic ash layers the mean grain size of the normal lacustrine sediment is very fine and ranges between 4.5 µm and ~ 12.8 µm (Fig. IV-33). Between 84 cm and 80 cm two clear peaks in the mean curve parallel the records of sorting and the individual coarse grain fractions. Within the intercept between 114 cm to 90 cm sediments are constantly moderate to poorly sorted with little variance in the curve (Fig. IV-33). Up until 70 cm depth sorting fluctuates strongly. Sediments again become moderately to poorly sorted until the top of the core with small variances between 52 cm to 33 cm depth.

Comparison of the individual grain fractions shows that clay and fine silt fraction parallel almost throughout the entire core from the bottom to the top (Fig. IV-34), and both curves follow inversely to medium silt. Influx of clay

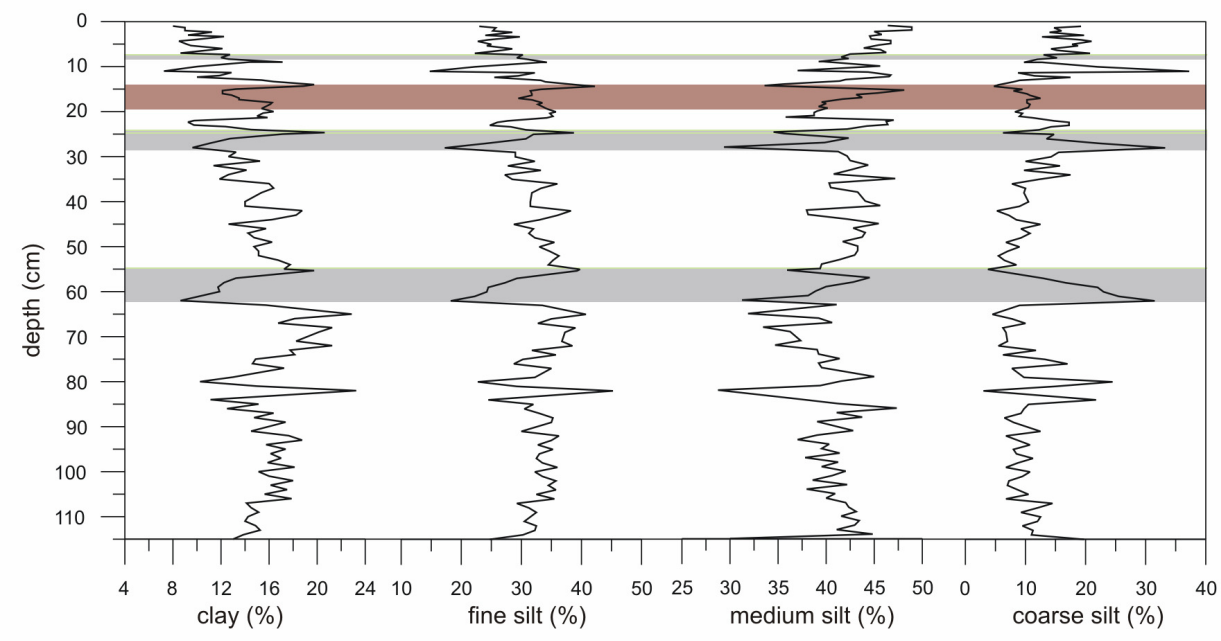

Fig. IV-34: Grain size distribution of individual grain size fractions for core LVR4s. Shaded and coloured bands indicate lithology, presented in Fig. IV-32.

and fine silt increases from the bottom until 93 cm and decreases for the subsequent 8 cm. Up until the base of the first ash layer in 62 cm depth both curves again record a steady increase, which inflects after ash layers to a continuous decrease in fine mode records (Fig. IV-34). Medium and coarse silt fractions mimic their general large-scale pattern quite continuous from the bottom to the top of the core. For the benefit of the fine mode both coarse fractions show the inverse trend throughout the

entire core intercept (Fig. IV-34). As the increasing and decreasing trends of each grain size fraction is clearly traceable in the individual concentration profiles a comparison of proportionate concentration variance by grain-size ratio maps can be abandoned.

6.2.5 Carbon and nitrogen

Neither in Lago Villarrica carbonate compounds had been identified, concluding total carbon corresponds entirely to TOC. Nitrogen and TOC curves are parallel, following the same trends throughout the core (Fig. IV-35). Lowest TOC values occur in the volcano-clastic ash layers with 0.884%. Highest values are measured in the surficial layers with 6.119%. Nitrogen ranges with highest values of 0.473% at the top of the core to lowest values of 0.09% in volcanic ash layers. Both curves are relatively constant but show a slight decreasing trend until 39 cm. The intercept between 39 cm and 22 cm depth reveals an increasing trend until the base of the second ash layer but inflects to a sudden decrease until the base of the third ash layer in 15 cm depth. These trends are clearly reflected by the C/N atomic ratio. With a total range from 3.34 to 31.30 the C/N atomic ratio achieves lowest values in a coarse ash layer and highest in surficial layers at the bottom of the core, corresponding the TOC course. The C/N atomic ratio does not show any larger diversification except in 47 cm depth, where a sudden shift in the C/N atomic ratio is recorded.

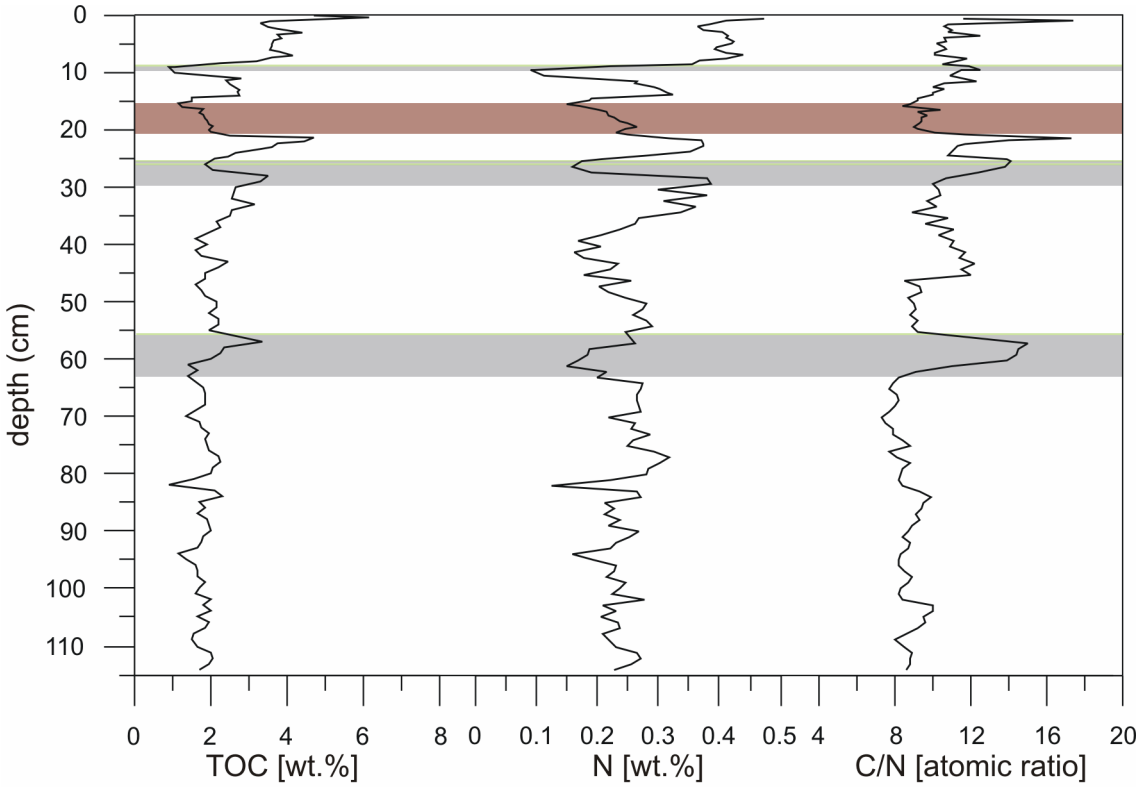

Fig. IV-35: Total organic carbon (TOC) and nitrogen (N), plots as a percent of the total weight, and the C/N atomic ratio for core LVR4s. Shaded and coloured bands indicate lithology, presented in Fig. IV-32.

6.2.6 Biogenic silica

With an average value of 28.38% biogenic silica concentrations of Lago Villarrica are somewhat smaller than those measured in Lago Calafquén. Biogenic silica concentration in core LVR4s decreases continuously from the bottom to the base of the first ash layer in 62 cm depth

(Fig. IV-36). Values vary from 28% to 45% excluding extreme lows at 95 cm and 85 cm, thus giving an average concentration of 34.83%. Although BSi concentration pattern rises after recovery of the ash impact, concentration range remains lower in the core intercept between 56 cm and 27 cm depth. Here, BSi values range from 20% to max. 40%, showing a decreased average of 28.68% in comparison with the downcore intercept. For the upper 24 cm core length until the top BSi concentration ranges from 11% to 37% with a somewhat lower average value of 27.9%, lacking larger fluctuations. Overall BSi fluctuations in core LVR4s reflect large-scale trends but are lacking complex internal patterns as they have been recorded and described for Lago Calafquén. A comparison of BSi and TOC concentrations shows an almost parallel trend of TOC to BSi (Fig. IV-37). Within the intercepts of centimetres 15 to 20, 47 to 52, 71 to 79, and 86 to 89 TOC concentrations develop inversely to an increase of BSi concentration.

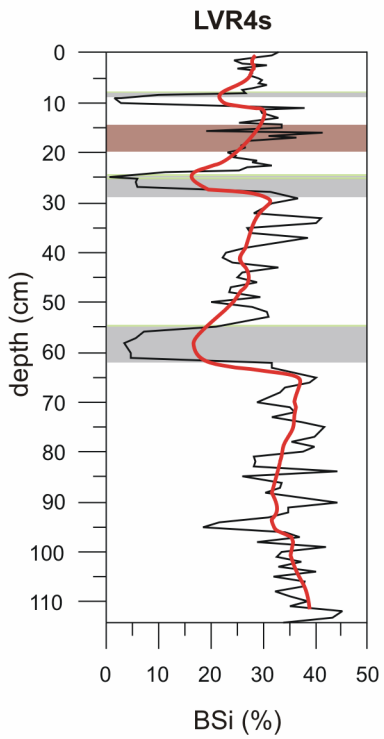

Fig. IV-36: Biogenic silica (BSi) curve with 11 samples running mean (red line) for core LVR4s. Shaded and coloured bands indicate lithology, presented in Fig. IV-32. Shaded and coloured bands indicate lithology, presented in Fig. IV-32.

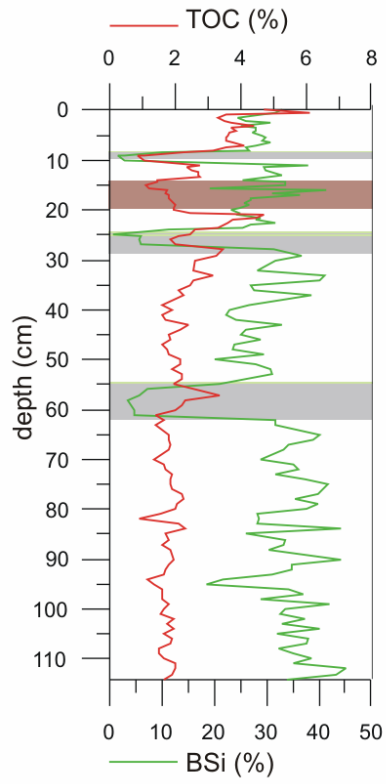

Fig. IV-37: Comparison of biogenic silica (BSi) to total organic carbon (TOC) for short core LVR4s. Shaded and coloured bands indicate lithology, presented in Fig. IV-32.

6.2.7 Inorganic geochemistry

Upwards until the base of the first ash layer in 62 cm core depth the Na/Ti and Ca/Ti ratio show a slight increasing trend, which turn into a decreasing upward until the top of the core (Fig. IV-38). Some major fluctuation occurs within the intercept 56 cm to 40 cm, showing an internal increase within the large-scale decreasing pattern of the curves. These fluctuations correspond to an undulation in magnetic susceptibility which is recorded in the same core intercept (cf. Fig. IV-31).

The Fe/Ti ratio slightly decreases from the bottom up to 62 cm depth. Within the intercept between 54 and 33 cm depth the Fe/Ti ratio increases clearly. Although the curve shows some larger

fluctuations the way up the core its average value remains quite constant. This can also be deduced by the Fe/Mn ratio which remains quite in line except some positive peaks within the volcanic ash layers. Peaks of the Fe curve mostly meet peaks of the Fe/Mn ratio.

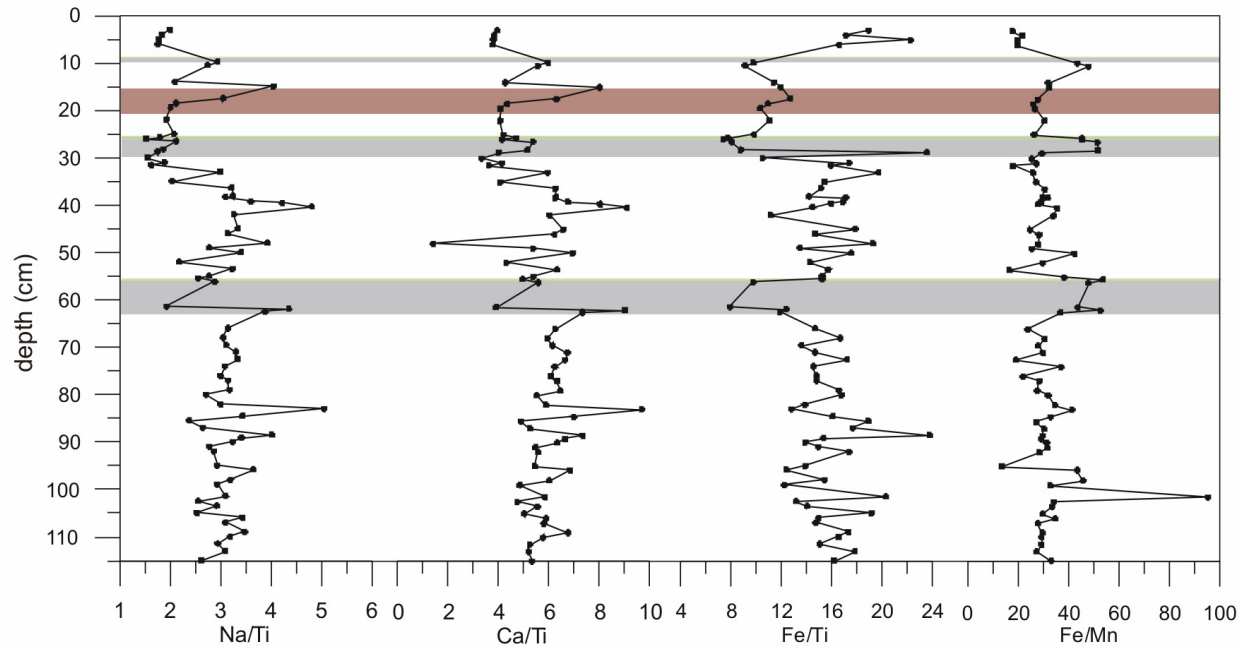

Fig. IV-38: Ti-normalized profiles of Na, Ca, and Fe, and Fe/Mn ratio for short core LVR4s. Shaded and coloured bands indicate lithology, presented in Fig. IV-32.

6.2.8 Age-depth model

For Lago Villarrica radio-isotope dating with ^{210}Pb and ^{137}Cs for the uppermost 10 cm of the core was neither significant (see Appendix, Fig. B-22). The age-depth model (Fig. IV-39) for Lago Villarrica was established by ^{14}C-AMS dating of plant material and organic residue of the normal lacustrine sediment. Ages have been

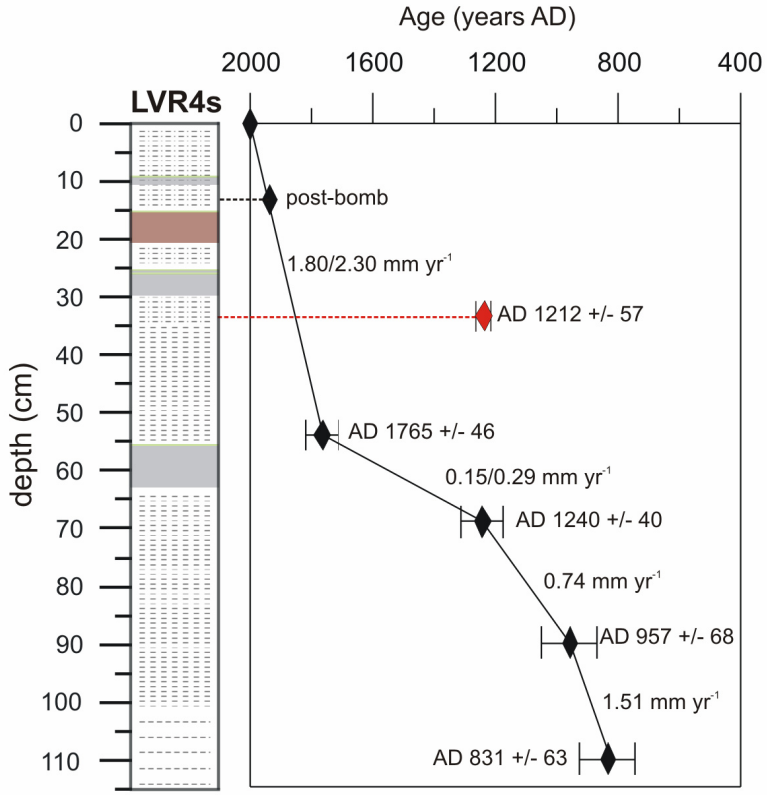

Fig. IV-39: Age-depth model for LVR4s (in years Anno Domini (AD)) for short core LVR4s established on ^{14}C-AMS dating of bulk organics from the normal lacustrine sediment. Numbers before slash indicate sedimentation rates excluding tephra sedimentation, behind the slash including tephra layers. Red rhombus marks indicate refused age. Post-bomb age refers to a date after the 1963 maximum in atmospheric weapons testing. Core lithology is that presented in Fig. IV-32.

calibrated to AD/BC ages with 2-sigma error. Core LVR4s only reveal ages of the AD period, which increase with depth. They range from AD 831 ±63 until post-bomb age in 13 cm core depth. Age inversion was detected once within 33-34 cm depth. This sample was excluded, indicated by a red rhombus (Fig. IV-39). The individual ages are listed in Table IV-3. Sedimentation rates and mass accumulation rates including and excluding volcanic ash layers are given in Table IV-4.

depth (cm)	^{14}C age BP	calendar yr. BP	calibrated age AD/BC	years
13	postbomb	-	>AD 1954	
33	882 ±31	740 ±57		
54	236 ±39	185 ±46	AD 1765 ±46	236
69	837 ±31	710 ±40	AD 1240 ±40	525
90	1129 ±40	993 ±68	AD 957 ±68	283
109	1200 ±28	1120±63	AD 831 ±63	126

Tab. IV-3: Uncalibrated and calibrated ^{14}C-AMS data for Lago Villarrica. Red lines mark excluded ages.

Depth (cm)	av. SR (cm a^{-1}) incl. tephra	av. MAR (mg cm^{-2} a^{-1}) incl. tephra	av. SR (cm a^{-1}) excl. tephra	av. MAR (mg cm^{-2} a^{-1}) excl. tephra
0-54	0.23	93.5	0.180	73.18
54-69	0.029	15.7	0.015	8.12
69-90	0.074	23.04	0.074	23.04
90-109	0.151	47.05	0.151	47.05

Tab. IV-4: Average sedimentation rates (SR) and mass accumulation rates (MAR) for Lago Villarrica including and excluding tephra layers.

6.2.9 Concentration versus mass accumulation rates

The comparison of individual grain size fractions with BSi and TOC concentrations shows that both biogenic parameters mainly follow inversely to clastic sediment input. Within some intercepts biogenic silica correlates positively with clay, medium and coarse silt fraction, whereas hardly any correlation within the fine silt mode can be observed (Fig. IV-40). Clay, medium and coarse silt fraction show an apparent but small positive correlation with BSi from 22 cm to 17 cm depth. The same can be observed from 35 cm to 33 cm, but here clay follows an inverse trend to the coarse fraction and BSi. TOC concentration aligns with grain size in some larger intercepts (Fig. IV-41). From the lowermost section up to 62 cm core depth TOC largely mimics the coarse silt mode. Within the subsequent intercepts TOC correlates positively from 47 cm to 40 cm, 35 cm to 33 cm, 25 to 20 cm and from 9.2 cm to present day.

MAR values for BSi decrease continuously from the bottom of the core towards 62 cm depth from a maximum of ~ 18 mg yr^{-1} to lowest values < 5 mg yr^{-1}, but concentration remains constant (Fig. IV-42). The TOC MAR follow the same trend within the same core intercept, but this trend turns after the first ash accumulation, where BSi MAR and TOC MAR and their concentrations align positively. Within the subsequent intercept TOC fluxes nearly doubles up until 43 cm depth. This trend achieves a maximum within the subsequent intercept over the second ash layer. Between 25 cm to 16 cm TOC fluxes invert from BSi fluxes but align within the uppermost 9 cm until the top of the core.

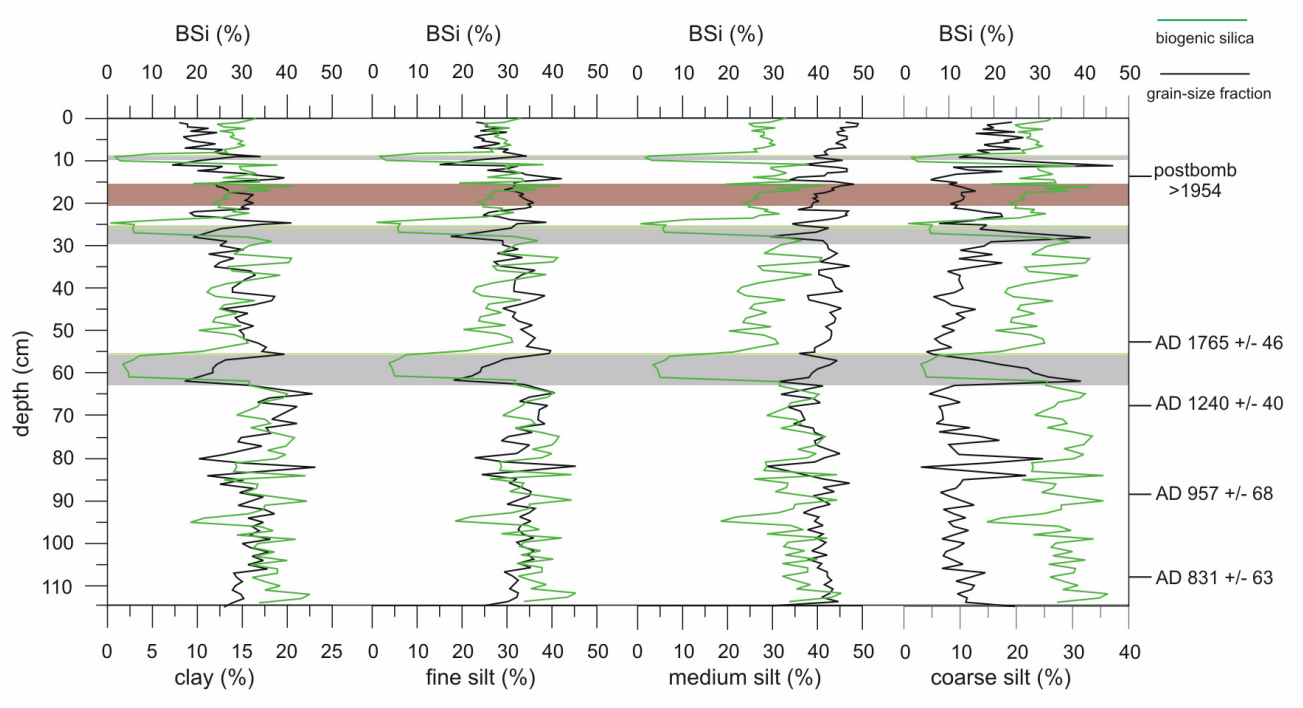

Fig. IV-40: Comparison of biogenic silica (BSi) with individual grain size fractions (percent clay, fine silt, medium silt, and coarse silt) for short core LVR4s. Dates are those obtained using the age-depth model presented in Fig. IV-39. Shaded and coloured bands indicate lithology, presented in Fig. IV-32.

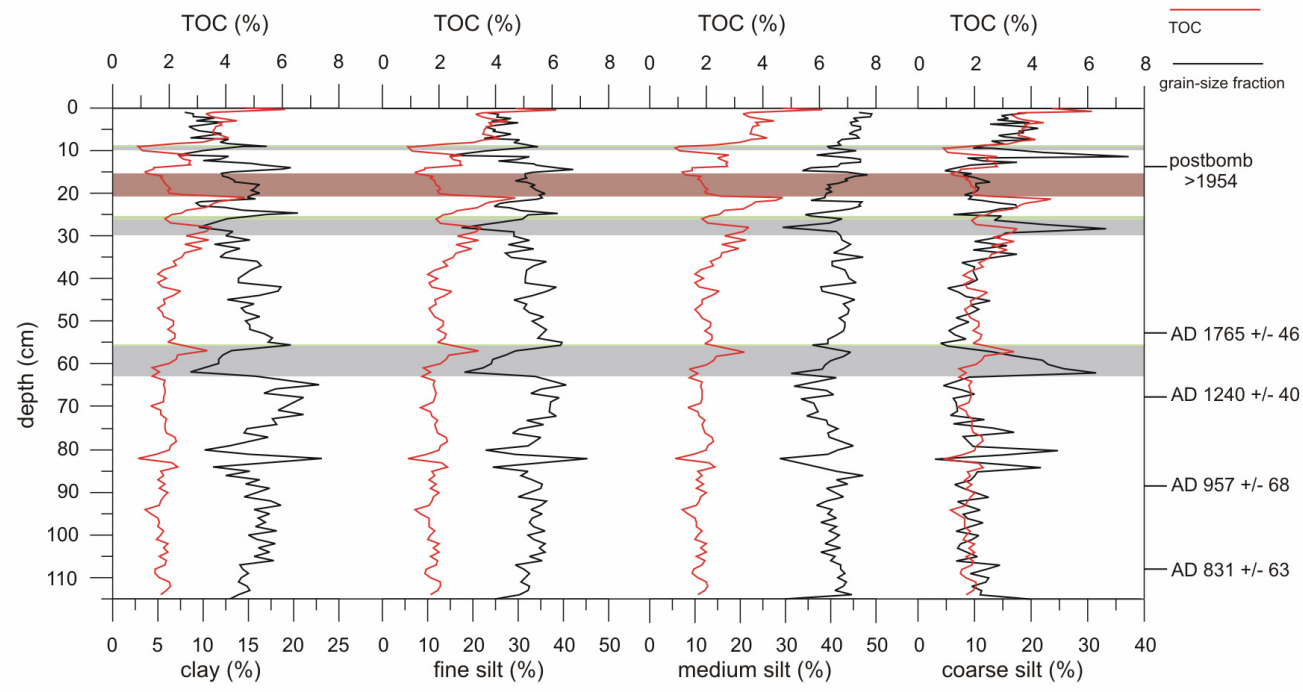

Fig. IV-41: Comparison of total organic carbon (TOC) with individual grain size fractions (percent clay, fine silt, medium silt, and coarse silt) for short core LVR4s. Dates are those obtained using the age-depth model presented in Fig. IV-39. Shaded and coloured bands indicate lithology, presented in Fig. IV-32.

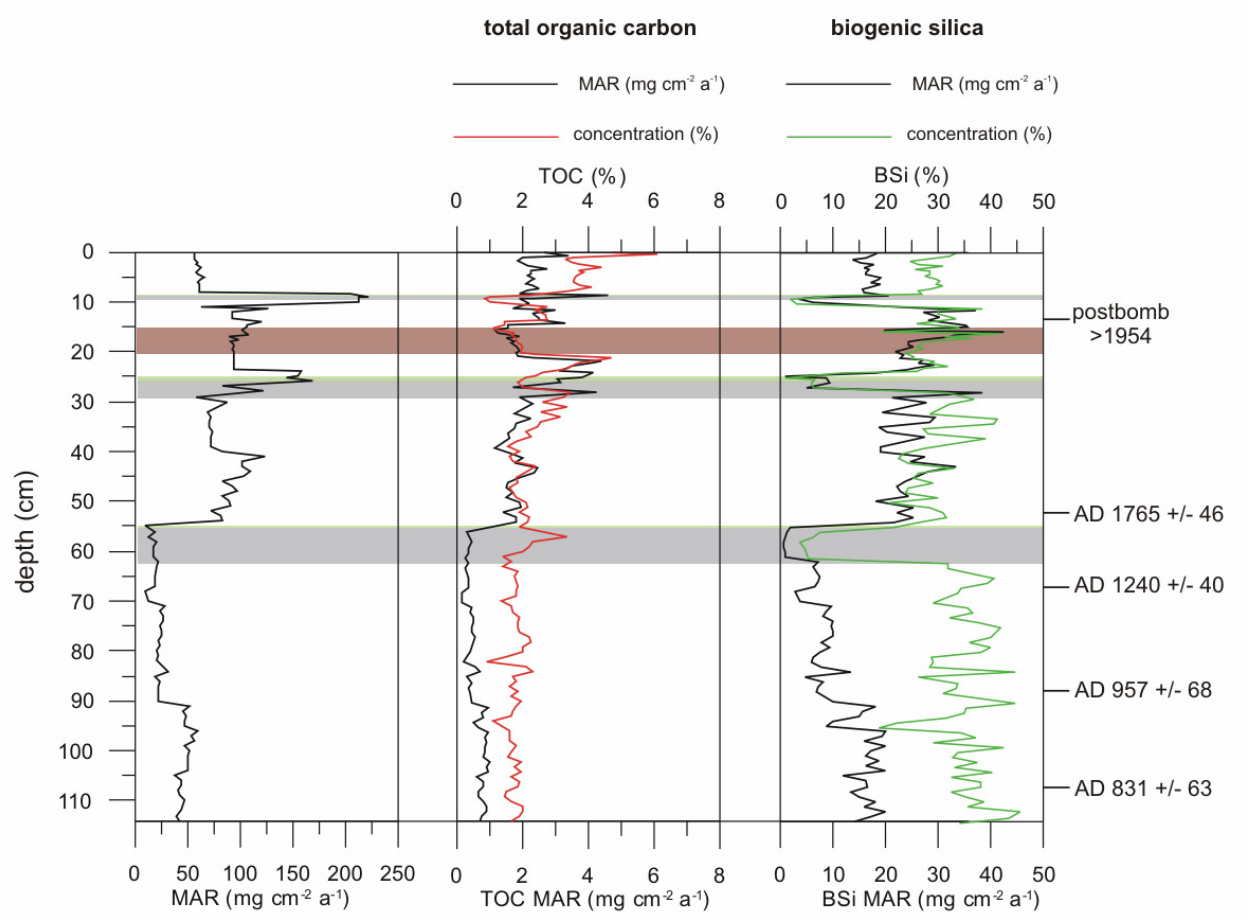

Fig. IV-42: Total mass accumulation rates (MAR), MAR of total organic carbon (TOC) versus TOC concentration, and MAR biogenic silica (BSi) versus BSi concentration profiles of Lago Villarrica, short core LVR4s. Dates are those obtained using the age-depth model presented in Fig. IV-39. Shaded and coloured bands indicate lithology, presented in Fig. IV-32.

7. Lake history

To unravel a lake's history in terms of environmental and in the broadest sense also of climatic reconstruction it is primarily necessary to investigate sedimentary processes in terms of sediment dynamic like it is recorded in sediment patterns and texture. Based on the proxies described in the previous Chapter an attempt is made to characterize phases of development and changes of each lake by its continuous sedimentological, geochemical and biological record, and to compare the records of both lakes as far as it is possible.

7.1 Lago Calafquén

Repeated volcanic disturbances in the sediment succession of Lago Calafquén are obvious as can be deduced by the minimum of 15 visible tephra layers that settled within a time span of ~ 3,000 years. Enriched in magnetized minerals magnetic susceptibility is high, and largely follows the patterns of grain size. According to ^{14}C-AMS dating the general patterns and events in Lago Calafquén can be chronologically confined for some further interpretation.

The period BC 1385 to BC 100 is characterized by strong volcanic activity. At least nine tephra layers are recorded during this period resulting in an 'artificial' enlargement of 'normal' lacustrine sedimentation rate as can be deduced by the increasing SR values given in Table IV-2.

Sedimentation processes through time leave a complex pattern in Lago Calafquén. Between AD 474 and AD 1216 two distinct small-scale increases of coarse grain size (Fig. IV-20,27) are recorded. These signals are followed by peaks in magnetic susceptibility and in main elements Na and Ca. Clear changes in all records can be observed beginning in 45 cm depth, around AD 1140, a period which is marked by continuous and obvious decrease in the flux rates (Fig. IV-43). This turns into an opposite but increasing trend after AD 1300. Inorganic geochemical data for the conservative elements Na and Ca trace this variance from 45 cm to 40 cm depth (Fig. IV-25), ~ AD 1140 to ~ AD 1216, and also the following increasing sediment fluxes (Fig. IV-43).

This development could have several reasons. Generally, the range of energetic controlled input and sedimentary processes give rise to sedimentary 'signals' (Dearing, 1997). Relating the decreasing terrigenous influx ~ AD 1140 to ~ AD 1216 to somehow 'environmental and/or climatic changes' can be one explanation. But this can also be the result of processes other than climate effects, such as shifts in sediment dynamics that result from hydrological changes within the catchment or from different reasons. Especially for Lago Calafquén and its somehow complex recent sedimentation patterns (see Chapter 4) the assumption of short-termed climate resonance to flux rates should be made very carefully. This assumption corroborates with Dearing (1997) and Dearing and Foster (1993) who state that "…varied dynamics of sedimentation probably causes sedimentation patterns to vary far more through time than sediment loads and accumulation rates at any one point in the lake bed".

Nevertheless, geochemical analyses of the biogenic components on sediments of Lago Calafquén could be used as proxies for deducing large-scale changes within the environment in the broadest sense. The biogenic silica concentration represents the remanent silicious skeletal substance of diatom valves and fecal pellets produced by grazing (see Part 3, Chapter 6,7) after dissolution during sinking and settling out of the water column. As dissolution and primary productivity for Si-rich environments mostly is in a somehow equilibrium, biogenic silica can be taken as indicator for productivity. The close C/N atomic ratio around 12 is characteristic for autochthonous production (Wetzel, 1975). TOC in Lago Calafquén is rather controlled by autochthonous production than by terrestrial supply, and therefore can be used as a further proxy for reconstructing the sub-recent lake's history. In the following discussion changes in these parameters are depicted using chronological total and biogenic MAR (BSi, TOC) (Fig. IV-43).

Total and biogenic MAR shows low values between BC 1385 and BC 100. From BC 50 to the present day total and biogenic MAR exhibit large-scale changes with internal small-scale fluctuations. Seven periods can be identified, mainly based on variations of MAR BSi which are correlated with total MAR and MAR TOC:

- BC 100 to ~ AD 160: BSi and TOC fluxes increase rapidly and remain constant. Total MAR decreases after a tephra-related increase;
- ~ AD 160 to ~ AD 370: Total and biogenic MARs decline and remain on a constant low level;
- ~ AD 370 to ~ AD 570: MAR BSi shows a strong increase which is also traced by MAR TOC. Total MAR only increases slightly, which is mainly referred to a continuous accumulation of fine-sized sediment (Fig. IV-44);
- ~ AD 570 to ~ AD 900: total and biogenic MAR decline continuously. Strikingly, decline of total MAR is only traced by decreasing MAR of fine-sized sediment, whereas medium to coarse silt remain constant;

- ~ AD 900 to ~ AD 1080: all fluxes increase strongly. MAR BSi and TOC still follow the same trend and are highest within the core during this period;
- ~ AD 1080 to ~ AD 1850: MAR BSi decreases constantly during this period but stagnates on a constant level between ~ AD 1170 to ~ AD 1550. During the latter period total MAR and MAR TOC decline and overall trace the course of MAR BSi, but from ~ AD 1350 to ~ AD 1600 they increase continuously, conversely to MAR BSi. The increase in MAR TOC is constant until present-day including some small-scale fluctuations, whereas total MAR decreases inversely to MAR TOC;
- ~ AD 1850 to present: MAR BSi rises again and shows a maximum around 1950. This record matches with a stronger shift in MAR TOC and a small bulge in total MAR.

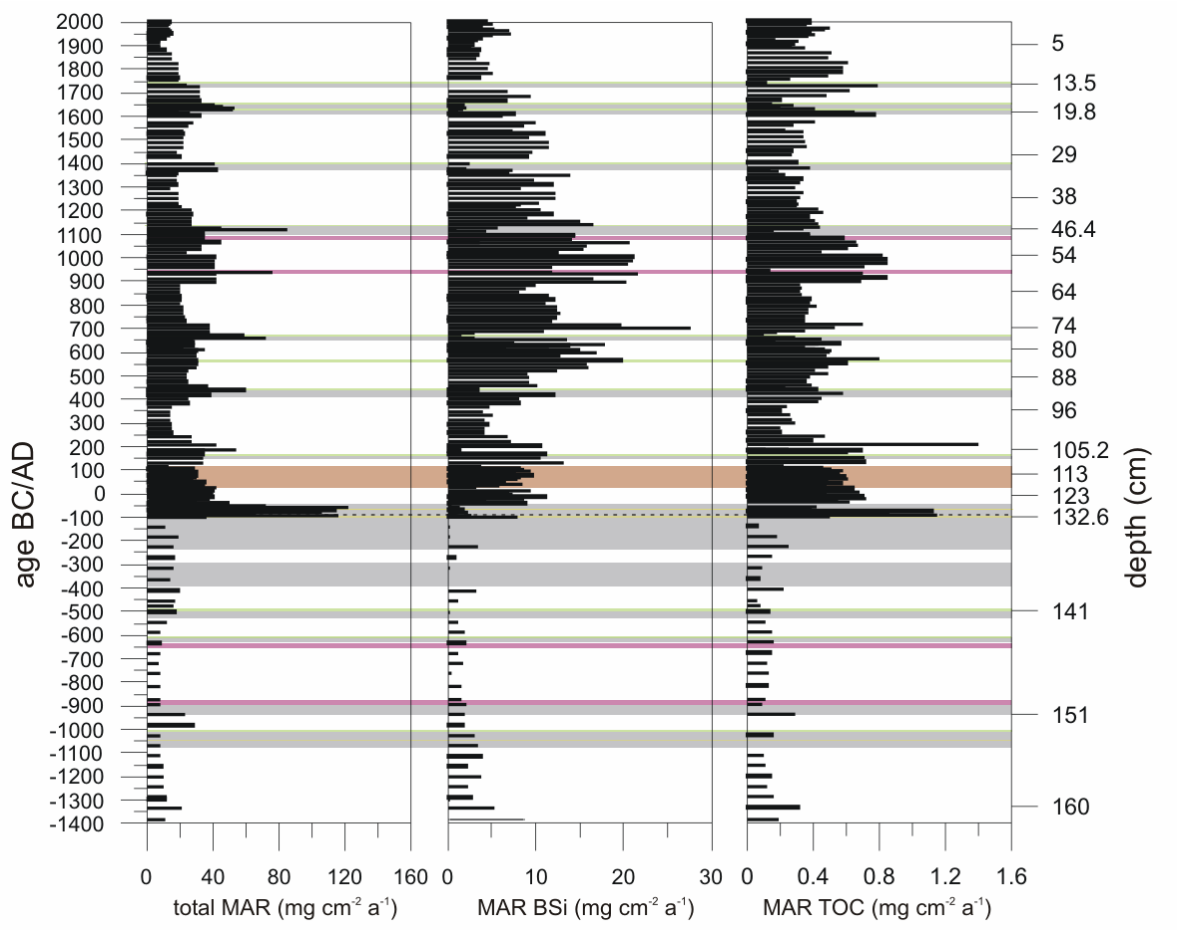

Fig. IV-43: Total mass accumulation rate (MAR), biogenic silica (BSi) MAR, and total organic carbon (TOC) of Lago Calafquén, short core LCQ2s based on ages obtained using the age-depth model presented in Fig. IV-26. Shaded and coloured bands indicate lithology, presented in Fig. IV-18.

High values for MAR BSi and MAR TOC are interpreted as high lake productivity. Increasing total MAR apparently result from higher erosion rates that might be linked to higher availability of sediment in the catchment or considerable atmospheric moisture changes, such as increased precipitation

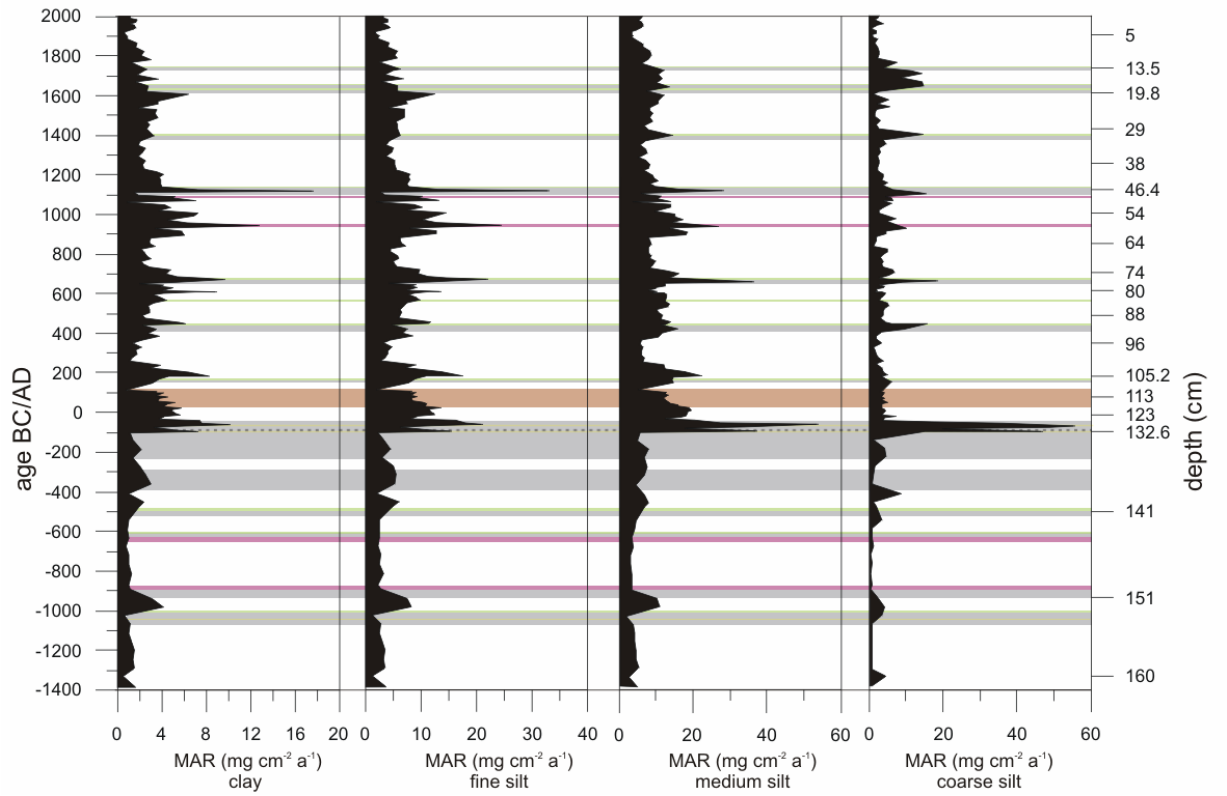

Fig. IV-44: Mass accumulation rates (MAR) for individual grain size fractions of Lago Calafquén, short core LCQ2s, based on ages obtained using the age-depth model presented in Fig. IV-26. Shaded and coloured bands indicate lithology, presented in Fig. IV-18.

For the BC 100 – AD 160 period high MAR BSi is interpreted as a sudden rise in productivity. After a tephra-related increase total MAR declines continuously. MAR TOC seems to be controlled by both variables, as on one hand it mimics the total MAR course overall but also seems to follow a general course of the MAR BSi. Interpretation of these MARs seems doubtful as this core intercept is affected by a sediment internal disturbance, probably a turbidite-like deposit (in 111 - 120 cm depth; see photographic documentation, Appendix, Fig. A-5).

The period AD 160 – AD 370 is characterized by a sudden regression of productivity. All MARs are declining, at last remaining constant on a low level during this period. This might be due to a reduced nutrient influx of allochthonous material.

Productivity strongly increases during the period AD 370 – AD 570, marked by a strong rise in MARs BSi and TOC. Supply of allochthonous material increases moderately. Rising flux rates are traced by a continuous increasing accumulation of fine-sized sediment. Medium silt fluxes remain nearly constant. The supply of fine-sized sediment obviously results in favourable productivity conditions within the lake.

During the period between AD 570 and AD 900 MAR BSi strongly decreases, followed by a decrease in MAR TOC that suggests a clear deterioration in productivity. This might be referred to a reduced supply of allochthonous clastic material from the catchment as it is depicted by the continuous decreasing total MAR during this time.

All MARs increase strongly, hence suggesting a sudden rise in productivity, during the time from AD 900 to AD 1080. A clear enhanced supply of allochthonous material marked by a sudden shift in total MAR results in high productivity, which is recorded in highest MAR BSi and MAR TOC during this period for the entire core. This is consistent with highest flux rates for clay and fine silt. Medium and coarse silt fluxes decrease clearly.

Productivity clearly declines during the period AD 1080 – AD 1850, marked by a continuous reduction in MAR BSi, which remains constant during AD 1170 – AD 1550. Total MAR and MAR TOC follow this trend, but from AD 1350 to AD 1600 they clearly rises which correlates negatively with MAR BSi. This is referred to increased allochthonous influx that maybe indicates a wet period, which would result in less favourable productivity conditions in the lake. Total MAR decreases from ~ AD 1670 on until the early AD 1900's, whereas MAR TOC continuously increases from ~ AD 1600 on until present-day, including small-scale fluctuations.

During AD 1850 to present-day increasing MAR BSi suggests a constant rise in productivity, which matches with a clear rise in MAR TOC and a small bulge in total MAR.

An assessment of these frequent changes with regard to short-termed environmental and climatic changes is difficult. A classification of these results into reference records is necessary but will be reviewed carefully.

From high-resolution marine sediment core analysis recovered at 41°S in front of the Chilean coast Lamy et al. (2002) report a continuous increase of palaeoproductivity for the late Holocene at ~ 2000 cal. BP with a most significant increase ~ 1500 cal. BP. Although a direct comparison between their dates and the lacustrine chronology of Lago Calafquén should be considered carefully, nevertheless, coincidences with the gradually increase around BC 100 (2 050 cal. BP) and rising productivity around AD 470 (~ 1470 cal. BP) in Lago Calafquén can be observed. Lamy et al. (2002) report a strong cooling during this time.

For central Chile at ~ 32°S Villagrán and Varela (1990) deduce a change to more humid conditions around AD 360 from peatbog analyses. An assumed similar change within the moisture budget would slightly coincide with a moderate increase of total MAR in Lago Calafquén and the registered increasing productivity rates recorded by BSi and TOC MARs.

For Northern Patagonia Villalba (1990) inferred four main and two minor climatic episodes from tree-ring records during the last 1000 years:

- AD 900-1070 – cold and moist;
- AD 1080-1250 – warm-dry, correlative with the Medieval warm period (MWP) of Europe;
- AD 1270-1670 – long, cold-moist peaking around AD 1340 and 1650. The latter two are contemporaneous with two principal Little Ice Age (LIA) events in the Northern Hemisphere;
- AD 1720-1790 – warmer conditions;
- Early AD 1800's – cold period;
- AD 1850-1890 – warmer period.

The record of Lago Calafquén during the periods AD 1350 – AD 1650 almost matches with the cold and moist peaking period for the LIA described by Villalba (1990). In Lago Calafquén this time is characterized by increased allochthonous influx, recorded in increasing total and TOC MARs with decreasing biogenic silica production. Increased fluxes of fine to medium grain fractions suggest higher erosion due to wet climate, which could be a local signature for the LIA around the setting of Lago Calafquén. A local signal of the MWP around AD 1080 – AD 1250 could probably be associated with less allochthonous influx that is recorded in decreasing MARs of all grain fractions, indicating less erosion caused by reduced precipitation. If this signal is taken as a marker for warm-dry conditions, further periods with similar patterns also prevailed during BC 90 – AD 50 and ~ AD 200 – AD 360 around Lago Calafquén. These are subordinated small-scale trends within a large-scale

increase of MAR BSi, recorded for the period AD 50 – AD 1000. Assuming more humid conditions within this long-term period the increased supply of 'nutrient enriched' fine clastic material (cf. Fig. IV-21,44) would lead to increased productivity rates, which eventually are recorded as high MAR BSi. From Laguna Acuelo (33°S) Jenny et al. (2002) report high lake levels for the period AD 200 – AD 950. Comparing the deduced environmental conditions around Lago Calafquén's with their records for this period suggest that cool and moist conditions would have prevailed spanning a large transect. However, assessing large-scale environmental and climatic trends based on local records is very doubtable "…as proxies that are used for studies on changes in environmental and climatic systems are individual and therefore local, as they differ greatly in nature" (Soon and Baliunas, 2003).

The constant rise in productivity during AD 1850 to present-day would indicate enhanced conditions for primary productivity during this period. This might be due to either climate fluctuations, due to a general warming trend described by Villalba (1990) and/or additionally to anthropogenic influence from beginning permanent settlements in the lake surroundings.

7.2 Lago Villarrica

Sedimentological and geochemical analyses of short core LVR4s showed several proxies that represent parallel trends. As terrigenous sediment in the catchment of Lago Villarrica is predominantely composed of volcanic material, which is naturally enriched in magnetic minerals, magnetic susceptibility (MS) is high. The MS background noise (Fig. IV-31b) largely correlates positively with the general pattern of grain size (Fig. IV-34), implicating that both parameters can be used as a proxy characterizing probable changes of the mode of sediment influx that at last are triggered by changes in the environment. Chronological comparison of total and biogenic MAR (BSi, TOC) (Fig. IV-45) allows a chronological narrowing into four periods on the base of the proxy data:

- ~ AD 800 to ~ AD 950: total and biogenic MARs are constant through this period with small fluctuations but do not show distinct peaks;
- ~ AD 980 to ~ AD 1230: all MARs decrease strongly. After dropping back total MAR remains constant on a lower level than the previous period, whereas biogenic MARs increase until AD 1220;
- ~ AD 1270 to ~ AD 1740: all MARs note a further slight decrease and the lowest values throughout the entire core during this period, but they remain constant between ~ AD 1310 and ~ AD 1480. Anytime during AD 1500 and AD 1700 (< AD 1765, see Age-depth model, Chapter 6.2.8; Fig. IV-39) a characteristic large tephra layer settles in the lake basin (56 – 62 cm depth), resulting in low MAR BSi and slight increasing MAR TOC but leaves no signal in total MAR;
- ~ AD 1760 to ~ AD 1950: all MARs increase with a sudden and strong shift. Total MAR increase steadily between AD 1770 and AD 1830 but since then drops back and decreases until the present day. MAR BSi increases gradually from AD 1770 to AD 1880, but declines ~ AD 1900 until present-day. A continuous rise from AD 1770 to present-day is noted in the MAR TOC with some internal decreasing small-scale flucutations. Periods around AD 1880 and AD 1960/70 show strong fluctuations for all MARs.

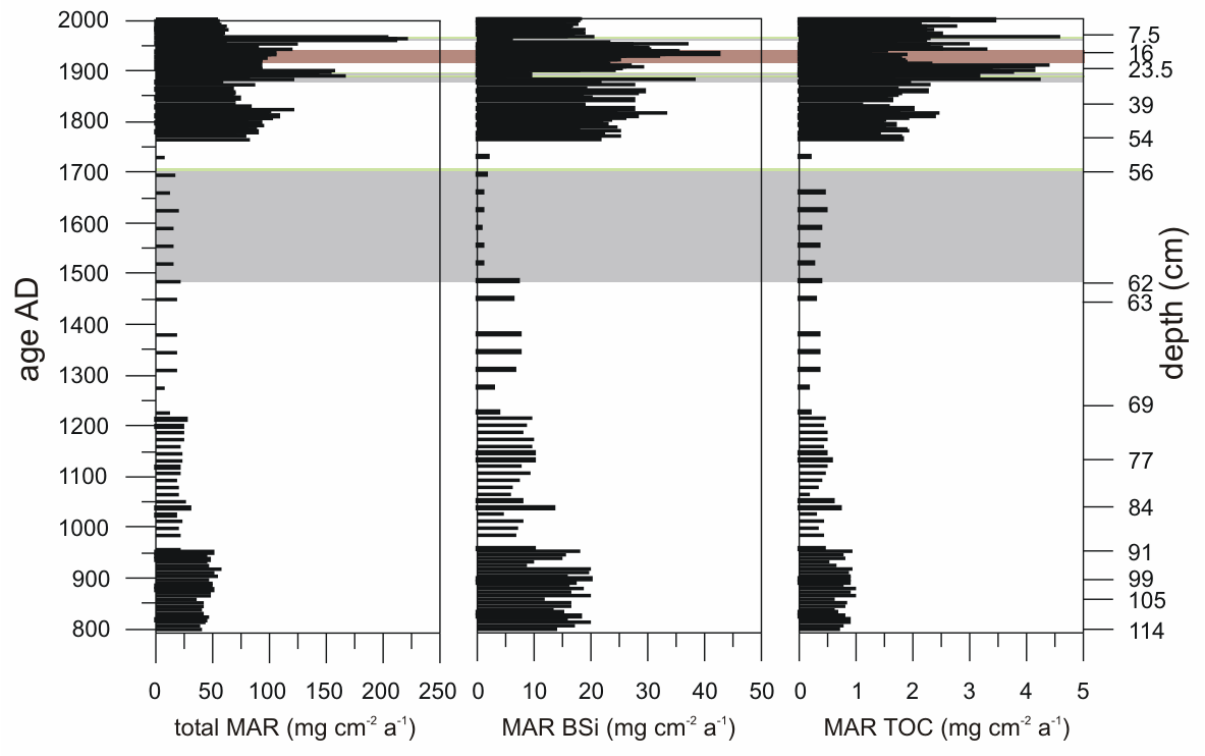

Fig. IV-45: Total mass accumulation rate (MAR), biogenic silica (BSi) MAR, and total organic carbon (TOC) MAR of Lago Villarrica, short core LVR4s, based on ages obtained using the age-depth model presented in Fig. IV-39. Shaded and coloured bands indicate lithology, presented in Fig. IV-32.

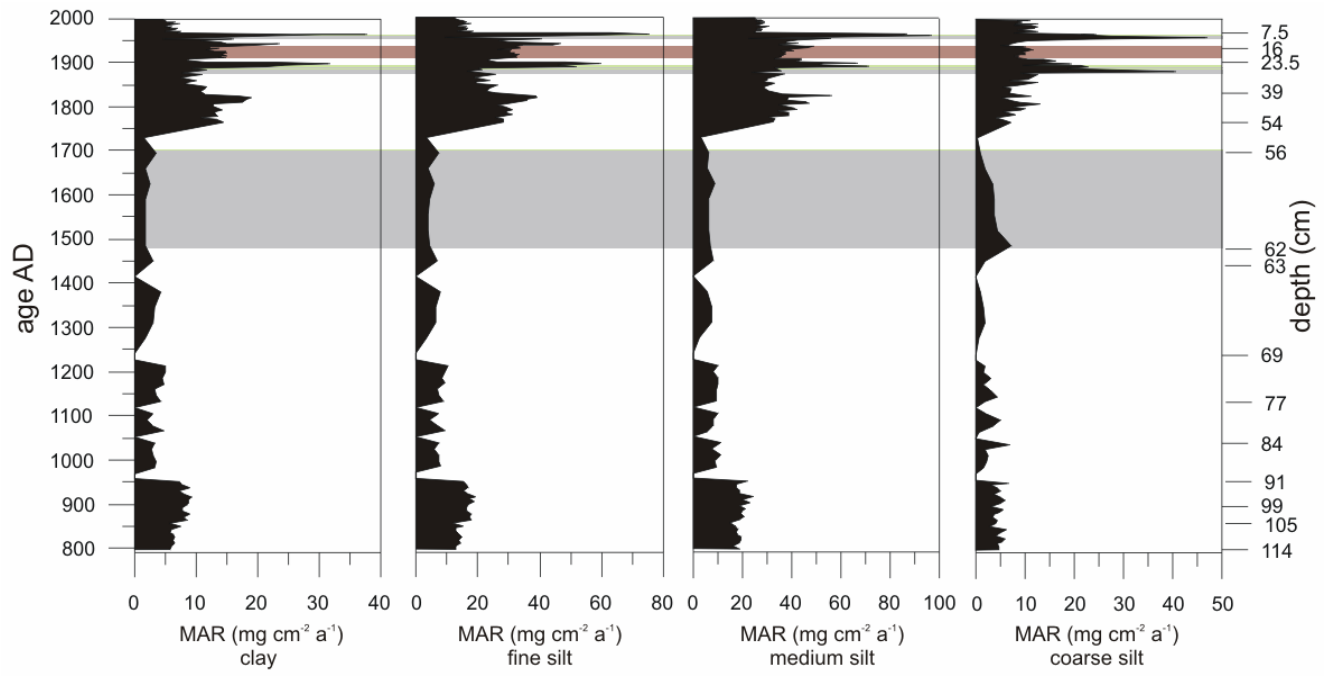

Fig. IV-46: Mass accumulation rates (MAR) for individual grain size fractions of Lago Villarrica, short core LVR4s, based on ages obtained using the age-depth model presented in Fig. IV-39.

The period AD 800 – AD 950 is characterized by a continuous supply of allochthonous clastic material, resulting in steady moderate productivity, which is traced in the constant MARs BSi and TOC. Sediment fluxes during this period are characterized by a constant supply of fine to medium grain mode (Fig. IV-46) and constant to moderate fining upward (Fig. IV-33,46).

The period AD 950 – AD 1230 starts with a clear decline of productivity, which increases moderately until AD 1220, traced by MARs BSi and TOC though allochthonous supply remains constantly low for this period with slight increases in fine-sized sediment fluxes.

Less influx of allochthonous material characterizes the period ~ AD 1270 – AD 1740. This period is marked by low accumulation rates of TOC. Compared to the previous period productivity slightly decreases but remains overall constant. Interpretation of the subsequent core intercept from AD 1500 – AD 1700 (56 – 62 cm depth) is doubtful as a large volcanic eruption encompass the latter period. MAR of fine-sized material continuously increases due to decreasing MARs of medium to coarse-sized material between AD 1230 and AD 1410, which would be consistent with low total MAR values. Slight increased influx of fine-sized material could be explanatory for little fluctuations in productivity though a drop back to a lower level is noted.

For the AD 1760 – AD 1950 period allochthonous influx suddenly increases, coincidently with a strong rise in lake productivity between AD 1770 and AD 1830. Since then, terrigenous influx and biogenic silica production decline until present-day. This contrasts with continuous increasing TOC fluxes from AD 1770 until-present day. The periods around AD 1880 and AD 1960/70 are characterized by the deposition of several tephra layers, which cause larger fluctuation within the MAR values, and should not be interpretated in terms of changes in the catchment. The sudden rise in allochthonous influx during this period matches the decrease of fine- to medium silt for the benefit of increasing fluxes of coarse silt (Fig. IV-46). Geochemical data of the conservative elements Ca and Na support this observation.

A chronological classification of the observed large-scale fluctuations for Lago Villarrica into the climatic reference records after Villalba (1990) (cf. Chapter 7.1, this Part) is rather difficult and will be assessed carefully. In Lago Villarrica the core investigated comprises a continuous sediment record spanning the time before the onset of the MWP and the entire LIA period. But apparently the latter is not fully resolved due to a large volcanic or turbiditic impact.

According to the environmental and climatic reference models the moderate increased allochthonous influx in Lago Villarrica with constant moderate productivity during the period AD 800-– AD 950 would match with the proposed cool and moist environmental conditions. A turn to warmer-dry conditions describing the MWP around AD 1080 – AD 1250 (Villalba, 1990) would then have set in earlier at Lago Villarrica, probably around AD 960, where a clear decrease of allochthonous influx occurred. This would be consistent with the general decreased sediment concentration (Fig. IV-34) and MARs (Fig. IV-46). Decreased but steadily low productivity would support these assumptions. The LIA, encompassing the time span during AD 1270 – AD 1670 apparently does not leave clear signals in the lake sediments investigated. Bertrand et al. (2005) propose increased terrigenous influx during the LIA period AD 1490 – AD 1700 for Lago Puyehue in the Chilean Lake District, located south of Lago Villarrica. In Lago Villarrica this period is characterized by very low total MAR values, connected with low MAR TOC and constantly low productivity rates, contrasting the generally expected higher total and TOC MARs for the LIA. This could have several reasons. On one hand deep lake basins tend to be inert to short term changes, depending on the lake and the catchment dynamic. Furthermore, Lago Villarrica has an open drainage basin with a high flushing rate. Reconstructing precipitation-erosion (p-e) changes in open drainage freshwater lakes of temperate regions is considerably difficult as for those basins a positive p-e balance prevails (Battarbee, 2000). A further reason for less allochthonous supply to Lago Villarrica and reduced productivity during the suggested LIA epoch could be a reduced availability of sediment in the catchment which would result in low erosion rates though increased precipitation rates might have prevailed. Slight increased sediment fluxes (Fig. IV-46) during this time interval would indicate a slight signal of the onset of the LIA. The sudden return to high influxes together with sudden increased

productivity in Lago Villarrica beginning ~ AD 1760 is consistent with warmer conditions reported by Villalba (1990). Lara and Villalba (1993) report dry conditions for the most recent period between AD 1740 and AD 1900. Bertrand et al. (2005) report a drying climate during this period around Lago Puyehue. Furthermore, anthropogenic influence on the catchment by beginning settlements and mining activity around Lago Villarrica should also be considered to have an additional impact affecting total and TOC MARs.

However, this discussion only attempts an approach to bring the observed patterns into a chronological and environmental relation but is not considered to be exhaustive.

7.3 Inter-Lake correlation

The preceding discussion in Chapters 4 to 6 have clearly pointed out that both lakes, Calafquén and Villarrica, differ greatly in their sedimentation texture, patterns, source, mode of supply, and chronological succession. Lago Calafquén comprises ~ 3000 years within 162 cm, whereas Lago Villarrica only includes a continuous record of 1200 years within 114 cm. Both cores were taken from areas with prevailing normal lacustrine sedimentation, largely free of strong underflow influence, at 144 m depth (LCQ2s) and 167 m depth (LVR4s), respectively. This assures quite similar premises of sedimentation conditions and gives rise to a vague comparison of the sedimentological records.

The difference of catchment size for both lakes is clearly recorded in the sediment succession. Lago Calafquén's catchment is about two-third smaller than that of Villarrica. Furthermore, terrestrial influx of Lago Calafquén mostly results from seasonal surficial runoffs or catastrophic events like subaerial debris flows and volcanic eruptions. The permanent natural tributary hardly delivers large amounts of riverrine sediment into Calafquén's basin, as it forms the outlet of Lago Pellaifa, the latter functioning as a sediment trap itself. The small catchment plus the lack of large overflowing tributaries result in a minor supply of sediment (see Tab. IV-2, SR), which in turn results in a concentrated chronological sediment succession that is then recorded within a given core length. Conversely, the large catchment and the continuous overflow tributary of Lago Villarrica, Río Trancura, transport more sediment into the large lake basin. Therefore, a younger sediment succession is retrieved within a given core length on a short time interval. This sedimentation process is furthermore 'artificially' amplified by large turbidites resulting from any kind of debris flows as well as by subaerial tephra fall-out.

Though these ubiquitous differences of regional characteristic control the normal lacustrine sedimentation the question arises, whether evidences of large-scale changes within the catchments, triggered by climatic fluctuations are found in both lakes. An approach to this question could be made by comparing the MAR BSi of both lakes (Fig. IV-47). The coloured background in Fig. IV-47 marks the different environmental conditions after Villalba (1990). Compared on a small-scale biogenic fluxes do not show direct but rather suggestively comparable trends. Assuming a locally contemporaneous onset of the described climatic short-termed periods for both lakes, productivity in both lakes obviously reacts different to the impact of environmental changes suggested in the previous Chapter, but reveal an overall common large-scale upward decrease between AD 800 and AD 1500. For both lakes the period of the MWP would be marked by stagnant or decreased productivity. The long cold and moist peaking of the LIA period would be characterized by decreasing mass accumulations rates in both lakes (Fig. IV-47). As catchments of both lakes are very different, primary the variable flushing rate and sediment dynamics and associated sediment availability for erosion within the catchment would be a substantial explanation for the differing small-scale signals recorded in both lakes

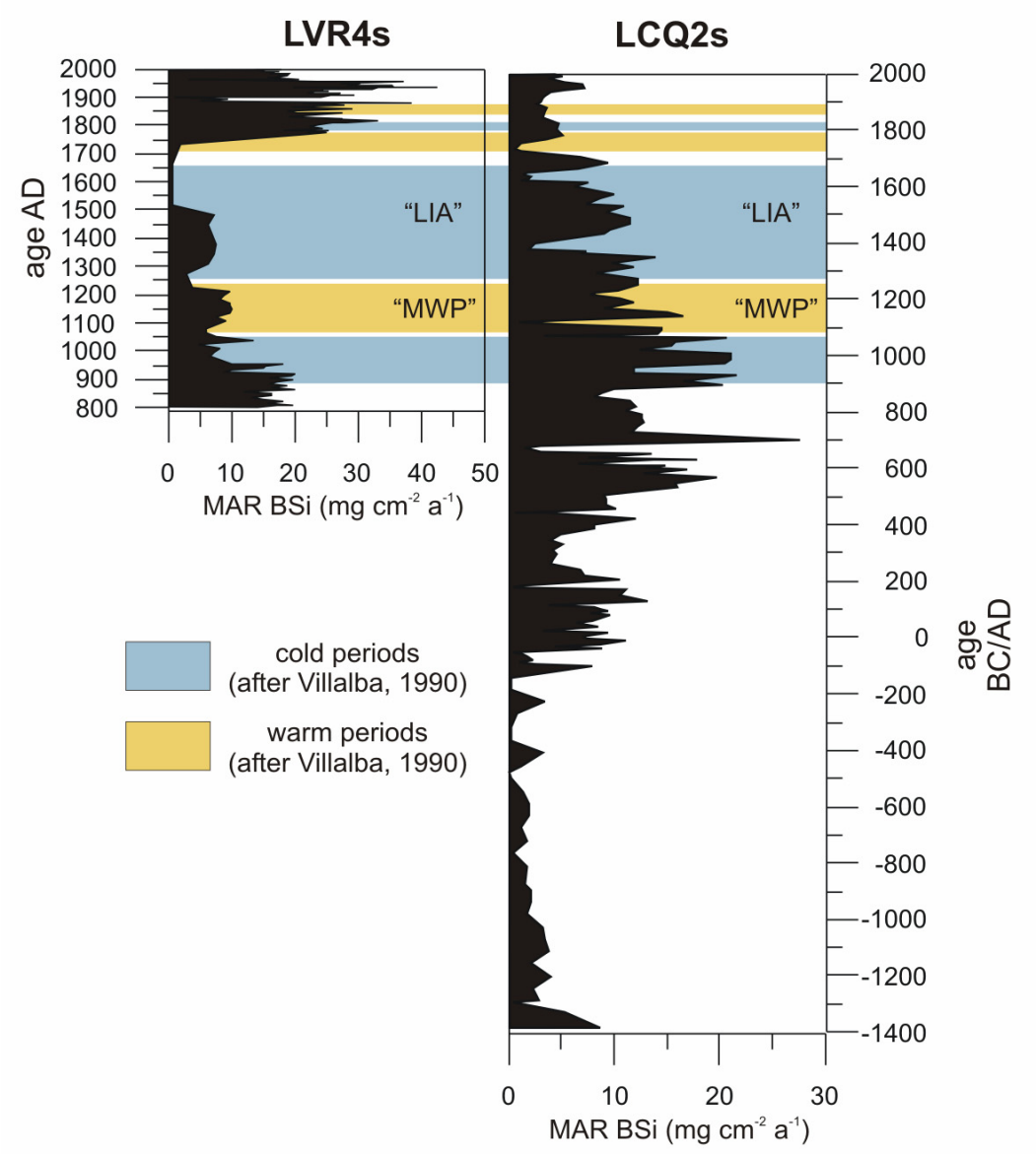

Fig. IV-47: Inter-core correlation of biogenic silica mass accumulation rate (MAR BSi) of Lago Villarrica (core LVR4s) and Lago Calafquén (core LCQ2s), based on age-depth models presented in Figs. IV-26 and IV-39.

To sum up: The multiproxy studies on short sediment cores in both lakes gave a general overview of chronological sedimentation processes in each lake basin. The analyzed proxies have shown significant responses of each lake to changes in its local catchment. As catchments of both lakes differ greatly, responses to regional spanning changes in environmental conditions are individual, but a general large-scale trend during AD 800 to AD 1500 is obvious, which is associated with a general driving force that control productivity in both lakes, such as climatic fluctuations. Therefore, applying a high-resolution limnogeological analysis with short dating intervals on long sediment cores from both lakes could contribute to a general better understanding of large-scale sedimentation processes and long-term changes within certain time intervals with respect to local catchment characteristics. This would enable reconstruction of past environmental and climatic changes including an evaluation of sustained effects of volcanic impacts on sedimentation processes of the lake systems.

PART 3

V. Diatom assemblages: Considerations in assessing environmental change

1. Introduction

Diatoms, siliceous microalgae, are recognized as excellent biological indicators for assessing past limnetic conditions. Diatom community composition changes during the shift from oligotrophic to eutrophic states. The remains of individuals are preserved in the lake sediments such that it is possible to reconstruct the patterns of community change. As water quality may change over centuries, investigating those patterns are done using palaeolimnological techniques (e. g. Klee and Schmidt, 1987; Alefs, 1997; Salmaso et al., 1999). Because diatoms have relatively short life cycles and respond rapidly to environmental changes, they are especially suitable for short-term palaeoenvironmental studies (Bradbury, 1999). Based on diatom community succession, numerous studies have reconstructed climate-driven environmental changes (e. g. Bradbury, 1988; Hickman and Reasoner, 1998; Anderson, 2000; Baier et al., 2004; Battarbee et al., 2000, 2005; Mackay et al., 2005; etc.). However, the reconstruction's accuracy depends on understanding lake-specific taphonomic and sedimentological processes, e. g. the degree to which processes like turbidite deposition disturbs the sediment record (Battarbee et al., 2005) and interrupts the recorded variation in the diatom population. Another problem is differential diatom preservation in lake sediments, resulting in biased interpretations of environmental and climate changes (Battarbee et al., 2005). The diatom record must therefore be considered critically.

Lago Calafquén and Lago Villarrica are subject to recurring tephra deposition. Volcanic eruptions may cause important changes in lake chemistry, sediment deposition, and in their catchment (Haberle et al., 2000; Zielinski, 2000). Depending on scale, deposition of hot tephra proximal to the volcano can immediately affect the ecology of local habitats, as reported from the 1980 Mt. St. Helens's blast zone (USA) (Wissmar et al., 1982a,b) or from the 1995/96 Mt. Ruapehu eruption on Lake Taupo (NZ) (Edgar and Keeley, 1998). There are ongoing discussions about the sustained effects of cold, distal tephra deposition on ecology in lacustrine systems (Hickman and Reasoner, 1994; Birks and Lotter, 1994; Lotter et al., 1995; Telford et al., 1999, 2004; Barker et al., 2000, 2003; Bertrand et al., 2005; etc.).

Since the beginning of the past century, both lakes were also subjected to the impacts of tourism. Their lake sediments contain a succession of well-preserved diatom frustules throughout the entire core lengths (LCQ2s, LVR4s, cf. Part 2, Chapter 6), such that it is expected to find evidence of environmental changes and anthropogenic stress.

This chapter will focus on the ecological analyses of fossil diatom communities retrieved from short gravity cores (described in the previous chapter) from both Lago Calafquén and Lago Villarrica, rather than on strict palaeoclimate reconstruction. Previous studies on the modern phytoplankton composition of both lakes have been performed by Campos (1983, 1984) and Rivera (1983). Rumrich et al. (2000) reviewed cosmopolitan and endemic diatom species occurring in South-American lakes, including Lago Calafquén and Lago Villarrica from the Chilean Lake District. These studies described the spatial distribution of living samples collected from the water column.

After a general introduction into diatom biology, a brief description of the diatom assemblages observed in the sediment sequences will be given. Further considerations on diatom preservation in the sediment and on the probable ecological effects of volcanism will be discussed. A careful attempt will be made to classify the observed stratigraphic patterns into a probable, time-related environmental development pattern.

2. Diatom biology

A comprehensive overview on diatom biology is given by Round et al. (1990) and van den Hoek et al. (1995), and their fossil history by Lipps (1993). In the following a brief outline of general key aspects of diatom biology is described.

2.1 Structure

Diatoms are unicellular algae encased in a siliceous cell wall, and are classified in the division Bacillariophyta. Their cell wall structures or ornamentation are highly variable and are therefore used as taxonomic characteristics. Diatom cells, commonly called frustules, consists of two *thecae*, the epi- and hypotheca, which fit within one another. The thecae comprise two overlapping *valves* (epi- and hypovalve) that are connected by the *cingulum*, or girdle band (Fig. V-1). Most of the taxonomic features are expressed on the valve surface. All freshwater diatoms contain *areolae*, or indentations within the cell wall (Battarbee et al., 2001), usually arranged in rows (*striae*) running at right angles to the margin. These striae are an additional characteristic feature for taxonomic identification, as their spacing is usually consistent within species, but varies among species. Though diatoms are primarily solitary, some species may form colonies or chains (e. g. *Aulacoseira*, *Fragilaria*, *Asterionella, Tabellaria,* etc.), linked together by spines.

Diatoms are sub-divided into two groups, the centric (Centrales) diatoms, having a radial symmetry, and pennate (Pennales) diatoms, with a bilateral symmetry. Centric diatoms appear generally circular or sometimes as elongated cylinders. They have long valve mantles and form filamentous chains. Ornamentation in the valve centre may be different from that at the margin. Centric diatoms are characterized by their tube-like labiate (*rimoportulae*) and strutted (*fultoportulae*) processes that penetrate the siliceous cell wall. The rimoportula is associated with mucilage secretion (Pickett-Heaps et al., 1986). Chitin secretion of crystalline fibrils occurs via the fultoportula. The strutted processes likely aid in flotation and prevent them from being grazed by zooplankton. The position of these processes on the valve is used in taxonomic identification. Within the pennate diatoms, at least one valve of the frustule has a *raphe*, a long slit through the cell wall. It is sometimes short and restricted to the poles, and some species lack a raphe altogether (araphid). Pennales also have ornamentation on their valves that is often interrupted along the longitudinal median axis, aiding in their identification.

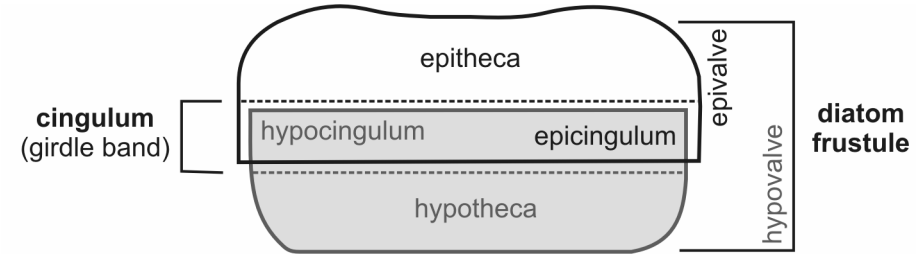

Fig. V-1: Illustration of a centric diatom cell with radial symmetry.

2.2 Mobility and habitats

Given the size and density of diatoms, water serves as a preponderant viscous environment, allowing only slow or no movement at all. Centric diatoms are normally considered immobile, moving passively as buoyant, free floating objects, however Pickett-Heaps et al. (1986) reported a weak form of

movement in some species. Mobility in pennate diatoms is restricted to those possessing a raphe. By the excretion of mucilage through the raphe, they attach themselves to particles or substratum (Lind et al., 1997), gliding across surfaces whilst maintaining their attachment. The secreted mucilage forms a trail behind the gliding cell (Lind et al., 1997).

Diatoms are found in all lake habitats. They commonly grow in the littoral and benthic zones. Other diatoms are planktonic, spending their entire life cycle suspended in the water column. After death, their remains tend to circulate through the water column, eventually sinking to the lake bottom, thus forming the source communities for the sediment record (Battarbee at al., 2001).

2.3 Physical and chemical factors

Diatoms react sensitively to physical and chemical factors, which is why they serve as good indicators of large- and fine-scale environmental and climate change (Battarbee, 2000; Battarbee et al., 2001; Mackay et al., 2005). Temperature is a potentially important variable which explains differences in diatom composition between lakes (Vyvermann and Sabbe, 1995; Lotter et al., 1997). Light penetration, perhaps also via ice cover duration (Lotter and Bigler, 2000), regulates photosynthesis and therefore plays a vital role in forcing algal productivity (Reynolds, 1984; Battarbee et al., 2001). Turbulent mixing of the water body locally influences species composition, as benthic species are suspended into the water column by upwelling where they mix with planktonic species.

Whilst some nutrients are excessively abundant, others such as C, N, and P may limit biomass production and affect the growth rate of phytoplankton. In case of diatoms, Si is also important in regulating diatom size, and influences species composition, as planktonic species have differential abilities to compete for Si and P. The supply and concentrations of silicon in a lake are driven by catchment weathering rates and silica recycling within the lake. Diatom productivity is often controlled by phosphorous availability (Hall and Smol, 1999), especially in eutrophic lakes, and is therefore responsible for increased biomass production (Sommer, 1994). Growth rates are dependent on dissolved nutrient concentrations, meaning how much of a dissolved nutrient is still available determines future growth. Nutrient limitation in eutrophic systems is far more important than in oligotrophic systems (Sommer, 1994). Species poorly adapted to low nutrient availability do not occur in oligotrophic systems, whereas they find favorable growth conditions in eutrophic systems. In many lakes, various nutrient limitations occur concomitantly (Sommer, 1994), nitrogen, phosphorous, silicon, and light-limited species, as well as species with maximum growth rates, may co-exist, and therefore the 'principle of the minimum' after Liebig might only refer to individual species (Sommer, 1994).

In freshwater, pH is the most significant controlling variable on species composition. It controls many chemical processes, such as metal and element solution, as well as biochemical processes, like the regulation of nutrient uptake by algae. The importance of the relationship between diatom production and pH, as well as salinity and dissolved organic matter, is discussed in detail in Battarbee et al. (1999, and references therein; 2001).

3. Diatom preservation and taphonomy

The interpretation of diatom-inferred environmental change is dependant upon the integrity of the relationships between fossil assemblages in sediment records and their original source communities. Comparisons between water column and sediment records may exhibit substantial differences in abundance and composition, as reported from Lake Baikal (Battarbee et al., 2001). Understanding this nonconformity requires an investigation into taphonomy, or 'what may happen to a diatom cell after its

death until its discovery as a fossil'. This includes affects of chemical, biological, or physical activity on the valves stored in the sediment, as well as affects via the transport through the water column to the sediment surface.

In addition to the loss of diatom remains via a lake's outflow, resuspension and reworking of older sediments within the lake basin, and/or contamination of upstream sources (Battarbee, 1986), the most disconcerting problem is the dissolution of frustules. Diatoms preserve differentially in lake sediments, suggesting that lightly silicified valve species may be more susceptible to dissolution than heavily silicified valves (Battarbee et al., 2005). This important observation implies that bias can occur in the reconstruction of the palaeolimnological record (Battarbee et al., 2005). In a sediment trap investigation of Lake Baikal, Ryves et al. (2003) observed frustule dissolution of fragile taxa occurred in the water column and further dissolution of robust taxa on the sediment surface. They suggested that only about 1% of valves are preserved in the sediments of Lake Baikal. Several studies that focus on diatom valve preservation in lacustrine and marine systems (Battarbee et al., 2001, 2005, and references therein; Ryves et al., 2003; etc.) give a preservation degree between 1 and 3%.

To minimize the problems of bias in palaeolimological reconstructions, Battarbee et al. (2005) introduced correction factors for individual diatom taxa, calculating the probable composition of the source population. To do this correctly, continuous comparisons between the modern (using sediment traps) and fossil communities from sediment cores must be done – an actualistic method which has not been applied on the Chilean lakes studied in this thesis.

4. Methods

Diatom composition of Lago Calafquén and Lago Villarrica sediment cores was determined qualitatively and semi-quantitatively using a light microscope (LM). Tentative identifications or unknown species were confirmed or identified, respectively, with a scanning electron microscope (SEM).

Core samples from both lakes are diatomaceous mud with a high percentage of well-preserved diatom valves. Minerogenic material did not prevent good slide preparation and therefore was not removed. As diatom valves were relatively small, sieving and elutriating would have had no effect on sample separation, as valves were found in all grain fractions. Regular strewn mounts were prepared for composition determination.

About 0.1 ml of diatom suspension was dropped by pipette onto a clean, tempered coverslip. Water was evaporated at room temperature, concurrent with diatom settling. When dry, the coverslips were mounted using Naphrax™ mounting media on glass microscope slides, and then heated for a few minutes on a hotplate and cooled slowly. For SEM examination, a 0.1 ml drop of diatom suspension was dried on a coverslip and later fixed to a specimen stub. Each sample was treated with gold vapour in a sputter coater and examined under a SEM.

Taxonomic identification was based primarily on Krammer and Lange-Bertalot (1986, 1988, 1991, 1996) and Rumrich et al. (2000). Due to the over-abundance of some species, between 600 to 1200 diatom valves per sample were counted using a Zeiss photo-microscope with oil immersion objectives having magnifications of 63 × (NA 0.9) and 100 × (NA 1.25). LM photos were taken at the 'Bayerische Landesamt für Wasserwirtschaft (now: Bayerisches Landesamt für Umweltschutz)', using a Zeiss Axioskop 2 with DIC (Digital Image Capture) and a Sensicam 12-Bit cooled imaging apparatus. Percent data for each taxa identified were determined using the total number of valves counted. Difficulties in differentiating the very small valves of *Cyclotella stelligera* and *Cyclostephanos sp.* occurred, as the resolution limit of light microscope was reached. During LM counting, identity was established using the appearance of their central area during focussing. In some samples, this was hardly

possible. Taxonomic identification of these species was made by SEM analyses. However, this technique provides poor results for semi-quantitative analyses, and interpretations based on a variation between these two taxa therefore might be considered carefully.

5. Diatom assemblages

Sediments of Lago Calafquén and Lago Villarrica contain similar diatom assemblages, therefore the diatom communites of both lakes will be described together. Species that are confined to one of the lakes will be mentioned separately. The sediment samples from both lakes were taken from pelagic areas, thus the communties should be comparable. The diatom assemblages from Lago Calafquén come from a sediment core sampled at 144 m water depth, which does not mark the profundal, but an area of deposition dominated by normal lacustrine sedimentation. Diatom assemblages from Lago Villarrica are from a sediment core retrieved from the profundal area, in 167 m depth (cf. Part 2, Chapter 6).

The diatom assemblages of both lakes are characterized by a poor variety of cosmopolitian genera, by species also known from freshwaters in Central Europe, and by species endemic to Chile or South America. Identification of all rare species occurring was not done, as this is beyond the scope of this thesis. Fossil diatom assemblages of both lakes are dominated by the planktonic centric species *Aulacoseira granulata* (Ehr.) Simonsen, and *Cyclotella stelligera* Cleve & Grunow, in varying abundances throughout the cores. The presence of the genus *Cyclostephanos* sensu Theriot, Stoermer & Håk. in both lakes is described here for the very first time. *Cyclostephanos patagonicus* Guerrero & Echenique (cf. Guerrero and Echenique, 2002) was identified all samples from both lakes. *Cyclostephanos sp*. was found only in the diatom flora of Lago Villarrica, which exhibits the characteristics of *Cyclostephanos* cf. *tholiformis* Stoermer, Håk. & Theriot (cf. Stoermer et al, 1987). An unknown species of the genus *Cyclotella* (Kütz.) de Brébisson, here named as *Cyclotella sp*., was found in abundance in Lago Villarrica, but only twice in Lago Calafquén as a single valve (and is therefore not listed in Calafquén's stratigraphy, Chapter 6, this Part). The littoral-inhabiting species *Melosira varians* Agardh formed significant portions of the pelagial assemblages. Colonies were identified in several samples (LVR4s 30-31, 38.1-38.3, 112-113 (cf. Appendix, Fig. C-4)).

Pennate diatoms were dominated by the genus *Fragilaria* Lyngb., *Gomphonema* Ehrenberg, and *Gomphoneis* Cleve. *Fragilaria construens* var. *binodis* (Ehrenb.) Grunow, and *Fragilaria construens* var. *venter* Grunow in Van Heurck were the dominant species of the *Fragilaria* genus. The former was found in both lakes in similar frequencies, whereas the latter was common in Lago Calafquén and rarely found in Lago Villarrica (and is therefore not listed in the subsequent stratigraphy of Villarrica). In Lago Villarrica, *Gomphonema* formed significant portions of the assemblage in some samples, but was rarely abundant in Lago Calafquén.

In both lakes, a discrete bloom of *Asterionella formosa* Hass. and *Fragilaria crotonensis* Kitton species occurred, suggesting an external source as a cause for this event. A single bloom occurred at 6 to 5 cm depth in Lago Calafquén, whereas in Lago Villarrica, *Asterionella* flourished from 8.8 to 6 cm depth. *Fragilaria crotonensis* was observed from 8.8 to 2 cm depth, declining signficantly from 6 to 4 cm depth.

Pennales occurring only rarely in low abundance have been summarized under the groups 'others' in the stratigraphic analyses. This group contains genera such as *Rhopalodia* O.Müll., *Cymbella* Agardh, *Synedra* Ehrenberg, *Cocconeis* Ehrenberg, *Epithemia* Kütz., *Gyrosigma* Hass., *Nitzschia* Hass., *Hantzschia* Grunow, etc. In some cases, their total increased to a significant amount.

A partial list of identified fossil diatom species is given in Tab. V-1. Taxonomic hierarchy was listed on the base of the Integrated Taxonomic Information System (ITIS), available under http://www.itis.usda.gov.

TAXONOMIC CLASSIFICATION	GENUS	SPECIES	LCQ2s	LVR4s
DIVISION: BACILLARIOPHYTA SUB-DIVISION: CENTRALES - CENTRALES -				
CLASS: COSCINODISCOPHYCEAE ORDER: THALASSIOSIRALES Glezer and Makarova FAMILY: STEPHANODISCACEAE Glezer and Makarova				
	Cyclotella (Kütz.) de Brébisson	*Cyclotella stelligera* (Cleve & Grunow) Van Heurck	++	++
		Cyclotella (nov.) sp.	-	+
	Cyclostephanos Theriot, Stoermer & Håk			
		Cyclostephanos patagonicus Guerrero & Echenique	+	+
		Cyclostephanos tholifomis auct. partim		+/++
ORDER: AULACOSEIRALES Crawford FAMILY: AULACOSEIRACEAE Crawford				
	Aulacoseira Twaites			
		Aulacoseira granulata (Ehrenb.) Simonsen	++	+/++
		Aulacoseira distans (Ehrenb.) Simonsen	+	+/++
ORDER: MELOSIRALES Crawfort FAMILY: MELOSIRACEAE Kütz.				
	Melosira Agardh			
		Melosira varians Agardh	+	+

Tab. V-1: Partial list of identified diatom species in Lago Calafquén and Lago Villarrica. Symbols in the columns LCQ2s and LVR4s indicate the relative frequency in which valves were found on the slides. ++ = prevalent, + = common, - = moderate or little, ○ = abundant, ● = event.

TAXONOMIC CLASSIFICATION	GENUS	SPECIES	LCQ2s	LVR4s
ORDER: RHIZOSOLENIALES Silva FAMILY: RHIZOSOLENIACEAE Petit				
	Rhizosolenia			
		Rhizosolenia erensis H.L. Smith	○	○
SUB-DIVISION: PENNALES - ARAPHIDINEAE -				
CLASS: FRAGILARIOPHYCEAE ORDER: FRAGILARIALES Silva FAMILY: FRAGILARIACEAE Grev.				
	Fragilaria Lyngb.			
		Fragilaria construens var. *binodis* (Ehrenb.) Grunow	+	+
		Fragilaria construens var. *venter* (Ehrenb.) Grunow	+/-	○
		Fragilaria crotonensis Kitton	●	●/+
		Fragilaria brevistriata Grunow in Van Heurck	○	○
		Fragilaria pinnata Ehrenberg	○	○
		Fragilaria arcus (Ehrenb.) Cleve	○	○
		Fragilaria ulna var. acus (Kütz.) Lange-Bertalot	○	○
		Fragilaria capucina Desm.	○	○
		Fragilaria capucina var. vaucheriae (Kütz.) Lange-Bertalot	○	○
	Asterionella Hass.			
		Asterionella formosa Hass.	●	●
SUB-DIVISION:				

Tab. V-1: Partial list of identified diatom species in Lago Calafquén and Lago Villarrica. Symbols in the columns LCQ2s and LVR4s indicate the relative frequency in which valves were found on the slides. ++ = prevalent, + = common, - = moderate or little, ○ = abundant, ● = event.

TAXONOMIC CLASSIFICATION	GENUS	SPECIES	LCQ2s	LVR4s
PENNALES - RAPHIDIOIDINEAE -				
CLASS: BACILLARIOPHYCEAE ORDER: RHOPALODIALES Mann FAMILY: RHOPALODIACEAE Topachevs'kyj & Oksiyuk				
	Rhopalodia O.Müll.	*Rhopalodia gibba* (Ehrenb.) O.Müll.	○	○
	Epithemia (Kütz.)	*Epithemia adnata* (Kütz.) Brébisson	○	○
ORDER: CYMBELLALES D.G. Mann FAMILY: GOMPHONEMATACEAE Kütz.				
	Gomphonema Ehrenberg			
		Gomphonema cf. *parvulum* (Kütz.) Kütz.		+
		Gomphonema gracile auct. partim		○
		Gomphonema (nov.) sp.		○
	Gomphoneis P.T. Cleve			
		Gomphoneis cf. *olivacea (Hornemann)* P.A. Dawson ex R.Ross & P.A. Sims	○	○
		Gomphoneis sp.	○	○
FAMILY: CYMBELLACEAE Grev.				
	Cymbella Agardh			
		Cymbella cistula (Ehrenb.) Kirchner	○	○
		Cymbella cymbiformis Agardh	○	○
ORDER: NAVICULALES Bessey FAMILY: PLEUROSIGMATACEAE Mersechk.				
	Gyrosigma Hass.			
		Gyrosigma spencerii (Queck.) Griff. & Henf.	○	○

Tab. V-1: Partial list of identified diatom species in Lago Calafquén and Lago Villarrica. Symbols in the columns LCQ2s and LVR4s indicate the relative frequency in which valves were found on the slides. ++ = prevalent, + = common, - = moderate or little, ○ = abundant, ● = event.

TAXONOMIC CLASSIFICATION	GENUS	SPECIES	LCQ2s	LVR4s
FAMILY: PINNULARIACEAE D.G. Mann				
	Pinnularia Ehrenberg			
		Pinnularia sp.	○	○
ORDER: ACHNANTHALES Silva				
FAMILY: COCCONEIDACEAE Kütz.				
	Cocconeis Ehrenberg			
		Cocconeis placentula Ehrenberg	○	○
ORDER: BACILLIARES Hendey				
FAMILY: BACILLARIACEAE Ehrenberg				
	Nitzschia Hass.			
		Nitzschia frustulm auct partim (Kütz.) Grunow	○/-	○
		Nitzschia fonticola Grunow	○/-	○
		Nitzschia pumila Hust.	○/-	○
		Nitzschia amphibia Grunow	○/-	
		Nitzschia capitellata Hust.	○/-	○
	Hantzschia Grunow			
		Hantschia amphioxys (Ehrenb.) Grunow	○	○

Tab. V-1: Partial list of identified diatom species in Lago Calafquén and Lago Villarrica. Symbols in the columns LCQ2s and LVR4s indicate the relative frequency in which valves were found on the slides. ++ = prevalent, + = common, - = moderate or little, ○ = abundant, ● = event.

6. Diatom stratigraphy

In the stratigraphic records of both lakes, diatoms of a minimum percentage ~ 1% are shown. Results of the stratigraphic analyses are displayed separately for each lake. For both lakes, several diatom sections (DS) have been subjectively identified by a relatively high fluctuation in diatom species and not by any statistical analysis, e. g. cluster analyses, etc. Therefore, the term 'zone' for creating 'diatom assemblage zones' has been avoided, as no mathematical basis was used to establish these findings. Establishing the DS was problematic, especially for Lago Villarrica, therefore the results displayed are summarized and indicate large-scale fluctuations rather than single events.

6.1 Lago Calafquén

The diatom record was separated into six DS (Fig. V-2) and compared with the biogenic silica concentration (cf. Part 2, Chapter 6).

DS-A from *BC 1385 to ~ AD 50* (162 cm to 105 cm)

This section is characterized by frequent volcanic impacts, marked by tephra layers and one large turbidite, possibly caused by a strong seismic activity. Diatom assemblages are dominated by the relatively consistent occurrence of *Aulacoseira granulata* and *Cyclotella stelligera*, with abundances up to 38% and 54%, respectively. *Cyclostephanos patagonicus* is present in low abundances, with a maximum of 1.8%. The base of the section is marked by a strong presence of 'other' species and a core maximum of *Fragilaria construens* var. *binodis*. This basal assemblage coincides with the highest peak in biogenic silica. *Aulacoseira granulata* and *Cyclostephanos patagonicus* attained highest abundances ~ AD 50, though is considered suspect as it occurred in the slump-layer and is likely the result of remobilization and focussing.Biogenic silica shows moderate concentrations through the middle of this section, and is frequently interrupted by tephra layers. A clear increase in silica towards the top of *DS-A* is noted.

DS-B from ~ *AD 190* to ~ *AD 460* (105 cm to 90 cm)

A clear dominance of *Cyclotella stelligera* occurs in this section. *Aulacoseira granulata* decreases relative to the previous section, with minimum values of 12.7%, coincident with increases in *Nitzschia* and *Gomphoneis,* forming the dominant portions of 'other' species at 96 cm depth. Highest abundance of 'others' is achieved together with the highest abundance of *Cyclotella stelligera* and lowest of *Aulacoseira granulata*. Biogenic silica is found in similar concentrations as at the end of *DS-A*.

DS-C from ~ *AD 460* to ~ *AD 1210* (90 cm to 40 cm)

A distinct large-scale shift occurs within the species that dominate the fossil diatom assemblage. Although abundance of *Aulacoseira granulata* is generally less than that of *Cyclotella stelligera*, increases in *Aulacoseira granulata* cause a relative drop in *Cyclotella stelligera*. The occurrence of *Cyclostephanos patagonicus* also occurs coincident with changes in *Cyclotella stelligera*. The occurrence of 'other' species is difficult to interpret, but it appears that a slight adaptation to the relative increase of *Aulacoseira granulata* has occurred, which would be consistent with the relative decrease in *Cyclostephanos patagonicus* and *Cyclotella stelligera*. Biogenic silica is higher than in preceding sections, though it decreases slightly towards the top of DS-C and follows the decline of *Aulacoseira granulata*, coeval with the increase in *Cyclotella stelligera*.

DS-D ~ AD 1210 to ~ *AD 1410* (40 cm to 33 cm)

This section is characterised by a sudden occurrence of *Aulacoseira distans* at 40 to 39 cm depth and an increase in *Fragilaria construens* var. *venter* relative to the previous section. *Cyclotella stelligera* and *Aulacoseira granulata* remain the most abundant species whereas the abundance of 'other' species remains low. The biogenic silica concentrations attain their highest values of the core.

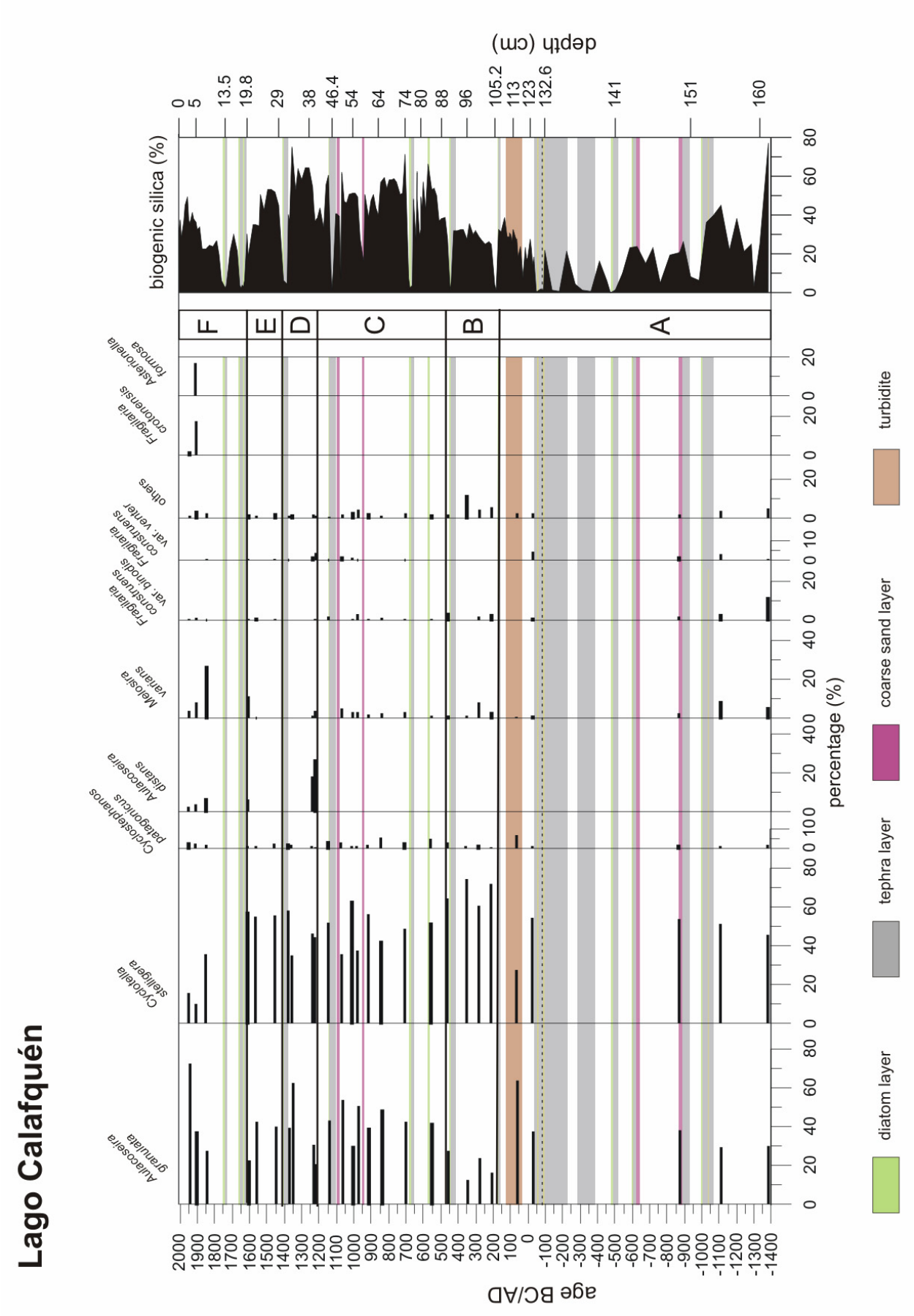

Fig. V-2: Diatom stratigraphy of Lago Calafquén with sediment biogenic silica concentration. Relative percent abundance of the major taxa is shown.

DS-E from ~ *AD 1410* to ~ *AD 160* (31 cm to 19 cm)

This section is characterised by consistently abundant *Cyclotella stelligera*. *Aulacoseira granulata* remain in similar abundance as the previous section. A marked decrease in the biogenic silica concentration occurs towards the end of this section.

DS-F from ~ AD 160 to present (19 cm to 0 cm)

DS-F is marked by two larger tephra fall-out events in the beginning of this section. This section is marked by a strong increase in *Melosira varians* and a moderate of 'other' species. Increases are also observed in *Aulacoseira granulata.* A single bloom of *Asterionella formosa* and *Fragilaria crotonensis* occurs at 6 to 5 cm depth. *Cyclotella stelligera* decreases in this section. From 6 to 2 cm depth, biogenic silica concentrations increases strongly towards the top of the core, coincident with a stepwise increase of 'other' species and a fluctuation of *Melosira varians*.

6.2 Lago Villarrica

Diatom stratigraphy of Lago Villarrica (Fig. V-3) is characterized by strong small-scale fluctuations. Separation into three DS was performed by subjective observation and determination of prominent changes.

DS-A from ~ *AD 800* to ~*AD 1750* (114 to 52 cm)

This section is dominated by up to 60% *Cyclotella stelligera* , and < 20% abundance of *Aulacoseira granulata,*. From ~ AD 880 to ~ AD 1160, *Cyclotella stelligera* declines as *Aulacoseira granulata* increases. This trend reverses from ~ AD 1230 to ~AD 1450 (72 to 62 cm depth). *Cyclostephanos sp*. fluctuates around 10%. *Cyclostephanos patagonicus*, at < 10% abundance, declines to < 1% at the point of tephra deposition, whereas 'other' species increase over the same period. A similar trend is observed in *Gomphonema* cf. *parvulum* and *Melosira varians*. The fluctuations in abundance do not appear correlated with changes in the biogenic silica concentration.

DS-B from ~ *AD 1760* to ~ *AD 1950* (52 to 13 cm)

This section is dominated by > 60% *Cyclotella stelligera* and < 40% *Aulacoseira granulata*. *Gomphonema* cf. *parvulum* increases up to 6%, surpassing the relative abundance of *Cyclostephanos patagonicus*. *Fragilaria construens* var. *binodis* follows this shift from 38 to 30 cm depth. *Cyclostephanos sp*. fluctuates between < 5 and 20%, but and does not follow one of the major centric species. This finding has to be considered carefully, as *Cyclotella stelligera* and *Cyclostephanos sp.* are both very small (down to 2.5 µm, see Appendix, Fig. C-1). 'Other' species apparently respond to the same conditions as *Aulacoseira granulata,* but show a sudden increase to > 5% at 23 cm depth. *Melosira varians* is present in this section at or below 5%. Biogenic silica concentrations generally range between 25 and 40%.

DS-C ~ AD 1950 to present day (13 to 0 cm)

This section represents the diatom communites of modern day. *Aulacoseira granulata* dominates the assemblage and *Cyclotella stelligera* clearly drops relative to previous sections. A strong single bloom of *Asterionella formosa* and *Fragilaria crotonensis* occur from 8.8 to 7 cm depth and fades from 7 to 6 cm depth. *Fragliaria crotonensis* remains abundant and dominates with *Aulacoseira granulata* the surface layers from 4 to 2 cm depth. The abundance of *Aulacoseira distans* remains constant around 3%. Biogenic silica occurs at concentrations similar to those observed in *DS-B*.

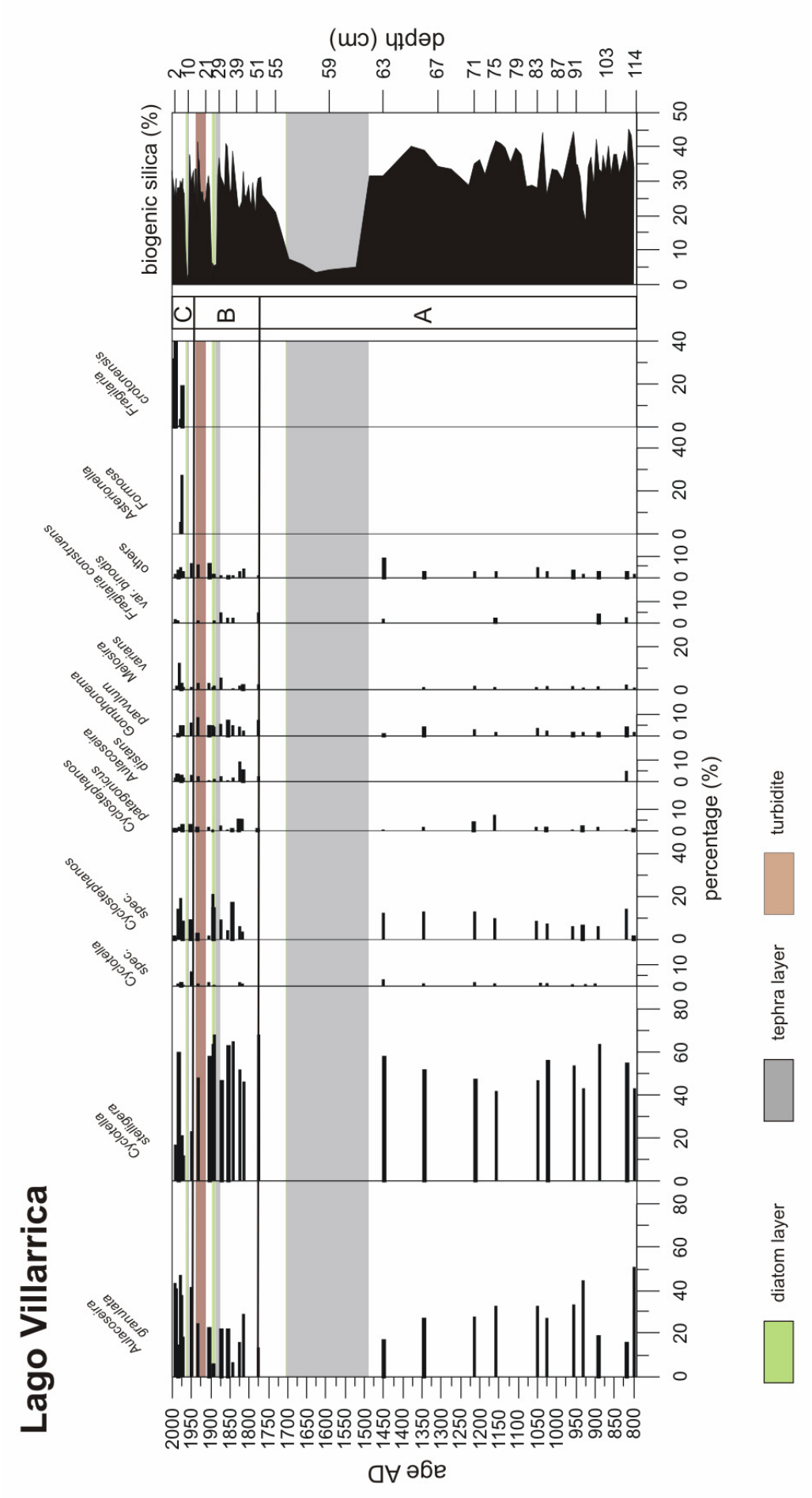

Fig. V-3: Diatom stratigraphy of Lago Villarrica with sediment biogenic silica concentration. Relative percent abundance of the major taxa is shown..

7. Biogenic silica, diatom production and grazing

Comparing the succession of diatom assemblages with the biogenic silica concentration from both lakes suggests that the variance in biogenic silica is related to the fluctuation of major diatom species.

In Lago Calafquén, large-scale fluctuations of biogenic silica concentration seems to be mainly triggered by the variance in the abundance of the heavy, large and robust diatom species *Aulacoseira granulata*, *Aulacoseira distans*, *Fragilaria construens* var. *binodis* or *Fragilaria construens*. var. *venter*, subordinately supported in single events by lighter species such as *Asterionella formosa, Fragilaria crotonensis* or those of the genus *Nitzschia*. This assumption is not directly verifiable for Lago Villarrica. There, light valve species such as *Cyclotella stelligera*, *Cyclostephanos sp*. and stronger silicified valves of *Cyclostephanos patagonicus* seem to control the fluctuation of biogenic silica concentration. *Gomphonema* cf. *parvulum* seems to play a remarkable role in the positive shift of biogenic silica concentration, at least in DS-B.

Preserved fossil diatom abundance in these lake sediments cannot be considered the only factor driving the biogenic silica concentration (Fig. V-2,3). A key aspect responsible for the high values is the amount of fecal material produced by grazing zooplankton. During elutriating lake sediments of Lago Calafquén and Lago Villarrica in the laboratory of the TU München, an agglomeration of white to light brownish substance separated from the heavy minerals of the lake sediment after settling and evaporation of the elutriation water. The proportions of this substance varied within the core lengths and comprised up to 25% of the elutriated sediment. SEM scanning of this substance revealed that it consists mainly of small scoria particles, conglutinated fine-sized materials, e.g. dust and/or clay-like minerals, and large fecal pellets (Fig. V-4a). The latter comprise digested diatom valves (Fig. V-4b). Originally, sediments were elutriated for the purpose of grain size analysis (after Atterberg, based on Stoke's law), but as aggregates of fecal pellets occurred preferentially in the fine to medium silt fraction, the inappropriateness of this method for grain size separation of biogenic controlled sediments was shown.

An enormous amount of grazing activity by meso-zooplankton in both lakes must be assumed, given the large proportion of fecal material in the sediment. Chilean zooplankton assemblages are characterized by calanoid copepods, with *Boeckella* as the dominant genus (Soto and Zuniga, 1991). Menu-Marque et al. (2000) describe *Boeckella gracilipes* Daday as the dominant grazing species in Lago Calafquén and Lago Villarrica. In response to diatom blooms, or generally high diatom growth rates, the biomass of diatoms consumed by copepods increases (Schultes, 2004). In doing so, their feces restore a significant amount of biogenic silica to the sediment, hence recycling silica and explaining its high preservation in both lakes. Thus, fecal pellets must be considered as an additional form and significant part of the biogenic silica concentration, apart from the preserved non-grazed fossil diatom valves. The observed fossil diatom assemblage retrieved from sediments is a subset of the original community after diatom dissolution (cf. Chapter 3, this part) and selective elimination by grazing. These taphonomic and grazing effects should therefore be considered when deducing productivity or other environmental changes by percentages or presence/absence of diatoms preserved in lake sediments.

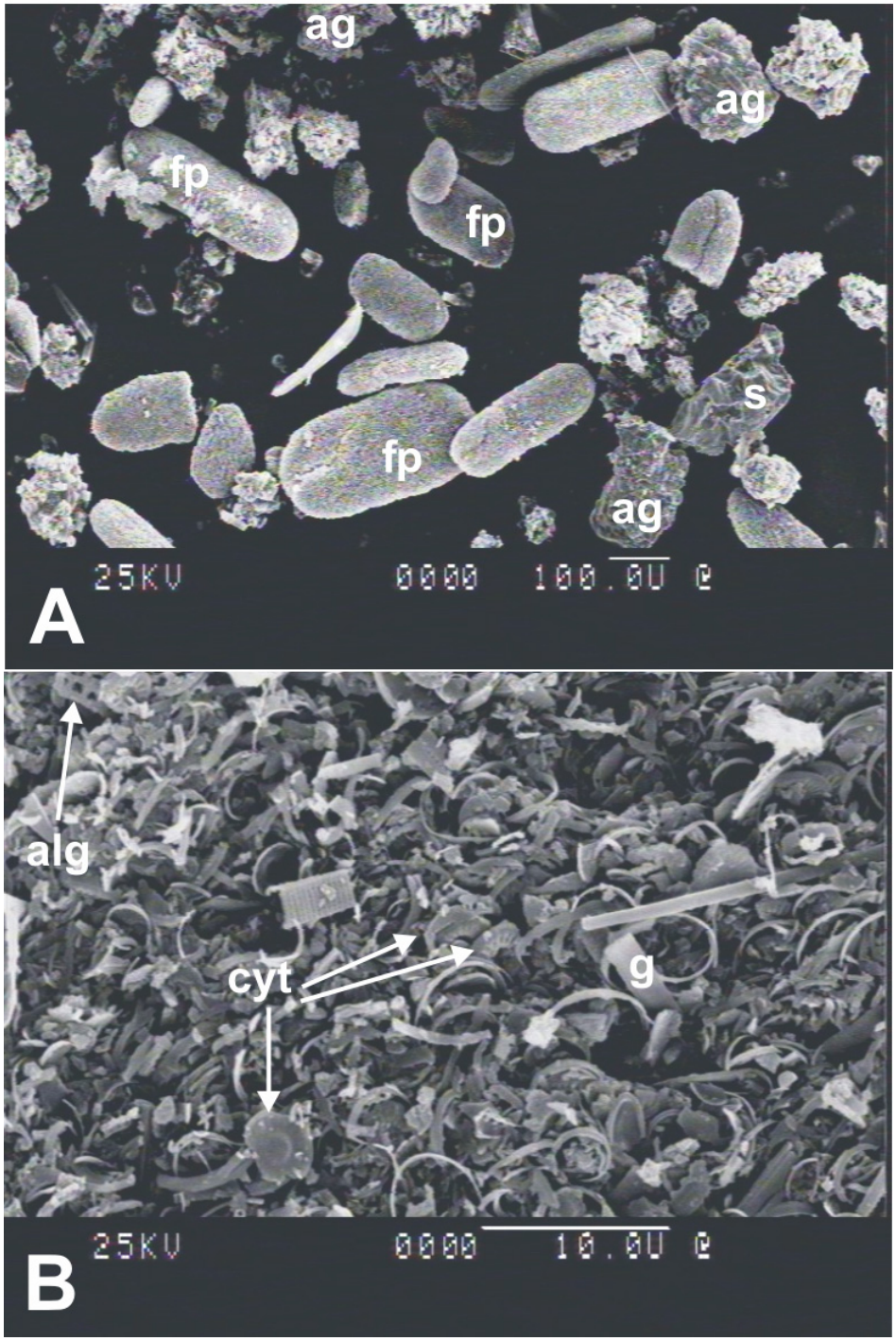

Fig. V-4: White to light brownish substance of the sediments of Lago Calafquén and Lago Villarrica that separated from the heavy minerals after elutriation. A) ag=conglutinated aggregrates, fp=fecal pellets, s=scoria. B) Magnification: pellets are made up of digested diatoms consisting of valve residue and girdle bands. g=girdleband, cyt=*Cyclotella stelligera*, alg=*Aulacoseira granulata*.

8. Volcanic impact and ecological response

Volcanic eruptions generate various profound effects on terrestrial and aquatic ecosystems. Barsdate and Dugdale (1972) report diatom blooms above ash layers in lakes in Alaska/USA, suggesting an increase of diatom productivity occurred after tephra deposition. The return to pre-deposition conditions required several hundred years. A diatom response to Mt. Mazama tephra

deposited in British Columbia, Canada, is reported by Hickman and Reasoner (1994) and Heinrichs et al. (1997). A short, decadal-scale recovery time is reported for the diatom response to Laacher See tephra in Lake Holzmaar (Lotter et al., 1995). Lakes located proximal to the eruption centre are affected immediately and destructively, as reported for the many lakes near the 1980 Mt. St. Helens blast zone (Wissmar et. al., 1982a,b) or from the devastating impact of the 1995/96 Mt. Ruapehu eruption on Lake Taupo, which caused measurable alteration of the water quality, fish kills, and the disappearance of phytoplankton (Edgar and Keeley, 1998). They estimated that Lake Taupo would need several years to return to pre-eruption conditions. Birks and Lotter (1994) did not observe significant impacts on a lake distal from the Laacher See eruption centre. In a study on lacustrine responses to tephra deposition in Mexico, Telford et al. (2004) found changes in proxies by tephra input analogous to those of climate forcing. According to their findings, tephra impact was insufficient to perturb underlying long-term climate forcing signals in their investigated lake systems.

The first and direct ecosystem response to volcanic ash fall-out in Lago Calafquén and Lago Villarrica resulted in an intense, monocultural diatom bloom of *Aulacoseira granulata* (Fig.V-5). A similar bloom occurred after almost each tephra impact. For estimating sustained effects on both lakes due to long-time leaching and reworking processes, Telford et al. (2004) premise the recognition of four criterias:

- A change in diatom stratigraphy greater than natural variation and distinguishable from pre-eruption assemblages should be observed, either in composition or diatom concentration;
- The assemblage change should start directly after tephra input;
- A recovery towards pre-tephra state (in absence of other perturbation) should be detected, depending on the time span of response (decadal, annual, seasonal);
- Similar responses should be shown by more than one tephra event (cf. Barker, 2003). This aspect is important, as it reduces the probability of co-incidences with tephra impact and other events unrelated to the former.

Analysing the diatom results for Lago Calafquén and Lago Villarrica with the criteria established by Telford et al. (2004), it has to be stated that the expression 'greater than natural variation' is a little bit misleading. Since both lakes are frequently influenced by tephra fall-out, a so-called pristine state is not determinable. The distinctions between a sustained response to tephra impact, recovery, and natural condition are difficult to assess. Thus, small scale variation in diatom assemblages in lacustrine sediment has to be considered as 'natural variance'. It could therefore be stated that in Lago Calafquén and Lago Villarrica, no change in diatom stratigraphy greater than the 'natural variation' was detected (Fig. V-2,3). The only similar responses that occur are the diatom blooms after tephra impact. Conversely, signals independent of tephra impact seem to be deducible. Much of the observed variations in the diatom assemblages might be considered as long-term responses to various mechanisms, internal and/or external (e.g. climate).

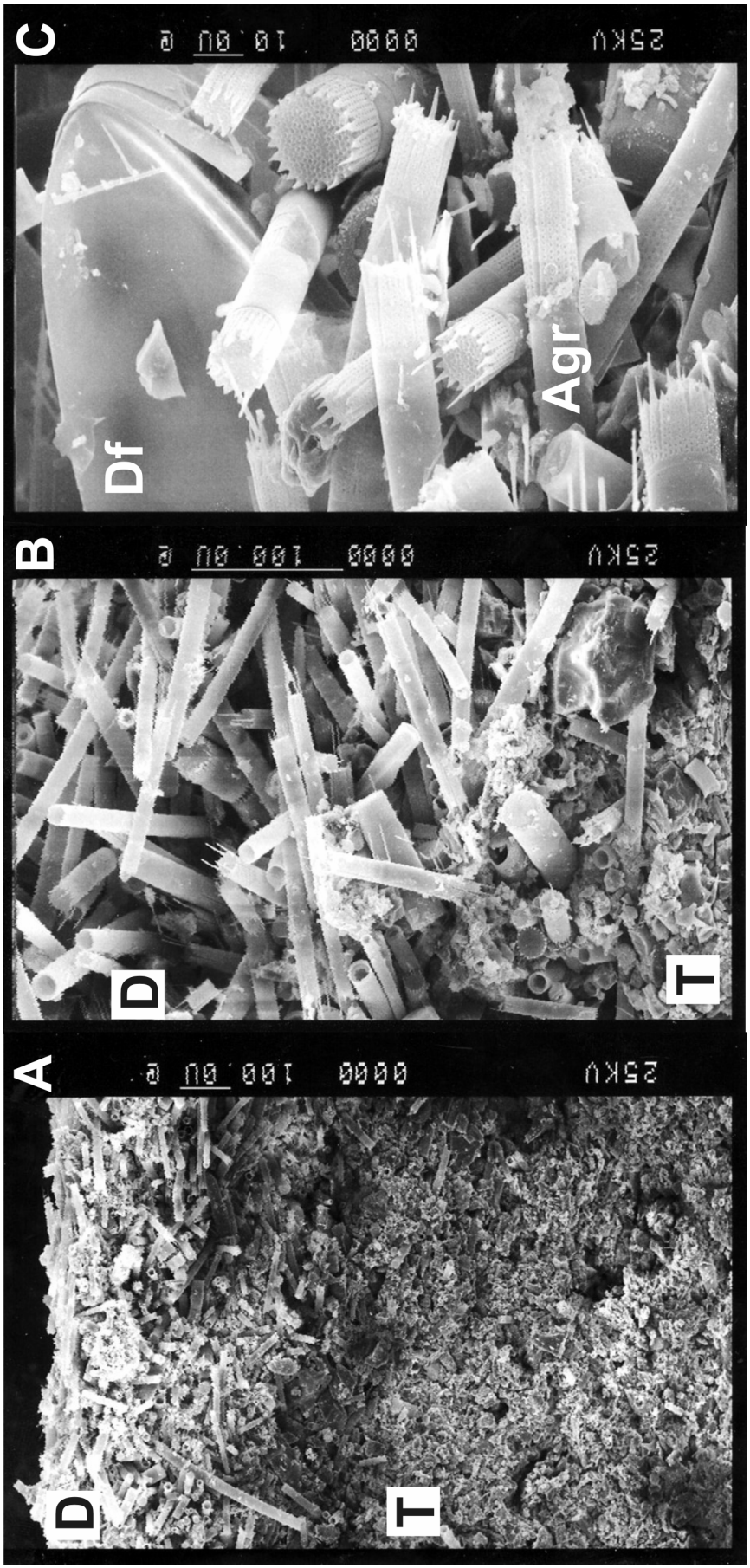

Fig. V-5: After tephra impact, a monospecific diatom layer accumulates above the tephra layers in both lakes. A) Boundary between tephra (T) and diatom layer (D). B) Magnification of the boundary layer. C) Monospecific growth of *Aulacoseira granulata* (Agr), with a dinoflagellate (Df) in the background.

9. Considerations in assessing environmental change

The results of the stratigraphical diatom analyses presented in the previous chapters provide information on basic aquatic and sedimentological processes controlling assemblage development. These processes may be triggered by environmental conditions outside the lake system or be generated in the lake itself. A last and careful attempt will be made to interpret the diatom results, illuminating possible changes of limnological conditions, ultimately forced by environmental change.

The 3000 and 1200 year records of Lago Calafquén and Lago Villarrica are dominated by planktonic diatoms. Within this community, the percentages of *Aulacoseira granulata, Cyclotella stelligera* and other species vary significantly, reflected on a larger scale by biogenic silica production, especially in Lago Calafquén. The driving force in biogenic silica production will be discussed below.

9.1 Nutrients

The relative increase in biogenic silica production in *Lago Calafquén* between ~ BC 50 and ~ AD 1350 indicates a rise in primary productivity. This is also reflected by the relative increase in *Aulacoseira granulata*, as this species prefers a light- and nutrient-rich habitat, blooming in late summer. It may also tolerate nutrient fluctuations better than *Cyclotella stelligera*. *Aulacoseira granulata* can be used to indicate eutrophication under different hydrological conditions, e. g. in conjunction with species such as *Stephanodiscus minutulus*, etc. in Lake Ammer (Ammersee) and Lake Starnberg (Starnberger See) (Alefs, 1997).

9.1.1 Silicon

Nutrient uptake not only controls primary production, i. e., the number or biomass of diatoms, but also diversity within diatom communities. Dissolved silica availability is known to affect algal productivity and growth (Wetzel, 1975; Sommer, 1994). Among the limiting nutrients controlling algal growth in Lago Calafquén and Lago Villarrica (cf. Chapter 2, this Part), silicon and phosphorus seem to be the most important. Si-limited conditions are reflected by the low diversity within each diatom community, conditions that are prominent in the studied lakes. Si-limitation for diatoms in stable, stratified lake-systems is not prone to strong fluctuations and may last for the entire period of stratification (Sommer, 1994). Silicon is released by inflowing suspended allophanes, volcanic materials, and other Si-bearing minerals. Though their dissolution rates are slow they form an ubiquitous available-but-limiting nutrient. One positive criterion for silicon limitation in both lakes is the high primary production that is reflected in the high BSi content of the sediments.

9.1.2 Phosphorus

Phosphorus limitation controls the diversity of assemblages (cf. Barbiero et al., 2002, and references therein). Aquatic organisms can remove phosphorus from lake sediment in sufficient amounts to satisfy their requirements (Syers, 1973).

The precise role of phosphorus in the studied lakes is difficult to estimate, as phosphorus concentrations in the sediments and Redfield ratios were not determined. Regardless, implications of phosphorus to algal growth within this special volcanic environment have been described in the literature and are considered in the following paragraphs.

Volcanic soils in Chile are characterized as andisoils, as the clay-sized fraction contains abundant allophane. These soils have a high P-adsorption capacity concomitant with low P-availability (Borie and Rubio, 2003). McCull (1974) examined phosphorus availability from lake sediments in a similar volcanic catchment in New Zealand and found that adsorption on volcanic soil particles did not appear to reduce the availability of dissolved P for algal growth. Soil phosphorus availability increased with increasing levels of dissolved phosphorus, increased inorganic phosphorus, and increased algal density. McCull (1974) suggested this occurred because the transfer rate of phosphorus between soil particles and algae occurred during close contact of soil particles in the water column, probably enhanced by turbulence. Additional chemical changes in the lake could also have caused mobilisation of otherwise unavailable phosphorus. Water-depth at which the sediments had been taken had no apparent effect on phosphorus availability.

The availability of sediment phosphorus to aquatic plants is less clearly defined, as phosphorus is either chemically bound and removed from the water by the incoming sediment, or released from the sediment to the water, depending on environmental conditions (McCull, 1974). Suspended matter, especially from volcanic topsoil and ash erosion, is regarded as a significant nutrient source for algal growth in the studied lakes. Powdered allophanic clay materials have the capacity to bind phosphorus (Wilson and Taylor, 1973), and can rapidly reduce dissolved phosphorus concentrations. This does not significantly reduce availability of phosphorus for algae in the surface waters, unless allophanes settle out of the photic zone soon after adsorption of phosphorus has occurred (McCull, 1974). This may have occurred in Lago Calafquén with the slight relative long-term increase in the clay-sized fraction (cf. Part 2, Chapter 6), observed during AD 370 and AD 1240. In Lago Calafquén and Lago Villarrica, reduced phosphorus availability for plankton growth may have resulted from the formation of flaky, clustered agglomerates comprised of dust, phytoplankton, senescent zooplankton, and/or clay minerals (cf. Chapter 7, this part, Fig. V-4a). The conglutination of fine (inorganic phosphorus-bearing and releasing) particles into large aggregates likely increased the water column particle flux rate and possibly increased the removal of limiting nutrients like phosphorus from the water column.

High amounts of dissolved phosphorus in fresh water usually indicate nutrient enrichment and a change in trophic status. Planktonic diatoms from areas experiencing active volcanic impacts, especially in Chile, suggest eutrophication trends in lakes located in these settings (Rumrich et al., 2000). Consequently, increased phosphorus availability for algal growth in the studied Chilean lakes should indicate a change in lake trophy. This may be oversimplified, as McCull (1974) observed that neither phosphorus content in the water column or sediment of oligotrophic lakes accurately reflected trophic status. His examined lakes had higher phosphorus contents in their volcanic lake sediments than some mesotrophic lakes have shown. Investigations by Flint (1977) in Lake Okataina, New Zealand, showed phyto- and zooplankton assemblages characteristic of mesotrophic water but chemically the lake was oligotrophic. Similar inconsistencies between biological and chemical findings occur in Lago Villarrica, where Thomasson (1959, in Flint, 1977) suggested that "…higher temperatures and persistent wind may cause a more rapid recycling and redistribution of nutrients and stimulate a richer phytoplankton than the chemical content of the water would indicate."

9.1.3 Iron

The onset of the biogenic silica increase in Lago Calafquén around AD 460 is consistent with an increase in the Fe:Ti ratio (cf. Part 2, Chapter 6). Fluctuations in Fe/Ti correspond with the phase of high productivity in Lago Calafquén. Iron likely originates from the strongly-weathered volcanic soils in the catchment. Precipitation of flocculated, colloidal particles of ferric hydroxide $Fe(OH)_3$ were

observed along the creek tributaries during field campaigns, indicating significant iron transport into Lago Calafquén occurs. As shown from iron fertilisation experiments in marine ecosystems, Fe stimulates algal Si-uptake (cf. Anderson, article from IGBP NL 56; also Schulte, 2004). Manganese is often associated with ferric iron compounds, and also stimulates diatom growth (Wetzel, 1975). As shown in Part 2, Chapter 6 of this investigation, the peaks of the Fe:Mn ratio in the sediments of Lago Calafquén could indicate changes in the redox-potential (sensu Mackereth, 1966). Redox-potential may be affected by increased primary productivity, resulting in decreased oxygen concentrations in the hypolimnion. Only slight, if any, fluctuations in the oxygen budget can be inferred for Lago Calafquén due to increased productivity, and no evidence for meromixis was observed.

9.1.4 Anthropogenic influence

The sudden occurrence of *Asterionella formosa* and *Fragilaria crotonensis,* along with *Aulacoseira granulata* in the sediment surface (6 to 5 cm depth Lago Calafquén, see above), indicates a rapid and significant shift in the environment. *Asterionella formosa* usually occurs with abundant dissolved silicon, but is also a good competitor for phosphorus. Pennate diatoms, especially those of the genus *Fragilaria,* dominate at high Si:P ratios. Similar diatom trends occur in the uppermost core samples from Lago Villarrica (8 to 2 cm depth), however *Fragilaria crotonensis* persists until present day, and is not restricted to a single bloom as observed in Lago Calafquén. Furthermore, these shifts in diatom assemblages correspond to a strong peak in the Fe:Ti ratio (cf. Part 2, Chapter 6, Figs. IV-25, 38). These findings suggest anthropogenic impact, as both lakes have been popular tourism destinations for nearly one century. Increasing settlement and associated land-clearing in the catchment have also occurred and are subject of discussion among the national environmental monitoring institutes for several years. Expected increases in Si and P are reflected in the sudden shift of species composition of diatom assemblages. Currently, eutrophication problems in Lago Villarrica are apparent (Woelfl, 2003), and were firstly described (Campos et al., 1983).

9.1.5 Summary of considerations of the role of nutrients

Though phophorus content was not measured in either lake investigated, the low diatom species diversity in each sample suggests silicon to be the first limiting nutrient, ranking higher than phosphorus, as the former is ubiquitously available from many sources. The diatoms presented tend to be good nutrient competitors, suggesting that phosphorus is a subordinate limiting nutrient. Phosphorus is available for algal growth only when it is released from P-bearing suspended matter in the photic zone (clay-sized volcanic soil and ash particles). Suspended matter tends to form large, conglutinated aggregates that rapidly settle out of the water column. These aggregates bind and remove fine-sized particles, effectively removing available phosphorus. For both lakes, nitrogen is not considered to be a main limiting nutrient, as the C:N ratios for sediments of Lago Calafquén and Lago Villarrica fluctuate around 12, corresponding to autochthonous organic matter produced by the decomposition of plankton within the lake (Wetzel, 1975). The assumptions on iron influx and its effect on primary productivity on Lago Calafquén are only hypothetical and only imply that Fe-limitation may play a role in Si-uptake. This would confirm that Si is the dominant limiting nutrient, consistent with the surrounding geology of the catchment.

9.2 Environmental conditions

The discussion on nutrient availability for algal growth in the previous chapter requires considerations on possible driving mechanisms. A range of environmental interpretations can be made based upon the diatoms life histories, habitats and ecological preferences (Bradbury, 1999). Assessing environmental change from fluctuations in diatom assemblages can also be difficult, as the same signal may display changes in opposite directions (Wolin and Duthie, 1999).

Among the many environmental variables that might force time-related fluctuations on diatom assemblages (*e. g*. droughts, fluctuations in temperature, long-term climate patterns or precipitation) wind action may be an important consideration in the entire complex scenaria of palaeoenvironmental reconstructions for both lakes investigated. Associated with wind might also be changes in lake-level. Palaeophycological approaches offer the possibility to interpret changes in lake-level as they provide a continuous chronological record over a variety of time scales (Smol and Cumming, 2000, and references therein). Some lakes may be more responsive to changes in the environment than others, dependent on basin morphometry (Håkanson, 2005) and local hydrology (Smol and Cumming, 2000). Comparisons between Lago Calafquén and Lago Villarrica involve potential regional difficulties, as even lakes that are in close proximity can have different properties and respond differently to environmental changes in the surroundings (Battarbee, 2000). This is apparent from the results of the multi-proxy sedimentological analysis in Part 2, Chapter 6, of this investigation. Hence, observed diatom signals are open to alternative interpretations.

9.2.1 Lago Calafquén

Several aspects of the above described findings would indicate wind action, in combination with lake-level fluctuation, as the driving forces producing the observed biological signals in Lago Calafquén. Wind action can transport non-planktonic species into pelagial waters. A temporary increase in littoral material can also indicate a rise or fall in lake level, signals that are mostly found in deep-water cores because of sediment focussing (Wolin and Duthie, 1999). Wolin (1996) describes an increase in fine particles occuring during high water stages. She based her findings on "…a deep-water core taken at 15.25 m" water depth. It must be stated that at the shallow water depths described by Wolin (1996), wave action still affects bottom sediments and sediment focussing effects would likely occur along the profundal plain. In the diatom records of both lakes investigated, fluctuations of littoral species are observed to occur with the planktonic community. The presence of *Melosira varians* colonies (see Appendix, Fig. C-4) indicate littoral erosion, likely caused by strong wave action triggered by wind. Littoral erosion in Lago Calafquén may be reflected in the variation of pennate diatoms found in the deep water cores, but it remains open if this could also be a result of large-scale lake-level fluctuation.

Additional evidence of wind activity might be the ubiquitous presence of *Aulacoseira granulata*, as this heavy diatom has rapid sinking velocities. Bradbury (1975) suggests this genus requires turbulence to maintain its presence in the water column using the effects of changing buoyancy. Increased turbulence – and hence increased wind activity – as well as corresponding nutrient increases during low water stages can favour this genus over other planktonic species (Wolin and Duthie, 1999). Owen and Crossley (1992) stated that *Aulacoseira* filaments favour up-welling conditions. In Lake Malawi, Africa, Pilskaln and Johnson (1991) reported that *Aulacoseira* dominated assemblages during dry-wind periods, where it takes advantage of high-nutrient and high turbulence conditions, though it must be also stated that this is a relatively shallow lake.

In both Lago Calafquén and Lago Villarrica, periods of high wind activity provide increased turbulence and therefore also high nutrient conditions by up-welling, favouring the growth of *Aulacoseira* genus. This genus is resistant against such kind of dynamic external forcing due to their thick, strong, and heavy cells. Furthermore, high primary productivity reflected by the high sediment biogenic silica concentration and the concomitant high amount of zooplankton fecal pellet aggregates implies nutrient enriched conditions. In Lago Calafquén between ~ BC 50 to ~ AD 1350, nutrients ultimately might have been generated by fluctuating lake levels.

9.2.2 Lago Villarrica

In Lago Villarrica, recurring fluctuations between species occurred on short time scales. Oscillations between *Aulacoseira granulata* and *Cyclotella stelligera* in DS-A might have been driven by repeated events. However, the consistent abundance of *Gomphonema* cf. *parvulum* during this interval likely reflects uniform nitrogen and phosphorus levels, and hence little change in lake productivity. During DS-B (cf. Fig. V-3), the step-wise increases in *Gomphonema* cf. *parvulum* and *Fragilaria construens* var. *binodis* might indicate phases of higher productivity, which is also reflected by higher sediment biogenic silica concentrations. *Gomphonema* cf. *parvulum* is considered to favour high nitrogen, phosphorus and organic matter concentrations (Werner, 1977), and in Lago Villarrica, indicate several important changes. Increased nitrogen concentrations around AD 1830 (~ 40 cm depth, Fig. IV-35 (Part 2, Chapter 6)) could be associated with increased soil erosion and influx of nitrogen from outside the lake system. Enhanced erosion of volcanic soils and ashes into Lago Villarrica would also increase phosphorus availablility. Erosion is also reflected by the increasing Fe:Ti ratio (Fig. IV-38, Part 2, Chapter 6). These findings could indicate the onset of permanent colonization around Lago Villarrica. Permanent settlement of the southern Lake District around Lago Villarrica started around the end of the 18th century (Schindler, 1990) and probably earlier than at Lago Calafquén, aside from Neolithic settlements (Pino et al., 2004). The continuous, relatively high abundance of *Gomphonema* cf. *parvulum* to present-day would support the assumption of anthropogenic changes in the catchment.

9.2.3 Assessing environmental change

The discussion is one possible interpretation of environmental conditions that might have prevailed around the lakes investigated. Stratigraphical diatom analyses have revealed that significant variation in the biota of Lago Calafquén and Lago Villarrica occurred, suggesting environmental changes. The current assessment of environmental changes from both lakes is still subject to interpretation, as additional data that could support these findings is lacking. Above all, the effects of selective grazing by zooplankton are one aspect that obviously is significant in both lakes. Changes in abundances should also be discussed including absolute diatom concentrations, which were not determined. Nevertheless, the diatom analyses for both lakes have shown some interesting and promising results that should be further investigated.

VI. Conclusions and outlook

1. Major conclusions

Lago Calafquén and Lago Villarrica, northern Chilean Lake District, were investigated to characterize the composition of basin infill, to determine modern and pre-historic sedimentation processes, and to estimate lake productivity. Furthermore, these analyses were performed to test the lakes' archive potential for assessing palaeoenvironmental and palaeoclimatic changes. Both lakes are located in a geodynamically active setting, where earthquakes and volcanic eruptions occur frequently, impacting the lakes and surrounding catchments. Assessing these effects on general sedimentation processes was a secondary aim of the presented study.

Seismic investigations of both lakes provided general information on basin geometry, morphology, and large-scale sedimentation processes. Lago Calafquén is divided into two sub-basins that give rise to diverse sedimentation processes. These basins are strongly affected by seismic and volcanic events. Inferred from seismic stratigraphic analyses various deformation features are recognized that are related to earthquake induced soft sediment deformation. Repeated, large mass-flow deposits are recognized in corresponding seismic stratigraphic horizons from various parts of Lago Calafquén's basin, hence implying coeval deposition associated with earthquake events. Large-scale liquefaction structures reveal large-scale injections and vertical migrating fluid escape pipes. Such structures indicate earthquakes as a trigger mechanism, but can also be generated by sediment overload or mass failure. Large turbidites of various origins are distributed in the lake basin. Seismic investigation has shown strongest deformation structures in the south-western part of Lago Calafquén's basin, where sediments are more acoustically penetrable. In the southern proximity of the lake basin, massive sub-aerial rockslides have occurred in prehistoric time and confine the present-day shore line of adjacent Lago Pullinque.

Nearby Lago Villarrica lacks such drastic events, as seismic investigation reveals that the lake basin is primarily affected by recurring, large mass-movements originating from the smooth slopes along the catchment's southern side, which is prone to landslides. Mass-flows are deposited in corresponding seismic stratigraphic units, hence implying they were triggered by seismic events. Locally, liquefaction processes in the mass-flow affected areas are likely caused by sediment overload. The deep plain of the simple U-shaped lake basin is affected by large turbidites and mass movements, sourced from the volcanically-active environment. Acoustic penetration was hampered in this area.

The basements of both lake basins are made up of large chaotically distributed blocks in the southern to south-western part of each basin. These structures imply that massive rock-slope failures, rockslides and earth spreads caused by debuttressed sidewalls from the detachment area control the basin morphology. The estimated accumulated rock volume is comparable with large sub-aerial landslides and rock-falls in various alpine regions that are caused by tension release, initially triggered by isostatic uplift. However, severe earthquakes are considered as the main triggers responsible for the large sidewall failures in the lake basins of Lago Calafquén and Lago Villarrica.

The heterogenous structures of both lake basins, as well as geodynamic effects, are also traced in sedimentological basin analyses. Surface sediments were analyzed to investigate modern sedimentation processes in Lago Calafquén and Lago Villarrica. They provided information as to pathways of sediment dispersal, which in turn has been used to reconstruct hydrodynamics and catchment related sedimentation processes. These analyses have shown that the lakes differ in their sediment deposition, and their catchments also differ in size and sediment availability. Little sediment is delivered to Lago Calafquén by the tributary Río Pellaifa flowing year-round, which forms the outlet of Lago Pellaifa. Seasonal runoffs drain the flanks of Volcano Villarrica, periodically delivering vast amounts of sediment to the lake basin, sometimes as sub-aerial debris flows that spread in the basin as turbidites. Sediment dispersal in Lago Calafquén is not uniform between the various

individual sub-basins. The deep basin plains of the eastern and central sub-basin are frequently affected by high-energy, large underflow deposits. They dilute the biogenically-controlled normal laucstrine sediments, which is reflected in low TOC values in these areas. Normal laucstrine sedimentation controls the south-western part of the central sub-basin, which is mostly characterized by interflow and surface flow deposits. TOC and TOC/TS ratios suggest production is controlled by autochthonous processes. Sediment dispersal is not controlled by sediment focusing, but by thermal stratification patterns. Despite the large permanently flowing E-W trending tributary, the strongest imprints on depositional patterns in Lago Villarrica are caused by small tributaries from the southern side. Some of them occasionally operate as debris flow trajectories, cross-cutting normal lacustrine sedimentation patterns. Due to lake-floor morphology, only the western part of the lake basin is less affected by strong turbidites, favouring deposition of normal lacustrine sediment, which is distributed by low-energy, interflow currents.

Chronological sedimentation patterns and their coupling to catchment-related processes, with respect to environmental and climatic changes, were analyzed by multi-proxy studies on sediment cores from Lago Calafquén and Lago Villarrica, covering ~ 3000 and ~ 1200 years, respectively. Various tephra layers recorded in the sediment succession imply frequent volcanic activity, especially between BC 1385 and BC 100. Sedimentation and mass accumulation rates reflect the different catchment sizes that in turn generate individual sedimentation patterns in each lake system. Environmental fluctuations, traced by comparing biogenic and sedimentary proxies, also show that both lakes have different small-scale sedimentation patterns. Age-related 'proxy-data', based on mass accumulation rates of biogenic silica, TOC, and sediment grain-size fractions, follow a long-term trend occurring in both lakes. This can obviously be a result of a general driving force, such as climate change. Increasing productivity between AD 360 to AD 1080 characterize conditions in Lago Calafquén, reflecting variable allochthonous influx by fluctuations in catchment erosion, ultimately due to possible increases in moisture. Decreasing allochthonous influx and moderate productivity characterize the period between ~ AD 1080 and AD 1270 of both lakes. After Villalba (1990), this time period is synchronous with the warm-dry 'Medieval Warm Period'. Faint signals of the 'Little Ice Age', between ~ AD 1350 and ~ AD 1650, are found in both lakes by increased allochthonous influx and decreased productivity. A sudden increase in all flux rates in Lago Villarrica at the end of the 18^{th} /beginning 19^{th} century marks distinct changes in environmental conditions, which might indicate warmer or moister climate, or the beginning of permanent settlements around the lake. This is consistent with the diatom analysis, which shows a strong increase in *Gomphonema* cf. *parvulum*, suggestive of increased soil erosion and influx by clearing.

Diatom analyses have shown that after nearly every tephra impact, a sudden, short, and prevalent monospecific development of *Aulacoseira granulata* occurs. No new species appear after such events, only shifts in relative abundance. Biogenic silica analyses indicate that tephra impacts do not cause long-term catastrophic effects on the ecosystems of Lago Calafquén and Lago Villarrica. Normal lacustrine sediments of both lakes are characterized by high biogenic silica concentrations that break down during each volcanic impact. Recovery to pre-state conditions occurs within decades, as suggested by the clear increase in biogenic silica within decades after tephra impact.

2. Outlook

This thesis provides baseline information on the general spatial- and chronological sedimentation processes and lake productivities during the late Holocene. Although the lake basins of Lago Calafquén and Lago Villarrica are affected by strong geodynamic activity, they have sufficient archive potential to unravel past environmental changes. From the dated short cores of both lakes,

basic sedimentation models were established describing lake-bottom sedimentation patterns and probable catchment-related environmental changes.

Based on this study, future multi-proxy investigations of long-term environmental and climatic changes should yield promising results. Long sediment cores taken from suitable coring sites of both lakes could be used to reconstruct the environmental history from the Late Glacial to present day. Applying detailed seismic stratigraphic studies, comprising the entire lake basin with a denser grid than employed in this study, could support reconstructed time-related sedimentation processes on a larger scale. Palaeoecological studies, and especially absolute diatom concentration analyses, could support assessment of long-term palaeoenvironmental and palaeoclimatic change.

Sedimentological and diatom-based palaeolimnological studies on Lago Calafquén and Lago Villarrica have shown some interesting preliminary results, and should be investigated further in the future.

VII. References

References

Abbott, M.B., Wolfe, B.B., Wolfe, A.P., Seltzer, G.O., Aravena, R., Mark, B.G., Polissar, P.J., Rodbell, D.T., Rowe, H.D., Vuille, M. 2003. Holocene paleohydrology and glacial history of the central Andes using multiproxy lake sediment studies. Palaeogeography, Palaeoclimatology, Palaeoecology 194, 123-138.

Abele, G. 1997. Influence of glacier and climatic variation on rockslide activity in the Alps. In: Matthews, J.A., Brunsden, D., Frenzel, B., Gläser, B., Weiss, M.J. (eds.). Rapid mass movement as a source of climatic evidence for the Holocene. Paläoklimaforschung 19, 1-6.

Acharya, H. 1982. Volcanic activity and large earthquakes. Journal of Volcanology and Geothermal Research 13, 373-378.

Alefs, J. 1997. Feinstratigraphie und Diatomeensukzession in den Profundalsedimenten des Ammersees und Starnberger Sees (Oberbayern). Dissertation, Technische Universität München, 165 p.

Anderson, D.M., Archer, R.B. 1999. Preliminary evidence of early deglaciation in southern Chile. Palaeogeography, Palaeoclimatology, Palaeoecology 146, 295-301.

Anderson, N.J. 2000. Diatoms, temperature and climate change. European Journal of Phycology 35, 307-314.

Anderson, R. What regulates the efficiency of the biological pump in the Southern Ocean? Article from IGBP NL 56.
http://www.igbp.kva.se/cgi-bin/php/list.show.php?section_id=63&article_id=343&onearticle=

Anderson R.Y., Soutar A., Johnson T.C. 1992. Long-term changes in El Niño/Southern Oscillation; evidence from marine and lacustrine sediments. In: Diaz, H.F., Markgraf, V. (eds.). El Niño; historical and paleoclimatic aspects of the Southern Oscillation. Camebridge University Press, 419-433.

André, M.F. 2001. Tors et roches moutonnées en Laponie suédoise: antagonisme ou filiation ? Geographie Physique et Quaternaire 55 (3), 229-242.

Andrello, A.C., Appoloni, C.R. 2004. Spatial variability and Cesium-137 inventories in native forest. Brazilian Journal of Physics 34 (3A), 800-803.

Appleby, P.G. 1997. Sediment records of fallout radionuclides and their application to studies of sediment-water interactions. Water, Air, and Soil Pollution 99 (1-4), 573-586.

Araneda, M., Avendaño, M.S., Götze, H.J., Schmidt, S., Muñoz, J. 2000. Gravedad en los Andes del Sur, correlación del residual isostático con rasgos estructurales mayores (37°-42°S). 9° Congreso Geológico Chileno, Actas Vol. 2, 399-403. Puerto Varas.

Ariztegui, D., Bianchi, M.M., Masaferro, J., Lafargue, E., Niessen, F. 1997. Interhemispheric synchrony of late-glacial climatic instability as recorded in proglacial Lake Mascardi, Argentina. Journal of Quaternary Science 12, 333-338.

Ashworth, A.C., Hoganson, J.W. 1993. Magnitude and rapidity of the climate change marking the end of the Pleistocene in the mid-latitudes of South America. Palaeogeography, Palaeoclimatology, Palaeoecology 101, 263-270.

Baier, J., Lücke, A., Negendank, J.F.W., Schleser, G.H., Zolitschka, B. 2004. Diatom and geochemical evidence of mid- to late Holocene climatic changes at Lake Holzmaar, West-Eifel (Germany). Quaternary International 113, 81-96.

Baillie, M.G.L., Munro, M.A.R. 1988. Irish tree rings, Santorini and volcanic dust veils. Nature 332 (6162), 344-346.

Ballantyne, C.K. 1997. Holocene rock-slope failures in the Scottish Highlands. Paläoklimaforschung 19, 197-205.

Ballantyne, C.K. 2002. Paraglacial geomorphology. Quaternary Science Reviews 21, 1935-2017.

Barazangi, M., Isacks, B.L. 1976. Spatial distribution of earthquakes and subduction of Nazca Plate beneath South America. Geology 4, 686-692.

Barbiero, R.P., Tuchman, M.L., Warren, G.J., Rockwell, D.C. 2002. Evidence of recovery from phosphorus enrichment in Lake Michigan. Canadian Journal of Fisheries and Aquatic Sciences 59, 1639-1647.

Barker, P., Telford, R., Merdaci, O., Williamson, D., Taieb, M., Vincens, A., Gibert, E. 2000. The sensitivity of a Tanzanian crater lake to catastrophic tephra input and four millennia of climate change. Holocene 10, 303-310.

Barker, P.A.., Williamson D., Gasse, F., Gibert, E. 2003. Climatic and volcanic forcing revealed in a 50,000 year diatom record from Lake Massoko, Tanzania. Quaternary Research 60, 368-376.

Barrientos, S.E., Ward, S.N. 1990. The 1960 Chile earthquake: inversion for slip distribution from surface deformation. Geophysical Journal International 103, 589-598.

Barsdate, R.J., Dugdale, R.C. 1972. Effects of volcanic ashfalls on chemical and sediment characteristics of two Alaskan lakes. Journal of the Fisheries Research Board of Canada 29 (3), 229-236.

Battarbee, R.W. 1986. Diatom analysis. In Berglund, B.E. (ed.). Handbook of Holocene Palaeoecology and Palaeohydrology. Wiley, Chichester, 527-570.

Battarbee, R.W., Charles, D.F., Dixit, S., Renberg, I. 1999. Diatoms as indicators of surface water acidity. In: Stoermer, E., Smol, H.P. (eds.). The Diatoms: Applications for the Environmental and Earth sciences. Cambridge University Press, Cambridge, 85-127.

Battarbee, R.W. 2000. Palaeolimnological approaches to climate change, with special regard to the biological record. Quaternary Science Reviews 19, 107-124.

Battarbee, R.W., Jones, V.J., Flower, R.J., Cameron, N.G., Bennion, H., Carvalho, L., Juggins, S. 2001. In: Smol, J.P., Birks, H.J.B., Last, W.M. Tracking environmental change using lake sediments. Vol. 3: Terrestrial, Algal, and Siliceous Indicators. Kluwer Academic Publishers, Dordrecht, Netherlands. 155-202.

Battarbee, R.W., Mackay, A.W., Jewson, D.H., Ryves, D.B., Sturm, M. 2005. Differential dissolution of Lake Baikal diatoms: correction factors and implications for palaeoclimatic reconstruction. Global and Planetary Change 46, 75-86.

Belousov, A., Belousova, M. 1996. Large scale landslides on active volcanoes in the 20th century – Examples from the Kurile-Kamchatka region (Russia). In: Senneset, K. (ed.). Landslides Vol. 2, Balkema, Rotterdam, 953-957.

Benn, D.I. 1992. The genesis and significance of 'hummocky moraine': evidence from the Isle of Skye, Scotland. Quaternary Science Reviews 11, 781-799.

Benn D.I., Clapperton C.M. 2000. Glacial sediment-landform associations and paleoclimate during the last glaciation, Strait of Magellan, Chile. Quaternary Research 54 (1), 13-23.

Bennett, M.R., Boulton, G.S. 1993. A reinterpretation of Scottish 'hummocky moraine' and its significance for the deglaciation of the Scottish Highlands during the Younger Dryas or Loch Lomond Stadial. Geological Magazine 130, 301-318.

Bennett, K.D., Haberle, S.G., Lumley, S.H. 2000. The Last Glacial–Holocene transition in Southern Chile. Science 290, 325-328.

Bentley, M. 1996. The role of lakes in moraine formation, Chilean Lake District. Earth Surface Processes and Landforms 21, 493-507.

Bertrand, S. 2005. Sédimentation lacustre postérieure au dernier maximum glaciaire dans les lac Icalma et Puyehue (Chili meridonial): Reconstitution de la variabilité climatique et des evenements sismo-tectoniques. Université de Liège, Dissertation, 268 p.

Bertrand, S., Boës, X., Castiaux, J., Charlet, F., Urrutia, R., Espinoza, C., Lepoint, G., Charlier, B., Fagel, N. 2005. Temporal evolution of sediment supply in Lago Puyehue (Southern Chile) during the last 600 yr and its climatic significance. Quaternary Research 64 (2), 163-175.

Besoain, E., Sepúlveda, G. 1984. Minerales secundarios. In: Institúto de Investigaciones Agropecuarias (INIA). Suelos volcanicos de Chile. Santiago.

Beylich, A.A. 2000. Geomorphology, sediment budget, and relief development in Austdalur, Austfiroir, East Iceland. Arctic Antarctic and Alpine Research 32 (4), 466-477.

Birks, H.H., Battarbee, R.W., Birks, H.J.B. 2000. The development of the aquatic ecosystem at Kråkenes Lake, western Norway, during the late glacial and early Holocene – a synthesis. Journal of Paleolimnology 23 (1), 91-114.

Birks, H.J.B. 1994. Did Icelandic volcanic eruptions influence the postglacial vegetational history of the British Isles. Trends Ecol. Evol. 9, 312-314.

Birks, H.J.B., Lotter, A.F. 1994. The impact of the Laacher See Volcano (11000 yr B.P.) on terrestrial vegetation and diatoms. Journal of Paleolimnology 11, 313-322.

Blunier, T., Chappelaz, J., Schwander, J., Dällenbach, A., Stauffer, B., Stocker, T.F., Raynaund, D., Jouzel, J., Clausen, H.B., Hammer, C.U., Johnsen, S.J. 1998. Asynchrony of Arctic and Greenland climate change during the last glacial period. Nature 394, 730-743.

Bohm, M., Lüth, S., Echtler, H., Asch, G., Bataille, K., Bruhn, C., Rietbrock, A., Wigger, P. 2002. The Southern Andes between 36° and 40°S latitude: seismicity and average seismic velocities. Tectonophysics 356, 279-289.

Borie, F., Rubio, R. 2003. Total and organic phosphorus in Chilean volcanic soils. Gayana Botanica 60 (1), 69-78.

Boyle, J.F. 2001. Inorganic geochemical methods in palaeolimnology. In: Last, W.M., Smol, J.P. (eds.). Tracking environmental change using lake sediments. Vol. 2: Physical and Geochemical methods. Kluwer Academic Publishers, Dordrecht, Netherlands, 504 p.

Bradbury, J.P. 1975. Diatom stratigraphy and human settlement in Minnesota. Geological Society of America, Special Paper 171, Colorado, 74 p.

Bradbury, J.P. 1988. A climatic-limnological model of diatom succession for paleolimnological interpretation of varved sediments at Elk Lake, Minnesota. Journal of Paleolimnology 1, 115-131.

Bradbury, J.P. 1999. Continental diatoms as indicators of long-term environmental change. In: Stoermer, E.F., Smol, J.P. (eds.). The Diatoms: Applications for the Environmental and Earth Sciences. Cambridge University Press, Cambridge, 169-182.

Branconnot, P., Harrison, S.P., Joussaume, S., Hewitt, C.D., Kitoh, A., Kutzbach, J.E., Liu, Z., Otto-Bliesner, O., Syktus, J., Weber, N. 2004. Evaluation of PMIP Coupled Ocean-Atmosphere Simulations of the Mid-Holocene. In: Battarbee R.W., Gasse F., and Stickley C.E. (eds.). Developments in Paleoenvironmental Research. Vol. 6: Past Climate Variability through Europe and Africa. Springer-Verlag.

Bryant, C.L., Farmer, J.G., MacKenhzie, A.B., Bailey-Watts, A.E., Kirika, A. 1997. Manganese behaviour in the sediments of diverse Scottish freshwater lochs. Limnology and Oceanography 42, 918-929.

Brueckl, E., Paroditis, M. 2001. Estimation of large-scale mechanical properties of a large landslide on the basis of seismic results. International Journal of Rock Mechanics & Mining Science 38, 877-883.

Campbell, C. 1998. Late Holocene lake sedimentology and climate change in Southern Alberta, Canada. Quaternary Research 49, 96-101.

Campos, H., Arenas, J., Steffen, W., Agüero, G. 1980. Limnologische Untersuchungen an den Seen Pellaifa und Calafquén in Chile. Beiträge zur Hydrologie 7, 99-137.

Campos, H., Steffen, W., Román, C., Zúñiga, L., Agüero, G. 1983. Limnological studies in Lake Villarrica – morphometric, physical, chemical, planktonical factors and primary productivity. Archiv für Hydrobiologie 65 (4), 371-406.

Campos, H. 1984. Limnological study of Araucanian lakes (Chile). Verhandlungen der Internationalen Vereinigung für Limnologie 22, 1319-1327.

Caseldine, C., Hatton, J., Huber, U., Chiverrell, R., Wooley, N. 1998. Assessing the impact of volcanic activity on mid-Holocene climate in Ireland: the need for replicate data. Holocene 8 (1), 105-111 (7).

Cembrano, J., Hervé, F., Lavenu, A. 1996. The Liquiñe Ofqui fault zone : a long-lived intra-arc fault system in southern Chile. Tectonophysics 259, 55-66.

Cembrano, J., Schermer, E., Lavenu, A., Sanhueza, A. 2000. Contrasting nature of deformation along intra-arc shear zone, the Liquiñe-Ofqui fault zone, southern Chilean Andes. Tectonophysics 319, 129-149.

Chapron, E., Beck, C., Pourchet, M., Deconinck, J.F. 1999. 1822 earthquake-triggered homogenite in Lake Le Bourget (NW Alps), Terra Nova 11 (2-3), 86-92.

Chapron, E., Bertrand, S., Charlet, F., Boes, X., De Batist, M., Fagel, N., Magand, O., Arnaud, F., Melieres, M.A., Pino, M., Urrutia, R. 2004a. Sedimentary processes in Lake Puyehue over the last 500 years: Implications for paleoenvironmental reconstructions in the Chilean Lake District (41°S). Bolletino di Geofisica 45(2), 238-242.

Chapron, E., Van Rensbergen, P., De Batist, M., Beck, C., Henriet, J.P. 2004b. Fluid-escape features as a precursor of a large sublacustrine sediment slide in Lake Le Bourget, NW Alps, France. Terra Nova 16 (5), 305-311.

Charlet, F., Marchant, C., Volland, S., Pino, M., Urrutia, R., Mueller, J., Chapron, E., De Batist, M. 2003. Reflection-seismic study of six lakes in South-Central Chile (37°S-42°S): Lagos Laja, Lleulleu, Icalma, Villarrica, Puyehue & Todos los Santos. 10° Congreso Geológico Chileno, Actas, Concepción, Session 3.

Charlet, F., Marchand, C., Bertrand, S., Chapron, E., Pino, M., Urrutia, R., De Batist, M. 2004. Geophysical reconstruction of the sedimentary infill of Lago Icalma (39°S, Chilean Lake District) since the last deglaciation. Bolletino di Geofisica 45(2),179-184.

Cifuentes, I.L. 1989. The 1960 Chilean earthquakes. Journal of Geophysical Research 94 (B1), 665-680.

Clapperton, C.H. 1994. The quaternary glaciation of Chile: a review. Revista Chilena de Historia Natural 67, 369-383.

Clapperton, C.M., Sudgen, D.E., Kaufman, D.S., McCulloch, R.D. 1995. The last glaciation in central Magellan-Strait, southernmost Chile. Quaternary Research 44 (2), 133-148.

Clavero, J., Moreno, H. 1994. Ignimbritas Licán y Pucón: Evidencias de erupciones explosivas andesitico-basalticas postglaciales del Volcán Villarrica, Andes del Sur, 39°25'S. 7° Congreso Geológico Chileno, Actas Vol.1, 250-254, Universidad de Concepción.

Cook, E.R. 1992. Using tree rings to study past El Niño/Southern Oscillation influences on climate. – In: Diaz, H.F., Markgraf, V. (eds.). El Niño; historical and paleoclimatic aspects of the Southern Oscillation. Camebridge University Press, United Kingdom. 476 p.

Dearing, J.A., Foster, I.D.L., 1993. Lake sediments and geomorphological processes: some thoughts. In: McManus, J., Duck, R.W. (eds.). Geomorphology and sedimentology of lakes and reservoirs. John Wiley, Chichester, 5–14.

Dearing, J.A. 1997. Sedimentary indicators of lake-level changes in the humid temperate zone: A critical review. Journal of Paleolimnology 18 (1), 1-14.

DeMets, C., Gordon, R.G., Argus, D.F., Stein, S. 1994. Effect of recent revisions of the geomagnetic reversal time scale on estimates of current plate motions. Geophysical Research Letters 21, 2191-2194.

Denton, G.H., Lowell, T.V., Heusser, C.J., Schlüchter, C., Andersen, B.G., Heusser, L.E., Moreno, P.J., Marchant, D.R. 1999a. Geomorphology, stratigraphy, and radiocarbon chronology of Llanquihue drift in the area of the southern Lake District, Seno Reloncavi, and Isla Grande de Chiloé, Chile. Geografiska Annaler Series A - Physical Geography 81A (2), 167-229.

Denton, G.H., Heusser, C.J., Lowell, T.V., Moreno, P.J., Andersen, B.G., Heusser, L.E., Schlüchter, C., Marchant, D.R. 1999b. Interhemispheric linkage of paleoclimate during the last glaciation. Geografiska Annaler Series A - Physical Geography 81A (2), 107-153.

Diaz, H.F., Markgraf, V. (eds.). 1992. El Niño; historical and paleoclimatic aspects of the Southern Oscillation. Camebridge University Press, United Kingdom. 476 p.

Diaz, H.F., Markgraf, V. (eds.). 2000. El Niño and the Southern Oscillation – multiscale variability and global and regional impacts. Camebridge University Press, United Kingdom. 496 p.

Edgar, N., Keeley, N. 1998. Effects of the 1995/1996 Mt. Ruapehu eruptions on Lake Taupo and other aquatic ecosystems, New Zealand. LakeLine 18 (3), 20-31.

Einsele, G., Hinderer, M. 1998. Quantifying denudation and sediment-accumulation systems (open and closed lakes): basic concepts and first results. Palaeogeography, Palaeoclimatology, Palaeoecology 140, 7-21.

Emparán, C. 1980. Áreas sometidas a riesgos naturales en la zona Villarrica-Pucón. Revista Geológica de Chile 9, 27-35.

Flint, E.A. 1977. Phytoplankton in seven monomictic lakes near Rotorua, New Zealand. New Zealand Journal of Botany 15, 197-208.

Förstner, U., Wittmann, G.T. 1979. Metal Pollution in the Aquatic Environment. Springer, New York, 486 p.

Folk, R.L. 1980. Petrology of sedimentary rocks. Hemphill Publishing Co., Austin, Texas, 184 p.

Frutos, J., Alfaro, G. 1985. El complejo ofiolítico del ambito eugeosynclinál palaeozoico en la Cordillera de la Costa del sur de Chile. 4° Congreso Geológico Chileno, Actas, 29-64, Antofagasta.

Gallimore, R., Kutzbach, J.E., Jacob, R.L. 2005. Coupled atmosphere-ocean-vegetation simulations for modern and mid-Holocene climates: Role of extratropical vegetation cover feedbacks. Climate Dynamics, accepted.

Gasse, F., Fontes, J.C., Plaziat, J.C., Carbonel, P., Kaczmarska, I., de Dekker, P., Soulié-Märsche, I., Callot, Y., Dupeuple, P.A. 1987. Biological remains, geochemistry and stable isotops for the reconstruction of environmental and hydrological changes in the Holocene lakes from Northern Sahara. Palaeogeography, Palaeoclimatology, Palaeoecology 60, 1-46

Gersonde, R., Abelmann, A., Brathauer, U., Sieger, R., Zielinski, U. 1996. Das Südpolarmeer, ein Schlüsselgebiet für Klimaveränderungen in vergangener Zeit. Die Geowissenschaften 14, 17-21.

Giovanoli, F., Kelts, K.R., Finckh, P., Hsü, K.J. 1984. Geological framework, site survey and seismic stratigraphy. In: Hsü, K.J., Kelts, K.R. (eds.). Quaternary Geology of Lake Zurich: an interdisciplinary investigation by deep-lake drilling. Contributions to Sedimentology 13, 5-20.

Glasser, N.F., Harrison, S., Winchester, V., Aniya, M. 2004. Late Pleistocene and Holocene paleoclimate and glacier fluctuations in Patagonia. Global and Planetary Change 43, 79-101.

Gonzales-Ferran, O. 1995. Volcanes de Chile. Instituto Geográfico Militar. Santiago de Chile. 640 p.

v. Grafenstein, U., Erlenkheuser, H., Müller, J., Trimborn, P., Alefs, J. 1996. A 200 year mid-European air temperature record preserved in lake sediments: An extension of the $\delta^{18}O_p$-air temperature relation into the past. Geochim. Cosmochim. Acta 60 (21), 4025-4036.

v. Grafenstein, U., Erlenkheuser, H., Müller, J., Jouzel, J., Johnsen, S. 1998. The cold event 8200 years ago documented in oxygen isotope records of precipitation in Europe and Greenland. Climate Dynamics 14, 73-81.

Grosjean, M., Cartajena, I., Geyh, M.A., Nuñez, L. 2003. From proxy data to paleoclimate interpretation: the mid-Holocene paradox of the Atacama Desert, northern Chile. Palaeogeography, Palaeoclimatology, Palaeoecology 194, 247-258.

Guerrero, J.M., Echenique, R.O. 2002. Cyclostephanos patagonicus sp. nov., a new freshwater diatom from western Patagonia (Argentina). Diatom Research 17 (1), 141-151.

Haberle, S.G., Szeicz, J.M., Bennett, K.D. 2000. Late Holocene vegetation dynamics and lake geochemistry at Laguna Miranda, XI. Region, Chile. Revista Chilena de Historia Natural 73, 655-669.

Haflidason, H., Einarsson, Á. 1989. Repeated tephra falls and their effect on the nutrient loading in a volcanogenic eutrophic lake, north Iceland. Terra Abstracts 1, 227.

Håkanson, L. 1977. The influence of wind, fetch and water epth on the distribution of sediments in Lake Vanern, Sweden. Canadian Journal of Earth Sciences 14, 397-412.

Håkanson, L. 1981. Determination of characteristic values for physical and chemical lake sediment parameters. Water Resources Research 17, 1625-1640.

Håkanson, L., Jansson, M. 1983. Principles of lake sedimentology. Springer, Berlin, 316 p.

Håkanson, L. 2005. The importance of lake morphometry for the structure and functions of lakes. International Review of Hydrobiology 90 (4), 433-461.

Hall, V.A., Pilcher, J.R., McCormac, F.G. 1994. Icelandic volcanic ash and the mid Holocene Scots pine *(Pinus sylvestris)* decline in the north of Ireland: no correlation. Holocene 4, 79-83.

Hall, V.A., Smol, J.P. 1999. Diatoms as indicators of lake eutrophication. In: Stoermer, E.F., Smol, J.P. (eds.). The Diatoms: Applications for the Environmental and Earth Sciences. Cambridge University Press, Cambridge, 128-168.

Hambrey, M.J., 1994. Glacial environments. University College London Press, London. 296 p.

Hardardóttir, J., Geirsdóttir, A., Thórdarson, T. 2001. Tephra layers in a sediment core from Lake Hestvatn, southern Iceland: implications for evaluating sedimentation processes and environmental impacts on a lacustrine system caused by tephra fall deposits in the surrounding watershed. In: White J.D.L. and Riggs N.R. (eds.). Sedimentation in volcaniclastic settings. International Association of Sedimentologists (IAS) Special Publications 30, 225-246.

Heim, A. 1932. Bergsturz und Menschenleben. Vierteljahresschrift der Naturforschenden Gesellschaft Zürich, Zürich, 218 p.

Heinrichs, M.L., Wilson, S.E., Walker, I.R., Smol, J.P., Mathewes, R.W., Hall, K.J. 1997. Midge- and diatom-based paleosalinity reconstructions for Mahoney Lake, Okanagan Valley, British Columbia, Canada. International Journal of Salt Lake Research 6, 249-267.

Heinrichs, M.L., Walker, I.R., Mathewes, R.W., Hebda, R.J. 1999. Holocene chironomid-inferred salinity and paleovegetation reconstruction from Kilpoola Lake, British Columbia. Geographie Physique et Quaternaire 53 (2), 211-221.

Hervé, F. 1994. The Southern Andes between 39° and 44°S latitude: the geological signature of a transpressive tectonic regime related to a magmatic arc. In: Reutter, K.J., Scheuber, E., Wigger, P.J. (eds.). Tectonics of the Southern Central Andes: structure and evolution of an active continental margin. Springer, Berlin, Heidelberg, 243-247.

Hervé, F., Demant, A., Ramos, V.A., Pankhurst, R.K., Súarez, M. 2000. The Southern Andes. In: Cordiani, U.G., Milani, E.J., Thomas Filho, A., Campos, D.A. (eds.). Tectonic evolution of South America. Rio de Janeiro. 605-634.

Heusser, C.J. 1974. Vegetation and climate of the southern Chilean lake district during and since the Last Interglaciation. Quaternary Research 4, 290-315.

Heusser, C.J., Rabassa, J. 1987. Cold climatic episode of Younger Dryas age in Tierra del Fuego. Nature 328, 609-611.

Heusser, C.J. 1995. 3 Late-Quaternary pollen diagrams from southern Patagonia and their paleoecological implications. Palaeogeography, Palaeoclimatology, Palaeoecology 118 (1-2), 1-24.

Heusser, C.J., Lowell, T.V., Heusser, L.E., Hauser, A., Andersen, B.G., Denton, G.H. 1996. Full-glacial-late-glacial palaeoclimate of the southern Andes: Evidence from pollen, beetle and glacial records. Journal of Quaternary Science 11 (3), 173-184.

Heusser, C.J., Heusser, L.E., Lowell, T.V. 1999. Paleoecology of the southern Chilean Lake District-Isla Grande de Chiloé during middle-late Llanquihue glaciation and deglaciation. Geografiska Annaler Series A - Physical Geography 81A (2), 231-284.

Hickey-Vargas, R., Moreno, H., López-Escobar, L., Frey, F. 1989. Geochemical variations in Andean basaltic and silicic lavas from the Villarrica-Lanín volcanic chain (39.5°S): an evaluation of source heterogeneity, fractional crystallization and crustal assimilation. Contributions to Mineralogy and Petrology 103 (3), 361-381.

Hickman, M., Reasoner, M.A. 1994. Diatom responses to late Quaternary vegetation and climate change, and to deposition of two tephras in an alpine and a sub-alpine lake in Yoho National Park, British Columbia. Journal of Paleolimnology 11, 173-188.

Hickman, M., Reasoner, M.A. 1998. Late Quaternary diatom response to vegetation and climate change in a subalpine lake in Banff National Park, Alberta. Journal of Paleolimnology 20, 253-265.

Hoganson, J.W., Ashworth, A.C. 1992. Fossil beetle evidence for climatic change 18,000-10,000 years BP in South-Central Chile. Quaternary Research 37 (1), 101-116.

Hulton, N.R.J., Purves, R.S., McCulloch, R.D., Sudgen, D.E., Bentley, M.J. 2002. The last glacial maximum and deglaciation in southern South America. Quaternary Science Reviews 21, 233-241.

Hutchinson, G.E. 1957. A treatise on Limnology. I. Geography, Physics, and Chemistry. John Wiley & Sons, New York, 1015 p.

Hutchinson, S.M. 1994. Chernobyl radiocaesium in upland watershed-lake systems, Galloway, south west Scotland. Journal of Paleolimnology 10, 169-180.

Illies, H. 1967. Randpazifische Tektonik und Vulkanismus im südlichen Chile. Geologische Rundschau 57, 81-101.

Ivins, E.R., James, T.S. 1999. Simple models for late Holocene and present-day Patagonian glacier fluctuations and predictions of a geodetically detectable isostatic response. Geophysical Journal International 138, 601-624.

Jarman, D. 2002. Rock slope failure and landscape evolution in the Caledonian Mountains, as exemplified in the Abisko area, northern Sweden. Geografiska Annaler, 84A, 213-224.

Jenny, B., Valero-Garcés, B.L., Urrutia, R., Kelts, K., Veit, H., Appleby, P.G., Geyh, M. 2002. Moisture changes and fluctuations of the Westerlies in mediterranean central Chile during the last 2000 years: The Laguna Acuelo record (33°50'). Quaternary International 87, 3-18.

Jones, B.F., Bowser, C.J. 1978. The mineralogy and related chemistry of lake sediments. In: Lerman, A. (ed.). Lakes – Chemistry, Geology, Physics. Springer, New York, 363 p.

Kaplan, M.R., Douglass, D.C., Singer, B.S., Caffee, M.W. 2005. Cosmogenic nuclide chronology of pre-last glacial maximum moraines at Lago Buenos Aires, 46 degrees S, Argentina. Quaternary Research 63 (3), 301-315.

Keefer, D.K. 1999. Earthquake-iduced landslides and their effects on alluvial fans. Journal of Sedimentary Research 69 (1), 84-104.

Kilian, R., Hohner, M., Biester, H., Wallrabe-Adams, H.J., Stern, C.R. 2003. Holocene peat and lake sediment tephra record from the southernmost Chilean Andes (53-55 degrees S). Revista Geológica de Chile 30 (1), 23-37.

Kimura, M. 1978. Significant eruptive activities related to large interplate earthquakes in the northwestern Pacific margin. Journal of Physics of the Earth 26 (Suppl.), S557-S570.

Klee, R., Schmidt, R. 1987. Eutrophication of Mondsee (upper Austria) as indicated by the diatom stratigraphy of a sediment core. Diatom Research 2 (1), 55-76.

Kleman, J. 1992. The palimpsest glacial landscape in northwestern Sweden. Geografiska Annaler 74A, 305-325.

Koch, J., Kilian, R. 2005. 'Little Ice Age' glacier fluctuations, Gran Campo Nevado, southernmost Chile. The Holocene 15 (1), 20-28.

Korup, O. 2005. Large landslides and their effect on sediment flux in South Westland, New Zealand. Earth Surface Processes and Landforms 30, 305-323.

Krammer, K., Lange-Bertalot, H. 1986 (Nachdr. 1997). Bacillariophyceae 1. Teil Naviculaceae. In: Ettl, H., Gerloff, J., Heynig, H., Mollenhauer, D. (eds.). Süsswasserflora von Mitteleuropa. Band 2/1. Gustav Fisher, Jena, 876 p.

Krammer, K., Lange-Bertalot, H. 1988 (Nachdr. 1997). Bacillariophyceae 2. Teil Bacillariaceae, Epithemiaceae, Surirellaceae.In: Ettl, H., Gerloff, J., Heynig, H., Mollenhauer, D. (eds.). Süsswasserflora von Mitteleuropa. Band 2/2. Gustav Fisher, Jena, 611 p.

Krammer, K., Lange-Bertalot, H. 1991. Bacillariophyceae 3. Teil Centrales, Fragilariaceae, Eunotiaceae. In: Ettl, H., Gerloff, J., Heynig, H., Mollenhauer, D. (eds.). Süsswasserflora von Mitteleuropa. Band 2/3. Gustav Fisher, Jena, 576 p.

Krammer, K., Lange-Bertalot, H. 1996 Bacillariophyceae 4. Teil Achnantaceae. Kritische Ergänzungen zu Navicula (Lineolatae) und Gomphonema. In: Ettl, H., Gerloff, J., Heynig, H., Mollenhauer, D. (eds.). Süsswasserflora von Mitteleuropa. Band 2/4. Gustav Fisher, Jena, 437 p.

La Marche, V.C., Hirschboeck, K.K. 1984. Frost rings in trees as records of major volcanic-eruptions. Nature 307 (5947), 121-126.

Lamb, H.F., Gasse, F., Benkaddour, A., El Hamoutl, N., van der Kaars, S., Perkins, W.T., Pearce, N.J., Roberts, C.N. 1995. Relation between century-scale Holocene arid intervals in tropical and temperate zones. Nature 373, 134-137.

Lamy, F., Hebbeln, D., Röhl, U., Wefer, G. 2001. Holocene rainfall variability in southern Chile: a marine record of latitudinal shifts of the Southern Westerlies. Earth and Planetary Science Letters 185 (3-4), 369-382.

Lamy, F., Ruhlemann, C., Hebbeln, D. 2002. High- and low-latitude climate control on the position of the southern Peru-Chile Current during the Holocene. Paleoceanography 17 (2), 1028.

Lara, A., Villalba, R. 1993. A 3620-year temperature record from *Fitzroya cupressoides* tree rings in southern South America. Science 260, 1104-1106.

Lauer, W. 1968. Die Glaziallandschaft des südchilenischen Seengebietes. Acta Geographica 20, 215-236.

Laugenie, C.J. 1982. La région des lacs, Chili meridional, recherches sur l'évolution géomorphologique d'un piédmont glaciaire quaternaire andin. Thése de doctorat d'état presentée devant l'Université de Bordeaux. Maître-Assistant à l'Université de Pau et des Pays de l'Adour. Volume I, 332 p.

Lavenue, A., Cembrano, J. 1999. Compressional- and transpressional-stress pattern for Pliocene and Quaternary brittle deformation in fore-arc and intra-arc zones (Andes of Central and Southern Chile). Journal of Structural Geology 21, 1669-1691.

Lind, J.L., Heimann, K., Miller, E.A., van Vliet, C., Hoogenraad, N.J., Wetherbee, R. 1997. Substratum adhesion and gliding in a diatom are mediated by extracellular proteoglycans. Planta 203, 213-221.

Lindhorst, S. 2004. Morphotektonische und sedimentologische Analyse des Gewässernetzes im südlichen Zentralchile zwischen Concepción und Valdivia. Diplomarbeit. Universität Hamburg, 218 p.

Lipps, J.H. 1993. Fossil Prokaryotes and Protists. Blackwell Scientific Publications, Boston, 342 p.

López-Escobar, L., Cembrano, J., Moreno, H. 1995. Geochemistry and tectonics of the Chilean Southern Andes basaltic Quaternary Volcanism (37°-46°S). Revista Geológica de Chile 22, 219-234.

Lotter, A.F., Birks, H.J.B. 1993. The impact of the Laacher See tephra on terrestrial and aquatic ecosystems in the Black-Forest, southern Germany. Journal of Quaternary Science 8 (3), 263-276.

Lotter, A., Sturm, M. 1994. High-resolution paleoenvironmental studies: an editorial note. Journal of Paleolimnology 11, 311-312.

Lotter, A., Birks, H.J.B., Zolitschka, B. 1995. Late-glacial pollen and diatom changes in response to two different environmental perturbations: volcanic eruption and Younger Dryas cooling. Journal of Paleolimnology 14, 23-47.

Lotter, A.F., Birks, H.J.B., Hofmann, W., Marchetto, A. 1997. Modern diatom, cladocera, chironomid and chrysophyte cyst assemblages as quantitative indicators for the reconstruction of past environmental conditions in the Alps. II. Nutrients. Journal of Paleolimnology 19, 443-463.

Lotter, A.F., Bigler, C. 2000. Do diatoms in the Swiss Alps reflect the length of ice-cover? Aquatic Sciences 62 (2), 125-141.

Lowe, D.R. 1975. Water escape structures in coarse-grained sediments. Sedimentology 22, 157-204.

Lowell, T.V., Heusser, C.J., Andersen, B.G., Moreno, P.I., Hauser, A., Denton, G.H., Heusser, L.E., Schlüchter, C., Marchant, D.R. 1995. Interhemispheric correlation of late Pleistocene glacial events. Science 269, 1541-1549.

Lukas, S. 2003. Scottish Landform Example No. 31. The moraines around the Pass of Drumochter. Scottish Geographical Journal 119, 383-393.

Lukas, S. 2004. The pattern of deglaciation around the Pass of Drumochter. In: Lukas, S., Merritt, J.W. and Mitchell, W.A. (eds.). The Quaternary of the Central Grampian Highlands: Field Guide. Quaternary Research Association: London, 68-77.

Mackay, A.W., Ryves, D.B., Battarbee, R.W., Flower, R.J., Jewson, D.H., Rioual, P., Sturm, M. 2005. 1000 years of climate variability in central Asia: assessing the evidence using Lake Baikal (Russia) diatom assemblages and the application of a diatom-inferred model of snow cover on the lake. Global and Planetary Change 46, 281-297.

Mackereth, F.J.H. 1966. Some chemical observations on post-glacial lake sediments. Philosophical Transactions of the Royal Society of London. Series B 250, 165-213.

Maltman, A.J., Bolton, A. 2003. How sediments become mobilized. In: Van Rensbergen, P., Hillis, R.R., Maltman, A.J., Morley, C.K. (eds.). Subsurface Sediment Mobilization. Geological Society London Special Publications 216, 9-20.

Markgraf, V. 1989. Reply to Heusser's "Southern Westerlies during the Last Glacial Maximum". Quaternary Research 31, 426-432.

Markgraf, V. 1991. Younger Dryas in southernmost South America – an update. Quaternary Science Reviews 12, 351-355.

Markgraf, V. 1993. Paleoenvironments and paleoclimates in Tierra-Del-Fuego and southernmost Patagonia, South America. Palaeogeography, Palaeoclimatology, Palaeoecology 102 (1-2), 53-68.

Martin, M.W., Duhart, P., McDonough, M., Campos, A., Kato, T.T., Rodriguez, C., Godoy, E. 1999. Evolution of the late Paleozoic accretionary complex and overlying forarc-magmatic arc, south central Chile (38°-41°S): Constraints for the tectonic setting along the southwestern margin of Gondwana. Tectonics 18, 582-605.

Marwan, N., Trauth, M.H., Vuille, M., Kurths, J. 2003. Nonlinear time-series analysis on present-day and Pleistocene data from the NW Argentine Andes. Climate Dynamics 21, 371-326.

McCull, R.H.S. 1974. Availability of soil and sediment phosphorus to a planktonic alga. New Zealand Journal of Marine and Freshwater Research 9 (2), 169-182.

McCulloch, R.C., Bentley, M.J., Purves, R.S., Hulton, N.R.J., Sudgen, D.E., Clapperton, C.M. 2000. Climatic inferences from glacial and paleoecological evidence at the last glacial termination, southern South America. Journal of Quaternary Science 15 (4), 409-417.

McCulloch, R.D., Bentley, M.J., Tipping, R.M., Clapperton, C.M. 2005. Evidence for late-glacial ice dammed lakes in the central Strait of Magellan and Bahia Inutil, southernmost South America. Geografiska Annaler Series A - Physical Geography 87A (2), 335-362.

McDonough, M., Duhart, P., Crinogla, P. 1997. Naturaleza del alzamiento del basamiento costero y la apertura de la cuenca Osorno-Llanquihue, X^{a} región: nuevos antecendentes sísmicos y observaciones de terreno. 8° Congreso Geológico Chileno, Actas Vol.1, 164-168, Antofagasta.

McDougall, D.A. 2001. The geomorphological impact of Loch Lomond (Younger Dryas) Stadial plateau icefields in the central Lake District, northwest England. Journal of Quaternary Science 16, 531-544.

Meischner, D., Rumohr, J. 1974. A light-weight, high-momentum gravity corer for subaqueous sediments. Seckenbergiana Maritima 6, 105-117.

Melnick, D., Folguera, A., Rosenau, M., Echtler, H., Potent, S. 2002. Tectonics from the northern segment of the Liquiñe-Ofqui fault system (37°-39°S), Patagonian Andes. Abstract presented at the ISAG International Symposium on Andean Geodynamics, Toulouse, 413-416.

Menu-Marque, S., Morrone, J.J., Locascio de Mitrovich, C. 2000. Distributional patterns of the South American species of *Boeckella* (Copepoda: Centropagidae): A track analysis. Journal of Crustacean Biology 20 (2), 262-272.

Mercer, J.H. 1976. Glacial History of Southernmost South America. Quaternary Research 6, 125-166.

Mercer, J.H. 1983. Cenozoic glaciation in the southern hemisphere. Annual Review of Earth Planetary Science 11, 99-132.

Monecke, K., Anselmetti, F.S., Becker, A., Sturm, M., Giardini, D. 2004. The record of historic earthquakes in lake sediments of Central Switzerland. Tectonophysics 394, 21-40.

Monecke, K., Anselmetti, F.S., Becker, A., Schnellmann, M., Sturm, M., Giardini, D. Earthquake-induced deformation structures in lake deposits – A Late Pleistocene to Holocene paleoseismic record for Central Switzerland. Eclogae Geologicae Helvetiae, in press.

Mordjovich, C. 1974. Geology of a part of the Pacific margin of Chile. In: Burke, C.A., Drake, C.L. (eds.). The geology of continental margins. Springer, New York, 591-598.

Moreno, H. 1993. Volcan Villarrica: Geología y evaluacion del riesgo volcanico, regiones IX y X, 39°25'S. Servicio Nacional de Geología y Mineria (SERNAGEOMIN), Temuco, 112p.

Moreno, H., Clavero, J., Lara, L. 1994a. Actividad explosiva postglacial del Volcán Villarrica, Andes del Sur (39°25'S). 7° Congreso Geológico Chileno, Actas Vol.1, 329-333, Universidad de Concepción.

Moreno, H., López-Escobar, L., Cembrano, J. 1994b. The Villarrica-Quetrupillán-Lanín volcanic chain: A review and probable significance in the Southern Andes, 39.4°S, Chile. 7° Congreso Geológico Chileno, Actas Vol.1, 339-341, Universidad de Concepción.

Moreno, H. 2000. Mapa de peligros del Volcán Villarrica. Regiones de la Araucania y de los Lagos. Servicio Nacional de Geología y Mineria (SERNAGEOMIN), Temuco, No. 17. Escala 1:75000.

Moreno, P.I., Lowell, T.V., Jacobson jr., G.L., Denton, G.H. 1999. Abrupt vegetation and climate changes during the last glacial maximum and the last termination in the Chilean Lake District: a case study from Canal de la Puntilla (41°S). Geografiska Annaler Series A - Physical Geography 81A (2), 285-311.

Moreno, P.I., Jacobson jr., G.L, Lowell, T.V., Denton, G.H. 2001. Interhemispheric climate links revealed by a late-glacial cooling episode in southern Chile. Nature 409, 804-808.

Moya, J., Vilaplana, J.M., Corominas, J. 1997. Late Quaternary and historical landslides in the south-eastern Pyrenees. Paläoklimaforschung 19, 55-73.

Müller, J., Sigl, W. 1977. Morphologie und rezente Sedimentation des Ammersees. N. Jb. Geol. Paläont. Abh. 154 (2), 155-185.

Muñoz, J., Araneda, M. 2000. Extension cortical en el Oligoceno-Mioceno entre los 39° y 42°Sur, Región de los Lagos, Chile: Antecendentes geológicos y geofisicos. 9° Congreso Geológico Chileno, Actas Vol.2, 609-612, Puerto Varas.

Muñoz Christi. 1956. In: Weischet, W. 1970. Chile, seine länderkundliche Individualität und Struktur. Wissenschaftliche Buchgesellschaft, Darmstadt, 618 p.

Nelson, C.S. 1983. Bottom sediments of Lake Rotoma. New Zealand Journal of Marine and Freshwater Research 17, 185-204.

Nelson, C.S., Lister, G.S. 1995. Surficial bottom sediments of Lake Taupo, New Zealand: texture, composition, provenance, and sedimentation rates. New Zealand Journal of Geology and Geophysics 38, 61-79.

Nelson, M.R., Forsythe, R., Arit, I. 1994. Ridge collision tectonics in terrane development. Journal of South American Earth Sciences 7, 271-278.

Notaro, M., Liu, Z.Y., Gallimore, R., Vavrus, S.J., Kutzbach, J.E., Prentice, I.C., Jacob, R.L. 2005. Simulated and observed preindustrial to modern vegetation and climate changes. Journal of Climate 18 (17), 3650-3671.

Noverraz, F., Bonnard, C. 1991. L'écroulement rocheux de Randa, près de Zermat. In: Bell, D.H. (ed.). Landslides. Vol. 1, Balkema, Rotterdam, 165-170.

Oberhänsli, H., Mackay, A.W. 2005. Introduction to "Progress towards reconstructing past climate in Central Eurasia, with special emphasis on Lake Baikal". Global and Planetary Change 46, 1-7.

Obermeier, S.F., Martin, J.R., Frankel, A.D., Youd, T.L., Munson, P.J., Munson, C.A., Pond, E.C. 1993. Liquefaction evidence for one or more strong Holocene earthquakes in the Wabash Valley of southern Indiana and Illinois, with a preliminary estimate of magnitude. U.S. Geological Survey Professional Paper, Report: P 1536, 1-27.

Ohlendorf, C., Sturm, M. PM-BSi: A progressive method for Biogenic Silica determination. Journal of Paleolimnology, in press.

Ortlieb, L., Marchare, J. 1993. Former El Niño events; records from western South America. In: Faure, H., Faure, D.L., Liu, T. (eds.). Quaternary Earth system changes. Global and Planetary Change 7, 181-202.

Owen, R.B., Crossley, R. 1992. Spatial and temporal distribution of diatoms in sediments of Lake Malawi, Central Africa, and ecological implications. Journal of Paleolimnology 7, 55-71.

Paskoff, R. P. 1977. Quaternary of Chile – The state of research. Quaternary Research 8, 2-31.

Patzelt, G., Poscher, G. 1993. Der Tschirgant-Bergsturz. Geologie des Oberinntaler Raumes. Arbeitstagung der Geologischen Bundesanstalt, Mieming, Tirol.

Penck, A., Brückner, E. 1901/1909. Die Alpen im Eiszeitalter. Leipzig, Tauchnitz.

Pendall, E., Markgraf, V., White, J.W.C., Dreier, M., Kenny, R. 2001. Multiproxy record of late Pleistocene-Holocene climate and vegetation changes from a peat bog in Patagonia. Quaternary Research 55 (2), 168-178.

Petit-Breuilh, M.E., Lobato, J. 1994. Análisis comparativo de la cronología eruptiva historica de los Volcanes Llaima y Villarrica (38°-39°L.S.). 7° Congreso Geológico Chileno, Actas Vol.1, 366-370, Universidad de Concepción.

Pickett-Heaps, J.D., Hill, D.R.A., Wetherbee, R. 1986. Cellular movement in the centric diatom *Odontella sinensis*. Journal of Phycology 22, 334-339.

Pilskaln, C.H., Johnson, T.C. 1991. Seasonal signals in Lake Malawi sediments. Limnology and Oceanography 36, 544-557.

Pino, M. 2003. Last interglacial volcanic sediments at the coast of Valdivia, south of Chile. Terra Nostra 3, 52-53.

Pino, M., Adán, L., Seguel, O. 2004. Geoarcheology of the Area of Calafquén lake, Southwestern flank of Villarrica Volcano. In: Lara, L., Clavero, J. (eds.). Villarrica Volcano (39.5°S), Southern Andes, Chile. Servicio Nacional de Geología y Minería, Boletín 61, 61-67.

Pino, M., Adán, L., Seguel, O., Mera, R., Brümmer, R. Entre lagos, bosques y volcanes: Geoarqueología del Valle Marifilo, Distrito de Los Lagos Araucanos, Chile. Latin American Antiquity. submitted.

Plafker, G., Savage, J.C. 1970. Mechanism of the Chilean earthquakes of May 21 and 22, 1960. Geological Society of America Bulletin 81, 1001-1030.

Pollet, N., Cojean, R., Couture, R., Schneider, J.L., Strom, A.L., Voirin, C., Wassmer, P. 2005. A slab-on-slab model for the Flims rockslide (Swiss Alps). Canadian Geotechnical Journal 42 (2), 587-600.

Porter, S.C. 1981. Pleistocene glaciation in the southern lake district of Chile. Quaternary Research 16, 263-292.

Potent, S. 2003. Kinematik und Dynamik neogener Deformationsprozesse des südchilenischen Subduktionssystems, nördlichste Patagonische Anden (37°-40°S). Dissertation, Universität Hamburg, 169 p.

Rabassa, J., Clapperton, C.M. 1990. Quaternary glaciations of the southern Andes. Quaternary Science Reviews 9, 153-174.

Ramos, V.A. 1989. The birth of southern South America. American Scientist 77, 444-450.

Ramos, V.A. 2000. The Southern Central Andes. In: Cordani, U., Milani, E.J., Thomaz Filho, A., Campos, D.A. (eds.). Tectonic Evolution of South America. Rio de Janeiro, 561-604.

Rapela, C.W., Pankhurst, R.J. 1992. The granites of northern Patagonia and the Gastre Fault system in relation to the break-up of Gondwana. In: Storey, B.C., Alabaster, T., Pankhurst, R.J. (eds.). Magmatism and the causes of continental break-up. Geological Society Special Publication 68, 209-220.

Reynolds, C.S. 1984. The Ecology of Freshwater Phytoplankton. Cambridge University Press, Cambridge, 384 p.

Rivera Ramirez, P. 1983. A guide for references and distribution for the class Bacillariophyceae in Chile between 18°28'S and 58'S. Bibliotheca diatomologica, Vol. 3. Cramer, Vaduz, 386 p.

Round, F.E., Crawford, R.M., Mann, D.G. 1990. The diatoms. Biology and morphometry of the genera. Cambridge University Press, Cambridge, 747 p.

Rumrich, U., Lange-Bertalot, H., Rumrich, M. 2000. Diatomeen der Anden – von Venezuela bis Patagonien/Feuerland. Iconographica diatomologica. Vol. 9. Phytogeography, Diversity, Taxonomy. Gantner ARG, Vaduz, 672 p.

Ryves, D.B., Jewson, D.H., Sturm, M., Battarbee, R.W., Flower, R.J., Mackay, A.W., Granin, N.G. 2003. Quantitative and qualitative relationships between planktonic diatom communities and diatom assemblages sedimenting material and surface sediments in Lake Baikal, Siberia. Limnology and Oceanography 48, 1643-1661.

Salmaso, N., Decet, F., Cordella, P. 1999. Understanding deep oligotrophic subalpine lakes for efficient management. Hydrobiologia 396, 253-263.

Schindler, C., Cuénod, Y., Eisenlohr, T., Joris, C.L. 1993. Die Ereignisse vom 18. April und 9. Mai 1991 bei Randa (VS) – ein atypischer Bergsturz in Raten. Eclogae Geologicae Helvetiae 86 (3), 643-665.

Schindler, H. 1990. Bauern und Reiterkrieger: Die Mapuche-Indianer im Süden Amerikas. Hirmer Verlag, München, 196 p.

Schnellmann, M., Anselmetti, F.S., Giardini, D., McKenzie, J.A., Ward, S.N. 2002. Prehistoric earthquake history revealed by lacustrine slump deposits. Geology 30 (12), 1131-1134.

Schnellmann, M., Anselmetti, F.S., Giardini, D., McKenzie, J.A. 2005. Mass movement-induced fold-and-thrust belt structures in unconsolidated sediments in Lake Lucerne (Switzerland). Sedimentology 52, 271-289.

Schultes, S. 2004. The role of mesozooplankton grazing in the biochemical cycle of silicon in the Southern Ocean. Dissertation, Universität Hamburg, 168 p.

Servicio Nacional de Geología y Mineria (SERNAGEOMIN). 1982. Mapa Geológico de Chile 1:1000000, Hoja 4.

Siebert, L. 1984. Large volcanic debris avalanches; characteristics of source areas, deposits and associated eruptions. Journal of Volcanology and Geothermal Research 22, 163-197.

Siegenthaler, C., Finger, W., Kelts, K., Wang, S. 1987. Earthquake and seiche deposits in Lake Lucerne, Switzerland. Eclogae Geologicae Helvetiae 80 (1), 241-260.

Sissons, J. B. and Cornish, R. 1982: Differential glacio-isotstatic uplift of crustal blocks at Glen Roy, Scotland. Quaternary Research 18, 268-288.

Smith, G.A., Lowe, D.R. 1991. Lahars: Volcano-hydrologic events and deposition in the debris flow-hyperconcentrated flow continuum. In: Fisher, R.V., Smith, G.A. (eds.). Sedimentation in volcanic settings, SEPM Special Publication 45, 59-70.

Smol, J.P., Walker, I.R., Leavitt, P.R. 1991. Paleolimnology and hindcasting climatic trends. Verhandlungen der Internationalen Vereinigung für Theoretische und Angewandte Limnologie 24, 1240-1246.

Smol, J.P., Cumming, B.F. 2000. Tracking long-term changes in climate using algal indicators in lake sediments. Journal of Phycology 36, 986-1011.

Sommer, U. 1994. Planktologie. Springer Verlag, Berlin, Heidelberg, New York, 274 p.

Soon, W., Baliunas, S. 2003. Proxy climatic and environmental changes of the past 1000 years. Climate Research, 23, 89-110.

Soto, D., Zuniga, L. 1991. Zooplankton assemblages of Chilean temperate lakes – A comparison with North-American counterparts. Revista Chilena de Historia Natural 64 (3), 569-581.

Stern, C. 1989. Pliocene to present migration of the volcanic front, Andean Southern Volcanic Zone. Revista Geológica de Chile 16, 145-162.

Stingl, V., Purtscheller, F., Brunner P., Ennemoser, O. 1993. Bergstürze, Schwemmfächer und Radonverteilung im äußeren Ötztal (Tirol, Österreich). Geologica et Palaeontologica, 27, 299-300.

Stoermer, E.F., Håkansśon, H., Theriot, E.C. 1987. Cyclostephanos species newly reported from North America: C. tholiformis sp. nov. and C. costatilimbus comb. nov. British Phycological Journal 22, 349-358.

Storey, B.C., Curtis, M.L., Ferris, J.K., Hunter, M.A., Livermore, R.A. 1999. Reconstruction and break-out model for the Falkland Islands within Gondwana. Journal of African Earth Sciences 29 (1), 153-163.

Stuiver, M., Pollach, H.A. 1977. Discussion: Reporting of ^{14}C data. Radiocarbon 19, 355-363.

Stuiver, M., Reimer, P.J. 1993. Extended ^{14}C database and revised CALIB radiocarbon calibration program. Radiocarbon 35, 215-230.

Sturm, M., Matter, A. 1978. Turbidites and varves in Lake Brienz (Switzerland): deposition of clastic detritus by densitiy currents. In: Matter, A., Tucker, M.E. (eds.), Modern and Ancient Lake Sediments. International Association of Sedimentologists Special Publication 2, 147-168.

Sudgen, D.E, Hulton, N.R.J., Purves, R.S. 2002. Modelling the inception of the Patagonian icesheet. Quaternary International 95-96, 55-64.

Syers, J.K., Harris, R.F., Armstrong, D.E. 1973. Phosphate chemistry in lake sediments. Journal of Environmental Quality 2, 1-14.

Telford, R.J., Lamb, H.F. 1999. Groundwater-mediated response to Holocene climatic change recorded by the diatom stratigraphy of an Ethiopian crater lake. Quaternary Research 52, 63-75.

Telford, R.J., Barker, P., Metcalfe, S., Newton, A. 2004. Lacustrine responses to tephra deposition: examples from Mexico. Quaternary Science Reviews 23, 2337-2353.

Thomasson, K. 1959. Nahuel Huapi. Plankton of some lakes in an Argentine National Park, with notes on terrestrial vegetation. Acta Phytogeographica Suecica, 42, 1-83. In: Flint, E.A. 1977. Phytoplankton in seven monomictic lakes near Rotorua, New Zealand. New Zealand Journal of Botany, 15, 197-208.

Thomasson, K. 1963. Araucarian Lakes. Plankton studies in North Patagonian with notes on terrestrial vegetation. Acta Phytogeographica Suecica 47, 1-139.

Thornburg, T.M., Kulm, L.D., Hussong, D.M. 1990. Submarine-fan development in the southern Chile trench: A dynamic interplay of tectonics and sedimentation. Geological Society of America Bulletin 102, 1658-1680.

Thuro, K., Berner, C., Eberhardt, E. 2005. Der Bergsturz von Goldau 1806 – Versagensmechanismen in wechsellagernden Konglomeraten und Mergeln. In: Moser, M. (ed.) 2005. Veröffentlichungen von der 15. Tagung Ingenieurgeologie, 6.-9. April 2005, Erlangen, 303-308.

Van Asch, T.W.J. 1997. The temporal activity of landslides and its climatological signals. In: Matthews, J.A., Brunsden, D., Frenzel, B., Gläser, B., Weiss, M.J. (eds.). Rapid mass movement as a source of climatic evidence for the Holocene. Paläoklimaforschung 19, 7-16.

Van den Hoeck, C., Mann, D.G., Jahns, H.M. 1995. Algae: an Introduction to Phycology. Cambridge University Press, Cambridge, 627 p.

Van der Meer, J. J. M., Kjær, K. H. and Krüger, J. 1999: Subglacial water-escape structures and till structures, Sléttjökull, Iceland. Journal of Quaternary Science 14, 191-205.

Van Rensbergen, P., De Batist, M., Beck, C., Chapron, E. 1999. High-resolution seismic stratigraphy of glacial to interglacial fill of a deep glacigenic lake: Lake Le Bourget, northwestern Alps, France. Sedimentary Geology 128, 99-129.

Villagrán, C., Varela, J. 1990. Palynological evidence for increased aridity on the Central Chilean coast during the Holocene. Quaternary Research 34, 198-207.

Villagrán, C., Leon, A., Roig, F.A. 2004. Paleodistribution of the alerce and cypres of the Guaitecas during the interstadial stages of the Llanquihue glaciation: Llanquihue and Chiloe provinces, Los Lagos Region, Chile. Revista Geologica de Chile 31 (1), 133-151.

Villalba, R. 1990. Latitude of the surface high-pressure belt over western South America during the last 500 years as inferred from tree-ring analysis. Quaternary of South America and Antarctic Peninsula 7, 273–303.

Villalba, R. 1994. Tree-ring and glacial evidence for the medieval warm epoch and the little ice age in southern South America. Climate Change 26, 183-197.

Viner, A.B. 1989. Distribution of carbon, nitrogen, and phosphorous in Lake Taupo surface sediment. New Zealand Journal of Marine and Freshwater Research 23, 393-399.

Voight, B., Glicken, H., Janda, R.L., Douglass, P.M. 1981. Catastrophic rockslide avalanche of May 18. In: Lipman, W.P. and Mullineaux, D.R. (eds.). The 1980 eruptions of Mount St. Helens, Washington, U.S. Geological Survey Professional Papers 1250, 347-378.

Volland, S., Sturm, M., Lukas, S., Pino, M., Müller, J. 2007. Geomorphological and sedimentological evolution of a lake basin under strong volcano-tectonic influence: Lago Calafquén (South Central Chile). Quaternary International, 161, in press.

Vyverman, W., Sabbe, K. 1995. Diatom-temperature transfer functions based on the altitudinal zonation of diatom assemblages in Papua New Guinea: a possible tool in the reconstruction of regional palaeoclimatic changes. Journal of Paleolimnology 13, 65-77.

Waldron, E.H. 1967. Debris flow and erosional control problems caused by the ash eruptions of Irazu volcano, Costa Rica. U.S. Geological Survey Bulletin 101, 278-291.

Weischet, W. 1970. Chile, seine länderkundliche Individualität und Struktur. Wissenschaftliche Buchgesellschaft, Darmstadt, 618 p.

Werner, D. (ed.). 1977. The biology of diatoms. Blackwell Scientific Publications, Oxford, 498 p.

Wetzel, R.G. 1975. Limnology. Saunders Company, Philadelphia, London, Toronto, 743 p.

Wieczorek, G.F. 1996. Landslide triggering mechanisms. In: Turner, K.A., Schuster, R.L., (eds.), Landslides: Investigation and mitigation, Special Report 247, National Academy Press, Washington, 76-90.

Willner, A., Hervé, F., Massonne, H.J. 2000. Mineral chemistry and pressure-temperature evolution of two contrasting high-pressure-low-temperature belts in the Chonos Archipelago, Southern Chile. Journal of Petrology 41, 309-330.

Wilson, A.T., Taylor, D.H. 1973. Potential use of allophane for effluent treatment. In: McCull, R.H.S. 1974. Availability of soil and sediment phosphorus to a planktonic alga. New Zealand Journal of Marine and Freshwater Research 9 (2), 169-182.

Wissmar, R.C., Devol, A.H., Nevissi, A.E., Sedell, J.R. 1982a. Chemical changes of lakes in the Mount St. Helens blast zone. Science 216 (9), 175-178.

Wissmar, R.C., Devol, A.H., Staley, J.T., Sedell, J.R. 1982b. Biological responses of lakes in the Mount St. Helens blast zone. Science 216 (9), 178-181.

Woelfl, S., Villalobos, L., Parra, O. 2003. Trophic parameters and method validation in Lake Riñihue (North Patagonia: Chile) from 1978 trough 1997. Revista Chilena de Historia Natural 76, 459-474.

Wolin, J.A. 1996. Late Holocene lake-level fluctuations in Lower Herring Lake, Michigan, U.S.A. Journal of Paleolimnology 15, 19-45.

Wolin, J.A., Duthie, H.C. 1999. Diatoms as indicators of water level change in freshwater lakes. In: Stoermer, E., Smol, H.P. (eds.). The Diatoms: Applications for the Environmental and Earth sciences. Cambridge University Press, Cambridge, 182-202.

Yan, P., Shi, P., Gao, S., Chen, L., Zhang, X., Bai, L. 2002. ^{137} Cs dating of lacustrine sediments and human impacts on Dalian Lake, Qinghai Province, China. Catena 47, 91-99.

Zeil, W. 1964. Geologie von Chile – Beiträge zur regionalen Geologie der Erde. Gebrüder Bornträger, Berlin. 233 p.

Zielinski, G.A. 2000. Use of paleo-records in determining variability within the volcanism-climate system. Quaternary Science Reviews 19, 417-438.

Web Sites

http://www.igbp.kva.se/cgi-bin/php/list.show.php?section_id=63&article_id=343&onearticle=
Anderson, R. What regulates the efficiency of the biological pump in the Southern Ocean? Article from IGBP NL 56.

http://www.itis.usda.gov

http://www.mtsu.edu/~scientia/journals/vol1/issue2/ehmann.html

http.//ngdc.noaa.gov/image/2minrelief.htm

http://www1.phys.uu.nl/ams/method.htm

http://www.povi.org

http://www.sinia.cl/mapas/ix_region.html

http://www.sinia.cl/mapas/ x_region.html.

http://ssn.dgf.uchile.cl/home/sismohisto.html

http://www.volcano.si.edu

Appendix A – Photographic documentation, illustration, seismic lines and data

Fig. A-1: Satellite image of Lago Villarrica and its surrounding: glacial landforms, such as moraine ridges are mapped with yellow lines. Source satellite image: *www.sinia.cl.*

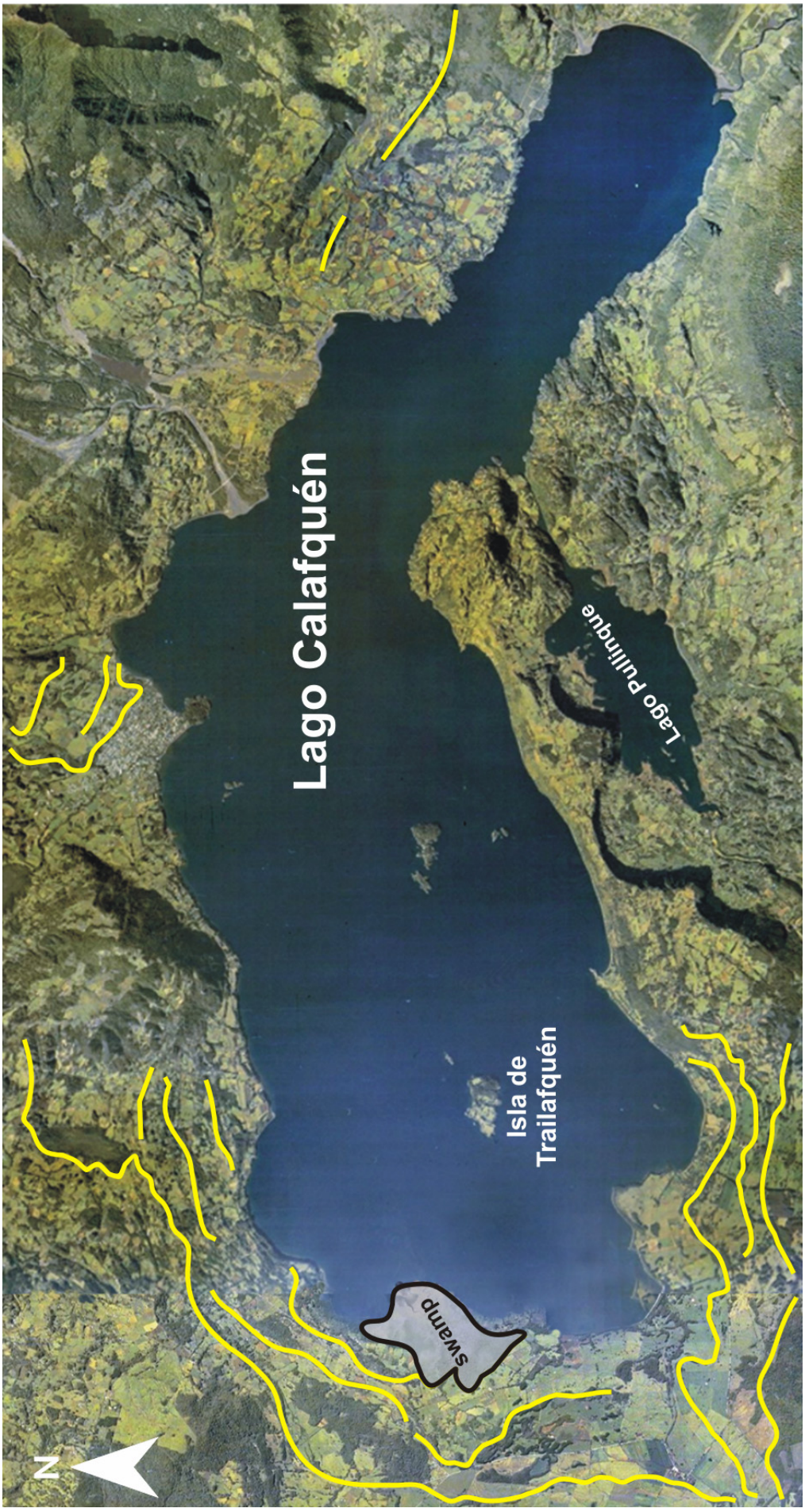

Fig. A-2: Satellite image of Lago Calafquén and its surrounding: glacial landforms, such as moraine ridges are mapped with yellow lines. Grey area mark a zone of swampy stagnant water at the uppermost western shore. Source satellite image: *www.sinia.cl.*

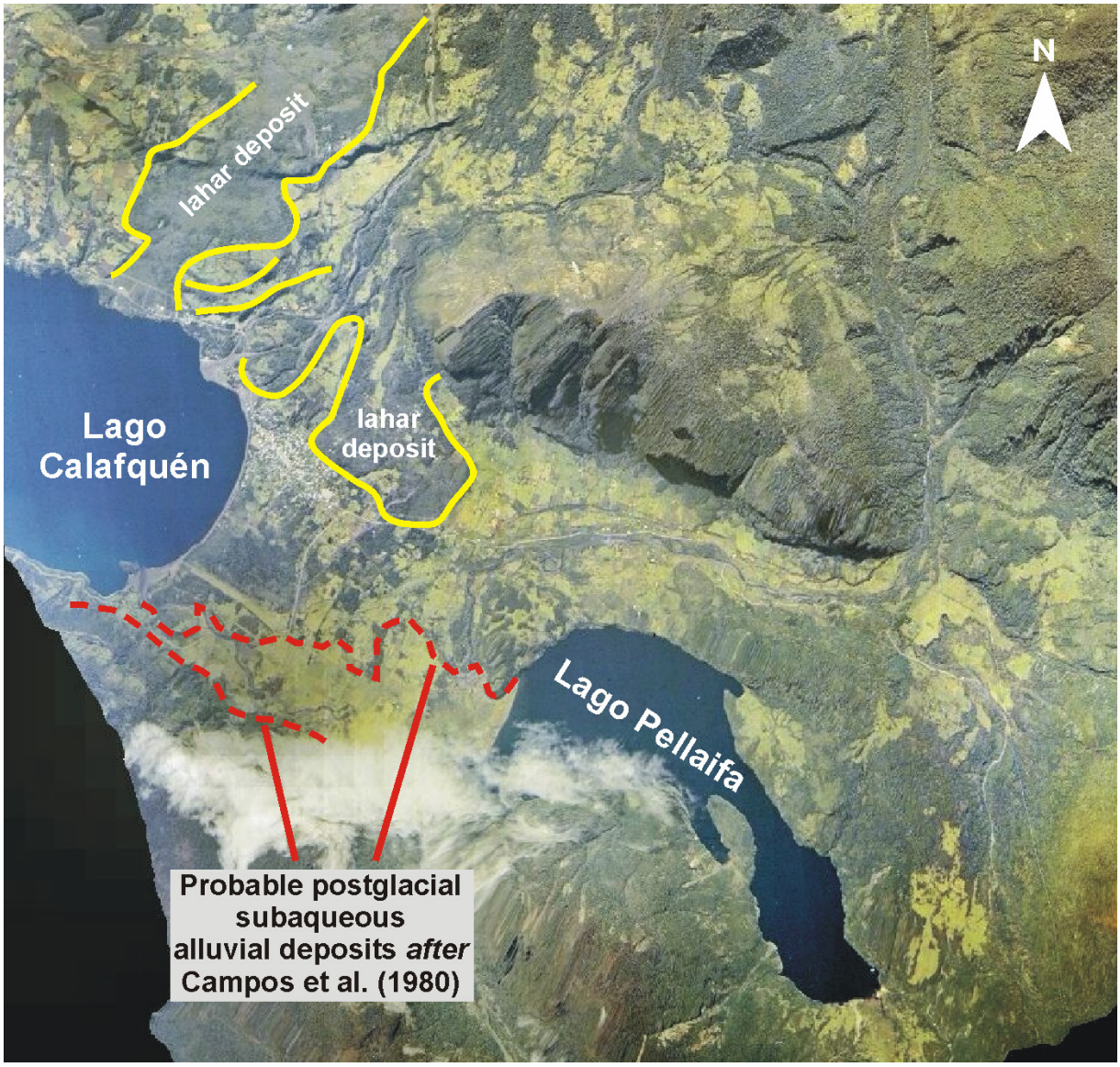

Fig. A-3: Satellite picture of Lago Pellafia that forms the tributary of Lago Calafquén. After Campos et al. (1980) Lago Pellafia once was a part of the Calafquén basin but was separated in postglacial time from the main basin. Separation is referred to a large subaqueous alluvial cone in the lake basin, which appeared after drop of lake level (Campos et al., 1980), but probably might have occurred in two or more stages. The red dashed lines mark at least two contours of alluvial cones and some additional (not marked) also could be recognized, which are referred to sliding events. Yellow lines mark lahar deposits of Volcano Villarrica that enter the lake basin on the north-eastern shore. Source satellite image: *www.sinia.cl.*

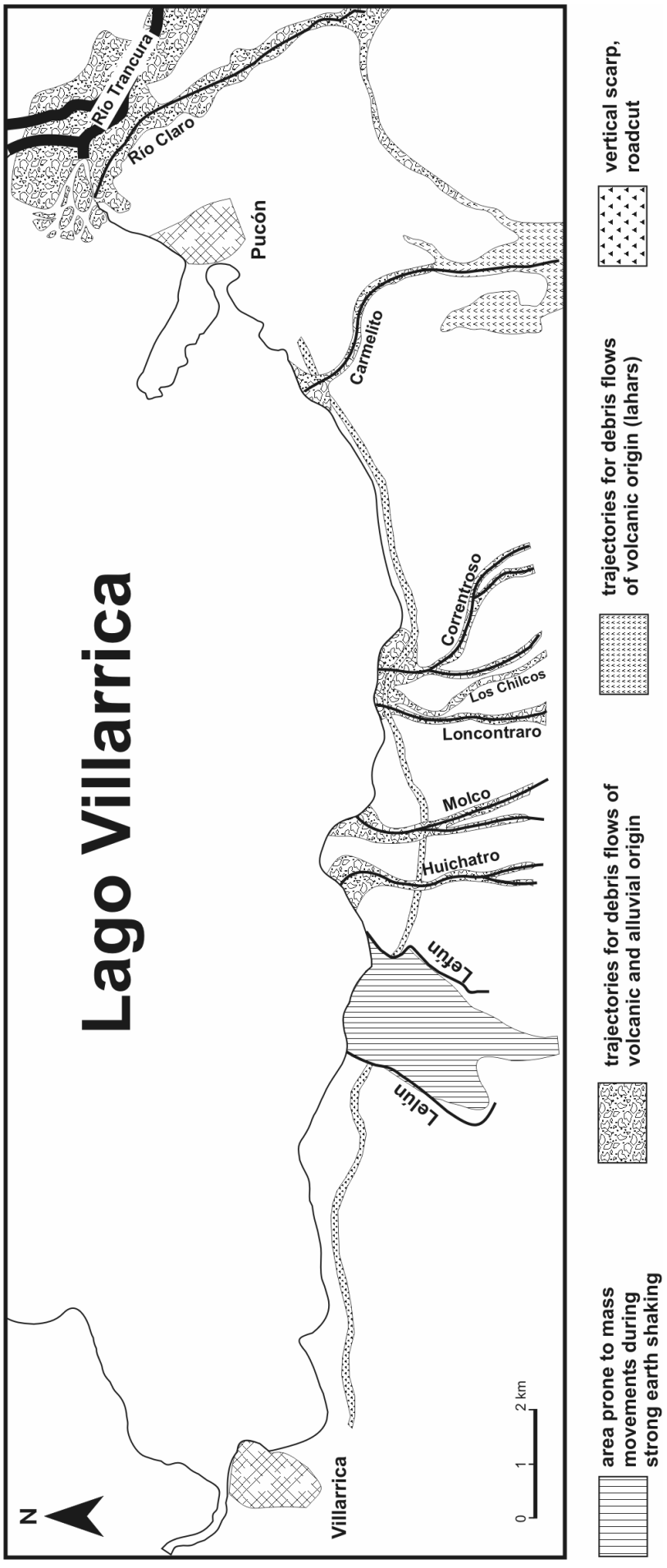

Fig. A-4 Area of risk for natural hazards along the southern side of Lago Villarrica (*modified after* Emparán, 1980).

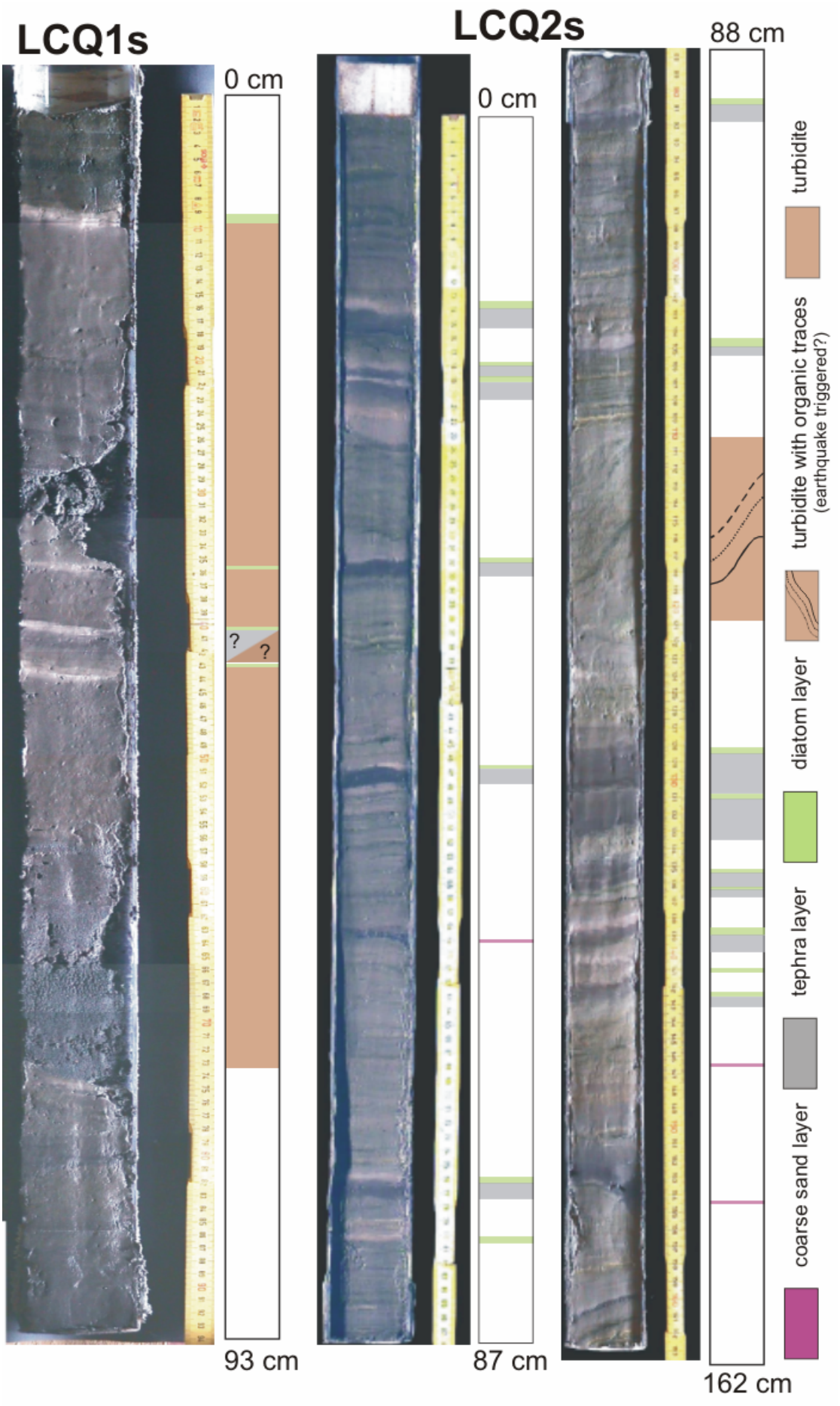

A-5: Sediment cores from Lago Calafquén: LCQ1s was taken from eastern sub-basin, strongly affected by underflow currents. The core was retrieved from the deep basin plain in 192 m depth. LCQ2s was taken from an area less affected by turbidites, controlled by normal lacustrine sedimentation. The core was taken from the elevated rise in 144 m depth. For coring sites see site map, Part 2, Fig. IV-3a.

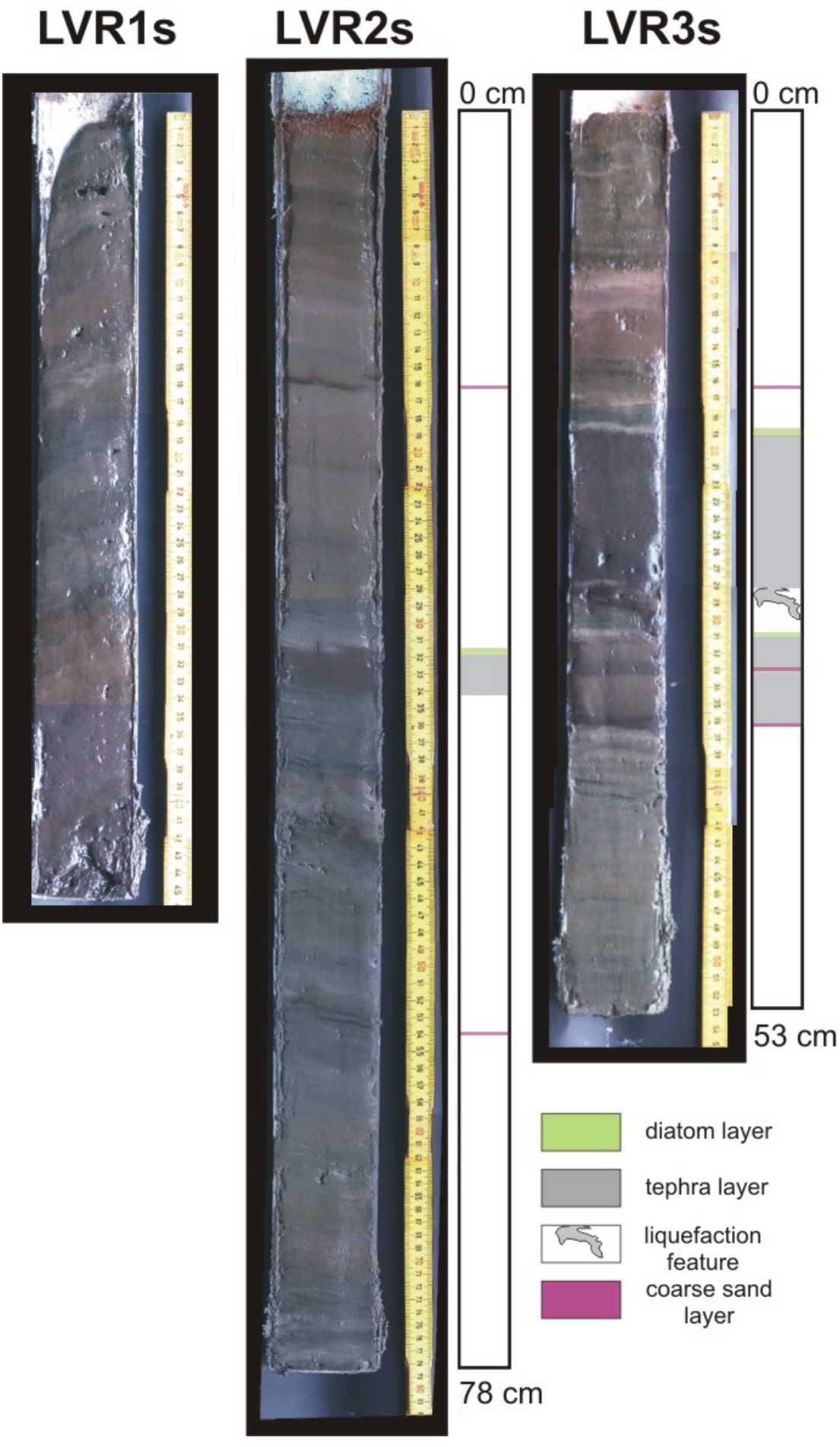

A-6: Sediment cores from Lago Villarrica: LVR1s was taken from 123 m depth at the shore of the city of Pucón. LVR2s was taken from the western shelf in 90 m depth. LVR3s was retrieved from the deep basin plain in the central basin at 160 m depth. For coring sites see sitemap, Part 2, Fig. IV-3b.

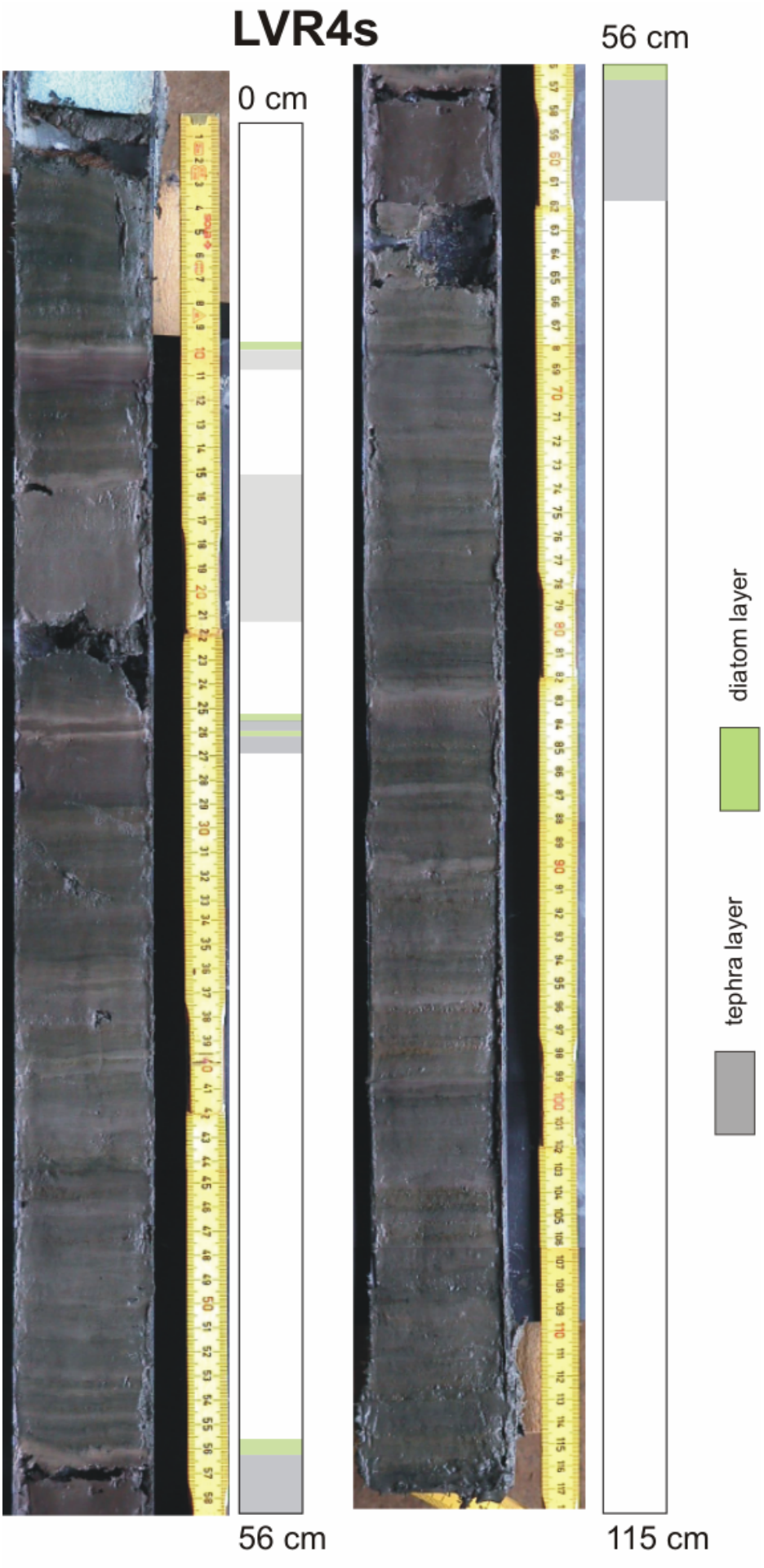

A-7: Sediment core LVR4s from Lago Villarrica was taken from the deep basin plain at 167 m depth, in front of the island Isla de Allaquillén in the western lake basin. The area is affected by turbidite deposition but controlled by normal lacustrine sedimentation. For coring sites see site map, Part 2, Fig. IV-3b.

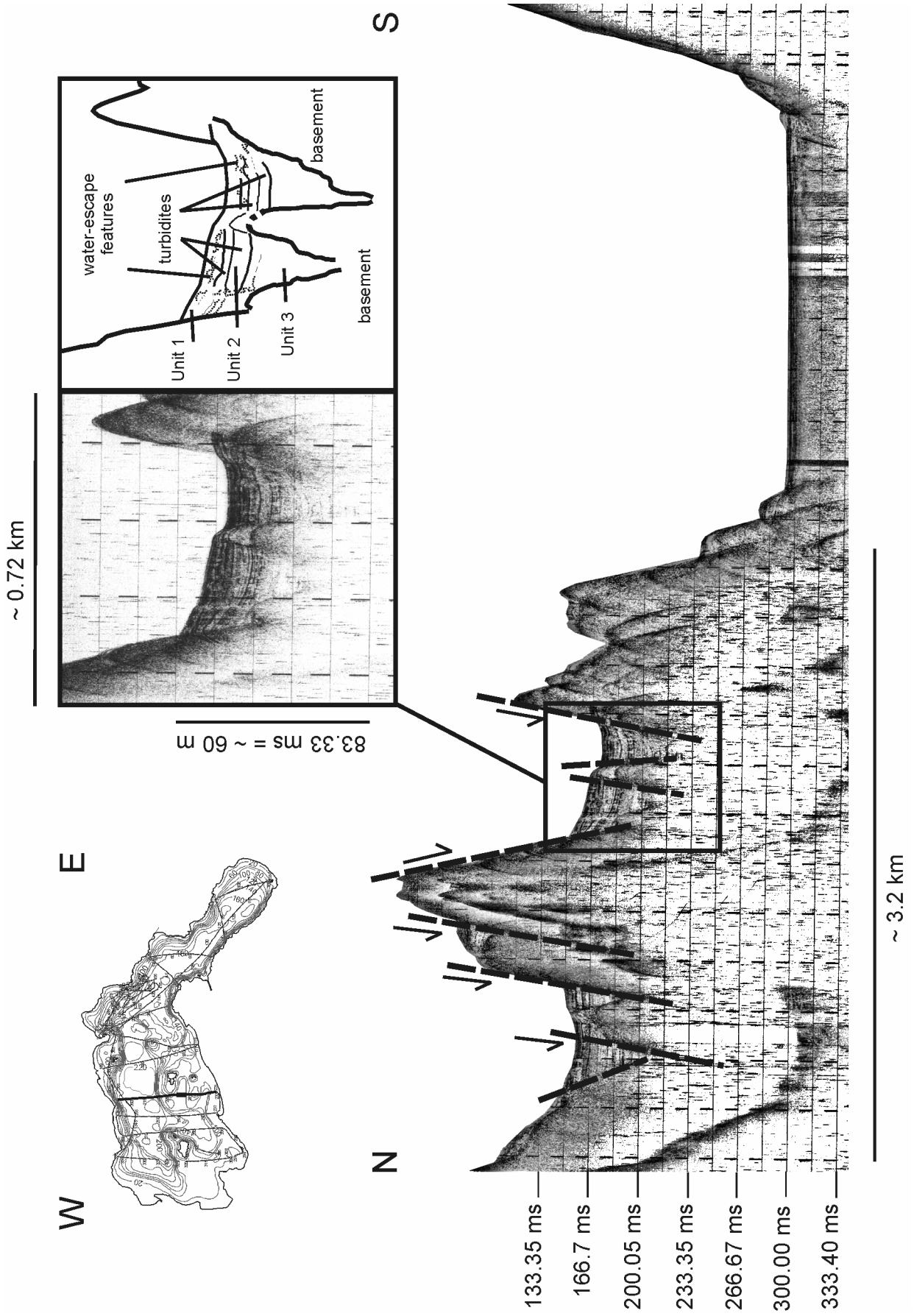

Fig. A-7: Longitudinal profile westward of Fig. III-12, see Part 1, Chapter 4.1.1. The Basement reveals enlarged voids for sediment deposition with a slightly increased inclination of 3.5% over a distance of ~ 3 km. The depressions are filled by > 30 m of sediment.

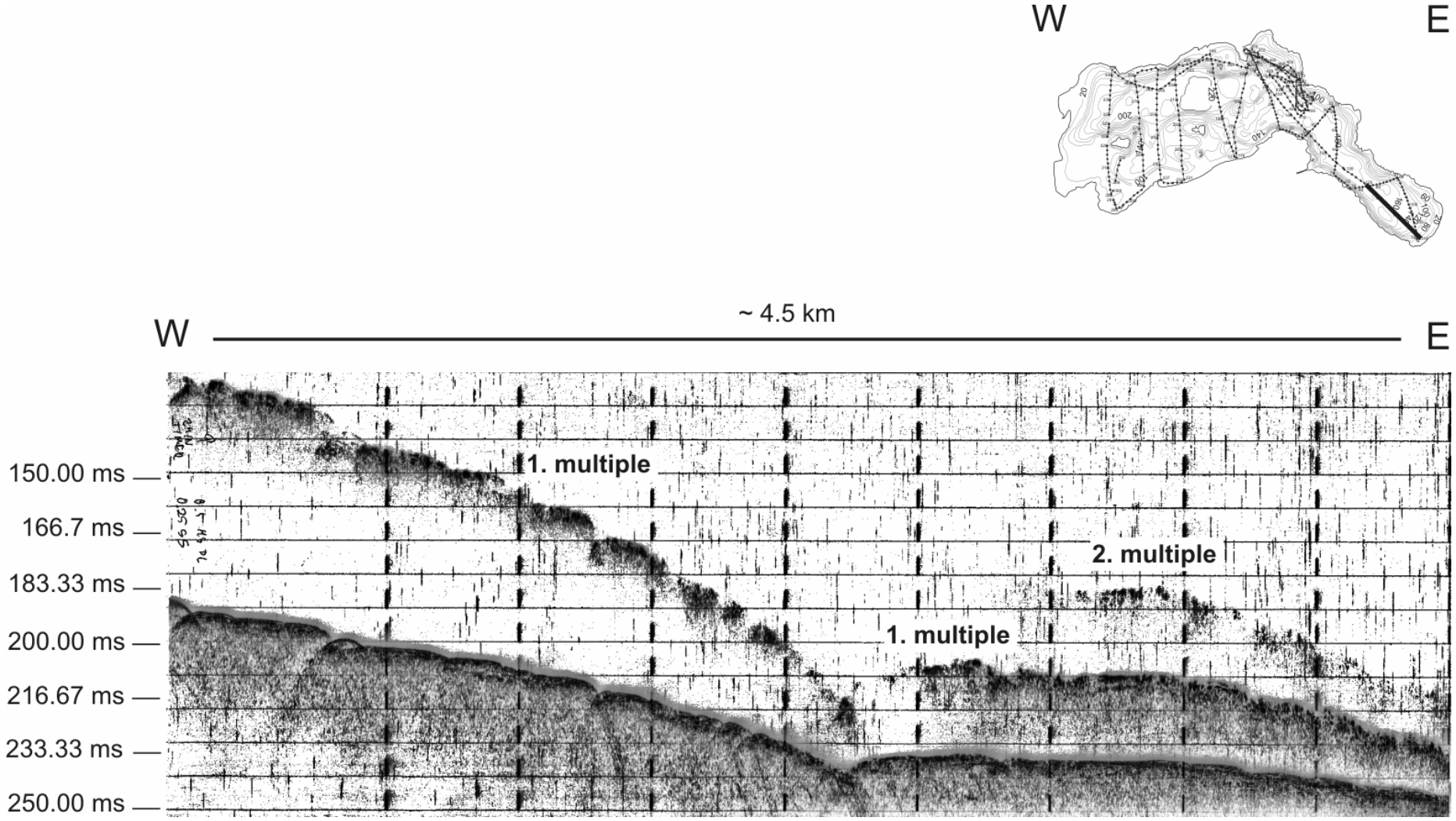

Fig. A-8: Seismic line from the eastern sub-basin of Lago Calafquén (shotpoints 110-124) is acoustically opaque. Sedimentation in this area is influenced by underflows, depositing medium- to coarse-sized materials (see Part 2, and photographic documentation of sediment core LCQ1s.

Seismic Data (Shotpoints and Coordinates) – Lago Calafquén

Shot-point No.	Longitude GPS (decimal)	Latitude GPS (decimal)	Depth [m]	Depth [m] (NN 208)	Shot-point No.	Longitude GPS (decimal)	Latitude GPS (decimal)	Depth [m]	Depth [m] (NN 208)
1	-72.1501	-39.493	192.585	15.415	30	-72.1253	-39.5261	25.450	182.550
2	-72.1488	-39.4923	197.858	10.142	31	-72.1248	-39.5278	28.695	179.305
3	-72.1476	-39.493	186.905	21.095	32	-72.1236	-39.5296	152.018	55.982
4	-72.1465	-39.4933	157.697	50.303	33	-72.1218	-39.5296	155.263	52.737
5	-72.146	-39.4941	136.603	71.397	34	-72.1193	-39.53	124.433	83.567
6	-72.145	-39.4955	109.829	98.171	35	-72.1171	-39.5305	120.376	87.624
7	-72.1443	-39.4965	92.385	115.615	36	-72.115	-39.5311	130.923	77.077
8	-72.1435	-39.4975	88.734	119.266	37	-72.1128	-39.5318	106.583	101.417
9	-72.1426	-39.4986	100.904	107.096	38	-72.1105	-39.5325	139.037	68.963
10	-72.1416	-39.4998	130.112	77.888	39	-72.1083	-39.5331	167.433	40.567
11	-72.141	-39.5008	109.017	98.983	40	-72.1075	-39.5333	172.301	35.699
12	-72.1403	-39.502	62.771	145.229	41	-72.1056	-39.5321	165.811	42.189
13	-72.1395	-39.503	44.111	163.889	42	-72.1046	-39.5313	114.697	93.303
14	-72.1385	-39.5041	5.572	202.428	43	-72.1028	-39.5301	15.714	192.286
15	-72.1375	-39.5053	5.572	202.428	44	-72.101	-39.529	15.714	192.286
16	-72.1366	-39.5065	5.978	202.022	45	-72.0993	-39.5276	15.714	192.286
17	-72.1363	-39.5068	5.978	202.022	46	-72.0976	-39.5263	15.308	192.692
18	-72.1355	-39.508	5.978	202.022	47	-72.0961	-39.5248	15.308	192.692
19	-72.1348	-39.509	5.978	202.022	48	-72.0943	-39.5233	16.931	191.069
20	-72.1338	-39.5103	5.978	202.022	49	-72.0928	-39.5221	21.799	186.201
21	-72.1331	-39.5113	6.789	201.211	50	-72.0911	-39.5206	41.271	166.729
22	-72.1321	-39.5128	57.092	150.908	51	-72.0895	-39.5193	87.111	120.889
23	-72.131	-39.5148	42.488	165.512	52	-72.0878	-39.518	154.452	53.548
24	-72.1301	-39.5163	37.214	170.786	53	-72.0868	-39.518	177.981	30.019
25	-72.1293	-39.518	52.224	155.776	54	-72.0866	-39.5186	157.697	50.303
26	-72.1285	-39.5196	10.846	197.154	55	-72.0861	-39.5205	117.536	90.464
27	-72.1276	-39.5213	10.846	197.154	56	-72.0856	-39.5221	81.432	126.568
28	-72.1268	-39.5228	11.252	196.748	57	-72.0851	-39.524	46.545	161.455
29	-72.126	-39.5245	14.091	193.909	58	-72.0848	-39.5261	29.101	178.899

Tab. A-1: GPS coordinates and water depth at shotpoints of the seismic survey on Lago Calafquén.

Shot-point No.	Longitude GPS (decimal)	Latitude GPS (decimal)	Depth [m]	Depth [m] (NN 208)	Shot-point No.	Longitude GPS (decimal)	Latitude GPS (decimal)	Depth [m]	Depth [m] (NN 208)
59	-72.0845	-39.5278	25.450	182.550	91	-72.0415	-39.5505	164.188	43.812
60	-72.0843	-39.5295	25.450	182.550	92	-72.0408	-39.5505	161.754	46.246
61	-72.084	-39.5311	22.610	185.390	93	-72.04	-39.5515	121.187	86.813
62	-72.0838	-39.5331	23.016	184.984	94	-72.0388	-39.553	94.413	113.587
63	-72.0836	-39.535	22.205	185.795	95	-72.0376	-39.5546	78.187	129.813
64	-72.0836	-39.5366	20.988	187.012	96	-72.0365	-39.5561	64.394	143.606
65	-72.0836	-39.5385	20.582	187.418	97	-72.0355	-39.5578	63.177	144.823
66	-72.0838	-39.5405	20.176	187.824	98	-72.0343	-39.5595	62.366	145.634
67	-72.084	-39.5423	20.176	187.824	99	-72.0335	-39.5611	61.554	146.446
68	-72.0841	-39.5441	19.365	188.635	100	-72.0325	-39.5628	61.960	146.040
69	-72.0845	-39.546	20.988	187.012	101	-72.0315	-39.5645	63.583	144.417
70	-72.0848	-39.5478	20.582	187.418	102	-72.0305	-39.5661	63.583	144.417
71	-72.0853	-39.5496	94.413	113.587	103	-72.0296	-39.5678	72.102	135.898
72	-72.0838	-39.5508	139.848	68.152	104	-72.029	-39.5696	76.564	131.436
73	-72.0816	-39.5518	133.763	74.237	105	-72.0283	-39.5713	83.866	124.134
74	-72.0796	-39.5528	106.583	101.417	106	-72.0276	-39.5731	89.545	118.455
75	-72.0776	-39.5538	117.131	90.869	107	-72.027	-39.575	98.470	109.530
76	-72.0756	-39.555	96.036	111.964	108	-72.0263	-39.5766	112.263	95.737
77	-72.0738	-39.5561	117.131	90.869	109	-72.026	-39.5785	129.301	78.699
78	-72.0731	-39.5563	110.640	97.360	110	-72.0241	-39.5785	151.207	56.793
79	-72.07	-39.5561	40.054	167.946	111	-72.0266	-39.576	109.829	98.171
80	-72.0673	-39.5556	25.044	182.956	112	-72.0303	-39.5738	86.300	121.700
81	-72.065	-39.5553	25.044	182.956	113	-72.0338	-39.5716	70.073	137.927
82	-72.0625	-39.5551	27.478	180.522	114	-72.0373	-39.5695	60.256	147.744
83	-72.0601	-39.5548	30.318	177.682	115	-72.039	-39.5683	56.000	152.000
84	-72.0578	-39.5543	31.129	176.871	116	-72.0413	-39.5668	52.555	155.445
85	-72.0553	-39.5541	31.129	176.871	117	-72.0438	-39.5651	43.029	164.971
86	-72.053	-39.5536	32.346	175.654	118	-72.0465	-39.5635	40.395	167.605
87	-72.0506	-39.5531	35.997	172.003	119	-72.049	-39.562	39.787	168.213
88	-72.0483	-39.5525	39.648	168.352	120	-72.0516	-39.5605	39.381	168.619
89	-72.046	-39.5518	89.545	118.455	121	-72.0541	-39.559	36.341	171.659
90	-72.0436	-39.5511	144.310	63.690	122	-72.0568	-39.5576	33.301	174.699

Tab. A-1: GPS coordinates and water depth at shotpoints of the seismic survey on Lago Calafquén.

Shot-point No.	Longitude GPS (decimal)	Latitude GPS (decimal)	Depth [m]	Depth [m] (NN 208)	Shot-point No.	Longitude GPS (decimal)	Latitude GPS (decimal)	Depth [m]	Depth [m] (NN 208)
126	-72.0663	-39.5525	24.639	183.361	158	-72.1476	-39.5013	129.301	78.699
127	-72.0698	-39.551	23.016	184.984	159	-72.1481	-39.5038	53.847	154.153
128	-72.0726	-39.5496	22.205	185.795	160	-72.1488	-39.5045	1.516	206.484
129	-72.0753	-39.5486	21.393	186.607	161	-72.1493	-39.5086	1.516	206.484
130	-72.078	-39.5475	20.176	187.824	162	-72.1501	-39.511	1.516	206.484
131	-72.079	-39.5468	19.771	188.229	163	-72.1508	-39.5131	1.110	206.890
132	-72.0833	-39.5445	19.365	188.635	164	-72.1513	-39.5155	1.110	206.890
133	-72.0863	-39.543	18.959	189.041	165	-72.1518	-39.5178	93.602	114.398
134	-72.0888	-39.5413	18.148	189.852	166	-72.1525	-39.5201	139.037	68.963
135	-72.0913	-39.5396	18.148	189.852	167	-72.153	-39.5225	113.074	94.926
136	-72.0943	-39.5376	18.554	189.446	168	-72.1538	-39.5248	47.356	160.644
137	-72.0963	-39.5361	26.261	181.739	169	-72.1548	-39.527	33.969	174.031
138	-72.099	-39.5345	35.186	172.814	170	-72.1555	-39.5295	60.743	147.257
139	-72.1021	-39.5323	41.271	166.729	171	-72.1565	-39.5318	138.225	69.775
140	-72.1038	-39.531	90.762	117.238	172	-72.1556	-39.5341	117.131	90.869
141	-72.1063	-39.5293	28.695	179.305	173	-72.1548	-39.5366	38.431	169.569
142	-72.1088	-39.5276	18.148	189.852	174	-72.154	-39.5393	107.395	100.605
143	-72.1113	-39.526	26.261	181.739	175	-72.1538	-39.5415	141.471	66.529
144	-72.1138	-39.5243	28.695	179.305	176	-72.1536	-39.5438	159.320	48.680
145	-72.1163	-39.5226	12.063	195.937	177	-72.155	-39.5431	155.669	52.331
146	-72.1193	-39.5206	11.252	196.748	178	-72.1561	-39.5408	143.093	64.907
147	-72.1213	-39.5193	11.252	196.748	179	-72.1573	-39.5388	94.413	113.587
148	-72.1236	-39.5173	11.657	196.343	180	-72.1585	-39.537	98.470	109.530
149	-72.1258	-39.5155	10.846	197.154	181	-72.1596	-39.5346	138.631	69.369
150	-72.1283	-39.5136	9.223	198.777	182	-72.1606	-39.5328	86.300	121.700
151	-72.1306	-39.5118	7.601	200.399	183	-72.1616	-39.5308	126.867	81.133
152	-72.1333	-39.5096	6.384	201.616	184	-72.1628	-39.5286	83.866	124.134
153	-72.136	-39.508	5.978	202.022	185	-72.164	-39.5256	95.225	112.775
154	-72.1378	-39.5063	5.167	202.833	186	-72.1645	-39.5245	40.054	167.946
155	-72.14	-39.5046	4.355	203.645	187	-72.1653	-39.5223	26.261	181.739
156	-72.1425	-39.5028	78.187	129.813	188	-72.1661	-39.5201	-0.513	208.513
157	-72.1473	-39.4995	177.169	30.831	189	-72.167	-39.518	-0.513	208.513

Tab. A-1: GPS coordinates and water depth at shotpoints of the seismic survey on Lago Calafquén.

Shot-point No.	Longitude GPS (decimal)	Latitude GPS (decimal)	Depth [m]	Depth [m] (NN 208)	Shot-point No.	Longitude GPS (decimal)	Latitude GPS (decimal)	Depth [m]	Depth [m] (NN 208)
190	-72.1678	-39.5158	-0.918	208.918	222	-72.193	-39.5343	112.263	95.737
191	-72.1686	-39.5136	-0.918	208.918	223	-72.1926	-39.5365	88.734	119.266
192	-72.1693	-39.5115	-0.918	208.918	224	-72.1925	-39.539	96.847	111.153
193	-72.1698	-39.5058	-1.324	209.324	225	-72.1921	-39.5413	147.556	60.444
194	-72.1705	-39.507	-1.324	209.324	226	-72.192	-39.5438	177.981	30.019
195	-72.1713	-39.5041	96.847	111.153	227	-72.1918	-39.5461	148.773	59.227
196	-72.1716	-39.5021	130.923	77.077	228	-72.1915	-39.5485	103.338	104.662
197	-72.1721	-39.5	166.216	41.784	229	-72.1908	-39.55	100.498	107.502
198	-72.1728	-39.4976	122.810	85.190	230	-72.1905	-39.5525	111.046	96.954
199	-72.1741	-39.4955	178.792	29.208	231	-72.1896	-39.555	136.603	71.397
200	-72.1765	-39.4958	173.113	34.887	232	-72.1915	-39.5563	172.301	35.699
201	-72.179	-39.4971	157.697	50.303	233	-72.1945	-39.5565	155.263	52.737
202	-72.1818	-39.4985	130.923	77.077	234	-72.1976	-39.5568	169.462	38.538
203	-72.1843	-39.4991	126.055	81.945	235	-72.2008	-39.557	192.990	15.010
204	-72.187	-39.5	106.583	101.417	236	-72.2038	-39.5568	199.887	8.113
205	-72.1898	-39.5006	103.338	104.662	237	-72.2058	-39.5555	189.339	18.661
206	-72.1926	-39.5013	57.903	150.097	238	-72.2063	-39.5528	183.660	24.340
207	-72.1955	-39.501	80.215	127.785	239	-72.2068	-39.5508	158.509	49.491
208	-72.1973	-39.5021	129.301	78.699	240	-72.2071	-39.5485	76.564	131.436
209	-72.198	-39.5031	55.875	152.125	241	-72.2076	-39.5458	62.771	145.229
210	-72.1978	-39.5058	2.733	205.267	242	-72.2081	-39.5438	56.281	151.719
211	-72.1975	-39.5081	-1.730	209.730	243	-72.2085	-39.5411	48.573	159.427
212	-72.1973	-39.5105	-2.135	210.135	244	-72.2086	-39.5391	51.413	156.587
213	-72.197	-39.513	-2.135	210.135	245	-72.209	-39.5361	51.818	156.182
214	-72.1965	-39.5153	-2.541	210.541	246	-72.2088	-39.5345	36.809	171.191
215	-72.1961	-39.5176	-2.541	210.541	247	-72.2093	-39.5321	18.959	189.041
216	-72.1956	-39.52	-2.541	210.541	248	-72.2096	-39.5295	31.941	176.059
217	-72.195	-39.5225	-2.135	210.135	249	-72.21	-39.5273	6.789	201.211
218	-72.1946	-39.5248	10.846	197.154	250	-72.2101	-39.525	-2.541	210.541
219	-72.1941	-39.5271	61.960	146.040	251	-72.2101	-39.5225	-2.947	210.947
220	-72.1938	-39.5295	106.583	101.417	252	-72.2101	-39.5201	-2.947	210.947
221	-72.1933	-39.5318	104.149	103.851	253	-72.2103	-39.5171	-2.947	210.947

Tab. A-1: GPS coordinates and water depth at shotpoints of the seismic survey on Lago Calafquén.

Shot-point No.	Longitude GPS (decimal)	Latitude GPS (decimal)	Depth [m]	Depth [m] (NN 208)	Shot-point No.	Longitude GPS (decimal)	Latitude GPS (decimal)	Depth [m]	Depth [m] (NN 208)
254	-72.2103	-39.515	-2.947	210.947	286	-72.2175	-39.5588	174.330	33.670
255	-72.2105	-39.513	-2.541	210.541	287	-72.2191	-39.5606	185.688	22.312
256	-72.2105	-39.5106	-2.541	210.541	288	-72.2218	-39.562	179.198	28.802
257	-72.2103	-39.5083	-1.324	209.324	289	-72.2243	-39.5633	176.764	31.236
258	-72.2101	-39.506	59.526	148.474	290	-72.2268	-39.565	174.735	33.265
259	-72.2098	-39.5036	147.556	60.444	291	-72.2291	-39.5665	174.330	33.670
260	-72.2115	-39.5028	184.471	23.529	292	-72.2316	-39.568	175.547	32.453
261	-72.2146	-39.5035	182.037	25.963	293	-72.2343	-39.5693	176.358	31.642
262	-72.2178	-39.504	168.650	39.350	294	-72.2366	-39.5696	189.745	18.255
263	-72.221	-39.5043	180.415	27.585	295	-72.2373	-39.568	201.509	6.491
264	-72.224	-39.5053	193.396	14.604	296	-72.2378	-39.567	201.104	6.896
265	-72.2261	-39.507	170.679	37.321	297	-72.2385	-39.5658	194.207	13.793
266	-72.2255	-39.5095	97.659	110.341	302	-72.2345	-39.547	87.111	120.889
267	-72.2248	-39.512	86.300	121.700	303	-72.2356	-39.5493	83.866	124.134
268	-72.2241	-39.5145	24.639	183.361	304	-72.2365	-39.5516	89.545	118.455
269	-72.2236	-39.5168	-2.135	210.135	305	-72.237	-39.5541	98.470	109.530
270	-72.2231	-39.5193	-2.947	210.947	306	-72.2376	-39.5565	117.131	90.869
271	-72.2228	-39.5218	-2.947	210.947	308	-72.239	-39.5613	146.339	61.661
272	-72.2225	-39.5243	-3.352	211.352	309	-72.2403	-39.563	181.045	26.955
273	-72.222	-39.5268	6.789	201.211	310	-72.241	-39.561	177.195	30.805
274	-72.2218	-39.5293	112.263	95.737	311	-72.2415	-39.5588	182.464	25.536
275	-72.2218	-39.5318	173.924	34.076	312	-72.2418	-39.557	136.661	71.339
276	-72.221	-39.5343	156.075	51.925	313	-72.2423	-39.555	126.528	81.472
277	-72.2205	-39.5368	82.243	125.757	314	-72.2425	-39.5528	125.515	82.485
278	-72.2198	-39.5398	64.800	143.200	315	-72.2428	-39.5508	137.067	70.933
279	-72.2195	-39.5416	61.149	146.851	316	-72.2431	-39.5486	140.107	67.893
280	-72.219	-39.5441	60.337	147.663	317	-72.2435	-39.5466	141.728	66.272
281	-72.2188	-39.5465	60.337	147.663	318	-72.2438	-39.5445	144.160	63.840
282	-72.2186	-39.549	60.743	147.257	319	-72.244	-39.5425	148.011	59.989
283	-72.2183	-39.5515	63.177	144.823	320	-72.244	-39.5403	172.533	35.467
284	-72.218	-39.5538	90.357	117.643	322	-72.2438	-39.536	111.531	96.469
285	-72.2176	-39.5563	135.791	72.209	323	-72.2436	-39.5338	64.917	143.083

Tab. A-1: GPS coordinates and water depth at shotpoints of the seismic survey on Lago Calafquén.

Shot-point No.	Longitude GPS (decimal)	Latitude GPS (decimal)	Depth [m]	Depth [m] (NN 208)	Shot-point No.	Longitude GPS (decimal)	Latitude GPS (decimal)	Depth [m]	Depth [m] (NN 208)
324	-72.2431	-39.5318	20.582	187.418	358	-72.1816	-39.4993	112.263	95.737
325	-72.2431	-39.53	3.138	204.862	359	-72.179	-39.4983	134.169	73.831
327	-72.2431	-39.5256	34.375	173.625	360	-72.1761	-39.4975	159.320	48.680
328	-72.243	-39.5231	58.715	149.285	361	-72.1731	-39.4978	137.414	70.586
329	-72.243	-39.5211	57.216	150.784	362	-72.17	-39.4981	123.216	84.784
330	-72.243	-39.5188	52.960	155.040	363	-72.1671	-39.4986	128.084	79.916
331	-72.2428	-39.5165	75.861	132.139	364	-72.1638	-39.499	134.980	73.020
332	-72.2428	-39.5141	86.197	121.803	365	-72.1603	-39.4991	141.876	66.124
333	-72.2426	-39.5118	84.373	123.627	366	-72.1548	-39.5001	144.310	63.690
334	-72.2425	-39.5095	104.235	103.765	367	-72.1518	-39.5008	153.641	54.359
335	-72.2421	-39.5071	118.016	89.984	368	-72.149	-39.501	156.886	51.114
336	-72.2418	-39.5045	187.328	20.672	369	-72.1463	-39.5	175.547	32.453
337	-72.2398	-39.5056	169.056	38.944	370	-72.1406	-39.4985	83.055	124.945
338	-72.2373	-39.5071	174.735	33.265	371	-72.1408	-39.4961	62.366	145.634
339	-72.2345	-39.5083	159.320	48.680	372	-72.1408	-39.4938	79.404	128.596
340	-72.2313	-39.5095	126.867	81.133	374	-72.1448	-39.4923	153.641	54.359
341	-72.2281	-39.5103	115.102	92.898	375	-72.1431	-39.4938	108.206	99.794
342	-72.2256	-39.511	89.951	118.049	376	-72.1403	-39.4948	70.073	137.927
343	-72.2226	-39.5115	54.658	153.342	377	-72.1375	-39.4958	55.189	152.811
344	-72.2195	-39.512	10.846	197.154	378	-72.1346	-39.497	83.968	124.032
345	-72.2163	-39.5123	-2.135	210.135	379	-72.1335	-39.4981	87.211	120.789
346	-72.2135	-39.5126	-2.947	210.947	380	-72.129	-39.4995	61.269	146.731
347	-72.2103	-39.513	-2.947	210.947	381	-72.1261	-39.5006	17.337	190.663
348	-72.2075	-39.5125	-2.541	210.541	382	-72.1235	-39.502	23.827	184.173
349	-72.2045	-39.5111	-2.541	210.541	383	-72.1208	-39.5033	42.488	165.512
350	-72.2021	-39.5098	-2.541	210.541	384	-72.1185	-39.505	75.753	132.247
351	-72.1995	-39.5081	-2.135	210.135	385	-72.1165	-39.507	106.583	101.417
353	-72.1945	-39.5051	3.544	204.456	386	-72.1148	-39.5091	106.583	101.417
354	-72.1921	-39.504	44.111	163.889	387	-72.1126	-39.511	81.432	126.568
355	-72.1895	-39.5026	62.771	145.229	388	-72.1108	-39.513	69.262	138.738
356	-72.187	-39.5015	68.451	139.549	389	-72.1086	-39.5146	46.545	161.455
357	-72.1843	-39.5005	87.923	120.077	390	-72.1056	-39.5158	40.865	167.135

Tab. A-1: GPS coordinates and water depth at shotpoints of the seismic survey on Lago Calafquén.

Shot-point No.	Longitude GPS (decimal)	Latitude GPS (decimal)	Depth [m]	Depth [m] (NN 208)	Shot-point No.	Longitude GPS (decimal)	Latitude GPS (decimal)	Depth [m]	Depth [m] (NN 208)
391	-72.1028	-39.5171	27.884	180.116	423	-72.1191	-39.5145	18.959	189.041
392	-72.1011	-39.5153	66.828	141.172	424	-72.1211	-39.5126	27.478	180.522
393	-72.1011	-39.5145	97.659	110.341	425	-72.1231	-39.5108	30.318	177.682
394	-72.1025	-39.5138	81.432	126.568	426	-72.1253	-39.509	21.393	186.607
395	-72.1053	-39.513	87.923	120.077	427	-72.1275	-39.5071	15.714	192.286
396	-72.1075	-39.5116	122.810	85.190	428	-72.1298	-39.5055	14.091	193.909
397	-72.1098	-39.5103	138.225	69.775	429	-72.1321	-39.504	13.686	194.314
398	-72.1113	-39.5083	140.254	67.746	430	-72.1321	-39.5043	12.469	195.531
399	-72.1126	-39.5061	162.565	45.435	431	-72.129	-39.5046	14.091	193.909
400	-72.1135	-39.5038	154.452	53.548	432	-72.1266	-39.5048	19.771	188.229
401	-72.1151	-39.502	117.942	90.058	433	-72.1233	-39.5051	29.507	178.493
402	-72.1173	-39.5005	107.395	100.605	434	-72.121	-39.5061	42.894	165.106
403	-72.1196	-39.4993	95.630	112.370	435	-72.1185	-39.5068	74.645	133.355
404	-72.122	-39.5001	73.319	134.681	436	-72.1156	-39.5073	113.152	94.848
405	-72.1241	-39.5016	19.771	188.229	437	-72.1128	-39.5061	159.360	48.640
406	-72.1265	-39.5031	20.582	187.418	438	-72.1115	-39.5056	176.789	31.211
407	-72.1266	-39.5048	18.554	189.446	439	-72.111	-39.5055	187.733	20.267
408	-72.124	-39.506	26.261	181.739	440	-72.1111	-39.506	183.275	24.725
409	-72.1213	-39.5073	46.139	161.861	441	-72.1133	-39.507	148.011	59.989
410	-72.1191	-39.5091	76.564	131.436	442	-72.1131	-39.5091	113.963	94.037
411	-72.1173	-39.511	61.960	146.040	443	-72.1131	-39.5103	91.669	116.331
412	-72.1155	-39.513	39.648	168.352	444	-72.1131	-39.5115	71.200	136.800
413	-72.1131	-39.5146	26.261	181.739	445	-72.113	-39.5126	52.757	155.243
414	-72.1115	-39.5168	17.337	190.663	446	-72.113	-39.5138	36.139	171.861
415	-72.1091	-39.5183	16.525	191.475	448	-72.113	-39.5161	18.148	189.852
416	-72.1066	-39.5196	16.931	191.069	449	-72.113	-39.5173	15.308	192.692
417	-72.1073	-39.5215	14.903	193.097	450	-72.113	-39.5185	13.686	194.314
418	-72.1095	-39.5228	14.091	193.909	451	-72.1118	-39.5191	13.280	194.720
419	-72.1118	-39.5221	12.874	195.126	452	-72.1108	-39.5201	13.280	194.720
420	-72.1135	-39.5201	12.874	195.126	453	-72.1093	-39.5205	13.686	194.314
421	-72.1153	-39.5183	13.280	194.720	454	-72.1076	-39.5203	14.903	193.097
422	-72.1171	-39.5163	14.497	193.503	455	-72.1061	-39.5201	15.714	192.286

Tab. A-1: GPS coordinates and water depth at shotpoints of the seismic survey on Lago Calafquén.

Shot-point No.	Longitude GPS (decimal)	Latitude GPS (decimal)	Depth [m]	Depth [m] (NN 208)	Shot-point No.	Longitude GPS (decimal)	Latitude GPS (decimal)	Depth [m]	Depth [m] (NN 208)
456	-72.1045	-39.5201	16.525	191.475	476	-72.12	-39.5023	52.352	155.648
457	-72.1051	-39.5186	18.148	189.852	477	-72.1216	-39.5016	70.592	137.408
458	-72.1055	-39.5178	23.422	184.578	478	-72.1231	-39.5008	45.461	162.539
459	-72.1061	-39.5166	30.318	177.682	479	-72.1246	-39.5003	19.771	188.229
460	-72.107	-39.5153	42.488	165.512	480	-72.1256	-39.5001	16.931	191.069
461	-72.1075	-39.5145	54.379	153.621	481	-72.1271	-39.4996	25.450	182.550
462	-72.1081	-39.5133	74.645	133.355	482	-72.1286	-39.4993	66.017	141.983
463	-72.109	-39.5121	103.019	104.981	483	-72.1301	-39.4988	68.971	139.029
464	-72.1091	-39.511	126.933	81.067	484	-72.1316	-39.4985	83.968	124.032
465	-72.1096	-39.5098	149.227	58.773	485	-72.1331	-39.498	71.808	136.192
466	-72.11	-39.5086	166.656	41.344	486	-72.1346	-39.4976	77.888	130.112
467	-72.1103	-39.5073	169.493	38.507	487	-72.1361	-39.4971	59.243	148.757
468	-72.1105	-39.5061	186.923	21.077	488	-72.1376	-39.4966	46.069	161.931
469	-72.1108	-39.5055	199.893	8.107	489	-72.1393	-39.4963	51.947	156.053
470	-72.1115	-39.5055	184.896	23.104	490	-72.1408	-39.4958	63.701	144.299
471	-72.113	-39.505	166.453	41.547	491	-72.1425	-39.4955	82.347	125.653
472	-72.1145	-39.5046	145.984	62.016	492	-72.1436	-39.4951	97.749	110.251
473	-72.1158	-39.5041	116.800	91.200	493	-72.1451	-39.495	111.936	96.064
474	-72.1173	-39.5036	90.048	117.952	494	-72.1466	-39.4945	130.987	77.013
475	-72.119	-39.5028	65.323	142.677	----	----	----	----	----

Tab. A-1: GPS coordinates and water depth at shotpoints of the seismic survey on Lago Calafquén.

Seismic Data (Shotpoints and Coordinates) – Lago Villarrica

Shot-point No.	Longitude GPS (decimal)	Latitude GPS (decimal)	Depth (m)	Depth [m] (NN 208)	Shot-point No.	Longitude GPS (decimal)	Latitude GPS (decimal)	Depth (m)	Depth [m] (NN 217)
1	-39.1643	-71.5928	203.827	13.173	30	-39.141	-72.0035	77.160	139.840
2	-39.1644	-71.5936	190.653	26.347	31	-39.1402	-72.0035	77.363	139.637
3	-39.1647	-71.5946	168.360	48.640	32	-39.1356	-72.0037	77.565	139.435
4	-39.165	-71.5956	115.059	101.941	33	-39.1349	-72.0039	83.240	133.760
5	-39.165	-72.0007	88.915	128.085	34	-39.134	-72.0038	71.688	145.312
6	-39.165	-72.0016	85.875	131.125	35	-39.1332	-72.0036	111.208	105.792
7	-39.1652	-72.0025	83.645	133.355	36	-39.1328	-72.004	194.301	22.699
8	-39.1652	-72.0035	79.592	137.408	37	-39.1335	-72.0039	94.995	122.005
9	-39.1647	-72.0038	88.509	128.491	38	-39.1342	-72.004	75.336	141.664
10	-39.164	-72.0041	76.349	140.651	39	-39.1349	-72.0041	75.539	141.461
11	-39.1631	-72.0041	88.915	128.085	40	-39.1402	-72.0047	75.741	141.259
12	-39.1624	-72.0043	118.909	98.091	41	-39.141	-72.005	75.944	141.056
13	-39.1617	-72.0044	155.187	61.813	42	-39.1417	-72.0053	74.728	142.272
14	-39.1609	-72.0045	154.984	62.016	43	-39.1425	-72.0057	73.309	143.691
15	-39.1603	-72.0044	157.416	59.584	44	-39.1432	-72.0058	73.917	143.083
16	-39.1557	-72.0029	76.552	140.448	45	-39.144	-72.01	73.715	143.285
18	-39.1541	-72.0046	77.768	139.232	46	-39.1447	-72.102	73.917	143.083
19	-39.1533	-72.0043	77.363	139.637	47	-39.1455	-72.0105	73.107	143.893
20	-39.1521	-72.0035	77.768	139.232	48	-39.1501	-72.011	73.309	143.691
21	-39.1514	-72.0035	76.147	140.853	49	-39.1508	-72.0116	71.688	145.312
22	-39.1508	-72.0035	75.539	141.461	50	-39.1515	-72.012	70.675	146.325
23	-39.1501	-72.0035	76.755	140.245	51	-39.1522	-72.0125	70.269	146.731
24	-39.1451	-72.0035	77.160	139.840	52	-39.1531	-72.0129	68.851	148.149
25	-39.1445	-72.0036	76.755	140.245	53	-39.1535	-72.0129	68.648	148.352
26	-39.1437	-72.0033	77.363	139.637	54	-39.1538	-72.0137	67.635	149.365
27	-39.1429	-72.0034	77.363	139.637	55	-39.1544	-72.0143	67.027	149.973
28	-39.1423	-72.0034	77.160	139.840	56	-39.155	-72.0143	66.419	150.581
29	-39.1417	-72.0034	75.539	141.461	57	-39.1558	-72.0149	66.013	150.987

Tab. A-2: GPS coordinates and water depth at shotpoints of the seismic survey on Lago Villarrica.

Shot-point No.	Longitude GPS (decimal)	Latitude GPS (decimal)	Depth (m)	Depth [m] (NN 208)	Shot-point No.	Longitude GPS (decimal)	Latitude GPS (decimal)	Depth (m)	Depth [m] (NN 217)
58	-39.1615	-72.0156	65.000	152.000	90	-39.1629	-72.0408	58.515	158.485
59	-39.162	-72.0203	63.784	153.216	91	-39.1622	-72.0411	58.109	158.891
60	-39.1628	-72.0208	62.568	154.432	92	-39.1614	-72.0412	57.907	159.093
61	-39.1634	-72.0213	62.163	154.837	93	-39.1608	-72.0411	57.501	159.499
62	-39.164	-72.0217	61.960	155.040	94	-39.1558	-72.0414	57.096	159.904
63	-39.165	-72.0225	61.757	155.243	95	-39.155	-72.0415	56.893	160.107
64	-39.1656	-72.0231	72.701	144.299	96	-39.1543	-72.0416	56.691	160.309
65	-39.1702	-72.0238	95.805	121.195	97	-39.1536	-72.0414	56.691	160.309
66	-39.1708	-72.0244	99.656	117.344	98	-39.1528	-72.0412	56.488	160.512
67	-39.1714	-72.0249	98.237	118.763	99	-39.152	-72.0413	56.488	160.512
68	-39.1721	-72.0256	70.675	146.325	100	-39.1512	-72.0414	56.285	160.715
69	-39.1728	-72.0301	69.864	147.136	101	-39.1505	-72.0412	56.488	160.512
70	-39.1734	-72.035	71.080	145.920	102	-39.1458	-72.0411	56.691	160.309
71	-39.1734	-72.0305	71.891	145.109	103	-39.1451	-72.0413	56.893	160.107
72	-39.1738	-72.0308	75.539	141.461	104	-39.1443	-72.0411	56.893	160.107
73	-39.1749	-72.0317	90.333	126.667	105	-39.1435	-72.0408	57.096	159.904
74	-39.1755	-72.0325	113.032	103.968	106	-39.1427	-72.0409	57.299	159.701
75	-39.1801	-72.0329	133.096	83.904	107	-39.1419	-72.0407	57.501	159.499
76	-39.1807	-72.0336	166.739	50.261	108	-39.1411	-72.0405	56.893	160.107
77	-39.1805	-72.0344	194.099	22.901	109	-39.1405	-72.0403	56.488	160.512
78	-39.1759	-72.0341	155.997	61.003	110	-39.1358	-72.0401	56.285	160.715
79	-39.1752	-72.0341	115.464	101.536	111	-39.1349	-72.0359	56.285	160.715
80	-39.1746	-72.0341	92.563	124.437	112	-39.1342	-72.04	56.488	160.512
81	-39.1739	-72.0343	79.997	137.003	113	-39.1335	-72.04	56.083	160.917
82	-39.1725	-72.0346	73.309	143.691	114	-39.1326	-72.0401	55.475	161.525
83	-39.172	-72.0349	67.432	149.568	115	-39.132	-72.04	56.083	160.917
84	-39.173	-72.0352	65.203	151.797	116	-39.1314	-72.0359	59.325	157.675
85	-39.1705	-72.0354	63.581	153.419	117	-39.1309	-72.0356	94.995	122.005
86	-39.1658	-72.0357	62.365	154.635	118	-39.13	-72.0354	142.621	74.379
87	-39.1651	-72.0401	61.352	155.648	119	-39.1241	-72.0353	191.667	25.333
88	-39.1644	-72.0405	60.339	156.661	120	-39.1235	-72.054	212.744	4.256
89	-39.1636	-72.0407	59.528	157.472	121	-39.124	-72.0404	212.538	4.462

Tab. A-2: GPS coordinates and water depth at shotpoints of the seismic survey on Lago Villarrica.

Shot-point No.	Longitude GPS (decimal)	Latitude GPS (decimal)	Depth (m)	Depth [m] (NN 208)	Shot-point No.	Longitude GPS (decimal)	Latitude GPS (decimal)	Depth (m)	Depth [m] (NN 217)
122	-39.1246	-72.0411	190.226	26.774	154	-39.162	-72.0543	57.573	159.427
123	-39.1248	-72.0421	151.688	65.312	155	-39.1628	-72.0549	59.601	157.399
124	-39.1249	-72.0431	143.980	73.020	156	-39.1637	-72.0552	61.630	155.370
125	-39.1257	-72.0437	115.178	101.822	157	-39.1643	-72.0555	62.847	154.153
126	-39.1304	-72.0437	59.601	157.399	158	-39.165	-72.0556	65.281	151.719
127	-39.131	-72.0438	54.733	162.267	159	-39.1658	-72.0558	71.771	145.229
128	-39.1316	-72.0443	54.328	162.672	160	-39.1707	-72.0601	82.724	134.276
129	-39.1322	-72.0446	54.328	162.672	161	-39.1715	-72.0603	100.979	116.021
130	-39.1331	-72.0447	53.922	163.078	162	-39.1723	-72.0601	136.678	80.322
131	-39.1337	-72.0448	53.922	163.078	163	-39.1729	-72.0604	178.056	38.944
132	-39.1344	-72.045	53.922	163.078	164	-39.1728	-72.0613	198.745	18.255
133	-39.1353	-72.0453	53.922	163.078	165	-39.1722	-72.0617	146.820	70.180
134	-39.1401	-72.0455	53.516	163.484	166	-39.1714	-72.0618	103.819	113.181
135	-39.141	-72.0501	53.922	163.078	167	-39.1707	-72.062	83.130	133.870
136	-39.1414	-72.0506	53.922	163.078	168	-39.1702	-72.0622	72.988	144.012
137	-39.1422	-72.0508	54.328	162.672	169	-39.1655	-72.0624	68.120	148.880
138	-39.1428	-72.0507	53.922	163.078	170	-39.165	-72.0627	65.281	151.719
139	-39.1437	-72.0509	53.922	163.078	171	-39.1644	-72.0626	62.847	154.153
140	-39.1443	-72.0513	53.922	163.078	172	-39.1632	-72.0623	61.630	155.370
141	-39.1449	-72.0514	54.328	162.672	173	-39.1626	-72.0617	60.007	156.993
142	-39.1455	-72.0517	54.328	162.672	174	-39.1617	-72.0616	57.979	159.021
143	-39.1504	-72.0519	53.922	163.078	175	-39.161	-72.0616	56.762	160.238
144	-39.1511	-72.0522	53.922	163.078	176	-39.1559	-72.0616	55.950	161.050
145	-39.1516	-72.0527	53.922	163.078	177	-39.155	-72.0618	55.139	161.861
146	-39.1525	-72.0532	54.328	162.672	178	-39.1544	-72.0617	54.328	162.672
147	-39.1534	-72.0531	54.328	162.672	179	-39.1536	-72.0619	54.328	162.672
148	-39.1541	-72.0524	54.733	162.267	180	-39.1529	-72.062	53.922	163.078
149	-39.1546	-72.0526	54.733	162.267	181	-39.1521	-72.0622	53.922	163.078
150	-39.1554	-72.0525	55.139	161.861	182	-39.1516	-72.0624	53.516	163.484
151	-39.1601	-72.0531	55.545	161.455	183	-39.1508	-72.0624	53.111	163.889
152	-39.1609	-72.0537	55.545	161.455	184	-39.1459	-72.0628	53.111	163.889
153	-39.1616	-72.054	56.356	160.644	185	-39.1453	-72.063	52.705	164.295

Tab. A-2: GPS coordinates and water depth at shotpoints of the seismic survey on Lago Villarrica.

Shot-point No.	Longitude GPS (decimal)	Latitude GPS (decimal)	Depth (m)	Depth [m] (NN 208)	Shot-point No.	Longitude GPS (decimal)	Latitude GPS (decimal)	Depth (m)	Depth [m] (NN 217)
186	-39.1447	-72.027	52.705	164.295	218	-39.1502	-72.074	54.733	162.267
187	-39.1438	-72.0626	52.705	164.295	219	-39.1509	-72.0744	70.960	146.040
188	-39.1431	-72.0627	52.299	164.701	220	-39.1516	-72.0749	53.516	163.484
189	-39.1426	-72.0629	52.299	164.701	221	-39.1521	-72.0751	53.111	163.889
190	-39.1418	-72.0627	52.299	164.701	222	-39.1528	-72.0754	53.111	163.889
191	-39.1409	-72.0625	51.894	165.106	223	-39.1537	-72.0755	53.111	163.889
192	-39.1402	-72.0627	51.894	165.106	224	-39.1544	-72.0756	53.111	163.889
193	-39.1354	-72.0628	51.894	165.106	225	-39.155	-72.0758	60.818	156.182
194	-39.1344	-72.0626	51.894	165.106	226	-39.1556	-72.0759	77.451	139.549
195	-39.1338	-72.0627	51.894	165.106	227	-39.1603	-72.08	110.715	106.285
196	-39.1334	-72.063	51.894	165.106	228	-39.161	-72.0802	137.084	79.916
197	-39.1326	-72.0632	52.299	164.701	229	-39.1616	-72.0806	125.319	91.681
198	-39.132	-72.0632	71.366	145.634	230	-39.1623	-72.0808	118.829	98.171
199	-39.1316	-72.0633	120.451	96.549	231	-39.163	-72.081	115.989	101.011
200	-39.1309	-72.0636	165.886	51.114	232	-39.1637	-72.0813	120.046	96.954
201	-39.1311	-72.064	153.716	63.284	233	-39.1646	-72.0814	94.083	122.917
202	-39.1319	-72.0643	94.489	122.511	234	-39.1653	-72.0818	94.489	122.511
203	-39.1327	-72.0645	53.111	163.889	235	-39.1703	-72.0825	94.894	122.106
204	-39.1334	-72.0647	51.894	165.106	236	-39.1703	-72.0831	95.300	121.700
205	-39.134	-72.065	51.894	165.106	237	-39.1711	-72.0835	96.923	120.077
206	-39.1347	-72.0656	51.894	165.106	238	-39.1717	-72.084	105.036	111.964
207	-39.1356	-72.0702	52.299	164.701	239	-39.1723	-72.0846	149.659	67.341
208	-39.1359	-72.0702	52.299	164.701	240	-39.1728	-72.0853	197.949	19.051
209	-39.1407	-72.0707	52.299	164.701	241	-39.1645	-71.5932	199.165	17.835
210	-39.1415	-72.0713	52.299	164.701	242	-39.1649	-71.5943	169.373	47.627
211	-39.142	-72.0716	52.299	164.701	243	-39.165	-71.5953	122.557	94.443
212	-39.1425	-72.072	52.299	164.701	244	-39.1652	-72.0004	96.616	120.384
213	-39.1432	-72.0725	52.299	164.701	245	-39.1656	-72.0016	94.184	122.816
214	-39.1437	-72.0728	52.299	164.701	246	-39.1659	-72.0026	92.563	124.437
215	-39.1444	-72.0731	52.299	164.701	247	-39.1702	-72.0038	96.008	120.992
216	-39.1451	-72.0739	52.299	164.701	248	-39.1704	-72.0049	88.509	128.491
217	-39.1457	-72.0742	52.299	164.701	249	-39.1705	-72.0059	83.240	133.760

Tab. A-2: GPS coordinates and water depth at shotpoints of the seismic survey on Lago Villarrica.

Shot-point No.	Longitude GPS (decimal)	Latitude GPS (decimal)	Depth (m)	Depth [m] (NN 208)	Shot-point No.	Longitude GPS (decimal)	Latitude GPS (decimal)	Depth (m)	Depth [m] (NN 217)
250	-39.1709	-72.0111	82.227	134.773	282	-39.1719	-72.0729	80.808	136.192
251	-39.1711	-72.0122	72.701	144.299	283	-39.1717	-72.0741	86.685	130.315
252	-39.1713	-72.0135	70.472	146.528	284	-39.1715	-72.0751	92.765	124.235
253	-39.1713	-72.0144	79.389	137.611	285	-39.1714	-72.081	92.968	124.032
254	-39.1715	-72.015	109.181	107.819	286	-39.1713	-72.0811	94.589	122.411
255	-39.1713	-72.0204	131.880	85.120	287	-39.1711	-72.0824	95.400	121.600
256	-39.1714	-72.0217	104.115	112.885	288	-39.1709	-72.0835	96.211	120.789
257	-39.1717	-72.0229	95.197	121.803	289	-39.1702	-72.0839	96.819	120.181
258	-39.1717	-72.0241	89.725	127.275	290	-39.1653	-72.084	96.616	120.384
259	-39.1719	-72.0253	71.080	145.920	291	-39.1643	-72.0838	98.237	118.763
260	-39.172	-72.0306	68.445	148.555	292	-39.1638	-72.083	100.669	116.331
261	-39.1719	-72.0318	67.635	149.365	293	-39.1626	-72.0828	106.952	110.048
262	-39.1717	-72.0329	67.635	149.365	294	-39.1608	-72.0834	107.965	109.035
263	-39.1716	-72.0338	67.635	149.365	295	-39.1559	-72.0834	111.208	105.792
264	-39.1713	-72.0345	67.027	149.973	296	-39.1555	-72.0832	97.224	119.776
265	-39.1716	-72.0359	69.053	147.947	297	-39.1546	-72.0834	58.109	158.891
266	-39.1717	-72.0414	68.851	148.149	298	-39.154	-72.0838	55.069	161.931
267	-39.1717	-72.0425	69.864	147.136	299	-39.1532	-72.0839	55.880	161.120
268	-39.1717	-72.0436	69.661	147.339	300	-39.1523	-72.084	57.096	159.904
269	-39.1717	-72.045	70.675	146.325	301	-39.1513	-72.084	81.619	135.381
270	-39.1718	-72.0503	72.904	144.096	302	-39.1512	-72.0838	113.843	103.157
271	-39.1718	-72.0513	78.376	138.624	303	-39.1502	-72.0836	97.427	119.573
272	-39.1718	-72.0526	83.443	133.557	304	-39.1453	-72.0834	54.259	162.741
273	-39.1718	-72.0538	100.264	116.736	305	-39.1443	-72.0831	52.029	164.971
274	-39.1717	-72.0551	120.531	96.469	306	-39.1436	-72.0831	51.421	165.579
275	-39.1717	-72.0602	141.608	75.392	307	-39.1425	-72.0828	51.016	165.984
276	-39.1716	-72.0614	141.608	75.392	308	-39.1417	-72.0827	50.813	166.187
277	-39.1714	-72.0626	126.003	90.997	309	-39.1408	-72.0827	50.813	166.187
278	-39.1714	-72.0638	112.829	104.171	310	-39.1359	-72.0828	50.813	166.187
279	-39.1716	-72.0651	95.603	121.397	311	-39.1341	-72.0818	50.813	166.187
280	-39.172	-72.0704	90.333	126.667	312	-39.1335	-72.0824	50.813	166.187
281	-39.1719	-72.0717	78.376	138.624	313	-39.1334	-72.0833	51.219	165.781

Tab. A-2: GPS coordinates and water depth at shotpoints of the seismic survey on Lago Villarrica.

Shot-point No.	Longitude GPS (decimal)	Latitude GPS (decimal)	Depth (m)	Depth [m] (NN 208)	Shot-point No.	Longitude GPS (decimal)	Latitude GPS (decimal)	Depth (m)	Depth [m] (NN 217)
314	-39.1326	-72.0834	51.624	165.376	346	-39.1602	-72.0938	121.341	95.659
315	-39.1316	-72.0835	51.624	165.376	347	-39.161	-72.094	116.477	100.523
316	-39.1307	-72.0833	52.232	164.768	348	-39.1619	-72.094	114.045	102.955
317	-39.1259	-72.083	60.947	156.053	349	-39.1626	-72.0945	111.816	105.184
318	-39.125	-72.0828	116.477	100.523	350	-39.1634	-72.095	109.992	107.008
319	-39.1245	-72.0837	137.555	79.445	351	-39.1643	-72.0952	108.776	108.224
320	-39.1244	-72.0849	137.960	79.040	352	-39.1652	-72.0952	107.763	109.237
321	-39.1245	-72.0901	128.840	88.160	353	-39.1702	-72.0952	109.992	107.008
322	-39.1242	-72.0912	125.395	91.605	354	-39.171	-72.0958	119.720	97.280
323	-39.1243	-72.0924	135.325	81.675	355	-39.1718	-72.1	174.845	42.155
324	-39.1249	-72.093	116.072	100.928	356	-39.172	-72.1012	171.197	45.803
325	-39.1258	-72.0931	85.672	131.328	357	-39.182	-72.1022	157.213	59.787
326	-39.1307	-72.0932	57.096	159.904	358	-39.1719	-72.1032	133.096	83.904
327	-39.1316	-72.0934	54.461	162.539	359	-39.171	-72.1038	125.395	91.605
328	-39.1326	-72.0934	53.245	163.755	360	-39.1702	-72.1038	123.773	93.227
329	-39.1334	-72.0934	52.435	164.565	361	-39.1653	-72.1038	122.760	94.240
330	-39.1342	-72.0935	52.029	164.971	362	-39.1644	-72.1035	122.152	94.848
331	-39.135	-72.0935	51.624	165.376	363	-39.1636	-72.1032	120.531	96.469
332	-39.1358	-72.0935	51.219	165.781	364	-39.1626	-72.1031	119.112	97.888
333	-39.1406	-72.0935	51.421	165.579	365	-39.1618	-72.1028	116.680	100.320
334	-39.1416	-72.0934	64.595	152.405	366	-39.1609	-72.1026	117.693	99.307
335	-39.1425	-72.0934	107.560	109.440	367	-39.16	-72.1026	121.544	95.456
336	-39.1433	-72.0935	142.419	74.581	368	-39.1544	-72.1025	126.205	90.795
337	-39.1441	-72.0934	132.083	84.917	369	-39.1537	-72.1022	132.285	84.715
338	-39.145	-72.0935	139.987	77.013	370	-39.1526	-72.102	135.528	81.472
339	-39.1459	-72.0935	148.904	68.096	371	-39.1517	-72.1019	137.555	79.445
340	-39.1508	-72.0934	155.389	61.611	372	-39.1509	-72.102	139.987	77.013
341	-39.1516	-72.0937	163.496	53.504	373	-39.1501	-72.1017	143.229	73.771
342	-39.1525	-72.0936	150.728	66.272	374	-39.1452	-72.1016	115.464	101.536
343	-39.1532	-72.0939	143.229	73.771	375	-39.1443	-72.1019	104.317	112.683
344	-39.1542	-72.0938	131.475	85.525	376	-39.1431	-72.1019	93.981	123.019
345	-39.1554	-72.0937	120.125	96.875	377	-39.142	-72.1019	70.675	146.325

Tab. A-2: GPS coordinates and water depth at shotpoints of the seismic survey on Lago Villarrica.

Shot-point No.	Longitude GPS (decimal)	Latitude GPS (decimal)	Depth (m)	Depth [m] (NN 208)	Shot-point No.	Longitude GPS (decimal)	Latitude GPS (decimal)	Depth (m)	Depth [m] (NN 217)
378	-39.141	-72.1017	68.851	148.149	410	-39.1531	-72.1044	131.677	85.323
379	-39.1401	-72.1016	55.069	161.931	411	-39.154	-72.1046	125.597	91.403
380	-39.1352	-72.1016	54.867	162.133	412	-39.155	-72.1049	122.557	94.443
381	-39.1341	-72.1016	55.272	161.728	413	-39.1558	-72.1055	123.368	93.632
382	-39.1332	-72.1014	58.515	158.485	414	-39.1607	-72.1055	122.963	94.037
383	-39.1324	-72.1013	76.755	140.245	415	-39.1617	-72.1056	124.179	92.821
384	-39.1317	-72.1012	94.387	122.613	416	-39.1623	-72.1101	139.581	77.419
385	-39.1311	-72.1014	113.235	103.765	417	-39.163	-72.1104	172.413	44.587
386	-39.1304	-72.1013	101.075	115.925	418	-39.164	-72.1112	142.419	74.581
387	-39.1253	-72.1013	133.907	83.093	419	-39.1648	-72.1118	135.528	81.472
388	-39.1241	-72.1009	145.661	71.339	420	-39.1655	-72.1126	133.907	83.093
389	-39.1236	-72.1008	172.616	44.384	421	-39.1705	-72.1132	151.133	65.867
390	-39.1244	-72.1015	147.283	69.717	422	-39.1708	-72.1139	173.629	43.371
391	-39.1252	-72.1016	135.528	81.472	423	-39.1711	-72.1144	200.381	16.619
392	-39.1259	-72.1021	110.803	106.197	424	-39.1705	-72.1149	193.085	23.915
393	-39.1309	-72.1023	127.016	89.984	425	-39.1658	-72.1202	149.512	67.488
394	-39.1318	-72.1025	134.515	82.485	426	-39.165	-72.1211	165.523	51.477
395	-39.1325	-72.1031	118.504	98.496	427	-39.1643	-72.1214	182.141	34.859
396	-39.1334	-72.1031	92.157	124.843	428	-39.1635	-72.1216	203.016	13.984
397	-39.1344	-72.1034	65.000	152.000	429	-39.1628	-72.122	201.395	15.605
398	-39.1352	-72.1025	58.920	158.080	430	-39.162	-72.1223	192.477	24.523
399	-39.1359	-72.1026	61.960	155.040	431	-39.1613	-72.123	160.861	56.139
400	-39.1406	-72.1028	66.419	150.581	432	-39.1605	-72.124	168.765	48.235
401	-39.1415	-72.1031	97.427	119.573	433	-39.1559	-72.1244	183.763	33.237
402	-39.1423	-72.1034	92.360	124.640	434	-39.1552	-72.1251	196.531	20.469
403	-39.1431	-72.1035	102.696	114.304	435	-39.1541	-72.1252	208.488	8.512
404	-39.1443	-72.1038	125.597	91.403	436	-39.1542	-72.124	210.109	6.891
405	-39.1452	-72.1037	121.949	95.051	437	-39.1544	-72.1231	202.611	14.389
406	-39.15	-72.1038	131.475	85.525	438	-39.1548	-72.1219	169.981	47.019
407	-39.1509	-72.104	139.784	77.216	439	-39.1546	-72.1208	149.715	67.285
408	-39.1517	-72.1046	137.960	79.040	440	-39.1545	-72.1159	142.419	74.581
409	-39.1525	-72.1047	134.717	82.283	441	-39.1545	-72.1147	137.555	79.445

Tab. A-2: GPS coordinates and water depth at shotpoints of the seismic survey on Lago Villarrica.

Shot-point No.	Longitude GPS (decimal)	Latitude GPS (decimal)	Depth (m)	Depth [m] (NN 208)	Shot-point No.	Longitude GPS (decimal)	Latitude GPS (decimal)	Depth (m)	Depth [m] (NN 217)
442	-39.1546	-72.1138	133.704	83.296	474	-39.1559	-72.0544	55.139	161.861
443	-39.1551	-72.1129	130.056	86.944	475	-39.1559	-72.0532	55.139	161.861
444	-39.155	-72.1116	129.043	87.957	476	-39.1603	-72.052	55.545	161.455
445	-39.1549	-72.1104	125.800	91.200	477	-39.1604	-72.051	55.950	161.050
446	-39.1549	-72.1052	123.571	93.429	478	-39.1605	-72.05	56.356	160.644
447	-39.1546	-72.1039	120.936	96.064	479	-39.1605	-72.045	56.762	160.238
448	-39.1547	-72.1029	121.949	95.051	480	-39.1606	-72.044	57.167	159.833
449	-39.155	-72.102	124.584	92.416	481	-39.1607	-72.0428	57.573	159.427
450	-39.155	-72.1008	129.853	87.147	482	-39.1611	-72.0418	57.573	159.427
451	-39.1549	-72.0956	131.677	85.323	483	-39.1613	-72.0407	57.979	159.021
452	-39.155	-72.0946	134.920	82.080	484	-39.1615	-72.0356	57.979	159.021
453	-39.1552	-72.0934	127.827	89.173	485	-39.1621	-72.0349	58.384	158.616
454	-39.1552	-72.0923	107.560	109.440	486	-39.1625	-72.0339	58.790	158.210
455	-39.1552	-72.0913	86.483	130.517	487	-39.1625	-72.0326	58.790	158.210
456	-39.1551	-72.0902	67.432	149.568	488	-39.162	-72.0315	59.196	157.804
457	-39.155	-72.0849	64.392	152.608	489	-39.1622	-72.0304	59.601	157.399
458	-39.155	-72.084	60.947	156.053	490	-39.1623	-72.0254	60.007	156.993
459	-39.155	-72.0829	57.096	159.904	491	-39.1628	-72.0242	60.413	156.587
460	-39.1552	-72.0819	55.475	161.525	492	-39.1629	-72.0232	61.224	155.776
461	-39.1554	-72.0808	55.880	161.120	493	-39.1631	-72.0219	62.035	154.965
462	-39.1551	-72.0755	56.691	160.309	494	-39.1634	-72.0211	62.441	154.559
463	-39.1551	-72.0744	54.259	162.741	495	-39.1636	-72.0159	62.847	154.153
464	-39.1552	-72.0732	50.677	166.323	496	-39.1638	-72.0149	63.658	153.342
465	-39.1552	-72.072	54.733	162.267	497	-39.1641	-72.0132	65.281	151.719
466	-39.1554	-72.0713	55.545	161.455	498	-39.1642	-72.0126	65.686	151.314
467	-39.1553	-72.0657	56.356	160.644	499	-39.1642	-72.0115	67.715	149.285
468	-39.1553	-72.0647	55.545	161.455	500	-39.1643	-72.0102	68.526	148.474
469	-39.1554	-72.0637	54.733	162.267	501	-39.1541	-72.0038	77.856	139.144
470	-39.1555	-72.0626	54.733	162.267	502	-39.1543	-72.0028	79.885	137.115
471	-39.1555	-72.0615	54.733	162.267	503	-39.1545	-72.0016	83.536	133.464
472	-39.1557	-72.0604	54.733	162.267	504	-39.1546	-72.0003	86.375	130.625
473	-39.1559	-72.0553	55.139	161.861	505	-39.1555	-71.5919	100.168	116.832

Tab. A-2: GPS coordinates and water depth at shotpoints of the seismic survey on Lago Villarrica.

Shot-point No.	Longitude GPS (decimal)	Latitude GPS (decimal)	Depth (m)	Depth [m] (NN 208)	Shot-point No.	Longitude GPS (decimal)	Latitude GPS (decimal)	Depth (m)	Depth [m] (NN 217)
506	-39.1546	-71.5914	100.574	116.426	538	-39.1541	-72	87.187	129.813
507	-39.1538	-71.5914	102.196	114.804	539	-39.1552	-71.5956	87.998	129.002
508	-39.1529	-71.5911	109.904	107.096	540	-39.154	-72.0021	83.130	133.870
509	-39.152	-71.5909	107.470	109.530	541	-39.155	-72.0034	79.885	137.115
510	-39.151	-71.5907	110.310	106.690	542	-39.1555	-72.0045	77.045	139.955
511	-39.1502	-71.5906	115.989	101.011	543	-39.1555	-72.0057	73.394	143.606
512	-39.1453	-71.5902	111.932	105.068	544	-39.1552	-72.0107	71.771	145.229
513	-39.1441	-71.5857	109.904	107.096	545	-39.1551	-72.0117	68.932	148.068
514	-39.1432	-71.5856	107.064	109.936	546	-39.1551	-72.0126	68.120	148.880
515	-39.1424	-71.59	111.121	105.879	547	-39.1552	-72.0139	67.309	149.691
516	-39.1416	-71.5859	109.498	107.502	548	-39.1553	-72.0149	66.903	150.097
517	-39.1408	-71.5859	102.602	114.398	549	-39.1555	-72.0204	64.875	152.125
518	-39.1359	-71.5859	111.527	105.473	550	-39.155	-72.0214	64.469	152.531
519	-39.1353	-71.5858	164.263	52.737	551	-39.1549	-72.0226	62.847	154.153
520	-39.1351	-71.5901	182.113	34.887	552	-39.1554	-72.0239	62.035	154.965
521	-39.1351	-71.5911	191.037	25.963	553	-39.1552	-72.0248	61.224	155.776
522	-39.1351	-71.5923	182.518	34.482	554	-39.1547	-72.0256	60.413	156.587
523	-39.135	-71.5934	165.886	51.114	555	-39.155	-72.031	59.601	157.399
524	-39.1347	-71.5943	148.037	68.963	556	-39.1549	-72.0313	59.196	157.804
525	-39.1346	-71.5953	120.857	96.143	557	-39.1548	-72.0324	58.790	158.210
526	-39.1349	-71.5955	83.941	133.059	558	-39.1548	-72.0336	58.384	158.616
527	-39.1356	-71.5956	84.347	132.653	559	-39.1549	-72.0347	57.573	159.427
528	-39.1411	-72.0001	84.753	132.247	560	-39.1547	-72.0359	57.167	159.833
529	-39.142	-72.0002	83.941	133.059	561	-39.1548	-72.0411	57.167	159.833
530	-39.1429	-72.0003	84.753	132.247	562	-39.1547	-72.0423	56.356	160.644
531	-39.1438	-72.0002	84.347	132.653	563	-39.1546	-72.0434	56.356	160.644
532	-39.1447	-72.0004	84.347	132.653	564	-39.1544	-72.0447	56.356	160.644
533	-39.1455	-72.0004	84.753	132.247	565	-39.1538	-72.0456	55.545	161.455
534	-39.1508	-71.5956	84.347	132.653	566	-39.1535	-72.0502	55.545	161.455
535	-39.1517	-71.5956	83.941	133.059	567	-39.1534	-72.0513	54.733	162.267
536	-39.1526	-71.5956	83.536	133.464	568	-39.1532	-72.0524	54.733	162.267
537	-39.1533	-71.5959	83.941	133.059	569	-39.1531	-72.0536	54.328	162.672

Tab. A-2: GPS coordinates and water depth at shotpoints of the seismic survey on Lago Villarrica.

Shot-point No.	Longitude GPS (decimal)	Latitude GPS (decimal)	Depth (m)	Depth [m] (NN 208)	Shot-point No.	Longitude GPS (decimal)	Latitude GPS (decimal)	Depth (m)	Depth [m] (NN 217)
570	-39.1527	-72.0546	53.922	163.078	602	-39.1348	-72.1058	109.384	107.616
571	-39.1523	-72.0557	53.922	163.078	603	-39.1347	-72.1047	112.019	104.981
572	-39.152	-72.0611	53.922	163.078	604	-39.1349	-72.1037	100.264	116.736
573	-39.1517	-72.062	53.516	163.484	605	-39.1347	-72.1026	72.093	144.907
574	-39.1514	-72.063	53.516	163.484	606	-39.1344	-72.1017	61.149	155.851
575	-39.1513	-72.0641	53.111	163.889	607	-39.1342	-72.1009	56.893	160.107
576	-39.151	-72.0653	53.111	163.889	608	-39.1338	-72.0959	54.056	162.944
577	-39.1507	-72.0703	52.705	164.295	609	-39.1337	-72.095	53.245	163.755
578	-39.1504	-72.0715	52.299	164.701	610	-39.1337	-72.0938	53.043	163.957
579	-39.1502	-72.0726	52.299	164.701	612	-39.1329	-72.091	52.637	164.363
580	-39.1459	-72.0735	52.029	164.971	613	-39.1326	-72.0858	52.299	164.701
581	-39.1457	-72.0747	52.232	164.768	614	-39.1325	-72.0846	51.894	165.106
582	-39.1453	-72.0758	92.360	124.640	615	-39.1326	-72.0844	51.894	165.106
583	-39.1452	-72.081	57.704	159.296	616	-39.1325	-72.0838	51.488	165.512
584	-39.1449	-72.082	52.029	164.971	617	-39.1325	-72.0827	51.488	165.512
585	-39.1446	-72.083	52.232	164.768	618	-39.1325	-72.0816	51.488	165.512
586	-39.1442	-72.0841	53.651	163.349	619	-39.1322	-72.0807	51.082	165.918
587	-39.1437	-72.085	53.043	163.957	620	-39.132	-72.0758	51.082	165.918
588	-39.1433	-72.0901	52.840	164.160	621	-39.1322	-72.0749	51.082	165.918
589	-39.143	-72.0911	74.525	142.475	622	-39.1322	-72.0738	51.488	165.512
590	-39.1426	-72.0923	128.232	88.768	623	-39.1325	-72.0721	51.488	165.512
591	-39.1423	-72.0936	107.155	109.845	624	-39.1328	-72.0707	51.488	165.512
592	-39.1423	-72.0947	89.117	127.883	625	-39.1329	-72.0658	51.488	165.512
593	-39.1421	-72.0958	89.928	127.072	626	-39.133	-72.0649	51.488	165.512
594	-39.1419	-72.101	56.893	160.107	627	-39.1332	-72.0639	51.488	165.512
595	-39.1417	-72.1021	57.299	159.701	628	-39.133	-72.0628	51.894	165.106
596	-39.1417	-72.1031	87.496	129.504	629	-39.1329	-72.0618	51.894	165.106
597	-39.1414	-72.1043	93.171	123.829	630	-39.1332	-72.0608	52.299	164.701
598	-39.1414	-72.105	104.317	112.683	631	-39.1335	-72.06	52.705	164.295
599	-39.141	-72.1059	116.883	100.117	632	-39.1333	-72.0549	52.705	164.295
600	-39.1403	-72.1107	131.880	85.120	633	-39.1332	-72.0537	52.705	164.295
601	-39.1356	-72.1109	151.944	65.056	634	-39.1333	-72.0525	53.111	163.889

Tab. A-2: GPS coordinates and water depth at shotpoints of the seismic survey on Lago Villarrica.

Shot-point No.	Longitude GPS (decimal)	Latitude GPS (decimal)	Depth (m)	Depth [m] (NN 208)	Shot-point No.	Longitude GPS (decimal)	Latitude GPS (decimal)	Depth (m)	Depth [m] (NN 217)
635	-39.1328	-72.0515	53.111	163.889	654	-39.1405	-72.0154	66.092	150.908
636	-39.1329	-72.0504	53.516	163.484	655	-39.1408	-72.0146	67.309	149.691
637	-39.133	-72.0453	53.922	163.078	656	-39.141	-72.0135	68.120	148.880
638	-39.1331	-72.0444	54.328	162.672	657	-39.1412	-72.0125	69.337	147.663
639	-39.1331	-72.0435	54.733	162.267	658	-39.1413	-72.0113	70.149	146.851
640	-39.133	-72.0424	54.733	162.267	659	-39.1417	-72.0105	72.583	144.417
641	-39.1335	-72.0416	55.545	161.455	660	-39.1419	-72.0055	73.394	143.606
642	-39.134	-72.0402	55.950	161.050	661	-39.1424	-72.0046	73.800	143.200
643	-39.134	-72.0352	56.356	160.644	662	-39.1426	-72.0034	77.045	139.955
644	-39.1344	-72.034	57.167	159.833	663	-39.1428	-72.0022	79.479	137.521
645	-39.1347	-72.0329	57.979	159.021	664	-39.143	-72.0013	81.507	135.493
646	-39.135	-72.0317	58.384	158.616	665	-39.1431	-72.0002	83.130	133.870
647	-39.135	-72.0305	59.196	157.804	666	-39.1434	-71.595	86.375	130.625
648	-39.135	-72.0256	60.007	156.993	667	-39.1437	-71.5941	88.809	128.191
649	-39.1353	-72.0246	61.224	155.776	668	-39.1438	-72.5934	92.866	124.134
650	-39.1359	-72.0235	62.035	154.965	669	-39.144	-72.5922	98.951	118.049
651	-39.1401	-72.0226	62.847	154.153	670	-39.1445	-72.5911	100.168	116.832
652	-39.1403	-72.0215	63.658	153.342	671	-39.1453	-71.5902	107.064	109.936
653	-39.1404	-72.0205	70.311	146.689	672	-39.1456	-71.5852	122.074	94.926

Tab. A-2: GPS coordinates and water depth at shotpoints of the seismic survey on Lago Villarrica.

Appendix B – Sedimentology, geochemistry and dating

Grain size parameters

Grab Samples - Lago Calafquén

				Grain Size Parameters						
Sample	Longitude (decimal)	Latitude (decimal)	Depth (m)	Clay 0.01 - 2 µm	Fine Silt 2 - 6 µm	Medium Silt 6 - 20 µm	Coarse Silt 20 - 63 µm	Fine Sand 63 - 125 µm	Medium Sand 125 - 250 µm	Coarse Sand 250 - 500 µm
LCQ BG2	-72.030	-39.564	143	8.962	18.314	39.567	31.238	1.918	0	0
LCQ BG3	-72.019	-39.575	71	9.193	18.426	39.224	30.954	2.204	0	0
LCQ BG4	-72.012	-39.563	10	4.259	7.5	22.23	45.972	17.718	2.32	0
LCQ BG6	-72.054	-39.557	174	1.272	1.923	4.502	21.349	30.855	20.897	7.83
LCQ BG7	-72.070	-39.560	4.3	6.874	15.789	40.246	32.017	5.074	0	0
LCQ B10	-72.060	-39.556	178	7.596	15.617	20.113	22.83	14.796	6.631	4.742
LCQ BG11	-72.092	-39.546	188	6.758	12.738	24.167	37.608	17.205	1.525	0
LCQ BG12	-72.091	-39.534	191	18.725	32.329	32.555	14.01	2.263	0.117	0
LCQ BG13	-72.089	-39.524	176	12.734	26.663	36.391	19.461	3.71	0.268	0.647
LCQ BG14	-72.133	-39.528	196	6.071	10.978	22.522	31.837	18.542	7.782	1.98
LCQ BG15	-72.135	-39.511	204	3.608	6.407	14.973	32.211	30.423	11.068	0.976
LCQ BG16	-72.171	-39.516	210	4.171	7.469	20.826	38.793	20.499	6.999	1.151
LCQ BG17	-72.204	-39.519	212	9.331	18.407	35.139	33.252	3.871	0	0
LCQ BG18	-72.240	-39.514	137	7.901	15.068	32.581	37.379	7.072	0	0
LCQ BG19	-72.253	-39.513	88.7	22.619	38.493	33.711	5.177	0	0	0
LCQ BG23	-72.261	-39.520	64.6	24.51	38.804	26.725	9.226	0.735	0	0
LCQ BG24	-72.259	-39.529	131	29.482	35.383	24.974	7.374	1.382	0.582	0.733

Tab. B-1: Granulometric results of grab samples of Lago Calafquén. Particles were measured by laser diffraction with Malvern Mastersizer.

				Grain Size Parameters						
Sample	Longitude (decimal)	Latitude (decimal)	Depth (m)	Clay 0.01 - 2 µm	Fine Silt 2 - 6 µm	Medium Silt 6 - 20 µm	Coarse Silt 20 - 63 µm	Fine Sand 63 - 125 µm	Medium Sand 125 - 250 µm	Coarse Sand 250 - 500 µm
LCQ BG26	-72.254	-39.545	----	100	0	0	0	0	0	0
LCQ BG29	-72.238	-39.557	61	27.973	34.498	26.253	9.303	1.344	0.576	0.052
LCQ BG30	-72.210	-39.550	126	25.179	36.725	25.401	9.331	2.235	0.507	0.48
LCQ BG31	-72.188	-39.551	101	21.317	38.325	30.892	8.334	1.133	0	0
LCQ BG32	-72.160	-39.540	120	22.783	41.534	29.795	5.359	0.529	0	0
LCQ BG33	-72.144	-39.498	86.9	11.104	19.104	27.935	27.343	10.904	2.315	0.989
LCQ BG34	-72.121	-39.503	164	3.859	6.918	21.45	39.8	21.64	5.48	0.673
LCQ BG35	-72.116	-39.503	101	7.627	14.236	23.699	27.216	11.589	7.455	6.334
LCQ BG36	-72.113	-39.504	44	6.033	14.172	22.251	25.936	18.037	10.633	2.745
LCQ BG38	-72.113	-39.507	53	3.284	5.322	12.107	22.519	14.723	19.008	18.943
LCQ BG39	-72.116	-39.507	97	1.814	3.147	9.531	24.218	22.782	20.051	13.147
LCQ BG40	-72.119	-39.508	126	2.112	3.73	12.738	33.361	28.514	12.219	4.783
LCQ BG41	-72.124	-39.511	182	4.851	11.156	24.023	39.308	17.789	2.873	0
LCQ BG42	-72.114	-39.516	193	10.803	21.923	37.665	25.991	3.084	0.117	0.303
LCQ BG43	-72.112	-39.511	170	8.081	17.599	27.29	28.755	13.457	3.583	0.963
LCQ BG44	-72.111	-39.508	53	6.871	15.4	32.865	35.464	8.331	1.069	0

Tab. B-1: Granulometric results of grab samples of Lago Calafquén. Particles were measured by laser diffraction with Malvern Mastersizer.

Grain Size Statistics						Carbon-Sulfur Analysis		
Sample	Mediane	Mean	Mode	Sorting	Skewness	Carbon	Sulfur	c/s ratio
LCQ BG2	12.8437	16.1991	18.189	2.1401	0.8167	1.87	0.0059	316.95
LCQ BG3	12.792	16.2165	18.205	2.1597	0.8116	1.58	0.0647	24.42
LCQ BG4	31.1796	36.6742	42.956	1.9773	0.8163	0.46	0.0090	51.11
LCQ BG6	100.5584	151.0589	94.413	1.8423	1.0694	1.14	0.0149	76.51
LCQ BG7	14.1634	18.8274	16.286	2.0686	0.9265	7.25	0.0000	
LCQ BG10	28.8733	61.9148	73.488	3.7227	0.7466	1.23	0.0050	246.00
LCQ BG11	25.2049	32.6989	50.734	2.5092	0.7003	3.53	0.0058	608.62
LCQ BG12	5.7988	9.324	4.813	2.3278	1.0395	1.96	0.0093	210.75
LCQ BG13	8.4212	13.1324	8.854	2.3241	0.9824	0.72	0.0075	96.00
LCQ BG14	30.2298	44.2848	60.512	2.6623	0.7759	0.64	0.0091	70.00
LCQ BG15	53.2164	59.0707	78.364	2.142	0.6489	0.42	0.0073	57.12
LCQ BG16	35.5619	45.2595	52.74	2.192	0.8015	0.63	0.0070	89.29
LCQ BG17	13.5809	18.1626	22.655	2.3193	0.8165	0.71	0.0087	81.38
LCQ BG18	16.9521	22.0321	28.207	2.2793	0.7993	1.42	0.0008	1775.00
LCQ BG19	4.4104	6.0685	4.226	2.0452	1.003	3.51	0.0032	1096.88
LCQ BG23	4.12	6.3251	3.716	2.0905	1.0627	2.63	0.0067	392.54
LCQ BG24	3.7003	6.1613	2.702	2.2527	1.1196	1.57	0.0111	141.44
LCQ BG26	1.138	1.1488	1.155	1.1633	0.992	2.97	0.0038	781.58
LCQ BG29	3.9539	6.7483	2.778	2.3162	1.1324	2.96	0.0024	1233.33
LCQ BG30	4.1923	7.035	3.623	2.2007	1.0894	2.17	0.0032	678.13
LCQ BG31	4.6703	6.523	5.02	2.0246	0.9755	2.38	0.0132	180.30
LCQ BG32	4.2346	5.5081	4.716	1.9249	0.9572	1.15	0.0086	133.72
LCQ BG33	14.1466	25.3101	41.451	2.9533	0.943	0.85	0.0114	74.12
LCQ BG34	35.4599	43.9272	56.541	2.1351	0.8065	0.76	0.0132	57.27
LCQ BG35	24.1819	49.9404	34.137	3.118	0.8681	1.93	0.0144	134.03
LCQ BG36	29.1069	48.8918	77.964	3.191	0.7486	0.88	0.0144	60.90
LCQ BG38	86.1263	137.2826	264.021	2.9995	0.828	0.75	0.0164	45.98
LCQ BG39	89.4531	130.1546	104.46	2.2902	0.8893	1.07	0.0199	53.77
LCQ BG40	60.2389	72.7369	74.724	1.9579	0.8255	1.74	0.0194	89.69
LCQ BG41	28.2243	35.4134	48.838	2.3441	0.7178	1.14	0.0195	58.46
LCQ BG42	10.7665	15.113	14.704	2.2994	0.8749	2.86	0.0381	75.07
LCQ BG43	17.596	30.0718	48.466	2.8943	0.9117	1.77	0.0139	127.34
LCQ BG44	17.1687	23.1164	24.903	2.2796	0.8298	1.24	0.0160	77.50

Tab. B-2: Grain size statistics and carbon-sulfur (C-S) analysis of grab samples of Lago Calafquén. Particles were measured by laser diffraction; C-S analysis was done by infra-red spectroscopy with LECO CS 125.

Grab Samples - Lago Villarrica

				Grain Size Parameters						
Sample	Longitude (decimal)	Latitude (decimal)	Depth (m)	Clay 0.01 – 2 µm	Fine Silt 2 - 6 µm	Medium Silt 6 – 20 µm	Coarse Silt 20 - 63 µm	Fine Sand 63 - 125 µm	Medium Sand 125 – 250 µm	Coarse Sand 250 – 500 µm
LVR BG1	-71.983	-39.263	118	5.966	13.236	31.033	35.494	12.389	1.882	0
LVR BG2	-72.021	-39.266	150	7.321	16.84	36.013	32.782	6.877	0.167	0
LVR BG3	-72.045	-39.267	158	5.692	11.896	26.376	40.076	14.042	1.918	0
LVR BG4	-72.069	-39.268	161	12.539	27.065	40.208	18.173	1.997	0.018	0
LVR BG5	-72.091	-39.268	162	7.583	16.548	31.62	32.249	9.388	1.47	0.92
LVR BG6	-72.115	-39.270	160	12.933	28.156	43.139	15.321	0.451	0	0
LVR BG7	-72.138	-39.272	107	18.19	35.979	37.274	8.29	0.266	0	0
LVR BG8	-72.208	-39.280	30	20.091	36.12	23.925	11.285	5.841	2.51	0.228
LVR BG9	-72.182	-39.278	91	16.531	32.804	34.948	13.74	1.978	0	0
LVR BG10	-72.160	-39.277	110	15.451	33.038	41.245	10.06	0.206	0	0
LVR BG11	-72.157	-39.245	81	25.674	44.545	25.95	3.631	0.201	0	0
LVR BG12	-72.151	-39.233	167	17.123	33.211	34.548	12.405	1.183	0.924	0.608
LVR BG13	-72.126	-39.236	167	14.439	33.066	39.788	11.601	1.107	0	0
LVR BG14	-72.100	-39.236	166	15.081	32.254	34.873	16.315	1.478	0	0
LVR BG15	-72.081	-39.238	164	12.023	26.495	37.074	21.108	3.163	0.137	0
LVR BG16	-72.052	-39.240	157	6.975	14.062	34.717	40.553	3.694	0	0
LVR BG17	-72.027	-39.242	150	9.289	23.982	39.782	23.638	3.162	0.146	0
LVR BG18	-72.064	-39.244	137	6.036	12.677	31.688	38.845	10.029	0.725	0

Tab. B-3: Granulometric results of grab samples of Lago Villarrica. Particles were measured by laser diffraction with Malvern Mastersizer.

Grain Size Statistics						Carbon-Sulfur Analysis		
Sample	Mediane	Mean	Mode	Sorting	Skewness	Carbon	Sulfur	c/s ratio
LVR BG1	19.8509	27.9674	29.013	2.3307	0.8868	2.91	0.0413	70.460
LVR BG2	14.794	20.4729	18.6	2.2456	0.8932	3.24	0.0664	48.795
LVR BG3	24.3545	30.8957	40.669	2.3137	0.7424	1.22	0.0244	50.000
LVR BG4	8.1316	11.4199	9.54	2.1567	0.9241	2.49	0.0483	51.553
LVR BG5	16.4149	24.4798	27.798	2.4736	0.8867	1.12	0.0257	43.580
LVR BG6	7.6624	9.9536	9.599	2.0511	0.892	2.35	0.0531	44.256
LVR BG7	5.3857	7.1175	6.334	2.0127	0.9372	2.71	0.0433	62.587
LVR BG8	4.9618	12.0407	3.902	2.3794	1.2927	3.22	0.0143	225.175
LVR BG9	6.1145	9.2543	6.35	2.1661	0.9957	3.36	0.0424	79.245
LVR BG10	6.2397	8.0491	7.663	2.0037	0.9134	2.61	0.0658	39.666
LVR BG11	3.7146	4.7341	4.037	1.8647	0.9679	2.31	0.0195	118.462
LVR BG12	5.9415	8.9988	5.761	2.1986	1.0132	2.15	0.0375	57.333
LVR BG13	6.3928	8.5718	7.057	1.9965	0.9499	2.31	0.0451	51.220
LVR BG14	6.4916	10.1096	5.77	2.223	1.0482	2.27	0.0469	48.401
LVR BG15	8.5463	13.2151	8.375	2.2827	1.0038	3.09	0.0537	57.542
LVR BG16	17.2603	20.4713	26.432	2.079	0.773	2.59	0.036	71.944
LVR BG17	9.9634	14.2883	10.664	2.1793	0.967	3.2	0.0868	36.866
LVR BG18	19.7736	25.603	27.76	2.1771	0.8364	3.14	0.0668	47.006

Tab. B-4: Grain size statistics and carbon-sulfur (C-S) analysis of grab samples of Lago Villarrica. Particles were measured by laser diffraction; C-S analysis was done by infra-red spectroscopy with LECO CS 125.

Gravity Core - Lago Calafquén

		Grain Size Statistics					Grain Size Parameters				
Sample	depth (cm)	Mediane	Mean	Mode	Sorting	Skewness	Clay (%) 0.01 – 2 µm	fine silt (%) 2 - 6 µm	medium silt (%) 6 – 20 µm	coarse silt (%) 20 - 63 µm	fine sand (%) 63 - 125 µm
LCQ2s 0-0.5	0	9.8229	12.5119	11.215	1.9332	0.9249	8.35	22.912	46.834	19.037	1.54
LCQ2s 0.5-1	0.5	9.4966	12.32	10.662	1.9521	0.9344	8.728	23.8	46.042	18.105	1.66
LCQ2s 1-1.5	1	7.005	9.3084	8.046	2.0131	0.9295	13.498	30.552	41.576	11.776	1.338
LCQ2s 1.5-2	1.5	8.2851	11.1973	9.315	2.0326	0.9373	11.133	26.875	42.928	15.092	1.289
LCQ2s 2-2.5	2	11.7029	16.4069	12.296	2.0752	0.9646	7.596	19.598	42.274	23.796	2.857
LCQ2s 2.5-3	2.5	8.5759	11.2604	9.885	1.998	0.9244	10.415	26.175	44.389	15.567	1.316
LCQ2s 3-3.5	3	6.7258	8.1456	7.784	1.8218	0.9234	11.601	33.278	45.889	7.332	0.751
LCQ2s 3.5-4	3.5	6.2666	7.7457	7.108	1.8457	0.934	12.905	35.165	42.922	7.127	0.771
LCQ2s 4-4.5	4	10.2739	13.6192	11.43	2.0196	0.9397	8.269	22.483	44.062	22.495	1.656
LCQ2s 4.5-5	4.5	10.8413	14.7797	11.442	2.009	0.9674	7.208	21.424	44.175	21.924	2.511
LCQ2s 5-5.5	5	7.3509	9.0614	8.275	1.8298	0.9383	10.032	31.035	46.904	8.947	0.898
LCQ2s 5.5-6	5.5	8.0908	10.4153	9.337	1.9575	0.9233	10.719	27.616	45.09	13.829	0.938
LCQ2s 6-6.5	6	10.7684	14.2832	12.116	2.0291	0.9318	8.224	21.245	43.759	23.01	1.938
LCQ2s 6.5-7	6.5	8.4235	10.3849	9.986	1.8946	0.9059	9.979	26.351	47.897	13.513	0.381
LCQ2s 7-7.5	7	7.5047	9.6755	8.611	1.9388	0.9242	11.66	29.32	44.245	9.707	0.675
LCQ2s 7.5-8	7.5	7.8881	9.8126	9.462	1.9244	0.9023	11.112	27.971	46.501	12.875	0.688
LCQ2s 8-8.5	8	8.0494	10.4458	9.248	1.9916	0.9224	11.395	27.389	44.323	15.979	0.915
LCQ2s 8.5-9	8.5	7.71505	9.95545	8.9785	1.98435	0.91735	11.972	28.3815	44.1505	14.601	0.888
LCQ2s 9-9.5	9	7.3807	9.4651	8.709	1.9771	0.9123	12.549	29.374	43.978	13.223	0.861

Tab. B-5: Granulometric results of gravity core LCQ2s of Lago Calafquén. Particles were measured by laser diffraction with Malvern Mastersizer.

		Grain Size Statistics					Grain Size Parameters				
Sample	depth (cm)	Mediane	Mean	Mode	Sorting	Skewness	Clay (%) 0.01 – 2 µm	fine silt (%) 2 - 6 µm	medium silt (%) 6 – 20 µm	coarse silt (%) 20 - 63 µm	fine sand (%) 63 - 125 µm
LCQ2s 9.5-10	9.5	7.7581	9.86775	9.198	1.96595	0.9096	11.822	28.2285	44.9025	13.8995	0.821
LCQ2s 10-11	10	8.1355	10.2704	9.687	1.9548	0.9069	11.095	27.083	45.827	14.576	0.781
LCQ2s 11-12	11	6.7136	8.7238	9.269	2.0954	0.8793	15.746	30.267	41.708	11.934	0.346
LCQ2s 12-13.5	12	19.5068	24.6993	30.01	2.1815	0.8104	6.472	12.878	31.523	39.894	9.152
LCQ2s 13.5-14	13.5	8.4093	10.7065	10.07	1.9774	0.906	11.015	26.183	45.413	16.038	0.883
LCQ2s 14-15	14	15.0693	17.8233	22.004	2.0345	0.789	7.41	15.621	38.695	36.274	1.999
LCQ2s 15-16	15	19.6406	22.0358	26.311	1.8695	0.8087	5.642	10.902	34.281	45.526	3.648
LCQ2s 16-17	16	11.2755	14.836	18.735	2.3314	0.7776	11.703	20.954	37.12	27.723	2.393
LCQ2s 17-18	17	20.9268	24.3906	27.749	1.8951	0.8484	5.07	9.704	33.288	45.618	6.319
LCQ2s 18-19	18	17.4471	22.9457	24.706	2.1895	0.8547	6.766	13.972	34.043	36.873	8.181
LCQ2s 19-20	19	7.1215	9.6743	7.852	2.0413	0.9416	13.685	29.8	40.947	13.853	1.062
LCQ2s 20-21	20	4.9254	6.1036	6.037	1.9273	0.9075	19.776	38.477	38.233	3.514	0
LCQ2s 21-22	21	8.4078	13.5006	8.537	2.2722	1.0007	12.847	25.902	37.324	18.225	4.298
LCQ2s 22-23	22	6.8898	8.8542	8.236	1.9929	0.8971	14.5	30.073	42.551	10.109	0.71
LCQ2s 23-24	23	12.1091	18.3195	12	2.2545	0.9874	8.888	19.074	38.433	26.514	6.503
LCQ2s 24-25	24	6.2529	8.302	7.379	2.0344	0.9113	16.269	32.14	39.356	8.82	1.286
LCQ2s 25-26	25	6.2092	7.661	7.771	1.9486	0.8782	15.976	32.62	42.68	7.107	0.116
LCQ2s 26-27	26	6.0212	7.7721	7.381	2.0122	0.8926	17.002	32.86	39.686	7.423	1.063
LCQ2s 27-28	27	8.5038	11.5884	10.025	2.0918	0.9118	11.981	25.67	42.127	15.087	1.495
LCQ2s 28-29	28	6.6772	9.7654	7.281	2.1472	0.9535	15.795	30.364	37.279	11.445	1.733
LCQ2s 29-30.5	29	7.6343	10.7045	8.437	2.0894	0.9444	13.116	28.079	40.573	14.447	1.961

Tab. B-5: Granulometric results of gravity core LCQ2s of Lago Calafquén. Particles were measured by laser diffraction with Malvern Mastersizer.

		Grain Size Statistics					Grain Size Parameters				
Sample	depth (cm)	Mediane	Mean	Mode	Sorting	Skewness	Clay (%) 0.01 – 2 µm	fine silt (%) 2 - 6 µm	medium silt (%) 6 – 20 µm	coarse silt (%) 20 - 63 µm	fine sand (%) 63 - 125 µm
LCQ2s 30.5-32	30.5	16.267	20.7387	22.114	2.1865	0.7872	7.996	15.148	34.618	35.117	6.334
LCQ2s 32-33	32	10.2709	16.0945	10.527	2.2683	0.985	10.576	22.122	38.485	21.179	4.535
LCQ2s 33-34	33	12.7639	23.2381	10.58	2.752	1.0371	10.46	19.99	30.954	25.699	8.829
LCQ2s 34-35	34	7.9818	11.9014	9.097	2.218	0.9365	13.648	26.769	38.523	15.111	2.575
LCQ2s 35-36	35	8.4746	12.0041	9.56	2.1319	0.931	12.283	25.632	40.869	16.508	2.629
LCQ2s 36-37	36	8.3514	12.7786	8.879	2.2291	0.9693	12.829	26.059	38.307	16.603	2.721
LCQ2s 37-38	37	7.9147	11.8875	8.676	2.2059	0.9566	13.403	27.176	38.399	14.989	2.103
LCQ2s 38-39	38	7.9926	10.4299	9.419	2.0023	0.9136	11.706	27.448	43.924	14.031	1.375
LCQ2s 39-39.5	39	7.6712	10.38	8.789	2.035	0.9312	12.292	28.498	42.081	12.505	1.551
LCQ2s 39.5-40	39.5	7.1247	10.878	7.735	2.2081	0.9634	15.066	29.013	36.966	13.102	2.328
LCQ2s 40-41	40	6.5246	10.4005	6.856	2.2468	0.986	16.689	30.46	34.675	12.265	3.001
LCQ2s 41-42	41	6.9771	12.1101	6.965	2.2728	1.0295	15.241	29.598	34.456	14.009	4.732
LCQ2s 42-43	42	7.3915	12.985	7.341	2.2668	1.0371	14.099	28.732	35.338	14.292	5.235
LCQ2s 43-44	43	7.1907	10.1971	8.163	2.1163	0.9347	14.387	29.079	39.32	13.063	2.586
LCQ2s 44-45	44	7.8562	16.9499	6.463	2.6375	1.2056	14.371	27.586	30.805	17.701	7.125
LCQ2s 45-46	45	7.2425	11.237	7.679	2.2498	0.9764	14.959	28.731	36.434	14.379	2.09
LCQ2s 46-46.4	46	7.03	10.6169	8.234	2.3048	0.9472	16.238	28.741	36.075	14.678	1.323
LCQ2s 46.4-47	46.4	4.658	6.5656	4.211	2.0439	1.0276	20.673	38.583	33.058	7.484	0.201
LCQ2s 47-47.7	47	42.8592	47.6138	67.339	2.212	0.6242	4.333	7.897	17.566	36.951	27.69
LCQ2s 47.7-48.3	47.7	30.8293	35.5286	48.656	2.1789	0.6878	5.356	9.746	21.342	43.773	18.381
LCQ2s 48.3-49	48.3	7.2542	15.9655	6.565	2.4037	1.1405	14.551	29.157	32.472	13.359	7.704

Tab. B-5: Granulometric results of gravity core LCQ2s of Lago Calafquén. Particles were measured by laser diffraction with Malvern Mastersizer.

		Grain Size Statistics					Grain Size Parameters				
Sample	depth (cm)	Mediane	Mean	Mode	Sorting	Skewness	Clay (%) 0.01 – 2 µm	fine silt (%) 2 - 6 µm	medium silt (%) 6 – 20 µm	coarse silt (%) 20 - 63 µm	fine sand (%) 63 - 125 µm
LCQ2s 49-49.8	49	8.1189	19.5306	6.58	2.7528	1.2958	14.086	26.956	30.275	17.005	9.454
LCQ2s 49.8-50	49.8	6.7453	13.322	6.26	2.3964	1.0942	16.143	30.071	31.741	14.337	5.6
LCQ2s 50-51	50	221.0129	208.3603	300.816	3.1939	0.2247	2.48	5.911	11.497	11.066	3.082
LCQ2s 51-52	51	8.249	11.2493	9.589	2.1124	0.9118	12.875	25.888	41.589	17.984	1.664
LCQ2s 52-53	52	6.8513	9.0009	7.999	2.0217	0.9157	14.45	30.461	41.638	12.083	1.336
LCQ2s 53-54	53	6.745	8.822	8.12	2.0427	0.8997	15.336	30.235	41.438	11.01	0.871
LCQ2s 54-55	54	5.5903	7.3659	6.41	1.9872	0.9268	17.552	35.293	36.97	6.628	1.005
LCQ2s 55-56	55	6.4021	9.2107	7.176	2.1576	0.9421	16.724	30.973	37.021	11.919	1.069
LCQ2s 56-57	56	8.9682	12.629	9.717	2.0919	0.9507	11.046	24.592	41.886	17.282	1.961
LCQ2s 57-58	57	6.7845	11.3708	6.575	2.2367	1.0348	15.199	30.545	34.568	11.701	1.914
LCQ2s 58-58.9	58	6.1279	9.1713	6.444	2.1389	0.9782	16.801	32.432	35.234	10.327	1.728
LCQ2s 58.9-60	58.9	14.3236	27.9615	11.823	2.6774	1.0813	8.059	18.704	32.173	24.341	8.245
LCQ2s 60-61	60	7	8.9234	8.337	1.9702	0.9055	13.67	30.227	43.397	10.531	0.981
LCQ2s 61-62	61	6.9356	8.9279	8.399	2.0027	0.901	14.201	30.203	42.681	10.575	0.808
LCQ2s 62-63	62	6.4907	8.3064	7.927	2.0041	0.8973	15.447	31.495	41.997	10.317	0.73
LCQ2s 63-64	63	6.7999	8.7092	8.202	1.9925	0.9008	14.466	30.645	42.643	10.181	0.752
LCQ2s 64-65	64	6.4803	8.0914	7.786	1.9338	0.8989	14.616	32.209	43	8.178	0.718
LCQ2s 65-66	65	5.6544	7.0038	6.815	1.9184	0.9005	16.848	35.663	40.372	6.297	0.652
LCQ2s 66-67	66	10.355	14.6943	11.495	2.2133	0.9355	10.657	21.838	39.391	24.505	3.028
LCQ2s 67-68	67	10.0566	14.2863	11.371	2.2478	0.924	11.458	22.232	38.81	24.689	2.783
LCQ2s 68-69	68	8.3304	11.4159	9.36	2.104	0.9308	12.393	25.952	41.564	18.253	1.814

Tab. B-5: Granulometric results of gravity core LCQ2s of Lago Calafquén. Particles were measured by laser diffraction with Malvern Mastersizer.

		Grain Size Statistics					Grain Size Parameters				
Sample	depth (cm)	Mediane	Mean	Mode	Sorting	Skewness	Clay (%) 0.01 – 2 µm	fine silt (%) 2 - 6 µm	medium silt (%) 6 – 20 µm	coarse silt (%) 20 - 63 µm	fine sand (%) 63 - 125 µm
LCQ2s 69-70	69	7.6177	10.9327	8.636	2.153	0.9331	13.944	27.678	39.429	13.973	2.054
LCQ2s 70-71	70	9.6053	12.3977	11.033	1.9783	0.9157	9.819	22.713	45.61	18.331	1.751
LCQ2s 71-72	71	8.9204	12.2272	10.022	2.0676	0.9311	11.092	24.633	42.691	16.807	1.945
LCQ2s 72-73	72	8.6963	14.4036	8.565	2.3318	1.0136	12.699	25.35	36.464	17.416	3.531
LCQ2s 73-74	73	8.9219	18.64	7.982	2.5181	1.1431	12.238	25.467	33.846	17.063	7.578
LCQ2s 74-75	74	8.9824	12.1325	10.456	2.0861	0.9155	11.301	24.502	42.534	18.172	1.911
LCQ2s 75-75.5	75	7.2001	10.3599	7.847	2.1268	0.9564	14.042	29.416	38.87	13.666	3.116
LCQ2s 75.5-76	75.5	4.8848	6.545	5.329	2.0137	0.9615	20.202	37.698	35.116	6.984	0
LCQ2s 76-76.8	76	5.4238	7.6457	4.913	2.0241	1.0378	16.441	37.41	35.938	10.211	0
LCQ2s 76.8-77.3	76.8	12.0768	13.8711	14.64	1.7846	0.8873	7.317	16.015	50.995	25.616	0.057
LCQ2s 77.3-78	77.3	13.8505	16.2367	17.808	1.9035	0.8447	7.207	15.277	44.106	31.903	1.507
LCQ2s 78-78.2	78	6.6359	8.2656	8.322	1.9593	0.8908	14.485	31.5	43.877	9.551	0.571
LCQ2s 78.2-78.8	78.2	7.4195	11.5832	7.512	2.2015	1.0023	13.638	28.977	37.058	15.473	3.434
LCQ2s 78.8-79.5	78.8	5.9523	8.8539	6.281	2.1804	0.9757	17.83	32.45	34.941	12.945	1.808
LCQ2s 79.5-80	79.5	5.7435	8.1541	6.584	2.1191	0.9502	18.047	33.526	35.577	9.372	1.599
LCQ2s 80-80.2	80	4.1059	5.805	4.171	2.0595	0.9997	25.102	38.667	29.184	6.788	0.26
LCQ2s 80.2-80.4	80.2	4.324	5.8649	4.724	2.0187	0.9709	23.405	38.979	31.151	5.714	0.75
LCQ2s 80.4-81	80.4	6.9828	9.3303	8.38	2.0482	0.9194	13.847	30.517	41.098	11.097	1.479
LCQ2s 81-82	81	8.408	11.2912	9.53	2.0259	0.9291	11.19	26.246	43.344	15.311	2.092
LCQ2s 82-83	82	7.1065	8.9762	8.62	1.9587	0.9004	13.113	30.175	44.116	11.057	0.817
LCQ2s 83-84	83	6.3537	8.0076	7.687	1.9487	0.9034	14.828	32.845	42.231	8.899	0.816

Tab. B-5: Granulometric results of gravity core LCQ2s of Lago Calafquén. Particles were measured by laser diffraction with Malvern Mastersizer.

		Grain Size Statistics					Grain Size Parameters				
Sample	depth (cm)	Mediane	Mean	Mode	Sorting	Skewness	Clay (%) 0.01 – 2 µm	fine silt (%) 2 - 6 µm	medium silt (%) 6 – 20 µm	coarse silt (%) 20 - 63 µm	fine sand (%) 63 - 125 µm
LCQ2s 84-85	84	8.6787	11.1252	10.205	1.9798	0.9073	10.761	25.283	45.4	16.26	1.207
LCQ2s 85-86	85	9.5943	12.5372	10.921	1.9833	0.9231	9.304	23.284	45.307	18.469	1.971
LCQ2s 86-87	86	8.634	11.8044	9.904	2.0883	0.9247	11.493	25.582	42.124	17.554	1.779
LCQ2s 87-88	87	8.0803	10.5859	9.773	2.0377	0.9044	12.025	27.062	43.418	15.055	1.145
LCQ2s 88-89	88	8.7668	10.769	10.306	1.8813	0.9089	9.393	25.31	48.557	15.155	0.791
LCQ2s 89-90	89	8.435	10.2415	10.306	1.8998	0.884	10.734	25.662	48.358	13.528	0.65
LCQ2s 90-90.7	90	6.4911	9.1454	6.988	2.0798	0.963	15.092	31.976	38.163	12.577	1.164
LCQ2s 90.7-90.8	90.7	6.5482	10.1668	6.319	2.3227	1.0061	16.603	30.66	34.534	17.024	1.179
LCQ2s 90.8-92	90.8	19.9151	23.6909	29.445	2.0874	0.7701	6.318	12.566	31.278	42.85	6.963
LCQ2s 92-93	92	11.2666	15.0407	13.207	2.0956	0.8998	9.344	19.829	42.067	25.327	3.3
LCQ2s 93-94	93	8.1886	10.1733	9.797	1.9251	0.8965	11.022	26.642	46.864	13.429	0.629
LCQ2s 94-95	94	6.1466	7.6041	7.753	1.9324	0.8968	15.131	33.882	42.868	7.722	0.397
LCQ2s 95-96	95	6.9421	9.2922	8.24	2.0674	0.913	14.637	29.97	40.875	12.427	0.889
LCQ2s 96-97	96	10.3944	13.9501	12.384	2.1188	0.9132	9.671	22.045	41.606	24.369	1.594
LCQ2s 97-98	97	6.341	7.6797	7.971	1.9019	0.8841	14.635	33.039	44.496	7.436	0.394
LCQ2s 98-99	98	7.573	9.487	9.257	1.9539	0.894	12.287	28.566	45.362	11.783	0.687
LCQ2s 99-100	99	7.946	10.5776	9.199	2.0239	0.9186	12.041	27.416	43.062	12.8	1.146
LCQ2s 100-101	100	9.6311	12.2025	11.061	1.9219	0.918	8.618	23.184	47.256	17.131	1.446
LCQ2s 101-102	101	12.2986	17.2573	12.717	2.078	0.9685	7.597	18.193	41.966	25.424	3.566
LCQ2s 102-103	102	6.3618	7.6578	7.943	1.8827	0.8852	14.308	33.186	44.768	6.64	0.242
LCQ2s 103-104	103	8.1188	10.1288	9.952	1.9496	0.8896	11.302	26.956	46.268	13.289	0.806

Tab. B-5: Granulometric results of gravity core LCQ2s of Lago Calafquén. Particles were measured by laser diffraction with Malvern Mastersizer.

		Grain Size Statistics					Grain Size Parameters				
Sample	depth (cm)	Mediane	Mean	Mode	Sorting	Skewness	Clay (%) 0.01 – 2 µm	fine silt (%) 2 - 6 µm	medium silt (%) 6 – 20 µm	coarse silt (%) 20 - 63 µm	fine sand (%) 63 - 125 µm
LCQ2s 104-105	104	6.4124	8.1695	7.964	1.99	0.8996	15.199	32.204	42.005	8.941	0.303
LCQ2s 105-105.3	105	6.4189	8.3659	7.784	2.0147	0.9128	15.212	32.197	40.931	9.383	0.837
LCQ2s 105.3-106	105.3	6.5751	8.2334	7.492	1.9051	0.9246	13.601	32.543	43.677	10.096	0.083
LCQ2s 106-107	106	8.2756	11.4763	9.113	2.0366	0.9449	11.267	26.687	42.492	13.328	1.756
LCQ2s 107-109	107	9.8354	13.7859	10.372	2.0508	0.9658	9.165	22.968	43.127	18.403	1.464
LCQ2s 109-110	109	15.0594	20.3695	16.302	1.9961	0.9485	5.712	14.312	41.31	28.988	3.226
LCQ2s 110-110.5	110	7.4227	9.2215	8.931	1.9241	0.9011	12.231	29.163	45.789	11.068	0.759
LCQ2s 110.5-111	110.5	7.6046	9.7511	8.902	1.9712	0.9143	12.274	28.468	44.368	12.657	0.778
LCQ2s 111-112	111	7.351	10.0725	8.214	2.0725	0.9389	13.445	29.066	40.837	13.86	1.02
LCQ2s 112-113	112	7.8877	10.1597	9.048	1.9636	0.9203	11.649	27.624	44.729	13.556	1.113
LCQ2s 113-114	113	6.7241	8.9933	7.853	2.0537	0.918	15.036	30.68	40.512	11.463	1.061
LCQ2s 114-115	114	7.683	10.3139	8.87	2.0536	0.9238	12.833	28.032	42.096	13.943	1.219
LCQ2s 115-116	115	7.3205	9.1962	8.977	1.9647	0.8969	12.937	29.269	44.816	11.584	0.551
LCQ2s 116-117	116	7.1758	9.8661	8.32	2.1105	0.9187	14.647	28.897	40.145	13.808	1.56
LCQ2s 117-118	117	6.9463	8.5033	8.724	1.9131	0.8954	12.854	31.167	45.824	9.581	0.14
LCQ2s 118-119	118	7.2259	8.8353	8.653	1.8796	0.9075	11.773	30.417	46.624	10.103	0.481
LCQ2s 119-120	119	6.6206	8.1492	8.222	1.9187	0.8969	13.767	32.189	44.55	8.52	0.525
LCQ2s 120-121	120	7.4968	8.8816	9.676	1.8942	0.8617	12.512	28.364	48.624	10.296	0.204
LCQ2s 121-122	121	7.5076	9.2958	9.071	1.9201	0.8983	12.041	28.891	46.108	11.217	0.602
LCQ2s 122-123	122	7.1008	8.7298	8.7	1.9186	0.8912	12.999	30.108	45.65	9.935	0.66
LCQ2s 123-124	123	6.7986	8.3623	8.461	1.9312	0.8848	13.909	30.994	44.788	8.696	0.505

Tab. B-5: Granulometric results of gravity core LCQ2s of Lago Calafquén. Particles were measured by laser diffraction with Malvern Mastersizer.

		Grain Size Statistics					Grain Size Parameters				
Sample	depth (cm)	Mediane	Mean	Mode	Sorting	Skewness	Clay (%) 0.01 – 2 µm	fine silt (%) 2 - 6 µm	medium silt (%) 6 – 20 µm	coarse silt (%) 20 - 63 µm	fine sand (%) 63 - 125 µm
LCQ2s 124-125	124	9.0351	11.994	10.723	2.0799	0.9084	11.197	24.443	42.872	18.762	1.092
LCQ2s 125-126	125	7.8082	10.4844	9.055	2.0608	0.9215	12.711	27.637	42.161	14.675	1.216
LCQ2s 126-127	126	6.2302	7.8275	7.542	1.9461	0.9062	15.144	33.324	42.189	8.044	0.718
LCQ2s 127-128	127	9.5492	13.7368	12.022	2.2622	0.9294	10.643	24.951	38.197	23.417	2.792
LCQ2s 128-129	128	12.806	14.9235	17.783	1.9615	0.8084	8.271	17.236	44.171	29.92	0.402
LCQ2s 129-130	129	22.0749	24.4937	31.035	1.9175	0.7693	5.34	10.605	29.857	49.027	5.171
LCQ2s 130-131	130	41.0068	44.2975	56.903	1.8608	0.7647	3.069	5.89	16.859	46.205	25.794
LCQ2s 131-132	131	12.9741	15.1577	18.047	1.9601	0.8127	7.972	17.155	43.905	30.507	0.461
LCQ2s 132-132.6	132	19.0164	23.632	29.569	2.1524	0.8011	6.263	13.359	32.186	40.612	7.58
LCQ2s 132.6-133.5	132.6	43.7712	47.2813	62.494	1.9455	0.7189	3.2	6.453	16.27	42.069	28.068
LCQ2s 133.5-134.4	133.5	7.4302	9.3602	8.808	1.9359	0.912	12.031	29.398	45.133	12.002	0.423
LCQ2s 134.4-135.5	134.4	9.4656	12.2768	12.632	2.1023	0.8768	10.841	23.839	42.747	21.751	0.822
LCQ2s 135.5-136.5	135.5	12.1458	15.75	15.132	2.0767	0.8894	8.339	18.791	41.678	28.745	2.448
LCQ2s 136.5-137.5	136.5	7.0487	8.5141	8.876	1.8929	0.8893	12.454	30.875	46.966	9.705	0
LCQ2s 137.5137.8	137.5	6.1281	7.577	7.636	1.9292	0.8971	15.234	33.896	42.817	7.823	0.23
LCQ2s 137.8-138.7	137.8	4.6627	6.2431	5.947	2.0535	0.9563	21.943	37.206	35.227	5.624	0
LCQ2s 138.7-139.7	138.7	19.2675	22.0516	25.998	1.8773	0.8332	5.489	10.634	35.537	44.693	3.647
LCQ2s 139.7-140.5	139.7	6.3469	7.6368	7.924	1.8731	0.894	13.839	33.75	45.216	7.01	0.185
LCQ2s 140.5-142	140.5	7.2855	9.5317	8.312	1.9817	0.9358	12.07	30.374	43.047	13.501	1.007
LCQ2s 142-143	142	12.5032	18.0594	13.147	2.2249	0.95	8.351	18.913	38.491	28.2	5.986
LCQ2s 143-144	143	7.6067	8.9424	9.808	1.8489	0.8815	10.926	29.1	50.106	9.869	0

Tab. B-5: Granulometric results of gravity core LCQ2s of Lago Calafquén. Particles were measured by laser diffraction with Malvern Mastersizer.

		Grain Size Statistics					Grain Size Parameters				
Sample	depth (cm)	Mediane	Mean	Mode	Sorting	Skewness	Clay (%) 0.01 – 2 µm	fine silt (%) 2 - 6 µm	medium silt (%) 6 – 20 µm	coarse silt (%) 20 - 63 µm	fine sand (%) 63 - 125 µm
LCQ2s 144-145	144	6.8775	8.4802	8.138	1.8864	0.9126	12.416	31.823	45.246	9.008	0.418
LCQ2s 145-146	145	8.2574	10.1789	9.781	1.8937	0.9103	10.025	27.054	47.786	14.38	0.74
LCQ2s 146-147	146	5.9763	7.2064	7.139	1.8415	0.9104	14.23	35.947	43.208	6.051	0.564
LCQ2s 147-148.2	147	6.6697	8.7412	7.425	1.9447	0.9449	13.039	32.642	41.536	10.056	1.354
LCQ2s 148.2-149.5	148.2	5.6087	6.6603	6.797	1.8149	0.909	14.974	38.121	42.57	4.277	0.057
LCQ2s 149.5-150	149.5	7.4588	9.2012	9.1	1.9237	0.8933	12.33	28.888	46.178	11.364	0.618
LCQ2s 150-151	150	6.3685	7.839	7.964	1.9266	0.8946	14.598	32.956	43.937	8.177	0.332
LCQ2s 151-152	151	6.795	8.3832	8.069	1.8984	0.9036	13.233	31.529	44.748	9.682	0.809
LCQ2s 152-153	152	7.239	9.8805	9.132	2.1495	0.9071	14.559	28.992	40.131	15.388	0.93
LCQ2s 153-154	153	21.7821	28.2781	39.935	2.5244	0.6813	8.07	14.102	25.356	38.458	13.234
LCQ2s 154-155	154	6.7402	8.1302	8.376	1.8864	0.8865	13.37	31.713	45.973	8.194	0.659
LCQ2s 155-156	155	7.7139	9.1881	9.621	1.8697	0.882	11.409	28.142	48.998	11.395	0.056
LCQ2s 156-157	156	6.8177	8.3294	8.502	1.9162	0.8896	13.535	31.215	45.523	9.217	0.351
LCQ2s 157-158	157	6.4584	7.8207	8.113	1.9021	0.8855	14.278	32.636	45.069	7.883	0.134
LCQ2s 158-159	158	6.8873	8.2724	8.816	1.8964	0.8798	13.235	31.04	46.763	8.666	0.297
LCQ2s 159-159.8	159	6.5502	7.6656	8.517	1.8598	0.8661	13.931	32.266	47.522	6.281	0
LCQ2s 159.8-160	159.8	7.0261	8.4921	8.913	1.9074	0.8798	13.083	30.432	46.568	9.311	0.589
LCQ2s 160-161	160	83.7749	99.2067	139.713	2.4654	0.5888	2.331	5.309	12.986	21.393	23.015
LCQ2s 161-162	161	6.4911	7.8955	8.074	1.8997	0.8913	14.003	32.697	44.815	8.026	0.459
LCQ2s 162	162	8.3449	11.6508	9.134	2.0494	0.9491	11.263	26.489	42.237	14.519	3.055

Tab. B-5: Granulometric results of gravity core LCQ2s of Lago Calafquén. Particles were measured by laser diffraction with Malvern Mastersizer.

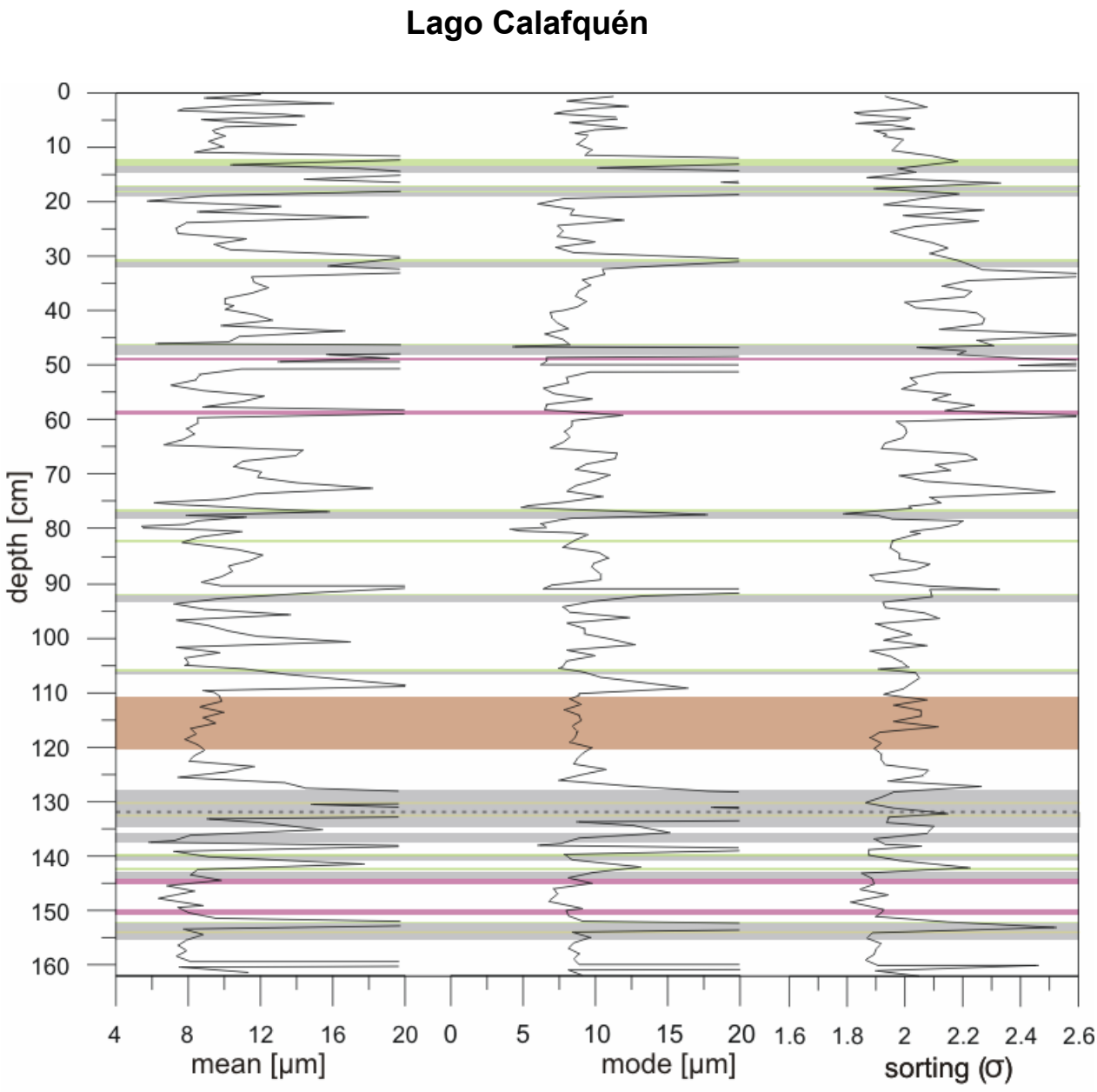

Fig. B-1: Mean and mode grain size (in µm) and sorting values (in standard deviation units) for short core LCQ2s in full resolution. Shaded and coloured bands indicate lithology, presented in Fig. IV-18.

Gravity Core - Lago Villarrica

		Grain Size Statistics					Grain Size Parameters					
Sample	Depth (cm)	Mediane	Mean	Mode	Sorting	Skewness	Clay (%) 0.01 – 2 µm	fine silt (%) 2 - 6 µm	medium silt (%) 6 – 20 µm	coarse silt (%) 20 - 63 µm	fine sand (%) 63 - 125 µm	medium sand (%) 63 - 125 µm
LVR4s 0.5-1	1	9.8968	12.8372	11.027	1.9422	0.9385	8.036	22.958	46.366	19.128	2.308	0.848
LVR4s 01-1.5	1.5	8.7501	10.7285	10.255	1.8667	0.9142	8.956	25.648	48.9	14.643	0.994	0.535
LVR4s 01.5-2	2	8.8562	10.8579	10.445	1.8766	0.9106	8.998	25.307	48.772	15.934	0.977	0.012
LVR4s 2-2.5	2.5	7.7949	9.9678	9.103	1.9549	0.9203	11.277	28.455	44.954	13.983	1.223	0.108
LVR4s 2.5-3	3	9.3636	12.0205	10.789	1.9685	0.9221	9.25	24.061	45.766	19.634	1.288	0
LVR4s 3-3.5	3.5	7.3619	9.3675	8.757	1.959	0.9151	12.197	29.753	44.436	12.742	0.86	0.013
LVR4s 3.5-4	4	9.2264	12.0128	10.813	2.0107	0.9182	9.817	24.485	44.555	19.195	1.427	0.385
LVR4s 4-4.5	4.5	10.0509	12.5537	12.212	1.9486	0.9003	8.428	22.567	46.661	21.025	1.301	0.017
LVR4s 4.5-5	5	9.093	11.523	10.612	1.9404	0.9191	9.144	24.91	46.581	17.576	1.224	0.498
LVR4s 5-5.5	5.5	9.3234	11.9643	11.063	1.9853	0.9111	9.486	24.256	45.412	18.739	1.315	0.483
LVR4s 5.5-6	6	7.7174	9.9884	9.165	2.0015	0.9151	12.107	28.352	43.874	14.224	0.827	0.615
LVR4s 6-6.5	6.5	8.3007	10.5273	10.01	1.97	0.9056	10.925	26.695	45.57	15.127	0.648	0.64
LVR4s 6.5-7	7	10.1246	12.8165	12.033	1.9622	0.9082	8.547	22.277	46.11	20.719	1.217	0.751
LVR4s 7-7.5	7.5	7.2064	9.4992	8.235	2.0035	0.9346	12.766	30.203	42.425	12.882	0.974	0.482
LVR4s 07.5-8-2	8	7.656	10.4514	8.409	2.052	0.9542	11.915	29.075	41.563	15.224	1.164	0.731
LVR4s 8-8.5	8.5	7.0858	9.3539	7.984	1.9849	0.9407	12.635	30.861	42.238	11.939	1.343	0.712
LVR4s 8.5-9	9	5.8107	7.716	7.068	2.0536	0.9358	17.02	34.163	39.201	9.617	0	0
LVR4s 9-9.2	9.2	6.398	8.7169	6.646	2.0382	0.9737	14.401	33.173	39.565	12.794	0.066	0
LVR4s 9.2-10	10	10.0505	12.3173	13.688	2.0161	0.8436	9.984	22.254	45.494	21.992	0.276	0

Tab. B-6: Granulometric results of gravity core LVR4s of Lago Villarrica. Particles were measured by laser diffraction with Malvern Mastersizer.

		Grain Size Statistics					Grain Size Parameters					
Sample	Depth (cm)	Mediane	Mean	Mode	Sorting	Skewness	Clay (%) 0.01 – 2 µm	fine silt (%) 2 - 6 µm	medium silt (%) 6 – 20 µm	coarse silt (%) 20 - 63 µm	fine sand (%) 63 - 125 µm	medium sand (%) 63 - 125 µm
LVR4s 10-11	11	15.9734	19.4536	22.891	2.0705	0.8087	7.22	14.747	36.904	37.22	3.909	0
LVR4s 11-11.5	11.5	6.7315	8.3574	7.905	1.8929	0.9158	12.865	32.281	44.337	8.586	0.875	0.401
LVR4s 11.5-12	12	7.4256	9.1155	9.051	1.9064	0.9013	11.84	29.468	46.664	11.457	0.554	0.017
LVR4s 12-12.5	12.5	8.7708	11.0391	10.426	1.9498	0.9106	9.986	25.475	46.438	17.487	0.614	0
LVR4s 12.5-13	13	6.2175	7.861	7.591	1.9641	0.9066	15.319	33.256	42.006	9.027	0.392	0
LVR4s 13-13.5	13.5	5.9597	7.5101	7.449	1.972	0.9002	16.353	33.915	41.38	7.91	0.441	0
LVR4s 13.5-14	14	4.8553	6.2078	5.616	1.9368	0.9358	19.668	39.053	35.53	5.449	0.299	0
LVR4s 14-14.5	14.5	4.6532	5.9346	4.938	1.8627	0.9704	18.828	42.209	33.562	4.651	0	0.291
LVR4s 14.5-15	15	6.5482	8.2312	7.391	1.8927	0.9327	13.161	33.12	43.316	9.466	0.762	0.174
LVR4s 15-15.5	15.5	6.9091	8.1716	8.177	1.8107	0.9041	12.129	31.492	48.035	7.901	0.444	0
LVR4s 15.5-16	16	6.927	8.572	7.781	1.8583	0.93	12.135	31.594	45.325	10.144	0.802	0
LVR4s 16-16.5	16.5	6.8259	8.7528	7.591	1.9205	0.9378	12.894	31.742	43.071	10.802	1.024	0.256
LVR4s 16.5-17	17	7.2419	9.2417	8.814	1.9923	0.8974	13.411	29.329	43.742	12.506	0.92	0.093
LVR4s 17-17.5	17.5	6.7588	8.8678	7.634	1.9667	0.9345	13.518	31.704	41.622	10.134	1.03	0.227
LVR4s 17.5-18	18	6.0298	7.95	7.047	2.0186	0.927	16.261	33.548	39.455	10.07	0.666	0
LVR4s 18-18.5	18.5	6.1974	8.1711	7.426	2.0331	0.9187	16.034	32.734	39.918	10.595	0.719	0
LVR4s 18.5-19	19	6.0997	8.1327	6.811	2.0056	0.9433	15.624	33.731	39.157	10.486	0.982	0.019
LVR4s 19-19.5	19.5	6.0778	7.8936	6.849	1.961	0.9353	15.337	34.14	40.143	9.791	0.589	0
LVR4s 19.5-20	20	5.7103	7.3482	6.544	1.9449	0.9314	16.288	35.748	38.966	8.198	0.799	0
LVR4s 20-20.5	20.5	5.9792	7.9208	6.594	1.9636	0.9476	15.416	34.725	38.637	9.349	1.282	0.436
LVR4s 20.5-21	21	6.006	7.9618	6.532	1.9483	0.9558	14.916	35.043	38.69	8.88	1.47	0.459

Tab. B-6: Granulometric results of gravity core LVR4s of Lago Villarrica. Particles were measured by laser diffraction with Malvern Mastersizer.

		Grain Size Statistics					Grain Size Parameters					
Sample	Depth (cm)	Mediane	Mean	Mode	Sorting	Skewness	Clay (%) 0.01 – 2 µm	fine silt (%) 2 - 6 µm	medium silt (%) 6 – 20 µm	coarse silt (%) 20 - 63 µm	fine sand (%) 63 - 125 µm	medium sand (%) 63 - 125 µm
LVR4s 21-21.5	21.5	6.0108	8.7363	6.249	2.0625	0.9879	15.862	34.07	35.691	11.157	2.801	0.419
LVR4s 21.5-22	22	8.177	10.2565	9.414	1.9026	0.9284	9.71	27.778	46.927	14.671	0.901	0.012
LVR4s 22-22.5	22.5	8.7553	11.2725	9.744	1.9349	0.9405	9.227	25.937	46.133	17.07	1.521	0.112
LVR4s 22.5-23	23	9.0927	11.469	10.846	1.9556	0.9038	9.723	24.559	46.417	17.291	0.877	0.117
LVR4s 23-23.5	23.5	7.7286	9.8858	9.578	2.007	0.8953	12.402	28.096	44.225	14.256	1.001	0.02
LVR4s 23.5-24	24	6.8435	8.8921	8.453	2.0338	0.9052	14.46	30.608	42.133	12.244	0.555	0
LVR4s 24-24.8	24.8	4.7326	6.3006	5.143	1.9921	0.9665	20.558	38.643	34.497	6.244	0.059	0
LVR4s 24.8-25.2	25.2	6.1697	9.1784	5.983	2.2388	0.9958	17.047	32.043	35.552	14.657	0.7	0
LVR4s 25.2-26	26	7.0905	9.3534	7.836	1.9835	0.9442	12.718	30.713	42.361	13.394	0.813	0
LVR4s 26-27	27	9.4342	13.2563	11.135	2.2015	0.9204	11.075	24.235	39.801	22.249	2.607	0.033
LVR4s 27-28	28	15.9	23.5815	36.771	2.6438	0.8199	9.594	17.301	29.305	33.04	10.069	0.692
LVR4s 28-29	29	7.4524	10.0948	8.515	2.0814	0.9316	13.278	28.852	41.23	15.508	1.121	0.012
LVR4s 29-30	30	7.4977	10.0123	8.531	2.0347	0.9328	12.601	29.045	42.195	14.142	1.205	0.562
LVR4s 30-31	31	6.4047	8.124	8.046	1.9917	0.899	15.204	32.258	42.469	9.874	0.196	0
LVR4s 31-32	32	8.0438	10.3869	9.512	1.9986	0.9181	11.294	27.663	44.35	15.624	0.698	0.322
LVR4s 32-33-2	33	6.4064	8.0872	7.55	1.9335	0.9189	14.112	33.203	42.679	9.58	0.427	0
LVR4s 33-34	34	8.0605	11.1757	9.077	2.1312	0.9351	12.558	27.125	40.674	17.492	1.239	0.501
LVR4s 34-35	35	7.665	9.3387	9.782	1.9252	0.8813	11.844	28.443	47.137	12.106	0.469	0
LVR4s 35-36	36	5.7235	7.2082	6.636	1.9167	0.9243	15.993	35.992	40.252	7.593	0.17	0
LVR4s 36-37	37	6.0687	7.8627	7.281	2.0097	0.9116	16.378	33.179	40.42	9.961	0.062	0
LVR4s 37-38	38	6.4943	8.1439	8.589	2.0002	0.8812	15.34	31.619	43.237	9.643	0.16	0

Tab. B-6: Granulometric results of gravity core LVR4s of Lago Villarrica. Particles were measured by laser diffraction with Malvern Mastersizer.

		Grain Size Statistics					Grain Size Parameters					
Sample	Depth (cm)	Mediane	Mean	Mode	Sorting	Skewness	Clay (%) 0.01 – 2 µm	fine silt (%) 2 - 6 µm	medium silt (%) 6 – 20 µm	coarse silt (%) 20 - 63 µm	fine sand (%) 63 - 125 µm	medium sand (%) 63 - 125 µm
LVR4s 39-40	40	6.7385	8.4298	8.197	1.9485	0.9012	13.99	31.341	43.955	10.482	0.231	0
LVR4s 40-41	41	6.7076	8.1533	8.565	1.9213	0.8808	13.92	31.518	45.551	8.964	0.046	0
LVR4s 41-42	42	5.094	6.3308	6.217	1.9161	0.9103	18.693	38.217	37.849	5.167	0.075	0
LVR4s 42-43	43	5.3949	6.9246	6.517	1.9783	0.9141	18.241	36.021	38.068	7.186	0.484	0
LVR4s 43-44	44	6.1153	7.6645	7.808	1.9813	0.8876	16.241	33.006	42.118	8.353	0.282	0
LVR4s 44-45	45	7.463	9.324	9.107	1.957	0.8933	12.629	28.784	45.375	12.507	0.552	0.153
LVR4s 45-46	46	6.3831	7.9935	8.03	1.9812	0.8834	15.683	31.867	42.786	9.145	0.404	0.115
LVR4s 46-47	47	6.7458	8.4446	8.321	1.9659	0.8937	14.261	31.091	43.946	10.605	0.097	0
LVR4s 47-48	48	6.4648	8.0207	8.015	1.9462	0.8916	14.75	32.227	43.682	9.18	0.161	0
LVR4s 48-49	49	5.775	7.1373	7.065	1.9197	0.9046	16.223	35.373	41.695	6.66	0.049	0
LVR4s 49-50	50	6.3596	7.9389	7.783	1.9436	0.9051	14.734	32.909	43.236	8.894	0.227	0
LVR4s 50-51	51	6.0326	7.3618	7.385	1.8938	0.9014	15.12	34.65	43.224	6.869	0.137	0
LVR4s 51-52	52	5.8187	6.9946	7.058	1.8522	0.9035	15.142	36.219	42.924	5.479	0.235	0
LVR4s 52-53	53	5.7179	7.0997	7.245	1.9417	0.8997	16.682	35.285	41.305	6.37	0.358	0
LVR4s 53-54	54	5.6916	7.3942	7.118	2.0275	0.9138	17.656	34.351	39.448	8.456	0.089	0
LVR4s 54-55	55	5.1746	6.1996	6.223	1.8341	0.9089	17.157	39.58	39.372	3.758	0.133	0
LVR4s 55-55.5	55.5	4.8356	6.1617	5.583	1.9343	0.937	19.709	39.171	35.941	5.129	0.05	0
LVR4s 56-57	57	7.326	9.2336	9.533	2.0044	0.8875	13.213	29.279	44.474	12.952	0.081	0
LVR4s 57-58	58	8.0917	10.6416	10.101	2.0736	0.8947	12.243	27.12	42.822	16.792	1.023	0
LVR4s 58-59	59	9.225	12.8508	11.168	2.2047	0.9048	11.677	24.378	39.949	21.992	2.004	0
LVR4s 59-60	60	9.4466	13.354	11.907	2.2593	0.8959	11.788	24.07	38.842	22.83	2.454	0.017

Tab. B-6: Granulometric results of gravity core LVR4s of Lago Villarrica. Particles were measured by laser diffraction with Malvern Mastersizer.

		Grain Size Statistics					Grain Size Parameters					
Sample	Depth (cm)	Mediane	Mean	Mode	Sorting	Skewness	Clay (%) 0.01 – 2 µm	fine silt (%) 2 - 6 µm	medium silt (%) 6 – 20 µm	coarse silt (%) 20 - 63 µm	fine sand (%) 63 - 125 µm	medium sand (%) 63 - 125 µm
LVR4s 60-61	61	10.5933	15.5707	11.488	2.2811	0.9426	10.211	22.141	38.053	25.515	4.038	0.043
LVR4s 61-62	62	14.7215	23.0467	39.643	2.5884	0.9507	8.641	18.136	31.25	31.49	10.021	0.461
LVR4s 62-63	63	6.1172	7.8311	7.502	1.9863	0.9113	15.751	33.489	41.096	8.844	0.799	0.021
LVR4s 64-65	65	4.3301	5.5258	5.088	1.9358	0.9298	22.815	40.661	31.777	4.441	0.306	0
LVR4s 65-66	66	5.5556	7.1683	6.978	2.0143	0.9113	18.064	34.9	39.158	7.664	0.215	0
LVR4s 66-67	67	6.075	7.9035	7.751	2.0489	0.9043	16.771	32.766	40.515	9.948	0	0
LVR4s 67-68	68	4.6727	6.1083	5.346	1.9714	0.9379	21.191	38.882	33.379	6.168	0.379	0
LVR4s 68-69	69	4.9775	6.5411	5.83	2.0098	0.936	20.139	37.102	36.147	6.612	0	0
LVR4s 70-71	71	5.3103	6.7911	6.251	1.9542	0.9186	18.255	36.762	37.262	6.854	0.867	0
LVR4s 71-72	72	4.7231	6.1044	5.561	1.976	0.9276	21.147	38.448	34.669	5.542	0.194	0
LVR4s 72-73	73	6.1234	8.2937	7.908	2.1447	0.9115	17.652	31.64	38.963	11.744	0	0
LVR4s 73-74	74	5.4731	6.9227	6.778	1.9728	0.9029	18.08	35.615	39.204	6.212	0.415	0.474
LVR4s 74-75	75	6.8744	9.0682	8.613	2.0773	0.9057	14.885	30.184	41.386	13.138	0.408	0
LVR4s 75-76	76	7.2764	10.19	8.281	2.1726	0.9355	14.632	28.754	39.196	16.862	0.555	0
LVR4s 76-77	77	5.6834	7.2542	6.826	1.9739	0.9103	17.221	34.958	39.517	7.775	0.529	0
LVR4s 78-79	79	6.7315	8.2958	7.864	1.8841	0.9137	13.021	32.075	44.882	9.643	0.379	0
LVR4s 79-80	80	10.0239	13.3893	12.161	2.1258	0.912	10.21	22.697	41.519	24.545	1.029	0
LVR4s 80-81	81	7.1273	9.8717	8.856	2.1726	0.9174	14.993	29.165	39.363	15.031	0.514	0.386
LVR4s 81-82	82	3.9524	4.9371	4.322	1.8344	0.9612	23.218	45.077	28.723	2.914	0.068	0
LVR4s 83-84	84	9.368	15.1527	8.86	2.3065	1.0352	11.095	24.383	37.209	21.734	5.172	0.406
LVR4s 84-85	85	6.4713	8.4153	7.726	2.0089	0.9117	15.121	31.949	41.216	10.506	0.712	0.359

Tab. B-6: Granulometric results of gravity core LVR4s of Lago Villarrica. Particles were measured by laser diffraction with Malvern Mastersizer.

		Grain Size Statistics					Grain Size Parameters					
Sample	Depth (cm)	Mediane	Mean	Mode	Sorting	Skewness	Clay (%) 0.01 – 2 µm	fine silt (%) 2 - 6 µm	medium silt (%) 6 – 20 µm	coarse silt (%) 20 - 63 µm	fine sand (%) 63 - 125 µm	medium sand (%) 63 - 125 µm
LVR4s 85-86	86	7.1411	8.5944	9.072	1.8934	0.8834	12.446	30.367	47.243	9.788	0.156	0
LVR4s 86-87	87	6.1114	7.833	7.801	2.0163	0.8984	16.342	32.954	41.107	9.231	0.366	0
LVR4s 87-88	88	6.0163	7.2707	7.264	1.8649	0.9036	14.763	35.118	43.628	6.491	0	0
LVR4s 88-89	89	5.6392	7.3201	6.891	2.0049	0.9209	17.389	35.014	39.023	8.072	0.502	0
LVR4s 90-91	91	6.9677	8.9691	8.973	2.0435	0.8893	14.5	29.969	42.683	12.367	0.481	0
LVR4s 91-92	92	5.4718	6.9008	6.62	1.9454	0.9113	17.546	36.243	39.058	6.81	0.343	0
LVR4s 92-93	93	5.4451	7.2891	6.515	2.052	0.9299	18.691	34.959	36.928	8.63	0.777	0.015
LVR4s 93-94	94	6.244	8.2212	7.492	2.0302	0.9225	15.7	32.788	40.232	10.785	0.496	0
LVR4s 94-95	95	5.6169	7.2653	6.803	1.9987	0.926	17.304	35.256	39.451	7.931	0.059	0
LVR4s 95-96	96	6.1611	7.8476	7.775	1.9997	0.8957	16.111	32.858	41.338	8.506	0.356	0.256
LVR4s 96-97	97	6.088	8.3815	7.177	2.0985	0.9307	16.952	32.517	37.789	11.288	1.433	0.021
LVR4s 97-98	98	6.1235	7.8045	7.579	1.9836	0.9047	15.836	33.361	41.197	8.8	0.792	0.014
LVR4s 98-99	99	5.4439	6.8898	6.863	1.9762	0.9061	18.075	35.795	39.509	6.621	0	0
LVR4s 99-100	100	6.4644	8.3155	7.895	2.0051	0.909	15.073	32.052	41.929	10.751	0.194	0
LVR4s 100-101	101	6.1039	7.8851	7.378	1.9984	0.9147	15.934	33.396	40.633	9.485	0.552	0
LVR4s 101-102	102	5.4751	7.0087	6.669	1.9806	0.9117	17.988	35.667	38.616	7.307	0.423	0
LVR4s 102-103	103	5.9094	7.283	7.453	1.9302	0.8921	16.079	34.55	42.106	6.914	0.352	0
LVR4s 103-104	104	5.5411	7.3093	6.319	1.9993	0.9416	17.412	35.703	37.929	8.739	0.218	0
LVR4s 104-105	105	6.3121	8.202	7.597	2.0145	0.9135	15.605	32.442	40.95	10.407	0.596	0
LVR4s 105-106	106	5.5523	6.9784	7.066	1.9713	0.8974	17.778	35.327	39.978	6.621	0.295	0
LVR4s 106-107	107	7.2356	9.522	8.924	2.0709	0.9052	14.053	29.149	42.024	14.417	0.357	0

Tab. B-6: Granulometric results of gravity core LVR4s of Lago Villarrica. Particles were measured by laser diffraction with Malvern Mastersizer.

		Grain Size Statistics					Grain Size Parameters					
Sample	Depth (cm)	Mediane	Mean	Mode	Sorting	Skewness	Clay (%) 0.01 – 2 µm	fine silt (%) 2 - 6 µm	medium silt (%) 6 – 20 µm	coarse silt (%) 20 - 63 µm	fine sand (%) 63 - 125 µm	medium sand (%) 63 - 125 µm
LVR4s 107-108	108	6.7359	8.7077	8.094	2.007	0.9103	14.416	31.13	42.237	11.884	0.332	0
LVR4s 108-109	109	6.396	8.0014	8.047	1.9663	0.8928	15.094	32.365	43.044	9.16	0.337	0
LVR4s 109-110	110	6.7422	8.868	7.901	2.0234	0.9247	14.242	31.324	41.516	12.425	0.494	0
LVR4s 110-111	111	6.929	8.828	8.484	1.9904	0.9021	13.906	30.517	43.351	11.815	0.41	0
LVR4s 111-112	112	6.4087	8.0422	7.903	1.9599	0.8981	14.902	32.458	42.88	9.414	0.346	0
LVR4s 112-113	113	6.4249	8.3994	7.637	2.0168	0.9175	15.198	32.171	40.971	11.206	0.453	0
LVR4s 113-114	114	6.9746	8.6694	8.94	1.971	0.8833	13.856	30.266	44.716	10.848	0.313	0
LVR4s 114-115	115	9.521	21.2394	7.556	2.8723	1.1932	12.924	24.769	29.956	19.656	9.929	2.766

Tab. B-6: Granulometric results of gravity core LVR4s of Lago Villarrica. Particles were measured by laser diffraction with Malvern Mastersizer.

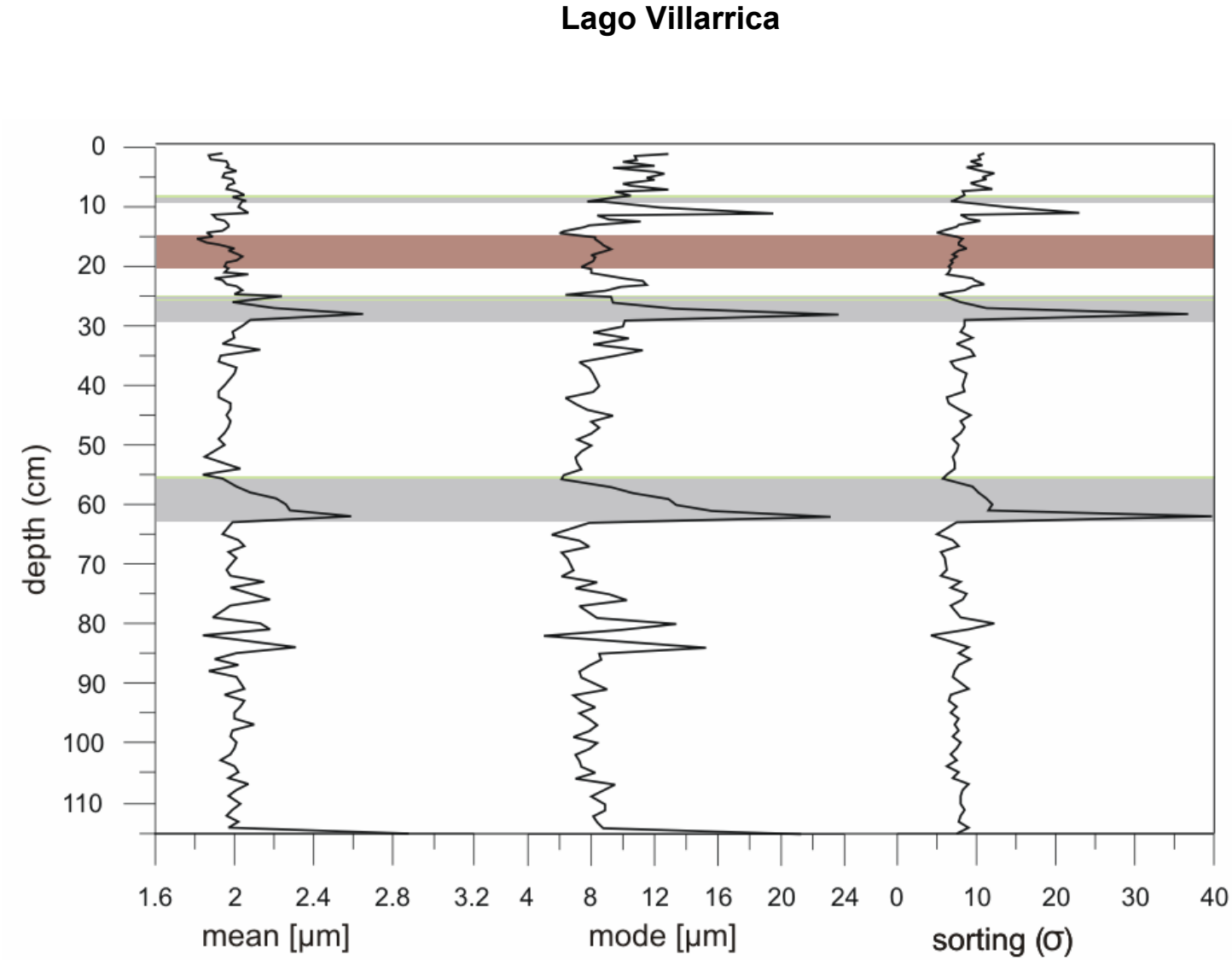

Fig. B-2: Mean and mode grain size (in µm) and sorting values (in standard deviation units) for short core LVR4s in full resolution. Shaded and coloured bands indicate lithology, presented in Fig. IV-32.

Water Content - Lago Calafquén

Sample	Depth (cm)	Water Content (%)	Sample	Depth (cm)	Water Content (%)
LCQ2s 0-1	0	0.9030	LCQ2s 90.8-91.5	90.8	0.6229
LCQ2s 1-2	1	0.9071	LCQ2s 92.5-92.6	92.5	0.7567
LCQ2s 2-3	2	0.8926	LCQ2s 95-96	95	0.9036
LCQ2s 3-4	3	0.9037	LCQ2s 98-99.5	98	0.9110
LCQ2s 4-5	4	0.9434	LCQ2s 100.5	100.5	0.9058
LCQ2s 5-6	5	0.9422	LCQ2s 101.5-102.5	101.5	0.9018
LCQ2s 6-7	6	0.9244	LCQ2s 104.5-105	104.5	0.7275
LCQ2s 7-8	7	0.8967	LCQ2s 105.1	105.1	0.6509
LCQ2s 8-9	8	0.8980	LCQ2s 109	109	0.9146
LCQ2s 13-14	13	0.8322	LCQ2s 111-112	111	0.8967
LCQ2s 18-18.5	18	0.7210	LCQ2s 115-116	115	0.9051
LCQ2s 18.5-18.6	18.5	0.6292	LCQ2s 119.5-121	119.5	0.8596
LCQ2s 18.6-18.8	18.6	0.6369	LCQ2s 124	124	0.8717
LCQ2s 19.5-20.5	19.5	0.8664	LCQ2s 125-126	125	0.9013
LCQ2s 20.5-21.5	20.5	0.7759	LCQ2s 127.5-128.5	127.5	0.7619
LCQ2s 22-23	22	0.8277	LCQ2s 128.5-130	128.5	0.5976
LCQ2s 28-29	28	0.8709	LCQ2s 130-130.2	130	0.6498
LCQ2s 31.2-31.5	31.2	0.7120	LCQ2s 130.7	130.7	0.7826
LCQ2s 31.5-32.5	31.5	0.7088	LCQ2s 130.8-132.7	130.8	0.6174
LCQ2s 36-37	35	0.8998	LCQ2s 132.8	132.8	0.8808
LCQ2s 40-41	40	0.8546	LCQ2s 134.1-134.5	134.1	0.7998
LCQ2s 46-46.5	46	0.7582	LCQ2s 134.5-136.1	134.5	0.6621
LCQ2s 46.5-47.5	46.5	0.5448	LCQ2s 138-138.5	138	0.7562
LCQ2s 49.5-49.6	49.5	0.7648	LCQ2s 138.5-139.5	138.5	0.6565
LCQ2s 53-54	53	0.8689	LCQ2s 140.2-140.7	140.2	0.7231
LCQ2s 58-58.7	58	0.5957	LCQ2s 141.6-142.6	141.6	0.6902
LCQ2s 62-63	62	0.8943	LCQ2s 143-143.5	143	0.8504
LCQ2s 67-68	67	0.8896	LCQ2s 146-147	146	0.8695
LCQ2s 72.5-73.5	72.5	0.8776	LCQ2s 148.8-150.3	148.8	0.8504
LCQ2s 76-76.5	76	0.6851	LCQ2s 151.3-152	151.3	0.5865
LCQ2s 76.5-77.5	76.5	0.6162	LCQ2s 151.5-152	151.5	0.5077
LCQ2s 79.5-80	79.5	0.8810	LCQ2s 155.5-156.5	155.5	0.8320
LCQ2s 80-80.7	80	0.8107	LCQ2s 159-160	159	0.8035
LCQ2s 86-87	86	0.8671	LCQ 2s160.5-161	160.5	0.6292
LCQ2s 89-90	89	0.8718	LCQ 2s162	162	0.9085

Tab. B-7: Water content of gravity core LCQ2s of Lago Calafquén.

Water Content - Lago Villarrica

Sample	Depth (cm)	Water Content (%)	Sample	Depth (cm)	Water Content (%)
LVR4s 2-3	2	0.9133	LVR4s 54-55	54	0.8944
LVR4s 3-4	3	0.9085	LVR4s 55.8-56.2	55.8	0.7747
LVR4s 4-5	4	0.9026	LVR4s 56.5-61.4	56.5	0.7514
LVR4s 5-6	5	0.9098	LVR4s 61.4-62	61.4	0.7266
LVR4s 6-7	6	0.8987	LVR4s 67-68	67	0.8960
LVR4s 7-8.8	7	0.9089	LVR4s 70-71	70	0.8847
LVR4s 9.4-9.8	9.4	0.6853	LVR4s 73-74	73	0.8887
LVR4s 9.8-10.5	9.8	0.6586	LVR4s 76-77	76	0.8959
LVR4s 12-13	12	0.9041	LVR4s 79-80	79	0.9048
LVR4s 14.7-15	14.7	0.8143	LVR4s 82.2-83	82.2	0.8692
LVR4s 17.5-18.5	17.5	0.8627	LVR4s 83-84	83	0.8531
LVR4s 18.5-19.5	18.5	0.8595	LVR4s 84.5-85.8	84.5	0.9132
LVR4s 25.5-25.7	25.5	0.7559	LVR4s 86-87	86	0.8963
LVR4s 25.7-26	25.7	0.7611	LVR4s 87-88.5	87	0.8935
LVR4s 26-26.5	26	0.7782	LVR4s 88.5-89.2	88.5	0.8925
LVR4s 26.5-28.2	26.5	0.7402	LVR4s 89.2-90	89.2	0.8786
LVR4s 28.2-28.8	28.2	0.8709	LVR4s 91-92	91	0.8949
LVR4s 30-31	30	0.9097	LVR4s 95-95.8	95	0.8622
LVR4s 32-33	32	0.8944	LVR4s 98-99	98	0.8887
LVR4s 34-35	34	0.8909	LVR4s 101.5-102.5	101.5	0.8819
LVR4s 39.2-39.6	39.2	0.8718	LVR4s 104-105	104	0.9128
LVR4s 39.6-40.4	39.6	0.8099	LVR4s 106-107	106	0.8973
LVR4s 42-43	42	0.8438	LVR4s 109-110	109	0.8894
LVR4s 45-46	45	0.8726	LVR4s 112-113	112	0.9065
LVR4s 48-49	48	0.8722	LVR4s 114-115	114	0.9262
LVR4s 51-52	51	0.8892	----	----	----

Tab. B-8: Water content of gravity core LVR4s of Lago Villarrica.

Magnetic Susceptibility - Lago Calafquén

Sample	Depth (cm)	Magn. Susc. (10^{-6} S.I.)	Sample	Depth (cm)	Magn. Susc. (10^{-6} S.I.)
LCQ2s 0-1	0	60.0	LCQ2s 74-75	74	62.5
LCQ2s 1-2	1	35.8	LCQ2s 75-76	75	57.6
LCQ2s 2-3	2	65.6	LCQ2s 76-77	76	101.6
LCQ2s 3-4	3	50.4	LCQ2s 77-78	77	215.0
LCQ2s 4-5	4	50.3	LCQ2s 78-79	78	543.2
LCQ2s 5-6	5	63.1	LCQ2s 79-80	79	182.3
LCQ2s 6-7	6	44.0	LCQ2s 80-81	80	87.4
LCQ2s 7-8	7	39.0	LCQ2s 81-82	81	74.6
LCQ2s 8-9	8	68.0	LCQ2s 82-83	82	109.8
LCQ2s 9-10	9	78.0	LCQ2s 83-84	83	72.1
LCQ2s 10-11	10	89.0	LCQ2s 84-85	84	61.4
LCQ2s 11-12	11	89.4	LCQ2s 85-86	85	120.6
LCQ2s 12-13	12	80.1	LCQ2s 86-87	86	54.8
LCQ2s 13-14	13	174.8	LCQ2s 87-88	87	62.7
LCQ2s 14-15	14	382.6	LCQ2s 88-89	88	78.5
LCQ2s 15-16	15	118.3	LCQ2s 89-90	89	72.1
LCQ2s 16-17	16	101.7	LCQ2s 90-91	90	54.7
LCQ2s 17-18	17	204.6	LCQ2s 91-92	91	135.4
LCQ2s 18-19	18	339.4	LCQ2s 92-93	92	112.3
LCQ2s 19-20	19	189.2	LCQ2s 93-94	93	237.2
LCQ2s 20-21	20	112.1	LCQ2s 94-95	94	515.2
LCQ2s 21-22	21	211.4	LCQ2s 95-96	95	205.1
LCQ2s 22-23	22	181.1	LCQ2s 96-97	96	69.8
LCQ2s 23-24	23	98.8	LCQ2s 97-98	97	57.6
LCQ2s 24-25	24	72.5	LCQ2s 98-99	98	74.5
LCQ2s 25-26	25	87.2	LCQ2s 99-100	99	81.3
LCQ2s 26-27	26	88.0	LCQ2s 100-101	100	90.2
LCQ2s 27-28	27	59.0	LCQ2s 101-102	101	64.5
LCQ2s 28-29	28	68.0	LCQ2s 102-103	102	57.2
LCQ2s 29-30	29	95.0	LCQ2s 103-104	103	77.9
LCQ2s 30-31	30	100.0	LCQ2s 104-105	104	78.5
LCQ2s 31-32	31	253.3	LCQ2s 105-106	105	96.2
LCQ2s 32-33	32	374.1	LCQ2s 106-107	106	90.7
LCQ2s 33-34	33	107.8	LCQ2s 107-108	107	102.6
LCQ2s 34-35	34	64.5	LCQ2s 108-109	108	304.4

Tab. B-9: Results of magnetic susceptibility analysis of gravity core LCQ2s of Lago Calafquén.

Sample	Depth (cm)	Magn. Susc. (10^{-6} S.I.)	Sample	Depth (cm)	Magn. Susc. (10^{-6} S.I.)
LCQ2s 109-110	109	80.3	LCQ2s 136-137	136	493.0
LCQ2s 110-111	110	59.1	LCQ2s 137-138	137	96.0
LCQ2s 111-112	111	52.5	LCQ2s 138-139	138	243.0
LCQ2s 112-113	112	42.2	LCQ2s 139-140	139	525.0
LCQ2s 113-114	113	117.8	LCQ2s 140-141	140	183.0
LCQ2s 114-115	114	75.6	LCQ2s 141-142	141	224.0
LCQ2s 115-116	115	68.3	LCQ2s 142-143	142	414.0
LCQ2s 116-117	116	78.8	LCQ2s 143-144	143	335.6
LCQ2s 117-118	117	74.6	LCQ2s 144-145	144	157.2
LCQ2s 118-119	118	63.4	LCQ2s 145-146	145	98.8
LCQ2s 119-120	119	67.3	LCQ2s 146-147	146	64.5
LCQ2s 120-121	120	88.1	LCQ2s 147-148	147	110.2
LCQ2s 121-122	121	154.6	LCQ2s 148-149	148	149.8
LCQ2s 122-123	122	157.3	LCQ2s 149-150	149	194.6
LCQ2s 123-124	123	124.1	LCQ2s 150-151	150	211.4
LCQ2s 124-125	124	90.8	LCQ2s 151-152	151	134.3
LCQ2s 125-126	125	202.5	LCQ2s 152-153	152	305.1
LCQ2s 126-127	126	196.2	LCQ2s 153-154	153	775.8
LCQ2s 127-128	127	192.0	LCQ2s 154-155	154	677.6
LCQ2s 128-129	128	444.0	LCQ2s 155-156	155	118.4
LCQ2s 129-130	129	393.0	LCQ2s 156-157	156	96.2
LCQ2s 130-131	130	291.0	LCQ2s 157-158	157	136.1
LCQ2s 131-132	131	434.0	LCQ2s 158-159	158	154.7
LCQ2s 132-133	132	512.0	LCQ2s 159-160	159	136.4
LCQ2s 133-134	133	126.0	LCQ2s 160-161	160	258.3
LCQ2s 134-135	134	278.0	LCQ2s 161-162	161	218.1
LCQ2s 135-136	135	631.0	LCQ2s 162	162	115.9

Tab. B-9: Results of magnetic susceptibility analysis of gravity core LCQ2s of Lago Calafquén.

Magnetic Susceptibility - Lago Villarrica

Sample	Depth (cm)	Magn. Susc. (10^{-6} S.I.)	Sample	Depth (cm)	Magn. Susc. (10^{-6} S.I.)
LVR4s 0-1	0	23.3	LVR4s 37-38	37	59.6
LVR4s 1-2	1	78.2	LVR4s 38-39	38	78.5
LVR4s 2-3	2	72.2	LVR4s 39-40	39	102.4
LVR4s 3-4	3	66.1	LVR4s 40-41	40	125.2
LVR4s 4-5	4	67.1	LVR4s 41-42	41	152.2
LVR4s 5-6	5	80.0	LVR4s 42-43	42	87.4
LVR4s 6-7	6	73.0	LVR4s 43-44	43	84.5
LVR4s 7-8	7	87.0	LVR4s 44-45	44	90.7
LVR4s 8-9	8	218.0	LVR4s 45-46	45	136.9
LVR4s 9-10	9	548.0	LVR4s 46-47	46	83.8
LVR4s 10-11	10	407.0	LVR4s 47-48	47	115.6
LVR4s 11-12	11	70.8	LVR4s 48-49	48	122.5
LVR4s 12-13	12	101.6	LVR4s 49-50	49	106.3
LVR4s 13-14	13	90.4	LVR4s 50-51	50	93.1
LVR4s 14-15	14	132.3	LVR4s 51-52	51	85.0
LVR4s 15-16	15	68.1	LVR4s 52-53	52	62.0
LVR4s 16-17	16	124.3	LVR4s 53-54	53	60.0
LVR4s 17-18	17	145.4	LVR4s 54-55	54	66.0
LVR4s 18-19	18	143.6	LVR4s 55-56	55	77.0
LVR4s 19-20	19	160.7	LVR4s 56-57	56	253.7
LVR4s 20-21	20	139.9	LVR4s 57-58	57	285.4
LVR4s 21-22	21	31.0	LVR4s 58-59	58	253.2
LVR4s 22-23	22	54.0	LVR4s 59-60	59	286.0
LVR4s 23-24	23	62.0	LVR4s 60-61	60	264.8
LVR4s 24-25	24	289.0	LVR4s 61-62	61	377.5
LVR4s 25-26	25	394.0	LVR4s 62-63	62	93.3
LVR4s 26-27	26	401.8	LVR4s 63-64	63	130.6
LVR4s 27-28	27	307.6	LVR4s 64-65	64	45.7
LVR4s 28-29	28	101.4	LVR4s 65-66	65	55.8
LVR4s 29-30	29	62.2	LVR4s 66-67	66	50.8
LVR4s 30-31	30	90.1	LVR4s 67-68	67	58.9
LVR4s 31-32	31	70.7	LVR4s 68-69	68	81.0
LVR4s 32-33	32	90.6	LVR4s 69-70	69	101.3
LVR4s 33-34	33	58.4	LVR4s 70-71	70	98.4
LVR4s 34-35	34	80.3	LVR4s 71-72	71	115.6

Tab. B-10: Results of magnetic susceptibility analysis of gravity core LVR4s of Lago Villarrica.

Sample	Depth (cm)	Magn. Susc. (10^{-6} S.I.)	Sample	Depth (cm)	Magn. Susc. (10^{-6} S.I.)
LVR4s 35-36	35	100.1	LVR4s 95-96	95	120.2
LVR4s 36-37	36	89.8	LVR4s 72-73	72	66.7
LVR4s 74-75	74	70.0	LVR4s 73-74	73	91.9
LVR4s 75-76	75	69.0	LVR4s 96-97	96	109.9
LVR4s 76-77	76	71.0	LVR4s 97-98	97	69.5
LVR4s 77-78	77	80.0	LVR4s 98-99	98	95.2
LVR4s 78-79	78	53.0	LVR4s 99-100	99	93.0
LVR4s 79-80	79	66.8	LVR4s 100-101	100	100.0
LVR4s 80-81	80	51.6	LVR4s 101-102	101	89.0
LVR4s 81-82	81	74.5	LVR4s 102-103	102	113.0
LVR4s 82-83	82	98.3	LVR4s 103-104	103	49.0
LVR4s 83-84	83	172.1	LVR4s 104-105	104	114.5
LVR4s 84-85	84	66.7	LVR4s 105-106	105	77.2
LVR4s 85-86	85	59.6	LVR4s 106-107	106	76.9
LVR4s 86-87	86	132.4	LVR4s 107-108	107	82.5
LVR4s 87-88	87	100.3	LVR4s 108-109	108	82.2
LVR4s 88-89	88	102.1	LVR4s 109-110	109	93.5
LVR4s 89-90	89	85.8	LVR4s 110-111	110	79.2
LVR4s 90-91	90	96.6	LVR4s 111-112	111	84.9
LVR4s 91-92	91	58.4	LVR4s 112-113	112	46.7
LVR4s 92-93	92	108.3	LVR4s 113-114	113	53.4
LVR4s 93-94	93	92.1	LVR4s 114-115	114	39.0
LVR4s 94-95	94	110.5	----	----	----

Tab. B-10: Results of magnetic susceptibility analysis of gravity core LVR4s of Lago Villarrica.

Carbon-Nitrogen Analysis - Lago Calafquén

Sample	Depth (cm)	C (%)	N (%)	Sample	Depth (cm)	C (%)	N (%)
LCQ2s 0-0.5	0	2.771	0.34	LCQ2s 24-25	24	1.622	0.215
LCQ2s 0.5-1	0.5	2.868	0.37	LCQ2s 25-26	25	1.619	0.224
LCQ2s 1-1.5	1	2.765	0.345	LCQ2s 26-27	26	1.652	0.23
LCQ2s 1.5-2	1.5	3.493	0.431	LCQ2s 27-28	27	1.701	0.245
LCQ2s 2-2.5	2	3.082	0.385	LCQ2s 28-29	28	1.461	0.201
LCQ2s 2.5-3	2.5	2.655	0.339	LCQ2s 29-30.5	29	1.351	0.205
LCQ2s 3-3.5	3	3.026	0.396	LCQ2s 30.5-31.8	30.5	0.722	0.083
LCQ2s 3.5-4	3.5	3.427	0.407	LCQ2s 31.8-32	31.8	0.925	0.097
LCQ2s 4-4.5	4	2.199	0.303	LCQ2s 32-32-5	32	0.786	0.101
LCQ2s 4.5-5	4.5	3.823	0.478	LCQ2s 32.5-33	32.5	1.066	0.156
LCQ2s 5-5.5	5	3.457	0.427	LCQ2s 33-34	33	1.246	0.192
LCQ2s 5.5-6	5.5	3.403	0.431	LCQ2s 34-35	34	1.783	0.267
LCQ2s 6-7	6	3.284	0.418	LCQ2s 35-36	35	1.752	0.263
LCQ2s 7-8	7	3.463	0.409	LCQ2s 36-37	36	2.043	0.287
LCQ2s 8-9	8	3.382	0.396	LCQ2s 37-38	37	1.802	0.266
LCQ2s 9-10	9	3.234	0.383	LCQ2s 38-39	38	1.687	0.239
LCQ2s 10-11	10	3.063	0.359	LCQ2s 39-39.5	39	1.544	0.218
LCQ2s 11-12	11	3.003	0.383	LCQ2s 39.5-40	39.5	1.66	0.239
LCQ2s 12-12.5	12	2.599	0.322	LCQ2s 40-41	40	1.463	0.2
LCQ2s 12.5-13	12.5	1.356	0.162	LCQ2s 41-42	41	1.597	0.218
LCQ2s 13-13.5	13	0.637	0.08	LCQ2s 42-43	42	1.693	0.251
LCQ2s 13.5-14	13.5	0.494	0.071	LCQ2s 43-44	43	1.373	0.201
LCQ2s 14-15	14	2.511	0.31	LCQ2s 44-45	44	1.51	0.221
LCQ2s 15-16	15	1.966	0.259	LCQ2s 45-46	45	1.597	0.231
LCQ2s 16-17	16	1.549	0.189	LCQ2s 46-46.4	46	0.986	0.141
LCQ2s 17-18	17	0.635	0.084	LCQ2s 46.4-47	46.4	0.404	0.048
LCQ2s 18-18.3	18	0.387	0.049	LCQ2s 47-47.7	47	0.453	0.049
LCQ2s 18.3-18.5	18.3	0.617	0.075	LCQ2s 47.7-48.3	47.7	1.085	0.184
LCQ2s 18.5-19	18.5	0.379	0.049	LCQ2s 48.3-49	48.3	1.096	0.18
LCQ2s 19-19.6	19	0.797	0.091	LCQ2s 49-50	49	1.643	0.221
LCQ2s 19.6-20.2	19.6	2.578	0.32	LCQ2s 50-51	50	1.976	0.262
LCQ2s 20.2-21.7	20.2	2.398	0.283	LCQ2s 51-52	51	2.012	0.267
LCQ2s 21.7-22.5	21.7	1.456	0.196	LCQ2s 52-53	52	1.856	0.24
LCQ2s 22.5-23.5	22.5	1.164	0.166	LCQ2s 53-54	53	1.877	0.238
LCQ2s 23.5-24	23.5	1.074	0.155	LCQ2s 54-55	54	1.994	0.251
LCQ2s 55-56	55	2.032	0.27	LCQ2s 87-88	87	2.025	0.274

Tab. B-11: Results of carbon-nitrogen (C-N) analysis of gravity core LCQ2s of Lago Calafquén; C-N content was measured chromatographically by EuroVector Elemental Analyzer.

Sample	Depth (cm)	C (%)	N (%)	Sample	Depth (cm)	C (%)	N (%)
LCQ2s 56-57	56	2.067	0.287	LCQ2s 88-89	88	1.595	0.203
LCQ2s 57-58.2	57	1.74	0.233	LCQ2s 89-90	89	1.474	0.191
LCQ2s 58.2-58.9	58.2	0.172	0.043	LCQ2s 90-90.66	90	1.074	0.144
LCQ2s 58.9-60	58.9	1.66	0.231	LCQ2s 90.6-90.7	90.6	0.622	0.078
LCQ2s 60-61	60	1.99	0.265	LCQ2s 90.7-90.9	90.7	0.44	0.053
LCQ2s 61-62	61	1.616	0.214	LCQ2s 90.9-92	90.9	0.72	0.091
LCQ2s 62-63	62	1.634	0.223	LCQ2s 92-93	92	1.541	0.209
LCQ2s 63-64	63	1.652	0.241	LCQ2s 93-94	93	1.789	0.235
LCQ2s 64-65	64	1.641	0.237	LCQ2s 94-95	94	1.728	0.221
LCQ2s 65-66	65	1.679	0.226	LCQ2s 95-96	95	1.665	0.223
LCQ2s 66-67	66	1.911	0.256	LCQ2s 96-97	96	1.423	0.195
LCQ2s 67-68	67	1.809	0.244	LCQ2s 97-98	97	1.85	0.247
LCQ2s 68-69	68	1.949	0.267	LCQ2s 98-99	98	1.999	0.248
LCQ2s 69-70	69	1.725	0.245	LCQ2s 99-100	99	2.089	0.278
LCQ2s 70-71	70	1.748	0.253	LCQ2s 100-101	100	1.427	0.219
LCQ2s 71-72	71	1.65	0.221	LCQ2s 101-102	101	1.35	0.2
LCQ2s 72-73	72	1.51	0.218	LCQ2s 102-103	102	1.731	0.239
LCQ2s 73-74	73	1.822	0.25	LCQ2s 103-104	103	1.467	0.211
LCQ2s 74-75	74	1.394	0.21	LCQ2s 104-105	104	3.312	0.464
LCQ2s 75-75.5	75	0.93	0.132	LCQ2s 105-105.2	105	0.474	0.085
LCQ2s 75.5-76	75.5	0.482	0.077	LCQ2s 105.2-105.3	105.2	0.342	0.052
LCQ2s 76-76.8	76	0.175	0.038	LCQ2s 105.3-106	105.3	2.037	0.286
LCQ2s 76.8-77.3	76.8	0.408	0.055	LCQ2s 106-107	106	1.814	0.238
LCQ2s 77.3-78	77.3	1.615	0.24	LCQ2s 107-108	107	2.109	0.283
LCQ2s 78-78.2	78	0.566	0.095	LCQ2s 108-109	108	2.089	0.278
LCQ2s 78.2-78.8	78.2	1.988	0.252	LCQ2s 109-110	109	1.676	0.225
LCQ2s 78.8-79.5	78.8	1.517	0.213	LCQ2s 110-110.5	110	1.595	0.206
LCQ2s 79.5-80	79.5	1.604	0.213	LCQ2s 1105-111	110.5	1.831	0.26
LCQ2s 80-80.2	80	1.344	0.181	LCQ2s 111-112	111	1.892	0.244
LCQ2s 80.2-80.4	80.2	1.383	0.193	LCQ2s 112-113	112	1.883	0.243
LCQ2s 80.4-81	80.4	1.737	0.246	LCQ2s 113-114	113	1.892	0.251
LCQ2s 81-82	81	1.702	0.237	LCQ2s 114-115	114	1.996	0.257
LCQ2s 82-83	82	1.643	0.216	LCQ2s 115-116	115	2.164	0.263
LCQ2s 83-84	83	2.69	0.25	LCQ2s 116-117	116	1.396	0.184
LCQ2s 84-85	84	2.04	0.264	LCQ2s 117-118	117	1.627	0.205
LCQ2s 85-86	85	1.664	0.242	LCQ2s 118-119	118	1.386	0.192
LCQ2s 86-87	86	1.696	0.238	LCQ2s 119-120	119	1.554	0.185
LCQ2s 120-121	120	1.604	0.223	LCQ2s 140.5-141	140.5	0.56	0.063

Tab. B-11: Results of carbon-nitrogen (C-N) analysis of gravity core LCQ2s of Lago Calafquén; C-N content was measured chromatographically with EuroVector Elemental Analyzer.

Sample	Depth (cm)	C (%)	N (%)	Sample	Depth (cm)	C (%)	N (%)
LCQ2s 121-122	121	1.684	0.223	LCQ2s 141-142	141	0.765	0.103
LCQ2s 122-123	122	1.21	0.174	LCQ2s 142-143	142	0.89	0.117
LCQ2s 123-124	123	1.733	0.241	LCQ2s 143-144	143	1.865	0.24
LCQ2s 124-125	124	1.876	0.231	LCQ2s 144-145	144	2.025	0.25
LCQ2s 125-126	125	1.879	0.242	LCQ2s 145-146	145	1.808	0.239
LCQ2s 126-128	126	1.286	0.158	LCQ2s 146-147	146	1.721	0.215
LCQ2s 128-129	128	0.349	0.043	LCQ2s 147-148.2	147	1.723	0.181
LCQ2s 129-130	129	0.348	0.045	LCQ2s 148.2-149.5	148.2	1.444	0.183
LCQ2s 130-131	130	1.059	0.085	LCQ2s 149.5-150	149.5	1.5	0.191
LCQ2s 131-132	131	1.32	0.11	LCQ2s 150-151	150	1.215	0.159
LCQ2s 132-132.6	132	0.993	0.114	LCQ2s 151-153	151	1.267	0.181
LCQ2s 132.6-133.5	132.6	1.417	0.186	LCQ2s 153-155	153	1.757	0.217
LCQ2s 133.5-134.5	133.5	0.609	0.062	LCQ2s 155-156	155	1.203	0.164
LCQ2s 134.5-135.5	134.5	0.986	0.092	LCQ2s 156-157	156	1.22	0.179
LCQ2s 135.5-136.5	135.5	1.559	0.197	LCQ2s 157-158	157	1.366	0.15
LCQ2s 136.5-137.5	136.5	0.958	0.121	LCQ2s 158-159	158	1.255	0.166
LCQ2s 137.5-138.6	137.5	0.55	0.074	LCQ2s 159-160	159	1.443	0.187
LCQ2s 138.6-138.7	138.6	0.532	0.062	LCQ2s 160-161	160	1.498	0.194
LCQ2s 138.7-139.7	138.7	1.167	0.166	LCQ2s 161-162	161	1.675	0.203
LCQ2s 139.7-140.5	139.7	0.386	0.044	----	----	----	----

Tab. B-11: Results of carbon-nitrogen (C-N) analysis of gravity core LCQ2s of Lago Calafquén; C-N content was measured chromatographically with EuroVector Elemental Analyzer.

Carbon-Nitrogen Analysis - Lago Villarrica

Sample	Depth (cm)	C (%)	N (%)	Sample	Depth (cm)	C (%)	N (%)
LVR4s 0-0.5	0	4.704	0.473	LVR4s 18.5-19	18.5	1.968	0.248
LVR4s 0.5-1	0.5	6.119	0.411	LVR4s 19-19.5	19	2.033	0.263
LVR4s 1-1.5	1	3.549	0.384	LVR4s 19.5-20	19.5	1.946	0.246
LVR4s 1.5-2	1.5	3.305	0.364	LVR4s 20-20.5	20	1.987	0.23
LVR4s 2-2.5	2	3.517	0.374	LVR4s 20.5-21	20.5	2.484	0.248
LVR4s 2.5-3	2.5	3.735	0.404	LVR4s 21-21.5	21	4.697	0.317
LVR4s 3-3.5	3	4.411	0.413	LVR4s 21.5-22	21.5	4.449	0.372
LVR4s 3.5-4	3.5	3.738	0.412	LVR4s 22-22.5	22	3.768	0.375
LVR4s 4-4.5	4	3.869	0.422	LVR4s 22.5-23.5	22.5	3.618	0.374
LVR4s 4.5-5	4.5	3.664	0.421	LVR4s 23.5-24	23.5	3.307	0.352
LVR4s 5-5.5	5	3.602	0.397	LVR4s 24-24.8	24	2.624	0.284
LVR4s 5.5-6	5.5	3.58	0.391	LVR4s 24.8-25.2	24.8	2.443	0.205
LVR4s 6-6.5	6	3.546	0.411	LVR4s 25.2-26	25.2	2.113	0.175
LVR4s 6.5-7	6.5	3.791	0.44	LVR4s 26-27	26	1.863	0.158
LVR4s 7-7.5	7	4.133	0.411	LVR4s 27-28	27	2.031	0.191
LVR4s 7.5-8	7.5	3.584	0.366	LVR4s 28-29	28	3.483	0.38
LVR4s 8-8.5	8	3.186	0.356	LVR4s 29-30	29	3.288	0.385
LVR4s 8.5-9	8.5	2.243	0.221	LVR4s 30-31	30	2.63	0.299
LVR4s 9-9.2	9	1.041	0.097	LVR4s 31-32	31	3.385	0.38
LVR4s 9.2-10	9.2	0.884	0.09	LVR4s 32-33	32	2.565	0.309
LVR4s 10-11	10	1.045	0.112	LVR4s 33-34	33	3.145	0.361
LVR4s 11-11.5	11	2.78	0.265	LVR4s 34-35	34	2.56	0.337
LVR4s 11.5-12	11.5	2.379	0.262	LVR4s 35-36	35	2.474	0.269
LVR4s 12-12.5	12	2.498	0.291	LVR4s 36-37	36	2.136	0.26
LVR4s 12.5-13	12.5	2.736	0.301	LVR4s 37-38	37	2.256	0.237
LVR4s 13-13.5	13	2.71	0.316	LVR4s 38-39	38	1.813	0.205
LVR4s 13.5-14	13.5	2.754	0.323	LVR4s 39-40	39	1.59	0.168
LVR4s 14-14.5	14	1.48	0.189	LVR4s 40-41	40	1.909	0.204
LVR4s 14.5-15	14.5	1.477	0.187	LVR4s 41-42	41	1.608	0.161
LVR4s 15-15.5	15	1.134	0.15	LVR4s 42-43	42	1.739	0.178
LVR4s 15.5-16	15.5	1.226	0.171	LVR4s 43-44	43	2.428	0.233
LVR4s 16-16.5	16	1.78	0.201	LVR4s 44-45	44	2.18	0.222
LVR4s 16.5-17	16.5	1.696	0.215	LVR4s 45-46	45	1.829	0.178
LVR4s 17-17.5	17	1.811	0.218	LVR4s 46-47	46	1.86	0.255
LVR4s 17.5-18	17.5	1.83	0.228	LVR4s 47-48	47	1.613	0.202
LVR4s 18-18.5	18	1.887	0.235	LVR4s 48-49	48	1.745	0.218

Tab. B-12: Results of carbon-nitrogen (C-N) analysis of gravity core LVR4s of Lago Villarrica; C-N content was measured chromatographically with EuroVector Elemental Analyzer.

Sample	Depth (cm)	C (%)	N (%)	Sample	Depth (cm)	C (%)	N (%)
LVR4s 49-50	49	1.825	0.246	LVR4s 82-83	83	2.106	0.265
LVR4s 50-51	50	2.14	0.279	LVR4s 83-84	84	2.296	0.271
LVR4s 51-52	51	2.15	0.275	LVR4s 84-85	85	1.718	0.212
LVR4s 51-52	52	1.933	0.257	LVR4s 85-86	86	1.824	0.228
LVR4s 52-53	53	2.22	0.281	LVR4s 86-87	87	1.631	0.21
LVR4s 53-54	54	2.189	0.288	LVR4s 87-88	88	1.876	0.237
LVR4s 54-55	55	1.941	0.247	LVR4s 88-89	89	1.66	0.217
LVR4s 55-57	57	3.355	0.262	LVR4s 89-90	90	1.974	0.266
LVR4s 57-58	58	2.324	0.188	LVR4s 90-91	91	1.804	0.252
LVR4s 58-59	59	2.236	0.182	LVR4s 91-92	92	1.728	0.229
LVR4s 59-60	60	2.013	0.169	LVR4s 92-93	93	1.644	0.222
LVR4s 60-61	61	1.407	0.149	LVR4s 93-94	94	1.142	0.16
LVR4s 61-62	62	1.67	0.215	LVR4s 94-95	95	1.351	0.192
LVR4s 62-63	63	1.402	0.199	LVR4s 95-96	96	1.615	0.229
LVR4s 63-64	64	1.851	0.273	LVR4s 97-98	97	1.639	0.226
LVR4s 64-65	65	1.792	0.271	LVR4s 98-99	98	1.631	0.215
LVR4s 65-66	66	1.834	0.265	LVR4s 99-100	99	1.826	0.245
LVR4s 66-67	67	1.859	0.264	LVR4s 100-101	100	1.682	0.237
LVR4s 67-68	68	1.83	0.266	LVR4s 101-102	101	1.582	0.225
LVR4s 68-69	69	1.801	0.272	LVR4s 102-103	102	1.973	0.276
LVR4s 69-70	70	1.354	0.217	LVR4s 103-104	103	1.787	0.209
LVR4s 70-71	71	1.685	0.261	LVR4s 104-105	104	1.974	0.23
LVR4s 71-72	72	1.727	0.256	LVR4s 105-106	105	1.665	0.205
LVR4s 72-73	73	1.929	0.286	LVR4s 106-107	106	1.924	0.234
LVR4s 73-74	74	1.853	0.257	LVR4s 107-108	107	1.867	0.238
LVR4s 74-75	75	1.881	0.25	LVR4s 108-109	108	1.527	0.208
LVR4s 75-76	76	1.92	0.293	LVR4s 109-110	109	1.493	0.217
LVR4s 76-77	77	2.206	0.318	LVR4s 110-111	110	1.671	0.23
LVR4s 77-78	78	2.254	0.301	LVR4s 111-112	111	2.016	0.264
LVR4s 78-79	79	2.041	0.283	LVR4s 112-113	112	2.034	0.271
LVR4s 79-80	80	1.994	0.281	LVR4s 113-114	113	1.923	0.255
LVR4s 80-81	81	1.541	0.22	LVR4s 114-115	114	1.686	0.228
LVR4s 81-82	82	0.898	0.125	----	----	----	----

Tab. B-12: Results of carbon-nitrogen (C-N) analysis of gravity core LVR4s of Lago Villarrica; C-N content was measured chromatographically with EuroVector Elemental Analyzer.

Biogenic Silica - Lago Calafquén

Sample	Depth (cm)	Biogenic Silica (%)	Sample	Depth (cm)	Biogenic Silica (%)
LCQ2s 0-0.5	0	31.8664556	LCQ2s 24-25	24	51.0074367
LCQ2s 0.5-1	0.5	37.7002338	LCQ2s 25-26	25	42.7973716
LCQ2s 1-1.5	1	28.4889089	LCQ2s 26-27	26	53.5141878
LCQ2s 1.5-2	1.5	36.8266679	LCQ2s 27-28	27	53.6003963
LCQ2s 2-2.5	2	45.1207927	LCQ2s 28-29	28	51.8021901
LCQ2s 2.5-3	2.5	49.6339005	LCQ2s 29-32	29	45.290516
LCQ2s 3-3.5	3	37.7718112	LCQ2s 32-32.5	32	39.8995719
LCQ2s 3.5-4	3.5	35.9716043	LCQ2s 32.5-33	32.5	36.9371093
LCQ2s 4-4.5	4	41.7639205	LCQ2s 33-34	33	75.470861
LCQ2s 4.5-5	4.5	38.3556904	LCQ2s 34-35	34	52.658557
LCQ2s 5-5.5	5	36.6026517	LCQ2s 35-36	35	64.1088543
LCQ2s 5.5-6	5.5	32.9588345	LCQ2s 36-37	36	58.0672127
LCQ2s 6-7	6	34.1111838	LCQ2s 37-38	37	64.6251284
LCQ2s 7-8	7	23.013208	LCQ2s 38-39	38	64.6405712
LCQ2s 8-9	8	22.6280867	LCQ2s 39-39.5	39	54.4113131
LCQ2s 9-10	9	24.3620477	LCQ2s 39.5-40	39.5	44.1931119
LCQ2s 10-11	10	23.8267237	LCQ2s 40-41	40	36.8443433
LCQ2s 11-12	11	27.0295553	LCQ2s 41-42	41	39.0002806
LCQ2s 12-12.5	12	19.3190444	LCQ2s 42-43	42	43.9425488
LCQ2s 12.5-13	12.5	6.52111735	LCQ2s 43-44	43	33.4175112
LCQ2s 15-16	15	21.6961616	LCQ2s 44-45	44	55.745706
LCQ2s 16-17	16	29.9013702	LCQ2s 45-46	45	61.0920566
LCQ2s 17-18	17	21.1822303	LCQ2s 46-47	46	12.6164057
LCQ2s 18-18.3	18	4.14497168	LCQ2s 47-47.7	47	12.1751233
LCQ2s 18.3-18.5	18.3	2.88904246	LCQ2s 47.7-48.3	47.7	41.0617107
LCQ2s 18.5-19	18.5	4.032175	LCQ2s 48.3-49	48.3	41.1258351
LCQ2s 19-19.6	19	3.48435892	LCQ2s 49-50	49	39.5820923
LCQ2s 19.3-19.8	19.3	6.18179857	LCQ2s 50-51	50	62.0963036
LCQ2s 19.8-20.2	19.8	30.2317486	LCQ2s 51-52	51	47.3699672
LCQ2s 20.2-21.7	20.2	19.0962386	LCQ2s 52-53	52	46.3186595
LCQ2s 21.7-22.5	21.7	35.5209813	LCQ2s 53-54	53	50.9130925
LCQ2s 22.5-23.5	22.5	35.3567759	LCQ2s 54-55	54	51.1578281
LCQ2s 23.5-24	23.5	34.4471672	LCQ2s 55-56	55	51.1986646
LCQ2s 56-57	56	49.4624883	LCQ2s 89-90	89	38.6504949
LCQ2s 57-58.2	57	28.6021758	LCQ2s 90-92	90	27.9629141

Tab. B-13: Results of biogenic silica (BSi) analysis of gravity core LCQ2s of Lago Calafquén; BSi content was measured by ICP-OES analysis.

Sample	Depth (cm)	Biogenic Silica (%)	Sample	Depth (cm)	Biogenic Silica (%)
LCQ2s 58.2-58.9	58.2	15.7547492	LCQ2s 92-93	92	32.0439333
LCQ2s 58.9-60	58.9	50.9019491	LCQ2s 93-94	93	32.1369004
LCQ2s 60-61	60	39.262622	LCQ2s 94-95	94	32.5107626
LCQ2s 61-62	61	47.7941529	LCQ2s 95-96	95	32.4144464
LCQ2s 62-63	62	51.0440639	LCQ2s 96-97	96	27.5502456
LCQ2s 63-64	63	44.2035814	LCQ2s 97-98	97	36.093508
LCQ2s 64-65	64	40.2470555	LCQ2s 98-99	98	30.2198576
LCQ2s 65-66	65	56.9050081	LCQ2s 99-100	99	31.9848253
LCQ2s 66-67	66	59.8416833	LCQ2s 100-101	100	28.7211251
LCQ2s 67-68	67	53.9100724	LCQ2s 101-102	101	26.696797
LCQ2s 68-69	68	58.0304878	LCQ2s 102-103	102	25.2210868
LCQ2s 69-70	69	58.0589255	LCQ2s 103-104	103	26.3137789
LCQ2s 70-71	70	59.006137	LCQ2s 104-105	104	24.9708319
LCQ2s 71-72	71	56.9441055	LCQ2s 105-106	105	2.64358547
LCQ2s 72-73	72	51.116632	LCQ2s 106-107	106	33.0032367
LCQ2s 73-74	73	51.2444173	LCQ2s 107-108	107	31.2256518
LCQ2s 74-75	74	71.6987414	LCQ2s 108-109	108	39.0137985
LCQ2s 75-75.5	75	28.5847787	LCQ2s 109-110	109	29.1684518
LCQ2s 75.5-76	75.5	7.90011996	LCQ2s 110-110.5	110	28.8028657
LCQ2s 77.3-78	77.3	48.1751144	LCQ2s 110.5-111	110.5	30.6316072
LCQ2s 78-78.5	78	26.4976982	LCQ2s 111-112	111	30.3323007
LCQ2s 78.5-78.8	78.5	62.9319153	LCQ2s 112-113	112	26.1228281
LCQ2s 78.8-79.5	78.8	48.2603915	LCQ2s 113-114	113	32.4874004
LCQ2s 79.5-80	79.5	29.6024486	LCQ2s 114-115	114	28.2120669
LCQ2s 80-80.2	80	32.503162	LCQ2s 115-116	115	27.9892638
LCQ2s 80.2-80.4	80.2	49.8079373	LCQ2s 116-117	116	18.1337856
LCQ2s 80.4-81	80.4	43.5821418	LCQ2s 117-118	117	23.9916203
LCQ2s 81-82	81	57.0680003	LCQ2s 118-119	118	16.51182
LCQ2s 82-83	82	42.8517218	LCQ2s 119-120	119	7.88085589
LCQ2s 83-84	83	66.4731499	LCQ2s 120-121	120	23.5464136
LCQ2s 84-85	84	53.5156661	LCQ2s 121-122	121	17.0867098
LCQ2s 85-86	85	53.8206912	LCQ2s 122-123	122	18.3476036
LCQ2s 86-87	86	50.3001524	LCQ2s 123-124	123	27.5219593
LCQ2s 87-88	87	37.3612139	LCQ2s 124-125	124	22.6978259
LCQ2s 88-89	88	38.1355038	LCQ2s 125-126	125	14.8073807
LCQ2s 126-128	126	18.0523393	LCQ2s 150-151	150	26.6236109
LCQ2s 132.6-133.5	132.6	22.0679495	LCQ2s 153-154	153	36.5950992

Tab. B-13: Results of biogenic silica (BSi) analysis of gravity core LCQ2s of Lago Calafquén; BSi content was measured by ICP-OES analysis.

Sample	Depth (cm)	Biogenic Silica (%)	Sample	Depth (cm)	Biogenic Silica (%)
LCQ2s 135.5-136.5	135.5	21.3106672	LCQ2s 154-155	154	40.0736778
LCQ2s 138.7-139.7	138.7	16.6853382	LCQ2s 155-156	155	45.0937998
LCQ2s 139.7-140.5	139.7	6.59429939	LCQ2s 156-157	156	21.8613353
LCQ2s 142-143	142	10.2977971	LCQ2s 157-158	157	38.03301
LCQ2s 143-144	143	23.2012992	LCQ2s 158-159	158	21.7134037
LCQ2s 144-145	144	23.8698328	LCQ2s 159-160	159	25.0433155
LCQ2s 145-146	145	15.0931823	LCQ2s 159.2-160	159.2	3.17070535
LCQ2s 146-147	146	23.1668537	LCQ2s 160-161	160	24.9792994
LCQ2s 148.2-149.5	148.2	19.6281278	LCQ2s 161-162	161	76.8447123
LCQ2s 149.5-150	149.5	20.6518996	----	----	----

Tab. B-13: Results of biogenic silica (BSi) analysis of gravity core LCQ2s of Lago Calafquén; BSi content was measured by ICP-OES analysis.

Biogenic Silica - Lago Villarrica

Sample	Depth (cm)	Biogenic Silica (%)	Sample	Depth (cm)	Biogenic Silica (%)
Lvr4s 0-0.5	0	33.0575226	Lvr4s 9.2-10	9.2	1.53042968
Lvr4s 0.5-1	0.5	31.8177164	Lvr4s 10-11	10	2.95166272
Lvr4s 1-1.5	1	29.2046417	Lvr4s 11-11.5	11	37.9684755
Lvr4s 1.5-2	1.5	24.5085048	Lvr4s 11.5-12	11.5	29.5546675
Lvr4s 2-2.5	2	25.9491421	Lvr4s 12-12.5	12	29.6983721
Lvr4s 2.5-3	2.5	30.6394035	Lvr4s 13-13.5	13	33.0947977
Lvr4s 3-3.5	3	25.1977944	Lvr4s 13.5-14	13.5	30.5781537
Lvr4s 3.5-4	3.5	27.9725825	Lvr4s 14-14.5	14	25.5156131
Lvr4s 4-4.5	4	28.0223213	Lvr4s 14.5-15	14.5	33.4472689
Lvr4s 4.5-5	4.5	27.1896843	Lvr4s 15-15.5	15	33.6608234
Lvr4s 5-5.5	5	29.2541626	Lvr4s 15.5-16	15.5	19.2032856
Lvr4s 5.5-6	5.5	29.9620679	Lvr4s 16-16.5	16	41.4863836
Lvr4s 6-6.5	6	29.2397466	Lvr4s 16.5-17	16.5	31.005466
Lvr4s 6.5-7	6.5	30.7329656	Lvr4s 17-17.5	17	36.3099564
Lvr4s 7-7.5	7	28.0636703	Lvr4s 17.5-18	17.5	26.8498094
Lvr4s 7.5-8	7.5	26.0086667	Lvr4s 18-18.5	18	26.8355025
Lvr4s 8-8.5	8	26.6182687	Lvr4s 18.5-19	18.5	25.7590179
Lvr4s 8.5-9	8.5	10.0405042	Lvr4s 19-19.5	19	26.7909698
Lvr4s 9-9.2	9	2.7919304	Lvr4s 19.5-20	19.5	24.9604738
Lvr4s 20-20.5	20	23.3881065	Lvr4s 54-55	54	25.9280399

Tab. B-14: Results of biogenic silica (BSi) analysis of gravity core LVR4s of Lago Villarrica; BSi content was measured by ICP-OES analysis.

Sample	Depth (cm)	Biogenic Silica (%)	Sample	Depth (cm)	Biogenic Silica (%)
Lvr4s 20.5-21	20.5	24.9667757	Lvr4s 56-57	56	7.27533044
Lvr4s 21-21.5	21	24.5938792	Lvr4s 57-58	57	5.81575002
Lvr4s 21.5-22	21.5	29.0035481	Lvr4s 58-59	58	3.55332234
Lvr4s 22-22.5	22	27.9991422	Lvr4s 59-60	59	4.23114514
Lvr4s 22.5-23	22.5	31.5480373	Lvr4s 60-61	60	4.63177042
Lvr4s 23-23.5	23	27.0894618	Lvr4s 61-62	61	4.85583987
Lvr4s 23.5-24	23.5	25.5657632	Lvr4s 62-63	62	31.6170627
Lvr4s 24-24.8	24	11.3340035	Lvr4s 64-65	63	31.5491569
Lvr4s 24.8-25.2	24.8	0.65658324	Lvr4s 65-66	65	40.1648717
Lvr4s 25.2-26	25.2	6.09117101	Lvr4s 66-67	66	39.0042532
Lvr4s 26-27	26	5.55361452	Lvr4s 67-68	67	34.1479951
Lvr4s 27-28	27	5.90310642	Lvr4s 68-69	68	33.3796128
Lvr4s 28-29	28	31.3702813	Lvr4s 70-71	70	28.8443926
Lvr4s 29-30	29	36.6258191	Lvr4s 71-72	71	35.1591744
Lvr4s 30-31	30	31.7121337	Lvr4s 72-73	72	36.219493
Lvr4s 32-33	32	28.2444043	Lvr4s 73-74	73	31.8096006
Lvr4s 33-34	33	41.0722593	Lvr4s 74-75	74	37.4814505
Lvr4s 34-35	34	40.2231177	Lvr4s 75-76	75	41.5894731
Lvr4s 35-36	35	26.8680273	Lvr4s 76-77	76	40.7179067
Lvr4s 36-37	36	27.7551512	Lvr4s 77-78	77	39.8160315
Lvr4s 37-38	37	38.6174445	Lvr4s 78-79	78	35.588583
Lvr4s 39-40	39	26.7447104	Lvr4s 79-80	79	39.8007554
Lvr4s 40-41	40	23.050049	Lvr4s 80-81	80	37.666836
Lvr4s 41-42	41	22.2627318	Lvr4s 81-82	81	28.3345705
Lvr4s 42-43	42	24.1765705	Lvr4s 82-83	82	28.6491419
Lvr4s 43-44	43	32.8981644	Lvr4s 83-84	83	28.2253414
Lvr4s 44-45	44	25.8910306	Lvr4s 84-85	84	44.2230717
Lvr4s 45-46	45	25.1044035	Lvr4s 85-86	85	25.9754151
Lvr4s 46-47	46	28.7651125	Lvr4s 86-87	86	33.4713139
Lvr4s 47-48	47	24.0110448	Lvr4s 87-88	87	33.1195802
Lvr4s 48-49	48	23.5308974	Lvr4s 88-89	88	30.4838823
Lvr4s 49-50	49	29.5957934	Lvr4s 90-91	90	44.3570022
Lvr4s 50-51	50	20.2335159	Lvr4s 91-92	91	34.9692602
Lvr4s 51-52	51	28.0668101	Lvr4s 92-93	92	34.7754196
Lvr4s 52-53	52	30.7573592	Lvr4s 93-94	93	31.210869
Lvr4s 53-54	53	31.1642886	Lvr4s 94-95	94	21.7337018
Lvr4s 55-55.5	55	21.0659676	Lvr4s 95-96	95	18.4379787

Tab. B-14: Results of biogenic silica (BSi) analysis of gravity core LVR4s of Lago Villarrica; BSi content was measured by ICP-OES analysis.

Sample	Depth (cm)	Biogenic Silica (%)	Sample	Depth (cm)	Biogenic Silica (%)
Lvr4s 96-97	96	34.1356271	Lvr4s 106-107	106	37.8240948
Lvr4s 97-98	97	36.9811878	Lvr4s 107-108	107	37.7242219
Lvr4s 98-99	98	28.7193097	Lvr4s 108-109	108	32.2306437
Lvr4s 99-100	99	42.0180518	Lvr4s 109-110	109	35.0487509
Lvr4s 100-101	100	33.5492797	Lvr4s 110-111	110	38.5408398
Lvr4s 101-102	101	32.5790361	Lvr4s 111-112	111	35.2077587
Lvr4s 102-103	102	37.223092	Lvr4s 112-113	112	45.1629011
Lvr4s 103-104	103	32.9326608	Lvr4s 113-114	113	43.1964768
Lvr4s 104-105	104	40.1285884	Lvr4s 114-115	114	33.7627756
Lvr4s 105-106	105	32.0804326	----	----	----

Tab. B-14: Results of biogenic silica (BSi) analysis of gravity core LVR4s of Lago Villarrica; BSi content was measured by ICP-OES analysis.

AAS Analysis - Lago Calafquén

Sample	Depth (cm)	Cd (ppm)	Cr (ppm)	Cu (ppm)	Fe (ppm)	Mn (ppm)	Ni (ppm)	Pb (ppm)	Zn (ppm)	Ca (ppm)
LCQ2s 0-1	0	0.170	11.06	57.95	37846	1601.2	9.40	8.80	22	8023
LCQ2s 1-2	1	0.100	12.29	69.09	36711	1618.5	8.25	6.70	46	7789
LCQ2s 2-3	2	0.090	10.39	63.03	33059	1364.4	11.03	6.79	35	7667
LCQ2s 3-4	3	0.090	12.13	53.04	24929	1041.0	9.09	6.18	29	6010
LCQ2s 4-5	4	0.090	10.19	53.15	46771	2158.3	7.96	7.07	28	6466
LCQ2s 5-6	5	0.100	12.47	55.00	35601	1654.5	6.61	6.63	30	6319
LCQ2s 6-7	6	0.110	8.76	51.73	45054	2229.6	7.81	5.41	35	5582
LCQ2s 7-8	7	0.090	12.08	63.95	34019	1479.8	7.73	5.81	43	6516
LCQ2s 8-9	8	0.090	13.03	66.46	39212	1517.1	8.82	5.37	39	7586
LCQ2s 13-14	13	0.050	26.26	131.21	34395	839.0	18.22	5.90	50	18491
LCQ2s 14.5-15	14.5	0.030	20.53	62.25	19013	300.3	20.07	1.95	18	12620
LCQ2s 15.5-17	16	0.098	15.6	88.1	29802	1213	11.8	7.11	38.5	9760
LCQ2s 24.5-26	25	0.054	11.1	52.7	17412	728	6.6	3.23	23.0	7680
LCQ2s 26-28	27	0.057	8.6	54.5	18594	688	5.6	3.63	23.4	8000
LCQ2s 28-29	28.5	0.05	11.96	44.77	22123	618.4	6.77	2.75	18	7030
LCQ2s 30-31	30	0.081	10.7	67.9	16782	597	8.0	3.21	25.2	9447
LCQ2s 31.2-31.5	31.2	0.03	31.06	125.17	23947	397.9	19.29	3.08	30	20155
LCQ2s 31.5-32.5	31.5	0.01	35.53	92.23	19308	242.1	28.62	1.77	19	14555
LCQ2s 32.5-34	32.5	0.031	13.4	72.3	17201	346	18.7	1.95	23.7	12206
LCQ2s 34-36	35.0	0.01	14.66	45.24	10802	175.2	13.95	2.46	20	7495
LCQ2s 37.5-40	38.5	0.075	11.2	59.2	18967	939	9.9	3.29	27.3	8361
LCQ2s 41.5-42.5	42	0.058	17.3	72.7	20029	607	11.1	3.45	28.8	10670

Tab. B-15: Results of geochemical analysis (Cd to Ca) of gravity core LCQ2s of Lago Calafquén; Elements were measured by atom adsorption spectrometry (AAS).

Sample	Depth (cm)	Cd (ppm)	Cr (ppm)	Cu (ppm)	Fe (ppm)	Mn (ppm)	Ni (ppm)	Pb (ppm)	Zn (ppm)	Ca (ppm)
LCQ2s 42.5-44.5	43.5	0.065	13.1	70.6	19417	658	12.5	3.08	28.2	10236
LCQ2s 45-45.1	45	0.059	18.6	81.5	20924	651	14.5	3.44	28.0	10936
LCQ2s 45-46	45.5	0.04	11.69	64.13	14903	313.5	4.19	2.39	21	7601
LCQ2s 46.5-47.5	47.0	0.01	15.44	78.55	18992	252.5	20.69	1.75	20	12336
LCQ2s 47.5-48.5	48.0	0.03	10.45	61.12	14821	279.0	5.38	2.26	22	8874
LCQ2s 48.5-48.7	48.5	0.028	12.7	58.4	15041	244	12.3	2.31	23.6	11193
LCQ2s 48.7-48.9	48.7	0.040	9.7	52.7	13624	335	5.3	3.06	21.4	8825
LCQ2s 49.5-49.6	49.5	0.031	5.3	21.1	10336	175	2.7	1.88	13.3	7701
LCQ2s 49.6-51.8	50.5	0.058	10.4	39.6	17401	554	6.0	2.53	20.6	7478
LCQ2s 53-55.8	54	0.076	11.6	57.8	17844	713	8.4	3.20	29.2	7794
LCQ2s 55.8-58	57	0.102	9.4	53.7	19658	817	7.7	3.08	28.1	7451
LCQ2s 58.7-60	59	0.089	11.4	62.6	18139	593	11.9	3.02	30.3	8208
LCQ2s 60-62	61	0.070	10.9	49.3	18012	733	11.0	2.77	24.4	6694
LCQ2s 63-65	64	0.073	12.6	71.1	22496	835	9.1	4.35	34.7	9477
LCQ2s 65-67	66	0.102	17.5	70.2	29279	1111	11.3	3.75	33.9	9604
LCQ2s 67.68	67.0	0.07	10.20	61.93	16940	734.1	5.09	0.02	22	7481
LCQ2s 68-69.5	68	0.079	15.0	58.4	19996	817	10.3	3.21	25.5	8292
LCQ2s 69.5-71.9	70	0.076	8.7	51.6	19202	836	8.0	2.99	27.0	7546
LCQ2s 73.5-74.5	73.5	0.070	11.7	45.7	16486	788	10.9	3.37	26.0	6105
LCQ2s 76-76.5	76.0	0.06	16.11	198.93	26082	606.9	11.69	5.84	51	15740
LCQ2s 76.5-77.5	77.0	0.05	14.15	132.39	19033	340.1	10.67	3.77	36	11939
LCQ2s 77.5-79.5	78.0	0.06	11.09	69.89	14943	601.0	2.78	3.14	29	8084
LCQ2s 80-80.7	80	0.074	9.4	103.4	24232	721	11.9	7.12	38.1	12548
LCQ2s 80.7-82.5	80.7	0.073	4.4	57.9	21192	794	6.2	4.19	26.9	6915

Tab. B-15: Results of geochemical analysis (Cd to Ca) of gravity core LCQ2s of Lago Calafquén; Elements were measured by atom adsorption spectrometry (AAS).

Sample	Depth (cm)	Cd (ppm)	Cr (ppm)	Cu (ppm)	Fe (ppm)	Mn (ppm)	Ni (ppm)	Pb (ppm)	Zn (ppm)	Ca (ppm)
LCQ2s 82.5-84	82.5	0.077	7.7	57.5	19306	735	7.7	4.60	29.5	6708
LCQ2s 84-85.5	84	0.084	10.0	49.0	23909	1107	7.1	3.70	26.3	6072
LCQ2s 86-87	86.0	0.08	10.32	61.18	16330	712.5	3.98	4.06	33	7102
LCQ2s 87-89	88	0.109	8.5	76.8	24030	1013	8.5	5.77	37.6	9491
LCQ2s 90-90.8	90	0.119	10.6	122.4	22815	564	11.9	5.55	37.3	15767
LCQ2s 90.8-91.5	90.8	0.039	12.6	118.8	22856	485	16.5	3.84	32.8	14795
LCQ2s 96-98	97	0.081	5.6	66.2	25191	1088	8.6	3.92	29.5	7863
LCQ2s 98-99.5	98	0.113	5.0	49.9	25340	1357	7.3	3.73	26.9	5833
LCQ2s 99.5-100.5	99.5	0.083	4.3	56.3	22882	1096	8.5	4.80	31.4	7632
LCQ2s 100.5-101.5	101	0.088	8.3	77.3	23524	1062	11.4	4.17	32.8	9418
LCQ2s 102.5-104.5	103.5	0.097	6.9	94.5	24885	837	12.7	4.04	30.9	11316
LCQ2s 104.5-105	104.5	0.058	17.2	136.0	23284	582	21.6	4.54	32.8	18049
LCQ2s 105-106	105	0.054	11.8	93.2	22307	674	14.3	3.52	30.2	15300
LCQ2s 106-107.5	106	0.103	6.1	53.2	25446	1713	10.5	3.60	27.6	6643
LCQ2s 107.5-109	108	0.059	5.1	50.5	21268	1084	7.5	2.99	22.2	5409
LCQ2s 109-111	110	0.087	6.3	75.9	22240	884	10.2	4.61	35.3	8654
LCQ2s 111-112	111.0	0.06	9.92	65.83	16394	532.4	6.65	2.85	27	8635
LCQ2s 112-113.5	112.5	0.079	9.5	60.7	20893	1146	8.4	3.37	28.2	8263
LCQ2s 113.5-114.5	114	0.086	8.1	56.8	23390	1169	8.3	3.60	28.4	7208
LCQ2s 116-117	116	0.107	6.6	63.9	26967	1530	7.6	4.58	33.5	6727
LCQ2s 117.5-119.5	118.5	0.110	8.3	108.8	29115	997	12.8	7.10	47.3	9862
LCQ2s 119.5-121	120	0.140	8.8	71.5	25231	1225	11.2	4.80	34.7	8549
LCQ2s 121-122.5	121	0.102	7.6	89.6	25600	782	11.8	5.39	36.3	10319
LCQ2s 122.5-124	123	0.217	8.6	71.8	26159	1098	7.8	4.44	30.5	6978

Tab. B-15: Results of geochemical analysis (Cd to Ca) of gravity core LCQ2s of Lago Calafquén; Elements were measured by atom adsorption spectrometry (AAS).

Sample	Depth (cm)	Cd (ppm)	Cr (ppm)	Cu (ppm)	Fe (ppm)	Mn (ppm)	Ni (ppm)	Pb (ppm)	Zn (ppm)	Ca (ppm)
LCQ2s 124-125	124	0.106	9.3	70.7	21956	874	8.5	3.11	28.1	8132
LCQ2s 126-127	126	0.116	9.2	92.6	25892	812	10.4	3.95	37.6	10330
LCQ2s 128.5-130	129.0	0.03	8.10	90.31	19903	256.4	4.46	2.43	22	7723
LCQ2s 130.8-132.7	131.0	0.04	8.84	104.46	16694	353.0	7.46	3.41	38	9118
LCQ2s 132.8-134	133.0	0.07	13.54	83.17	18260	601.8	5.44	3.70	33	8619
LCQ2s 134.5-136	135	0.072	9.1	110.2	22367	523	12.4	2.94	32.5	11039
LCQ2s 136-138	137	0.099	7.8	100.1	26563	835	12.7	4.21	37.7	9036
LCQ2s 138-138.5	138.0	0.06	20.47	171.99	27242	582.7	14.62	6.78	53	17891
LCQ2s 138.5-139.5	138.5	0.03	11.71	106.20	18462	302.4	12.33	3.57	35	13770
LCQ2s 139-140	139	0.090	8.2	125.1	30316	796	10.8	4.31	39.9	11498
LCQ2s 140-141	140	0.092	6.5	136.6	32406	833	13.1	5.63	48.2	10384
LCQ2s 41.6-142.6	142	0.060	5.9	108.0	23060	550	16.9	2.86	32.8	12482
LCQ2s 143.5-146	144.5	0.097	2.6	76.6	31347	1482	10.0	4.78	38.7	7030
LCQ2s 147.5-148.8	148	0.142	13.0	134.3	38846	1035	11.4	8.64	59.7	8767
LCQ2s 148.8-150.3	149	0.117	9.5	97.8	25393	906	10.3	4.23	43.0	7903
LCQ2s 150.3-151	150.3	0.107	7.1	94.0	26550	894	8.9	4.09	40.2	7071
LCQ2s 152-155.5	153.5	0.128	8.6	91.6	24577	1079	11.4	3.68	39.8	7174
LCQ2s 156-159	157.5	0.114	10.9	128.5	30489	867	14.5	4.21	45.4	8601
LCQ2s 161-162	161.0	0.09	13.13	132.58	21473	599.5	7.68	6.47	53	8965
LCQ2s 162-162.5	162	0.084	5.7	51.3	18891	843	8.2	2.80	24.6	5014

Tab. B-15: Results of geochemical analysis (Cd to Ca) of gravity core LCQ2s of Lago Calafquén; Elements were measured by atom adsorption spectrometry (AAS).

AAS Analysis - Lago Calafquén

Sample	Depth (cm)	K (ppm)	Mg (ppm)	Na (ppm)
LCQ2s 0-1	0	622.8	3742.0	3071
LCQ2s 1-2	1	687.6	3927.1	2827
LCQ2s 2-3	2	613.1	3760.0	2737
LCQ2s 3-4	3	575.2	2782.7	2076
LCQ2s 4-5	4	934.2	3041.5	2494
LCQ2s 5-6	5	472.9	2652.9	1950
LCQ2s 6-7	6	404.0	2365.2	1672
LCQ2s 7-8	7	871.3	2722.5	2287
LCQ2s 8-9	8	657.1	3003.8	2614
LCQ2s 13-14	13	714.0	5528.4	7467
LCQ2s 14.5-15	14.5	496.1	5006.0	4452
LCQ2s 15.5-17	16	1044	4958	4207
LCQ2s 24.5-26	25	675	3795	3492
LCQ2s 26-28	27	734	3645	3655
LCQ2s 28-29	28.5	1028.2	2566.7	2584
LCQ2s 30-31	30	898	4293	4479
LCQ2s 31.2-31.5	31.2	466.0	4529.5	6158
LCQ2s 31.5-32.5	31.5	782.5	4577.1	5292
LCQ2s 32.5-34	32.5	541	5839	5264
LCQ2s 34-36	35.0	356.3	4955.4	3406
LCQ2s 37.5-40	38.5	717	3777	3664
LCQ2s 41.5-42.5	42	883	5100	4958
LCQ2s 42.5-44.5	43.5	833	4813	4670
LCQ2s 45-45.1	45	936	5085	5323
LCQ2s 45-46	45.5	586.3	2265.7	2384
LCQ2s 46.5-47.5	47.0	618.7	5233.7	4449
LCQ2s 47.5-48.5	48.0	762.1	2364.3	3221
LCQ2s 48.5-48.7	48.5	563	6066	4879
LCQ2s 48.7-48.9	48.7	739	3506	3796
LCQ2s 49.5-49.6	49.5	400	1636	3744
LCQ2s 49.6-51.8	50.5	544	2449	3595
LCQ2s 53-55.8	54	771	3175	3464
LCQ2s 55.8-58	57	698	3044	3185
LCQ2s 58.7-60	59	689	3422	3611
LCQ2s 60-62	61	665	2696	2739
LCQ2s 63-65	64	996	4039	4082

Tab. B-16: Results of geochemical analysis (K to Na) of gravity core LCQ2s of Lago Calafquén; Elements were measured by atom adsorption spectrometry (AAS).

Sample	Depth (cm)	K (ppm)	Mg (ppm)	Na (ppm)
LCQ2s 65-67	66	932	4093	4136
LCQ2s 67.68	67.0	666.8	2338.0	2727
LCQ2s 68-69.5	68	723	3373	3679
LCQ2s 69.5-71.9	70	620	3041	3145
LCQ2s 73.5-74.5	73.5	569	2633	2638
LCQ2s 76-76.5	76.0	717.2	6340.1	6999
LCQ2s 76.5-77.5	77.0	1019.4	4454.9	5352
LCQ2s 77.5-79.5	78.0	560.3	2586.7	2731
LCQ2s 80-80.7	80	1294	5352	6202
LCQ2s 80.7-82.5	80.7	786	3280	2982
LCQ2s 82.5-84	82.5	745	3321	2991
LCQ2s 84-85.5	84	710	2975	2542
LCQ2s 86-87	86.0	407.2	2726.6	2561
LCQ2s 87-89	88	1025	4569	4395
LCQ2s 90-90.8	90	1177	6263	7596
LCQ2s 90.8-91.5	90.8	960	6583	7116
LCQ2s 96-98	97	866	3886	3521
LCQ2s 98-99.5	98	654	3055	2421
LCQ2s 99.5-100.5	99.5	856	4619	3510
LCQ2s 100.5-101.5	101	1070	4675	4560
LCQ2s 102.5-104.5	103.5	1089	5250	5401
LCQ2s 104.5-105	104.5	1514	8086	8739
LCQ2s 105-106	105	901	5791	6958
LCQ2s 106-107.5	106	697	2974	2670
LCQ2s 107.5-109	108	634	2534	2281
LCQ2s 109-111	110	982	4197	3911
LCQ2s 111-112	111.0	711.7	2905.0	2734
LCQ2s 112-113.5	112.5	756	3884	3829
LCQ2s 113.5-114.5	114	672	3403	3102
LCQ2s 116-117	116	847	3545	2786
LCQ2s 117.5-119.5	118.5	1260	6119	4716
LCQ2s 119.5-121	120	972	4602	3871
LCQ2s 121-122.5	121	1040	5110	4931
LCQ2s 122.5-124	123	993	3789	2862
LCQ2s 124-125	124	904	4224	3476
LCQ2s 126-127	126	1109	5651	4538
LCQ2s 128.5-130	129.0	2707.1	3928.4	3111
LCQ2s 130.8-132.7	131.0	424.8	4230.9	3336

Tab. B-16: Results of geochemical analysis (K to Na) of gravity core LCQ2s of Lago Calafquén; Elements were measured by atom adsorption spectrometry (AAS).

Sample	Depth (cm)	K (ppm)	Mg (ppm)	Na (ppm)
LCQ2s 132.8-134	133.0	918.0	3347.7	3218
LCQ2s 134.5-136	135	846	5615	5207
LCQ2s 136-138	137	1128	4923	3834
LCQ2s 138-138.5	138.0	626.0	5945.1	6672
LCQ2s 138.5-139.5	138.5	369.7	4417.7	4632
LCQ2s 139-140	139	1350	6243	5335
LCQ2s 140-141	140	1648	6485	4619
LCQ2s 41.6-142.6	142	872	6175	5419
LCQ2s 143.5-146	144.5	1029	4211	2402
LCQ2s 147.5-148.8	148	1496	6458	3322
LCQ2s 148.8-150.3	149	1198	6235	3693
LCQ2s 150.3-151	150.3	1184	6104	3478
LCQ2s 152-155.5	153.5	1123	5792	3214
LCQ2s 156-159	157.5	1247	7306	4127
LCQ2s 161-162	161.0	838.4	4875.8	3212
LCQ2s 162-162.5	162	618	3240	2007

Tab. B-16: Results of geochemical analysis (K to Na) of gravity core LCQ2s of Lago Calafquén. Elements were measured by atom adsorption spectrometry (AAS).

Lago Calafquén – AAS Analysis

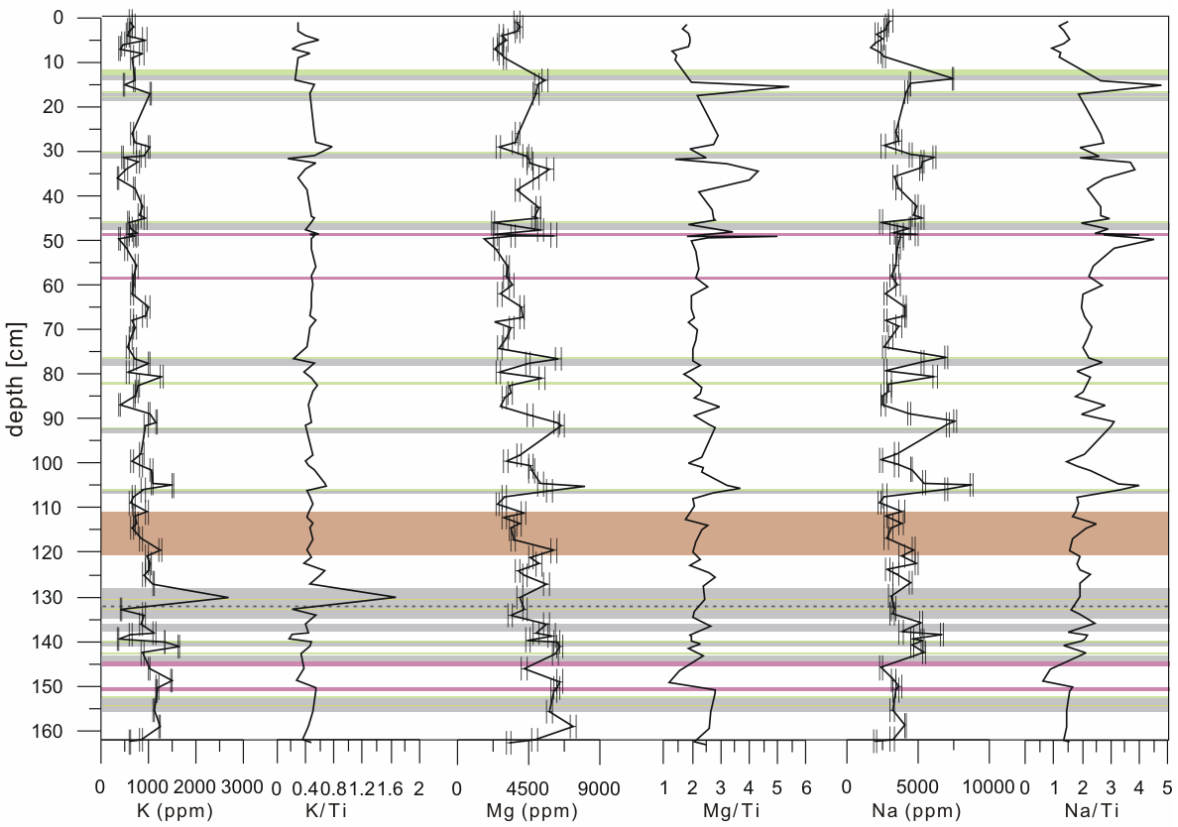

Fig. B-3: Concentration and Ti-normalized profiles of K, Mg, and Na for short core LCQ2s. Shaded and coloured bands indicate lithology, presented in Fig. IV-18.

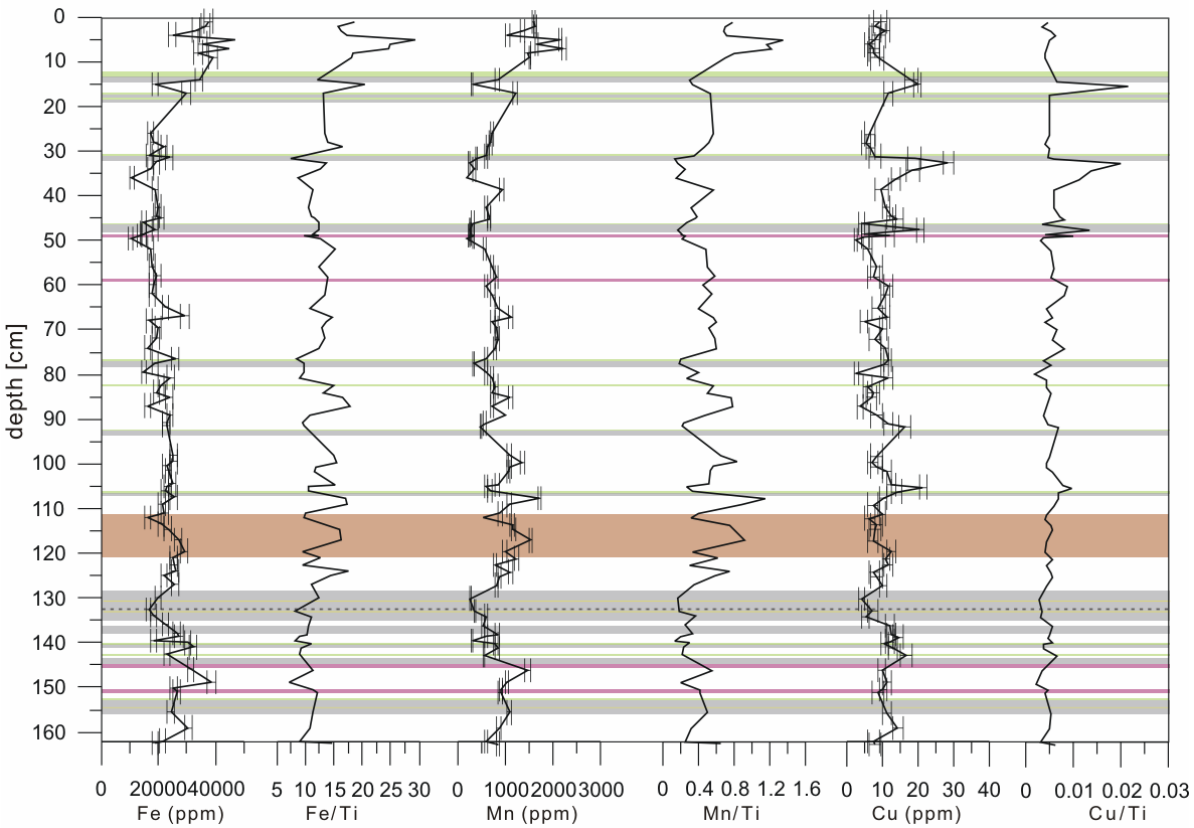

Fig. B-4: Concentration and Ti-normalized profiles of Fe, Mn, and Cu for short core LCQ2s. Shaded and coloured bands indicate lithology, presented in Fig. IV-18.

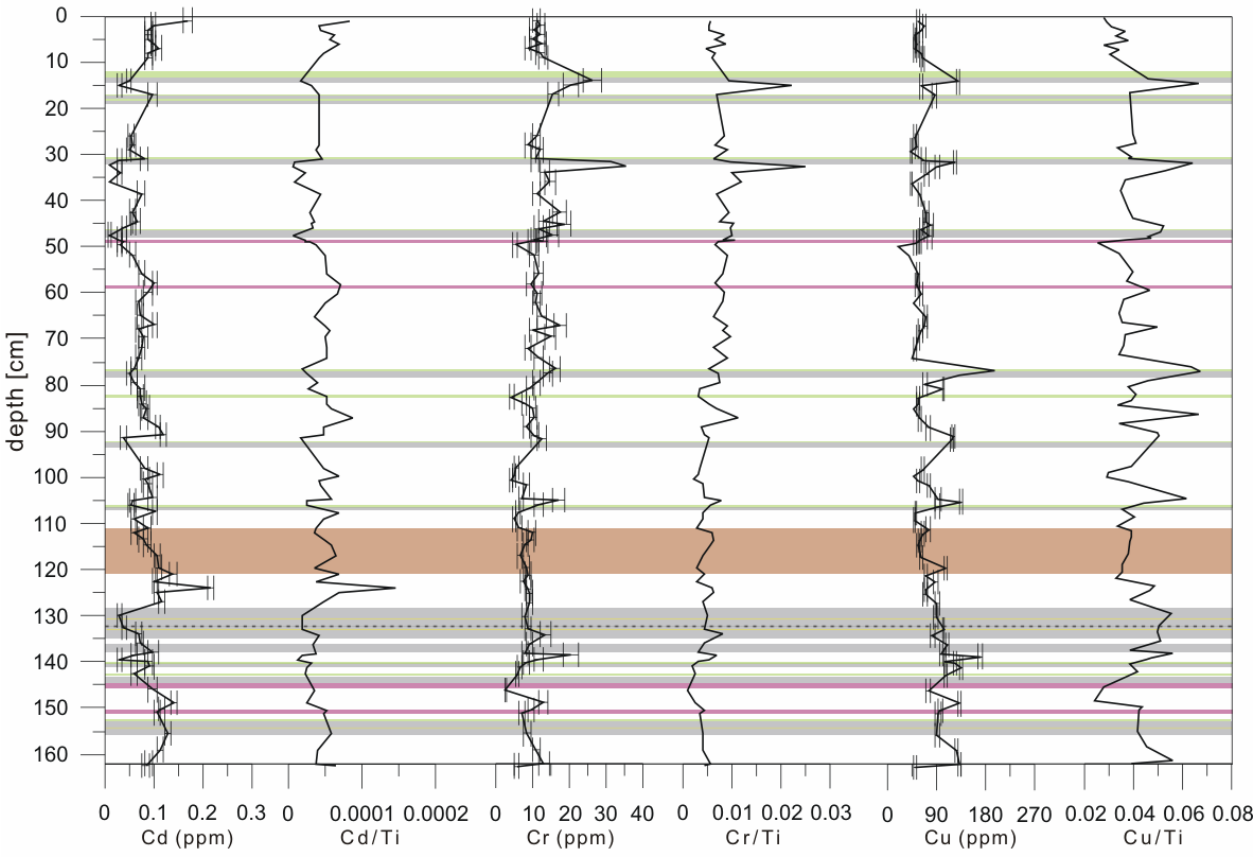

Fig. B-5: Concentration and Ti-normalized profiles of Cd, Cr, and Cu for short core LCQ2s. Shaded and coloured bands indicate lithology, presented in Fig. IV-18.

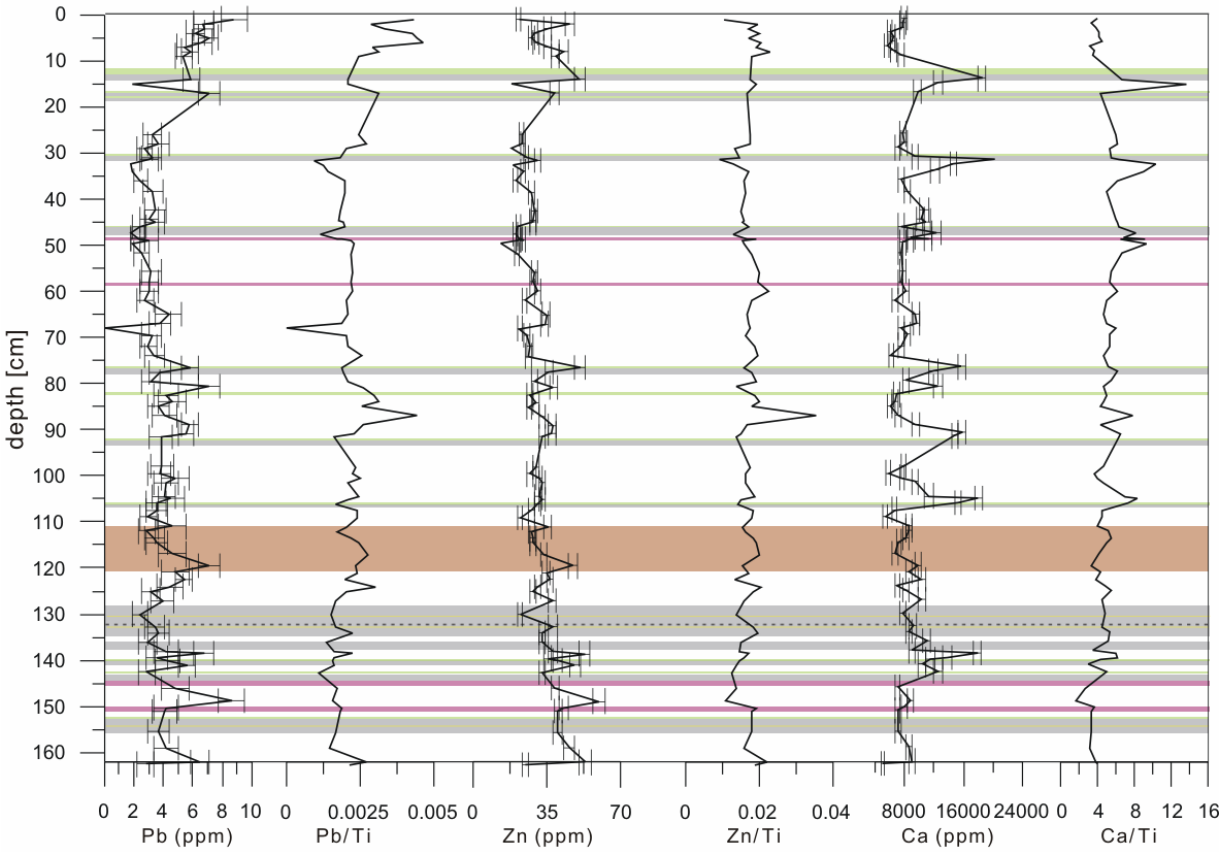

Fig. B-6: Concentration and Ti-normalized profiles of Pb, Zn, and Ca for short core LCQ2s. Shaded and coloured bands indicate lithology, presented in Fig. IV-18.

ICP-MS Analysis - Lago Calafquén

Sample	Depth (cm)	^{45}Sc (ppm)	^{47}Ti (ppm)	^{59}Co (ppm)	^{85}Rb (ppm)	^{88}Sr (ppm)	^{90}Zr (ppm)	^{133}Cs (ppm)	^{135}Ba (ppm)	^{139}La (ppm)
LCQ2s 0-1	1	7.0503	2038.4301	11.6619	4.6648	87.9191	15.9178	1.0922	96.0752	4.4276
LCQ2s 1-2	2	7.2838	2345.9716	9.6880	4.7305	102.4882	11.1078	1.1720	105.0553	4.5369
LCQ2s 2-3	3	6.8809	2023.2789	9.9294	4.6521	97.7836	10.1857	1.1854	98.4770	4.3611
LCQ2s 3-4	4	5.2717	1444.2935	9.4592	3.8261	61.8478	9.8220	1.0106	83.2745	3.9565
LCQ2s 4-5	5	5.7541	1599.9398	9.1692	3.8350	68.0163	11.3501	1.0126	82.8567	4.1797
LCQ2s 5-6	6	5.4648	1432.2493	11.8564	4.0745	65.8130	9.8401	1.0370	82.8184	4.0122
LCQ2s 6-7	7	5.0000	1834.2685	19.2814	3.4193	59.4519	11.4156	0.9203	72.4752	3.8293
LCQ2s 7-8	8	5.9404	1851.3278	9.3274	4.2773	84.0118	12.5816	1.1395	90.7270	4.6811
LCQ2s 8-9	9	6.4914	2178.1551	16.9792	4.5312	91.1936	14.7111	1.1631	87.4303	4.9518
LCQ2s 13-14	14	9.1725	2815.0894	9.7296	4.6838	247.7104	13.1705	0.8787	124.0733	5.4754
LCQ2s 14.5-15	15.0	2.8260	928.9428	8.5095	1.3811	155.2210	5.7247	0.2901	33.7197	1.9595
LCQ2s 15.5-17	17	6.7992	2276.9029	14.4619	4.9252	127.2178	8.1247	1.2278	75.5249	6.1535
LCQ2s 24.5-26	26	3.7583	1307.9470	8.0362	2.6707	100.7132	4.4129	0.6563	42.3077	3.4755
LCQ2s 26-28	28	3.8370	1325.1582	6.7590	2.9575	100.8966	4.3407	0.6566	45.2795	3.6933
LCQ2s 28-29	29.0	3.2509	1334.0695	6.2044	2.7164	75.3239	8.0094	0.6315	39.9588	2.6943
LCQ2s 30-31	31	4.3741	1729.8938	7.1409	3.3169	123.0020	5.4628	0.6390	57.9540	3.9568
LCQ2s 31.2-31.5	31.5	7.5532	3257.2172	9.0878	3.7683	279.1055	9.1706	0.5970	76.8339	3.5779
LCQ2s 31.5-32.5	32.5	2.7192	1425.7991	9.9007	1.2009	179.9087	5.4212	0.2499	41.2557	2.1164
LCQ2s 32.5-34	34	2.8035	1360.2015	9.5516	1.1482	153.1486	3.6474	0.2356	33.1612	2.7947
LCQ2s 34-36	36	2.9848	1234.5498	5.6167	2.3775	93.9132	6.3372	0.5477	42.0751	2.6505
LCQ2s 37.5-40	38.5	4.3943	1674.9751	8.7101	2.8514	108.8609	6.0369	0.6347	53.2777	3.9419
LCQ2s 41.5-42.5	42.5	4.7280	1888.3394	9.4781	3.0414	138.5997	6.2949	0.6096	59.2660	4.1671

Tab. B-17: Results of geochemical analysis (^{45}Sc to ^{139}La) of gravity core LCQ2s of Lago Calafquén; Elements were measured by inductive coupled plasma mass spectrometry (ICP-MS).

Sample	Depth (cm)	^{45}Sc (ppm)	^{47}Ti (ppm)	^{59}Co (ppm)	^{85}Rb (ppm)	^{88}Sr (ppm)	^{90}Zr (ppm)	^{133}Cs (ppm)	^{135}Ba (ppm)	^{139}La (ppm)
LCQ2s 42.5-44.5	44.5	4.5943	1748.6798	8.8478	2.8217	129.6207	6.1318	0.5875	56.6731	3.9990
LCQ2s 45-45.1	45	4.9419	1800.6506	9.3204	2.8625	142.6580	6.5033	0.5699	61.5822	3.9974
LCQ2s 45.1-46	46	3.2818	1213.8554	4.3439	2.3062	90.3353	6.8020	0.5837	41.7627	2.7541
LCQ2s 46.5-47.5	47.5	2.4556	1538.0435	9.5562	0.8499	154.0761	4.9257	0.1436	33.0254	1.8071
LCQ2s 47.5-48.5	48.5	3.3367	1313.4960	4.3264	2.5510	111.7032	6.4181	0.5298	51.2450	2.7229
LCQ2s 48.5-48.7	48.7	2.8109	1219.9828	8.6139	1.4408	143.0103	4.0512	0.2821	36.9854	2.6747
LCQ2s 48.7-48.9	48.9	3.8485	1379.8516	5.1241	2.7811	112.6712	6.0659	0.5525	54.8231	3.7215
LCQ2s 49.5-49.6	49.6	1.8531	825.7403	3.9021	1.2859	126.6515	3.7494	0.2620	30.5239	2.0923
LCQ2s 49.6-51.8	51.8	2.7817	1148.0177	5.7473	1.8284	107.9030	4.8970	0.4211	36.1763	2.9708
LCQ2s 53-55.8	55.8	4.0553	1436.8302	7.3153	3.1923	100.2256	6.1647	0.7036	53.1726	4.2950
LCQ2s 55.8-58	58	3.8638	1418.6296	6.4936	2.9698	94.1916	7.6298	0.6785	48.6081	4.1087
LCQ2s 58.7-60	60	4.1466	1339.0052	13.5079	3.3141	104.8298	6.4751	0.7080	58.8220	4.5275
LCQ2s 60-62	62	3.5782	1353.4624	6.5540	2.7331	83.5196	6.0374	0.6225	45.0654	3.7227
LCQ2s 63-65	65	4.8199	2058.2902	8.3899	4.8096	120.7772	8.6295	0.9211	76.0751	5.0168
LCQ2s 65-67	67	4.8720	1973.8844	9.5094	3.5890	123.1364	7.8664	0.7561	65.8849	4.6197
LCQ2s 67.68	68	3.2328	1242.9312	8.0113	2.6579	86.3219	6.3407	0.5838	44.1447	2.5943
LCQ2s 68-69.5	69.5	3.9514	1566.5357	6.7785	2.9015	103.5514	7.0354	0.6517	52.2179	4.1058
LCQ2s 69.5-71.9	71.9	3.7781	1431.9055	7.4080	2.6949	93.6711	6.8959	0.6249	47.7348	3.8207
LCQ2s 73.5-74.5	74	3.5754	1319.4780	6.2639	2.7453	79.1445	7.1387	0.6190	49.1542	3.7566
LCQ2s 76-76.5	76.5	8.9067	3118.3595	11.1560	4.3232	208.4573	17.4458	0.9204	143.3277	5.3740
LCQ2s 76.5-77.5	77.5	5.2091	1965.5732	10.7246	2.8307	155.7318	9.7332	0.5541	100.7570	3.2246
LCQ2s 77.5-79.5	79.5	3.6903	1512.4180	5.6619	2.9346	96.7315	9.5408	0.6931	52.5773	3.4196
LCQ2s 80-80.7	80.7	7.3396	2706.0288	8.9270	5.1272	175.3319	13.2895	1.0257	119.5935	6.7298
LCQ2s 80.7-82.5	82.5	4.3269	1406.0258	7.6554	3.8152	89.5385	7.7451	0.8058	58.9670	4.3807

Tab. B-17: Results of geochemical analysis (^{45}Sc to ^{139}La) of gravity core LCQ2s of Lago Calafquén; Elements were measured by inductive coupled plasma mass spectrometry (ICP-MS).

Sample	Depth (cm)	^{45}Sc (ppm)	^{47}Ti (ppm)	^{59}Co (ppm)	^{85}Rb (ppm)	^{88}Sr (ppm)	^{90}Zr (ppm)	^{133}Cs (ppm)	^{135}Ba (ppm)	^{139}La (ppm)
LCQ2s 82.5-84	84	4.4992	1466.7006	9.3073	3.5180	89.3238	8.9324	0.7641	63.3960	4.5920
LCQ2s 84-85.5	85	4.8252	1445.3883	8.9053	3.4818	76.1408	6.0716	0.9017	52.9490	3.9794
LCQ2s 86-87	87	3.7357	915.8542	6.9468	3.4633	86.5833	6.7253	0.8415	59.1882	3.4665
LCQ2s 87-89	89	5.6392	2220.4969	10.3753	4.1770	120.7298	7.9956	0.9748	74.9482	5.0647
LCQ2s 90-90.8	90.8	6.2352	2434.5146	10.6600	3.1972	208.3975	8.6158	0.6665	90.5624	4.8934
LCQ2s 90.8-91.5	91.5	5.2389	2356.3803	17.5267	2.1136	187.3411	6.5264	0.4160	64.9720	4.0963
LCQ2s 96-98	98	4.8418	1680.3055	8.7439	3.6129	101.4048	8.0756	0.8445	62.9705	4.4531
LCQ2s 98-99.5	99.5	4.0145	1644.3098	7.9825	3.3698	78.3103	6.9331	0.7762	47.5876	4.0405
LCQ2s 99.5-100.5	100.5	4.2778	1921.0897	9.7687	4.4293	108.5016	8.3396	0.9353	57.5975	4.8027
LCQ2s 100.5-101.5	101.5	5.2449	2012.7326	9.3438	3.8737	122.2209	8.4611	0.8695	72.4780	4.8739
LCQ2s 102.5-104.5	104.5	5.2278	1639.0998	9.7777	3.5317	148.0477	8.4192	0.7660	74.6204	4.4875
LCQ2s 104.5-105	105	6.3016	2187.8484	12.0192	3.5633	236.7614	9.1290	0.6438	105.5741	5.2174
LCQ2s 105-106	106	4.4415	2093.5583	10.7797	2.5882	197.8528	7.0974	0.5661	66.0276	3.9468
LCQ2s 106-107.5	107.5	4.0988	1491.8076	13.8214	3.2796	84.4477	9.0499	0.7846	52.7088	4.1279
LCQ2s 107.5-109	109	3.5280	1235.8583	7.8099	2.8910	57.6980	6.4990	0.6776	41.3797	3.4801
LCQ2s 109-111	111	5.3575	2242.4658	8.6973	4.5000	114.7671	11.0397	0.9968	76.6027	5.4027
LCQ2s 111-112	112	3.8827	1674.8112	7.6222	3.1519	105.0311	8.6550	0.8346	52.1879	3.0320
LCQ2s 112-113.5	113.5	4.1406	1529.7340	8.1847	3.1742	106.0250	8.3868	0.7836	52.8039	3.8211
LCQ2s 113.5-114.5	114.5	3.9357	1465.2956	8.2969	2.9653	90.6041	7.7211	0.7271	46.6452	3.6710
LCQ2s 116-117	117	5.0433	1668.4694	10.4164	4.1658	87.2228	9.8067	0.9893	60.7761	4.8486
LCQ2s 117.5-119.5	119.5	7.4901	3047.8700	12.5165	5.7795	136.6930	14.7782	1.1627	106.9939	6.5141
LCQ2s 119.5-121	121	5.2036	2013.5747	9.6217	4.1805	111.8527	9.7360	1.0031	68.0241	4.7989
LCQ2s 121-122.5	122.5	5.8874	2693.3237	9.3612	4.2267	142.4111	13.2685	0.9547	81.6643	5.4755
LCQ2s 122.5-124	124	5.3036	1477.3922	8.8683	4.2915	94.0983	8.2150	0.9953	71.2671	5.0079

Tab. B-17: Results of geochemical analysis (^{45}Sc to ^{139}La) of gravity core LCQ2s of Lago Calafquén; Elements were measured by inductive coupled plasma mass spectrometry (ICP-MS).

Sample	Depth (cm)	^{45}Sc (ppm)	^{47}Ti (ppm)	^{59}Co (ppm)	^{85}Rb (ppm)	^{88}Sr (ppm)	^{90}Zr (ppm)	^{133}Cs (ppm)	^{135}Ba (ppm)	^{139}La (ppm)
LCQ2s 124-125	125	4.9581	1507.1770	7.4940	3.7978	105.2512	8.9510	0.9264	61.4713	4.3888
LCQ2s 126-127	127	6.2741	2365.4822	10.7018	4.5381	140.9898	12.1624	1.0510	80.4315	5.4708
LCQ2s 128.5-130	130	3.2752	1615.4005	8.1379	1.9116	96.0157	5.6214	0.4289	43.1358	2.3028
LCQ2s 130.8-132.7	132.7	4.3696	2052.0764	9.0285	2.2966	118.6370	8.7186	0.4932	48.0821	3.1667
LCQ2s 132.8-134	134	3.9508	1660.6426	6.4251	3.4819	89.0562	10.3392	1.0131	63.4578	3.9702
LCQ2s 134.5-136	136	5.1290	2143.2015	10.6123	2.7375	144.4069	9.1538	0.5775	61.8370	4.3250
LCQ2s 136-138	138	6.7710	2581.5944	9.2416	5.9724	125.1605	16.1316	1.2483	87.6404	6.1865
LCQ2s 138-138.5	138.5	8.8595	3039.7471	12.2742	5.2958	239.6116	16.2602	1.0732	123.7579	5.9553
LCQ2s 138.5-139.5	139.5	4.4571	2230.5271	13.2179	3.0380	174.7640	7.1007	0.6452	55.5566	3.4668
LCQ2s 139-140	140	7.6881	2738.1470	10.7819	7.0944	160.5046	16.7355	1.2266	100.3915	6.3441
LCQ2s 140-141	141	9.4611	3486.9432	11.3774	11.4555	142.7291	23.5023	1.6833	128.7762	8.0056
LCQ2s 141.6-142.6	142.6	6.0213	2567.7638	11.2561	3.5987	164.9322	7.2701	0.7119	65.5010	4.5753
LCQ2s 143.5-146	146	6.7239	2744.4098	12.5819	5.6916	94.4618	12.0645	1.3326	81.2663	6.2585
LCQ2s 147.5-148.8	148.8	12.7808	5441.4838	11.6157	9.1066	128.3046	16.9018	1.6928	161.7032	10.1345
LCQ2s 148.8-150.3	150.3	6.5279	2229.8345	8.6711	4.8772	106.3987	11.6055	1.2397	74.8966	5.4124
LCQ2s 150.3-151	151	6.3511	2201.5735	8.4021	4.6514	97.2192	11.3728	1.1321	64.5279	5.7718
LCQ2s 152-155.5	155.5	5.9735	2188.6241	13.5117	4.6718	96.8750	10.7846	1.1646	65.8161	5.1360
LCQ2s 156-159	159	7.6838	2822.6496	12.5748	5.3013	125.5342	14.0705	1.2479	88.9744	5.9744
LCQ2s 161-162	162	7.6676	2363.2554	9.7640	5.7080	119.4310	13.5311	1.4358	99.4817	5.8458
LCQ2s 162-162.5	162.5	3.8739	1295.7075	6.7170	3.0803	54.2793	10.2040	0.8006	41.9184	3.4883

Tab. B-17: Results of geochemical analysis (^{45}Sc to ^{139}La) of gravity core LCQ2s of Lago Calafquén; Elements were measured by inductive coupled plasma mass spectrometry (ICP-MS).

ICP-MS Analysis - Lago Calafquén

Sample	Depth (cm)	^{140}Ce (ppm)	^{141}Pr (ppm)	^{146}Nd (ppm)	^{149}Sm (ppm)	^{151}Eu (ppm)	^{159}Tb (ppm)	^{160}Gd (ppm)	^{163}Dy (ppm)	^{165}Ho (ppm)
LCQ2s 0-1	1	10.3802	1.4462	6.3144	1.6276	0.4254	0.2715	1.7161	1.6294	0.3493
LCQ2s 1-2	2	10.5944	1.5018	6.6282	1.6499	0.4148	0.2763	1.7703	1.6815	0.3434
LCQ2s 2-3	3	10.2105	1.4252	6.4586	1.5565	0.4069	0.2722	1.6865	1.6444	0.3279
LCQ2s 3-4	4	9.1848	1.2817	5.6399	1.3601	0.3598	0.2298	1.4878	1.4266	0.3008
LCQ2s 4-5	5	9.6598	1.3420	6.0747	1.3933	0.3701	0.2498	1.5999	1.5608	0.3141
LCQ2s 5-6	6	9.1680	1.2762	5.6951	1.3767	0.3569	0.2374	1.5325	1.4675	0.2999
LCQ2s 6-7	7	8.7754	1.2322	5.3960	1.3066	0.3375	0.2189	1.4760	1.4005	0.2861
LCQ2s 7-8	8	10.9055	1.4998	6.6674	1.5977	0.4295	0.2754	1.7425	1.6913	0.3515
LCQ2s 8-9	9	11.5978	1.5978	7.1059	1.7157	0.4389	0.3026	1.8918	1.8386	0.3690
LCQ2s 13-14	14	13.5957	1.8873	8.6023	2.1489	0.5958	0.3609	2.2939	2.2340	0.4612
LCQ2s 14.5-15	15.0	4.7974	0.6622	2.9474	0.7423	0.2219	0.1234	0.7968	0.7475	0.1533
LCQ2s 15.5-17	17	12.6785	1.7375	7.6247	1.8202	0.4919	0.2919	1.8740	1.8530	0.3996
LCQ2s 24.5-26	26	5.7998	0.8714	3.8869	0.9237	0.2603	0.1494	0.9675	0.9440	0.2052
LCQ2s 26-28	28	6.3172	0.9234	4.0796	0.9579	0.2669	0.1499	0.9925	0.9740	0.2079
LCQ2s 28-29	29.0	5.9217	0.8547	3.8619	0.9181	0.2566	0.1592	1.0137	0.9695	0.2039
LCQ2s 30-31	31	7.1750	1.0522	4.6662	1.1127	0.3083	0.1765	1.1423	1.1187	0.2451
LCQ2s 31.2-31.5	31.5	8.6465	1.2139	5.4851	1.3322	0.4094	0.2291	1.4718	1.4399	0.2903
LCQ2s 31.5-32.5	32.5	5.2021	0.7106	3.2237	0.8057	0.2581	0.1366	0.8768	0.8372	0.1656
LCQ2s 32.5-34	34	4.8438	0.6866	3.0743	0.7223	0.2194	0.1137	0.7481	0.7300	0.1528
LCQ2s 34-36	36	5.8524	0.8416	3.7094	0.8827	0.2544	0.1493	1.0095	0.9534	0.1941
LCQ2s 37.5-40	38.5	7.1074	1.0406	4.5875	1.1019	0.3028	0.1746	1.1365	1.1336	0.2420
LCQ2s 41.5-42.5	42.5	7.6510	1.1206	4.9558	1.1986	0.3336	0.1881	1.2193	1.2103	0.2616

Tab. B-18: Results of geochemical analysis (^{140}Ce to ^{165}Ho) of gravity core LCQ2s of Lago Calafquén; Elements were measured by inductive coupled plasma mass spectrometry (ICP-MS).

Sample	Depth (cm)	^{140}Ce (ppm)	^{141}Pr (ppm)	^{146}Nd (ppm)	^{149}Sm (ppm)	^{151}Eu (ppm)	^{159}Tb (ppm)	^{160}Gd (ppm)	^{163}Dy (ppm)	^{165}Ho (ppm)
LCQ2s 42.5-44.5	44.5	7.3812	1.0738	4.7756	1.1366	0.3159	0.1831	1.1861	1.1811	0.2504
LCQ2s 45-45.1	45	7.5337	1.1128	4.9628	1.1942	0.3413	0.1924	1.2372	1.2256	0.2649
LCQ2s 45.1-46	46	6.0071	0.8618	3.8436	0.9402	0.2656	0.1566	1.0194	0.9530	0.2052
LCQ2s 46.5-47.5	47.5	4.5371	0.6148	2.8614	0.6967	0.2327	0.1198	0.7945	0.7579	0.1556
LCQ2s 47.5-48.5	48.5	6.1927	0.8607	3.9554	0.9218	0.2595	0.1525	0.9878	0.9461	0.1912
LCQ2s 48.5-48.7	48.7	4.7298	0.6692	2.9556	0.6969	0.2128	0.1114	0.7302	0.7095	0.1521
LCQ2s 48.7-48.9	48.9	6.5596	0.9344	4.0939	0.9569	0.2644	0.1503	0.9727	0.9655	0.2043
LCQ2s 49.5-49.6	49.6	3.1264	0.4482	1.9533	0.4539	0.1581	0.0690	0.4707	0.4659	0.0970
LCQ2s 49.6-51.8	51.8	4.7587	0.7023	3.0764	0.7162	0.2037	0.1094	0.7284	0.7119	0.1487
LCQ2s 53-55.8	55.8	7.5578	1.1153	4.8646	1.1536	0.3034	0.1789	1.1777	1.1591	0.2511
LCQ2s 55.8-58	58	7.2564	1.0851	4.7578	1.1151	0.3098	0.1749	1.1472	1.1285	0.2412
LCQ2s 58.7-60	60	8.5445	1.2326	5.3665	1.2542	0.3399	0.1954	1.2754	1.2539	0.2691
LCQ2s 60-62	62	6.3918	0.9393	4.1508	0.9678	0.2541	0.1514	1.0023	1.0029	0.2135
LCQ2s 63-65	65	9.6347	1.4080	6.1606	1.4430	0.3755	0.2302	1.4676	1.4585	0.3166
LCQ2s 65-67	67	8.5560	1.2667	5.6554	1.3463	0.3602	0.2141	1.3831	1.3425	0.2897
LCQ 2s 67.68	68	5.8824	0.8483	3.8042	0.9477	0.2671	0.1669	1.0670	1.0608	0.2135
LCQ2s 68-69.5	69.5	7.1701	1.0512	4.6392	1.1065	0.2942	0.1764	1.1568	1.1360	0.2473
LCQ2s 69.5-71.9	71.9	6.6776	0.9959	4.4028	1.0309	0.2725	0.1647	1.0921	1.0611	0.2300
LCQ2s 73.5-74.5	74	6.7218	0.9900	4.3475	1.0306	0.2633	0.1636	1.0698	1.0495	0.2258
LCQ2s 76-76.5	76.5	13.1003	1.8604	8.3298	2.1451	0.5745	0.3701	2.3247	2.3502	0.4869
LCQ2s 76.5-77.5	77.5	8.1083	1.1148	5.0514	1.2635	0.3495	0.2206	1.4104	1.4393	0.2857
LCQ2s 77.5-79.5	79.5	7.9042	1.1051	4.9930	1.1985	0.3087	0.1978	1.3238	1.2172	0.2535
LCQ2s 80-80.7	80.7	13.4748	1.9718	8.6297	2.0838	0.5368	0.3422	2.1972	2.1668	0.4725
LCQ2s 80.7-82.5	82.5	8.3046	1.1940	5.1901	1.2243	0.3076	0.1925	1.2410	1.2076	0.2572

Tab. B-18: Results of geochemical analysis (^{140}Ce to ^{165}Ho) of gravity core LCQ2s of Lago Calafquén; Elements were measured by inductive coupled plasma mass spectrometry (ICP-MS).

Sample	Depth (cm)	^{140}Ce (ppm)	^{141}Pr (ppm)	^{146}Nd (ppm)	^{149}Sm (ppm)	^{151}Eu (ppm)	^{159}Tb (ppm)	^{160}Gd (ppm)	^{163}Dy (ppm)	^{165}Ho (ppm)
LCQ2s 82.5-84	84	8.7913	1.2811	5.6660	1.3498	0.3353	0.2178	1.3943	1.3663	0.2970
LCQ2s 84-85.5	85	7.1335	1.0966	4.5364	1.1034	0.3341	0.2405	1.2184	1.1579	0.2936
LCQ2s 86-87	87	7.7808	1.1043	5.0413	1.1901	0.2912	0.2018	1.3438	1.2728	0.2593
LCQ2s 87-89	89	9.6506	1.4325	6.0947	1.4997	0.4018	0.2791	1.6084	1.5373	0.3513
LCQ2s 90-90.8	90.8	9.7791	1.4060	6.1364	1.4972	0.4412	0.2578	1.5973	1.5498	0.3363
LCQ2s 90.8-91.5	91.5	8.2130	1.1754	5.2618	1.2900	0.3795	0.2284	1.3841	1.3650	0.3029
LCQ2s 96-98	98	8.2815	1.2197	5.3587	1.2883	0.3273	0.2141	1.3283	1.3107	0.2885
LCQ2s 98-99.5	99.5	7.5563	1.1110	4.8020	1.1099	0.2813	0.1816	1.1532	1.1283	0.2477
LCQ2s 99.5-100.5	100.5	9.1851	1.3105	5.5848	1.2729	0.3179	0.2048	1.2905	1.2588	0.2740
LCQ2s 100.5-101.5	101.5	9.1026	1.3271	5.9035	1.4153	0.3663	0.2409	1.5071	1.4863	0.3215
LCQ2s 102.5-104.5	104.5	8.5629	1.2405	5.5342	1.3339	0.3629	0.2234	1.3910	1.3652	0.2923
LCQ2s 104.5-105	105	10.4822	1.4967	6.6388	1.6263	0.4695	0.2815	1.7517	1.7238	0.3703
LCQ2s 105-106	106	7.4450	1.0782	4.7559	1.1346	0.3337	0.1892	1.1895	1.1497	0.2509
LCQ2s 106-107.5	107.5	7.3692	1.0991	4.8362	1.1553	0.3048	0.1956	1.2400	1.2006	0.2674
LCQ2s 107.5-109	109	6.1633	0.9099	3.9892	0.9453	0.2486	0.1620	1.0021	0.9721	0.2141
LCQ2s 109-111	111	10.4945	1.5137	6.6562	1.5767	0.3968	0.2612	1.6370	1.6096	0.3484
LCQ2s 111-112	112	6.7936	0.9765	4.4014	1.0512	0.2851	0.1911	1.1906	1.1417	0.2356
LCQ2s 112-113.5	113.5	6.8284	1.0063	4.4236	1.0716	0.2866	0.1823	1.1453	1.1168	0.2389
LCQ2s 113.5-114.5	114.5	6.4177	0.9423	4.1671	1.0026	0.2677	0.1695	1.0731	1.0440	0.2251
LCQ2s 116-117	117	9.0251	1.3245	5.7639	1.3588	0.3486	0.2301	1.4508	1.4116	0.3048
LCQ2s 117.5-119.5	119.5	13.4497	1.9466	8.5419	2.0608	0.5223	0.3497	2.1805	2.1542	0.4696
LCQ2s 119.5-121	121	9.1390	1.3399	5.8899	1.4002	0.3622	0.2338	1.4731	1.4279	0.3128
LCQ2s 121-122.5	122.5	11.0134	1.5946	7.0125	1.6739	0.4224	0.2770	1.7267	1.7015	0.3700
LCQ2s 122.5-124	124	9.5662	1.3920	6.1238	1.4511	0.3619	0.2391	1.4932	1.4774	0.3247

Tab. B-18: Results of geochemical analysis (^{140}Ce to ^{165}Ho) of gravity core LCQ2s of Lago Calafquén; Elements were measured by inductive coupled plasma mass spectrometry (ICP-MS).

Sample	Depth (cm)	^{140}Ce (ppm)	^{141}Pr (ppm)	^{146}Nd (ppm)	^{149}Sm (ppm)	^{151}Eu (ppm)	^{159}Tb (ppm)	^{160}Gd (ppm)	^{163}Dy (ppm)	^{165}Ho (ppm)
LCQ2s 124-125	125	8.3971	1.2249	5.3720	1.2715	0.3317	0.2114	1.3361	1.3074	0.2844
LCQ2s 126-127	127	10.9150	1.5964	7.0381	1.6954	0.4339	0.2854	1.7830	1.7335	0.3796
LCQ2s 128.5-130	130	5.7370	0.7966	3.5116	0.8721	0.2321	0.1485	0.9593	0.9222	0.1934
LCQ2s 130.8-132.7	132.7	7.8392	1.0678	4.8250	1.1801	0.3073	0.2098	1.3526	1.2998	0.2773
LCQ2s 132.8-134	134	9.3497	1.2762	5.8102	1.3397	0.3393	0.2280	1.4507	1.4190	0.2866
LCQ2s 134.5-136	136	8.8597	1.2512	5.5919	1.3778	0.3726	0.2338	1.4501	1.4429	0.3128
LCQ2s 136-138	138	12.9160	1.8031	7.8973	1.8713	0.4803	0.3052	1.9061	1.8767	0.4089
LCQ2s 138-138.5	138.5	14.5777	1.9964	8.7760	2.1669	0.6168	0.3736	2.4187	2.3509	0.4871
LCQ2s 138.5-139.5	139.5	8.4648	1.1576	5.2085	1.3316	0.3657	0.2255	1.4103	1.4270	0.2841
LCQ2s 139-140	140	13.6690	1.9106	8.3351	1.9943	0.5219	0.3279	2.0465	1.9965	0.4350
LCQ2s 140-141	141	17.3195	2.4219	10.4391	2.5154	0.6491	0.4265	2.6523	2.5832	0.5576
LCQ2s 141.6-142.6	142.6	9.4857	1.3081	5.6304	1.4230	0.4246	0.2736	1.5634	1.5053	0.3461
LCQ2s 143.5-146	146	12.9082	1.7720	7.6196	1.8227	0.4778	0.3188	1.9332	1.8526	0.4030
LCQ2s 147.5-148.8	148.8	22.3354	3.0969	13.3098	3.3033	0.8541	0.5742	3.5789	3.4535	0.7436
LCQ2s 148.8-150.3	150.3	11.0199	1.5680	6.8653	1.6572	0.4063	0.2826	1.7877	1.6973	0.3609
LCQ2s 150.3-151	151	11.8692	1.7173	7.4973	1.8435	0.4314	0.3123	1.9818	1.8367	0.3832
LCQ2s 152-155.5	155.5	10.4092	1.5198	6.6648	1.6266	0.3956	0.2780	1.7525	1.6817	0.3599
LCQ2s 156-159	159	12.5427	1.7863	7.7511	1.8900	0.4652	0.3278	2.0534	1.9776	0.4250
LCQ2s 161-162	162	13.6524	1.9012	8.7064	2.1813	0.5337	0.3717	2.3952	2.3710	0.4815
LCQ2s 162-162.5	162.5	6.3010	0.9066	3.8580	0.9185	0.2348	0.1604	1.0164	0.9687	0.2063

Tab. B-18: Results of geochemical analysis (^{140}Ce to ^{165}Ho) of gravity core LCQ2s of Lago Calafquén; Elements were measured by inductive coupled plasma mass spectrometry (ICP-MS).

ICP-MS Analysis - Lago Calafquén

Sample	Depth (cm)	^{166}Er (ppm)	^{169}Tm (ppm)	^{172}Yb (ppm)	^{175}Lu (ppm)	^{232}Th (ppm)	^{238}U (ppm)
LCQ2s 0-1	1	0.0046	0.1413	0.8849	0.1304	0.8933	0.6766
LCQ2s 1-2	2	0.9838	0.1418	0.8974	0.1327	0.9752	0.7556
LCQ2s 2-3	3	0.9663	0.1387	0.8918	0.1290	0.8259	0.7597
LCQ2s 3-4	4	0.8512	0.1258	0.7789	0.1202	0.7721	0.6832
LCQ2s 4-5	5	0.9052	0.1306	0.8525	0.1218	0.8049	0.7134
LCQ2s 5-6	6	0.8907	0.1213	0.7962	0.1167	0.7691	0.8104
LCQ2s 6-7	7	0.8279	0.1232	0.7846	0.1170	0.7792	0.7972
LCQ2s 7-8	8	1.0096	0.1438	0.9358	0.1417	1.1330	0.8366
LCQ2s 8-9	9	1.0992	0.1526	0.9987	0.1542	1.0281	0.7978
LCQ2s 13-14	14	1.3094	0.1899	1.2669	0.1827	1.0179	0.4421
LCQ2s 14.5-15	15.0	0.4474	0.0606	0.4130	0.0609	0.3271	0.1448
LCQ2s 15.5-17	17	1.1096	0.1622	1.0490	0.1601	1.3425	0.6545
LCQ2s 24.5-26	26	0.5819	0.0806	0.5325	0.0786	0.5092	0.4123
LCQ2s 26-28	28	0.5890	0.0827	0.5338	0.0796	0.5426	0.3944
LCQ2s 28-29	29.0	0.5891	0.0833	0.5465	0.0807	0.4360	0.4639
LCQ2s 30-31	31	0.6849	0.0947	0.6342	0.0931	0.5811	0.3648
LCQ2s 31.2-31.5	31.5	0.8542	0.1203	0.7954	0.1171	0.5243	0.2918
LCQ2s 31.5-32.5	32.5	0.4967	0.0723	0.4574	0.0677	0.2845	0.1245
LCQ2s 32.5-34	34	0.4312	0.0581	0.3908	0.0554	0.3613	0.1354
LCQ2s 34-36	36	0.5711	0.0818	0.5158	0.0774	0.4060	0.3315
LCQ2s 37.5-40	38.5	0.6859	0.0967	0.6386	0.0942	0.5646	0.4342
LCQ2s 41.5-42.5	42.5	0.7307	0.1015	0.6672	0.1023	0.6828	0.4137
LCQ2s 42.5-44.5	44.5	0.7127	0.1008	0.6482	0.0989	0.5503	0.3815
LCQ2s 45-45.1	45	0.7416	0.1066	0.6831	0.1028	0.5640	0.3597
LCQ2s 45.1-46	46	0.5909	0.0845	0.5507	0.0809	0.3739	0.3988
LCQ2s 46.5-47.5	47.5	0.4418	0.0606	0.4238	0.0616	0.2707	0.1063
LCQ2s 47.5-48.5	48.5	0.5558	0.0792	0.5142	0.0746	0.4310	0.3181
LCQ2s 48.5-48.7	48.7	0.4233	0.0584	0.3945	0.0577	0.4872	0.1781
LCQ2s 48.7-48.9	48.9	0.5716	0.0788	0.5331	0.0779	0.5187	0.3272
LCQ2s 49.5-49.6	49.6	0.2855	0.0369	0.2543	0.0362	0.2631	0.1508
LCQ2s 49.6-51.8	51.8	0.4225	0.0582	0.3899	0.0569	0.3593	0.3340
LCQ2s 53-55.8	55.8	0.7038	0.0972	0.6450	0.0959	0.5526	0.5233
LCQ2s 55.8-58	58	0.6733	0.0950	0.6255	0.0941	0.5315	0.5625
LCQ2s 58.7-60	60	0.7448	0.1029	0.6890	0.1033	0.5839	0.4576
LCQ2s 60-62	62	0.6067	0.0844	0.5619	0.0844	0.4869	0.4671

Tab. B-19: Results of geochemical analysis (^{166}Er to ^{238}U) of gravity core LCQ2s of Lago Calafquén; Elements were measured by inductive coupled plasma mass spectrometry (ICP-MS).

Sample	Depth (cm)	^{166}Er (ppm)	^{169}Tm (ppm)	^{172}Yb (ppm)	^{175}Lu (ppm)	^{232}Th (ppm)	^{238}U (ppm)
LCQ2s 63-65	65	0.8821	0.1256	0.8176	0.1255	0.9856	0.5742
LCQ2s 65-67	67	0.8119	0.1142	0.7420	0.1121	0.6458	0.5816
LCQ2s 67.68	68	0.6170	0.0908	0.5906	0.0832	0.4308	0.4694
LCQ2s 68-69.5	69.5	0.6997	0.0966	0.6339	0.0971	0.5343	0.4926
LCQ2s 69.5-71.9	71.9	0.6512	0.0906	0.6010	0.0896	0.5206	0.5034
LCQ2s 73.5-74.5	74	0.6335	0.0909	0.5739	0.0868	0.5437	0.4834
LCQ2s 76-76.5	76.5	1.3802	0.1987	1.2548	0.1846	0.9584	0.3643
LCQ2s 76.5-77.5	77.5	0.8421	0.1241	0.7970	0.1150	0.5458	0.2113
LCQ2s 77.5-79.5	79.5	0.7327	0.1102	0.6608	0.0996	0.5332	0.4741
LCQ2s 80-80.7	80.7	1.3251	0.1897	1.2009	0.1867	1.1120	0.6012
LCQ2s 80.7-82.5	82.5	0.7219	0.0994	0.6578	0.0976	0.7009	0.4932
LCQ2s 82.5-84	84	0.8413	0.1183	0.7717	0.1154	0.6992	0.5033
LCQ2s 84-85.5	85	0.7121	0.1534	0.6721	0.1530	3.2718	0.8539
LCQ2s 86-87	87	0.7375	0.1063	0.6594	0.1029	0.5536	0.5058
LCQ2s 87-89	89	0.9247	0.1579	0.8547	0.1539	1.6149	0.7615
LCQ2s 90-90.8	90.8	0.9147	0.1434	0.8476	0.1338	1.0247	0.3832
LCQ2s 90.8-91.5	91.5	0.8321	0.1290	0.7712	0.1268	0.7562	0.2213
LCQ2s 96-98	98	0.7905	0.1170	0.7347	0.1177	0.8280	0.5397
LCQ2s 98-99.5	99.5	0.6728	0.1015	0.6211	0.1003	0.7092	0.5937
LCQ2s 99.5-100.5	100.5	0.7548	0.1112	0.6865	0.1096	0.9104	0.5464
LCQ2s 100.5-101.5	101.5	0.8860	0.1319	0.8244	0.1284	0.7919	0.5075
LCQ2s 102.5-104.5	104.5	0.8113	0.1203	0.7432	0.1170	0.7057	0.4311
LCQ2s 104.5-105	105	1.0247	0.1531	0.9438	0.1486	0.8087	0.3031
LCQ2s 105-106	106	0.6973	0.1006	0.6263	0.0984	0.6351	0.3241
LCQ2s 106-107.5	107.5	0.7438	0.1078	0.6809	0.1091	0.6601	0.5839
LCQ2s 107.5-109	109	0.5883	0.0877	0.5454	0.0862	0.5680	0.5571
LCQ2s 109-111	111	0.9664	0.1442	0.8996	0.1429	0.9510	0.6277
LCQ2s 111-112	112	0.6888	0.1037	0.6658	0.0958	0.5446	0.5875
LCQ2s 112-113.5	113.5	0.6555	0.0973	0.6132	0.0955	0.5743	0.5689
LCQ2s 113.5-114.5	114.5	0.6240	0.0931	0.5716	0.0893	0.5524	0.5578
LCQ2s 116-117	117	0.8613	0.1282	0.7943	0.1256	0.8503	0.8006
LCQ2s 117.5-119.5	119.5	1.3153	0.1948	1.2088	0.1871	1.2879	0.6912
LCQ2s 119.5-121	121	0.8639	0.1273	0.7859	0.1232	0.7464	0.5776
LCQ2s 121-122.5	122.5	1.0091	0.1490	0.9205	0.1447	0.9162	0.4595
LCQ2s 122.5-124	124	0.8866	0.1312	0.8107	0.1285	0.8605	0.6556
LCQ2s 124-125	125	0.7862	0.1153	0.7133	0.1133	0.6907	0.6672
LCQ2s 126-127	127	1.0496	0.1547	0.9647	0.1522	0.8924	1.3997

Tab. B-19: Results of geochemical analysis (^{166}Er to ^{238}U) of gravity core LCQ2s of Lago Calafquén; Elements were measured by inductive coupled plasma mass spectrometry (ICP-MS).

Sample	Depth (cm)	^{166}Er (ppm)	^{169}Tm (ppm)	^{172}Yb (ppm)	^{175}Lu (ppm)	^{232}Th (ppm)	^{238}U (ppm)
LCQ2s 128.5-130	130	0.5405	0.0810	0.5058	0.0736	0.4486	0.1661
LCQ2s 130.8-132.7	132.7	0.7509	0.1139	0.7143	0.1058	0.5409	0.2493
LCQ2s 132.8-134	134	0.8087	0.1174	0.7482	0.1125	0.7543	0.5465
LCQ2s 134.5-136	136	0.8723	0.1286	0.8135	0.1278	0.7011	0.2675
LCQ2s 136-138	138	1.1268	0.1675	1.0340	0.1645	1.1550	0.7158
LCQ2s 138-138.5	138.5	1.4182	0.2058	1.2816	0.1904	1.1868	0.4792
LCQ2s 138.5-139.5	139.5	0.8492	0.1222	0.7829	0.1132	0.7700	0.3054
LCQ2s 139-140	140	1.2125	0.1779	1.1114	0.1761	1.2016	0.5776
LCQ2s 140-141	141	1.5527	0.2337	1.4542	0.2249	1.6999	0.7605
LCQ2s 141.6-142.6	142.6	0.9211	0.1603	0.8652	0.1548	3.2732	0.5278
LCQ2s 143.5-146	146	1.0930	0.1724	1.0316	0.1646	1.8591	0.8281
LCQ2s 147.5-148.8	148.8	2.0703	0.3184	1.9684	0.3063	2.5980	1.0649
LCQ2s 148.8-150.3	150.3	0.9889	0.1462	0.8855	0.1374	1.0512	0.6542
LCQ2s 150.3-151	151	1.0440	0.1541	0.9471	0.1443	0.9829	0.5846
LCQ2s 152-155.5	155.5	0.9784	0.1453	0.8940	0.1396	0.8744	0.6914
LCQ2s 156-159	159	1.1656	0.1744	1.0769	0.1668	1.0780	0.6488
LCQ2s 161-162	162	1.3752	0.1994	1.3057	0.1932	1.0604	0.6844
LCQ2s 162-162.5	162.5	0.5652	0.0868	0.5386	0.0866	0.6411	0.6190

Tab. B-19: Results of geochemical analysis (^{166}Er to ^{238}U) of gravity core LCQ2s of Lago Calafquén; Elements were measured by inductive coupled plasma mass spectrometry (ICP-MS).

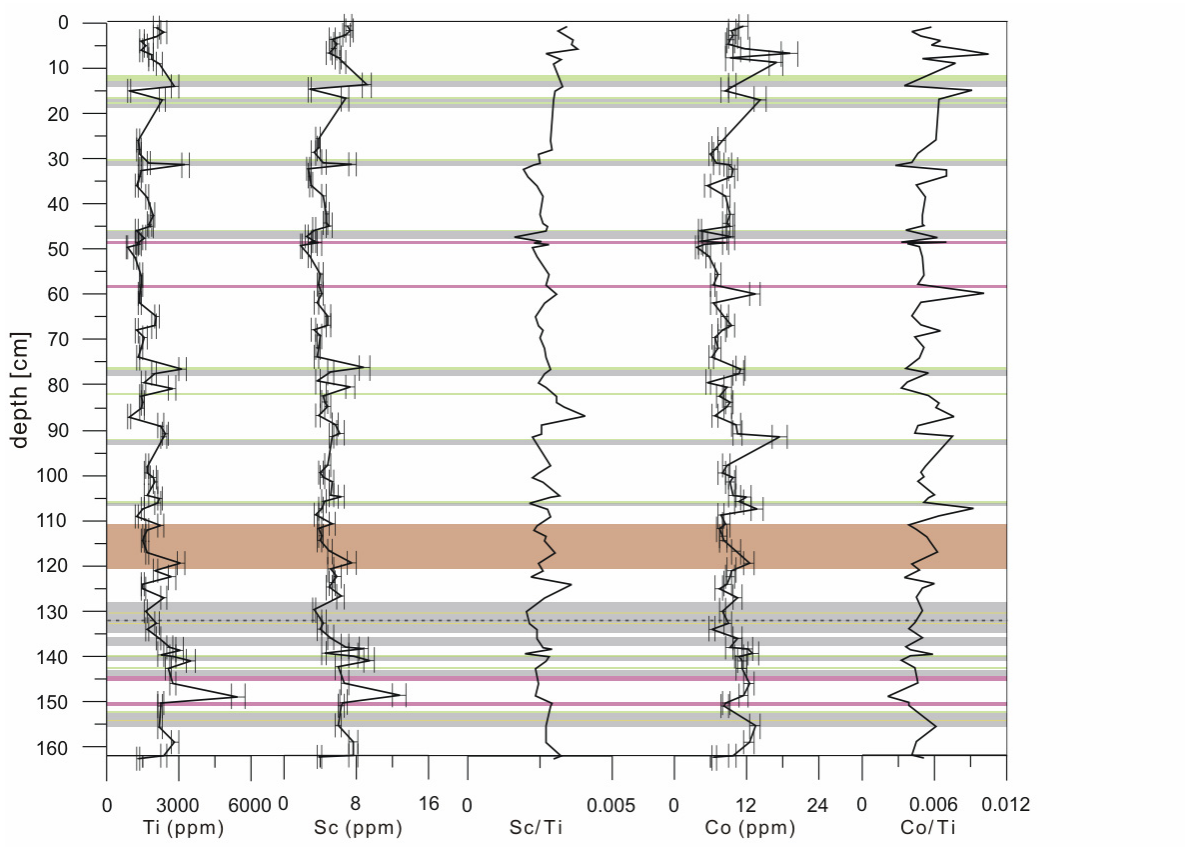

Fig. B-7: Concentration of Ti, and concentration and Ti-normalized profiles of Sc, and Co for short core LCQ2s. Shaded and coloured bands indicate lithology, presented in Fig. IV-18.

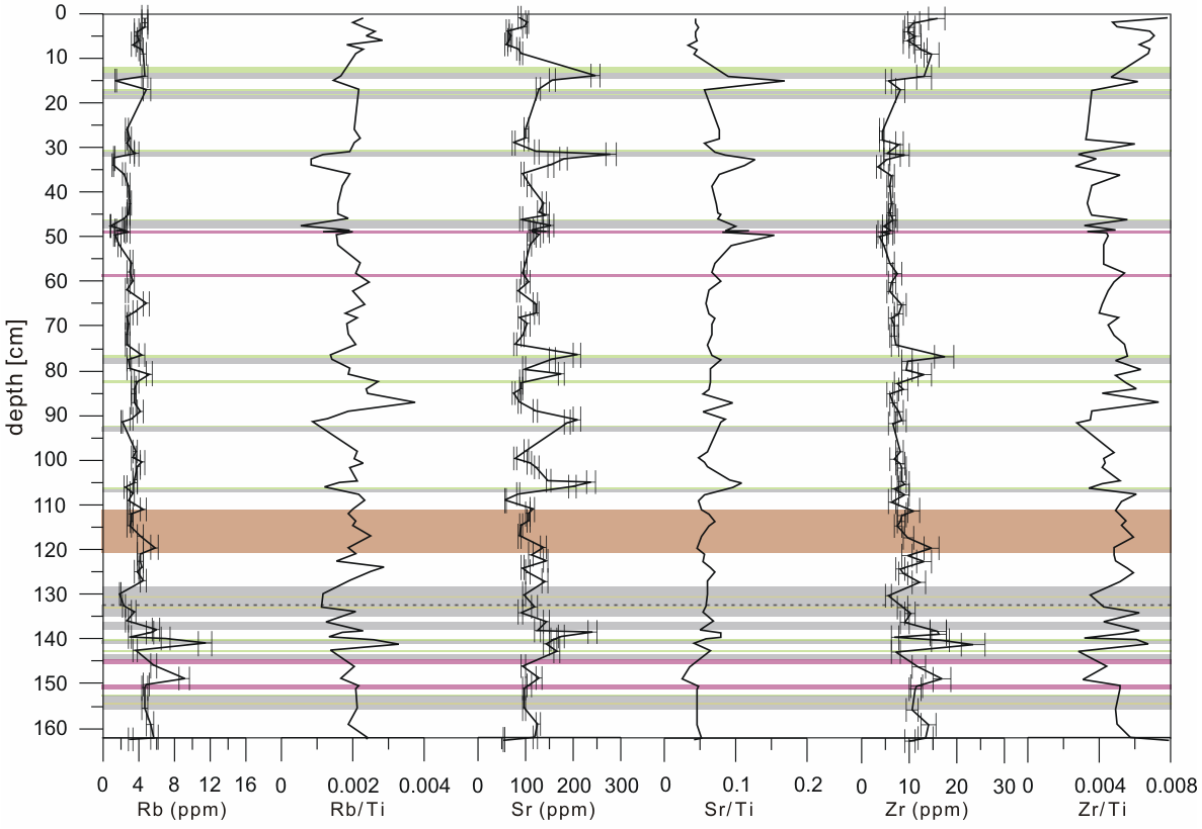

Fig. B-8: Concentration and Ti-normalized profiles of Rb, Sr, and Zr for short core LCQ2s. Shaded and coloured bands indicate lithology, presented in Fig. IV-18.

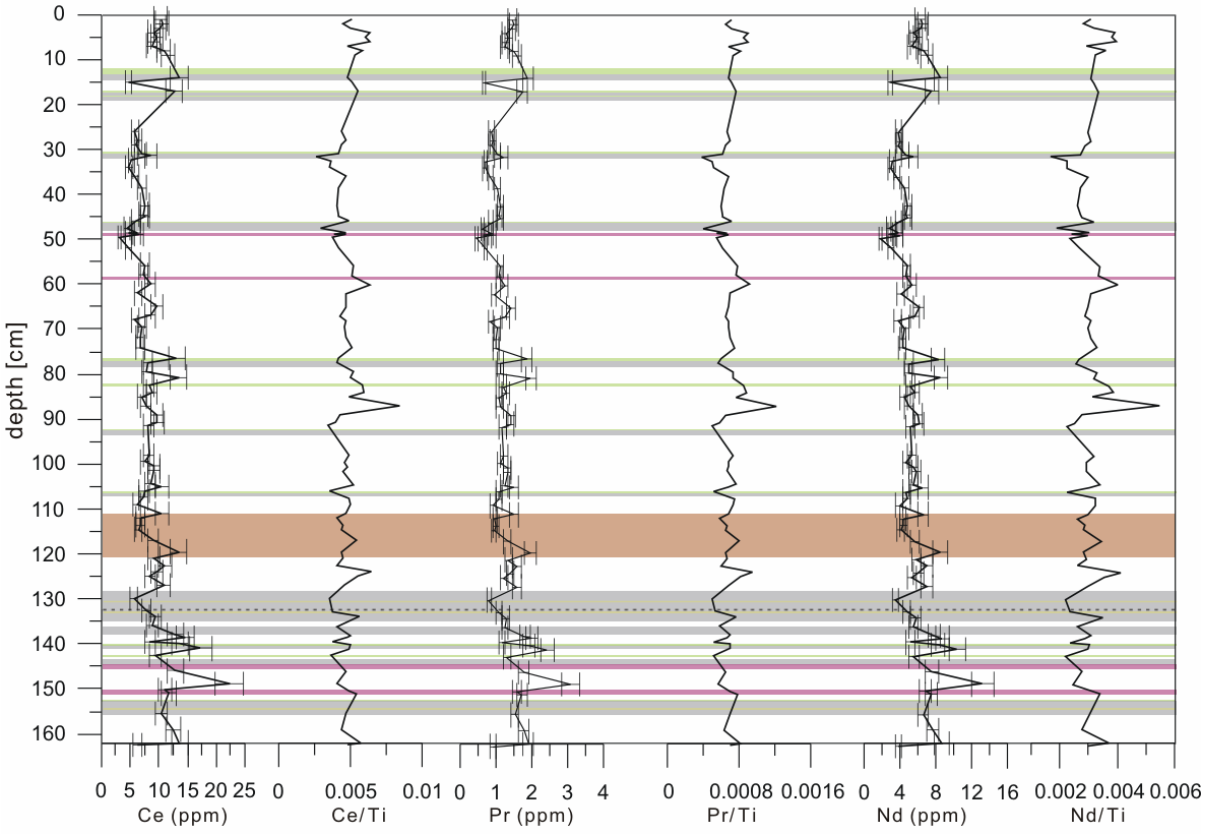

Fig. B-9: Concentration and Ti-normalized profiles of Ce, Pr, and Nd for short core LCQ2s. Shaded and coloured bands indicate lithology, presented in Fig. IV-18.

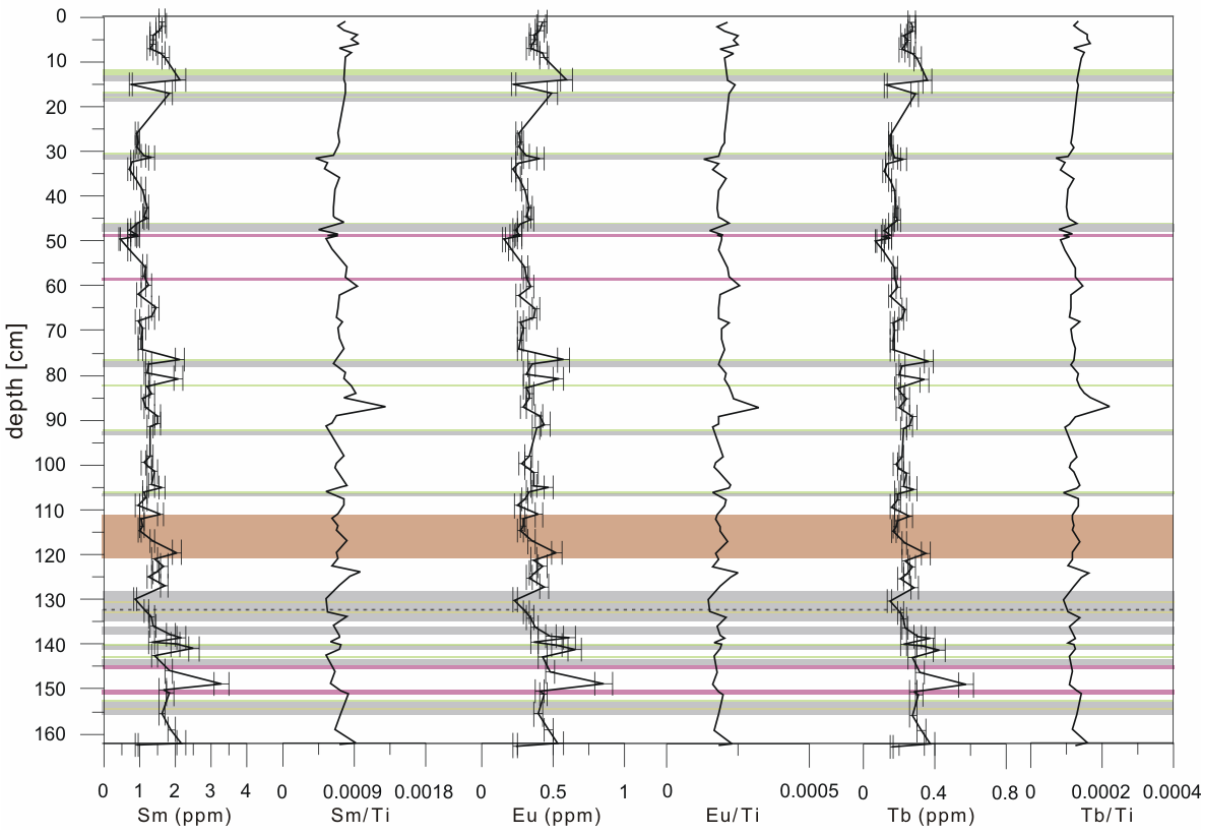

Fig. B-10: Concentration and Ti-normalized profiles of Sm, Eu, and Tb for short core LCQ2s. Shaded and coloured bands indicate lithology, presented in Fig. IV-18.

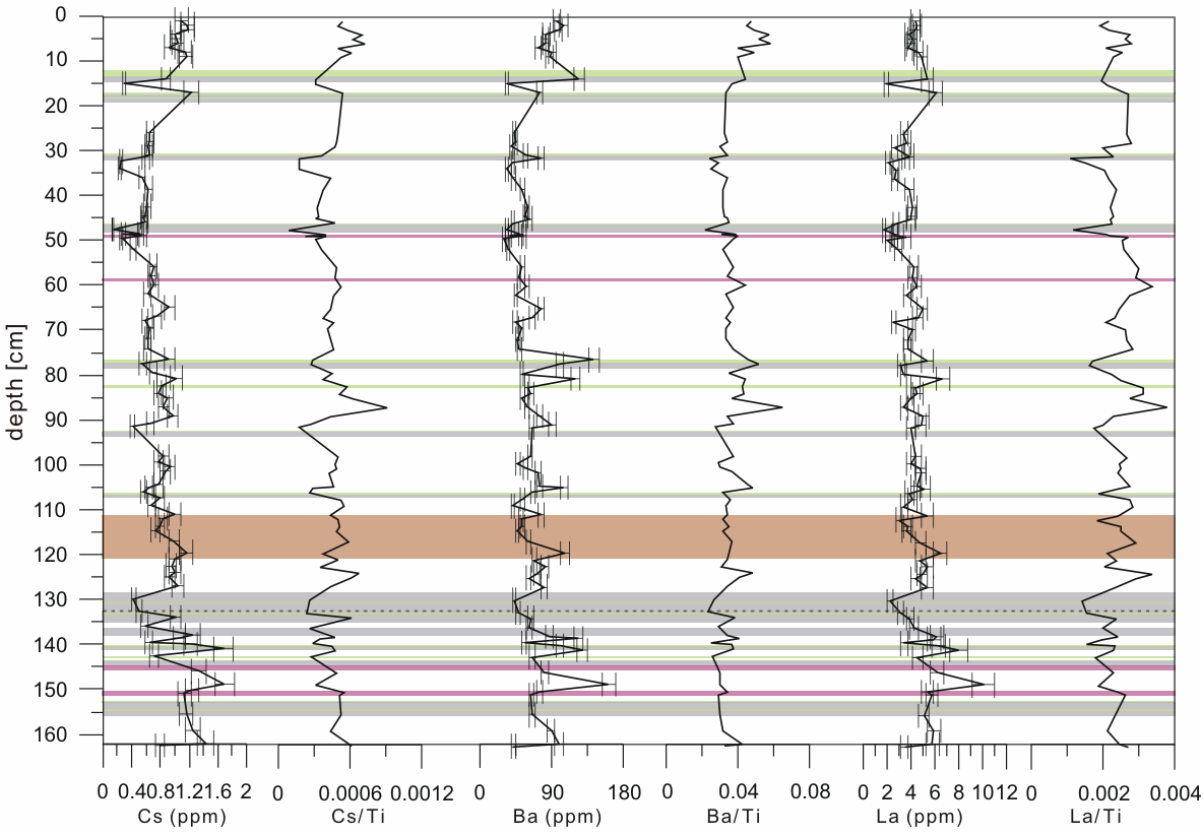

Fig. B-11: Concentration and Ti-normalized profiles of Cs, Ba, and La for short core LCQ2s. Shaded and coloured bands indicate lithology, presented in Fig. IV-18.

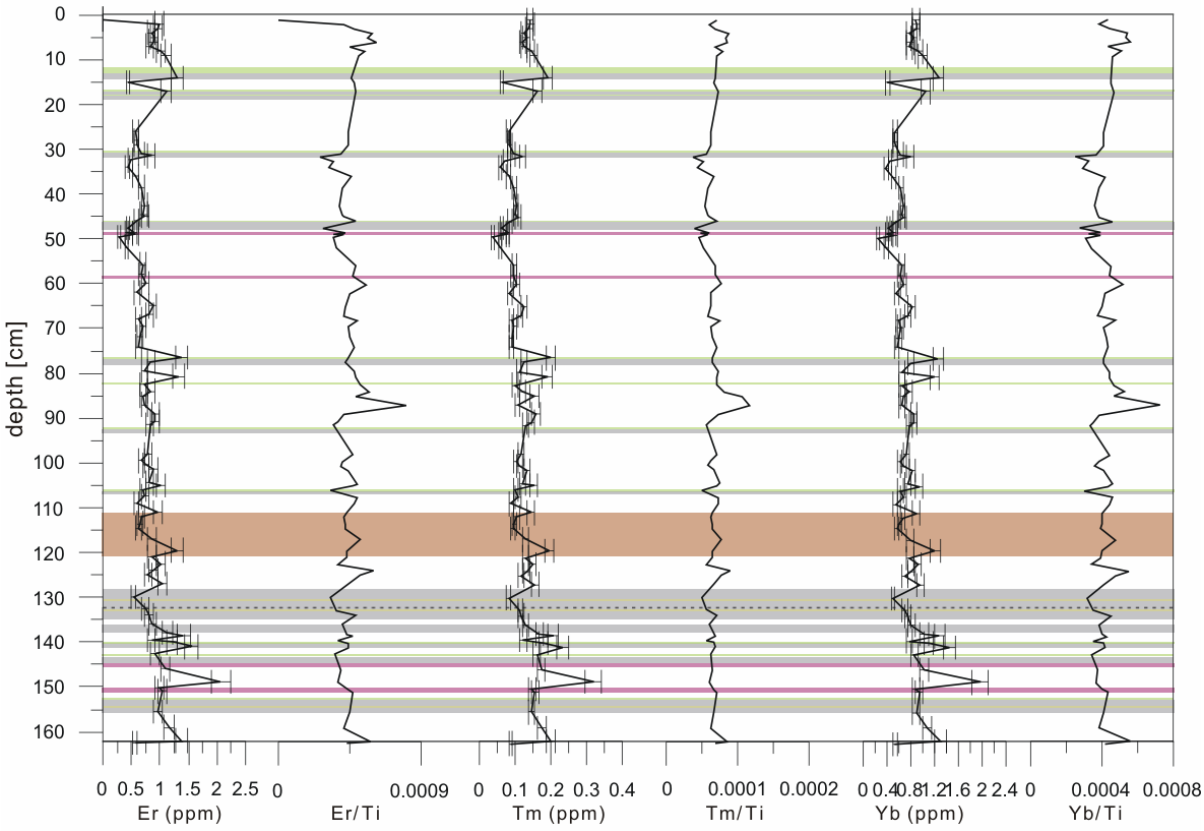

Fig. B-12: Concentration and Ti-normalized profiles of Er, Tm, and Yb for short core LCQ2s. Shaded and coloured bands indicate lithology, presented in Fig. IV-18.

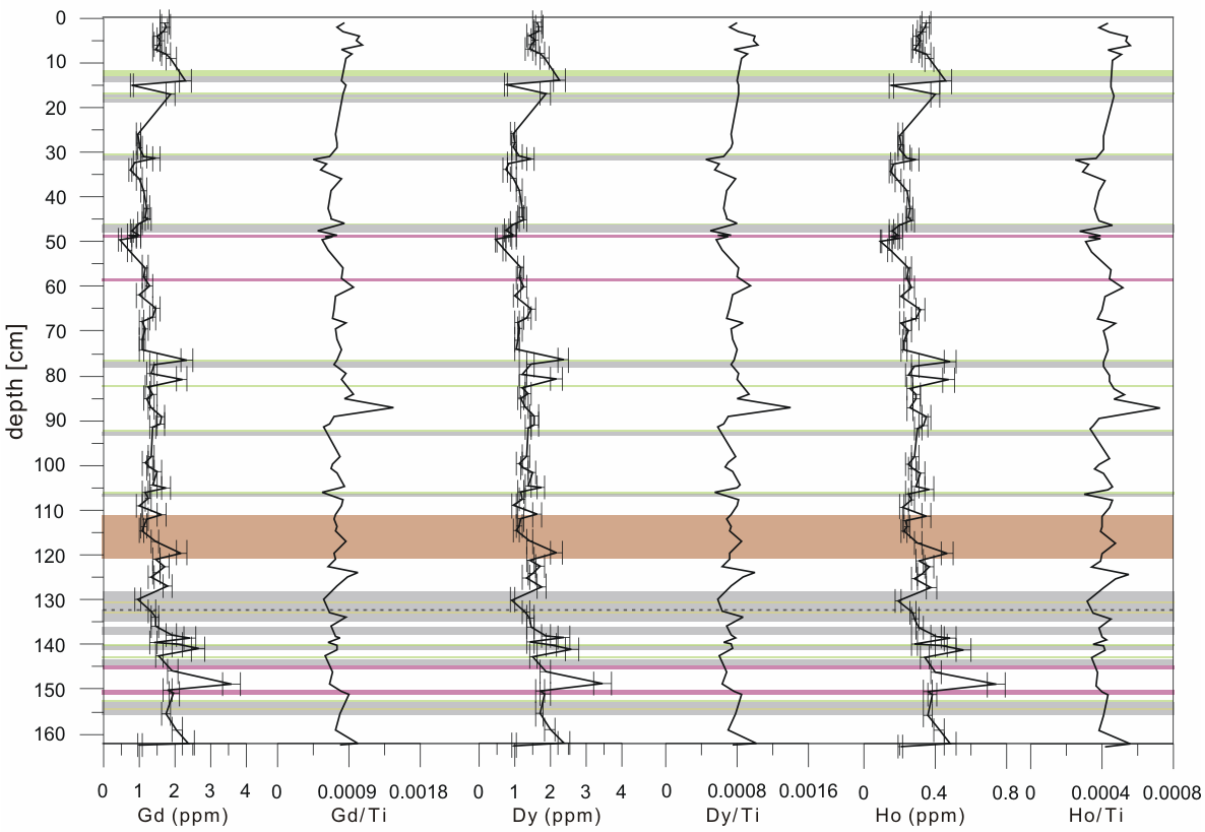

Fig. B-13: Concentration and Ti-normalized profiles of Gd, Dy, and Ho for short core LCQ2s. Shaded and coloured bands indicate lithology, presented in Fig. IV-18.

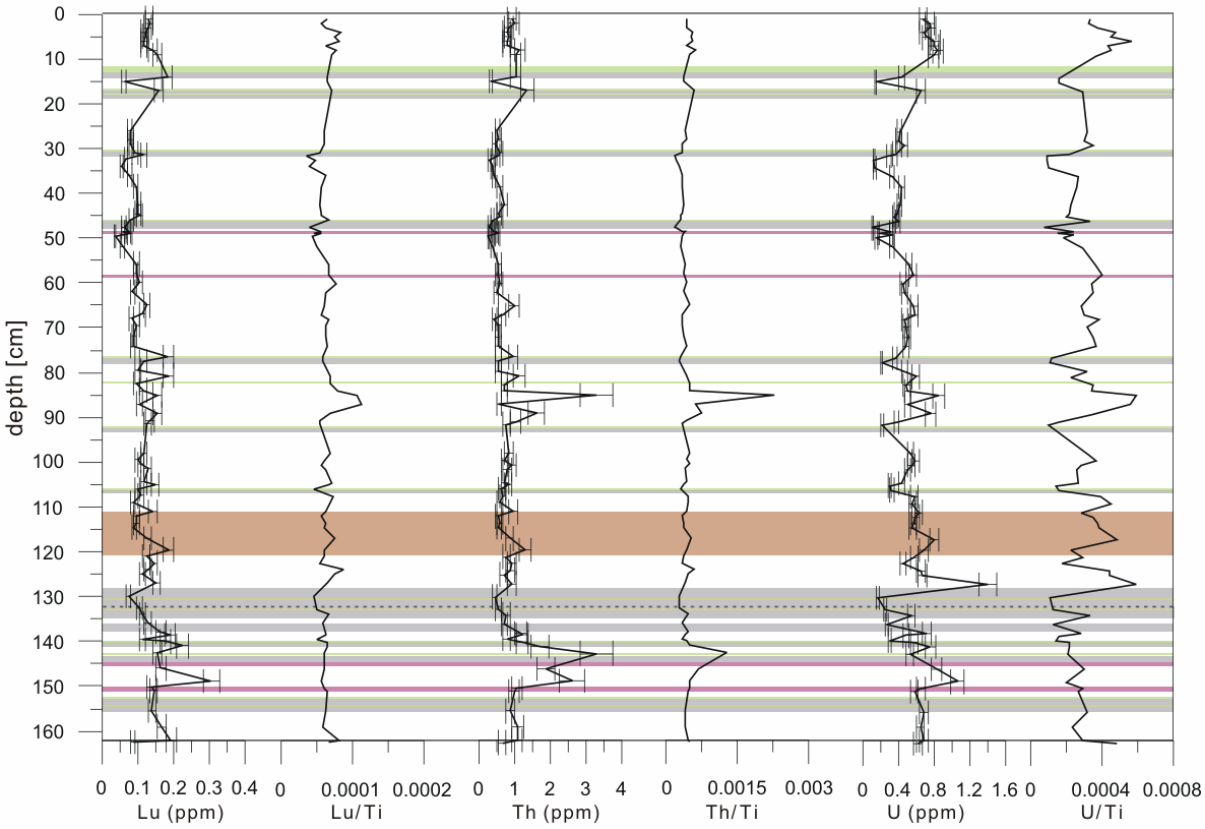

Fig. B-14: Concentration and Ti-normalized profiles of Lu, Th, and U for short core LCQ2s. Shaded and coloured bands indicate lithology, presented in Fig. IV-18.

AAS Analysis - Lago Villarrica

Sample	Depth (cm)	Cd (ppm)	Cr (ppm)	Cu (ppm)	Fe (ppm)	Mn (ppm)	Ni (ppm)	Pb (ppm)	Zn (ppm)	Ca (ppm)
LVR4s 2-3	3	0.176	14.3	71.7	42001	2381	9.7	7.20	50.9	8742
LVR4s 4-5	4	0.216	16.0	73.2	39296	1833	12.8	8.77	57.4	8815
LVR4s 5-6	5	0.203	12.7	72.1	47144	2436	10.1	7.75	50.9	8041
LVR4s 6-7	6	0.213	16.9	75.3	38290	1959	14.6	7.28	53.1	8721
LVR4s 9.4-9.8	9.8	0.066	25.4	162.8	28762	666	17.6	4.19	39.1	17573
LVR4s 9.8-10.5	10.5	0.049	22.6	152.1	26687	558	18.4	4.18	36.9	16288
LVR4s 13-14	14	0.150	16.6	80.1	28211	888	13.0	5.16	40.6	10586
LVR4s 14.7-15	15	0.087	18.9	80.1	21574	670	17.9	3.94	31.4	14476
LVR4s 15.7-17.5	17.5	0.095	14.6	64.8	20688	746	12.7	3.85	29.7	10237
LVR4s 17.5-18.5	18.5	0.122	17.3	74.9	24503	942	12.9	5.30	38.9	9734
LVR4s 18.5-19.5	19.5	0.152	18.0	88.5	27814	1049	16.6	7.24	45.1	10973
LVR4s 20.5-22	22	0.145	17.5	85.9	31150	1024	16.0	6.44	50.6	11420
LVR4s 22-25	25	0.141	19.8	106.5	28447	1086	15.1	7.56	47.5	12122
LVR4s 25.5-25.7	25.7	0.05	22.8	156.2	24805	547	20.0	5.46	48.0	15113
LVR4s 25.7-26	26	0.06	20.8	148.6	22835	507	17.6	4.75	44.1	12751
LVR4s 26-26.5	26.5	0.05	20.3	148.8	24974	487	14.6	5.21	47.1	16750
LVR4s 26.5-28.2	28.2	0.04	23.1	104.4	21336	414	18.6	4.01	40.3	12580
LVR4s 28.2-28.8	28.8	0.140	14.6	58.3	44487	1519	8.7	6.54	39.1	7549
LVR4s 29-30	30	0.160	16.8	67.7	26895	1063	14.0	7.34	47.8	8538
LVR4s 30-31	31	0.163	14.7	61.7	33180	1218	12.4	6.95	44.9	7874
LVR4s 31-31.5	31.5	0.193	15.7	58.9	30990	1743	13.7	7.61	49.1	7010
LVR4s 32-33	33	0.147	17.9	72.0	34148	1333	14.9	6.40	44.2	10316

Tab. B-20: Results of geochemical analysis (Cd to Ca) of gravity core LVR4s of Lago Villarrica; Elements were measured by atom adsorption spectrometry (AAS).

Sample	Depth (cm)	Cd (ppm)	Cr (ppm)	Cu (ppm)	Fe (ppm)	Mn (ppm)	Ni (ppm)	Pb (ppm)	Zn (ppm)	Ca (ppm)
LVR4s 34-35	35	0.217	13.8	72.3	31326	1167	14.5	5.77	42.6	8238
LVR4s 36.2-36.4	36.4	0.144	20.0	83.0	29826	977	15.6	5.29	41.8	12344
LVR4s 36.4-38.1	38.1	0.148	24.1	76.7	25649	869	18.7	4.37	43.9	11349
LVR4s 38.1-38.3	38.3	0.127	20.7	72.3	27383	862	14.4	4.39	34.1	9987
LVR4s 38.3-39.2	39.2	0.129	19.7	90.8	30146	1043	15.5	4.19	35.7	12041
LVR4s 39.2-39.6	39.6	0.094	21.9	84.4	30044	1086	16.5	4.01	36.1	15158
LVR4s 39.6-40.4	40.4	0.088	20.1	79.7	24530	693	16.4	3.27	34.3	15416
LVR4s 42-43	42	0.122	20.6	92.8	27294	810	17.3	4.95	41.2	14766
LVR4s 43.5-45	45	0.177	23.5	80.2	33680	1370	18.7	3.60	44.3	12397
LVR4s 45-46	46	0.152	21.6	85.6	32477	1155	21.2	4.15	46.0	13794
LVR4s 46.5-48	48	0.131	25.5	84.5	32689	1170	17.9	3.59	40.7	2370
LVR4s 48-49	49	0.118	22.1	94.1	35013	1380	18.1	4.35	42.7	13953
LVR4s 49-50	50	0.101	20.9	89.3	33415	789	15.6	4.09	45.1	13229
LVR4s 51-52	52	0.150	17.8	81.2	37125	1260	13.3	4.82	50.2	11200
LVR4s 52-53.5	53.5	0.140	17.1	77.3	29105	1772	13.3	4.40	41.6	11678
LVR4s 54-55	55	0.140	17.5	83.6	31907	838	14.5	4.48	45.4	11258
LVR4s 55-55.5	55.5	0.085	19.6	105.6	32024	599	10.9	5.24	42.4	10450
LVR4s 55.5-56.2	56.2	0.037	19.0	147.3	28175	590	14.8	3.72	37.8	16076
LVR4s 56.5-61.4	61.4	0.049	19.0	130.9	27912	641	14.0	3.70	39.2	13786
LVR4s 61.4-62	62	0.062	19.1	91.2	19668	375	17.2	2.35	28.4	14344
LVR4s 62-62.5	62.5	0.102	19.7	110.6	24058	657	17.2	3.68	36.7	14893
LVR4s 63-66	66	0.125	14.2	67.8	25213	1066	9.9	3.27	34.4	10707
LVR4s 67-68	68	0.134	13.5	73.3	30093	987	10.3	3.76	38.6	10691
LVR4s 68-69.5	69.5	0.158	15.5	72.5	25468	914	12.5	3.37	41.6	11536

Tab. B-20: Results of geochemical analysis (Cd to Ca) of gravity core LVR4s of Lago Villarrica; Elements were measured by atom adsorption spectrometry (AAS).

Sample	Depth (cm)	Cd (ppm)	Cr (ppm)	Cu (ppm)	Fe (ppm)	Mn (ppm)	Ni (ppm)	Pb (ppm)	Zn (ppm)	Ca (ppm)
LVR4s 70-71	71	0.137	16.9	72.5	25654	864	13.4	3.03	40.6	11789
LVR4s 71-72.5	72.5	0.128	16.4	70.7	28725	1530	11.7	2.93	36.8	11092
LVR4s 73-74	74	0.148	17.9	74.6	27911	755	12.3	3.37	42.4	11976
LVR4s 74-76	76	0.123	17.5	68.5	27955	1279	12.5	3.25	38.0	11505
LVR4s 76-77	77	0.137	17.8	71.3	26169	926	12.4	2.83	37.4	11210
LVR4s 77.5-79	79	0.149	16.2	69.0	27100	987	13.1	2.95	39.0	10538
LVR4s 79-80	80	0.147	14.7	67.7	30123	948	10.2	3.88	40.5	9912
LVR4s 81-82	82	0.136	13.6	78.3	24708	719	10.6	4.19	42.2	10495
LVR4s 82.2-83	83	0.051	13.3	74.1	18739	454	11.4	2.59	26.8	14192
LVR4s 83-84.5	84.5	0.066	14.4	72.4	27147	827	12.6	2.39	30.7	11809
LVR4s 84.5-85.5	85.5	0.167	15.3	69.4	31105	1156	8.8	3.90	43.1	8039
LVR4s 86-87	87	0.130	14.7	77.7	36221	1203	10.7	3.54	40.4	10773
LVR4s 87-88.5	88.5	0.134	16.7	83.5	31910	1085	11.2	3.70	43.6	9843
LVR4s 88.5-89.2	89.2	0.139	20.6	103.4	31068	1071	15.8	5.61	42.9	13430
LVR4s 89.2-90	90	0.153	15.8	98.0	29440	943	14.6	5.00	51.3	13445
LVR4s 90.5-91	91	0.142	17.0	69.0	28134	894	14.2	4.14	46.1	10310
LVR4s 91-92	92	0.134	17.0	72.1	31712	1120	13.6	3.77	41.1	10146
LVR4s 93-95	95	0.189	15.9	84.7	27902	2089	13.3	4.25	42.8	10893
LVR4s 95-95.8	95.8	0.105	17.3	108.4	26535	613	14.8	3.80	40.0	14642
LVR4s 96-98	98	0.086	15.1	77.2	30317	665	14.1	3.96	37.0	11835
LVR4s 98-99	99	0.133	16.3	85.1	25895	796	16.7	4.78	43.7	10274
LVR4s 99.5-101.5	101.5	0.088	16.9	69.5	31577	332	12.0	3.48	38.2	9079
LVR4s 101.5-102.5	102.5	0.137	19.0	77.3	27077	795	14.7	4.66	42.8	9764
LVR4s 103-103.5	103.5	0.124	16.7	66.9	24873	746	13.7	3.54	40.7	9848

Tab. B-20: Results of geochemical analysis (Cd to Ca) of gravity core LVR4s of Lago Villarrica; Elements were measured by atom adsorption spectrometry (AAS).

Sample	Depth (cm)	Cd (ppm)	Cr (ppm)	Cu (ppm)	Fe (ppm)	Mn (ppm)	Ni (ppm)	Pb (ppm)	Zn (ppm)	Ca (ppm)
LVR4s 104-105	105	0.118	13.9	61.3	33619	1138	8.1	3.72	37.4	8838
LVR4s 105-106	106	0.119	14.5	68.6	25638	743	9.5	3.81	39.0	10118
LVR4s 106-107	107	0.115	16.4	76.5	27391	991	10.6	3.34	38.9	10788
LVR4s 107.5-109	109	0.126	18.4	76.6	28957	984	12.3	3.25	39.2	11306
LVR4s 109-110	110	0.128	17.3	83.1	31386	1073	10.4	3.65	43.0	10978
LVR4s 111-111.5	111.5	0.107	18.1	74.3	28381	976	8.8	3.37	39.7	9897
LVR4s 112-113	113	0.119	16.0	70.5	28674	1052	8.8	3.59	39.9	8340
LVR4s 114-115	115	----	16.6	57.3	25776	780	10.7	3.56	36.6	8504

Tab. B-20: Results of geochemical analysis (Cd to Ca) of gravity core LVR4s of Lago Villarrica; Elements were measured by atom adsorption spectrometry (AAS).

AAS Analysis - Lago Villarrica

Sample	Depth (cm)	K (ppm)	Mg (ppm)	Na (ppm)
LVR4s 2-3	3	1380	5188	4403
LVR4s 4-5	4	1514	5282	4214
LVR4s 5-6	5	1177	4706	3750
LVR4s 6-7	6	1308	4899	4034
LVR4s 9.4-9.8	9.8	1123	6961	8648
LVR4s 9.8-10.5	10.5	956	6883	8031
LVR4s 13-14	14	1245	5139	5169
LVR4s 14.7-15	15	1303	5555	7298
LVR4s 15.7-17.5	17.5	1012	4539	4942
LVR4s 17.5-18.5	18.5	1174	5042	4718
LVR4s 18.5-19.5	19.5	1352	5738	5378
LVR4s 20.5-22	22	1321	6105	5398
LVR4s 22-25	25	1321	5831	5981
LVR4s 25.5-25.7	25.7	467	4623	5740
LVR4s 25.7-26	26	451	4289	4686
LVR4s 26-26.5	26.5	691	4709	6609
LVR4s 26.5-28.2	28.2	385	4527	4517
LVR4s 28.2-28.8	28.8	949	4298	3293
LVR4s 29-30	30	1248	4710	3957
LVR4s 30-31	31	1240	4433	3584
LVR4s 31-31.5	31.5	1362	4280	3146
LVR4s 32-33	33	1474	5380	5171
LVR4s 34-35	35	1298	4530	4123
LVR4s 36.2-36.4	36.4	1369	5592	6343
LVR4s 36.4-38.1	38.1	1395	5638	5854
LVR4s 38.1-38.3	38.3	1095	4536	4943
LVR4s 38.3-39.2	39.2	1432	5377	6418
LVR4s 39.2-39.6	39.6	1464	6242	7938
LVR4s 39.6-40.4	40.4	1339	6443	8157
LVR4s 42-43	42	1581	7117	7980
LVR4s 43.5-45	45	1226	5994	6302
LVR4s 45-46	46	1405	6829	6934
LVR4s 46.5-48	48	1419	6055	6656
LVR4s 48-49	49	1480	6891	7188
LVR4s 49-50	50	1400	6645	6478
LVR4s 51-52	52	1603	6261	5639

Tab. B-21: Results of geochemical analysis (K to Na) of gravity core LVR4s of Lago Villarrica; Elements were measured by atom adsorption spectrometry (AAS).

Sample	Depth (cm)	K (ppm)	Mg (ppm)	Na (ppm)
LVR4s 52-53.5	53.5	1343	5395	5974
LVR4s 54-55	55	1498	5897	5789
LVR4s 55-55.5	55.5	1605	5630	5355
LVR4s 55.5-56.2	56.2	1149	6544	8303
LVR4s 56.5-61.4	61.4	943	6047	6763
LVR4s 61.4-62	62	962	6451	6919
LVR4s 62-62.5	62.5	1351	6356	7851
LVR4s 63-66	66	1204	4967	5375
LVR4s 67-68	68	1280	5222	5469
LVR4s 68-69.5	69.5	1372	5442	5813
LVR4s 70-71	71	1304	5337	5754
LVR4s 71-72.5	72.5	1198	4986	5561
LVR4s 73-74	74	1394	5618	5927
LVR4s 74-76	76	1216	5033	5678
LVR4s 76-77	77	1151	4948	5554
LVR4s 77.5-79	79	1129	4690	5174
LVR4s 79-80	80	1264	5045	4853
LVR4s 81-82	82	1349	4841	5340
LVR4s 82.2-83	83	1345	5144	7389
LVR4s 83-84.5	84.5	874	5098	5791
LVR4s 84.5-85.5	85.5	1099	4228	3892
LVR4s 86-87	87	1253	5167	5412
LVR4s 87-88.5	88.5	1477	5303	5385
LVR4s 88.5-89.2	89.2	1451	6263	6898
LVR4s 89.2-90	90	1440	6162	6849
LVR4s 90.5-91	91	1416	5257	5222
LVR4s 91-92	92	1340	5198	5213
LVR4s 93-95	95	1445	5714	5867
LVR4s 95-95.8	95.8	1430	6352	7805
LVR4s 96-98	98	1199	6101	6265
LVR4s 98-99	99	1997	5401	6190
LVR4s 99.5-101.5	101.5	1357	4899	4810
LVR4s 101.5-102.5	102.5	1585	5210	5242
LVR4s 103-103.5	103.5	1358	5083	5169
LVR4s 104-105	105	1127	4703	4425
LVR4s 105-106	106	1461	5133	5882
LVR4s 106-107	107	1236	5187	5739
LVR4s 107.5-109	109	1228	5295	5800

Tab. B-21: Results of geochemical analysis (K to Na) of gravity core LVR4s of Lago Villarrica; Elements were measured by atom adsorption spectrometry (AAS).

Sample	Depth (cm)	K (ppm)	Mg (ppm)	Na (ppm)
LVR4s 109-110	110	1316	5442	6041
LVR4s 111-111.5	111.5	1298	4921	5551
LVR4s 112-113	113	1263	4728	4962
LVR4s 114-115	115	1189	4382	4154

Tab. B-21: Results of geochemical analysis (K to Na) of gravity core LVR4s of Lago Villarrica; Elements were measured by atom adsorption spectrometry (AAS).

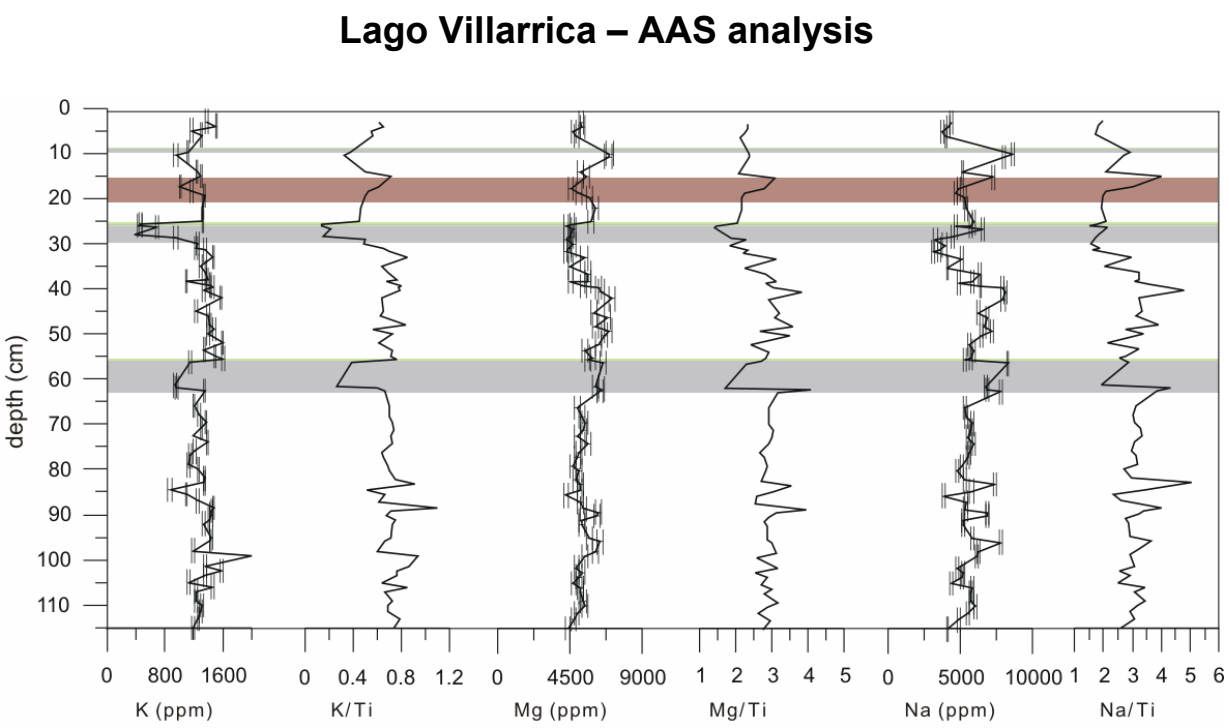

Fig. B-15: Concentration and Ti-normalized profiles of K, Mg, and Na for short core LVR4s. Shaded and coloured bands indicate lithology, presented in Fig. IV-32.

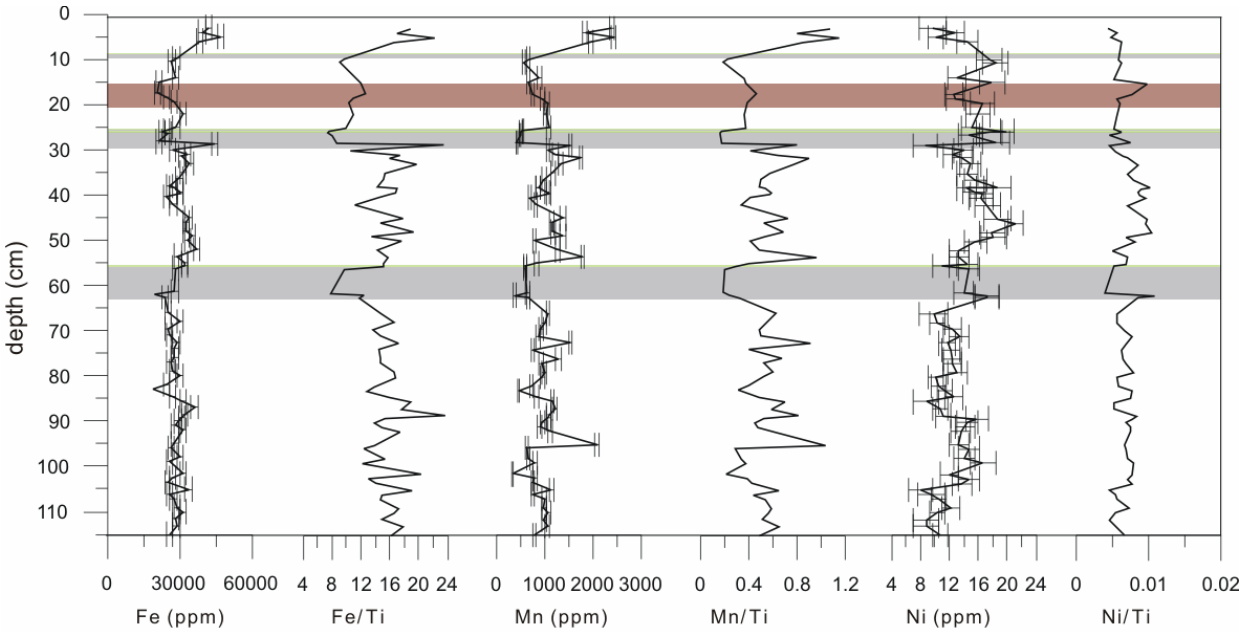

Fig. B-16: Concentration and Ti-normalized profiles of Fe, Mn, and Cu for short core LVR4s. Shaded and coloured bands indicate lithology, presented in Fig. IV-32.

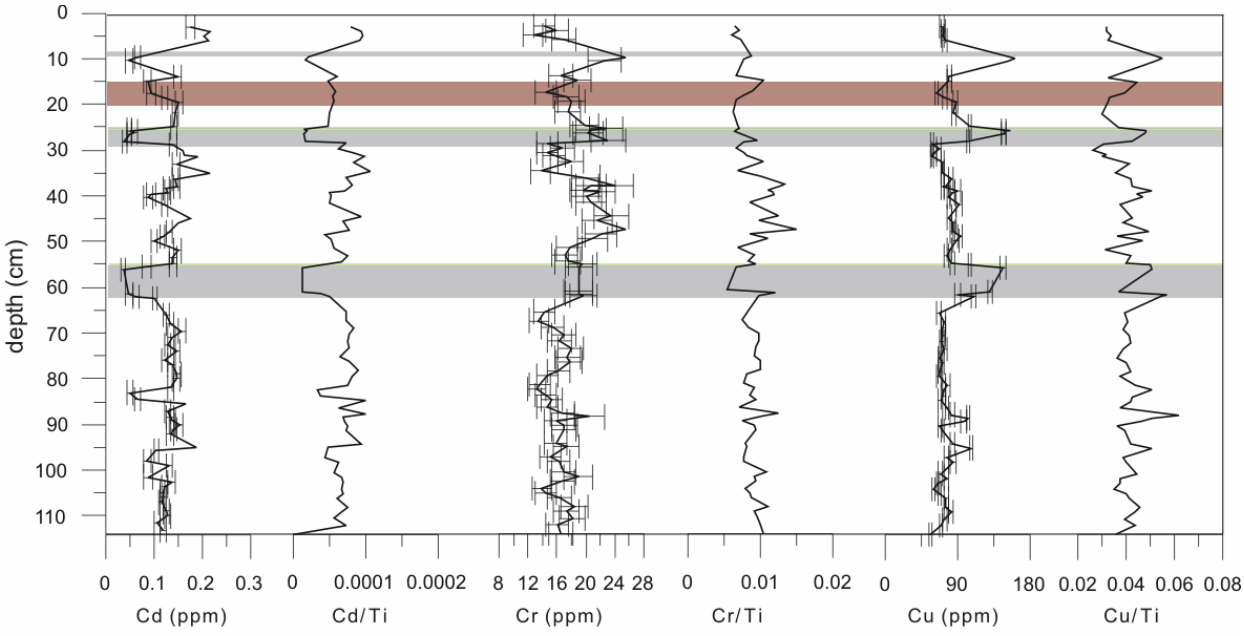

Fig. B-17: Concentration and Ti-normalized profiles of Cd, Cr, and Cu for short core LVR4s. Shaded and coloured bands indicate lithology, presented in Fig. IV-32.

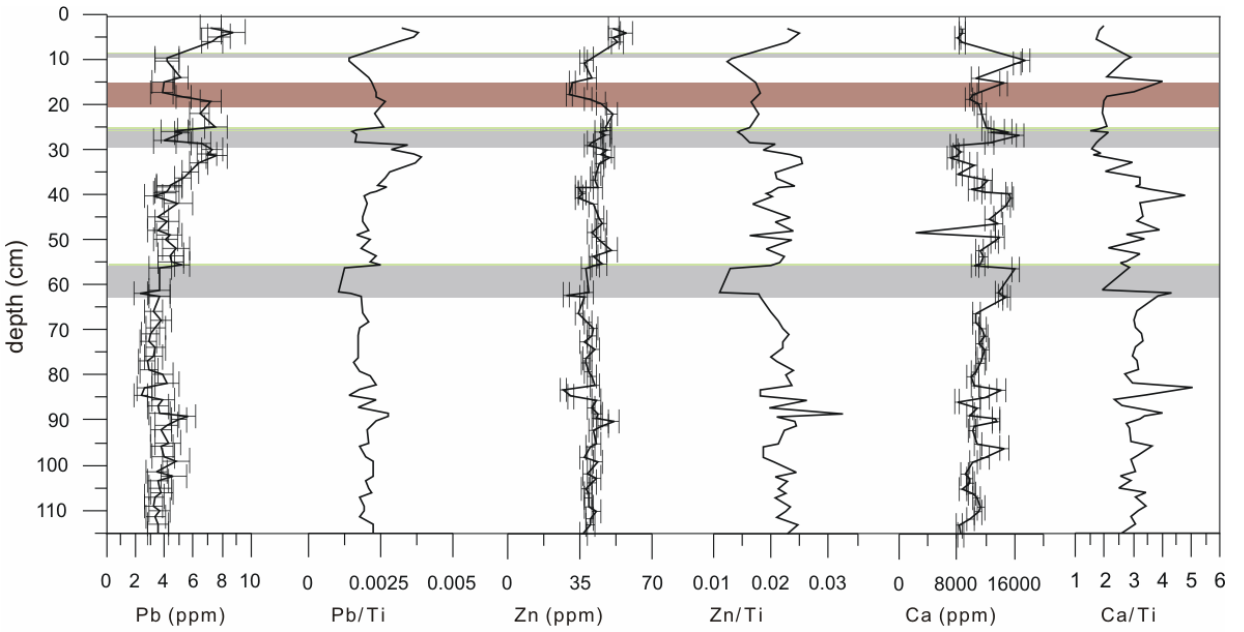

Fig. B-18: Concentration and Ti-normalized profiles of Pb, Zn, and Ca for short core LVR4s. Shaded and coloured bands indicate lithology, presented in Fig. IV-32.

ICP-MS Analysis - Lago Villarrica

Sample	Depth (cm)	^{45}Sc (ppm)	^{47}Ti (ppm)	^{59}Co (ppm)	^{85}Rb (ppm)	^{88}Sr (ppm)	^{90}Zr (ppm)	^{133}Cs (ppm)	^{135}Ba (ppm)	^{139}La (ppm)
LVR4s 2-3	3	6.0108	2222.2222	11.2506	5.0722	120.3744	12.4816	1.2653	139.2560	6.7768
LVR4s 4-5	4	6.7261	2300.5811	12.2161	6.0367	123.9567	17.6440	1.5954	149.7623	7.5608
LVR4s 5-6	5	5.9701	2123.5268	13.0292	4.6148	113.3784	5.6624	1.3084	113.9241	6.3117
LVR4s 6-7	6	6.4680	2311.9777	12.7451	5.4540	122.1588	14.8607	1.5487	124.1783	7.1671
LVR4s 9.4-9.8	9.8	6.9457	2952.7991	9.3043	2.4328	238.7486	11.3241	0.5683	99.6158	5.3005
LVR4s 9.8-10.5	10.5	6.1021	2939.3093	10.0635	2.0315	224.8603	11.1592	0.4968	83.9132	4.7753
LVR4s 13-14	14	6.1172	2481.5983	10.4666	4.4519	144.5846	15.0631	1.3486	99.4742	6.2592
LVR4s 14.7-15	15	4.9658	1808.2192	10.3781	3.8438	196.7123	10.1219	1.0971	98.3151	4.9192
LVR4s 15.7-17.5	17.5	4.2838	1630.0000	8.1388	3.6250	141.2500	9.0275	1.1308	80.8250	4.5463
LVR4s 17.5-18.5	18.5	5.1455	2248.8636	8.3795	4.1955	135.3409	10.1443	1.1943	92.8523	5.5364
LVR4s 18.5-19.5	19.5	6.0587	2697.1279	9.6723	4.8773	154.5692	13.0444	1.3747	106.5535	6.5574
LVR4s 20.5-22	22	6.0820	2827.0424	12.1342	4.9108	158.9969	13.2368	1.3663	101.1763	6.7955
LVR4s 22-25	25	7.1151	2900.7937	13.0370	4.5860	165.7407	16.2566	1.2015	112.8439	6.7063
LVR4s 25.5-25.7	25.7	7.1901	3221.3684	12.2744	2.4021	193.2325	12.6549	0.6282	92.6128	5.1289
LVR4s 25.7-26	26	6.5267	3097.3257	12.7576	1.8457	166.9224	11.6616	0.5066	75.7014	4.5846
LVR4s 26-26.5	26.5	7.4087	3128.1281	11.0836	3.2570	221.9720	14.1266	0.7902	110.9234	5.0050
LVR4s 26.5-28.2	28.2	4.6866	2446.5090	10.1633	2.0242	170.5143	9.8442	0.5184	65.4842	3.7200
LVR4s 28.2-28.8	28.8	5.5188	1889.4472	8.0854	4.0603	104.6357	13.4925	1.1361	80.3518	5.6193
LVR4s 29-30	30	6.1799	2568.2382	9.9591	5.5012	124.5658	17.2829	1.4553	114.0571	7.0707
LVR4s 30-31	31	5.5902	1913.7750	9.9132	5.3063	109.5952	14.7345	1.3670	98.7513	6.4235
LVR4s 31-31.5	31.5	6.3650	1945.0317	11.9794	6.2645	98.0708	11.9173	1.6517	115.6184	6.8023
LVR4s 32-33	33	5.8969	1736.1822	8.9688	4.9156	141.5046	9.4844	1.2588	123.0169	6.3485

Tab. B-22: Results of geochemical analysis (^{45}Sc to ^{139}La) of gravity core LVR4s of Lago Villarrica; Elements were measured by inductive coupled plasma mass spectrometry (ICP-MS).

Sample	Depth (cm)	^{45}Sc (ppm)	^{47}Ti (ppm)	^{59}Co (ppm)	^{85}Rb (ppm)	^{88}Sr (ppm)	^{90}Zr (ppm)	^{133}Cs (ppm)	^{135}Ba (ppm)	^{139}La (ppm)
LVR4s 34-35	35	6.1257	2035.3107	13.1709	5.1215	116.1299	15.1412	1.3322	121.5537	7.1511
LVR4s 36.2-36.4	36.4	5.8366	1976.8084	12.8700	4.2725	171.4522	10.7717	1.0592	133.6002	5.6184
LVR4s 36.4-38.1	38.1	5.1762	1809.5123	9.4411	4.4845	155.1183	10.3030	1.0878	125.5432	5.5070
LVR4s 38.1-38.3	38.3	4.4797	1603.1545	8.1128	3.3031	131.9616	10.0707	0.8281	97.4801	4.5286
LVR4s 38.3-39.2	39.2	5.3945	1788.4828	8.9922	3.8192	163.0676	10.9759	0.9363	109.6484	5.7184
LVR4s 39.2-39.6	39.6	5.4699	1887.3168	8.7784	3.7822	206.7964	9.8914	0.8642	124.5831	4.6299
LVR4s 39.6-40.4	40.4	4.4524	1698.0519	9.3571	3.3344	210.3896	8.2695	0.7581	106.2987	4.1212
LVR4s 42-43	42	5.2832	2453.5935	10.9674	4.3384	207.2822	11.2744	0.9548	130.4141	5.7532
LVR4s 43.5-45	45	5.0874	1889.4602	11.1967	3.5398	165.5527	11.1594	0.8661	95.9769	4.4987
LVR4s 45-46	46	5.7573	2219.0020	11.3735	4.3838	186.4919	12.0161	1.0696	106.3130	5.8682
LVR4s 46.5-48	48	5.2713	1699.6744	9.5795	3.6720	168.7466	9.2390	0.8581	102.2518	4.3190
LVR4s 48-49	49	5.9838	2604.8118	11.5210	4.4986	192.5917	11.2351	1.0428	123.5112	5.0655
LVR4s 49-50	50	6.0952	1907.7880	10.1379	4.5646	178.6101	10.5462	1.0823	120.5246	5.2826
LVR4s 51-52	52	6.1419	2609.3156	11.8453	5.7391	154.8241	14.5318	1.3070	124.0494	6.0361
LVR4s 52-53.5	53.5	5.2539	1854.1280	13.3581	4.3588	162.8015	12.2565	1.0296	109.1721	5.0615
LVR4s 54-55	55	6.1937	2099.0688	9.9651	3.4571	212.7522	13.9550	0.7340	114.0973	4.6107
LVR4s 55-55.5	55.5	6.6465	2106.2020	10.6957	5.3965	144.7585	16.8496	2.5851	125.0686	23.2162
LVR4s 55.5-56.2	56.2	7.0939	2896.1809	11.8415	2.6844	203.0290	11.2599	0.5752	113.2572	5.6124
LVR4s 56.5-61.4	61.4	6.5284	3540.1096	10.7536	2.2210	185.6004	15.1221	0.7748	95.8645	4.6849
LVR4s 61.4-62	62	4.1297	1594.3442	8.0570	2.1404	189.7855	8.2960	0.4422	79.1931	3.0059
LVR4s 62-62.5	62.5	5.4575	2028.9318	10.1644	4.7020	150.9644	14.2186	1.1052	115.4921	5.9619
LVR4s 63-66	66	4.4540	1718.3908	9.2678	3.6828	145.0575	10.6575	1.0810	87.4253	4.6977
LVR4s 67-68	68	4.9270	1806.0366	8.6108	4.0735	147.5755	11.9186	0.9485	99.4310	5.3414
LVR4s 68-69.5	69.5	4.9919	1878.7808	9.0007	4.4300	159.6091	12.5407	1.0605	108.4225	5.4816

Tab. B-22: Results of geochemical analysis (^{45}Sc to ^{139}La) of gravity core LVR4s of Lago Villarrica; Elements were measured by inductive coupled plasma mass spectrometry (ICP-MS).

Sample	Depth (cm)	^{45}Sc (ppm)	^{47}Ti (ppm)	^{59}Co (ppm)	^{85}Rb (ppm)	^{88}Sr (ppm)	^{90}Zr (ppm)	^{133}Cs (ppm)	^{135}Ba (ppm)	^{139}La (ppm)
LVR4s 70-71	71	4.8329	1753.4247	9.1260	4.1329	157.3973	11.0425	1.0299	102.6986	5.0890
LVR4s 71-72.5	72.5	4.6318	1672.4138	11.3793	3.5012	147.1675	10.3190	0.8287	88.5591	4.2278
LVR4s 73-74	74	5.0889	1926.4943	9.6177	4.3646	158.3199	12.1661	1.0183	108.3603	5.0633
LVR4s 74-76	76	4.8064	1897.7030	11.6653	3.7019	153.4455	12.1541	0.8741	93.2158	4.2788
LVR4s 76-77	77	5.2092	1775.3984	8.9504	3.5869	148.2819	7.7664	0.9155	101.4816	4.4696
LVR4s 77.5-79	79	4.9752	1635.6185	9.4349	3.6115	138.2265	9.1580	0.9744	94.4486	4.3145
LVR4s 79-80	80	4.9781	1801.1667	8.7579	4.5941	135.6344	10.4096	1.2076	108.9694	5.2613
LVR4s 81-82	82	4.9756	1786.7611	7.5843	4.3796	141.6707	11.6720	1.0752	109.8192	4.9365
LVR4s 82.2-83	83	3.9116	1467.3087	8.3426	3.3186	187.0248	7.4316	0.7917	99.6199	3.4339
LVR4s 83-84.5	84.5	3.6692	1692.9995	8.9195	2.4392	159.2124	9.0982	0.6545	75.0851	3.2110
LVR4s 84.5-85.5	85.5	4.9122	1648.1207	8.7562	4.0418	109.3225	10.6677	1.1950	107.6039	4.8417
LVR4s 86-87	87	5.0994	2056.4837	9.7633	3.8962	109.6261	13.0390	1.0177	104.9324	4.9841
LVR4s 87-88.5	88.5	5.0128	1343.6968	10.1555	4.2462	132.5596	3.6190	0.9656	107.4319	4.8041
LVR4s 88.5-89.2	89.2	6.1780	2028.0980	10.1777	4.4104	181.7963	11.2068	1.0790	143.8521	5.0624
LVR4s 89.2-90	90	6.0744	2125.3264	11.5183	4.5535	177.9373	13.3420	1.0858	141.7755	5.3460
LVR4s 90.5-91	91	4.9710	1887.7551	9.4884	4.9545	137.1760	10.6343	1.0993	104.7435	5.1696
LVR4s 91-92	92	4.8894	1829.5292	9.2630	4.2737	134.9263	5.3840	1.0078	105.2901	4.8229
LVR4s 93-95	95	5.2198	2010.8195	15.6768	4.3865	148.0203	12.1202	0.9625	113.9157	5.2785
LVR4s 95-95.8	95.8	5.3349	2145.9611	8.5647	3.7947	194.5297	11.5976	0.8073	118.4560	4.8671
LVR4s 96-98	98	4.7378	1970.6759	8.9277	3.7438	163.6431	11.1282	0.8755	97.5149	4.5042
LVR4s 98-99	99	5.5869	2122.0330	10.1174	5.5160	148.7358	13.6481	1.4164	119.1692	5.6450
LVR4s 99.5-101.5	101.5	4.8027	1558.4416	6.1538	4.4855	116.9206	9.4918	1.1552	93.1444	4.5654
LVR4s 101.5-102.5	102.5	5.4403	2063.5942	10.1699	5.8509	142.2503	13.2853	1.2383	116.0530	5.8007
LVR4s 103-103.5	103.5	4.7993	1778.2882	8.5348	4.7776	131.8907	13.1044	1.0791	103.3245	5.1971

Tab. B-22: Results of geochemical analysis (^{45}Sc to ^{139}La) of gravity core LVR4s of Lago Villarrica; Elements were measured by inductive coupled plasma mass spectrometry (ICP-MS).

Sample	Depth (cm)	^{45}Sc (ppm)	^{47}Ti (ppm)	^{59}Co (ppm)	^{85}Rb (ppm)	^{88}Sr (ppm)	^{90}Zr (ppm)	^{133}Cs (ppm)	^{135}Ba (ppm)	^{139}La (ppm)
LVR4s 104-105	105	4.6822	1758.5551	8.4845	4.2653	119.0386	9.7148	0.9871	93.4818	4.5750
LVR4s 105-106	106	4.7160	1717.4549	8.1680	4.6270	136.1531	10.7752	1.0455	102.2306	4.9842
LVR4s 106-107	107	4.8913	1864.7343	10.2729	3.9855	143.1159	10.6920	0.9516	102.6449	4.6703
LVR4s 107.5-109	109	4.6402	1674.8527	8.1262	3.6690	116.7608	10.6201	0.9129	95.9479	4.0803
LVR4s 109-110	110	4.9555	1901.2865	10.3773	4.1131	149.1836	11.7256	0.9567	97.2909	4.5621
LVR4s 111-111.5	111.5	5.4504	1893.1298	9.6807	4.1196	146.1832	11.0102	0.9427	109.3639	4.7341
LVR4s 112-113	113	5.2209	1609.7884	9.6534	3.7116	130.0529	9.9669	0.9108	104.5370	4.2487
LVR4s 114-115	115	4.4739	1597.1475	8.5414	4.2653	113.2535	7.0950	1.0393	96.2460	4.4349

Tab. B-22: Results of geochemical analysis (^{45}Sc to ^{139}La) of gravity core LVR4s of Lago Villarrica; Elements were measured by inductive coupled plasma mass spectrometry (ICP-MS).

ICP-MS Analysis - Lago Villarrica

Sample	Depth (cm)	^{140}Ce (ppm)	^{141}Pr (ppm)	^{146}Nd (ppm)	^{149}Sm (ppm)	^{151}Eu (ppm)	^{159}Tb (ppm)	^{160}Gd (ppm)	^{163}Dy (ppm)	^{165}Ho (ppm)
LVR4s 2-3	3	13.6686	1.8710	7.7435	1.7230	0.4235	0.2826	1.8062	1.6875	0.3573
LVR4s 4-5	4	15.2668	2.0853	8.5922	1.9387	0.4778	0.3118	1.9783	1.8806	0.3967
LVR4s 5-6	5	12.5818	1.7634	7.2774	1.6467	0.4143	0.2719	1.7307	1.6445	0.3484
LVR4s 6-7	6	14.1922	1.9708	8.1170	1.8482	0.4604	0.2996	1.9053	1.8148	0.3831
LVR4s 9.4-9.8	9.8	11.2184	1.5615	6.7741	1.6548	0.4796	0.2870	1.7755	1.7495	0.3702
LVR4s 9.8-10.5	10.5	10.1866	1.3916	6.0170	1.4830	0.4336	0.2565	1.5668	1.5439	0.3324
LVR4s 13-14	14	12.5591	1.7258	7.2805	1.7008	0.4406	0.2773	1.7639	1.6562	0.3508
LVR4s 14.7-15	15	9.6342	1.3286	5.5753	1.3055	0.3660	0.2184	1.3575	1.2785	0.2737
LVR4s 15.7-17.5	17.5	8.8100	1.2141	5.0950	1.1870	0.3179	0.1910	1.2071	1.1446	0.2448
LVR4s 17.5-18.5	18.5	11.0659	1.5364	6.4420	1.4886	0.3876	0.2442	1.5455	1.4455	0.3089

Tab. B-23: Results of geochemical analysis (^{140}Ce to ^{165}Ho) of gravity core LVR4s of Lago Villarrica; Elements were measured by inductive coupled plasma mass spectrometry (ICP-MS).

Sample	Depth (cm)	^{140}Ce (ppm)	^{141}Pr (ppm)	^{146}Nd (ppm)	^{149}Sm (ppm)	^{151}Eu (ppm)	^{159}Tb (ppm)	^{160}Gd (ppm)	^{163}Dy (ppm)	^{165}Ho (ppm)
LVR4s 18.5-19.5	19.5	13.1070	1.8146	7.6423	1.7546	0.4570	0.2863	1.8211	1.7010	0.3615
LVR4s 20.5-22	22	13.4566	1.8601	7.7934	1.8033	0.4629	0.2916	1.8537	1.7154	0.3643
LVR4s 22-25	25	14.0873	1.9272	8.1706	1.9246	0.5243	0.3255	2.0251	1.9140	0.4104
LVR4s 25.5-25.7	25.7	13.0020	1.8133	8.0801	1.9782	0.5616	0.3532	2.1133	2.0749	0.4114
LVR4s 25.7-26	26	11.6506	1.6078	7.2096	1.7832	0.5099	0.3141	1.9224	1.8775	0.3752
LVR4s 26-26.5	26.5	12.4049	1.7480	7.7127	1.9507	0.5389	0.3296	1.9845	1.9795	0.3864
LVR4s 26.5-28.2	28.2	9.1629	1.2387	5.4655	1.2969	0.3631	0.2278	1.3992	1.3316	0.2669
LVR4s 28.2-28.8	28.8	11.0490	1.5101	6.2802	1.4711	0.3751	0.2361	1.4962	1.4020	0.3003
LVR4s 29-30	30	14.5533	1.9690	8.1551	1.8660	0.4753	0.3036	1.9107	1.8065	0.3820
LVR4s 30-31	31	12.7603	1.7455	7.2792	1.6562	0.4180	0.2666	1.7074	1.5957	0.3417
LVR4s 31-31.5	31.5	14.3235	1.8803	7.7193	2.0336	0.4536	0.2964	1.7772	1.6530	0.3721
LVR4s 32-33	33	12.6958	1.7605	7.2441	1.9294	0.4191	0.2700	1.6876	1.5827	0.3417
LVR4s 34-35	35	14.3644	1.9605	8.0127	1.8079	0.4360	0.2953	1.8997	1.7740	0.3791
LVR4s 36.2-36.4	36.4	12.4531	1.7104	7.1231	1.8788	0.4183	0.2592	1.6441	1.5461	0.3295
LVR4s 36.4-38.1	38.1	11.9676	1.6647	6.8300	1.8035	0.3864	0.2488	1.5874	1.4643	0.3143
LVR4s 38.1-38.3	38.3	9.5631	1.3339	5.4405	1.4623	0.3173	0.2016	1.2933	1.1885	0.2498
LVR4s 38.3-39.2	39.2	10.9787	1.5545	6.4369	1.4729	0.3887	0.2434	1.5421	1.4563	0.3073
LVR4s 39.2-39.6	39.6	10.1124	1.4237	5.9272	1.6081	0.3837	0.2305	1.4477	1.3732	0.2869
LVR4s 39.6-40.4	40.4	9.0400	1.2706	5.2543	1.4102	0.3461	0.2004	1.2706	1.1851	0.2498
LVR4s 42-43	42	12.6606	1.7527	7.2632	1.8896	0.4108	0.2588	1.6635	1.5326	0.3254
LVR4s 43.5-45	45	9.7506	1.4036	5.9344	1.5784	0.3661	0.2220	1.4229	1.3483	0.2892
LVR4s 45-46	46	11.5083	1.6293	6.7981	1.5738	0.4163	0.2596	1.6444	1.5512	0.3289
LVR4s 46.5-48	48	9.2363	1.3536	5.7664	1.5220	0.3591	0.2189	1.3809	1.3226	0.2854
LVR4s 48-49	49	11.1315	1.5889	6.7115	1.8068	0.4212	0.2530	1.6210	1.5305	0.3287

Tab. B-23: Results of geochemical analysis (^{140}Ce to ^{165}Ho) of gravity core LVR4s of Lago Villarrica; Elements were measured by inductive coupled plasma mass spectrometry (ICP-MS).

Sample	Depth (cm)	^{140}Ce (ppm)	^{141}Pr (ppm)	^{146}Nd (ppm)	^{149}Sm (ppm)	^{151}Eu (ppm)	^{159}Tb (ppm)	^{160}Gd (ppm)	^{163}Dy (ppm)	^{165}Ho (ppm)
LVR4s 49-50	50	11.4048	1.6658	7.0849	1.8821	0.4281	0.2633	1.6779	1.6063	0.3441
LVR4s 51-52	52	13.4268	1.8809	7.8505	2.0639	0.4449	0.2845	1.8192	1.7182	0.3666
LVR4s 52-53.5	53.5	12.3493	1.5816	6.6257	1.7289	0.3888	0.2404	1.5399	1.4552	0.3087
LVR4s 54-55	55	10.6958	1.5184	6.5210	1.7680	0.4349	0.2553	1.5908	1.5416	0.3277
LVR4s 55-55.5	55.5	13.5140	1.8880	7.9185	2.0993	0.4687	0.2958	1.8702	1.7824	0.3813
LVR4s 55.5-56.2	56.2	11.6769	1.6341	7.1104	1.7702	0.5140	0.2999	1.8624	1.7823	0.3761
LVR4s 56.5-61.4	61.4	11.5272	1.5708	6.7850	1.9096	0.4643	0.2773	1.7215	1.6779	0.3610
LVR4s 61.4-62	62	7.0222	0.9951	4.2040	1.1358	0.2890	0.1647	1.0317	1.0048	0.2151
LVR4s 62-62.5	62.5	13.3408	1.8311	7.5210	1.9461	0.4091	0.2681	1.6976	1.6197	0.3436
LVR4s 63-66	66	10.5644	1.4529	6.0184	1.5310	0.3346	0.2120	1.3736	1.2805	0.2744
LVR4s 67-68	68	11.9174	1.6724	6.8926	1.7429	0.3783	0.2474	1.5685	1.4918	0.3180
LVR4s 68-69.5	69.5	12.5291	1.7078	7.1045	1.8195	0.3904	0.2512	1.6217	1.5100	0.3282
LVR4s 70-71	71	11.1123	1.5575	6.4562	1.6712	0.3726	0.2364	1.5014	1.4205	0.3027
LVR4s 71-72.5	72.5	9.6416	1.3387	5.6195	1.4852	0.3360	0.2076	1.3288	1.2562	0.2712
LVR4s 73-74	74	11.3382	1.5913	6.6559	1.7569	0.3870	0.2484	1.6007	1.5118	0.3247
LVR4s 74-76	76	9.4084	1.3662	5.6944	1.4944	0.3439	0.2127	1.3435	1.2902	0.2752
LVR4s 76-77	77	9.8581	1.4131	5.8616	1.5513	0.3550	0.2186	1.3882	1.3247	0.2841
LVR4s 77.5-79	79	9.5392	1.3748	5.7501	1.5400	0.3489	0.2178	1.3686	1.3189	0.2822
LVR4s 79-80	80	11.5216	1.6274	6.7064	1.7538	0.3791	0.2426	1.5386	1.4657	0.3149
LVR4s 81-82	82	10.9416	1.5388	6.4240	1.6939	0.3723	0.2330	1.4924	1.4021	0.3031
LVR4s 82.2-83	83	7.8016	1.0854	4.5819	1.2149	0.2980	0.1719	1.0834	1.0536	0.2225
LVR4s 83-84.5	84.5	7.1791	1.0220	4.3012	1.1746	0.2790	0.1648	1.0564	0.9854	0.2128
LVR4s 84.5-85.5	85.5	10.5341	1.4985	6.2871	1.6667	0.3645	0.2360	1.4936	1.4243	0.3065
LVR4s 86-87	87	11.0561	1.5579	6.5274	1.7257	0.3775	0.2377	1.5380	1.4336	0.3039

Tab. B-23: Results of geochemical analysis (^{140}Ce to ^{165}Ho) of gravity core LVR4s of Lago Villarrica; Elements were measured by inductive coupled plasma mass spectrometry (ICP-MS).

Sample	Depth (cm)	^{140}Ce (ppm)	^{141}Pr (ppm)	^{146}Nd (ppm)	^{149}Sm (ppm)	^{151}Eu (ppm)	^{159}Tb (ppm)	^{160}Gd (ppm)	^{163}Dy (ppm)	^{165}Ho (ppm)
LVR4s 87-88.5	88.5	10.7432	1.5226	6.3905	1.7036	0.3721	0.2412	1.5109	1.4427	0.3070
LVR4s 88.5-89.2	89.2	11.4433	1.6306	6.9524	1.8840	0.4515	0.2729	1.7171	1.6535	0.3569
LVR4s 89.2-90	90	11.9556	1.6997	7.2258	1.9321	0.4573	0.2799	1.7572	1.6893	0.3683
LVR4s 90.5-91	91	11.5582	1.6133	6.7705	1.7871	0.3908	0.2478	1.5761	1.5017	0.3245
LVR4s 91-92	92	10.8369	1.5228	6.4170	1.6893	0.3673	0.2336	1.5086	1.3944	0.3035
LVR4s 93-95	95	12.3158	1.6701	7.0051	1.8393	0.4000	0.2576	1.6218	1.5424	0.3292
LVR4s 95-95.8	95.8	11.1529	1.5746	6.7293	1.7868	0.4201	0.2519	1.5785	1.5158	0.3227
LVR4s 96-98	98	10.0845	1.4227	5.9667	1.5880	0.3565	0.2187	1.4103	1.3233	0.2835
LVR4s 98-99	99	12.7232	1.7699	7.3800	1.9621	0.4278	0.2673	1.7028	1.6086	0.3464
LVR4s 99.5-101.5	101.5	9.7827	1.4323	5.9865	1.5997	0.3513	0.2197	1.3886	1.3187	0.2827
LVR4s 101.5-102.5	102.5	13.1050	1.8100	7.5451	1.9683	0.4293	0.2718	1.7212	1.6233	0.3471
LVR4s 103-103.5	103.5	11.6526	1.6175	6.7070	1.7493	0.3768	0.2360	1.5256	1.4241	0.3034
LVR4s 104-105	105	10.1602	1.4272	5.9845	1.5752	0.3460	0.2146	1.3688	1.2883	0.2808
LVR4s 105-106	106	11.1580	1.5687	6.5200	1.7016	0.3718	0.2354	1.5041	1.4078	0.3031
LVR4s 106-107	107	10.4457	1.4783	6.1582	1.6341	0.3649	0.2284	1.4650	1.3708	0.2943
LVR4s 107.5-109	109	9.0766	1.2979	5.4666	1.4833	0.3336	0.2100	1.3372	1.2635	0.2757
LVR4s 109-110	110	10.2808	1.4510	6.0935	1.6341	0.3683	0.2276	1.4547	1.3830	0.2971
LVR4s 111-111.5	111.5	10.5891	1.5153	6.3830	1.7214	0.3866	0.2420	1.5382	1.4695	0.3156
LVR4s 112-113	113	9.4537	1.3611	5.8148	1.5569	0.3578	0.2253	1.3942	1.3519	0.2888
LVR4s 114-115	115	9.8237	1.3940	5.7495	1.5151	0.3372	0.2092	1.3384	1.2783	0.2744

Tab. B-23: Results of geochemical analysis (^{140}Ce to ^{165}Ho) of gravity core LVR4s of Lago Villarrica; Elements were measured by inductive coupled plasma mass spectrometry (ICP-MS).

ICP-MS Analysis - Lago Villarrica

Sample	Depth (cm)	^{166}Er (ppm)	^{169}Tm (ppm)	^{172}Yb (ppm)	^{175}Lu (ppm)	^{232}Th (ppm)	^{238}U (ppm)
LVR4s 2-3	3	0.9853	0.1493	0.9217	0.1427	1.3179	1.2531
LVR4s 4-5	4	1.0866	0.1644	1.0330	0.1570	1.7657	1.6337
LVR4s 5-6	5	0.9527	0.1436	0.9015	0.1388	1.1261	1.4666
LVR4s 6-7	6	1.0511	0.1584	0.9909	0.1552	1.3558	1.5655
LVR4s 9.4-9.8	9.8	1.0309	0.1542	0.9654	0.1498	0.8441	0.3714
LVR4s 9.8-10.5	10.5	0.9078	0.1356	0.8474	0.1290	0.7520	0.3240
LVR4s 13-14	14	0.9670	0.1450	0.8970	0.1395	1.0903	1.1987
LVR4s 14.7-15	15	0.7466	0.1112	0.6973	0.1075	0.8078	0.6381
LVR4s 15.7-17.5	17.5	0.6695	0.0986	0.6166	0.0958	0.8120	0.7265
LVR4s 17.5-18.5	18.5	0.8498	0.1277	0.7777	0.1205	1.0351	1.0623
LVR4s 18.5-19.5	19.5	0.9937	0.1492	0.9124	0.1402	1.1561	1.2465
LVR4s 20.5-22	22	1.0084	0.1479	0.9219	0.1428	1.2104	1.2965
LVR4s 22-25	25	1.1349	0.1675	1.0413	0.1574	1.2444	1.0721
LVR4s 25.5-25.7	25.7	1.1808	0.1808	1.1153	0.1673	0.8534	0.5299
LVR4s 25.7-26	26	1.1377	0.1685	1.0567	0.1550	0.7286	0.4564
LVR4s 26-26.5	26.5	1.1112	0.1660	1.0747	0.1584	0.8929	0.5459
LVR4s 26.5-28.2	28.2	0.7881	0.1178	0.7125	0.1070	0.6414	0.4366
LVR4s 28.2-28.8	28.8	0.8163	0.1235	0.7572	0.1182	1.0899	1.2676
LVR4s 29-30	30	1.0499	0.1598	0.9702	0.1517	1.4194	1.5571
LVR4s 30-31	31	0.9330	0.1377	0.8686	0.1341	1.2202	1.3736
LVR4s 31-31.5	31.5	0.9839	0.1648	0.9049	0.1587	3.8980	1.7442
LVR4s 32-33	33	0.9199	0.1409	0.8470	0.1337	1.7925	1.3204
LVR4s 34-35	35	1.0362	0.1566	0.9904	0.1523	1.4153	1.3562
LVR4s 36.2-36.4	36.4	0.9089	0.1354	0.8370	0.1317	1.3240	1.0843
LVR4s 36.4-38.1	38.1	0.8615	0.1304	0.7898	0.1212	1.1307	1.1529
LVR4s 38.1-38.3	38.3	0.6960	0.1048	0.6374	0.0988	0.9482	1.0934
LVR4s 38.3-39.2	39.2	0.8401	0.1269	0.7818	0.1239	0.9203	1.0363
LVR4s 39.2-39.6	39.6	0.7863	0.1196	0.7273	0.1137	0.8729	0.8487
LVR4s 39.6-40.4	40.4	0.6855	0.1028	0.6311	0.0965	0.7653	0.6680
LVR4s 42-43	42	0.8968	0.1324	0.8222	0.1258	1.0137	0.8853
LVR4s 43.5-45	45	0.8018	0.1189	0.7307	0.1141	0.8121	1.1716
LVR4s 45-46	46	0.9041	0.1352	0.8340	0.1324	1.0050	1.1187
LVR4s 46.5-48	48	0.7724	0.1149	0.7286	0.1157	0.8212	0.9699
LVR4s 48-49	49	0.9013	0.1339	0.8405	0.1314	1.0343	0.9946
LVR4s 49-50	50	0.9390	0.1395	0.8675	0.1347	1.0461	1.0548

Tab. B-24: Results of geochemical analysis (^{166}Er to ^{238}U) of gravity core LVR4s of Lago Villarrica; Elements were measured by inductive coupled plasma mass spectrometry (ICP-MS).

Sample	Depth (cm)	^{166}Er (ppm)	^{169}Tm (ppm)	^{172}Yb (ppm)	^{175}Lu (ppm)	^{232}Th (ppm)	^{238}U (ppm)
LVR4s 51-52	52	1.0048	0.1497	0.9234	0.1454	1.3272	1.3260
LVR4s 52-53.5	53.5	0.8445	0.1270	0.7817	0.1234	1.0308	1.1572
LVR4s 54-55	55	0.9018	0.1349	0.8460	0.1302	0.8416	0.7796
LVR4s 55-55.5	55.5	1.0456	0.1550	0.9554	0.1509	1.2947	1.2121
LVR4s 55.5-56.2	56.2	1.0583	0.1580	0.9754	0.1488	0.9236	0.4210
LVR4s 56.5-61.4	61.4	0.9827	0.1484	0.9154	0.1435	0.8645	0.5183
LVR4s 61.4-62	62	0.5864	0.0884	0.5434	0.0852	0.5408	0.4009
LVR4s 62-62.5	62.5	0.9372	0.1398	0.8629	0.1374	1.1936	1.1458
LVR4s 63-66	66	0.7547	0.1125	0.6993	0.1084	0.9141	1.2195
LVR4s 67-68	68	0.8627	0.1289	0.8112	0.1262	1.0141	1.1941
LVR4s 68-69.5	69.5	0.8970	0.1315	0.8211	0.1299	1.0396	1.2355
LVR4s 70-71	71	0.8382	0.1237	0.7689	0.1207	0.9863	1.1789
LVR4s 71-72.5	72.5	0.7389	0.1103	0.6841	0.1079	0.8075	1.0851
LVR4s 73-74	74	0.8982	0.1335	0.8308	0.1311	0.9657	1.2497
LVR4s 74-76	76	0.7597	0.1131	0.7069	0.1127	0.9020	1.1552
LVR4s 76-77	77	0.7840	0.1169	0.7239	0.1148	2.7141	1.3621
LVR4s 77.5-79	79	0.7753	0.1144	0.7158	0.1136	1.3003	1.3674
LVR4s 79-80	80	0.8517	0.1275	0.7861	0.1274	1.3041	1.2846
LVR4s 81-82	82	0.8267	0.1220	0.7538	0.1201	1.1279	1.2579
LVR4s 82.2-83	83	0.6094	0.0895	0.5598	0.0864	0.7269	0.4881
LVR4s 83-84.5	84.5	0.5811	0.0865	0.5309	0.0856	0.7025	0.6840
LVR4s 84.5-85.5	85.5	0.8485	0.1251	0.7737	0.1213	1.0424	1.5888
LVR4s 86-87	87	0.8469	0.1235	0.7800	0.1213	1.0388	1.1404
LVR4s 87-88.5	88.5	0.8493	0.1251	0.7730	0.1223	1.0272	1.0733
LVR4s 88.5-89.2	89.2	0.9739	0.1455	0.9163	0.1412	1.0355	1.0778
LVR4s 89.2-90	90	1.0108	0.1512	0.9377	0.1483	1.0863	1.0812
LVR4s 90.5-91	91	0.8890	0.1302	0.8122	0.1280	1.3569	1.1703
LVR4s 91-92	92	0.8338	0.1224	0.7599	0.1186	0.9496	1.2078
LVR4s 93-95	95	0.9038	0.1334	0.8270	0.1304	1.0832	1.0624
LVR4s 95-95.8	95.8	0.8940	0.1333	0.8193	0.1301	0.9095	0.7679
LVR4s 96-98	98	0.7668	0.1132	0.7135	0.1118	1.0905	1.0066
LVR4s 98-99	99	0.9435	0.1406	0.8842	0.1360	1.1984	1.1607
LVR4s 99.5-101.5	101.5	0.7725	0.1140	0.7163	0.1120	0.9874	1.1784
LVR4s 101.5-102.5	102.5	0.9591	0.1430	0.8759	0.1357	1.3517	1.2109
LVR4s 103-103.5	103.5	0.8357	0.1244	0.7582	0.1211	1.1410	1.2706
LVR4s 104-105	105	0.7615	0.1141	0.6995	0.1107	1.0686	1.2307
LVR4s 105-106	106	0.8248	0.1210	0.7594	0.1198	1.0151	1.1685

Tab. B-24: Results of geochemical analysis (^{166}Er to ^{238}U) of gravity core LVR4s of Lago Villarrica; Elements were measured by inductive coupled plasma mass spectrometry (ICP-MS).

Sample	Depth (cm)	^{166}Er (ppm)	^{169}Tm (ppm)	^{172}Yb (ppm)	^{175}Lu (ppm)	^{232}Th (ppm)	^{238}U (ppm)
LVR4s 106-107	107	0.8088	0.1193	0.7359	0.1163	0.9289	1.1395
LVR4s 107.5-109	109	0.7577	0.1121	0.7015	0.1085	0.8093	1.4293
LVR4s 109-110	110	0.8102	0.1216	0.7517	0.1176	1.0901	1.2209
LVR4s 111-111.5	111.5	0.8677	0.1284	0.7964	0.1253	0.9344	1.1760
LVR4s 112-113	113	0.8038	0.1194	0.7452	0.1149	0.8114	1.2556
LVR4s 114-115	115	0.7582	0.1114	0.6948	0.1101	0.8918	1.7398

Tab. B-24: Results of geochemical analysis (^{166}Er to ^{238}U) of gravity core LVR4s of Lago Villarrica; Elements were measured by inductive coupled plasma mass spectrometry (ICP-MS).

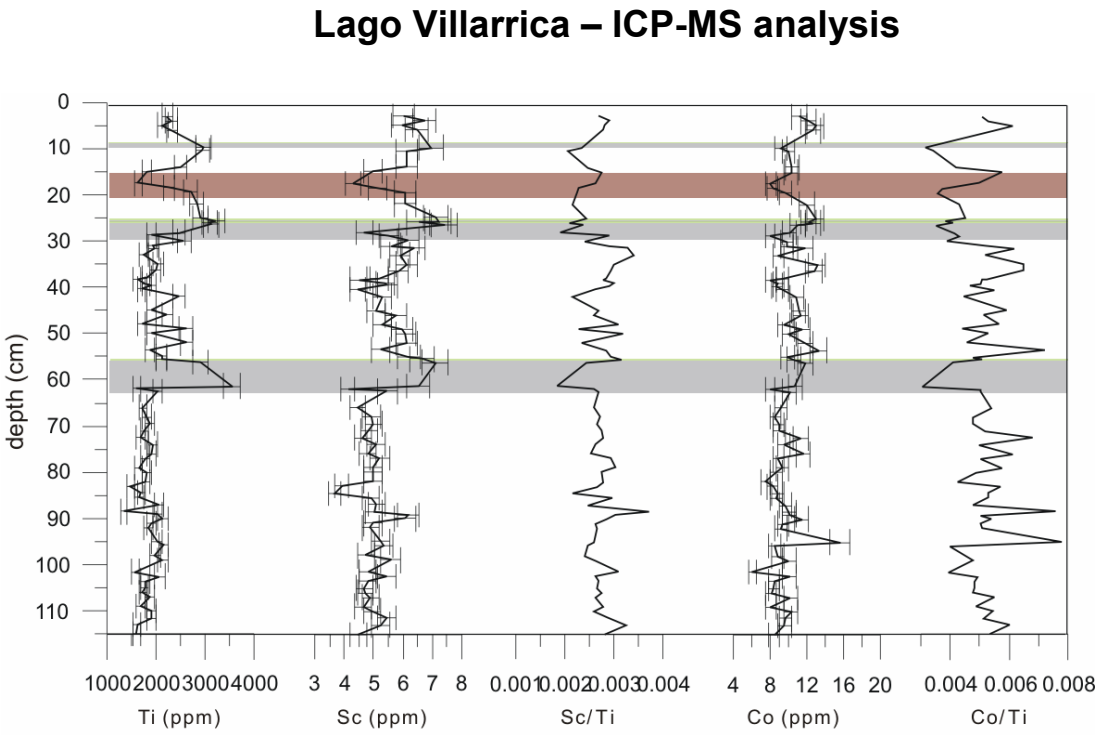

Fig. B-19: Concentration of Ti, and concentration and Ti-normalized profiles of Sc, and Co for short core LVR4s. Shaded and coloured bands indicate lithology, presented in Fig. IV-32.

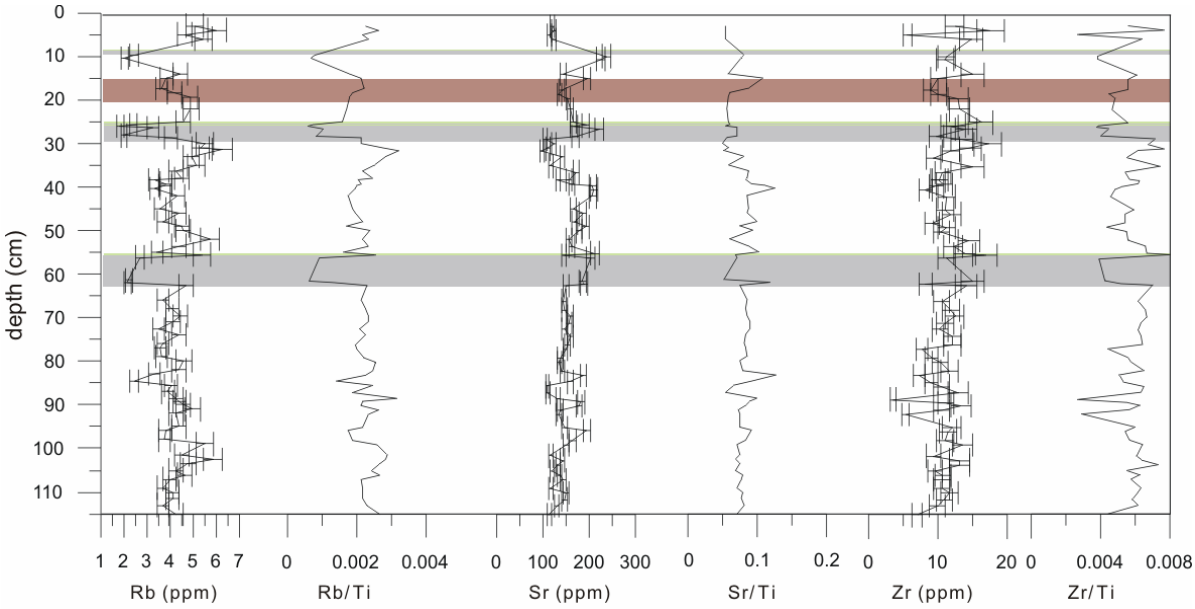

Fig. B-20: Concentration and Ti-normalized profiles of Rb, Sr, and Zr for short core LVR4s. Shaded and coloured bands indicate lithology, presented in Fig. IV-32.

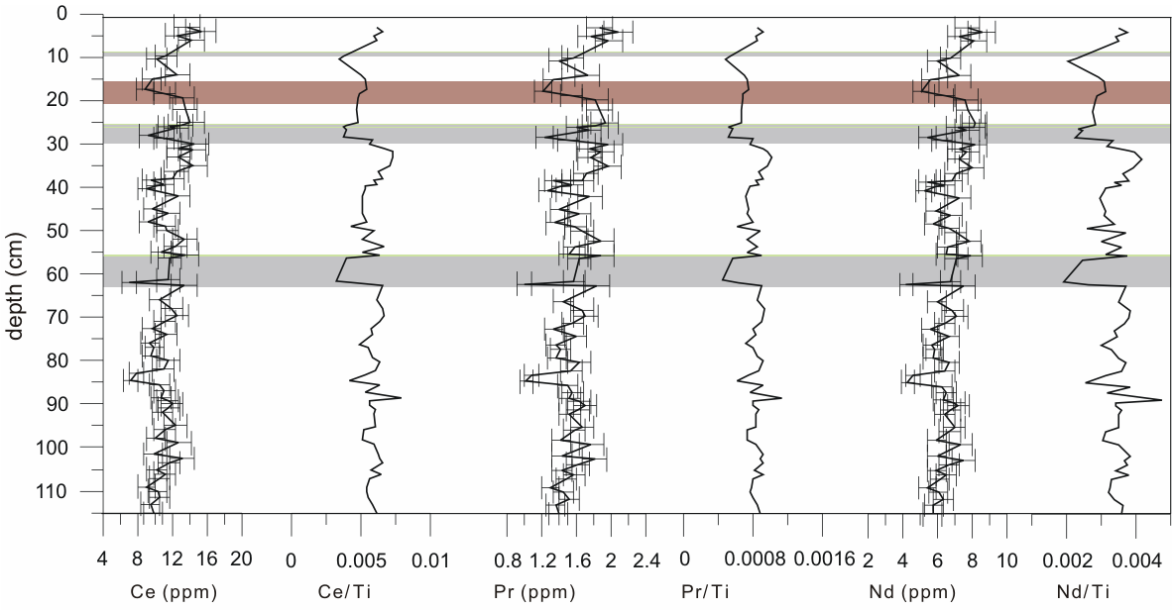

Fig. B-21: Concentration and Ti-normalized profiles of Ce, Pr, and Nd for short core LVR4s. Shaded and coloured bands indicate lithology, presented in Fig. IV-32.

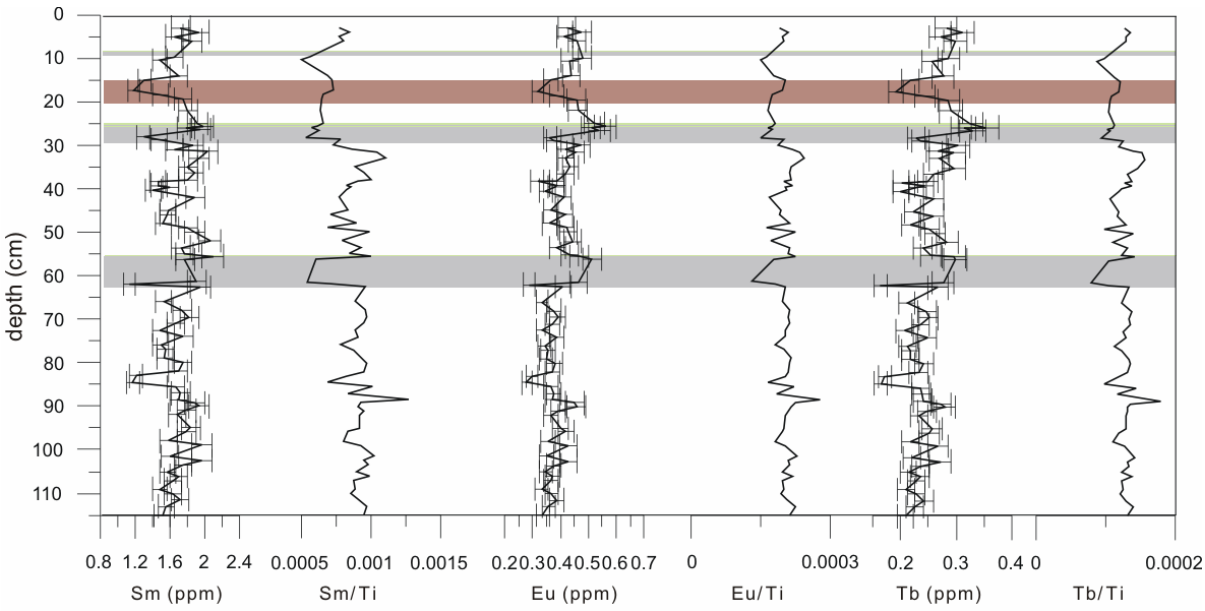

Fig. B-22: Concentration and Ti-normalized profiles of Sm, Eu, and Tb for short core LVR4s. Shaded and coloured bands indicate lithology, presented in Fig. IV-32.

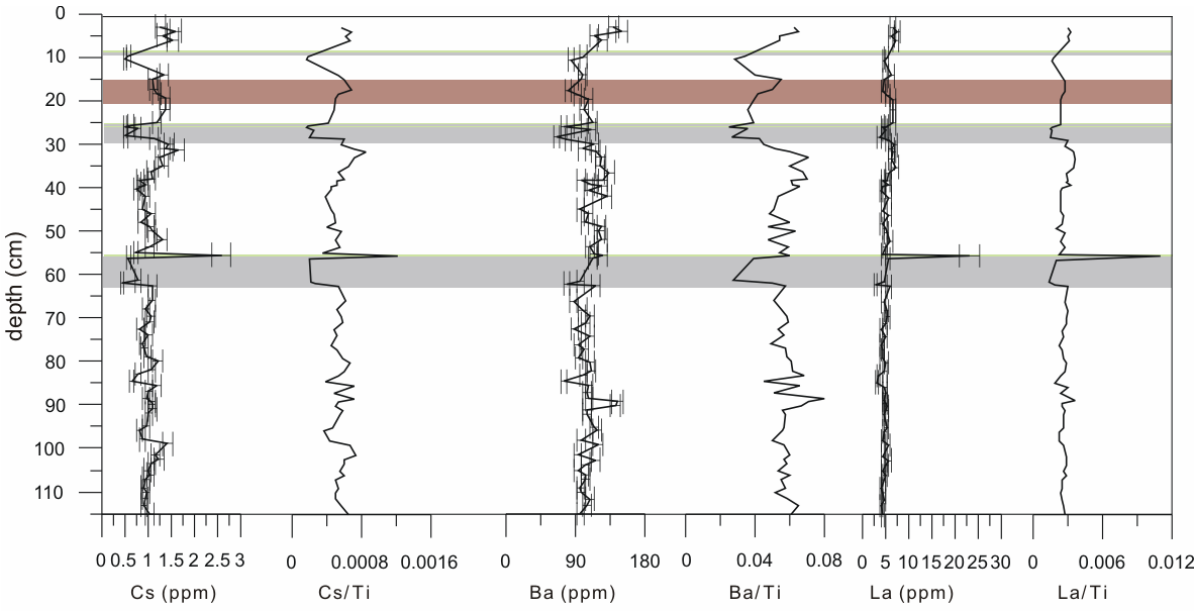

Fig. B-23: Concentration and Ti-normalized profiles of Cs, Ba, and La for short core LVR4s. Shaded and coloured bands indicate lithology, presented in Fig. IV-32.

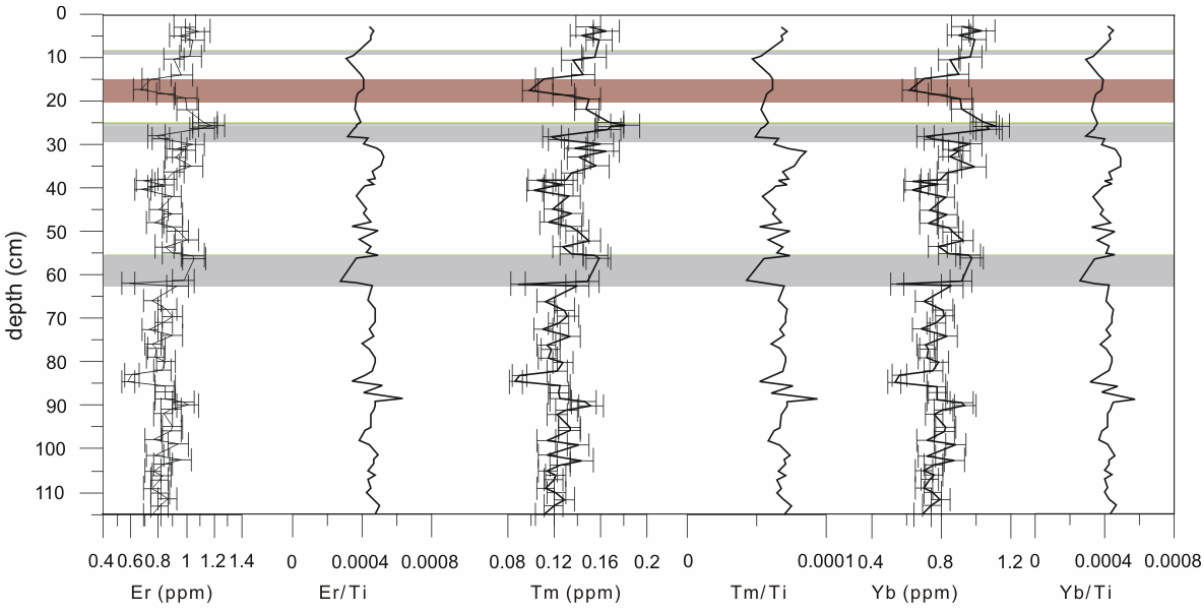

Fig. B-24: Concentration and Ti-normalized profiles of Er, Tm, and Yb for short core LVR4s. Shaded and coloured bands indicate lithology, presented in Fig. IV-32.

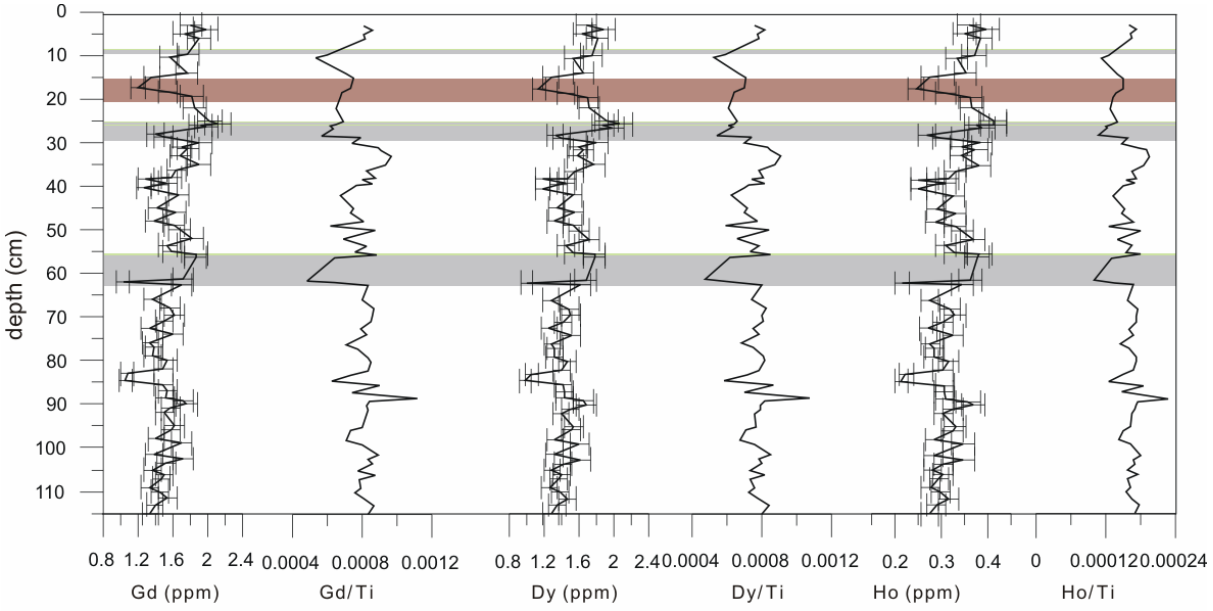

Fig. B-25: Concentration and Ti-normalized profiles of Gd, Dy, and Ho for short core LVR4s. Shaded and coloured bands indicate lithology, presented in Fig. IV-32.

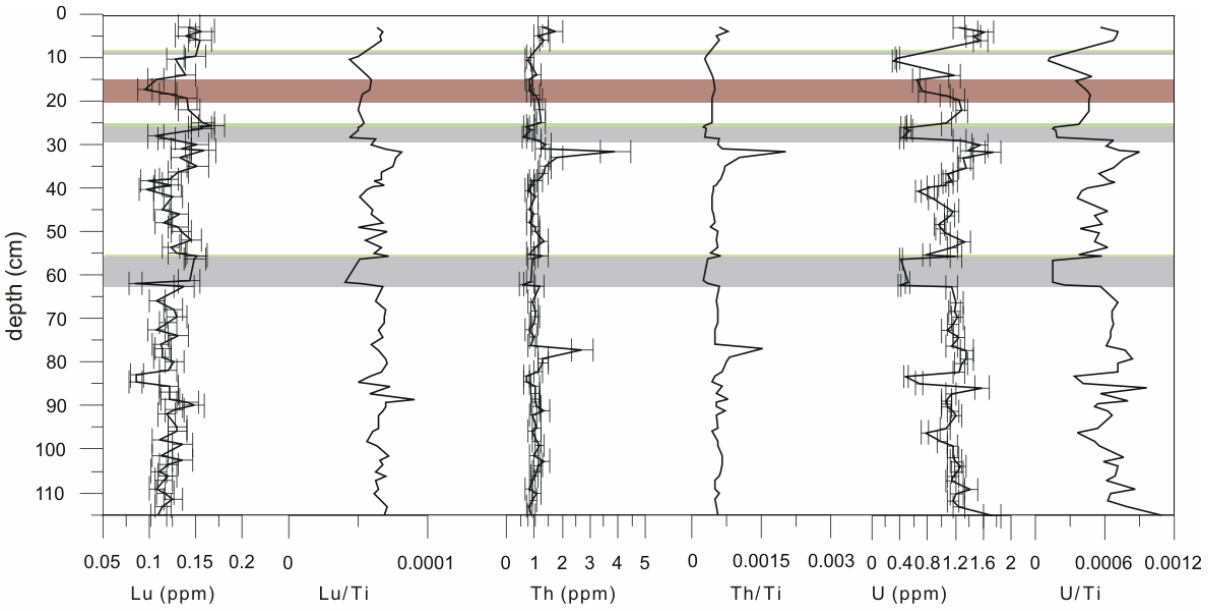

Fig. B-26: Concentration and Ti-normalized profiles of Lu, Th, and U for short core LVR4s. Shaded and coloured bands indicate lithology, presented in Fig. IV-32.

Total and biogenic mass accumulation rates (MAR) – Lago Calafquén –

Depth (cm)	MAR (mg/cm²/a)	BSi MAR (mg/cm²/a)	TOC MAR (mg/cm²/a)	Depth (cm)	MAR (mg/cm²/a)	BSi MAR (mg/cm²/a)	TOC MAR (mg/cm²/a)
0	13,8947711	4,42777105	0,38502411	22,5	24,7262356	8,74239971	0,28781338
0,5	13,5940205	5,12497752	0,38987651	23,5	21,5172063	7,41206805	0,2310948
1	13,2952294	3,78766579	0,36761309	24	21,5172063	10,9753754	0,34900909
1,5	14,3256704	5,27566705	0,50039567	25	21,5172063	9,20879876	0,34836357
2	15,3796047	6,93939953	0,47399942	26	21,5172063	11,5147582	0,35546425
2,5	14,5746963	7,23399024	0,38695819	27	21,5172063	11,5333079	0,36600768
3	13,7835269	5,20628774	0,41708952	28	18,5023612	9,58462831	0,2703195
3,5	10,8460446	3,90149623	0,37169395	29	19,9866293	9,05204753	0,27001936
4	8,09051111	3,37891463	0,17791034	31,2	41,4643966	2,57282372	0,29937294
4,5	8,18114938	3,13793632	0,31276534	31,5	41,9170561	1,84746028	0,38773277
5	8,27197842	3,02776345	0,28596229	32	18,5144213	7,38717483	0,14552335
5,5	8,18114938	2,69641148	0,27840451	32,5	18,5144213	6,83869201	0,19736373
6	10,815988	3,68946154	0,35519704	33	18,5144213	13,9729931	0,23068969
7	14,7918915	3,40408875	0,5122432	34	18,5144213	9,74942708	0,33011213
8	14,6051422	3,30486423	0,49394591	35	18,5144213	11,8693834	0,32437266
9	19,1091329	4,65537607	0,61798936	36	14,3514647	8,33349556	0,29320042
10	19,1091329	4,55308031	0,58531274	37	18,9734063	12,2615882	0,34190078
11	19,1091329	5,16511365	0,57384726	38	18,9734063	12,2645182	0,32008136
12	19,1091329	3,69170188	0,49664636	39	18,9734063	10,3236795	0,29294939
12,5	19,1091329	1,24612898	0,25911984	39,5	18,9734063	8,38493868	0,31495854
13,5	24,0729719	0,67344305	0,11892048	40	20,8537882	7,6834413	0,30509092
14	31,5292943	1,18600261	0,79170058	41	27,1241162	10,5784814	0,43317214
15	31,5292943	6,84064666	0,61986593	42	27,1241162	11,919028	0,45921129
16	31,5292943	9,42769101	0,48838877	43	27,1241162	9,06420457	0,37241412
17	31,5292943	6,67860774	0,20021102	44	27,1241162	15,1205301	0,40957415
18	40,1592333	1,66458885	0,15541623	45	27,1241162	16,5706804	0,43317214
18,3	46,4717981	1,34258998	0,28673099	46	44,9791535	5,67475248	0,44349445
18,5	53,496106	2,15705661	0,20275024	46,4	85,1962246	1,07233991	0,34419275
18,6	52,3743774	1,82491129	0,41742379	47	35,470549	4,31858307	0,16068159
19,5	19,1454657	1,18353413	----	47,7	35,470549	14,5648142	0,38485546
19,8	25,2640416	7,63776152	0,65130699	48,3	35,470549	14,5875595	0,38875722
20,2	32,204013	6,14975515	0,77225223	49	35,470549	14,0399854	0,58278112
21,7	28,3339776	10,0645069	0,41254271	49,5	43,7425661	3,36387581	----

Tab. B-25: Total (bulk sediment) and biogenic (BSi and TOC) mass accumulation rates of gravity core LCQ2s of Lago Calafquén.

Depth (cm)	MAR ($mg/cm^2/a$)	BSi MAR ($mg/cm^2/a$)	TOC MAR ($mg/cm^2/a$)	Depth (cm)	MAR ($mg/cm^2/a$)	BSi MAR ($mg/cm^2/a$)	TOC MAR ($mg/cm^2/a$)
50	33,3344641	20,6994701	0,65868901	81	29,7019619	16,9503157	0,50552739
51	33,3344641	15,7905247	0,67068942	82	29,7019619	12,7278021	0,48800323
52	33,3344641	15,440077	0,61868765	83	29,7019619	19,7438296	0,79898277
53	24,3218362	12,3829989	0,45652087	84	29,7019619	15,8952027	0,60592002
54	41,2697303	21,1126977	0,82291842	85	29,7019619	15,9858012	0,49424065
55	41,2697303	21,1295508	0,83860092	86	24,6559017	12,4019561	0,41816409
56	41,2697303	20,4130355	0,85304533	87	24,2137127	9,04653698	0,49032768
57	41,2697303	11,8040408	0,71809331	88	24,2137127	9,23402133	0,38620872
58,2	75,5705903	11,905957	0,12998142	89	23,7746223	9,18900917	0,35043793
58,9	42,3102677	21,536751	0,70235044	90	36,698279	10,2619082	0,39413952
60	42,3102677	16,6121205	0,84197433	90,6	36,698279	1,01096729	0,2282633
61	42,3102677	20,221834	0,68373393	90,7	36,698279	0,61478474	0,16147243
62	19,5887973	9,99891821	0,32008095	90,9	58,6899508	3,51966964	0,42256765
63	20,0208553	8,84993508	0,33074453	91,5	37,7246389	12,0884581	0,58133669
64	20,0208553	8,05780475	0,32854224	93	25,1252766	8,07448512	0,4494912
65	20,0208553	11,3928694	0,33615016	94	25,1252766	8,16841903	0,43416478
66	20,0208553	11,9808168	0,38259855	95	14,8850276	4,82489929	0,24783571
67	20,4560178	11,027854	0,37004936	96	14,3095573	3,94231819	0,203625
68	21,5705698	12,5175069	0,42041041	97	14,3095573	5,16482122	0,26472681
69	21,5705698	12,523641	0,37209233	98	13,7407293	4,15242883	0,27467718
70	21,5705698	12,72796	0,37705356	99	14,1395737	4,52251794	0,29537569
71	21,5705698	12,283168	0,3559144	100	14,541678	4,17653351	0,20750974
72,5	22,7057486	11,606414	0,3428568	101	15,1650021	4,04856983	0,20472753
73	38,4233786	19,6898365	0,70007396	102	27,0971659	6,83419973	0,46905194
74	38,4233786	27,5490789	0,5356219	103	27,0971659	7,13028832	0,39751542
75	38,4233786	10,9832377	0,35733742	104	42,2840909	10,5586893	1,40044909
75,5	38,4233786	3,035493	0,18520068	105	54,295639	1,43535162	0,25736133
76	58,7118958	1,60987145	0,10274582	105,2	33,9345196	1,41299414	0,11605606
76,8	71,6924194	3,01184088	0,29250507	105,3	33,9345196	0,44174882	0,69124617
77,3	28,2903544	13,6289106	0,45688922	106	33,9345196	11,1994898	0,61557219
78	28,2903544	7,49629271	0,16012341	107	33,9345196	10,596275	0,71567902
78,5	28,2903544	17,8036619	0,56241224	108	33,9345196	13,2391451	0,70889212
78,8	28,2903544	13,6530358	0,42916468	109	13,1853496	3,84596234	0,22098646
79,5	22,0720343	6,53386261	0,35403543	110	28,2849013	8,14686214	0,45114418
80	35,1698829	11,431324	0,47268323	110,5	28,2849013	8,66411987	0,51789654
80,2	29,7019619	14,7939345	0,41077813	111	31,0179117	9,40844627	0,58685889
80,4	29,7019619	12,9447511	0,51592308	112	29,7479284	7,77100021	0,56015349

Tab. B-25: Total (bulk sediment) and biogenic (BSi and TOC) mass accumulation rates of gravity core LCQ2s of Lago Calafquén.

Depth (cm)	MAR ($mg/cm^2/a$)	BSi MAR ($mg/cm^2/a$)	TOC MAR ($mg/cm^2/a$)	Depth (cm)	MAR ($mg/cm^2/a$)	BSi MAR ($mg/cm^2/a$)	TOC MAR ($mg/cm^2/a$)
113	29,7479284	9,66432861	0,56283081	138,7	19,4188965	3,24010856	0,22661852
114	29,7479284	8,39250548	0,59376865	139,7	17,4481725	1,15058473	0,06734995
115	28,4943987	7,97537243	0,61661879	140,5	15,6267434	0,07413956	0,08750976
116	35,1010552	6,36515009	0,49001073	141	17,5006936	0,26401951	0,13388031
117	35,1010552	8,42131188	0,57109417	142	12,482307	1,28540264	0,11109253
118	35,1010552	5,79582306	0,48650063	143	8,41145413	1,95156664	0,15687362
119	42,1779303	3,3239819	0,65544504	144	7,86512051	1,87739111	0,15926869
120	40,350156	9,50101462	0,6472165	145	7,86512051	1,18709697	0,14220138
121	40,350156	6,89451405	0,67949663	146	7,33386315	1,69902535	0,12621578
122	40,350156	7,4032867	0,48823689	147	7,8643864	0,38944124	0,13550338
123	40,350156	11,1051535	0,6992682	148,2	8,40994399	1,65071456	0,12143959
124	38,5545404	8,75104246	0,72328318	149,5	7,8643864	1,62414518	0,1179658
125	29,6319162	4,38771065	0,55678371	150	7,8643864	2,09378364	0,09555229
126	48,6169263	8,77649248	0,62521367	151	23,4225208	2,02085728	0,29676334
127,2	71,7351111	0,44902919	----	152	27,9490281	1,78189481	
128	121,80194	1,28938256	0,42508877	153	8,5636087	3,1338611	0,1504626
129	113,593213	1,6716292	0,39530438	154	8,5636087	3,43175296	
130	105,84323	2,31701311	1,1208798	155	8,5636087	3,86165656	0,10302021
131	65,4600843	1,02242151	0,86407311	156	9,44936996	2,06575845	0,11528231
132	115,74335	2,48803186	1,14933146	157	10,2415525	3,89517068	0,13989961
132,6	35,7993089	7,90017343	0,50727621	158	10,2415525	2,22378963	0,12853148
133,5	11,2736983	0,19399008	0,06865682	159	11,0656752	2,77121196	0,15967769
134,5	19,1036771	0,20672323	0,18836226	159,2	10,6495018	0,33766432	
135,5	16,2707799	3,46741175	0,25366146	160	20,9784447	5,24026851	0,3142571
136,5	16,2707799	0,75796416	0,15587407	161	11,2935484	8,67849481	0,18916694
137,5	16,2707799	0,23768284	0,08948929	162	5,13875268	----	-----
138,6	13,7431733	0,1360332	0,07311368	----	----	----	----

Tab. B-25: Total (bulk sediment) and biogenic (BSi and TOC) mass accumulation rates of gravity core LCQ2s of Lago Calafquén.

Mass accumulation rates (MAR) of grain size fractions
– Lago Calafquén –

Depth (cm)	MAR clay ($mg/cm^2/a$)	MAR fine silt ($mg/cm^2/a$)	MAR med. silt ($mg/cm^2/a$)	MAR coarse silt ($mg/cm^2/a$)	Depth (cm)	MAR clay ($mg/cm^2/a$)	MAR fine silt ($mg/cm^2/a$)	MAR med. silt ($mg/cm^2/a$)	MAR coarse silt ($mg/cm^2/a$)
0	1.16021339	3.18356995	6.50747709	2.64514757	14	2.33632071	4.92519107	12.2002604	11.4369362
0.5	1.18648611	3.23537688	6.25895893	2.46119741	15	1.77888279	3.43732367	10.8085574	14.3540265
1	1.79459006	4.06195848	5.52762457	1.56564621	16	3.68987332	6.60664833	11.7036741	8.74086627
1.5	1.59487688	3.85002391	6.14972378	2.16203017	17	1.59853522	3.05960272	10.4954715	14.3830335
2	1.16823477	3.01409492	6.50157407	3.65973072	18	2.71717372	5.61104807	13.6714078	14.8079141
2.5	1.51795461	3.81492674	6.46956192	2.26884297	19.5	2.62005698	5.70534879	7.83949385	2.65222137
3	1.59902695	4.58688207	6.32512264	1.01060819	20.2	6.3686656	12.3911381	12.3125603	1.13164902
3.5	1.39968205	3.81401157	4.65533925	0.7729976	21.7	3.6400661	7.33906688	10.5753738	5.16386742
4	0.66900436	1.81898961	3.564841	1.81996047	22.5	3.58530416	7.43592083	10.5212605	2.49957516
4.5	0.58969725	1.75272944	3.61402274	1.79363519	23.5	1.9124493	4.10419193	8.26970791	5.70507209
5	0.82984488	2.5672085	3.87988876	0.74009391	24	3.5006343	6.91563011	8.46831172	1.8978176
5.5	0.8769374	2.25930621	3.68888026	1.13137115	25	3.43758888	7.0189127	9.18354366	1.52922785
6	0.88950685	2.29785664	4.73296818	2.48875883	26	3.65835542	7.070554	8.5393185	1.59722223
7	1.72473454	4.33698257	6.54467237	1.4358489	27	2.57797649	5.52346686	9.06455351	3.24630092
8	1.66425595	4.00020239	6.47343716	2.33375567	28	2.92244795	5.61805695	6.89749523	2.11759524
9	2.39800509	5.6131167	8.40381448	2.52680065	29	2.62144629	5.61204563	8.10917509	2.88746833
10	2.1201583	5.17532647	8.75714234	2.78534721	31.2	3.31549315	6.2810268	14.3541448	14.5610522
11	3.00892407	5.78376126	7.97003716	2.28048392	32	1.95808519	4.09576027	7.12527502	3.92116928
12	1.23674308	2.46087414	6.02377197	7.62339749	33	1.93660846	3.70103281	5.73095396	4.75802112
13.5	2.65163786	6.30302624	10.9322587	3.86082324	34	2.52684821	4.95612543	7.1323105	2.7977142

Tab. B-26: Mass accumulation rates of individual grain size fractions of gravity core LCQ2s of Lago Calafquén.

Depth (cm)	MAR clay (mg/cm²/a)	MAR fine silt (mg/cm²/a)	MAR med. silt (mg/cm²/a)	MAR coarse silt (mg/cm²/a)	Depth (cm)	MAR clay (mg/cm²/a)	MAR fine silt (mg/cm²/a)	MAR med. silt (mg/cm²/a)	MAR coarse silt (mg/cm²/a)
35	2.27412636	4.74561646	7.56665883	3.05636066	54	7.24366307	14.5653259	15.2574193	2.73535773
36	1.84114941	3.7398482	5.4976156	2.38277369	55	6.9019497	12.7824736	15.2784669	4.91893916
37	2.54300565	5.1562129	7.28559829	2.84392387	56	4.55865441	10.1490521	17.2862392	7.1322348
38	2.22102694	5.20782056	8.33387899	2.66215864	57	6.27258631	12.6058391	14.2661204	4.82897115
39	2.3322111	5.40704133	7.98419911	2.37262446	58.2	12.6966149	24.5090538	26.6265418	7.80417486
39.5	2.85853339	5.50475437	7.01370938	2.48589569	58.9	3.40978448	7.91371248	13.6124824	10.2987423
40	3.4802887	6.35206387	7.23105104	2.55771712	60	5.7838136	12.7891246	18.3613869	4.4556943
41	4.13398655	8.02819592	9.34588549	3.79981744	61	6.00848112	12.7789702	18.0584454	4.47431081
42	3.82422915	7.79330107	9.58512019	3.87657869	62	3.02588152	6.16949171	8.2267072	2.02097622
43	3.9023466	7.88742176	10.6652025	3.5432233	63	2.89621693	6.13539112	8.53749334	2.03832328
44	3.89800674	7.4824587	8.355584	4.80123981	64	2.92624822	6.44851729	8.60896779	1.63730555
45	4.05749655	7.79302983	9.8824005	3.90017667	65	3.37311371	7.14003764	8.08281971	1.26071326
46	7.30371495	12.9274585	16.2262296	6.60204016	66	2.13362255	4.37215439	7.88641512	4.9061106
46.4	17.6126155	32.8712593	28.1641679	6.37608545	67	2.34385052	4.54778187	7.9389805	5.05038623
47	1.53693889	2.80110925	6.23075664	13.1067226	68	2.67324072	5.59799428	8.96559164	3.93727611
47.7	1.8998026	3.4569597	7.57012456	15.5265234	69	3.00780025	5.97030231	8.50505997	3.01405572
48.3	5.16131958	10.342148	11.5179967	4.73851064	70	2.11801425	4.89932352	9.83833689	3.95410115
49	4.99638153	9.56144119	10.7387087	6.03176686	71	2.3926076	5.31347846	9.20869196	3.62536567
49.5	7.06136244	13.153827	13.8843279	6.27137169	72.5	2.88340302	5.75590728	8.27942418	3.95443318
50	0.82669471	1.97040018	3.83246334	3.6887918	73	4.70225307	9.78528182	13.0047767	6.55618109
51	4.29181226	8.62962608	13.8634703	5.99487003	74	4.34222601	9.41449622	16.3429998	6.98229636
52	4.81683007	10.1540111	13.8798042	4.0278033	75	5.39541082	11.302621	14.9351673	5.25093892
53	3.7299968	7.35370717	10.0784825	2.67783416	75.5	7.76229094	14.4848453	13.4927536	2.68348876

Tab. B-26: Mass accumulation rates of individual grain size fractions of gravity core LCQ2s of Lago Calafquén.

Depth (cm)	MAR clay (mg/cm²/a)	MAR fine silt (mg/cm²/a)	MAR med. silt (mg/cm²/a)	MAR coarse silt (mg/cm²/a)	Depth (cm)	MAR clay (mg/cm²/a)	MAR fine silt (mg/cm²/a)	MAR med. silt (mg/cm²/a)	MAR coarse silt (mg/cm²/a)
76	9.65282279	21.9641202	21.0998811	5.99507168	93	2.76930799	6.69387619	11.7747096	3.37407339
76.8	5.24573433	11.481541	36.5595493	18.3647301	94	3.8017056	8.51294621	10.7707036	1.94017386
77.3	2.03888584	4.32191744	12.4777437	9.02547175	95	2.17872148	4.46104276	6.08425502	1.84976238
78	4.09785783	8.91146163	12.4129588	2.70201175	96	1.38387729	3.15454191	5.95363442	3.48709603
78.5	3.85823853	8.19769599	10.4838395	4.37736653	97	2.09420372	4.72773465	6.36718063	1.06405868
78.8	5.04417018	9.18021999	9.88493272	3.66218637	98	1.68832341	3.92517673	6.23306962	1.61907013
79.5	3.98334003	7.39987023	7.85256765	2.06859106	99	1.70254607	3.87650552	6.08878322	1.80986543
80	8.828344	13.5991386	10.2639786	2.38733165	100	1.25320181	3.37134262	6.87181534	2.49113485
80.2	6.95174418	11.5775277	9.25245815	1.6971701	101	1.15208521	2.75896884	6.36414479	3.85555014
80.4	4.11283066	9.06414771	12.2069123	3.29602671	102	3.87706249	8.99246547	12.1308592	1.79925181
81	3.32364954	7.79557692	12.8740184	4.54766739	103	3.06252169	7.30431203	12.5373167	3.60094237
82	3.89481826	8.962567	13.1033175	3.28414593	104	6.42675897	13.6171686	17.7614324	3.78062056
83	4.40420691	9.75560938	12.5434355	2.64317759	105	8.2594526	17.4815669	22.223748	5.0945598
84	3.19622812	7.50954702	13.4846907	4.829539	105.3	4.61543402	11.0433107	14.8215801	3.4260291
85	2.76347053	6.91580481	13.4570679	5.48565534	106	3.82340233	9.05610526	14.4194561	4.52279278
86	2.83370278	6.30747278	10.386052	4.32809699	107	3.11009873	7.79408047	14.6349403	6.24496965
87	2.91169895	6.55271493	10.5131098	3.64537445	109	0.75314717	1.88708724	5.44686792	3.82216915
88	2.27439403	6.12849068	11.7574525	3.66958816	110	3.45952628	8.24872577	12.9513735	3.13057288
89	2.55196796	6.10104358	11.4969319	3.2162309	110.5	3.47168879	8.0521457	12.549445	3.58001996
90	5.53850426	11.7346417	14.0051642	4.61554254	111	4.17035823	9.01566623	12.6667846	4.29908257
90.6	6.09301525	11.2516923	12.6733837	6.24751501	112	3.46533618	8.21756775	13.3059509	4.03262918
90.7	2.31859726	4.61150573	11.4784877	15.7252125	113	4.47289852	9.12666445	12.0514808	3.41000504
91.5	3.52499026	7.48041864	15.8696238	9.55451929	114	3.81755166	8.3389393	12.522688	4.14775366

Tab. B-26: Mass accumulation rates of individual grain size fractions of gravity core LCQ2s of Lago Calafquén.

Depth (cm)	MAR clay (mg/cm²/a)	MAR fine silt (mg/cm²/a)	MAR med. silt (mg/cm²/a)	MAR coarse silt (mg/cm²/a)	Depth (cm)	MAR clay (mg/cm²/a)	MAR fine silt (mg/cm²/a)	MAR med. silt (mg/cm²/a)	MAR coarse silt (mg/cm²/a)
115	3.68632036	8.34002556	12.7700497	3.30079115	137.5	2.47869061	5.51514355	6.96665982	1.27286311
116	5.14125156	10.1431519	14.0913186	4.8467537	138.6	3.01566451	5.11328504	4.84130764	0.77291606
117	4.51188964	10.9399459	16.0847075	3.3630321	138.7	1.06590323	2.06500545	6.90089325	8.67888741
118	4.13244723	10.676688	16.365516	3.54625961	139.7	2.41465259	5.88875821	7.88936567	1.22311689
119	5.80663566	13.576654	18.7902679	3.59355966	140.5	1.88614793	4.74646705	6.72684424	2.10976663
120	5.04861152	11.4449183	19.6198599	4.15445207	142	1.04239746	2.36077872	4.80456479	3.52001058
121	4.85856229	11.6575636	18.6046499	4.526077	143	0.91903548	2.44773315	4.21464321	0.83012641
122	5.24511678	12.148625	18.4198462	4.008788	144	0.97653336	2.5029173	3.55865243	0.70849006
123	5.6123032	12.5061274	18.0720279	3.50884957	145	0.78847833	2.1278297	3.75842649	1.13100433
124	4.31695189	9.42388632	16.5291026	7.23360287	146	1.04360873	2.63630379	3.16881559	0.44377206
125	3.76651287	8.18937268	12.4931122	4.3484837	147	1.02543734	2.56709301	3.26655154	0.7908427
126	7.36254733	16.2011045	20.5109951	3.91074556	148.2	1.25930501	3.20595475	3.58011316	0.3596933
127.2	7.63476787	17.8986276	27.4006604	16.798211	149.5	0.96967884	2.27186394	3.63161635	0.89370887
128	10.0742385	20.9937825	53.8011351	36.4431406	150	1.14804313	2.59178718	3.45537545	0.64307088
129	6.06587757	12.0465602	33.9155256	55.6913445	151	3.09950218	7.3848866	10.4811096	2.26776847
130	3.24832872	6.23416623	17.8441101	48.9048643	152	4.069099	8.10298223	11.2162245	4.30079645
131	5.21847792	11.2296775	28.74025	19.9699079	153	0.69108322	1.2076401	2.17138862	3.29339263
132	7.24900598	15.4621541	37.2531545	47.0056891	154	1.14495448	2.71577723	3.93694783	0.7017021
132.6	1.14557789	2.3101294	5.82454756	15.0604113	155	0.97702212	2.40997076	4.19599699	0.97582321
133.5	1.35633864	3.31424182	5.08815824	1.35306927	156	1.27897222	2.94962083	4.30163669	0.87094843
134.5	2.07102963	4.55412558	8.16624884	4.1552408	157	1.46228886	3.34243307	4.61576529	0.80734158
135.5	1.35682033	3.05744225	6.78133564	4.67703568	158	1.35546947	3.17897789	4.78925718	0.88753294
136.5	2.02636293	5.02360329	7.64173448	1.57907919	159	1.54155921	3.57045076	5.25863017	0.69503506

Tab. B-26: Mass accumulation rates of individual grain size fractions of gravity core LCQ2s of Lago Calafquén.

Depth (cm)	MAR clay (mg/cm²/a)	MAR fine silt (mg/cm²/a)	MAR med. silt (mg/cm²/a)	MAR coarse silt (mg/cm²/a)	Depth (cm)	MAR clay (mg/cm²/a)	MAR fine silt (mg/cm²/a)	MAR med. silt (mg/cm²/a)	MAR coarse silt (mg/cm²/a)
159.2	1.39327432	3.24085638	4.95925999	0.99157511	161	1.58143559	3.69265154	5.06120374	0.9064202
160	0.48900755	1.11374563	2.72426083	4.48791868	162	0.57877771	1.3612042	2.17045497	0.7460955

Tab. B-26: Mass accumulation rates of individual grain size fractions of gravity core LCQ2s of Lago Calafquén.

Mass accumulation rates (MAR) of grain size fractions – Lago Villarrica–

Depth (cm)	MAR clay (mg/cm²/a)	MAR fine silt (mg/cm²/a)	MAR med. silt (mg/cm²/a)	MAR coarse silt (mg/cm²/a)	Depth (cm)	MAR clay (mg/cm²/a)	MAR fine silt (mg/cm²/a)	MAR med. silt (mg/cm²/a)	MAR coarse silt (mg/cm²/a)
0	----	----	----	----	6	7.124322	16.683636	25.817503	8.370063
0.5	----	----	----	----	6.5	6.709734	16.395090	27.987422	9.290449
1	4.497308	12.848333	25.948506	10.704892	7	5.139011	13.394377	27.724322	12.457606
1.5	5.012182	14.353778	27.366647	8.194884	7.5	7.675747	18.160002	25.508661	7.745494
2	5.312933	14.942698	28.797773	9.408343	8	7.164071	17.481775	24.990370	9.153656
2.5	6.484198	16.361431	25.848244	8.040130	8.5	25.830037	63.089891	86.348168	24.407187
3	5.816756	15.130484	28.779424	12.346616	9	37.780300	75.833631	87.016777	21.347423
3.5	7.339425	17.903575	26.738926	7.667373	9.2	30.683939	70.681086	84.300400	27.259935
4	5.717762	14.260916	25.950382	11.179836	10	21.272721	47.416179	96.933209	46.857940
4.5	4.989922	13.361127	27.626337	12.448163	11	4.470452	9.130990	22.850076	23.045735
5	5.980289	16.291448	30.464549	11.494921	11.5	16.188355	40.620000	55.790370	10.803981
5.5	5.907949	15.106812	28.282921	11.670784	12	10.843820	26.988655	42.737838	10.493044

Tab. B-27: Mass accumulation rates of individual grain size fractions of gravity core LVR4s of Lago Villarrica.

Depth (cm)	MAR clay (mg/cm²/a)	MAR fine silt (mg/cm²/a)	MAR med. silt (mg/cm²/a)	MAR coarse silt (mg/cm²/a)	Depth (cm)	MAR clay (mg/cm²/a)	MAR fine silt (mg/cm²/a)	MAR med. silt (mg/cm²/a)	MAR coarse silt (mg/cm²/a)
13	14.030108	30.457945	38.471747	8.267497	24.8	31.846140	59.861386	53.438870	9.672502
13.5	14.977110	31.061499	37.898417	7.244477	25.2	24.495267	46.043399	51.085570	21.061015
14	23.640232	46.940307	42.705788	6.549503	26	21.431451	51.755321	71.383686	22.570598
14.5	19.853146	44.507192	35.389381	4.904237	27	9.241537	20.222903	33.211957	18.565685
15	13.877589	34.923315	45.674466	9.981404	28	11.723544	21.141238	35.809722	40.373766
15.5	12.359412	32.090248	48.947512	8.051094	29	7.737412	16.812760	24.025720	9.036887
16	12.436763	32.379653	46.452104	10.396252	30	11.079589	25.538185	37.100490	12.434533
16.5	13.796354	33.963384	46.085216	11.557951	32	7.704387	18.870769	30.254079	10.658168
17	11.899510	26.023468	38.812047	11.096508	33	10.036067	23.613062	30.352132	6.813033
17.5	13.204184	30.968001	40.655758	9.898742	34	8.851959	19.120034	28.670534	12.329866
18	14.773036	30.478188	35.844668	9.148544	35	8.283356	19.892223	32.966274	8.466591
18.5	15.110106	30.847836	37.617888	9.984506	36	11.741485	26.424031	29.551569	5.574507
19	14.723731	31.787388	36.900737	9.881787	37	11.658670	23.618452	28.772953	7.090732
19.5	14.240089	31.698287	37.271949	9.090742	39	10.919770	22.507967	30.778233	6.864364
20	15.168239	33.290411	36.287181	7.634407	40	11.590919	25.966475	36.417358	8.684490
20.5	14.345548	32.313775	35.954135	8.699827	41	17.130651	38.787633	56.057347	11.031548
21	13.880267	32.609694	36.003455	8.263393	42	19.079999	39.008202	38.632583	5.273972
21.5	14.851403	31.899338	33.417061	10.446167	43	18.428175	36.390619	38.458624	7.259737
22	9.043310	25.870760	43.704987	13.663688	44	17.621540	35.811622	45.698172	9.063033
22.5	8.593473	24.156163	42.965503	15.897972	45	13.024479	29.685375	46.795924	12.898658
23	9.156216	23.127379	43.711209	16.283054	46	12.916692	26.246014	35.239023	7.531923
23.5	11.679049	26.458197	41.646987	13.424973	47	13.191994	28.760416	40.651804	9.810048

Tab. B-27: Mass accumulation rates of individual grain size fractions of gravity core LVR4s of Lago Villarrica.

Depth (cm)	MAR clay ($mg/cm^2/a$)	MAR fine silt ($mg/cm^2/a$)	MAR med. silt ($mg/cm^2/a$)	MAR coarse silt ($mg/cm^2/a$)	Depth (cm)	MAR clay ($mg/cm^2/a$)	MAR fine silt ($mg/cm^2/a$)	MAR med. silt ($mg/cm^2/a$)	MAR coarse silt ($mg/cm^2/a$)
24	22.883032	48.437333	66.675711	19.376199	48	14.218713	31.066202	42.108599	8.849342
49	13.398251	29.213853	34.435066	5.500361	72	5.068279	9.214791	8.309082	1.328245
50	13.170003	29.415748	38.646549	7.949912	73	4.521908	8.105210	9.981141	3.008457
51	13.632302	31.240692	38.971073	6.193140	74	4.752900	9.362529	10.306011	1.633021
52	10.838103	25.924267	30.723467	3.921673	75	3.442428	6.980600	9.571267	3.038402
53	13.457247	28.464151	33.320440	5.138632	76	3.612552	7.099189	9.677256	4.163126
54	14.621962	28.448063	32.669186	7.002906	77	4.258482	8.644562	9.771931	1.922635
55	1.475433	3.403722	3.385835	0.323173	78	0.000000	0.000000	0.000000	0.000000
56	3.628191	7.210912	6.616308	0.944188	79	3.015590	7.428390	10.394419	2.233265
57	1.729444	3.832315	5.821182	1.695281	80	2.019645	4.489705	8.212894	4.855258
58	2.488927	5.513329	8.705449	3.413710	81	3.215861	6.255624	8.443002	3.224011
59	1.926097	4.021100	6.589504	3.627535	82	4.785200	9.290313	5.919774	0.600572
60	1.944406	3.970296	6.406907	3.765761	83	0.000000	0.000000	0.000000	0.000000
61	1.722413	3.734790	6.418859	4.303923	84	3.391599	7.453571	11.374314	6.643805
62	1.933245	4.057556	6.991542	7.045237	85	2.727104	5.762068	7.433391	1.894779
63	3.071806	6.531122	8.014661	1.724783	86	2.989117	7.293147	11.346203	2.350753
64	0.000000	0.000000	0.000000	0.000000	87	3.523076	7.104360	8.862017	1.990057
65	4.271633	7.612925	5.949581	0.831485	88	3.266279	7.769774	9.652591	1.436118
66	3.362966	6.497316	7.290026	1.426803	89	0.000000	0.000000	0.000000	0.000000
67	3.137054	6.128956	7.578424	1.860796	90	0.000000	0.000000	0.000000	0.000000
68	1.794082	3.291846	2.825948	0.522198	91	7.465373	15.429639	21.975484	6.367191
69	0.000000	0.000000	0.000000	0.000000	92	7.821559	16.156205	17.411060	3.035724
70	0.000000	0.000000	0.000000	0.000000	93	8.969565	16.776364	17.721262	4.141424

Tab. B-27: Mass accumulation rates of individual grain size fractions of gravity core LVR4s of Lago Villarrica.

Depth (cm)	MAR clay ($mg/cm^2/a$)	MAR fine silt ($mg/cm^2/a$)	MAR med. silt ($mg/cm^2/a$)	MAR coarse silt ($mg/cm^2/a$)	Depth (cm)	MAR clay ($mg/cm^2/a$)	MAR fine silt ($mg/cm^2/a$)	MAR med. silt ($mg/cm^2/a$)	MAR coarse silt ($mg/cm^2/a$)
71	4.984927	10.038669	10.175205	1.871635	94	7.264796	15.171856	18.616388	4.990499
95	8.155028	16.615445	18.592464	3.737721	105	5.764354	11.983797	15.126580	3.844257
96	9.424451	19.220943	24.181488	4.975754	106	7.671936	15.245050	17.252147	2.857233
97	8.933495	17.136058	19.914337	5.948637	107	6.120442	12.695136	18.302529	6.278973
98	8.799841	18.538236	22.892591	4.890036	108	5.936705	12.819758	17.393772	4.893993
99	8.529291	16.891063	18.643638	3.124339	109	6.465763	13.864079	18.438605	3.923836
100	7.734914	16.447918	21.516434	5.517021	110	6.680818	14.693859	19.474852	5.828477
101	7.845449	16.443242	20.006535	4.670145	111	6.237945	13.689298	19.446366	5.299966
102	9.010526	17.866268	19.343477	3.660213	112	6.546378	14.258646	18.836982	4.135526
103	7.985453	17.158866	20.911467	3.433760	113	6.022882	12.749187	16.236578	4.440875
104	8.647472	17.731490	18.837008	4.340125	114	5.786620	12.639855	18.674545	4.530402

Tab. B-27: Mass accumulation rates of individual grain size fractions of gravity core LVR4s of Lago Villarrica.

Total and biogenic mass accumulation rates (MAR) – Lago Villarrica–

Depth (cm)	MAR (mg/cm²/a)	BSi MAR (mg/cm²/a)	TOC MAR (mg/cm²/a)	Depth (cm)	MAR (mg/cm²/a)	BSi MAR (mg/cm²/a)	TOC MAR (mg/cm²/a)
0	55.9645131	18.5004815	2.63257069	18	90.8494945	24.3799184	1.66254575
0.5	55.9645131	17.80663	3.42446855	18.5	94.2379069	24.2747593	1.7782693
1	55.9645131	16.3442355	1.98618057	19	94.2379069	25.2472491	1.85460201
1.5	55.9645131	13.7160654	1.84962716	19.5	92.8479403	23.1752858	1.88759863
2	59.0457087	15.3218549	2.07663758	20	93.125241	21.7802306	1.81221719
2.5	57.4993198	17.6174486	2.1475996	20.5	93.056228	23.2331398	1.84902725
3	62.8838522	15.8453438	2.77380672	21	93.056228	22.8861363	2.3115167
3.5	60.1740158	16.8322262	2.24930471	21.5	93.6288164	27.1556788	4.3977455
4	58.2434782	16.3211746	2.25344017	22	93.1339898	26.0767182	4.1435312
4.5	59.206483	16.0980558	2.16932554	22.5	93.1339898	29.3819458	3.50928873
5	65.4012355	19.1325837	2.3557525	23	94.1706886	25.5103327	3.40709551
5.5	62.280722	18.6605922	2.22964985	23.5	94.1706886	24.0754553	3.11422467
6	58.8446522	17.2060272	2.08663137	24	158.250567	17.9361248	4.15249487
6.5	61.416332	18.8750602	2.32829314	24.8	154.908745	1.01710486	3.78442063
7	60.1264836	16.8736981	2.48502757	25.2	143.692536	8.75255808	3.03622328
7.5	60.1264836	15.6380967	2.15493317	26	168.512749	9.35854849	3.13939251
8	60.1264836	16.004629	1.91562977	27	83.4450305	4.92584895	1.69476857
8.5	204.432425	20.5260463	4.5854193	28	122.196627	38.3334256	4.25610853
9	221.975912	6.19741297	2.31076924	29	58.2724236	21.3427525	1.91599729
9.2	213.068117	3.2608577	1.88352215	30	87.9262702	27.8832964	2.31246091
10	213.068117	6.28905216	2.22656182	32	68.2166385	19.2673832	1.74975678
11	61.9176123	23.5091734	1.72130962	33	71.117253	29.2094626	2.23663761
11.5	125.832533	37.1893866	2.99355595	34	70.488603	28.3527137	1.80450824
12	91.5863145	27.1996445	2.28782614	35	69.9371493	18.7907324	1.73024507
13	91.5863145	30.3103055	2.50580156	36	73.4164	20.3768328	1.5681743
13.5	91.5863145	28.005404	2.48198912	37	71.1849417	27.4898053	1.60593228
14	120.196419	30.6688532	3.31020937	39	71.1849417	19.0382065	1.13184057
14.5	105.444792	35.2684033	1.56058293	40	82.8514561	19.0973012	1.5816343
15	105.444792	35.4935853	1.55741958	41	123.065021	27.3976354	1.97888553
15.5	101.899682	19.568087	1.1555424	42	102.070288	24.6770951	1.7750023
16	102.486716	42.5180322	1.25648714	43	101.026122	33.2357397	2.45291424
16.5	106.99825	33.175306	1.90456885	44	108.500338	28.0918557	2.36530737
17	88.7294749	32.2176337	1.50485189	45	103.131513	25.8905511	1.88627537
17.5	97.6785309	26.2264994	1.76895819	46	82.3611058	23.6912647	1.53191657

Tab. B-28: Total (bulk sediment) and biogenic (BSi and TOC) mass accumulation rates of gravity core LVR4s of Lago Villarrica.

Depth (cm)	MAR ($mg/cm^2/a$)	BSi MAR ($mg/cm^2/a$)	TOC MAR ($mg/cm^2/a$)	Depth (cm)	MAR ($mg/cm^2/a$)	BSi MAR ($mg/cm^2/a$)	TOC MAR ($mg/cm^2/a$)
47	92.5039915	22.2111748	1.49208938	81	21.4490811	6.07750501	0.33053034
48	96.3980569	22.6833278	1.68214609	82	20.6098732	5.90455182	0.18507666
49	82.5879993	24.4425737	1.50723099	83	27.1980518	7.67674297	0.57279097
50	89.3851154	18.0857515	1.91284147	84	30.5687183	13.5184262	0.70185777
51	90.1607272	25.3052401	1.93845563	85	18.0352062	4.68471967	0.30984484
52	71.5764306	22.0150199	1.3835724	86	24.0166856	8.03870022	0.43806435
53	80.6692663	25.140003	1.79085771	87	21.5584144	7.14005634	0.35161774
54	82.8158233	21.4725197	1.81283837	88	22.1247622	6.74448647	0.41506054
55	8.59960016	1.81158898	0.16691824	89	----	----	----
56	18.4088033	1.33930127	----	90	22.3422356	9.91034596	0.44103573
57	13.0889553	0.76122092	0.43913445	91	51.4853305	18.0040392	0.92879536
58	20.3293843	0.72236855	0.47245489	92	44.5774498	15.5019952	0.77029833
59	16.4947915	0.69791857	0.36882354	93	47.988685	14.9776856	0.78893398
60	16.4947915	0.76400087	0.33204015	94	46.2725879	10.0567462	0.52843295
61	16.8682081	0.81909318	0.23733569	95	47.1279923	8.68944917	0.63669918
62	22.3729355	7.07366504	0.37362802	96	58.4969948	19.968316	0.94472647
63	19.5022897	6.15280799	0.2734221	97	52.6987662	19.4886297	0.86373278
64	----	----	----	98	55.5685868	15.9589145	0.90632365
65	18.7229158	7.52003511	0.33551465	99	47.1883317	19.8276177	0.86165894
66	18.6169508	7.2614026	0.34143488	100	51.3163534	17.2162669	0.86314106
67	18.7052302	6.3874611	0.34773023	101	49.2371587	16.0409917	0.77893185
68	8.46624635	2.82600025	0.15493231	102	50.0918723	18.6457437	0.98831264
69	----	----	----	103	49.6638655	16.3556324	0.88749328
70	13.1339434	3.78840619	0.17783359	104	49.6638655	19.9294082	0.98036471
71	27.3071887	9.6009821	0.46012613	105	36.939145	11.8502375	0.61503676
72	23.9668923	8.68068685	0.41390823	106	43.1541033	16.3226489	0.83028495
73	25.6169727	8.1486567	0.4941514	107	43.552562	16.4298651	0.81312633
74	26.2881614	9.8531842	0.48711963	108	41.1813634	13.2730185	0.62883942
75	23.126823	9.61832384	0.43501554	109	42.8366428	15.0137082	0.63955108
76	24.6893961	10.0530053	0.47403641	110	46.9092679	18.0792258	0.78385387
77	24.7284233	9.8458768	0.54550902	111	44.857942	15.793476	0.90433611
78	21.6257062	7.69628241	0.48744342	112	43.9295278	19.8398492	0.8935266
79	23.1594382	9.21763132	0.47268413	113	39.6294396	17.1185217	0.76207412
80	19.781049	7.45089527	0.39443412	114	41.7625569	14.1001983	0.70411671

Tab. B-28: Total (bulk sediment) and biogenic (BSi and TOC) mass accumulation rates of gravity core LVR4s of Lago Villarrica.

^{137}Cs and ^{210} Pb radionuclide dating

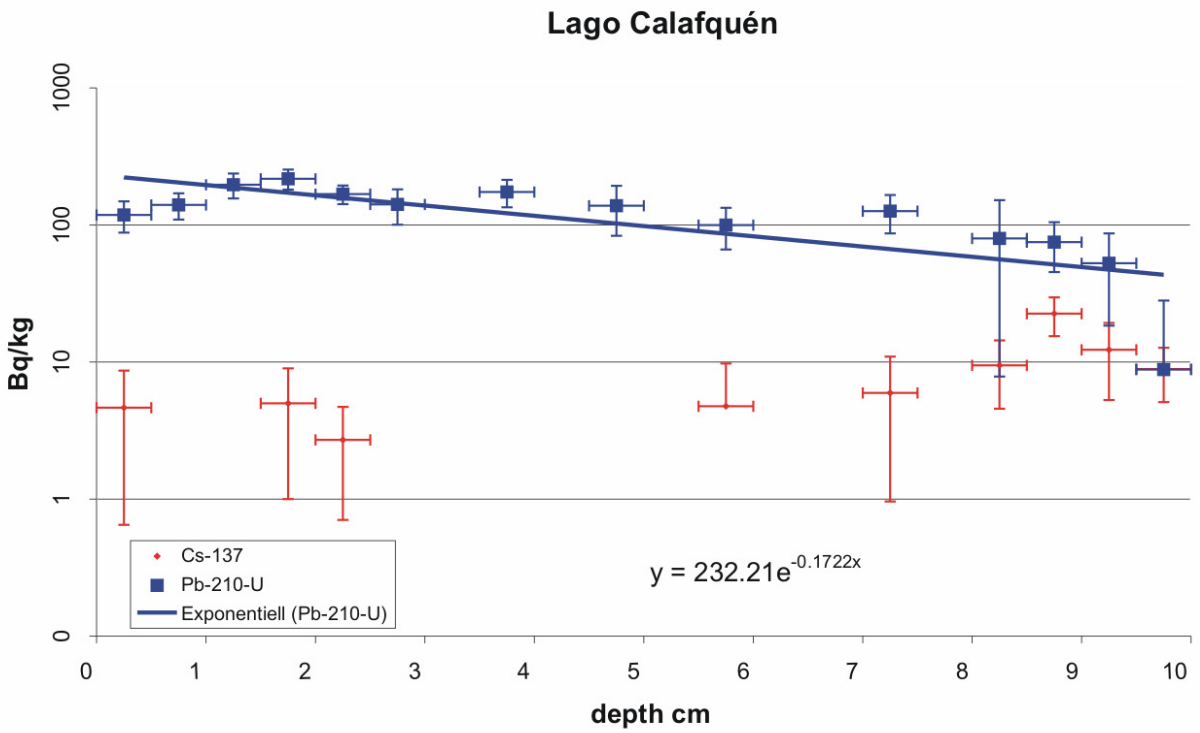

Fig. B-27: ^{137}Cs (red bars) and ^{210}Pb (blue bars) dating for 10 cm of surface sediments in Lago Calafquén analysed on short core LCQ2s.

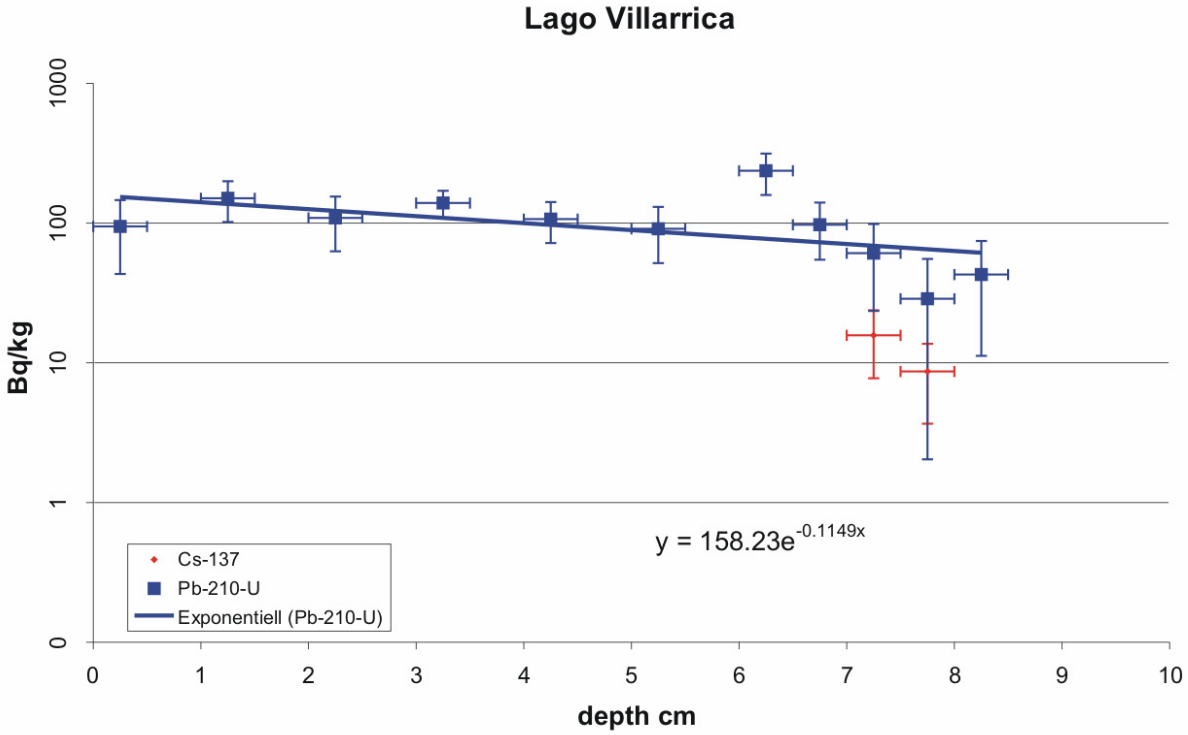

Fig. B-28: ^{137}Cs (red bars) and ^{210}Pb (blue bars) dating for 10 cm of surface sediments in Lago Villarrica analysed on short core LVR4s.

Appendix C – Tables of diatoms

TABLES OF DIATOMS

Genus: Cyclotella

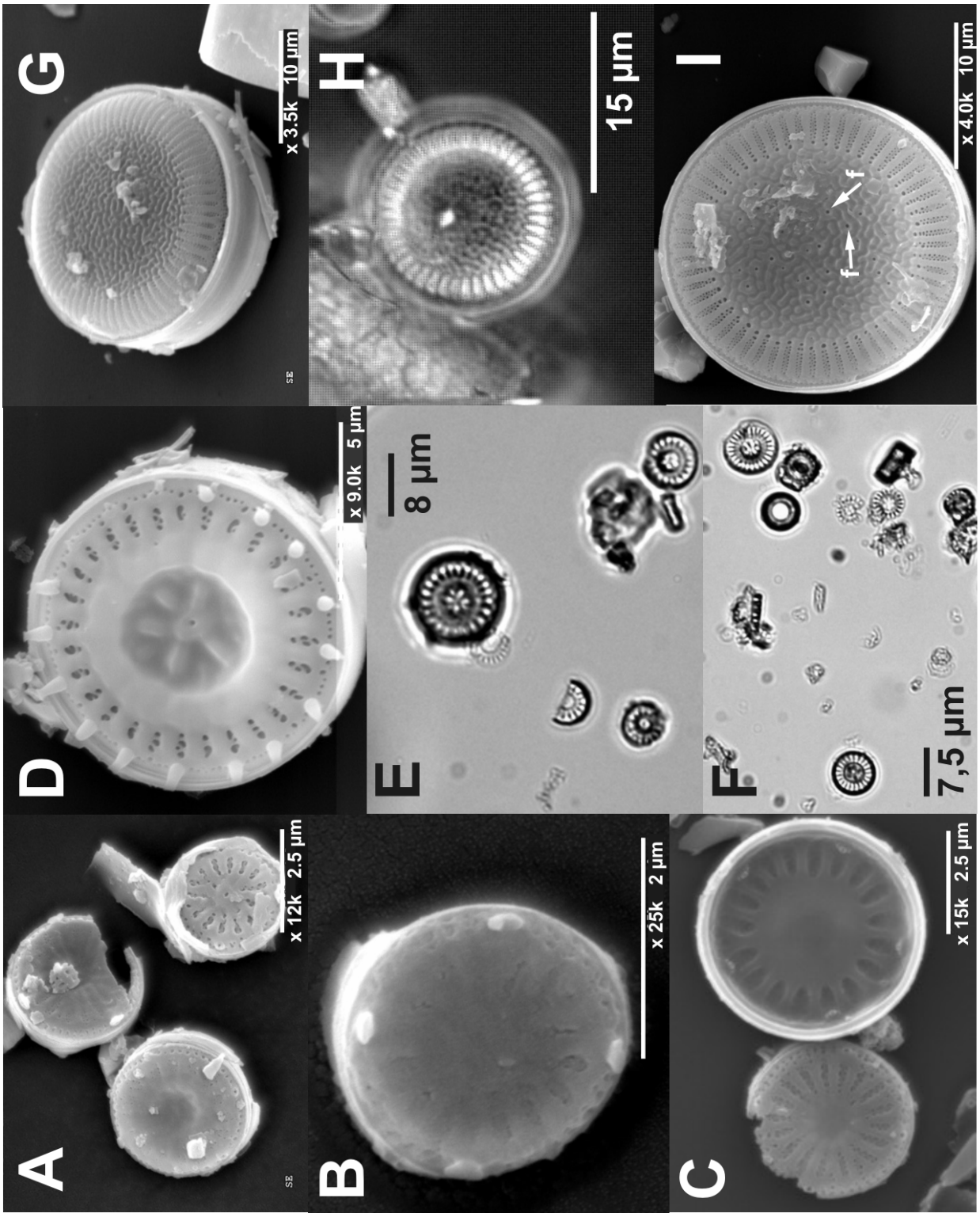

Fig. C-1: SEM photographs (A,B,C, and D) of *Cyclotella stelligera*. Valves are very small (down to ~ 2.5 µm) (A,B,C) and, therefore, difficult to identify in the light microscope (LM). LM pictures of *Cyclotella stellligera* (E, and F). Newly identified species *Cyclotella sp.* (SEM pictures G,H, and I, f=fultuportulae.).

Genus: Aulacoseira

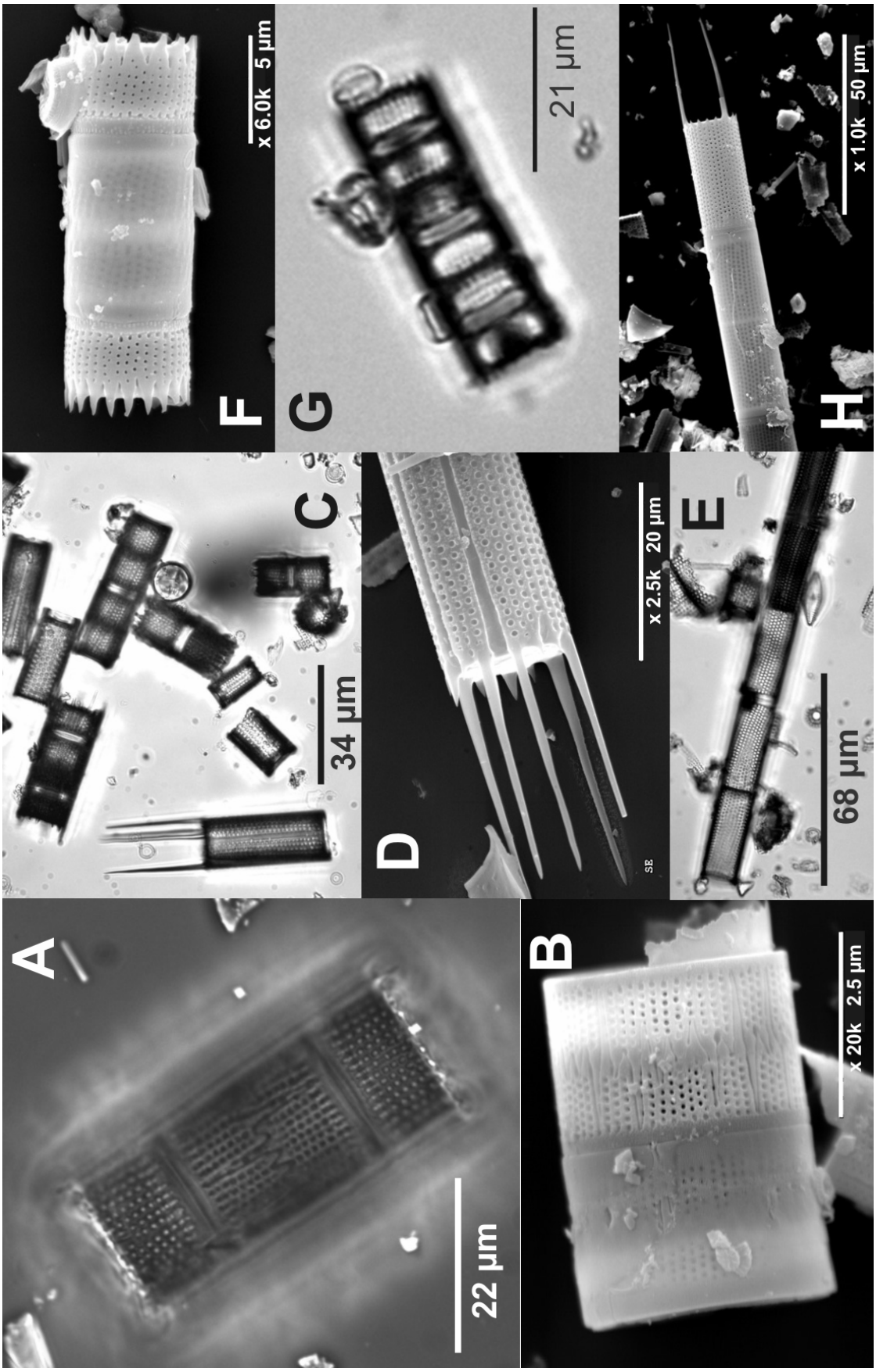

Fig. C-2: SEM photographs (A,B,D, and H) and LM pictures (C,E) of *Aulacoseira granulata.* Valves show a linear alignment of areolation. SEM (F) and LM picture of *Aulacoseira distans*.

Genus: Fragilaria

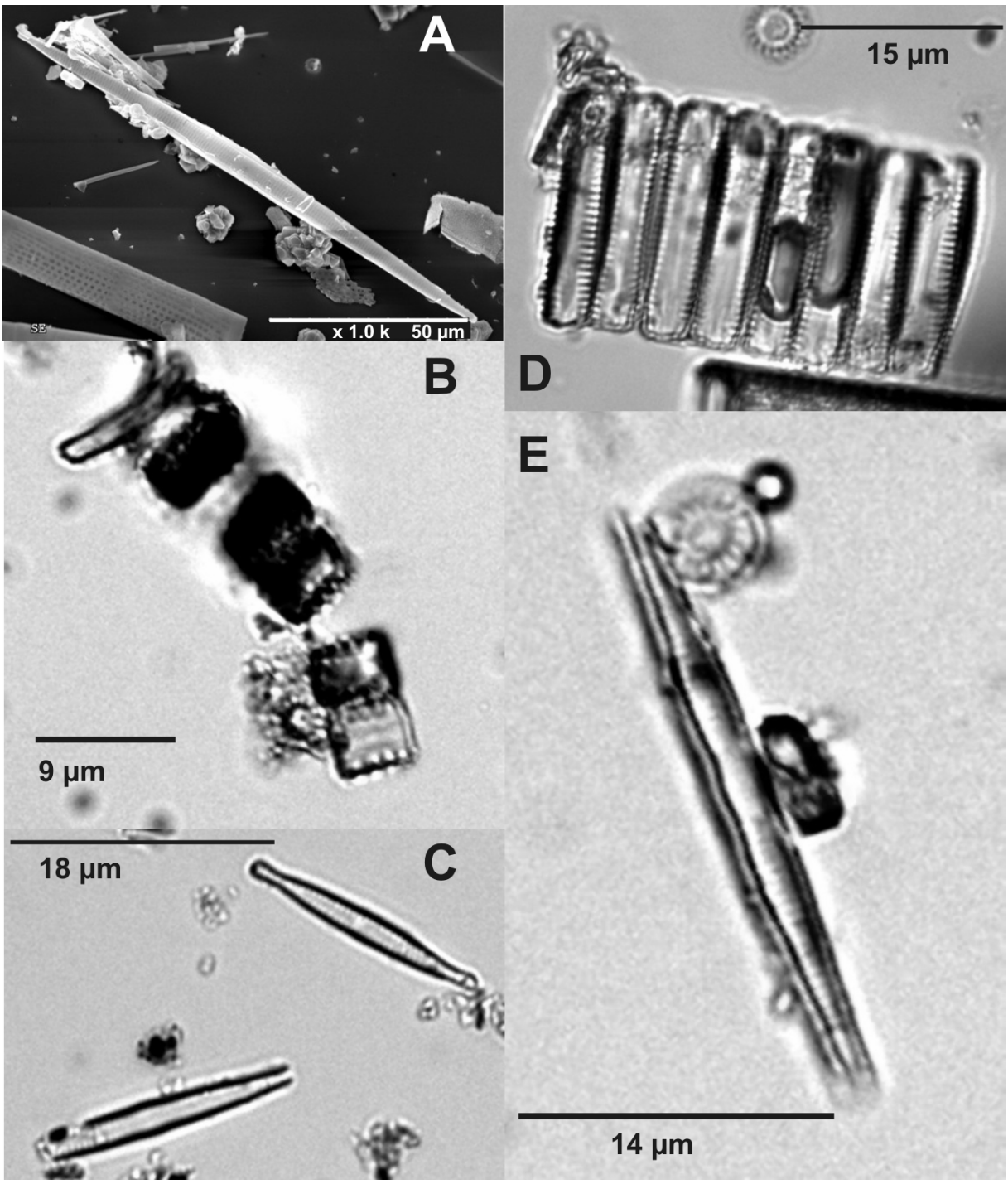

Fig. C-3: A) *Fragilaria acus* var. *ulna* (SEM photograph). B) *Fragilaria construens* var. *venter* (LM). C,E) *Fragilaria* cf. *capucina* (LM). D) *Fragilaria construens* var. *binodis* (LM).

Genus: Cyclostephanos

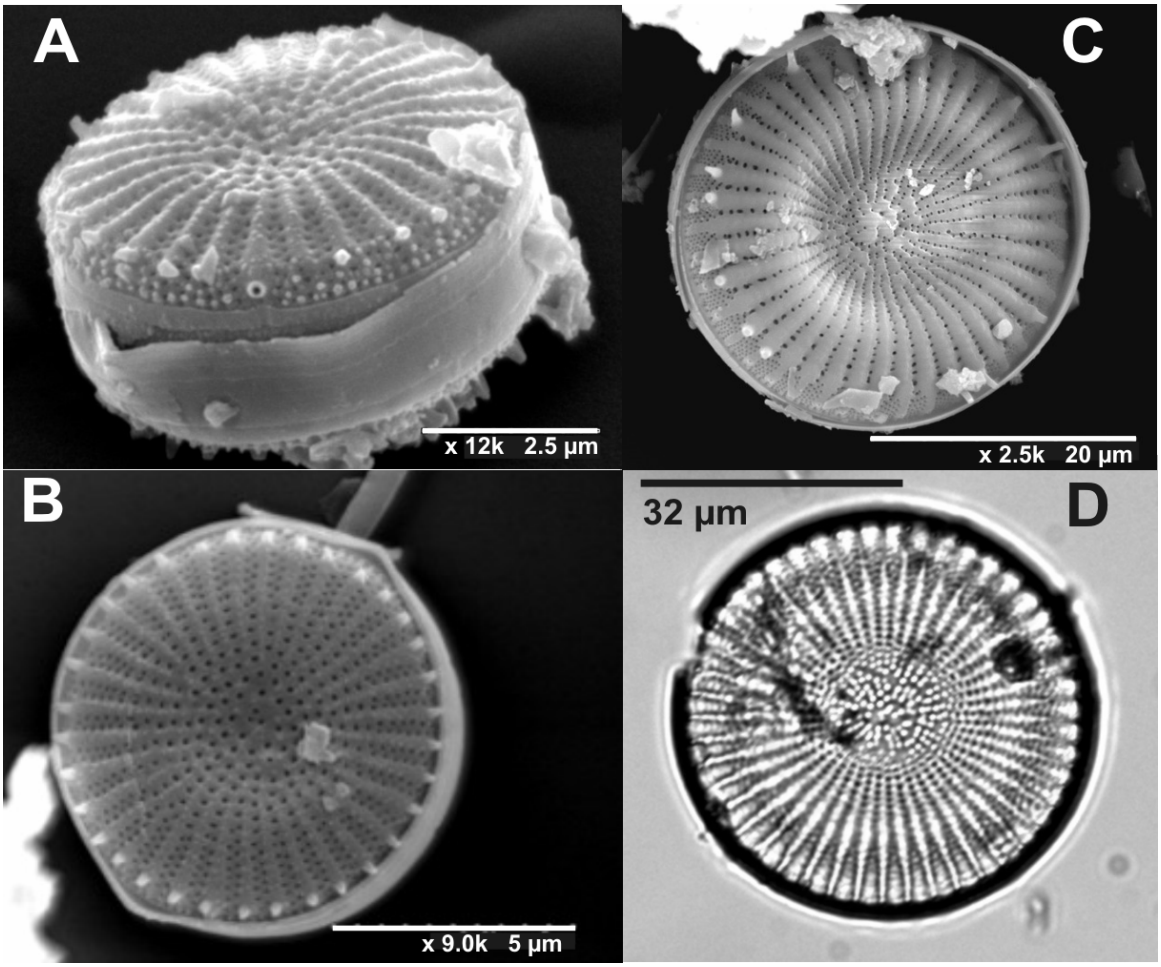

Fig. C-4: A,B) *Cyclostephanos* cf. *tholiformis* (SEM photograph). C,D) *Cyclostephanos patagonicus* (SEM and LM).

Genus: Melosira

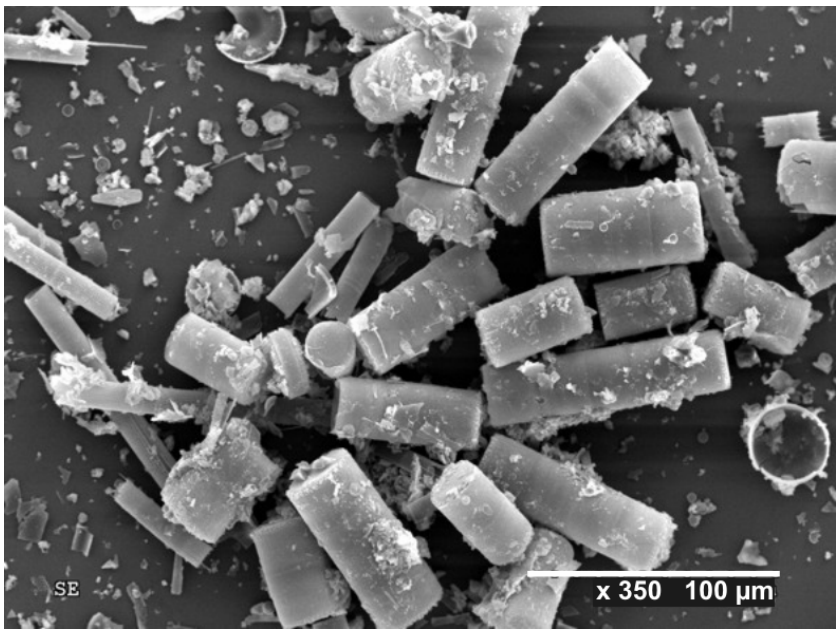

Fig. C-5: Colony of the benthic living species *Melosira varians* from the deep water core LVR4s from the profundal basin. Species agglomeration of sample LVR4s 111-112 cm.

Genus: Asterionella and Fragilaria

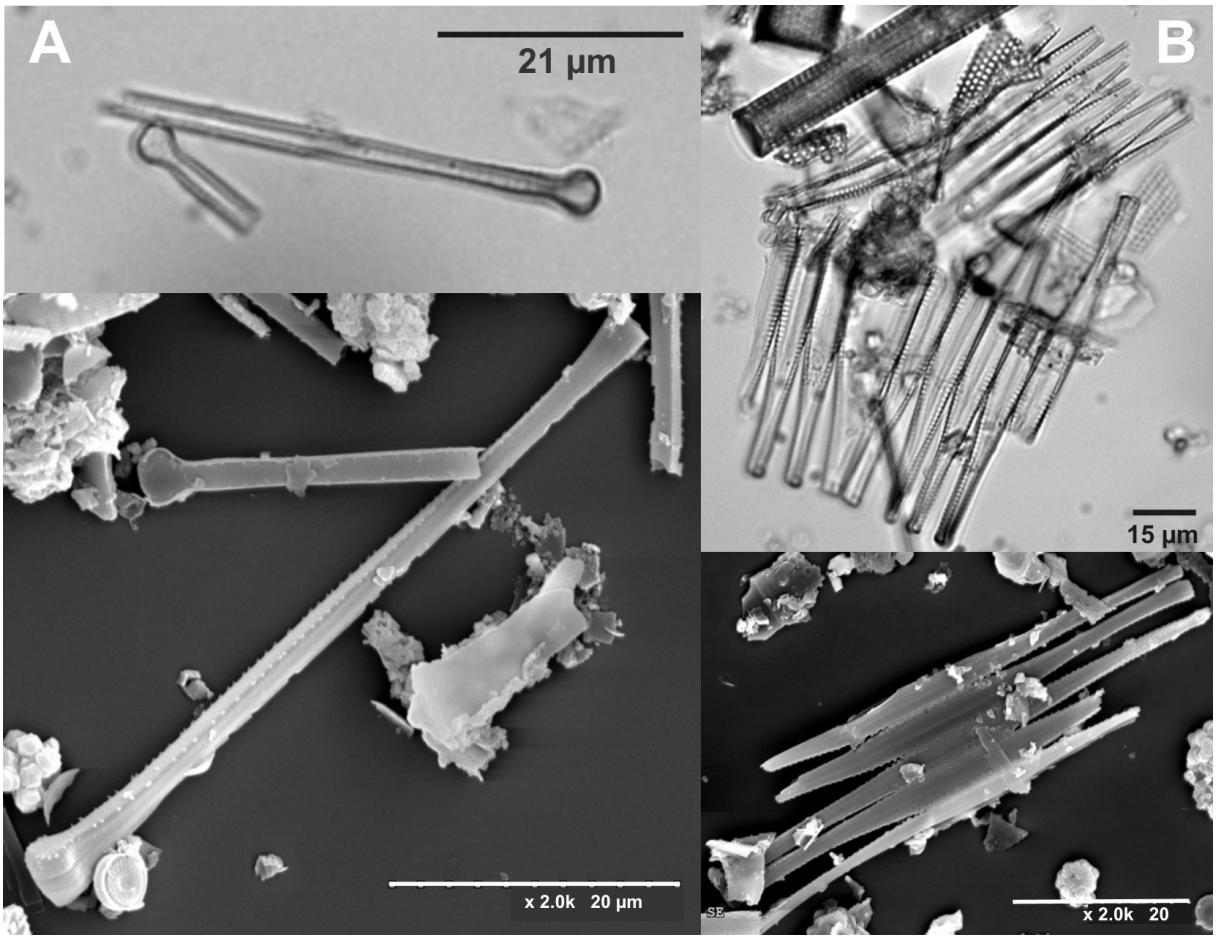

Fig. C-6: A) above LM and below SEM photograph of *Asterionella formosa*. B) above LM and below SEM photograph of *Fragilaria crotonensis.*

Genus: Gomphonema

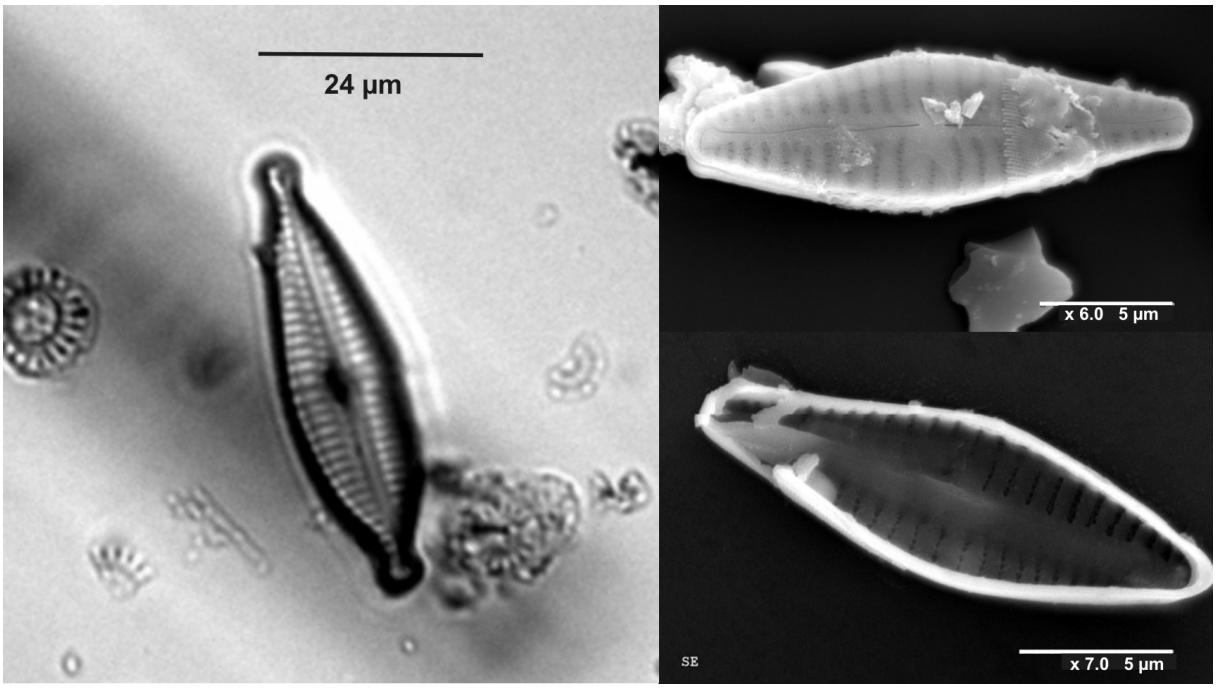

Fig. C-7: A) left LM and right SEM photograph of *Gomphonema parvulum* auct. partim.

Other species

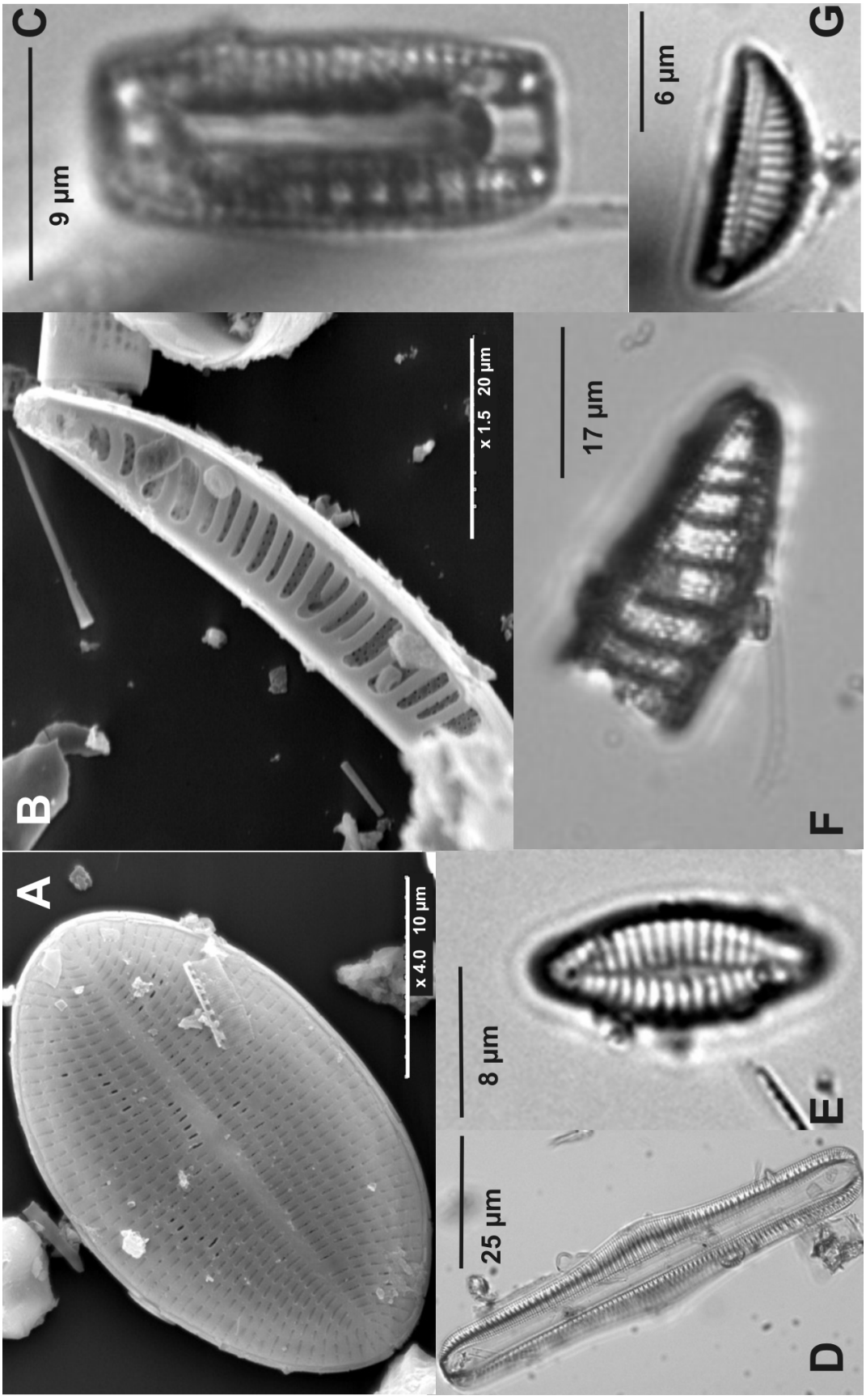

Fig. C-8: A) *Cocconeis placentula* (SEM photograph) , B) *Epithemia adnata* (SEM photograph), C) *Denticula sp.* in girdle view (LM), D) *Rhopalodia gibba* in girdle view (LM), E) *Fragilaria construens* var. *venter* in valve view, F) *Epithemia adnata* (LM), G) *Cymbella sp.* (LM).

Semiquantitative Diatom Analysis – Lago Calafquén

Sample	Depth (cm)	*Aulacoseira granulata* var. *granulata* (%)	*Cyclotella stelligera* (%)	*Cyclostephanos patagonicus* (%)	*Melosira varians* (%)	*Fragilaria crotonensis* (%)	*Aulacoseira subarctica* (%)	*Fragilaria construens* var. *binodis* (Ehrenb.) (%)	Others (%)	*Asterionella formosa* (%)	*Fragilaria construens* var. *venter* (%)
LCQ2s 3-4	3	72.71	15.52	2.12	3.59	1.31	2.78	0.65	1.31	0	0
LCQ2s 5-6	5	36.79	9.72	2.5	8.02	17.47	3.94	1.31	3.29	16.95	0
LCQ2s 8-9	8	27.38	35.41	1.8	26.39	0	6.39	0	2.3	0	0.33
LCQ2s 20.2	20.2	21.77	57.04	1.28	11.41	0	6.17	0.7	0.93	0	0.35
LCQ2s 22.5	22.5	42.52	54.79	0.98	0	0	0.082	0.41	1.22	0	0
LCQ2s 28-29	28	39.98	55.38	2.32	0	0	0	0.49	1.47	0	0.37
LCQ2s 32	32	39.31	58.15	1.47	0	0	0	0.08	0.9	0	0.08
LCQ2s 33	33	62.72	34.65	1.67	0	0	0	0	0.96	0	0
LCQ2s 39	39	30.93	46.12	0.78	1.55	0	17.96	0	1.77	0	0.89
LCQ2s 40	40	20.39	44.43	0.48	3.74	0	26	0.38	1.03	0	3.55
LCQ2s 45	45	42.96	51.49	2.98	0.1	0	0	1.64	0.72	0	0.1
LCQ2s 50	50	53.74	35.83	2.68	4.94	0.28	0	0	1.55	0	0.99
LCQ2s 53-54	54	29.28	62.5	1.2	3.08	0	0	0.34	2.23	0	1.37
LCQ2s 56	56	50.75	37.34	0.75	3.26	0.13	0	3	4.52	0	0
LCQ2s 60	60	38.53	56.01	1.56	2.12	0	0	0.33	1.48	0	0
LCQ2s 65-67	65	47.83	41.52	5.33	2.72	0	0	1.09	1.3	0	0.22
LCQ2s 74	74	42.76	48.81	2.28	3.19	0	0	0.68	2.28	0	0
LCQ2s 84	84	41.49	51.18	4.61	1.18	0	0	0.24	1.3	0	0

Tab. C-1: Semiquantitative diatom analysis of prevalent valves in gravity core LCQ2s of Lago Calafquén.

Sample	Depth (cm)	*Aulacoseira granulata* var. *granulata* (%)	*Cyclotella stelligera* (%)	*Cyclostephanos patagonicus* (%)	*Melosira varians* (%)	*Fragilaria crotonensis* (%)	*Aulacoseira subarctica* (%)	*Fragilaria construens* var. *binodis* (Ehrenb.) (%)	Others (%)	*Asterionella formosa* (%)	*Fragilaria construens* var. *venter* (%)
LCQ2s 90	90	27.47	64.21	2.98	0.79	0	0	2.67	1.88	0	0
LCQ2s 96	96	12.72	74.27	1.02	1.02	0	0	0	11.11	0	0
LCQ2s 100	100	23.99	60.59	1.07	8.18	0	0	1.61	4.56	0	0
LCQ2s 104	104	16.26	72.03	0.53	2.27	1.22	0	2.27	5.25	0	0
LCQ2s 115	115	63.9	27.12	6.39	0.35	0	0	0	2.07	0	0
LCQ2s 125	125	37.54	54.15	0.96	0.48	0	0	0.32	2.24	0	3.99
LCQ2s 149.5	149.5	37.93	53.51	0.97	2.21	0	0	1.79	1.93	0	1.38
LCQ2s 155	155	29.64	51.17	1.25	8.11	0	0	2.5	3.74	0	3.28
LCQ2s 161	161	30.29	45.62	1.83	5.11	0	0	11.31	5.11	0	0.73

Tab. C-1: Semiquantitative diatom analysis of prevalent valves in gravity core LCQ2s of Lago Calafquén.

Semiquantitative Diatom Analysis – Lago Villarrica

Sample	Depth (cm)	*Aulacoseira granulata* var. *granulata* (%)	*Cyclotella stelligera* (%)	*Cyclo-stephanos patagonicus* (%)	*Melosira varians (%)*	*Aulacoseira subarctica* (%)	*Fragilaria construens* var. *binodis* (Ehrenb.) (%)	Others (%)	*Gomphonema parvulum* (%)	*Cyclo-stephanos spec.* (*tholiformis?*) (%)	*Cyclotella spec.* (%)
LVR4s 2-3	2	43.65	16.83	1.11	0.48	1.9	1.9	1.75		0.95	
LVR4s 3-4	3	40.82	10.98	1.03	2.23	3.77	1.03	0.51		0.34	
LVR4s 4-5	4	14.15	59.62	0.79	0.95	3.82	0.95	3.02	0.32	14.31	1.43
LVR4s 5-6	5	46.86	20.57	1.9	12.57	2.48		4.95	4.76	5.71	0.19
LVR4s 6-7	6	38.05	21.22	1.72	2.49	2.68		2.68	2.1	19.12	1.15
LVR4s 7.8.8	7	18.24	12.05	2.93	1.72	1.89		2.58	4.99	8.09	0.69
LVR4s 12-13	12	41.47	23.52	2.69	1.26	3.05		6.46	5.92	8.44	7.18
LVR4s 16	16	24.4	48.4	1.63	3.26	2.76	1.38	5.83	8.83	2.13	1.12
LVR4s 23	23	22.44	57.86	2.46	3.28	0.41		5.61	4.24	1.78	1.92
LVR4s 25-25.5	25	5.66	63.63	0.51	1.37			1.89	5.15	20.75	
LVR4s 26-26.5	26	6.07	68.3	0.44	1.78	1.48	1.04	1.63	4.44	13.93	0.89
LVR4s 30-31	30	21.59	46.7	2.5	5.8	2.84	4.89	1.02	5.57	9.09	
LVR4s 34-35	34	21.28	62.64	0.97	0.36	0.97	2.66	0.61	6.41	4.11	
LVR4s 38.1-38.3	38.1	6.32	65.05	0.92	1.03	1.84	2.64	0.8	4.71	16.67	
LVR4s 41	41	15.74	51.9	5.54	1.9	9.69		2.94	4.15	6.23	1.9
LVR4s 43	43	29.23	46.74	5.93	2.32	5.07		3.91	2.32	3.18	1.3
LVR4s 52-53	52	13.28	68.04	1.11	2.49	2.21	4.98	0.83	7.05		
LVR4s 63	63	16.8	57.42	0.98			0.78	8.45	0.78	12.5	2.34

Tab. C-2: Semiquantitative diatom analysis of prevalent valves in gravity core LVR4s of Lago Villarrica.

Sample	Depth (cm)	*Aulacoseira granulata* var. *granulata* (%)	*Cyclotella stelligera* (%)	*Cyclo-stephanos patagonicus* (%)	*Melosira varians* (%)	*Aulacoseira subarctica* (%)	*Fragilaria construens* var. *binodis* (Ehrenb.) (%)	Others (%)	*Gomphonema parvulum* (%)	*Cyclo-stephanos spec.* (*tholiformis?*) (%)	*Cyclotella spec.* (%)
LVR4s 66	66	26.63	51.37	2.32	0.72			2.32	3.33	12.59	0.72
LVR4s 71	71	28.11	47.02	3.92	1.22			2.71	2.71	12.84	0.95
LVR4s 75	75	32.98	42.32	7.83	1.05		0.6	2.71	1.96	9.64	0.75
LVR4s 83	83	32.97	46.84	2.34	0.55			4.95	3.71	8.38	0.27
LVR4s 85	85	27.05	55.74	1.48	1.64			3.11	2.62	7.38	0.98
LVR4s 90	90	33.7	53.82	1.09	1.25			2.96	1.25	5.77	0.16
LVR4s 94	94	44.56	43.48	1.9	0.54			1.63	1.77	5.84	0.27
LVR4s 100	100	18.53	64.16	2.27	1.57		3.5	2.1	1.22	6.29	0.35
LVR4s 111-111.5	111	15.61	54.52	1.23	2.12	4.91	1.9	2	3.34	14.38	
LVR4s 114	114	51.17	43.34	0.82	0.55			1.51	1.51	1.1	

Tab. C-2: Semiquantitative diatom analysis of prevalent valves in gravity core LVR4s of Lago Villarrica.

Semiquantitative Diatom Analysis – Lago Villarrica

Sample	Depth (cm)	*Fragilaria crotonensis*	*Asterionella formosa*
LVR4s 2-3	2	31.43	0
LVR4s 3-4	3	39.28	0
LVR4s 4-5	4	0.64	0
LVR4s 5-6	5	0	0
LVR4s 6-7	6	3.63	5.16
LVR4s 7-8.8	7	18.76	27.36
LVR4s 12-13	12	0	0
LVR4s 16	16	0	0
LVR4s 23	23	0	0
LVR4s 25-25.5	25	0	0
LVR4s 26-26.5	26	0	0
LVR4s 30-31	30	0	0
LVR4s 34-35	34	0	0
LVR4s 38.1-38.3	38.1	0	0
LVR4s 41	41	0	0
LVR4s 43	43	0	0
LVR4s 52-53	52	0	0
LVR4s 63	63	0	0
LVR4s 66	66	0	0
LVR4s 71	71	0	0
LVR4s 75	75	0	0.15
LVR4s 83	83	0	0
LVR4s 85	85	0	0
LVR4s 90	90	0	0
LVR4s 94	94	0	0
LVR4s 100	100	0	0
LVR4s 111-111.5	111	0	0
LVR4s 114	114	0	0

Tab. C-3: Semiquantitative diatom analysis of *Fragilaria crotonensis* and *Asterionella formosa* valves in gravity core LVR4s of Lago Villarrica.